CORROSION PROTECTION SERVICE LIFE OF EPOXY COATED REINFORCING STEEL IN VIRGINIA BRIDGE DECKS

by

Michael Carey Brown

Dissertation submitted to the faculty of the

Virginia Polytechnic Institute and State University

in partial fulfillment of the requirements for the degree of

Doctor of Philosophy

in

Civil & Environmental Engineering

Committee Members

Richard E. Weyers, Chair
Sean G. Corcoran
Thomas E. Cousins
John G. Dillard
Alberto A. Sagüés
Michael M. Sprinkel

May 3, 2002
Blacksburg, Virginia

Keywords: corrosion, epoxy coating, concrete, reinforcement, impedance, service life

Copyright 2002, Michael C. Brown

CORROSION PROTECTION SERVICE LIFE OF EPOXY COATED REINFORCING STEEL IN VIRGINIA BRIDGE DECKS

Michael Carey Brown

ABSTRACT

The corrosion protection service life extension provided by epoxy-coated reinforcement (ECR) was determined by comparing ECR and bare bar from 10 bridge decks built between 1981 and 1995. The objective was to determine the corrosion protection service life time extension provided by ECR field specimens with various degrees of coating adhesion: disbonded, partially disbonded, and wholly bonded coatings.

The size and length distributions of cracks in Virginia bridge decks were investigated to assess the frequency and severity of cracks. Correlation of cracks with chloride penetration was used to characterize the influence of cracking on deck deterioration. Cracks influence the rate of chloride penetration, but the frequency and width distributions of cracks indicate that cracks are not likely to shorten the overall service life of most bridge decks in Virginia.

Altogether, 141 drilled cores, 102 mm (4 inches) in diameter, were employed in this study. For each of the decks built with ECR, 10 to 12 cores were drilled through a top reinforcing bar adjacent to the previous study core locations. In addition, approximately 3 cores were drilled through a top reinforcing bar at a surface crack location. Laboratory testing involved nondestructive monitoring using advanced electrochemical techniques to periodically assess the corrosion state of the steel bars during cyclic exposure to chloride-rich solution over 22 months of treatment. Time of corrosion initiation and time of cracking (where applicable), as well as chloride content of the concrete before and after treatment, were used in the analysis.

Less than 25 percent of all Virginia bridge decks built under specifications in place since 1981 is projected to corrode sufficiently to require rehabilitation within 100 years, regardless of bar type. The corrosion service life extension attributable to ECR in bridge decks was found to be approximately 5 years beyond that of bare steel.

ACKNOWLEDGEMENTS

I would first like to express my appreciation to Dr. Richard Weyers, who has guided me through my graduate experience. I want to thank the members of my doctoral committee, Dr. Sean Corcoran, Dr. Thomas Cousins, Dr. John Dillard, Dr. Alberto Sagüés, and Mr. Michael Sprinkel, who have contributed their time and expertise to this project.

I would like to express my sincere gratitude for the financial support of the National Science Foundation, under the Graduate Research Traineeship Program in Civil Infrastructure Systems at Virginia Tech. The Virginia Transportation Research Council provided funding and consultation over the duration of this project, and the Virginia Department of Transportation district residencies provided assistance during the field surveys in this study.

I wish to recognize my fellow students at Virginia Tech who assisted with portions of the study and made the working environment very enjoyable. Trevor Kirkpatrick was especially helpful in gathering and assessing data. I would like to thank my friends David Mokarem, Ryan Weyers, Rich Meyerson, and Ed Vincent for their support and companionship. I would like to express my appreciation to technicians Brett Farmer and Dennis Huffman for their skills, support and humor and to Julie Petruska for the many tests, consultations, and in-promptu chemistry lessons related to this and other projects. I also wish to recognize Dr. Christine Anderson-Cook for her invaluable assistance with the statistical analysis and probabilistic modeling portions of this study.

My parents are credited for their guidance and encouragement. Finally, I cannot overstate the importance of the love and support of my wife, Julie and my children, Alexander and Meghan.

TABLE OF CONTENTS

ABSTRACT ..... **ii**

ACKNOWLEDGEMENTS ..... **iii**

TABLE OF CONTENTS ..... **iv**

LIST OF TABLES ..... **vi**

LIST OF FIGURES ..... **viii**

INTRODUCTION **1**

BACKGROUND **2**

PURPOSE **4**

SCOPE **5**

REVIEW OF THE LITERATURE **6**
- Corrosion Deterioration of Concrete Structures 6
- Steel in Concrete: Passivity 6
- Corrosion of Steel in Concrete 7
  - Carbonation-Induced Corrosion 7
  - Chloride-Induced Corrosion 8
- Chloride Corrosion of Bare Steel In Concrete 8
  - Corrosion Initiation Concentrations 9
- Corrosion of the ECR in Concrete 10
  - Fusion Bonded ECR 10
  - Well Bonded Coatings 14
  - Disbonded Coatings (partially and wholly) 16
- Reinforcing Steel Corrosion-Induced Cracking of Cover Concrete 17
  - Process for Bare Reinforcement and ECR 17
  - Models for Bare Steel in Concrete 17
  - Applicability of Bare Steel Models to ECR 21
- Chloride-Induced Corrosion Assessment Methods for Steel in Concrete 22
  - Chloride Content 22
  - Corrosion Potential 23
  - Concrete Resistivity 24
  - Linear Polarization 25
  - Electrochemical Impedance Spectroscopy 27

METHODS AND MATERIALS **38**
- Field Survey and Sampling 38
  - Bridge Deck Selection 38
  - Sampling Plan 38
  - Field Evaluation 39
- Laboratory Testing 40
  - Sample Treatment and Exposure 40
  - Physical Testing 42
  - Post-cracking evaluation 47

RESULTS **48**
- Influence of Cracking 49
  - Field Survey 49
  - Laboratory Core Evaluations 50
- Corrosion Potential and Impedance Monitoring 53
  - Typical Impedance Plots 53
  - Determining Corrosion Initiation 54
- Chloride Concentrations at Time of Field Sampling and After Cracking 57

ANALYSIS AND DISCUSSION **70**
Crack Frequency and Influence on Durability 70
Field Crack Frequency 70
Crack Width and Depth in Cores 71
Chloride Concentration at Cracks and in Uncracked Locations 71
Accelerated Laboratory Treatment and Monitoring 74
Time to Corrosion Initation and Cracking 74
Propagation Time 77
Chloride Concentration at Reinforcement Depth after Cracking 78
Estimating Chloride Concentration at Reinforcement Depth at Corrosion Initiation 81
Probabilistic Model 84
Simulation Input Data 84
Estimating Service Life from Chloride Concentration at Corrosion Initiation 85
Estimating Service Life from Chloride Concentration after Cracking 86
Determining Corrosion Rate Ratios of ECR/Bare Steel 89
Stainless Steel as a Cost Effective Alternative 94

CONCLUSIONS **98**
Significance of Increased Chloride Penetration at Cracks 98
Service Life Extension of ECR 98
Benefits versus Risks of Corrosion Prevention Methods 95

RECOMMENDATIONS **99**

APPENDICES **108**

A SUPPORTING DATA **109**

B POTENTIAL AND IMPEDANCE TRENDS **127**

VITA **269**

LIST OF TABLES

Table 1 Interpretation of ASTM C 876-91 Corrosion Potential Readings 24
Table 2 Polarization Resistance and Corrosion Rates for Steel in Concrete (Sagüés, A. A. & Zayed, A. M., 1991) 27
Table 3 Impedance Circuit Elements (Geenen, F. M., 1991) 29
Table 4 ECR Decks to be Sampled (Pyc, W., 1998) 38
Table 5 Selection of ECR and Bare Steel Bridge Decks (Pyc, W., 1998) 39
Table 6 Core Sample Classification 48
Table 7 Bridge Superstructure Type and Reinforcing Steel Type 48
Table 8 Bridge Survey Area and Crack Length 49
Table 9 Initiation and Cracking Period (to date) – Bridge 1001/ECR 60
Table 10 Initiation and Cracking Period (to date) – Bridge 1004_3/ECR 60
Table 11 Initiation and Cracking Period (to date) – Bridge 1004_6/ECR 61
Table 12 Initiation and Cracking Period (to date) – Bridge 1015/ECR 61
Table 13 Initiation and Cracking Period (to date) – Bridge 1019/ECR 62
Table 14 Initiation and Cracking Period (to date) – Bridge 1136/ECR 62
Table 15 Initiation and Cracking Period (to date) – Bridge 2021/ECR 63
Table 16 Initiation and Cracking Period (to date) – Bridge 2262/ECR 63
Table 17 Initiation and Cracking Period (to date) – Bridge 6037/Bare 64
Table 18 Initiation and Cracking Period – Bridge 6128/Bare 64
Table 19 Chloride Concentrations – Bridge 1001/ECR 65
Table 20 Chloride Concentrations – Bridge 1004_3/ECR 65
Table 21 Chloride Concentrations – Bridge 1004_6/ECR 66
Table 22 Chloride Concentrations – Bridge 1015/ECR 66
Table 23 Chloride Concentrations – Bridge 1019/ECR 67
Table 24 Chloride Concentrations – Bridge 1136/ECR 67
Table 25 Chloride Concentrations – Bridge 2021/ECR 68
Table 26 Chloride Concentrations – Bridge 2262/ECR 68
Table 27 Chloride Concentrations – Bridge 6037/Bare 69
Table 28 Chloride Concentrations – Bridge 6128/Bare 69
Table 29 Bridge Crack Frequency 71
Table 30 Average Times to Initiation and Cracking for Bare Steel and ECR 75
Table 31 Percentiles of Propagation Times (ECR vs Bare) 90
Table 32 Critical Depth of Penetration for ECR vs Bare Steel 91
Table 33 Projected Mass Loss for Bare Steel 92
Table 34 Projected Mass Loss for ECR 93
Table 35 Estimated Propagation Times for ECR in Field Service 94
Table 36 Reinforcement Costs 95
Table 37 Unit Costs for Deck Reinforcement 95
Table 38 Summary Field Data for Bridge 1001 110
Table 39 Summary Field Data for Bridge 1004_3 111
Table 40 Summary Field Data for Bridge 1004_6 112
Table 41 Summary Field Data for Bridge 1015 113
Table 42 Summary Field Data for Bridge 1019 114

Table 43 Summary Field Data for Bridge 1136....115
Table 44 Summary Field Data for Bridge 2021....116
Table 45 Summary Field Data for Bridge 2262....117
Table 46 Summary Field Data for Bridge 6037....118
Table 47 Summary Field Data for Bridge 6128....120
Table 48 Density, Absorption, Permeable Voids and Saturation of Field Cores....121
Table 49 Potential and Impedance At Initiation – Bridges 1001 & 1004_3....122
Table 50 Potential and Impedance At Initiation – Bridges 1004_6 & 1015....123
Table 51 Potential and Impedance At Initiation – Bridges 1019 & 1136....124
Table 52 Potential and Impedance At Initiation – Bridges 2021 & 2262....125
Table 53 Potential and Impedance At Initiation – Bridges 6037 & 6128....126

LIST OF FIGURES

Figure 1 Service Life Model for Chloride-Induced Corrosion of Reinforced Concrete 2
Figure 2 Steel Corrosion Reactions in Concrete 8
Figure 3 Electrostatic Bar Coating Process 11
Figure 4 Representing Impedance in the Complex Plane (Geenen, F. M., 1991) 29
Figure 5 Potential versus Current in EIS Measurement 31
Figure 6 Bode Diagram 32
Figure 7 Nyquist Plot 32
Figure 8 Randles Equivalent Circuit Model 33
Figure 9 Constant Phase Element 35
Figure 10 Selected Bridge Locations 39
Figure 11 Core Section Plan 40
Figure 12 Core Observation 41
Figure 13 Ponding Specimen with Modified Ponding Reservoir 42
Figure 14 Test Probe and Cell Connections Design 44
Figure 15 Comparison of EIS at 10 Points(A) and 5 Points(B) per Decade Frequency 45
Figure 16 Post-cracking Sampling Plan for Laboratory Specimens 46
Figure 17 Predicting Chloride Content at the Bar Depth 51
Figure 18 Chloride Diffusion Parameters by Age – Surface Concentration, C_o 52
Figure 19 Chloride Diffusion Parameters by Age – Diffusion Coefficient, D_c 52
Figure 20 Typical Bode and Nyquist Plots for Bare Steel Before and After Initiation 55
Figure 21 Typical Bode and Nyquist Plots for ECR Before and After Initiation 56
Figure 22 Potential and Impedance Trends for Bare Steel Specimens (typical) 58
Figure 23 Potential and Impedance Trends for ECR Specimens (typical) 59
Figure 24. Crack Width and Depth 72
Figure 25 Comparisons of Chloride Concentration at 13mm Below Surface 73
Figure 26 Comparisons of Chloride Concentration at 19mm Above the Bar 73
Figure 27 Comparison of Time to Initiation Under Laboratory Exposure 76
Figure 28 Comparison of Time to Cracking Under Laboratory Exposure 76
Figure 29 Histograms of Corrosion Propagation Period for BS and ECR 77
Figure 30 Chloride Concentration at ECR Depth for Truncated Observations and Cracked Specimens 79
Figure 31 Chloride Concentration at Reinforcement Depth After Cracking 80
Figure 32 Chloride Concentration Diffrence: ECR minus Bare Steel (ΔCl^-_{cr}) Under Laboratory Treatment 80
Figure 33 Estimate of Chloride Concentration at Reinforcement Depth at Corrosion Initiation 83
Figure 34 Cumulative Time to Corrosion Initiation for Bare Steel 87
Figure 35 Cumulative Time to Corrosion Initiation for ECR 87
Figure 36 Cumulative Time to Cracking for Bare Steel 88
Figure 37 Cumulative Time to Cracking for ECR 88
Figure B-1 Potential and Impedance Summary for Specimen 1001_C1 128
Figure B-2 Potential and Impedance Summary for Specimen 1001_C2 129
Figure B-3 Potential and Impedance Summary for Specimen 1001_C3 130
Figure B-4 Potential and Impedance Summary for Specimen 1001_C4 131
Figure B-5 Potential and Impedance Summary for Specimen 1001_C5 132

Figure B-6 Potential and Impedance Summary for Specimen 1001_C6 133
Figure B-7 Potential and Impedance Summary for Specimen 1001_C7 134
Figure B-8 Potential and Impedance Summary for Specimen 1001_C8 135
Figure B-9 Potential and Impedance Summary for Specimen 1001_C9 136
Figure B-10 Potential and Impedance Summary for Specimen 1001_C10 137
Figure B-11 Potential and Impedance Summary for Specimen 1001_C11 138
Figure B-12 Potential and Impedance Summary for Specimen 1001_CR1 139
Figure B-13 Potential and Impedance Summary for Specimen 1001_CR2 140
Figure B-14 Potential and Impedance Summary for Specimen 1001_CR3 141
Figure B-15 Potential and Impedance Summary for Specimen 1004_3_C1 142
Figure B-16 Potential and Impedance Summary for Specimen 1004_3_C2 143
Figure B-17 Potential and Impedance Summary for Specimen 1004_3_C3 144
Figure B-18 Potential and Impedance Summary for Specimen 1004_3_C4 145
Figure B-19 Potential and Impedance Summary for Specimen 1004_3_C5 146
Figure B-20 Potential and Impedance Summary for Specimen 1004_3_C6 147
Figure B-21 Potential and Impedance Summary for Specimen 1004_3_C7 148
Figure B-22 Potential and Impedance Summary for Specimen 1004_3_C8 149
Figure B-23 Potential and Impedance Summary for Specimen 1004_3_C9 150
Figure B-24 Potential and Impedance Summary for Specimen 1004_3_C10 151
Figure B-25 Potential and Impedance Summary for Specimen 1004_3_C11 152
Figure B-26 Potential and Impedance Summary for Specimen 1004_3_C12 153
Figure B-27 Potential and Impedance Summary for Specimen 1004_3_CR2 154
Figure B-28 Potential and Impedance Summary for Specimen 1004_3_CR3 155
Figure B-29 Potential and Impedance Summary for Specimen 1004_6_C1 156
Figure B-30 Potential and Impedance Summary for Specimen 1004_6_C2 157
Figure B-31 Potential and Impedance Summary for Specimen 1004_6_C3 158
Figure B-32 Potential and Impedance Summary for Specimen 1004_6_C4 159
Figure B-33 Potential and Impedance Summary for Specimen 1004_6_C5 160
Figure B-34 Potential and Impedance Summary for Specimen 1004_6_C6 161
Figure B-35 Potential and Impedance Summary for Specimen 1004_6_C7 162
Figure B-36 Potential and Impedance Summary for Specimen 1004_6_C8 163
Figure B-37 Potential and Impedance Summary for Specimen 1004_6_C10 164
Figure B-38 Potential and Impedance Summary for Specimen 1004_6_C11/CR3 165
Figure B-39 Potential and Impedance Summary for Specimen 1004_6_C12 166
Figure B-40 Potential and Impedance Summary for Specimen 1004_6_CR1 167
Figure B-41 Potential and Impedance Summary for Specimen 1004_6_CR2 168
Figure B-42 Potential and Impedance Summary for Specimen 1015_C1 169
Figure B-43 Potential and Impedance Summary for Specimen 1015_C2 170
Figure B-44 Potential and Impedance Summary for Specimen 1015_C3 171
Figure B-45 Potential and Impedance Summary for Specimen 1015_C4 172
Figure B-46 Potential and Impedance Summary for Specimen 1015_C5 173
Figure B-47 Potential and Impedance Summary for Specimen 1015_C6 174
Figure B-48 Potential and Impedance Summary for Specimen 1015_C7 175
Figure B-49 Potential and Impedance Summary for Specimen 1015_C8 176

Figure B-50 Potential and Impedance Summary for Specimen 1015_C9 177
Figure B-51 Potential and Impedance Summary for Specimen 1015_C10 178
Figure B-52 Potential and Impedance Summary for Specimen 1015_CR1 179
Figure B-53 Potential and Impedance Summary for Specimen 1015_CR1b 180
Figure B-54 Potential and Impedance Summary for Specimen 1015_CR2 181
Figure B-55 Potential and Impedance Summary for Specimen 1015_CR3 182
Figure B-56 Potential and Impedance Summary for Specimen 1019_C1 183
Figure B-57 Potential and Impedance Summary for Specimen 1019_C2 184
Figure B-58 Potential and Impedance Summary for Specimen 1019_C3 185
Figure B-59 Potential and Impedance Summary for Specimen 1019_C4 186
Figure B-60 Potential and Impedance Summary for Specimen 1019_C5 187
Figure B-61 Potential and Impedance Summary for Specimen 1019_C6 188
Figure B-62 Potential and Impedance Summary for Specimen 1019_C7 189
Figure B-63 Potential and Impedance Summary for Specimen 1019_C8 190
Figure B-64 Potential and Impedance Summary for Specimen 1019_C9 191
Figure B-65 Potential and Impedance Summary for Specimen 1019_C10 192
Figure B-66 Potential and Impedance Summary for Specimen 1019_CR1 193
Figure B-67 Potential and Impedance Summary for Specimen 1019_CR2 194
Figure B-68 Potential and Impedance Summary for Specimen 1019_CR3 195
Figure B-69 Potential and Impedance Summary for Specimen 1136_C1 196
Figure B-70 Potential and Impedance Summary for Specimen 1136_C2 197
Figure B-71 Potential and Impedance Summary for Specimen 1136_C3 198
Figure B-72 Potential and Impedance Summary for Specimen 1136_C4 199
Figure B-73 Potential and Impedance Summary for Specimen 1136_C5 200
Figure B-74 Potential and Impedance Summary for Specimen 1136_C6 201
Figure B-75 Potential and Impedance Summary for Specimen 1136_C7 202
Figure B-76 Potential and Impedance Summary for Specimen 1136_C8 203
Figure B-77 Potential and Impedance Summary for Specimen 1136_C9 204
Figure B-78 Potential and Impedance Summary for Specimen 1136_C10 205
Figure B-79 Potential and Impedance Summary for Specimen 1136_C11 206
Figure B-80 Potential and Impedance Summary for Specimen 1136_C12 207
Figure B-81 Potential and Impedance Summary for Specimen 1136_CR1 208
Figure B-82 Potential and Impedance Summary for Specimen 1136_CR2 209
Figure B-83 Potential and Impedance Summary for Specimen 1136_CR3 210
Figure B-84 Potential and Impedance Summary for Specimen 2021_C1 211
Figure B-85 Potential and Impedance Summary for Specimen 2021_C2 212
Figure B-86 Potential and Impedance Summary for Specimen 2021_C3 213
Figure B-87 Potential and Impedance Summary for Specimen 2021_C4 214
Figure B-88 Potential and Impedance Summary for Specimen 2021_C5 215
Figure B-89 Potential and Impedance Summary for Specimen 2021_C6 216
Figure B-90 Potential and Impedance Summary for Specimen 2021_C7 217
Figure B-91 Potential and Impedance Summary for Specimen 2021_C8 218
Figure B-92 Potential and Impedance Summary for Specimen 2021_C9 219
Figure B-93 Potential and Impedance Summary for Specimen 2021_C10 220

Figure B-94 Potential and Impedance Summary for Specimen 2021_C11 221
Figure B-95 Potential and Impedance Summary for Specimen 2021_C12 222
Figure B-96 Potential and Impedance Summary for Specimen 2021_CR1 223
Figure B-97 Potential and Impedance Summary for Specimen 2021_CR2 224
Figure B-98 Potential and Impedance Summary for Specimen 2021_CR3 225
Figure B-99 Potential and Impedance Summary for Specimen 2262_C1 226
Figure B-100 Potential and Impedance Summary for Specimen 2262_C2 227
Figure B-101 Potential and Impedance Summary for Specimen 2262_C3 228
Figure B-102 Potential and Impedance Summary for Specimen 2262_C4 229
Figure B-103 Potential and Impedance Summary for Specimen 2262_C5 230
Figure B-104 Potential and Impedance Summary for Specimen 2262_C6 231
Figure B-105 Potential and Impedance Summary for Specimen 2262_C7 232
Figure B-106 Potential and Impedance Summary for Specimen 2262_C8 233
Figure B-107 Potential and Impedance Summary for Specimen 2262_C9 234
Figure B-108 Potential and Impedance Summary for Specimen 2262_C10 235
Figure B-109 Potential and Impedance Summary for Specimen 2262_C11 236
Figure B-110 Potential and Impedance Summary for Specimen 2262_C12 237
Figure B-111 Potential and Impedance Summary for Specimen 2262_CR1 238
Figure B-112 Potential and Impedance Summary for Specimen 2262_CR2 239
Figure B-113 Potential and Impedance Summary for Specimen 2262_CR3 240
Figure B-114 Potential and Impedance Summary for Specimen 6037_C1 241
Figure B-115 Potential and Impedance Summary for Specimen 6037_C2 242
Figure B-116 Potential and Impedance Summary for Specimen 6037_C3 243
Figure B-117 Potential and Impedance Summary for Specimen 6037_C4/CR1 244
Figure B-118 Potential and Impedance Summary for Specimen 6037_C5 245
Figure B-119 Potential and Impedance Summary for Specimen 6037_C6/CR2 246
Figure B-120 Potential and Impedance Summary for Specimen 6037_C7 247
Figure B-121 Potential and Impedance Summary for Specimen 6037_C8 248
Figure B-122 Potential and Impedance Summary for Specimen 6037_C9 249
Figure B-123 Potential and Impedance Summary for Specimen 6037_C10 250
Figure B-124 Potential and Impedance Summary for Specimen 6037_C11 251
Figure B-125 Potential and Impedance Summary for Specimen 6037_C12 252
Figure B-126 Potential and Impedance Summary for Specimen 6128_C1 253
Figure B-127 Potential and Impedance Summary for Specimen 6128_C2 254
Figure B-128 Potential and Impedance Summary for Specimen 6128_C3 255
Figure B-129 Potential and Impedance Summary for Specimen 6128_C4 256
Figure B-130 Potential and Impedance Summary for Specimen 6128_C5 257
Figure B-131 Potential and Impedance Summary for Specimen 6128_C6 258
Figure B-132 Potential and Impedance Summary for Specimen 6128_C7 259
Figure B-133 Potential and Impedance Summary for Specimen 6128_C8 260
Figure B-134 Potential and Impedance Summary for Specimen 6128_C9 261
Figure B-135 Potential and Impedance Summary for Specimen 6128_C10 262
Figure B-136 Potential and Impedance Summary for Specimen 6128_C11 263
Figure B-137 Potential and Impedance Summary for Specimen 6128_C12 264

Figure B-138 Potential and Impedance Summary for Specimen 6128_CR1.....265
Figure B-139 Potential and Impedance Summary for Specimen 6128_CR2.....266
Figure B-140 Potential and Impedance Summary for Specimen 6128_CR3.....267
Figure B-141 Potential and Impedance Summary for Specimen 6128_CR4.....268

INTRODUCTION

The Bridge Division of the Federal Highway Administration maintains the National Bridge Inventory, a database of highway bridges throughout the United States that are 6 meters (20 feet) or more in length. Bridges that are considered inadequate for current or projected use are classified as either structurally or functionally deficient. Structurally deficient bridges are those designated as needing significant maintenance attention, rehabilitation, or replacement. The National Transportation Statistics Report for 1999 states that in 1990, from a total of 572,205 rural and urban bridges over 24% (137,865) were considered structurally deficient (National Transportation Statistics 1999, 2000). A significant percentage of such deficiencies are due to reinforcing steel corrosion as a result of marine environment or deicing salt exposure.

A recent memorandum circulated within the Virginia Department of Transportation indicates that Virginia has a total of approximately 25 million square feet of bridge deck within 4,432 bridge structures that are eligible for maintenance replacement funding based on age and condition. Of this figure, 794 Virginia structures, comprising almost 14.7 million square feet of bridge deck, were considered part of the National Highway System (NHS) bridge inventory (Kerley, M., 1998).

In 1998, rehabilitation and replacement expenditures required for rehabilitation of existing bridge decks in Virginia were estimated to be $150 million. NHS structures accounted for nearly half, or $70 million, of the predicted rehabilitation costs. Meanwhile, the cost for replacement of NHS structures accounted for about $400 million dollars, or nearly 30% of the estimated $1.4 billion necessary for replacement of aged and structurally deficient bridge structures. These expenditures were above and beyond routine maintenance and inspection costs, which average over $10 million and $7 million per year, respectively (Kerley, M., 1998).

The Virginia Department of Transportation must address the growing need for maintenance and rehabilitation funding, in the face of shrinking revenues. Thus funded research has focused on corrosion prevention alternatives and life-cycle prediction for corrosion-related damage to Virginia bridge structures, in an effort to make informed decisions about rehabilitation and replacement alternatives.

BACKGROUND

In the late 1960s, corrosion of reinforcing steel in concrete bridges became a central point of concern in North America, as many bridges were in need of repair after only a few years of service (Manning, D. G., 1996). The rapid deterioration was attributed to the increased use of deicing salts (Cady, P. D., 1977). Swift improvements were made to increase concrete quality, depth of clear concrete cover, and to tighten quality assurance procedures. However, further research was deemed necessary for a long-term method of addressing reinforcing steel corrosion (Manning, D. G., 1996).

In 1972, the Federal Highway Administration (FHWA) and National Bureau of Standards (NBS, now National Institute of Standards and Technology, NIST) began a feasibility study of organic coatings to protect reinforcing steel in concrete bridge decks (Clear, K. C. et al., 1995; Weyers, R. E., 1995). By 1976, within four years of the placement of epoxy coated reinforcement (ECR) in the first test bridge deck in Pennsylvania, over 40 bridges in the U.S. had incorporated the material (Manning, D. G., 1996; Weyers, R. E., 1995). Epoxy coatings on steel became the prevalent corrosion prevention method by 1981.

In 1986, premature corrosion deterioration in 6-year-old bridge substructure components in the Florida Keys sparked a new debate over the long-term performance of ECR (Sagues, A. A. et al., 1994). As a result, studies in recent years have begun to question the long-term performance of epoxy coating systems toward corrosion prevention. Further work has been conducted by various state departments of transportation and independent researchers to characterize the life expectancy of structures built with ECR in a variety of climates. Meanwhile, some states, such as Florida and Oregon, have discontinued use of ECR altogether as an option for design and construction in coastal regions (Manning, D. G., 1996; Covino, B. S. et al., 2000).

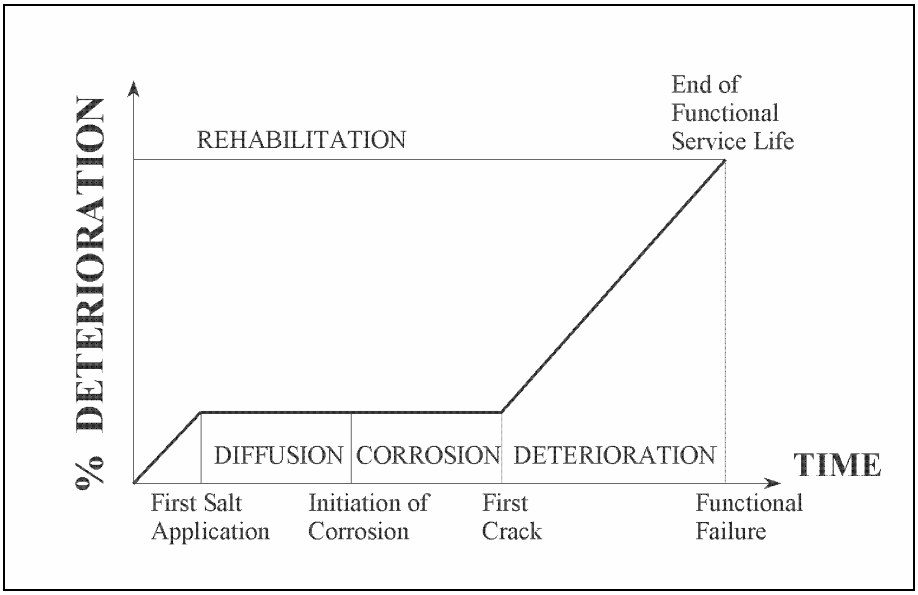

Figure 1 Service Life Model for Chloride-Induced Corrosion of Reinforced Concrete

Figure 1 illustrates a general service life model for reinforced concrete undergoing corrosion-related deterioration. Arguably, ECR has the same chloride initiation concentration at bare

locations (coating damage, holidays, and imperfections) as that of uncoated bars. This is supported by McDonald, et. al., who stated, "Half-cell potentials obtained for the damaged epoxy-coated bars were similar to that determined for black steel. Based upon this review, it was determined that the chloride threshold for damaged epoxy-coated bars is similar to that of black bars"(McDonald, D. B. et al., 1998). Therefore, the ECR service-life extension period will result from variations in the rate of metal dissolution and accumulation of corrosion product, and resultant differences in pressure being generated by the corrosion products over time during the active corrosion period.

PURPOSE

Information about service life, life-cycle costs and anticipated time to repair, rehabilitation, and/or replacement of bridge decks built with ECR would be useful to practicing bridge engineers and maintenance personnel. The purpose of the study was to compare ECR and bare bar from bridge decks built between 1981 and 1995 to determine the corrosion protection service life time extension provided by ECR field specimens with various degrees of coating adhesion: disbonded, partially disbonded, and wholly bonded coatings.

SCOPE

The extent of the research was limited to the sampling, preparation and testing of a series of concrete cores containing bare steel from 2 bridge decks, and ECR from 8 bridge decks. The samples were used in a laboratory investigation to assess the corrosion-related service life of ECR compared to bare steel. Laboratory testing involved nondestructive monitoring using advanced electrochemical techniques to periodically assess the corrosion state of the steel bars during cyclic exposure to chloride-rich solutions over 22 months of treatment.

To date, 27 of 28 bare steel and 21 of 113 ECR cores have developed cracks under cyclic ponding of chloride solution (treatment) and have been evaluated. In addition, treatment of 17 ECR specimens was terminated prior to cracking (truncated observations) to surmise the condition of the remaining uncracked ECR specimens. The present chloride content of the cores subject to truncation of observations was assessed. Time of corrosion initiation and time of cracking (where applicable), as well as chloride content of the concrete before and after treatment, were used in the analysis. At this time, 75 ECR cores remain under continued treatment and monitoring, and in this dissertation will only be analyzed with regard to whether and when corrosion initiated.

REVIEW OF THE LITERATURE

Corrosion Deterioration of Concrete Structures

Corrosion deterioration accounts for a significant percentage of annual expenditures by state and federal transportation agencies on bridge maintenance, repair or replacement. A review will be presented of the fundamentals of corrosion processes, as related to reinforced concrete, followed by discussion of ECR-specific phenomena, and evaluation techniques employed in current practice.

Steel in Concrete: Passivity

Corrosion of steel in concrete involves a complex series of reactions, the proportions of which may vary with environmental exposure and materials characteristics. However, for discussion, the overall process may be simplified into a series of general reactions. A model of the chemical reactions associated with corrosion deterioration of steel within concrete follows:

Generally, iron (Fe) atoms pass into solution as positively charged (Fe^{2+}) hydrated ions at the anodic site and the liberated electrons flow through the metal to cathodic sites, where dissolved oxygen is available to consume them.

In a high-pH environment, such as concrete, hydroxide (OH^-) is abundant in solution. Hydroxide ions may react with iron at the steel surface to create ferrous hydroxide ($Fe(OH)_2$). In electrochemical terms, this is the anodic reaction. Simultaneously, at an alternate location on the steel surface, dissolved oxygen (O_2) reacts with water (H_2O) and electrons released by the anodic reaction to form hydroxide ions (OH^-). This is the cathodic reaction. Together, the anodic reaction and the cathodic reaction form a corrosion cell, and the reactions proceed simultaneously. Further reaction of $Fe(OH)_2$ with water and oxygen results in transformation to the insoluble corrosion products, specifically hydrated iron oxide compounds in solution, which accumulate in the small pore spaces and the interfacial zone around the steel. The iron oxides include ferric oxide (Fe_2O_3, red-brown rust) and magnetite (Fe_3O_4, black rust). The above is a simplified description. Many other ions exist in concrete pore solution and the exact composition of the steel varies. Since the exact products may also vary with changes in pH, oxygen supply, and moisture content of concrete, Liu presented a generalized expression for corrosion products (Liu, Y. & Weyers, R. E., 1998):

$$m \cdot Fe(OH)_2 + n \cdot Fe(OH)_3 + p \cdot H_2O$$

Equation 1

Shortly after the bar is placed in fresh concrete, a thin "passive" layer of oxidized ferrous (Fe^{2+}) and ferric (Fe^{3+}) molecules naturally forms. The layer is a stratified film, with conductive magnetite at the steel surface covered by an insulating layer of ferric oxide, which is impermeable to ions (St. John, D.A., Poole, A.B., and Sims, I., 1998). Within the high-pH (~13) environment, and in the absence of aggressive ions, development of the passive layer, a corrosion process itself, continues at an ever-decreasing rate until the rate of iron dissolution becomes negligible. Once developed, the passive layer normally protects the reinforcement from

spontaneous corrosion in the moist concrete environment.(Bentur, A., Diamond, S., and Berke, N., 1997).

Corrosion of Steel in Concrete

Carbonation-Induced Corrosion

Carbonation is a process in which carbon dioxide, diffuses into the concrete from the air. Carbon dioxide dissolves into the available pore water to form carbonic acid and also reacts with calcium hydroxide, a component of portland cement, and cement phases to produce calcium carbonate (St. John, D.A., Poole, A.B., and Sims, I., 1998):

$$Ca(OH)_2 + CO_2 \rightarrow CaCO_3 + H_2O$$ **Equation 2**

$$Calcium\ silicate\ hydrates + CO_2 \rightarrow CaCO_3 + SiO_2nH_2O + H_2O$$ **Equation 3**

$$Aluminate\ hydrates + CO_2 \rightarrow CaCO_3 + hydrated\ alumina$$ **Equation 4**

$$Ferrite\ hydrates + CO_2 \rightarrow CaCO_3 + hydrated\ alumina\ and\ iron\ oxides$$ **Equation 5**

Carbonation induced corrosion of reinforcing steel is less prevalent in the United States than in European countries. Carbonation of moderate to good quality concrete is a slow process, and becomes significant in structures that are many decades of age, or exposed to environments containing high concentrations of carbon dioxide, such as transit tunnels. Poor quality concretes with porous internal structure allow faster diffusion of carbon dioxide, and therefore are more susceptible to carbonation. Carbonation occurs slowly in saturated concrete, but is accelerated in concrete where internal relative humidity decreases to 50 to 70 percent. The phenomenon is tied to a reduction of the pH of the concrete surrounding the reinforcing steel. The reaction product, calcium carbonate, has a pH of about 9.5, which is below the level necessary to sustain the passive layer (St. John, D.A., Poole, A.B., and Sims, I., 1998). Thus, once the carbonation "front" reaches the depth of reinforcement, so long as sufficient moisture and oxygen are present, spontaneous corrosion may occur, especially at locations where the passive layer may be damaged. The associated corrosion reactions are:

Anode: $3Fe + 8OH^- \rightarrow Fe_3O_4 + 4H_2O + 8e^-$ **Equation 6**

Cathode: $8e^- + 4H_2O + 2O_2 \rightarrow 8OH^-$ **Equation 7**

Chloride-Induced Corrosion

Chloride ions (Cl^-) that diffuse through liquid phases in the concrete to the steel surface can disrupt the passive layer and induce corrosion, even in a high-pH environment. Chloride ions may react with iron compounds in the passive layer to create an iron-chloride complex ($FeCl_2$). The iron-chloride subsequently reacts with hydroxide ions within the surrounding concrete to form ferrous hydroxide ($Fe(OH)_2$). The process is shown schematically in Figure 2. Then the available iron hydroxide continues the development of corrosion products and the chloride is released to further react with the passive layer (Bentur, A., Diamond, S., and Berke, N., 1997).

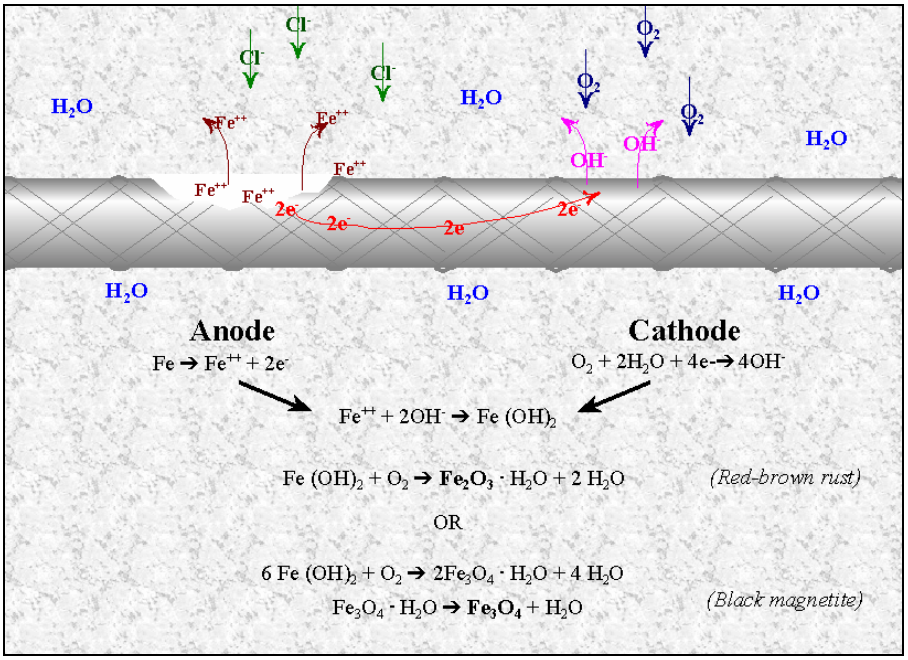

Figure 2 Steel Corrosion Reactions in Concrete

Many corrosion cells may exist within a concrete member simultaneously. Localized corrosion, or micro-cell corrosion cells, involves anode and cathode reactions occurring adjacent to one another on the same metal surface. Macro-cell corrosion cells involve anode and cathode reactions occurring at distant locations on the same or on different bars or metal elements that are electrically continuous. A particularly insidious form of micro-cell corrosion, termed pitting, is usually the observed phenomena in chloride-induced corrosion of reinforcing steel. In many cases corrosion initiates as pitting in highly localized areas of greater chloride concentration and/or inclusions in the steel surface or passive layer. The pitting continues until anodic areas are large enough to resemble or revert to general corrosion conditions.

Chloride Corrosion of Bare Steel In Concrete

The initiation and rate of chloride-induced corrosion is influenced by many factors, such as moisture content, chloride content, and concrete resistivity. For chloride-induced corrosion to initiate on an uncoated reinforcing steel bar in concrete with a mature passive layer, sufficient chloride must reach the surface to breach the passive layer or an inclusion must already exist. It has been reported that chloride displaces hydroxide in an ion exchange at the steel-concrete

interface. The hydroxide thus leaches out as the chloride diffuses in, causing a localized reduction in solution pH.(Byfors, K., 1986).

Corrosion Initiation Concentrations

The concentration of chloride necessary to initiate corrosion is not a fixed value, and significant variation exists between structures and within a structure. Indeed, depassivation remains nebulous, as potential shifts and sporadic corrosion may occur, but not be stable at lower concentrations. Thus the question remains: at what point does one define depassivation and the associated chloride threshold concentration? Further, the chloride concentration necessary to initiate corrosion in reinforced concrete may be influenced by many factors, including:(Alonso, C. et al., 2000)

- concrete mix proportions
- cement type
- tri-calcium aluminate (C_3A) content of the cement
- w/c ratio
- temperature
- relative humidity
- source of chloride penetration

A simple expression of chloride concentration is in terms of the mass of chloride per unit volume of concrete. Wide variations cement content, water content, air content, and unit weights of aggregates in the concrete mixture designs employed in practice make this a poor choice. Often researchers conducting solution studies refer to the ratio of chloride to hydroxide in solution as a more definitive measure. The argument has been made that this more directly addresses the relevant mechanism of sufficient quantity of chloride to overcome the passivation effect of hydroxide. However, determination of precise OH^- concentration in reinforced concrete can be difficult to assess. Therefore, pragmatic concrete researchers prefer to use the mass ratio of measured chloride to cement, since data of this type is far simpler to obtain.

The measured chloride may be derived from acid-soluble chloride concentration or water-soluble chloride concentration test methods. Many practitioners refer to acid-soluble as "total" chloride, although this may be a misnomer. Similarly, water-soluble chloride concentrations may be referred to as "free" chloride. The difference is termed "bound" chloride, which is chemically combined with the cement paste constituents or confined within aggregates. Significant differences of opinion exist among researchers concerning which is the more appropriate measure.

Researchers who have studied samples in solution, either filtered cement slurry solutions or synthetically simulated pore solutions, have indicated that a threshold quantity of chloride exists below which corrosion will not occur. In an analysis of literature on chloride threshold for corrosion initiation, Glass concluded that chloride threshold levels are best presented as a weight percentage of acid-soluble chloride to cement, finding that this expression results in the smallest range of values (Glass, G. K. & Buenfeld, N. R., 1997). However, the threshold is believed to be directly dependent upon pH and the ratio of free to fixed chloride, and therefore varies not only between different concretes, but also by location within a single structure (Vassie, P., 1984).

Glass also noted that variations in the interface between the steel and cement paste greatly influence the corrosion threshold, but that such variations are difficult to quantify. Some studies, by Haussman and others, indicate that corrosion risk increases in a nearly linear fashion with increasing chloride concentration, rather than a rapid increase in corrosion rate at a particular chloride concentration (Glass, G. K. & Buenfeld, N. R., 1997).

Commonly cited threshold concentration values are approximately 0.7 kg chloride per cubic meter of concrete (1.2 pcy) or 0.2% chloride by weight of cement. However, these represent a conservative approach that represents a low probability of corrosion initiation. Indeed, chloride thresholds may vary by an order of magnitude or more. Summary data from U.S. bridges indicated a range from 0.59 to 5.1 kg Cl^-/m^3 concrete, representing minimal to very high corrosion risk (Glass, G. K. & Buenfeld, N. R., 1997).

Corrosion of the ECR in Concrete

Fusion Bonded ECR

The first step in understanding of the performance of epoxy coatings on reinforcing steel in concrete, is to identify the properties of the coating which influence the corrosion process.

Materials (Epoxy and Steel Bar)

The organic material that has developed into most common usage in the United States, as a protective coating for steel reinforcement, is a bisphenol-amine epoxy. Epoxy resins, also referred to as ethyoxyline resins, are produced by the condensation of bis phenol A ($(HOC_6H_4)_2C(CH_3)_2$) and epichlorohydrin ($CH_2(O)CHCH_2Cl$). The material can be cured at ambient or elevated temperature with an amino resin (Seymour, R.B. & Mark, H.F., 1990). The epoxy is a thermo-setting plastic that is resistant to solvents, chemicals and water. This general material was identified as a potential corrosion resistive coating for reinforcing steel during the initial FHWA-funded study conducted at NBS. Research has shown that defect-free epoxy coatings resist the diffusion of chloride and oxygen, but are not impermeable to moisture (Clear, K. C. et al., 1995).

The bisphenol amine epoxy has mechanical properties, such as high ductility, low shrinkage during curing, and heat resistance, which make it desirable for use as a reinforcing steel coating (Manning, D. G., 1996). Most epoxies have a specific gravity of approximately 1.2 and withstand temperatures of 125°C. Epoxy coatings have a Rockwell M hardness of 90 (Seymour, R.B. & Mark, H.F., 1990).

Process

Epoxy coatings for reinforcing steel are generally prepared and applied by one of two methods: two-part liquid or powder.

Liquid Resin

Liquid epoxy is commonly prepared by mixing stoichiometrically balanced proportions of a two-part system, epoxy resin and polyamine. The liquid epoxy is applied by brushing or spraying, or by immersing the bars to be coated. The former method is most appropriate for field

dressing of observed damage on reinforcing bars prior to concrete placement. The liquid coatings commonly contain solvents that, upon evaporation, may result in pore formation within the cured coating. Shrinkage due to solvent loss and curing is also a concern with the use of liquid epoxy coatings (Salparanta, L., 1988).

Fusion-Bonded Powder

The most commonly used fabrication method for ECR involves fusion bonding of epoxy. The material, in the form of a powder (10-100 μm) bearing an electrostatic charge, is applied to the hot, freshly blasted reinforcing steel surface (Seymour, R.B. & Mark, H.F., 1990). The application temperature is commonly on the order of 204°C to 230°C (400°F to 446°F) (Manning, D. G., 1996; Sagues, A. A. & Zayed, A. M., 1991; Sagues, A. et al., 1990). The electrically charged powder particles are attracted to the preheated steel, and melt to form a continuous film, then the system is quenched to form a solid coating as shown in Figure 3.

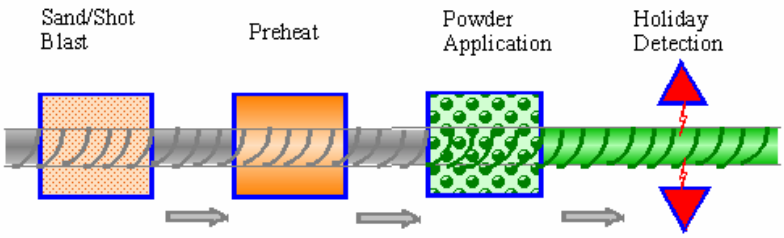

Figure 3 Electrostatic Bar Coating Process

The epoxy coating cures through a combination of physical and chemical curing. The physical process involves the melting and sintering of powdered constituents at elevated temperature, to form a continuous film from the separate powder particles. As the powder particles melt and fuse, a reactive cure is also initiated, where a polymer network is formed from the poly-addition reaction between components in the thermo-setting powder (Geenen, F. M., 1991). Curing time, shrinkage and pore development within the coating are significantly reduced, since powder epoxy coatings do not require solvents (Salparanta, L., 1988).

Corrosion Resistant Properties (ECR: Chemical and Physical)

Epoxy resins have characteristically excellent adhesion and corrosion resistance.
The fundamental mechanisms of corrosion control by coatings are as follows (Revie, R.W., 2000):

Barrier coatings that protect by:

- Resistance inhibition: provide electrical resistance to limit current transfer between anodic and cathodic sites.
- Oxygen deprivation: exclude oxygen to impede the cathodic reaction.
- Cathodic (galvanic) protection: introduce a less noble metal or pigment to perform as a sacrificial anode.

- Inhibition or aestivation: material is introduced into the interfacial environment that stimulates the development of passive or inhibitive surface films.

Physical Barrier

Theoretically, coatings form a physical barrier between metal substrate in the aqueous corrosive environment. This mechanism was the theoretical basis for implementation of ECR as a corrosion prevention strategy in reinforced concrete (Covino, B. S. et al., 2000).
Physical barrier properties are limited, since all organic coatings are known to be permeable to water and oxygen to some extent. Further, the barrier theory of protection is predicated on the existence of a uniform, defect-free coating, which has proven unachievable under practical construction conditions (Clear, K. C. et al., 1995). The particulars of this problem will be illustrated in the following sections.

Coating Thickness

The film thickness of typical epoxy coating on rebar is between 0.13mm and 0.30mm after curing, with an optimum value between 0.13 and 0.23mm (Manning, D. G., 1996; Bentur, A., Diamond, S., and Berke, N., 1997; Sagues, A. et al., 1990; Pyc, W., 1998). The "Interim Specifications for Epoxy-Coated Reinforcing Steel" used in the placement of the first production bridge decks containing ECR specified a uniform, smooth coating with thickness of 178 ± 51 μm (7 ± 2 mils), as recommended by NBS. ASTM standard A 775-89a, Epoxy Coated Reinforcing Steel Bars, specified at least 90% of thickness readings to be between 127μm and 305μm (5 and 12 mils.) In 1993, the specification limits changed to 90% within 178 to 305μm (7-12 mils), with no reading less than 127μm (5 mils), nor greater than 330μm (13 mils.) ASTM Specification D 3963, "Standard Specification for Epoxy-Coated Reinforcing Steel" progressed in much the same way over time (Weyers, R. E., 1995).

In 1983, Satake and others reported on ECR specimens in concrete under accelerated laboratory and tidal exposure. He concluded that an epoxy coating thickness of 200 μm was sufficient to protect the steel from chloride-induced corrosion (Satake, J. et al., 1983).

A 1984 study published by Kobayashi and Takewaka demonstrated that the occurrence of pinholes in epoxy coating was inversely proportional to coating thickness, with a subsequent influence on corrosion during laboratory testing (Kobayashi, K. & Takewaka, K., 1984).

Holidays

The "Interim" specifications permitted no visible holes, voids, cracks or deficient areas, and no more than 2 holidays per 0.3 m (linear foot) of coated bar, to be checked using a 67.5 volt holiday detector. ASTM A 775-89a reflected the same requirements, with total deficiencies totaling less than 0.5% of the surface area of the bar. In 1993, the total deficiencies requirement was removed.(Weyers, R. E., 1995).

Bending

The "Interim" specification required a 19mm diameter bar (No. 6) be bent 120° at room temperature over a mandrel of 76mm (3 inch) radius without visible cracking of the coating. ASTM A 775-89a requirements were similar, but a 152mm (6 inch) radius mandrel was employed. Notably, Ontario and British specifications were more stringent, requiring smaller mandrel radius and shorter bending times than the ASTM requirements (Weyers, R. E., 1995).

In 1989, an investigation of the influence of fabrication and service conditions on the corrosion protection performance of ECR was published. Sections of 22 mm bar were bent 180° around 112,133, and 165 mm diameter anvils, and cast into concrete specimens. After immersion in 5% NaCl for 300 days, corrosion potential chloride content, and EIS measurements were conducted, as well as destructive visual observation. Fabrication was found to cause coating disbondment, and corrosion occurred under the disbonded coating (Zayed, A. M. & Sagues, A. A., 1989; Sagues, A. A. & Zayed, A. M., 1989; Sagues, A. A. & Powers, R. G., 1990).

Coating damage

Minor damaged areas and sheared or cut ends were required to be repaired or patched using an appropriate material supplied by the epoxy coating manufacturer. Severely damaged bars were required to be replaced or returned to the manufacturer for shop repair. ASTM requirements limited total damage to 1% of total surface area per 0.3 meters (linear foot), and all damage was to be repaired with patch material (Weyers, R. E., 1995).

Storage

Sagüés studied the effects of outdoor exposure to marine environment and sunlight on performance of epoxy coating. Clear recommended a maximum of 2 months outdoor storage, regardless of environment or protective cover conditions (Clear, K. C. et al., 1995).

Pre-Placement Physical Damage

During early use, some surface damage was tolerated, so long as, after fabrication, no more than 2% of coated areas on straight bar and 5% of coated area on bent bar were damaged. Further, up to 3% damaged coating area was tolerated after placement of the bars (Manning, D. G., 1996). Later, ASTM specifications were revised to allow up to 2% bare areas, with no one area being greater than 58 mm^2 (0.09 in^2), on coated reinforcement. After the discovery of corrosion in Florida bridges, recommendations from FHWA were to reduce these permitted values to 0.25% area. More recently, in 1992, a report to the Concrete Reinforcing Steel Institute (CRSI) suggested a maximum of 0.0006% allowable bare area (Clear, K. C. et al., 1995).

Concrete Placement

In addition to inspection prior to concrete placement, specifications generally require the use of coated heads for probe-type concrete vibrating devices to reduce ECR damage due to abrasion.

Electrical Resistance

In addition to physical barrier mechanisms, epoxy coating is a dielectric. This, presumably, results in the restriction of electron or ion flow between the metal and the electrolyte, and inhibits charge transfer between anode and cathode (Geenen, F. M., 1991). Therefore, the coating may be effective in reducing the occurrence of macroscopic corrosion cells between reinforcing steel bars, and increases the electrical resistance between neighboring coated steel locations (Broomfield, J.P., 1997). The relatively good performance of non-specification bar in an FHWA study was attributed to high electrical resistance of the coating and reduced cathode area (Manning, D. G., 1996).

Adhesion of the coating to the substrate plays an important role in the reduction of corrosion. Once a coating has become disbonded from a metal substrate, highly conductive ion pathways may form beneath the coating, negating the benefits of the resistive coating on the corrosion micro-cell level (Geenen, F. M., 1991).

In addition, most coatings contain pigments and additives, some of which may induce corrosion-inhibitive properties to the coating. The green pigment, likely chromic oxide, found in most ECR imparts resistance to sunlight and corrosives (Seymour, R.B. & Mark, H.F., 1990). Covino reported 0.36 to 0.75 percent by weight Chromium measured by Energy-Dispersive X-ray Spectroscopy (EDS) of epoxy coatings from field ECR samples (Covino, B. S. et al., 2000).

Well Bonded Coatings

Many studies have been undertaken to evaluate the performance of new reinforcing bar with intact coatings in laboratory and field structures, using both natural and accelerated exposures. A number of factors have been identified which influence the longevity of the coating and the steel.

Moisture Uptake

Epoxy coatings are not impermeable to moisture (Clear, K. C. et al., 1995). The average transmission rate of water through the coating has been found to be 10 to 100 times that necessary to support corrosion (Geenen, F. M., 1991). Impermeability to water sufficient to prevent corrosion by resistance inhibition is not practical with most barrier coatings, except in very thick films, usually greater than 0.51μm (20 mils). Impermeability to ionic solutions and oxygen can readily be achieved and often can control the rate of corrosion beneath intact barrier films (Revie, R.W., 2000).

Adhesion Loss

A perfectly adhered coating will not experience under-film corrosion. Unfortunately, adhesion is imperfect in nearly all cases, as the coating material is heterogeneous, and weak bond areas will occur. Further, research has shown that long-term exposure to moisture results in the reduction or loss of adhesion of epoxy coating to steel (Sagues, A. A. & Powers, R. G., 1990; Pyc, W., 1998). In a moist environment, such as concrete, wet adhesion loss due to moisture diffusion will induce failure in an otherwise soundly adhered coating (Geenen, F. M., 1991). It has been shown that for epoxy coatings on a steel substrate, the secondary bond energy (~10 to 26 kJ/mole) between the surfaces is exceeded by the activation energy (32 kJ/mole) associated with

disbondment of the epoxy by water (Pyc, W., 1998). It has also been shown that adhesion loss can occur around breaks in a coating due to a phenomenon termed *cathodic disbondment* (Zayed, A. M. & Sagues, A. A., 1990; Sagues, A. A. et al., 1991; Pyc, W., 1998).

Once water has permeated the coating, it may collect in areas of weak adhesion, forming a blister. Leidheiser and Funke outlined two hypotheses for loss of coating adhesion due to water: chemical disbondment and mechanical (hydrodynamic) disbondment. Under extended exposure to an aqueous environment, water molecules in the vapor phase eventually permeate through the coating, reaching the steel surface. Under chemical disbondment, bonds between the polymer and metal oxide molecules at the coating-metal interface are broken as water molecules compete for bonds with the coating, the metal oxide, or both. Initial defects or poorly adhered regions may contribute, but are not a prerequisite for this mode of failure (Pyc, W., 1998; Geenen, F. M., 1991).

Mechanical disbondment is the result of the presence of contaminants or poorly adhered regions between the coating and metal surface, where water transmitted by the vapor phase through the coating can condensate beneath the coating in local sites of poor adhesion. Stress in these regions develops under osmotic pressure from dissolved ions in the condensate. Disbondment may be the result of both chemical and mechanical processes (Pyc, W., 1998; Geenen, F. M., 1991).

Field evaluation of ECR failures has shown that adhesion of the coating is commonly reduced or lost altogether, and often accompanied by disbonded areas with solution under the coating. The pH of this undercoating electrolyte is almost invariably on the order of 5 or 6, far less than the nominal 12 or 13 typical of sound, non-carbonated concrete (Sagues, A. A. & Powers, R. G., 1990).

Sagüés, Zayed, and others (Sagues, A. A. & Zayed, A. M., 1991; Sagues, A. A. et al., 1991; Zayed, A. M. & Sagues, A. A., 1990) have conducted a significant number of studies to determine the cause of coating disbondment, which has been clearly shown to contribute to the demise of ECR. One such study confirmed the negative influence of outdoor exposure to a marine environment during pre-construction storage.

The pore solution within concrete is primarily comprised of ionic solutions of calcium hydroxide, sodium hydroxide, and potassium hydroxide (Diamond, S., 1981). Laboratory studies have shown that saturated $Ca(OH)_2$ does not lead to corrosion or disbondment, NaOH solution will cause coating disbondment, but does not induce corrosion, and NaCl in solution causes active corrosion at damaged areas and holidays, but does not cause coating disbondment. Finally, a saturated solution of $Ca(OH)_2$ in conjunction with dissolved NaCl will cause significant coating disbondment, accompanied by active corrosion at breaches or holidays in the coating, especially under anodic polarization (Sagues, A. A. & Powers, R. G., 1990).

A good quality coating has been found to cathodically limit the progress of the corrosion reaction during short term tests, but the long-term performance of ECR has been questioned due to the uptake of moisture and resulting decline in coating resistance, as well as the progressive disbondment of the coating and creation of crevices with significantly lower pH and higher chloride concentration than the bulk solution. Bending of bars after coating application has been

found to cause disbonding of the coating at the bend and reduce the effectiveness of the coating in resisting corrosive attack (Sagues, A. A. & Powers, R. G., 1990; Aguilar, A. et al., 1990; McDonald, D. B. et al., 1998).

Disbonded Coatings (partially and wholly)

Effects of Chloride

It is understood that chloride depassivates steel and initiates corrosion, even at high pH. Research confirms that chloride is not directly deleterious to a sound epoxy coating, and that the coating will resist the penetration of chloride ions. However, where holidays, damage and other breaks exist in the coating, no barrier to chloride ion exists, and corrosion will initiate inside these areas, just as if the coating were not present. Unlike the corrosion of bare steel in concrete, which begins primarily as pitting corrosion, the presence of the coating changes the localized environment, such that crevice, or underfilm, corrosion occurs under the coating. Similarity exists, in that both mechanisms involve the formation of a localized region that is protected (within the pit or crevice) from the bulk pore solution.

In some areas, anodic dissolution of reinforcing steel proceeds at a coating breach, while at other exposed areas, the cathodic reaction occurs to support the balanced corrosion process. At the cathode(s), the coating further disbonds, increasing the available exposed surface area. Increased cathode surface area is known to support greater rates of dissolution at finite anodic sites. As both chloride concentrations and exposed steel surface increase, cathode and anode areas may develop adjacent to one another beneath the same coating defect. Localized reduction in pH occurs in the crevices under the coating, as the anodic area is protected from the high-pH bulk solution by the coating and accumulated corrosion product (Sagues, A. A. & Powers, R. G., 1990). Anodic dissolution proceeds, until sufficient corrosion product forms to displace the coating and create stress in the concrete cover.

It is interesting to note that epoxy coatings used for steel reinforcement contain a small amount of organically-bound chloride within the coating matrix. This is likely from the manufacture of the epoxy, an ingredient of which is ethylene chlorhydrin. Covino and others reported levels of approximately 0.12 to 0.28 percent by weight chloride in epoxy coatings within samples from the Perley bridge between Ontario and Quebec. Further, they concluded that the chloride did not diffuse either into or out of the epoxy matrix, as only small amounts of chloride were observed on the surface of the epoxy adjacent to the steel surface and no chloride diffusion profile was evident within the surrounding concrete (Covino, B. S. et al., 2000).

The chloride threshold concentration necessary to induce corrosion in ECR has been debated. McDonald and Sagüés have reported, independently, that the threshold concentration is the same or of the same order as that of bare steel reinforcement, especially where damage or holidays exist in the coating (McDonald, D. B. et al., 1998; Sagues, A. A. et al., 2001).

Reinforcing Steel Corrosion-Induced Cracking of Cover Concrete

Process for Bare Reinforcement and ECR

Generally the development of cracks in the cover concrete over reinforcing steel bars results from the expansive nature of the corrosion reaction. The volume of the corrosion products will exceed that of the original reactants, though the exact proportion will vary, depending upon the exact composition of corrosion products. Since the corrosion products occupy greater volume than the original steel, expansive stresses develop in the restricted spaces within the concrete (Bentur, A., Diamond, S., and Berke, N., 1997). Once these stresses exceed the tensile capacity of the cover concrete, cracks form above the steel bar. One form of cracking generally takes the form of a single crack, located almost directly over the bar, but through the weakest planes of the concrete material. If a large area of reinforcement, commonly several adjacent bar sections, all corrode simultaneously, the cracking may occur parallel to the concrete surface, extending between the bars in a plane. This creates a delamination. Subsequent loss of the concrete in this delaminated layer results in a spalled area, and the reinforcement surface is exposed.

Models for Bare Steel in Concrete

Several models have been developed to predict the time-to-cracking of concrete cover due to corroding reinforcement. The generally accepted model for chloride migration to the steel is a one-dimensional application of Fick's Second Law of diffusion. As a simplifying assumption, the boundary conditions are often assumed to be a concentration gradient at a single surface of semi-infinite dimension.

Diffusion of Chloride

Fick's First Law of Diffusion states that the rate of flow of molecules is proportional to the change in concentration per unit distance (called the concentration gradient), but does not specifically address time as a variable. Fick's Second Law of Diffusion addresses the time dimension of the diffusion problem and is expressed most simply as (Giancoli, D.C., 1989):

$$\frac{\partial C}{\partial t} = D_c \frac{\partial^2 C}{\partial x^2}$$ **Equation 8**

where; C = concentration at a given point along a path (kg/mm3)
D_c = diffusion coefficient
t = time (years)
x = distance (mm)

It is important to note that the diffusion coefficient, often referred to as the diffusion constant, is not constant at all, but changes over time, as pore structure and pore contents of the concrete change. Indeed, D_c for a given concrete is affected by many factors, primarily temperature, degree of hydration, relative humidity of the concrete, and concentration of chloride (Andrade, C. & Alonso, C., 1996).

Concrete researchers have refined the diffusion model, taking into consideration the boundary conditions in a concrete environment. The time dependent characteristic of near-surface chloride

concentration has been found to be appropriate for laboratory specimens that have not undergone extensive environmental exposure prior to testing (Weyers, R. E. et al., 1994).

$$C_{(x,t)} = k\sqrt{t}\left[e^{\frac{-x^2}{4D_c t}} - \frac{x\sqrt{\pi}}{2\sqrt{D_c t}}\left(1 - erf\,\frac{x}{2\sqrt{D_c t}}\right)\right] \qquad \textbf{Equation 9}$$

where; $C_{(x,t)}$ = chloride concentration at depth x after exposure time t
k = coefficient dependent upon concrete material and surface concentration
erf = mathematical error function (Rieger, P.H., 1994)

Using Equation 9, diffusion constants can be derived from a least-squares regression fit of chloride profiles obtained in laboratory testing.

In bridge decks exposed to a salt-laden environment, the chloride concentration becomes relatively stable below approximately 13 millimeters depth into the cover concrete, and becomes the driving concentration that causes diffusion (Weyers, R. E. et al., 1993; Cady, P. D. & Weyers, R. E., 1984). The near surface chloride content for field specimens that have been in service for several years may be modeled by a constant value of C_0. Therefore, the system may be modeled by the simplified equation:

$$C_{(x,t)} = C_0\left(1 - erf\,\frac{x}{2\sqrt{D_c t}}\right) \qquad \textbf{Equation 10}$$

where; C_0 = constant chloride concentration near the surface

Time-to-cracking

Reinforcement corrosion service life models generally involve integration of corrosion current density over time to estimate total charge transfer. The models employ Faraday's Law to convert total estimated charge transfer to mass of iron oxidized. Physical models are incorporated to explain the accumulation of corrosion product in interstitial spaces around the reinforcement and subsequent development of expansive pressures that eventually crack the concrete.

Bazant proposed an early mathematical model for predicting time-to-cracking of concrete cover for corrosion of reinforcement exposed to seawater (Bazant, Z. P., 1979). The model considered various chemical and physical phenomena regarding chloride-induced reinforcement corrosion, including:

- one-dimensional oxygen and chloride transport through concrete cover
- steady-state corrosion and rust production after depassivation
- density of original steel versus rust products

Thus, Bazant defined the time-to-cracking as a function of:

- electrochemical properties: corrosion rate
- dimensional properties: cover depth, bar spacing
- physical properties: density of steel, density of rust product
- mechanical properties of concrete: tensile strength, modulus of elasticity, Poisson's ratio, and creep coefficient.

The intent was to perform a finite element analysis of the corrosion system using these mathematical representations of the applicable phenomena.

The crux of the model was the derivation of time-to-cracking, t_{cr}, which is the sum of time to depassivation, t_p and time of active (steady-state) corrosion to induce cracking, t_{cor}. Time to depassivation, controlled by diffusion of chloride, was modeled using either the error function (Fickian diffusion) or approximated using a parabolic function. Time of active corrosion to induce cracking incorporated physical, mechanical and dimensional parameters, as shown in Equation 11

$$t_{cor} = \rho_{cor} \frac{D\Delta D}{sj_r}$$

Equation 11

where ρ_{cor} = density of corrosion products
D = original bar diameter
ΔD = addition to bar diameter by expansive products
s = bar spacing
j_r = rate of rust production

The increase in bar diameter, ΔD, necessary to induce failure of cover concrete, which may be either inclined cracking of the cover versus cover peeling, was defined as a function of cover depth and bar spacing. The Bazant model was proposed for seawater exposure, and has not been experimentally proven to apply to bridge decks in deicing environments.

Andrade summarized progress on the development of quantitative models for service life prediction based on carbonation and chloride-induced corrosion. Citing the conceptual model introduced by Tuutti, the modeling process was broken into two phases: time to corrosion initiation, t_i and time of corrosion propagation, t_p. Two diffusion models and one empirical model of the carbonation initiation phase were referenced. Discussion of chloride initiation was based on Fick's second Law, as previously discussed. Both chloride and carbonation diffusion models incorporate as the key determining factor, the "square root of time" function:

$$x = K\sqrt{t}$$

Equation 12

Assuming uniform corrosion measured by depth of penetration into the steel, the service life for carbonation-induced corrosion was modeled by:

$$t = t_i + t_p = K_c\sqrt{t} + \frac{PL}{CR}$$

Equation 13

where K_c = carbonation coefficient
PL = penetration limit (mm)
CR = corrosion rate (μm/year)

A penetration limit of 100-200μm was suggested (Andrade, C. & Alonso, C., 1996). No mathematical model for chloride-induced corrosion propagation was presented, but empirical analysis based on reduction of section was suggested.

Liu and Weyers have carried out further refinement of electrochemical and physical models for the chloride-induced corrosion propagation phase (Liu, Y. & Weyers, R. E., 1998). The propagation was described as consisting of three steps: (i) free expansion of corrosion products in the interstitial space around the bar up to a limiting quantity, W_p (ii) stress initiation after the available space has been consumed, and (iii) cracking induced by a critical quantity of corrosion product, W_{crit}.

The critical mass of corrosion product necessary to induce cracking was calculated as:

$$W_{crit} = \rho_{rust}\left(\pi\left[\frac{Cf'_t}{E_{ef}}\left(\frac{a^2+b^2}{b^2-a^2}+\nu_c\right)+d_o\right]D+\frac{W_{st}}{\rho_{st}}\right)$$

Equation 14

where ρ_{rust}, ρ_{st} = density of rust product and original steel, respectively
d_o = thickness of pore space around bar
C = cover depth
D = bar diameter
a = distance from bar center to outer pore face ($D/2+d_o$)
b = distance from center of bar to concrete surface ($a + C$)
W_{st} = weight of original steel consumed by corrosion
ν_c = Poisson's ratio for concrete
f'_t = tensile strength of concrete
E_{ef} = effective modulus of elasticity of concrete, $\left(\frac{E_c}{1+\varphi_{cr}}\right)$
E_c = elastic modulus of concrete
φ_{cr} = creep coefficient of concrete

Defining k_p as the rate of rust production:

$$k_p = 0.098\left(\frac{1}{\alpha}\right)\pi D i_{cor}$$

Equation 15

where α = ratio of mol. wt. of steel to mol. wt. of corrosion product
i_{cor} = annual mean corrosion current density

For a constant corrosion rate, the time to cracking, t_{cr}, can then be calculated as:

$$t_{cr} = \frac{W_{crit}^{\ 2}}{2k_p}$$

Equation 16

The model was validated against observed times-to-cracking of laboratory slabs containing admixed chloride and exposed outdoors for 5 years. Critical mass of corrosion product necessary to induce cracking, W_{crit}, was found to be primarily a function of cover depth, concrete

tensile strength and modulus, void space at the steel-concrete interface, type of corrosion products, and reinforcing steel bar diameter. Time-to-cracking, in turn, was a function of W_{crit} and corrosion rate.

Torres-Acosta and Sagüés published a study of cover cracking (Torres-Acosta, A. A. & Sagues, A. A., 1999). The study was based upon previous observation that corrosion in concrete begins as pitting, and anodic dissolution of steel occurs at discrete locations along the steel bar. The study specifically considered the cover cracking induced by concentration of corrosion products at discrete anodes, as opposed to the common assumption of uniform corrosion (Torres-Acosta, A. A., 1999). The study identified a range of values for the critical depth of steel penetration necessary to induce cover cracking, comparing generalized (uniform) corrosion to localized corrosion. The values of steel penetration for localized corrosion associated with cover cracking were found to be significantly greater (0.054 to 0.137 mm) than that of the uniform corrosion (0.015 to 0.075 mm.) The conclusions suggest that, where higher rates of corrosion occur near cracks, the amount of corrosion product necessary to disrupt the cover is also greater, due to the localized nature of the anode. The critical corrosion penetration depth was found to be clearly dependent upon the cover to bar diameter ratio (C/φ) and the ratio of cover depth to corrosion length (C/L), or degree of localization, of the corrosion.

Pantazopoulou presented a mathematical model in which cracking time was defined as a function of cover, concrete and corrosion product material properties, and corrosion rate (Pantazopoulou, S. J. & Papoulia, K. D.,). The paper uses information previously presented by Liu and Weyers, Bazant, and others, toward the formulation of a boundary value problem of an anisotropic hollow thick cylinder to be evaluated by the finite difference method. Correlation with data from Liu and Weyers was good, but specific research needs were identified to refine the model. Specifically, greater knowledge of the influence of open cracks to accommodate corrosion products and reduce the rate of pressure accumulation, as wells as effects of accelerated conditioning and seasonal variations of environmental variables.

Applicability of Bare Steel Models to ECR

Few attempts have been reported to apply time-to-cracking models to ECR. Sohanghpurwala and Scannell performed a study of epoxy-coated reinforcement in 80 bridge decks ranging from 3 to 19 years of age, located throughout Pennsylvania and New York (Sohanghpurwala, A. A. & Scannell, W. T., 1998). ECR bar specimens within concrete cores from the decks were evaluated using a variety of visual, chemical and electrochemical techniques. The study characterized the condition of the coatings, the pH, moisture and void properties of the concrete, and physical parameters, such as concrete cover depth. Corresponding information about the overall structural condition of the deck was obtained at the time of sampling. Results indicated a propensity for adhesion reduction or loss of the coating that increases with the age of the structure. Overall, the condition of the epoxy coating with respect to adhesion was considered poor, with less than 47% showing no reduction in adhesion. Specifically reported was the following probability of adhesion loss (rating of 1) for age groups 1 to 4, representing 0 to 20 years of age in 5-year increments, in increasing order:

$$P(Adh.red.) = -0.575 \times AgeGroup^2 + 0.4345 \times AgeGroup - 0.1275$$

Equation 17

However, progressive corrosion was only identified in 2 bars during the study. The authors could not clearly discern whether the observed lack of corrosion activity was a direct result of the epoxy coating. The relatively young average age (10 years) of the decks suggests that the long-term effect of chloride exposure for poorly adhered coatings has yet to be observed. The log EIS data, number of holidays, and number of bare spots within ECR coatings correlated most strongly with overall corrosion condition of the bars.

Fanous and Wu recently published the results of an Iowa DOT study of ECR in bridge decks (Fanous, F. S. et al., 2001; Fanous, F. S. et al., 2000). The study incorporated the model proposed by Liu & Weyers for bare steel. The assumed chloride initiation threshold for bare steel was 0.7 kg/m^3 concrete (1.2 lb Cl^-/cy concrete), but an increased initiation threshold of 2.1kg/m^3 concrete (3.6 lb Cl^-/cy concrete) was selected for ECR, based on an assumed, and rather arbitrary, range from a referenced study by Sagüés. The propagation period for ECR was assumed to be 5 to 8 years, versus 3 to 5 years for black bars, as extrapolated from a report by Larson and Cady on bridge deck concrete durability. The resulting calculations suggest that under conditions common to Iowa, decks constructed with black steel will reach the end of functional service life (EFSL) in approximately 22 years, versus approximately 65 years if ECR is used. The authors concluded from this study of 80 bridge decks that ECR significantly extends the service life of bridge decks, but that the presence of cracks had a significant effect. However, they also concluded that coating-to-reinforcement adhesion decreases with time due to high moisture and chloride. Finally, adequate concrete cover was found to significantly prolong the corrosion initiation period.

Clearly, more study is required to adequately model the corrosion initiation and time-to-cracking of epoxy coated reinforcement in field structures, and the present study will contribute toward that end.

Chloride-Induced Corrosion Assessment Methods for Steel in Concrete

Several commonly accepted methods exist for assessing the condition of a reinforced concrete structure with respect to chloride-induced corrosion. These methods involve destructive testing to determine the level of contamination with chloride and subsequent corrosion-related damage. In addition, some non-destructive techniques are used to estimate the general location and rate at which deterioration is occurring, based on monitoring of electrochemical processes.

Chloride Content

Acid-Soluble and Water-Soluble Chloride Tests

To determine the level of chloride contamination, profiles of chloride content within the cover concrete are measured. This involves the extraction of powdered concrete material from known depth ranges within the cover, or extraction of concrete core samples, which are subsequently cut into depth ranges and pulverized.

The powdered concrete is subject to chemical testing, most commonly by one of two techniques. The acid-soluble technique involves the digestion of the powdered concrete in an acidic solution, such that the cementitious compounds are dissolved and any chloride bound within the material matrix is released. The water-soluble technique involves boiling the concrete powder and

soaking in solution for approximately 24 hours, to allow the leaching of "soluble" chloride from the cementitious materials without necessarily inducing the complete dissolution of materials.

As noted previously, researchers and practitioners have debated the relative validity of both measurements. Some prefer the acid-soluble content, commonly referred to as total chloride, as an indication of the sum of chloride potentially available within the material to feed a deleterious reaction. Proponents of the water-soluble method argue that a significant portion of the chloride may be bound to or within the hydrated cement and aggregate, and will never be available to induce corrosion at the surface of the reinforcement. Therefore, it is argued, a water-soluble technique more accurately reflects that portion of the chloride that may actually induce corrosion.

Corrosion Potential

One of the basic electrochemical techniques for corrosion monitoring has been electrical potential measurement. From a simple point of view, the method involves the creation of an electrochemical cell, one half being composed of the reference electrode in an appropriate electrolyte. The second half of the cell is comprised of the steel or other metal (working electrode) being monitored, suspended in its own aqueous environment. An appropriate bridge, usually a porous ceramic, which allows ion flow but prevents mixing, joins the two electrolytes. The electrodes are connected to a voltmeter, which indicates the mixed potential created by the cell.

For laboratory use, the Standard Hydrogen Electrode (SHE) is commonly used as a benchmark for comparison. More frequently the Standard Calomel Electrode (SCE) is chosen, since it is relatively simple, inexpensive and stable for laboratory applications. For field applications involving saturated soil or concrete as the conductive medium between reference and working electrodes, the Copper-Copper Sulfate Electrode (CSE) is commonly used because it is inexpensive, rugged, and easily maintained.

Bare Steel

For concrete applications, the procedure is outlined in ASTM C 876-91 (ASTM, 1991). Electrical potential can be successfully used to determine the probability that active corrosion is occurring at the time of measurement. However, there are several limitations to the method. First, good electrical contact to and between the elements of the reinforcing steel mat in question is required. Next, the concrete between the surface being probed and the underlying steel bars in question must be sufficiently saturated to complete the electrical circuit. Surface coatings or overlays on the concrete, as well as epoxy coating on the reinforcing steel may make the potential method useless or unreliable, since electrical resistance of the coating is too high to permit proper measurement. Finally, the electrical potential method is only an indicator of the potential for corrosion activity, and gives no information about the extent or rate of corrosion activity in the subject reinforcing steel.

Interpretation of Values

Research has shown that the arrival of sufficient chloride to initiate sustained corrosion is marked shortly thereafter by a sharp increase in the magnitude of electrical potential of the

reinforcing steel, as measured against a standard reference probe, such as a copper-copper sulfate electrode (CSE) or standard calomel electrode (SCE) (Schiessl, P., 1988).

Although the magnitude of the electrical potential does not directly relate to the rate of corrosion, it may provide a reasonable indication of the probability that corrosion is occurring (ASTM, 1991). A summary of the ASTM C 876-91 interpretation guidelines for electrical potential readings versus CSE in bare-steel reinforced concrete is presented in Table 1.

Table 1 Interpretation of ASTM C 876-91 Corrosion Potential Readings

Potential Reading (mV CSE)	Probability of Corrosion
$x \geq -200$	<10 percent
$-200 > x > -350$	Indeterminate
$x \leq -350$	>90 percent

Concrete Resistivity

The resistivity of concrete is a general measure of the moisture content, as well as the size, continuity and tortuosity of the pore system within the cement paste (Revie, R.W., 2000). The electrical resistance of a conductor is (Jones, D.A., 1996):

$$R = \frac{\rho L}{A}$$

Equation 18

where ρ = resistivity
L = length of conductor (e.g. the path through concrete)
A = cross-sectional area of conductor (i.e. the path through concrete)

Solving for resistivity gives:

$$\rho = \frac{RA}{L}$$

Measuring resistance to an alternating current (impedance) and short test duration are used to prevent polarization of the reinforcing steel. A relatively low frequency (~50 to 500 Hz) is often used, which provides results very similar to direct current resistance measurements (Neville, A.M., 1996). Commonly, resistivity of concrete is measured in the field using the four-probe method (Wenner array) initially developed for soils.

Sagüés and others measured nominal concrete resistivity in laboratory column specimens by circulating a 10 μA, 200 Hz alternating current between unconnected rebar segments and recording the AC potential drop between reference electrodes at different elevations (Sagues, A. A. et al., 1991). Apparent resistivity, ρ, was then calculated as:

$$\rho = \frac{V_{AC} \cdot A_{CS}}{d \cdot I_{AC}}$$

Equation 19

where V_{AC} = AC potential drop between electrodes (V)
A_{CS} = cross-sectional area of the column (cm^2)
d = vertical distance between electrodes (cm)
I_{AC} = applied AC current (A)

"The following interpretation of resistivity measurements has been cited when referring to depassivated steel:

> 20	kΩ•cm	Low Corrosion rate
10-20	kΩ•cm	Low-to-moderate corrosion rate
5 -10	kΩ•cm	High corrosion rate
< 5	kΩ•cm	Very high corrosion rate" (Revie, R.W., 2000)

Therefore, concrete resistivity can be used as an empirical assessment of possible corrosion rate.

Linear Polarization

Theory

The polarization resistance, or linear polarization, method gives more direct information about the rate at which corrosion is occurring. Starting with the cell components described under electrical potential, a third electrode is introduced: the counter electrode. The counter electrode is used to induce a small potential change from the open-circuit potential of the corrosion cell. By measuring the amount of applied current, *I*, related to small, but known increments of potential change, a linear interpolation of the potential-current trend results in an estimate of polarization resistance. This polarization resistance, R_p, or charge-transfer resistance, in conjunction with the Tafel coefficients for the anode and cathode, and the Butler-Volmer, and Stern-Geary equations, can be used to estimate corrosion current.

$$I = I_{corr}\left(10^{\frac{2.303(E-E_{oc})}{\beta_a}} - 10^{\frac{-2.303(E-E_{oc})}{\beta_c}}\right)$$

Butler-Volmer: **Equation 20**

where; E = circuit potential (V)
E_{oc} = open-circuit potential (V, no induced current)
β_a and β_c = anodic and cathodic Tafel coefficients (V/decade current)

This equation can be converted to the more useful form:

$$I_{corr} = \frac{\beta_a \beta_c}{2.303(\beta_a + \beta_c)} \cdot \frac{1}{R_p} = \frac{B}{R_p}$$

Stern-Geary: **Equation 21**

R_p = polarization resistance

Corrosion current density, i_{corr}, is the calculated corrosion current, I_{corr}, taken over the surface area, A, of the working electrode, and can be used as an indication of overall corrosion intensity. Faraday's Law relates the transfer of current in an electrochemical reaction to the number of atoms of a material that reacts.

$$m = \frac{Ita}{nF}$$

Faraday's Law: **Equation 22**

where; m = mass reacted (g)
n = ionic charge, or number of equivalents exchanged
I = electrical current (amperes = 1 coulomb/sec =6.2×10^{18} electrons/sec)
F = Faraday's Constant = 96,500 electrons per mole
t = time (seconds)
a = atomic weight (g/mole)

Incorporating Faraday's Law, an estimate the rate of metal loss due to corrosion in simple corrosion cells may be obtained. Using Faraday's Law, the rate of corrosion, r, can be calculated as follows:

$$r = \frac{m}{tA}$$

Equation 23

where; A = surface area of metal involved in the reaction

One popular linear polarization method for concrete applications uses a Stern-Geary constant of B = 40.76, where Tafel constants β_a = 187.5 mV per decade, and β_c = 187.5 mV per decade, in converting the measured polarization resistance to an equivalent corrosion current density (Brown, M. C., 1999).

Unguarded and Guarded Counter Electrodes

Many linear polarization test devices (such as the three-electrode linear polarization device, 3LP) employ "unguarded" electrodes, which employ the reinforcing steel as the working electrode, a standard half-cell as a reference electrode, and a relatively noble metal rod or mesh as a counter electrode. In these systems, no attempt is made to constrain the area of influence of the counter electrode. Thus, in concrete structures where the working electrode is one section of a steel reinforcing bar, it is impossible to precisely assess the length of the bar that is polarized under the test.

As an attempt to address this issue, researchers have developed "guarded" electrodes, in which inner and outer electrodes are arranged in concentric circles, with reference electrode(s) located between. The driving current from the counter electrode used in the polarization process is balanced by an opposing current from the outer guard electrode, which serves to confine the area of influence of the counter electrode. This method is intended to provide some control over the length of bar, and hence the surface area of the working electrode which is polarized under the test. The primary research of this method has been conducted in Spain by Feliu, Andrade and others, resulting in the development of the GeoCor device (Feliu, S. et al., 1990). Experiments showed significant success using the method on systems undergoing corrosion at a significant rate. However, the results become more ambiguous in situations where corrosion is less active and corrosion current density is very low.

Research by Weyers and others has shown that the guarded electrode devices tend to underestimate corrosion rate, while unguarded devices overestimate the corrosion rate, with as

much as an order of magnitude difference in readings (Newhouse, C. D. & Weyers, R. E., 1996; Liu, Y. & Weyers, R. E., 1998).

Application and Interpretation of Values

Table 2 presents orders of magnitude associated with general corrosion states for measured, surface normalized polarization rate, and calculated corrosion current density of steel in concrete.

Table 2 Polarization Resistance and Corrosion Rates for Steel in Concrete (Sagues, A. A. & Zayed, A. M., 1991)

Corrosion State	R_p kΩ-cm^2	Corrosion Current Density* (μA/cm^2)	Corrosion Current Density (mA/ft^2)
Passive Steel	2600	0.01	0.009
Borderline Corrosion	260	0.1	0.09
Actively Corroding Steel	26	1	0.9

* Stern-Geary Constant, B, assumed to be 26 mV for steel in concrete.

ECR in Concrete

The linear polarization method does involve estimating the surface area of steel polarized by the test procedure, and this fact can have significant consequences when attempting to apply the procedure to coated steel bars that may or may not have holidays or bare areas. Further, the resistance of the coating may render the base open-circuit potential readings invalid. Therefore, the linear polarization method is not considered applicable to polymer coated reinforcing steel.

Electrochemical Impedance Spectroscopy

An increasingly popular, but substantially more complicated method is termed ac impedance or electrochemical impedance spectroscopy (EIS).

Theory

For direct current (dc) electrical circuits, Ohm's Law states that the electrical potential (E) in the circuit is the product of current (I) and resistance (R) in the circuit. Thus, a resistor is the only element in a dc circuit which resists the flow of electrons and the current and potential (EG&G Princeton Applied Research, 1989).

In an alternating current (ac) circuit, simple resistance is replaced by *impedance* (Z). Ohm's Law for dc circuits is replaced by the analogous equation:

$$E = I \cdot Z$$

Equation 24

In addition to resistors, reactive components, known as capacitors and inductors can resist the flow of electrons in an ac circuit. Capacitance involves the buildup of excess electrons at an interface, resulting in an electrostatic charge. A capacitor resists changes in electrical potential. Conversely, an inductor resists change in electrical current, and involves the storage of energy in an electromagnetic field about a conductive element, especially in a coiled configuration.

Unlike ideal resistors, which induce linearly proportional opposition to electron flow as potential changes, the opposition imposed by capacitance (C) and inductance (L) are dependent upon the frequency (f) of an ac signal.

$$Z = R + j\omega L + \frac{1}{j\omega C}$$

Equation 25

where *radial frequency*, $\omega = 2\pi f$

Note that the impedance resulting from an inductor increases with frequency, while impedance due to a capacitor is inversely proportional to frequency.

Impedance in real electrical circuits is usually the result of both resistive and reactive (capacitive reactance, X_c and/or inductive reactance, X_L) components. This is the case with most electrochemical cells. To simplify expression and computation, impedance data are often subject to vector analysis and converted to complex numbers, such that:

$$Z_{Total} = \frac{E' + E'' j}{I' + I'' j} = Z' + Z'' j$$

Equation 26

;where $j = \sqrt{-1}$

Simply put, the real component of impedance (Z') represents the resistance and the imaginary component (Z'') represents the reactance (EG&G Princeton Applied Research, 1989; Gamry Instruments, I., 1999).

Further, with ac circuits, the current and potential may not be synchronous; rather the two waveforms are often shifted in time. This temporal offset is termed *phase* (θ). Purely resistive circuits are in phase ($\theta = 0$), while for purely capacitive or inductive circuits, current is shifted 90° ahead or behind the potential waveform, respectively. Circuits exhibiting a limited capacitive behavior would have a phase angle less than 90°, but greater than 0° (EG&G Princeton Applied Research, 1989).

The absolute magnitude of the impedance (length of vector) and phase angle can be calculated according to the following equations, as shown in Figure 4:

$$|Z| = \sqrt{Z'^2 + Z''^2}$$

Equation 27

$$\theta = \tan^{-1}\left(\frac{Z''}{Z'}\right)$$

Equation 28

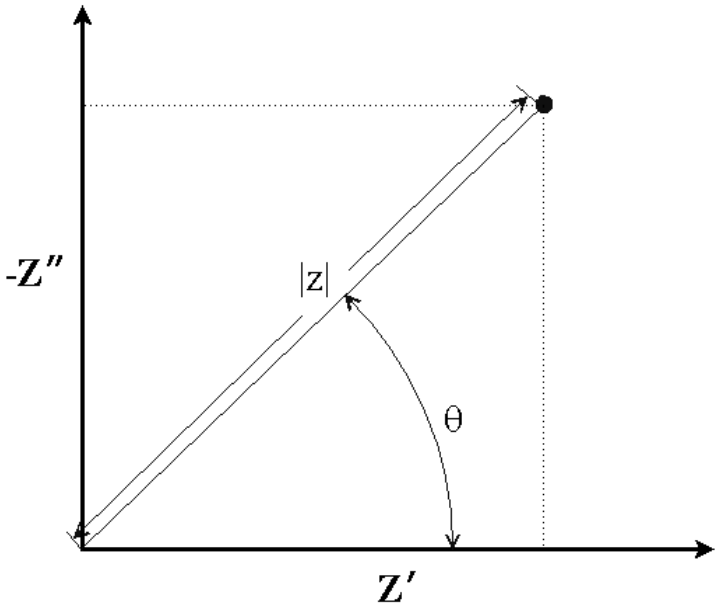

Figure 4 Representing Impedance in the Complex Plane (Geenen, F. M., 1991)

In addition to resistors, capacitors, and inductors common in ac circuit analysis, electrochemical impedance measurements often involve several other impedance elements, which may be employed to describe electrochemical behavior, see Table 3.

Table 3 Impedance Circuit Elements (Geenen, F. M., 1991)

Element	Symbol	Impedance Expression	
Resistance	R	R	
Capacitance	C	$\frac{1}{j\omega C}$	
Inductance	L	$j\omega L$	
Warburg[1,2]	W	$\frac{Y_o}{\sqrt{j\omega}}$	$\sigma = \frac{1}{Y_o\sqrt{2}}$
Bounded Finite length Diffusion Impedance (BFDI)[3]	T	$Coth\frac{B\sqrt{(j\omega)}}{Y_o\sqrt{(j\omega)}}$	$B = \frac{\delta_N}{\sqrt{D}}$
Open Finite length Diffusion Impedance (OFDI)[3]	O	$Tanh\frac{B\sqrt{(j\omega)}}{Y_o\sqrt{(j\omega)}}$	$B = \frac{\delta_N}{\sqrt{D}}$
Constant Phase Element (CPE)[1]	Q	$Y_o(j\omega)^n$	$-1 \le n \le 1$
Gerischer[4]	G	$\gamma\sqrt{\omega(p-jq)}$	

[1] Y_o = frequency independent part of admittance, Y (Y=1/Z)
[2] σ = Warburg coefficient
[3] δ_N = Nernst diffusion layer thickness, D = diffusion coefficient of electro-active species
[4] γ = Greischer coefficient, p and q are rate constant related quantities

A constant phase element, CPE, is so denoted because the phase angle, θ, between the steady state harmonic excitation potential and the current response is the same at all frequencies. The CPE may be viewed as resembling a capacitor-resistor series combination, where both values are frequency dependent (Sagues, A. A. & Zayed, A. M., 1991). It is interesting to note that the CPE can be used to represent every standard electrical circuit element by varying the factor *n*. For *n* = -1, *n* = -0.5, and *n* = 1, the CPE represents a capacitor, Warburg impedance, and an inductor, respectively (Geenen, F. M., 1991).

Sagüés conducted a study that discussed application of the CPE as a circuit element in EIS of reinforced concrete (Sagues, A. A. et al., 1996). In it he stated, "Complications can arise from uneven distribution of corrosion on the steel surface, uneven distribution of the polarization excitation signal, the presence of transport-limited polarization, limitations on the amount of time available to perform a test, uncertainty in the size of the steel surface sampled, the presence of corrosion macro-cells, the dielectric behavior of the concrete and the presence of large and non-ideal apparent interfacial capacitance at the steel-concrete interface."

Application and Interpretation of Values

This method uses the same working, reference and counter electrodes as described earlier for dc methods. Instead of varying the potential in a linear fashion, under dc conditions, an ac potential is generated, with variation of the frequency of the ac signal. To give the greatest probability of obtaining linear response between potential and current, the amplitude of the potential change is kept very small, on the order of ± 10 mV rms. Equipment demands are greater for this method, requiring a potentiostat and a frequency response analyzer and/or computer interface (Zemajtis, J. et al., 1998).

Data Presentation Methods

Lissajous Figure

If electrical potential is varied in a sinusoidal manner about a central value, the associated electrical current will likewise vary. Depending upon the resistive and reactive components of the electrical or electrochemical circuit involved, the current response may be larger or smaller in magnitude, in or out of phase with the potential waveform. A direct plot of the voltage versus current waveforms is termed a *Lissajous* figure, as shown in Figure 5 (Gamry Instruments, I., 1999).

The magnitude of the current will be a function of absolute impedance, and the "skew" of the resulting oval plot will be indicative of the phase angle. A plot of a purely resistive element would be a line, the slope of which indicates the resistance. A plot of a single, purely reactive element, with the same magnitude of voltage and current, would resemble a circle. Most real-life elements include parts of both, and result in a tilted oval shaped plot, as shown above.

Bode Diagrams

Summarizing the results of impedance measurements over a wide range of frequencies and plotting both the log of the modulus of impedance and the phase angle as functions of the log of the frequency results in a Bode diagram, as shown in Figure 6**.**

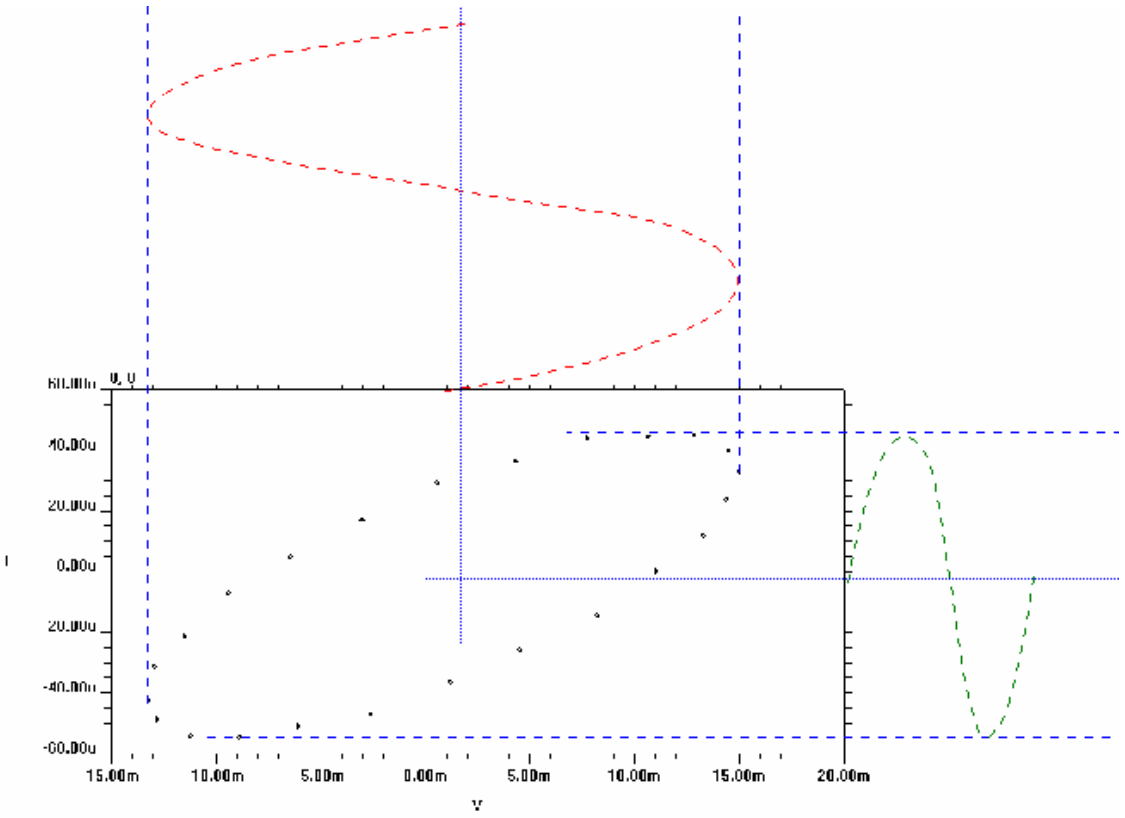

Figure 5 Potential versus Current in EIS Measurement

Nyquist Plots

If the real and imaginary components of impedance are plotted on x and y coordinates, respectively, the result is termed a Nyquist plot. Generally, impedance measurements may be made over a range of frequencies, from less than 1 mHz to 25 kHz or more. Low frequencies are generally limited by time and stability constraints, whereas high frequency is often limited by the capability of available instrumentation.

The electrochemical response of bare and coated metals in corrosive conditions is representative of many concurrent processes, including electrochemical reactions, chemical reactions, adsorption of intermediate products, and ion transport by diffusion, migration, or convection. Under ac potential stimulus, only those processes that have sufficient time to take place during the cycle of the electric field have a measurable effect. Slower reactions do not occur. Therefore, in order to determine the various physical phenomena associated with electrochemical measurements, it is necessary to measure impedance response over a range of frequencies. Each process can be separated according to its relaxation time, provided relaxation times of separate processes are measurably different (Piens, M. & Verbist, R., 1981).

On a Nyquist plot, typically the frequency will increase from right to left. Higher Z' is usually associated with the cumulative impedance of all elements in the system (such as the combined R_p + R_u), and is often observed at the lowest frequency. An example of a Nyquist plot is presented in Figure 7**.**

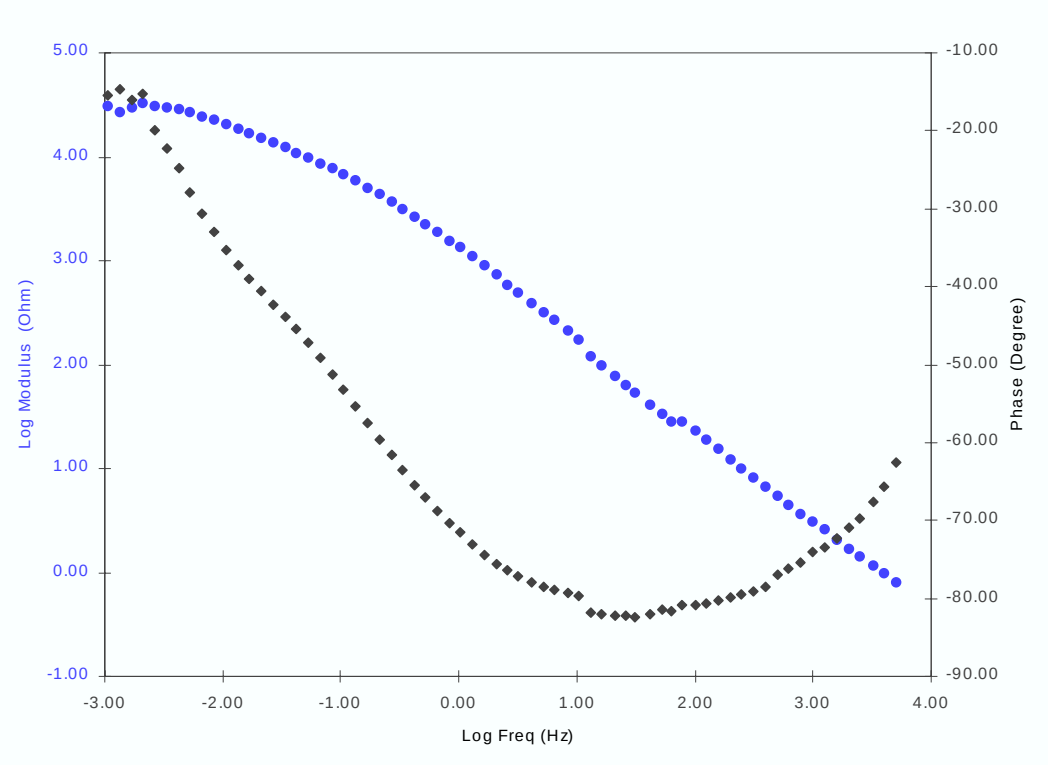

Figure 6 Bode Diagram

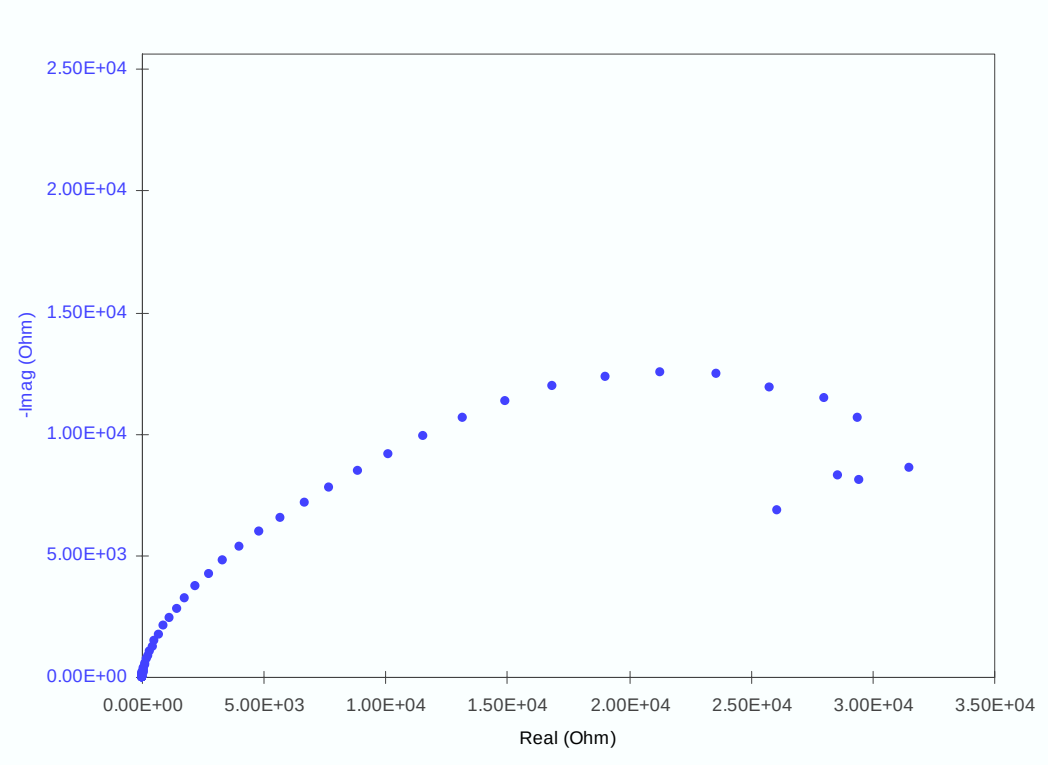

Figure 7 Nyquist Plot

Bare Steel in Concrete

Polarization Resistance of Simple Cells

For very simple electrochemical corrosion cells, where the measured impedance is primarily due to solution resistance and charge-transfer influences, R_u represents the electrolyte resistance. Provided that impedance data is obtained over a sufficiently large range of frequency, the polarization resistance, R_p, can be calculated by subtracting R_u, determined by the high-frequency impedance, from the sum of $R_p + R_u$, measured at low frequency (Pyc, W., 1998).

When more sophisticated phenomena are involved, such as the presence of coatings, inhibitive films or oxide layers, interpretation of impedance data becomes more difficult.

Equivalent Electrical Models

The advantage to EIS is that data can be obtained on both electrode capacitance and charge-transfer kinetics in an electrochemical cell. This information can be interpreted to model mechanistic parameters of the cell. This is most commonly achieved by fitting EIS data to one or more analogous equivalent electrical circuits, comprised of resistors and capacitors, by regression techniques. Proper selection of an equivalent circuit model will allow individual circuit components to be correlated with chemical or physical phenomena in the cell (Geenen, F. M., 1991).

One circuit used commonly to represent charge transfer reaction of a freely corroding surface is the Randles model. This circuit, as shown in Figure 8, is comprised of the uncompensated electrolyte resistance, R_u, the polarization resistance, R_p, of the corrosion reaction, and the faradaic capacitance, C_f, induced by the double layer at the electrode surface. This double layer forms instantaneously whenever a metal surface is exposed to water, and the polar water molecules are attracted to the conductive surface, aligning to create layers of positive and negative charge, as on the plates of a capacitor (Jones, D.A., 1996). The charged layer prevents the close approach of charged species from the bulk solution and impedes easy charge transfer. Depending upon the frequency of the ac potential applied, the double layer will provide varying impedance to electron flow.

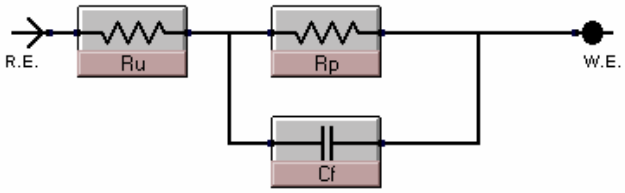

Figure 8 Randles Equivalent Circuit Model

This same simple circuit model can be used to describe the impedance of a well-adhered coating on a metal substrate, when there is no water beneath the coating, in contact with the metal surface. By definition, this precludes the occurrence of corrosion. The difference lies in the fact that the circuit components represent different mechanistic components of the cell. Components that were representative of corrosion at the metal surface are rather the resistance and capacitance of the polymer (R_{pf} and C_{pf}), where the coating is the dielectric.

Geenen offered the following description of physical phenomena associated with electrical elements of a coated system in solution under impedance measurement (Geenen, F. M., 1991):

> "R_u: Experimental resistance determined by conductivity of the electrolyte and the distance between reference and working electrode. It should remain constant during exposure, or otherwise indicate a fitting error.
>
> C_{pf}: From $C_{pf}(t)$ the values of [dielectric constant, solubility and diffusion] of a coating may be calculated, giving detailed information on the coating structure and composition. Furthermore [it] may indicate wet adhesion problems in an early stage.
>
> R_{pf}: Resistance related to the ohmic resistance of the paint film, but not its exact numeric value. $R_{pf}(t)$ gives a rough indication of the density and permeability of the polymer. In case a blister forms, R_{pf}, becomes R_b. R_b gives information on the density of the corrosion products formed in and under the defect.
>
> C_{dl}: As the capacitance of a double layer is a constant for a specific material in contact with an aqueous solution, from the measured value the total area of wetted metal under the coating may be calculated. It is thus a measure for the delaminated area, while $C_{dl}(t)$ gives the delamination rate.
>
> R_{ct}: Charge transfer resistance is coupled to the reaction rates of the rate determining steps of the anodic and cathodic corrosion reactions (R_{an}, R_{cat}).
>
> Z_{diff}: Impedance indicating the presence and quantity of a diffusion limitation of species to and from the corrosion sites (Z_{an}, Z_{cat}). Special cases of Z_{diff} (W,T,O) indicate special diffusion conditions."

On a Nyquist plot, Warburg impedance, Z_w, results in a characteristic 45° line at the low frequency (high real impedance, Z') end of the spectrum. In other words, the impedance is almost inversely proportional to the square root of frequency. This phenomenon most often represents an electrochemical process under complete diffusion control, but may alternatively be associated with current and interfacial capacitance distributions in a transmission-line configuration (Sagues, A. A. & Zayed, A. M., 1991).

A spectrum scan in Nyquist format will often take the form of one or more semi-circles, which may or may not overlap. The real component of impedance is often inversely proportional to frequency, and the imaginary component approaches zero at both low and high frequency, with a maximum in the intermediate frequency ranges. Each semicircle is indicative of a time-constant for which an equivalent electrical element can be defined, representing some physical phenomena, such as diffusion, capacitance, or charge transfer. When the time constant values for multiple elements are too close in value or the diameter of one resulting semicircle far exceeds the other(s), then it may be difficult or impossible to distinguish the separate time constants from the Nyquist plot (Pyc, W., 1998). Under such circumstances, observing directly the variation of phase and modulus on the Bode plot may provide a better indication of the elements involved.

Often the semicircles within a Nyquist plot are observed to be depressed below the x-axis, as shown in Figure 9. This is typical of a CPE, and is considered representative of a condenser relative to a rotated coordinate system (Geenen, F. M., 1991). The rotation angle is a function of the CPE factor (see Table 3), such that

$$\alpha = (1-n)\frac{\pi}{2}$$

Equation 29

The depression of the semi-circle, for coated systems, has been associated with unstable processes or heterogeneities in the system. For example, gradients in pH and ion concentrations are not uncommon, especially in crevices under coatings, and will cause gradients in conductivity and reaction rate, resulting in distributed time constants and CPE behavior. If the corroding system is not in steady state, the resulting instability will result in CPE-like response, but results in invalid impedance measurements. Therefore, stability of the system during measurement is crucial for impedance evaluation (Geenen, F. M., 1991).

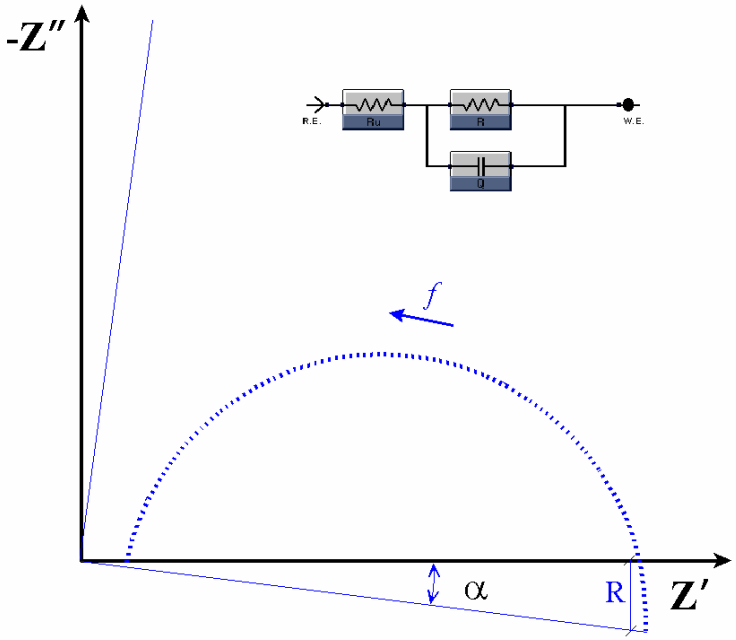

Figure 9 Constant Phase Element

Application to Coated Metals

Unfortunately, simple circuit models are often inadequate to describe the complex phenomena of corrosion occurring underneath a disbonded coating. As the complexity of the electrochemical cell and environment increases, the number of circuit elements necessary to model such behavior also increases, making it nearly impossible to exactly model the dynamic corrosion process. Further, individual circuit models do not uniquely fit impedance data. As the number of circuit

elements increases, the greater the likelihood of deriving a circuit model that fits the experimental data, but may bear no relation to the physicochemical phenomena involved.

If an anodic reaction extends into a crevice, such as under a coating, ohmic potential drops, mass transport issues, and large variations in local chemistry will complicate the impedance response. In such a case, the effective potential drops in the crevice so that most of the anodic reaction occurs near the opening. The impedance for the reduction reaction would then involve both activation and diffusion influences. The reduction related impedance in the crevice would be much larger at low frequencies, but may be overshadowed by parallel impedance components (Sagues, A. A. & Zayed, A. M., 1991).

Electrochemical impedance has been used successfully to monitor the uptake of water into coatings (in the absence of corrosion). This is accomplished by using the simple impedance model for a well-adhered coating, discussed previously. The capacitance of a plate-shaped capacitor can be calculated as follows (Geenen, F. M., 1991):

$$C = \frac{\varepsilon_o \varepsilon_r A}{l}$$

Equation 30

;where ε_o = dielectric constant (permittivity) of a vacuum
ε_r = relative dielectric constant of the dielectric
A = area of the plate
l = distance between the plates

The relative dielectric constant (permittivity) of water (ε_h ~80 @ 20°C) is much greater than that of an organic coating. Therefore, as water permeates and collects in the coating, consecutive impedance measurements will show an increase in capacitance over time, as the water leads to an increase in C_{pf}. If such increase is accompanied by changes in the corrosion potential, E_{corr}, of the cell, then it may be indicative of wet adhesion problems and the initiation of corrosion (Geenen, F. M., 1991).

Application to Reinforced Concrete and ECR

Testing of ECR via EIS procedures has revealed that for a perfect epoxy coating, the measured impedance values can be greater than 10^8 Ω/cm^2. Poor corrosion performance was associated with impedance values below 10^6 Ω/cm^2 (Clear, K. C. et al., 1995).

The uncompensated electrolyte resistance through concrete is much different from that of the bulk solution in an electrochemical test cell. Resistivity of concrete has been documented to range from less than 5 kΩ-cm to more than 100 kΩ-cm, depending upon permeability, degree of saturation, and other variables (Revie, R.W., 2000). Some concrete parameters which may influence electrolyte resistance may include the presence of pozzolans and admixtures of high ionic content.

Corrosion current density in reinforced concrete, and especially ECR, vary considerably from point to point on the bar surface. External measurements in concrete can only provide corrosion rates averaged over macroscopic regions, and a moderate nominal uniform corrosion rate,

estimated as a function of total surface area, may belie more severe localized corrosion (Sagues, A. A. & Zayed, A. M., 1991).

When considering the application of impedance measurements to concrete, some further complications arise. Ions in solution, such as those in concrete pore solution, will significantly decrease the dielectric constant of water. For example, a 5 M NaCl solution will have a dielectric constant less than half that of pure water (Geenen, F. M., 1991). This produces complications for the monitoring of coating water uptake in other than ideal laboratory test experiments.

EIS has been applied to ECR specimens in simulated solutions under laboratory conditions to characterize environmental influences on adhesion loss and corrosion (Sagues, A. A. & Powers, R. G., 1990). Sagüés reported that as-received ECR specimens in saturated $Ca(OH)_2$ solution remained in the passive potential range and electrochemical impedance at 1 mHz was reported to be on the order of 1 megohm. As-received specimens exposed to 3.5% NaCl evolved to corrosion potential of approximately -645 mV (SCE), and impedance at low frequency was on the order of 15,000 to 20,000 ohms after one month exposure. As-received specimens in solution of 3.5% NaCl + saturated $Ca(OH)_2$ gave open-circuit potentials around –625 mV (SCE) and impedance results were not reported.

METHODS AND MATERIALS

The study involved field sampling of bridge decks built with ECR and bare steel, followed by preparation of the specimens prior to cyclic exposure to chloride solution and electrochemical monitoring in the laboratory. Analysis of the relative corrosion response of ECR and bare steel specimens to cyclic chloride exposure provided an indication of the service life extension to be expected of the ECR system. The experimental procedures involved laboratory assessment of ECR specimens from a subset of 8 bridge decks from the previous study (Pyc, W., 1998) and 2 bridge decks with bare steel (uncoated) bars.

Field Survey and Sampling

Bridge Deck Selection

The decks were selected based upon relative adhesion rating and diffused chloride content, determined in the previous study, as shown in Table 4 (Pyc, W., 1998). Dry knife adhesion ratings ranged from 1 to 5, with 5 indicating no significant adhesion of the epoxy coating to the steel, and 1 corresponding to an adhesive bond greater than the cohesive strength of the epoxy coating.

Table 4 ECR Decks to be Sampled (Pyc, W., 1998)

Adhesion Groups	Decks	Specimens
4-4.5	2	24+6
3-3.5	2	24+6
1.5-2.5	2	24+6
1.0	2	24+6
Bare Steel	2	24+6
Total	8	150

Two bridge decks were sampled from each of four ranges of dry knife adhesion rating. In addition, two bridge decks constructed with bare steel bars, but constructed within the same time period as the ECR bridges and thus under the same concrete and cover depth specifications, were sampled and used as controls. Deck selection information is provided in Table 5 (Pyc, W., 1998) and Figure 10 presents the location of the bridge structures.

Sampling Plan

Altogether, 141 drilled cores, 102 mm (4 inches) in diameter, were employed in this study. For each of the decks built with ECR, 10 to 12 cores were drilled through a top reinforcing bar adjacent to the previous study core locations. In addition, approximately 3 cores were drilled through a top reinforcing bar at a surface crack location. Specific quantities of cracked and uncracked core samples for each deck are detailed in Table 5. For the 2 control decks, cores were drilled through a top reinforcing bar at locations that represent the 12-percentile shallowest concrete cover depth. The previous ECR study sample locations also represented the 12-percentile shallowest concrete cover depth.

Table 5 Selection of ECR and Bare Steel Bridge Decks (Pyc, W., 1998)

District	Structure Number	Year Built	Age (yrs)	Average Adhesion	Average Chlorides @ 13 mm, (kg/m^3)*
3	1004	1983	16	1.0	4.5
1	1136	1995	4	1.0	1.4
9	2262	1985	14	1.5	2.2
2	1015	1987	12	2.5	5.8
7	1001	1992	7	3.0	2.5
5	2021	1981	18	3.5	1.1
6	1004	1993	6	4.0	0.8
7	1019	1990	9	4.5	1.7
2	6128	1984	18	Bare Steel	-
1	6037	1983	16	Bare Steel	-

* Bare Steel decks were unique to the current study, thus no previous chloride data was available.

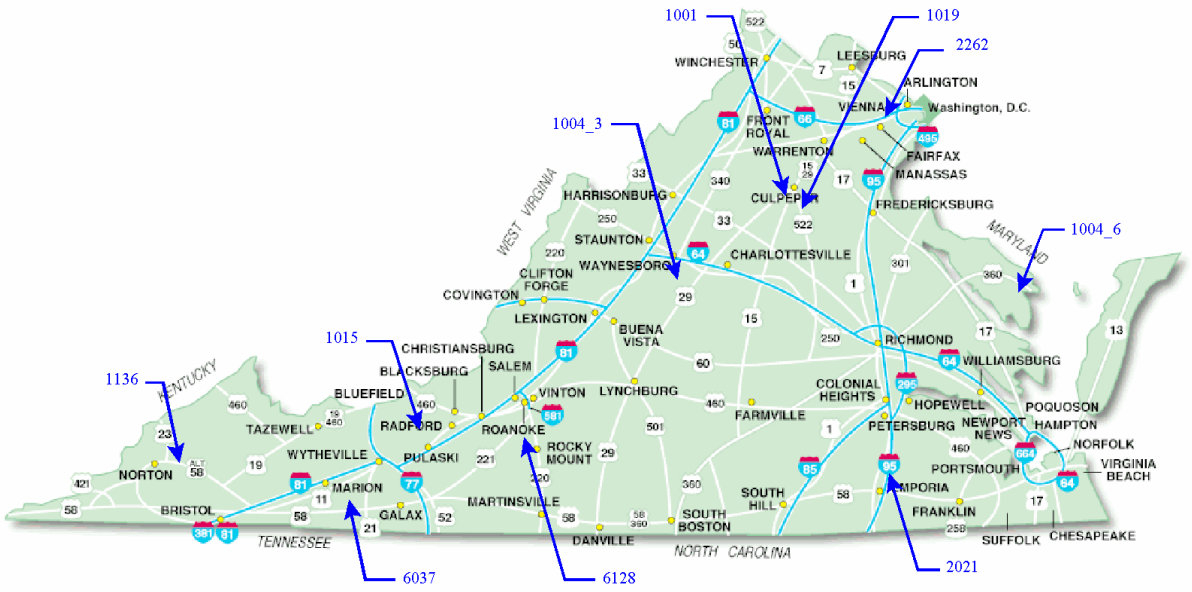

Figure 10 Selected Bridge Locations

Upon coring, each specimen was allowed to air dry only long enough for surface moisture to evaporate. The samples were then wrapped in multiple layers, consisting of a layer of 102-µm (4 mils) polyethylene sheet, followed by a layer of aluminum foil, and another layer of polyethylene sheet. Finally, the specimen and protective layers were wrapped tightly with duct tape. The purpose of the immediate wrapping of the cores was to maintain as closely as practical the in-place moisture condition of the concrete during transport and storage.

Field Evaluation

In addition to obtaining cores, as indicated above, additional information about bridge deck condition was obtained. A sounding survey, using chain drag and hammer, was conducted to identify delaminated areas, and visible spalls were noted. Powdered concrete samples were obtained using a hammer-drill and sampling bit, with attached filter collection device. The powdered samples were taken at 13 mm depth increments from 6 mm to 71 mm, in three

locations per bridge, adjacent to cores containing identified surface cracks. Powdered concrete samples were used for chloride concentration profiles and diffusion analyses.

The field survey was limited to the right travel lane because field experience has shown that this lane most often deteriorates first. The field survey of each deck consisted of 40 clear cover depth readings on each span and a visual crack survey. The crack survey consisted of the number and length of cracks in each span, categorizing them as either longitudinal or transverse/diagonal relative to the direction of traffic. Transverse and diagonal cracks were considered together, and differentiated from longitudinal cracks. Very few diagonal cracks were observed. Surface crack widths were measured visually with a crack comparator, generally at one-foot intervals along each crack. However, in all cases, no less than 5 crack widths were measured for a crack.

Laboratory Testing

All cores were visually examined for surface cracks. Cores that were taken in the field in visibly uncracked sections (crack widths << 0.08 mm were not visible in the field), but later discerned to contain surface cracks, were incorporated into the crack study. Crack widths and depths were measured, noting whether or not the crack extended to the depth of the reinforcing steel.

Sample Treatment and Exposure

Each core obtained from field sampling was divided into several parts for use in determining chloride and moisture content and subsequent laboratory corrosion assessment using electrochemical and visual techniques.

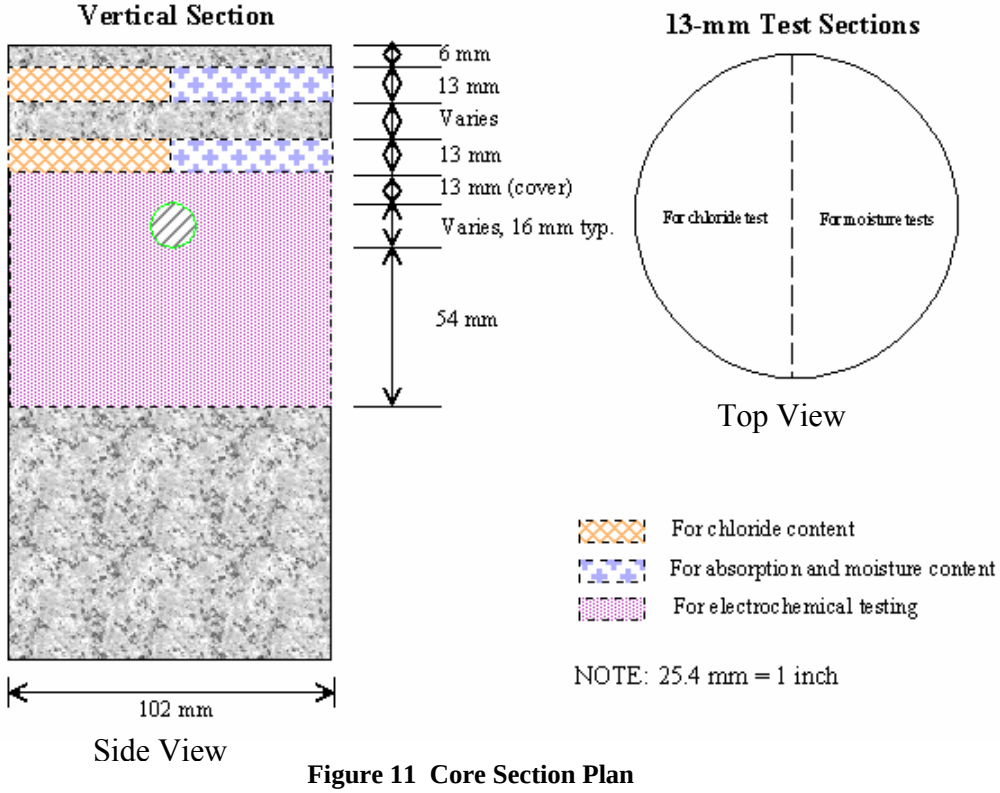

Figure 11 Core Section Plan

Core Preparation Procedure

For each core, the section of concrete 13 mm (½ inch) above the reinforcing steel was removed by dry sawing. Concrete chloride content, moisture content, percent absorption and percent saturation were determined for two 13-mm (½-inch) sections. A diagram of core sectioning is presented in Figure 11. Chloride contents were measured at two depths; one 13 mm below the surface and the other 19 mm above the reinforcing bar. Acid-soluble chloride concentrations were measured in crack sections and adjacent uncracked sections. Figure 11 presents the location of the chloride samples taken from field cores. Depending upon depth of clear cover, chloride samples were not retrievable for the whole core at some sample locations.

In general, chloride samples from cracked concrete sections were 19 mm wide, 13 mm thick, and 100 millimeters long and centered over the crack as shown in Figure 12. The samples were crushed to pass a #200 sieve, and sampled for chemical analysis. In addition, chloride contents were measured in the companion uncracked cores and in powdered-concrete sample profiles taken at three locations per deck adjacent to cracked cores.

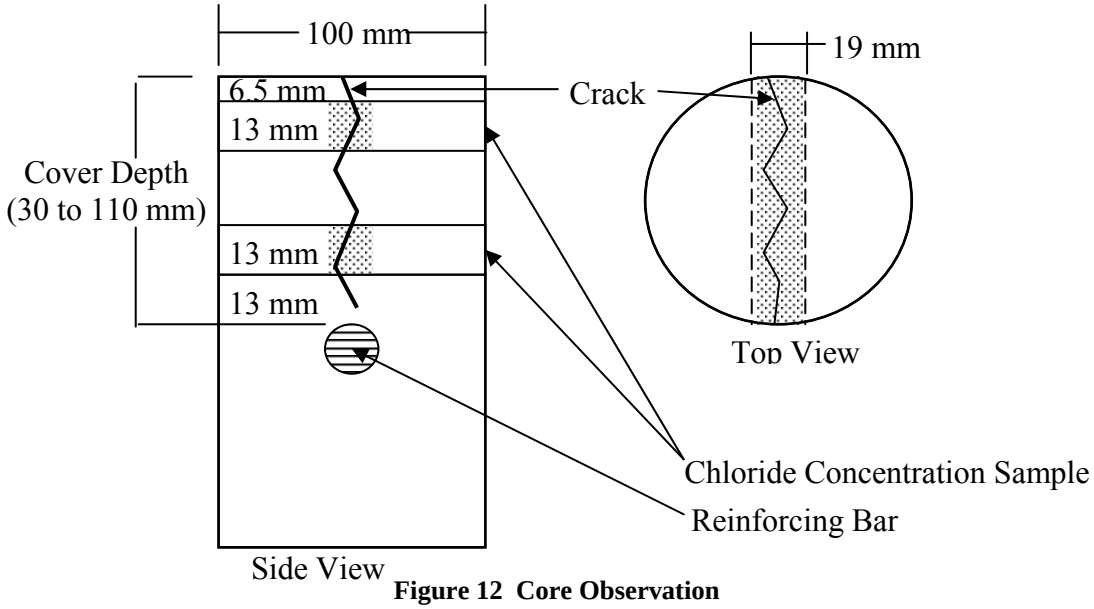

Figure 12 Core Observation

Electrochemical Specimen Preparation and Treatment

Dry saw-cutting and specimen preparation was conducted in groups by bridge, resulting in 10 groups. After the specimens were unwrapped, visual and photographic documentation of cores was accomplished. Exposed steel bar ends were cleaned and samples were obtained from the appropriate depths of the core by dry saw-cutting. Samples were obtained for chloride and moisture determination and sections containing the reinforcement bar were prepared for laboratory exposure to chloride solution and monitoring.

One end of the reinforcing bar was drilled and tapped (dry) and a stainless steel screw was inserted. The perimeter and bottom of the specimen were coated with paraffin wax, and the top remained exposed. A section of PVC pipe, 76-mm (3-inch) i.d., was fixed to the top of the core and sealed with silicone sealant to create a ponding reservoir. The reduced diameter of the

ponding dike was used to create a longer path of diffusion and migration for chloride to the ends of the bars at the core perimeter, which are more susceptible to corrosion (see Figure 13).

The length of core below the bar was kept constant at 54 mm for all specimens, where possible. Timing of core preparation and subsequent testing was staggered, with specimens divided into two to four major groups on alternate ponding cycles, to allow most efficient use of EIS equipment.

After preparation, the concrete core specimens were ponded with 3% NaCl solution. Chloride solution exposure was cycled on a weekly basis, by ponding for 2 days, followed by 3 to 5 days of drying under laboratory conditions, depending upon whether monthly testing was due for a given specimen. Testing occurred immediately after ponding solution was removed to assure good conductivity of the concrete cover.

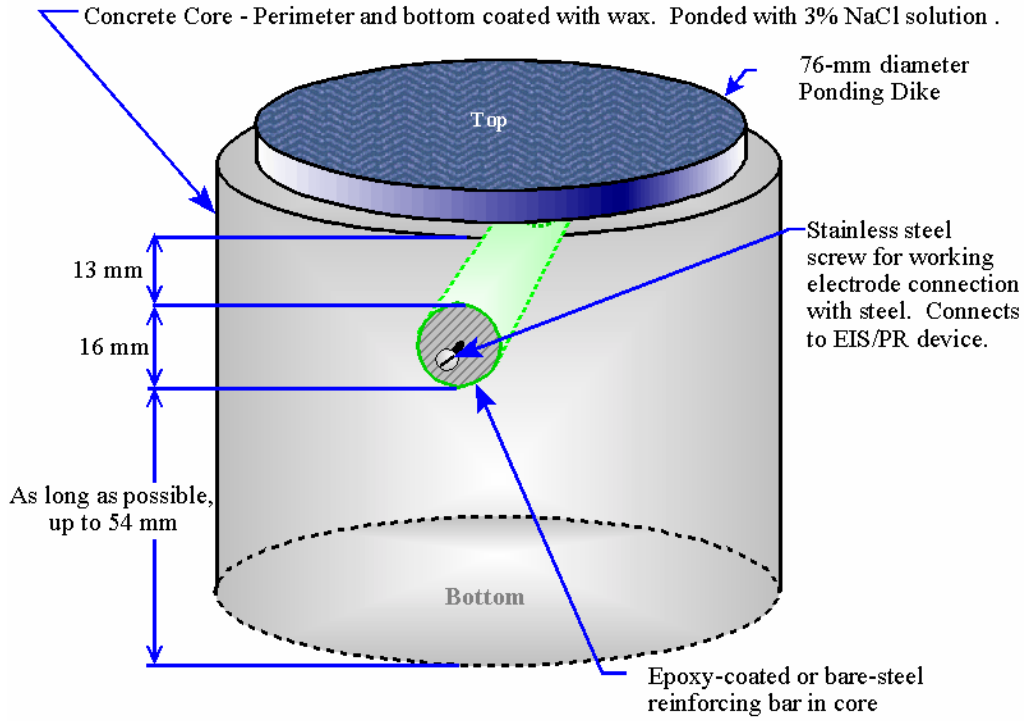

Figure 13 Ponding Specimen with Modified Ponding Reservoir

Physical Testing

Moisture Content

Moisture samples were weighed immediately after cutting. Percent absorption, and percent saturation of two 13-mm (½-inch) sections, centered at 19 mm (¾ inch) above the ECR bars and 10 mm ($^3/_8$ inch) from the surface, respectively, were determined in general accordance with ASTM C 642-97 (ASTM, 1997). One exception to the method involved individual sample size, which ranged from 21,000 to 131,000 mm^3, and is less than the 350,000 mm^3 per sample recommended by the method. However, determinations of mass, both in air and water, were

conducted on a mechanical balance, with a precision to the nearest $^{1}/_{10000}$ gram. The result was mass determination to the nearest 0.0002% or better of gross sample weight. Thus the 0.025% precision criterion outlined by the method was met. Initial percent saturation was estimated using the initial weight measurements in conjunction with absorption data from the test.

Chloride Testing

Concrete core sections scheduled for chloride analysis were obtained and stored during specimen cutting operations. The chloride sub-samples were pulverized and ground to a powder using rock-crushing equipment. Since the amount of material obtained from the rock crusher was much larger than that required for a single chloride test, the sample was quartered, using the procedures in ASTM C 702-98 until an appropriate sample was obtained (ASTM, 1998). After the initial mechanical crushing, any particles not passing the No. 20 sieve were crushed into a powder using a mortar and pestle. Acid soluble chloride content of powdered and core samples was measured in accordance with ASTM C 1152-90 (ASTM, 1990).

Chloride tests were also performed on powdered concrete samples, obtained by hollow-bore impact drill bit, from three locations of each bridge. The drill bit diameter was 29 mm (1.125 inches) and thus 1.5 times the maximum coarse aggregate size of 19 mm (¾ inch). Profiles were taken as five consecutive 13-mm depth ranges, the first of which was centered 13 mm below the deck surface. Apparent chloride diffusion constants were calculated from the powdered concrete profiles. The nominal background chloride content for a given bridge was determined from concentrations at the greatest depths that did not appear to be influenced by chloride ingress from the environment. All measured chloride concentrations from a given bridge were then adjusted by subtracting this nominal value, to reveal the concentration of "diffused" chloride.

Electrochemical Testing

Corrosion progress and coating properties were monitored using Electrochemical Impedance Spectroscopy (EIS). The major components of the test system included a computer-operated potentiostat and appropriate software. The Gamry Instruments PC3/300 Potentiostat / Galvanostat / ZRA system of integrated circuit cards for use in IBM-PC compatible computers was employed, along with the associated Framework software. The user interface and control of the PC cards and selection and manipulation of electrochemical techniques was coordinated through the Framework software, and analysis was performed via spreadsheets.

Custom probes were fabricated for use in the electrochemical tests to accommodate the new ponding reservoir. Each probe consists of a titanium mesh counter-electrode cut to 63-mm (2½-inch) diameter and sandwiched in an open cell sponge to maximize electrical surface contact. The sponge assembly is adhered to a probe housing fabricated to accommodate a pen-cell type Cu-Cu(SO_4) half-cell reference electrode. A small concrete weight was cast for each probe to enhance surface contact. Figure 14 is a schematic of a typical core specimen with connections and probe for EIS testing.

To permit efficient EIS testing of the prepared samples containing epoxy coated or reference bare steel bars, two multiplexed electrochemical testing systems were used. The two systems, based on Gamry Instruments Model PC3/300 potentiostats installed in separate IBM compatible personal computers, were each linked to a Gamry ECM8 eight-channel multiplexer. The two

systems, running in parallel, each perform potentiostatic EIS on eight specimens, to be tested consecutively over a one- to two-day period.

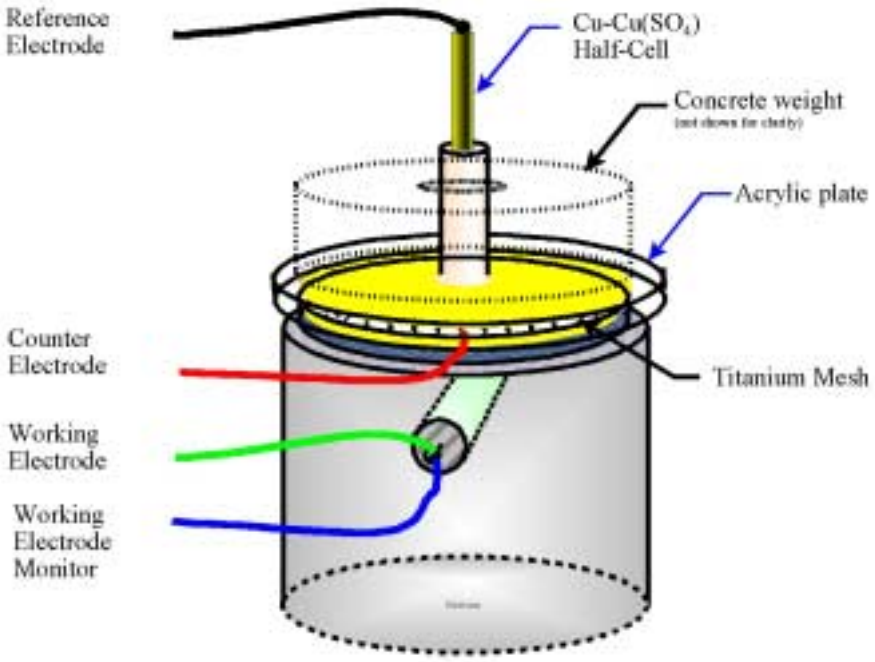

Figure 14 Test Probe and Cell Connections Design

EIS was performed using a frequency range of 0.001 Hertz to 5000 Hertz with ±10 mV RMS amplitude about the corrosion potential. The high frequency was limited by the capabilities of the potentiostat. The low frequency, which is equivalent to 1 cycle every 16 minutes, was selected as the most practical lower limit, based on available time for testing and the expected degree of stability in the corrosion system (Sagues, A. A. & Zayed, A. M., 1991). The sample rate was adjusted from 10 individual frequencies per decade to 5 frequencies per decade, reducing test time by almost half. The benefit is twofold:

a. The cumulative test time for a multiplexed series of eight specimens was reduced to approximately one day.
b. The length of test for an individual specimen is shorter, which would reduce error introduced by potential shift that may result from changes in the corrosion state of the specimen during the test.

This change reduced the number of data points, but sufficient data were acquired to describe the general frequency spectra of the samples, as demonstrated in Figure 15.

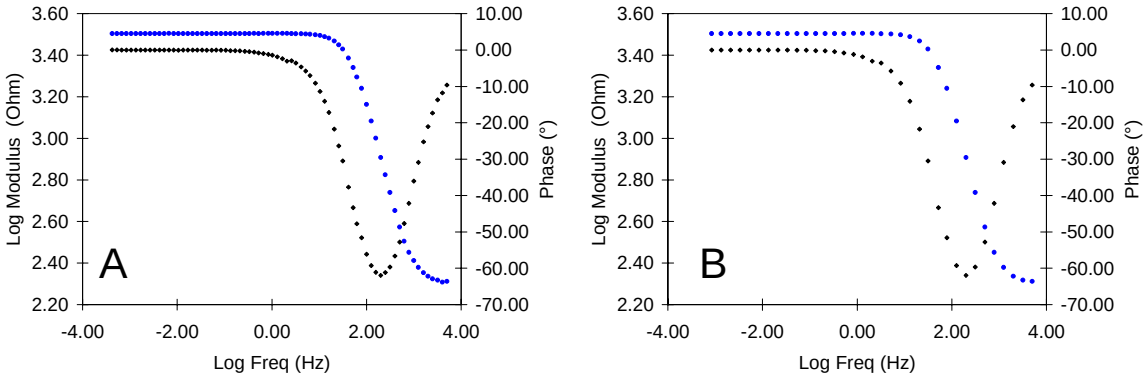

Figure 15 Comparison of EIS at 10 Points(A) and 5 Points(B) per Decade Frequency

Results can be analyzed graphically using Bode and Nyquist plots, which show the modulus of impedance and phase angle versus frequency, or the real versus imaginary impedance, respectively. The impedance values obtained at frequencies on the order of 0.001 Hz generally reflect the total of electrolyte resistance, the ECR coating resistance and other resistive and capacitive elements, whereas impedance values in the 5000 Hz range are more indicative of solely the concrete electrolyte characteristics. These are rather broad simplifications, for impedance response of epoxy coated reinforcement in a concrete medium is a very complex system (Sagues, A. A. & Zayed, A. M., 1991). For example, issues concerning impedance of the coating system at or away from holidays or breaks in the coating, current distribution through non-homogeneous concrete, the potential presence of a moisture layer beneath the coating, are only a few of the phenomena which will greatly influence current response over the frequency spectrum selected. Further, true electrolyte resistance is more likely to be characterized at frequencies of 100 kHz or greater, well beyond the capacity of the systems used. However, reasonable comparisons do seem to be possible between the two bar systems under investigation. In almost all cases, the time of initiation of corrosion could clearly be established by corroborating impedance and potential data.

The two multiplexed EIS systems, running in parallel, performed potentiostatic EIS over the selected frequency spectrum on a total of sixteen specimens in a 24-hour period. The preparation of specimens was performed in ten groups of sixteen specimens. The preparation occurred at two-day intervals over a four-week period. After preparation and curing of sealant, an EIS test was performed on each specimen prior to initiation of ponding with 3% NaCl. The specimens were then subject to a regular ponding cycle, including two days of ponding, and five days of drying under room temperature and relative humidity conditions each week. During every fourth week, immediately following ponding, the specimens were subject to EIS tests over one to two days and then the dry period was limited to three to four days. Ponding cycles for the specimens were divided into three major groups, to stagger the testing cycle as appropriate for three groups of up to sixteen tests per week. All 141 bridge specimens were prepared and tested in approximately four weeks. The specimens were then tested at four-week intervals.

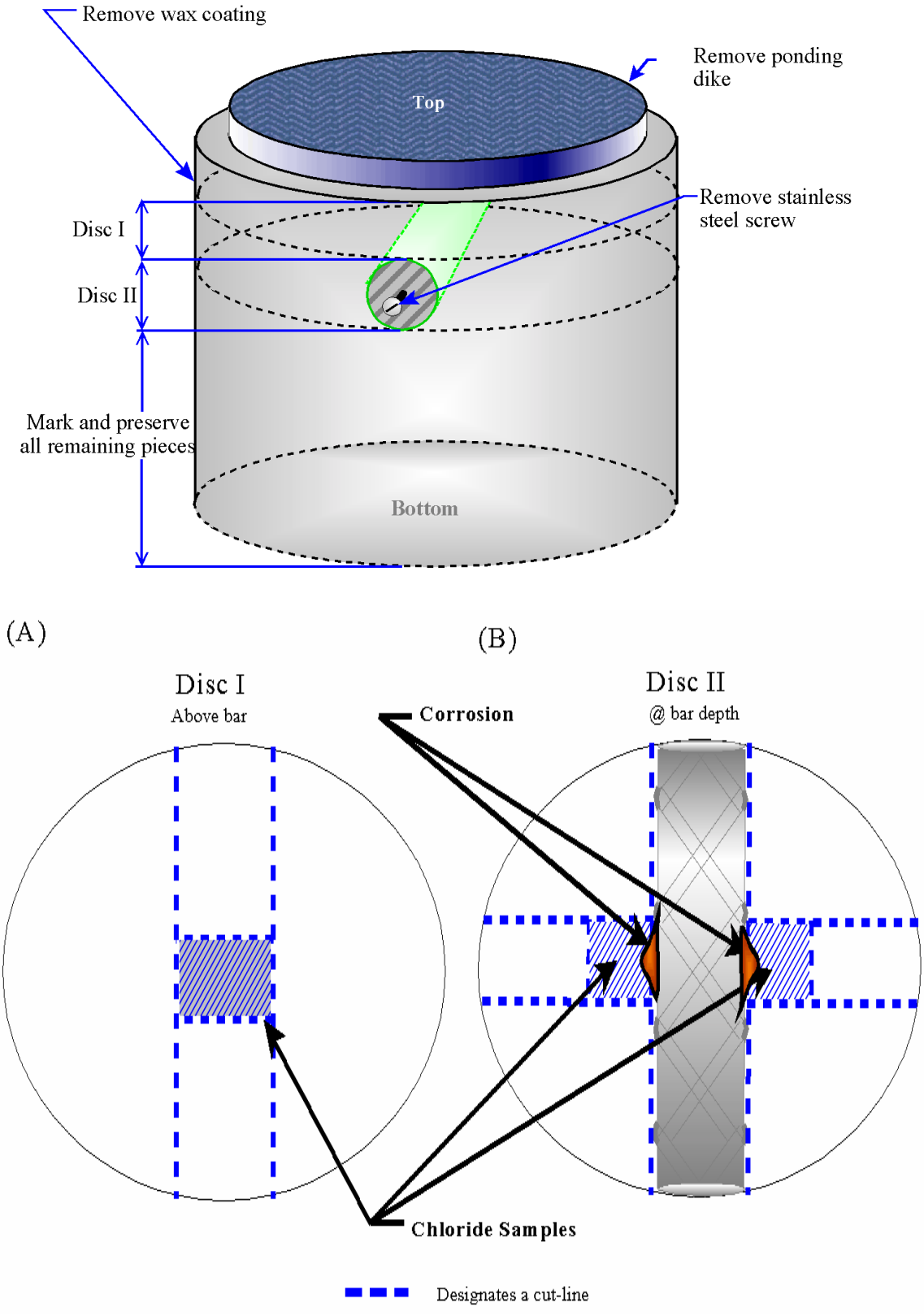

Figure 16 Post-cracking Sampling Plan for Laboratory Specimens

Post-cracking evaluation

Post-cracking observations of the cyclically ponded cores included documentation of the width, length, and orientation of the crack at the core surface. The core was then dry-cut in accordance with Figure 16 to permit visual observation and extraction of the reinforcement bar, as well as sampling of concrete adjacent to and above the site of active corrosion.

Adhesion rating

Immediately after exposure, the reinforcement was photographed, along with the bar trace of the surrounding concrete, to document the physical condition. For ECR samples, a knife adhesion test was performed, using the same criteria applied in a previous study (Pyc, W. A. et al., 2000). The adhesion rating was documented for six locations on each bar; three on the top and three on the bottom. In addition, the color of the bar surface beneath the coating was documented, also using similar ratings to those employed in the previous study. The adhesion and color rating results were also photographically documented.

Chloride analysis

Samples of concrete adjacent to and directly above the site of active corrosion along the bar were crushed to pass a # 20 sieve and subject to acid-soluble chloride concentration tests in accordance with ASTM C 1152-90. These values were taken to indicate the concentration of chloride at the corrosion site at the time of cracking. As before, values were adjusted by subtracting the nominal background chloride content of the concrete in the bridge. Samples were generally greater than 10.0 g, as specified, but a few samples were slightly less, depending upon the dimensions of the core, orientation of the reinforcing bar and the size of the active corrosion site.

Truncated Observations

After approximately 22 months of exposure, 27 of 28, or 96%, of the bare steel specimens had cracked and been subject to destructive assessment. Since only 21 of 113, or 19%, of ECR specimens had cracked at this time, more information was desired about the distribution of diffused chlorides in the remaining ECR cores. A group of 17 cores was selected at random from among all the remaining ECR cores. This group represented a set of "truncated observations", in which the post-cracking evaluation procedures were applied, even though a visible crack had not yet been identified. The observed bar condition, coating condition, and chloride contents for each specimen were then used to surmise the status of the remaining ECR cores. The set of ECR specimens allowed to proceed through cracking was reduced from 113 to 96 specimens.

RESULTS

Although the plan called for 15 cores from each deck, the exact number of cores with and without surface cracks varied based on field conditions. Table 6 presents the district bridge designations, route locations, ages at sampling, and exact numbers of samples from each deck.

Table 6 Core Sample Classification

Bridge	District-County	Route	Year Built	Age	Total Number of Cores	Uncracked Cores	Cores containing Surface Cracks
1136	1 - Wise	SR 72	1995	4	15	11	4
1004.6	6 - Northumberland	SR 200	1993	6	13	9	4
1001	7 - Culpeper	US 29	1992	7	14	11	3
1019	7 - Culpeper	US 522	1990	9	13	8	5
1015	2 - Giles	SR 100	1987	12	14	10	4
2262	9 - Fairfax	Vaden Drive	1985	14	15	10	5
6128	2 - Franklin	County 740	1984	15	16	11	5
1004.3	3 - Nelson	SR 6	1983	16	14	11	3
6037	1 - Grayson	County 662	1983	16	12	10	2
2021	5 - Greensville	I-95	1981	18	15	10	5
Total					141	101	40

Table 7 presents respective Virginia Engineering District, dates of construction and age at the time of the survey, number and length of spans, superstructure type, and reinforcing steel type for all bridges in the study. The bridges were built between 1981 and 1995 and were 4 to 18 years of age at the time of field survey. Bridge superstructures were primarily simply supported or continuous design steel girder systems with composite decks. One structure was prestressed concrete I-beams with continuous span design. Previous research has shown that transverse cracking is more frequent for steel girders and more frequent for continuous girders than simply supported girders (Krauss, P. D. & Rogall, E. A., 1996).

Table 7 Bridge Superstructure Type and Reinforcing Steel Type

District	Structure Number	Year Built	Survey Age (yrs)	No. Spans	Span Lengths (m)	Type	Reinforcing Type
1-Bristol	1136	1995	4	3	22/22/22	S/C	ECR
6-Fredericksburg	1004	1993	6	3	13/13/27	PI/C	ECR
7-Culpeper	1001	1992	7	3	23/23/24	S/C	ECR
7-Culpeper	1019	1990	9	3	15/26/15	S/S	ECR
2-Salem	1015	1987	12	3	15/24/15	S/S	ECR
9-Northern VA	2262	1985	14	4	21/20/25/23	S/S	ECR
1-Bristol	6037	1983	16	2	20/20	S/S	BS
3-Lynchburg	1004	1983	16	3	18/18/19	S/C	ECR
2-Salem	6128	1981	18	2	17/17	S/S	BS
5-Suffolk	2021	1981	18	3	21/21/21	S/C	ECR

S/S: steel girders, simply supported
S/C: steel girders, continuous design
PI/C: prestressed I-beams, continuous design
ECR: epoxy coated reinforced steel
BS: bare reinforcing steel

Span lanes were generally equivalent, with the shortest span of 13 m and the longest span of 27 m, both on Fredericksburg structure No. 1004. Eight of the decks were built with ECR and two with bare steel (BS). The two bare steel decks were 15 and 16 years old when the field survey was conducted. These two bridges are in the highest snowfall area of the state, but are located on County Routes, which have lower traffic counts than U.S. and Interstate routes.

Influence of Cracking

Field Survey

Table 8 presents the total longitudinal and transverse cracks for average crack width of less than and equal to 0.30 mm and greater than 0.30 mm. As shown, the total length of longitudinal cracks is significantly greater than the total length of transverse cracks, 1109 m and 172 m, respectively. Also, the greater percentages of the longitudinal and transverse cracks were less than 0.30 mm, 85 and 95 percent, respectively. The total length of cracks is less for the bare steel than any of the ECR decks. However, the subset of BS decks was too small to allow conclusions as to the influence of steel type.

Cover Depth Survey

Clear cover depths, 40 per span, were averaged to determine the cover depth distribution and were compared to the applicable construction specifications. These data were taken from the preceding study involving 21 bridges, all containing ECR (Pyc, W., 1998). The average clear cover was 65 mm with a standard deviation of 9.1 mm. The average cover depth of the two bare steel bridges in this study was 55 mm and standard deviation was 11.5 mm. Overall, field cover depths ranged from 43 mm to 116 mm, with no instances of "zero" cover observed. The average directly measured clear cover depth from 141 core samples in this study was 69 mm, with a standard deviation of 14.3 mm. The structures were built under the same concrete specification, with a maximum water-to-cement ratio (w/c) of 0.45 and a cover depth of 63 mm to 76 mm.

Table 8 Bridge Survey Area and Crack Length

Survey Age (years)	Survey Area (m^2)	Crack Length (mm) Longitudinal		Transverse	
		Width ≤ 0.30mm	Width > 0.30mm	Width ≤ 0.30mm	Width > 0.30mm
4	411.7	82.8	7.2	50.9	5.7
6	196.2	77.4	1.6	40.9	0.0
7	312.5	94.2	0.0	38.6	1.2
9	347.5	165.1	29.1	22.8	0.9
12	359.5	25.8	25.8	0.0	0.0
14	326.6	240.2	4.9	0.0	0.0
16*	285.4	0.0	0.0	0.0	0.0
16	372.0	154.8	41.1	0.0	0.0
18*	254.9	20.0	11.3	9.6	1.4
18	479.9	85.8	42.2	0.0	0.0
Total	3,346.2	946.1	163.2	162.8	9.2
	Percent	85.3%	14.7%	94.7%	5.3%

*Deck contains bare steel reinforcement, others were constructed with ECR.

Crack Frequency

The number of longitudinal cracks ranged from 0 to 4 in a span-lane and from 0 to 11 for a deck. The number of transverse/diagonal cracks ranged from 0 to 9 in a span-lane and from 0 to 16 for a deck. For the 8 decks built with ECR, there were 51 longitudinal and 56 transverse cracks. Of these decks, 4 span-lanes had no longitudinal cracks and 15 span-lanes had no transverse cracks from the sub-sample of 25 span-lanes. For the two BS decks, there were 6 longitudinal and 5 transverse cracks spread over the 2 span-lanes of structure 6128. Structure 6037 had no longitudinal or transverse cracks. The number of transverse and longitudinal cracks does not appear to be a function of span length.

Laboratory Core Evaluations

Crack Width and Depth in Cores

Although only 30 cores in the field were identified with surface cracks and targeted for sampling, several of the cores sampled from visibly uncracked concrete had apparent surface cracks after core sampling. The presence of these cracks, which were oriented vertically in the cores, is not attributed to the coring process, but more likely represents preexisting cracks that were not visible in the rough finished surface. These cracks became apparent after removal from the deck, possibly from the loss of confining pressure from the surrounding concrete. Thus, 40 cores contained cracks and were incorporated in the cracked cores subset for the study.

The crack widths for all the cores that contained a surface crack ranged from 0.08 mm to 0.33 mm and crack depths ranged from 3 mm to 162 mm. Only one of the 40 cores, core 2 from structure 1015, built in 1987, had a surface crack greater than 0.30 mm. Only 7.5% of the cracks in cores were greater than or equal to 0.30 mm in width. Only 5 of the cracks, or approximately 12.5%, penetrated to the depth of the reinforcing steel and all 5 cracks were from the 30 cores deliberately drilled over a crack identified in the field.

Moisture Content

A summary of results of the concrete density, absorption, and percent saturation tests is included in Appendix A. Tests indicate that the concrete specimens, although stored in multiple layers of polyethylene sheet and aluminum foil, likely did lose some moisture between field sampling and laboratory specimen preparation. From 275 determinations, the average moisture content for all specimens was 66% with a standard deviation of 7.8%. The highest average percent saturation for a bridge group was 76% and the lowest average percent saturation was 55%. The moisture content of sections 6 mm to 19 mm below the top surface was not different from that of the sections 13 mm to 26 mm above the reinforcement.

Chloride Content

The acid-soluble chloride content of concrete, extracted from slices of the cores at two depths, was determined by potentiometric titration. The ingress of chloride into concrete bridge decks is commonly modeled using a solution of Fick's Second Law of Diffusion, as approximated for one-dimensional diffusion into a semi-infinite slab:

$$C_{(x,t)} = C_0\left(1 - erf\frac{x}{2\sqrt{D_c t}}\right)$$

Equation 31

where; $C_{(x,t)}$ = chloride concentration at depth x after exposure time t
C_o = constant chloride concentration near the surface
D_c = effective diffusion coefficient
erf = mathematical error function (Rieger, P.H., 1994).

The rate of chloride ingress into the concrete is dependent upon the quality of the cement paste, including cement and water content, and degree of maturity, which in turn affect pore size distribution and tortuosity of the capillary pore system. Capillarity has an influence on the system, but is primarily observed in the outer few millimeters of concrete cover, especially for concrete in a saturated or near-saturated condition, as under the cyclic ponding process in this study. The above equation is a simplification of a complex process, and does not consider the influence of chloride binding, leaching, non-homogeneities of aggregate size, shape, and distribution, or variations in saturation and hydration through the depth of the paste matrix, as well as other chemical and physical processes (Sagues, A. A. et al., 2001; Kranc, S. C. et al., 2002). Therefore, it is recognized that the effective diffusion coefficient employed is not a pure scientific measure, but rather a nominal engineering indicator, which estimates a coefficient, fixed in space and time, to describe the long-term rate of chloride ingress.

Chloride concentrations at the two depths, centered 13 mm (½ inch) below surface and 19 mm (¾ inch) above the surface of the top reinforcing bar, in conjunction with profiles from powdered samples, were used to project the chloride content at each bar depth. A typical chloride profile is shown in Figure 17.

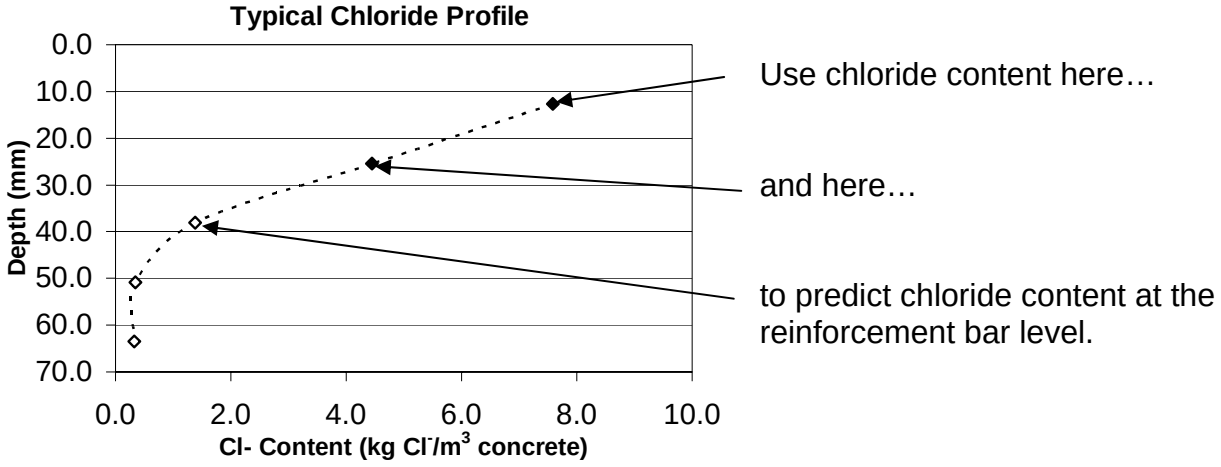

Figure 17 Predicting Chloride Content at the Bar Depth

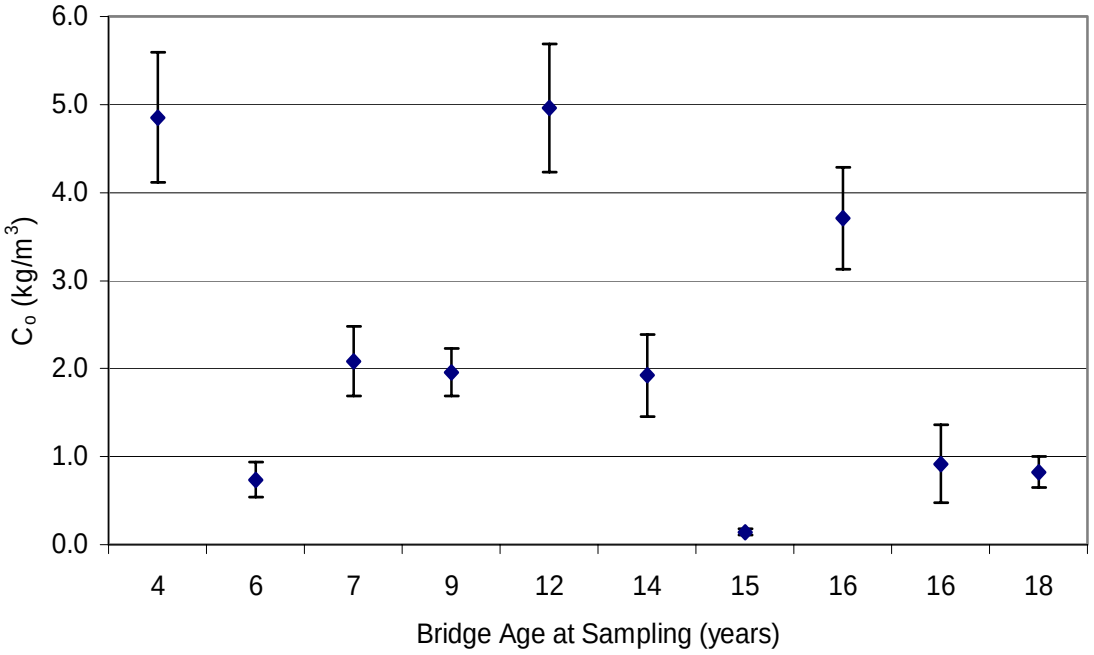

Figure 18 Chloride Diffusion Parameters by Age – Surface Concentration, C_o

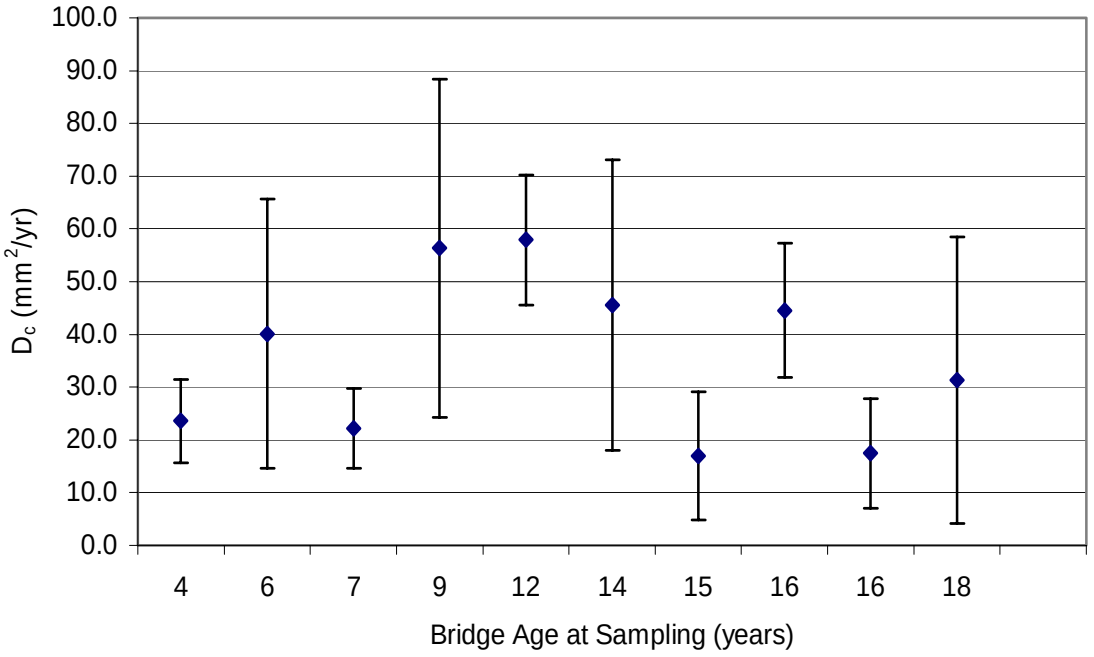

Figure 19 Chloride Diffusion Parameters by Age – Diffusion Coefficient, D_c

Analysis of the resulting chloride profiles has been presented elsewhere (Kirkpatrick, T. J. et al., 2000). Figure 18 presents the average and 95% confidence intervals for chloride concentrations at 13 mm depth, assumed to be the driving concentration, C_o, as a function of age. C_o was used in conjunction with an apparent field diffusion coefficient, D_c. The resulting estimated average D_c and 95% confidence interval is plotted in Figure 19. A few of the specimens that contained cracks resulted in very high estimated diffusion coefficients. Since these conditions were not solely related to the diffusion process, the samples were removed from the data presented.

Corrosion Potential and Impedance Monitoring

During the laboratory treatment period, the specimens were ponded, and tested periodically to monitor the condition of the coatings and the presence or absence of active corrosion. The open-circuit potential and selected impedance data were compiled and tracked as a function of time. Specifically, the modulus of impedance, as defined previously, and the associated phase angle were recorded at frequencies of 1 mHz, 1 Hz, and 5000 Hz.

Based on previous experience with EIS data for reinforced concrete specimens, the frequencies were selected to give general indications about components of the physical system (Pyc, W. A. et al., 2000). The impedance at 5000 Hz is indicative of the concrete and electrolyte between the reference/counter electrode and the bar specimen. Impedance response at 1 Hz may capture a small part but not all of the coating and corrosion impedance in addition to the electrolyte resistance. At 1 mHz, impedance values are more indicative of the cumulative effects of the concrete and the impedance induced by both the coating, if present, the passive oxide layer on the reinforcement, and the corrosion process.

Typical Impedance Plots

The potential, impedance and phase angle data from each EIS test across the chosen frequency spectrum could be plotted in several formats to reveal information about the system and its corrosion state. The first is a Bode plot, with the modulus of impedance and the phase angle plotted as a function of the frequency of the alternating current. The second is the Nyquist plot, which presents real and imaginary components of the complex impedance response. Each of the plots is useful for determining aspects of the system, including indications of corrosion state, coating saturation, and concrete resistivity.

Interpretation of electrochemical impedance spectroscopy results is difficult for any but the simplest experimental designs conducted under tightly controlled laboratory conditions. In simple solution, a good quality coating on a metallic substrate can be clearly characterized (Standish, J. V. & Leidheiser, Jr. H., 1981; Scantlebury, J. D. & Sussex, G. A. M., 1981). However, the concrete medium as an electrolyte introduces a host of complexities regarding current distribution, interface impedances, and alternate physical and chemical interactions. Further, partially or fully disbonded coatings with moisture between the coating and the substrate add more complexity to the system. Once corrosion has initiated, the accumulation of corrosion product will provide new barriers for ion and electron flow, making the system even more complex.

The frequency range used in this study is insufficient to completely capture aspects of the electrolyte and polarization resistance related to corrosion, even for bare steel. For example, to determine precisely the electrolyte resistance would require frequency of 10 kHz or greater, which is beyond the capacity of the system employed. Polarization resistance time constants are often represented by large arc-shaped response of high real impedance on the Nyquist plot. As can be seen from Figure 20, for bare steel, arc-shaped curves are suggested at high values of real impedance, but the frequency range (high real impedance typically corresponds with low frequency on the Nyquist plot) is insufficient to fully describe the curve. Attempts to extrapolate from the available data would induce considerable error in the resulting estimates. Therefore, it is not reasonable to determine precise polarization resistance values from the available data. However, this condition does not preclude the use of these data in determining the time of corrosion initiation.

Figure 20 presents both Bode and Nyquist diagrams of the available impedance spectrum for a typical bare steel specimen at selected times prior to (top) and after (bottom) the initiation of corrosion. The slope of the Nyquist plot (top-right) implies a very large polarization resistance, consistent with a well-developed passive layer(Sagues, A. A. & Zayed, A. M., 1991). Considering the modulus of impedance, as shown in the Bode plots (left), as well as the magnitude of real and imaginary impedance components in the Nyquist plots (right), a clear decrease in overall impedance can be observed at low frequencies as corrosion occurs. Projecting the arc at the high impedance portion of the Nyquist plot (bottom-right) suggests a much lower polarization resistance, and thus a higher corrosion rate, than observed in the prior test.

The same trends can be observed for a typical ECR specimen, as shown in Figure 21. The Nyquist plots for the ECR specimen before (top) and after (bottom) corrosion initiated correlate well with observations by Sagüés and Zayed of partially disbonded coatings in concrete (Sagues, A. A. & Zayed, A. M., 1991). The impedance in the complex plane prior to corrosion (top-right) resembles either a system under diffusion control, or more likely, a transmission line configuration, where moisture exists beneath the coating. Again, as corrosion occurs (bottom), the low frequency impedance decreases dramatically. The magnitude of the phase angle also decreases, but also becomes more complex, as additional phenomena occur related to corrosion and coating deterioration.

Determining Corrosion Initiation

For uncoated bars, active corrosion appeared to correspond to potential values more negative than -350 mV CSE, as outlined in ASTM C 876 (ASTM, 1991). For coated bars, a similar change in electrical potential was generally observed. However, active corrosion could not be assumed unless a corresponding decrease in impedance was observed. The value of impedance at 1 mHz was determined for ECR, recognizing that the coating has a strong influence on the impedance values, and the observed behavior would be a combination of coating and corrosion related impedance factors. However, the reduction of low frequency impedance were complimented by changes in open-circuit potential, and together reliably indicate the occurrence of corrosion in the specimens. This is consistent with observations by others of ECR systems involving disbonded or partially disbonded coating (Sagues, A. A. & Zayed, A. M., 1991).

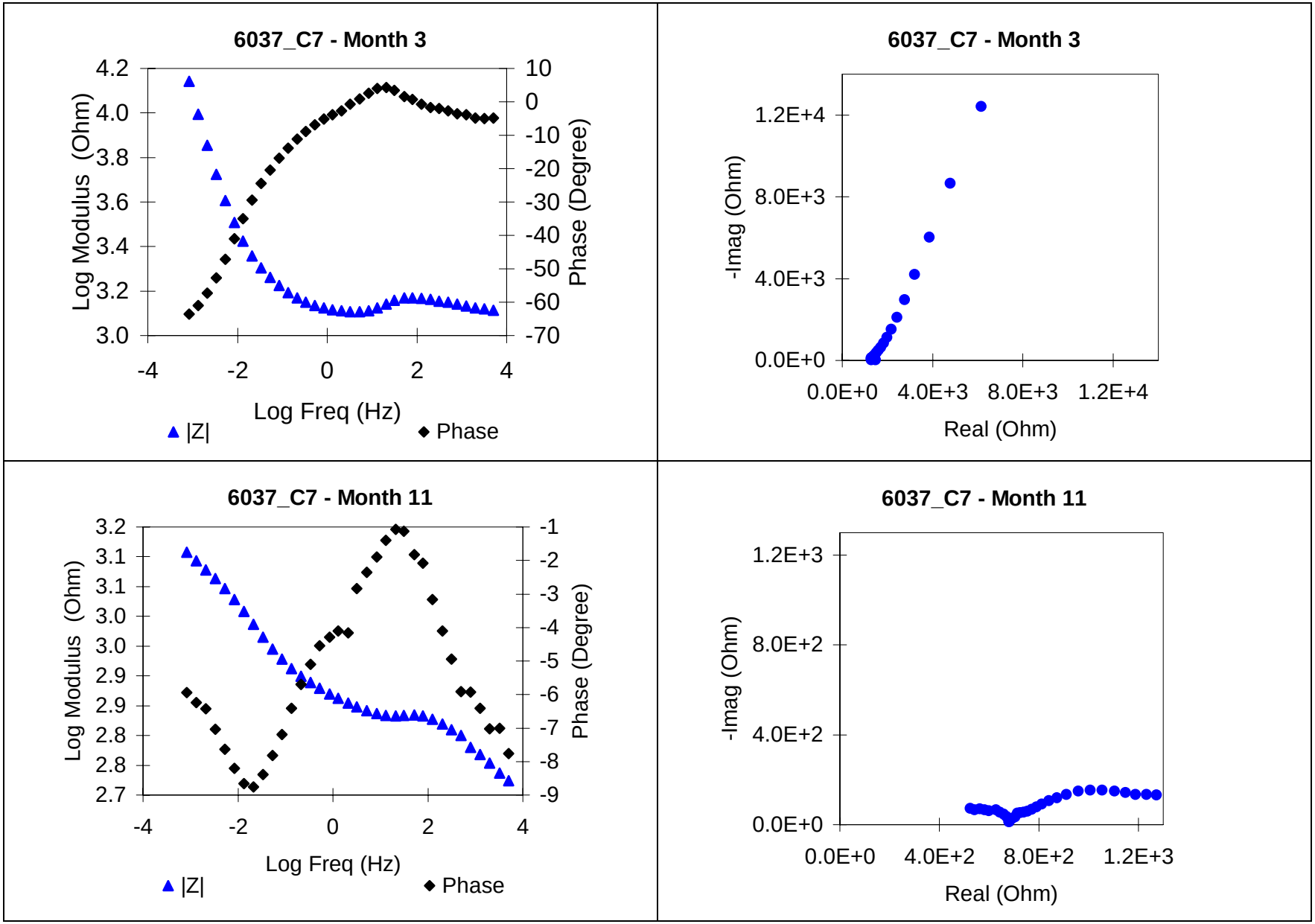

Figure 20 Typical Bode and Nyquist Plots for Bare Steel Before and After Initiation

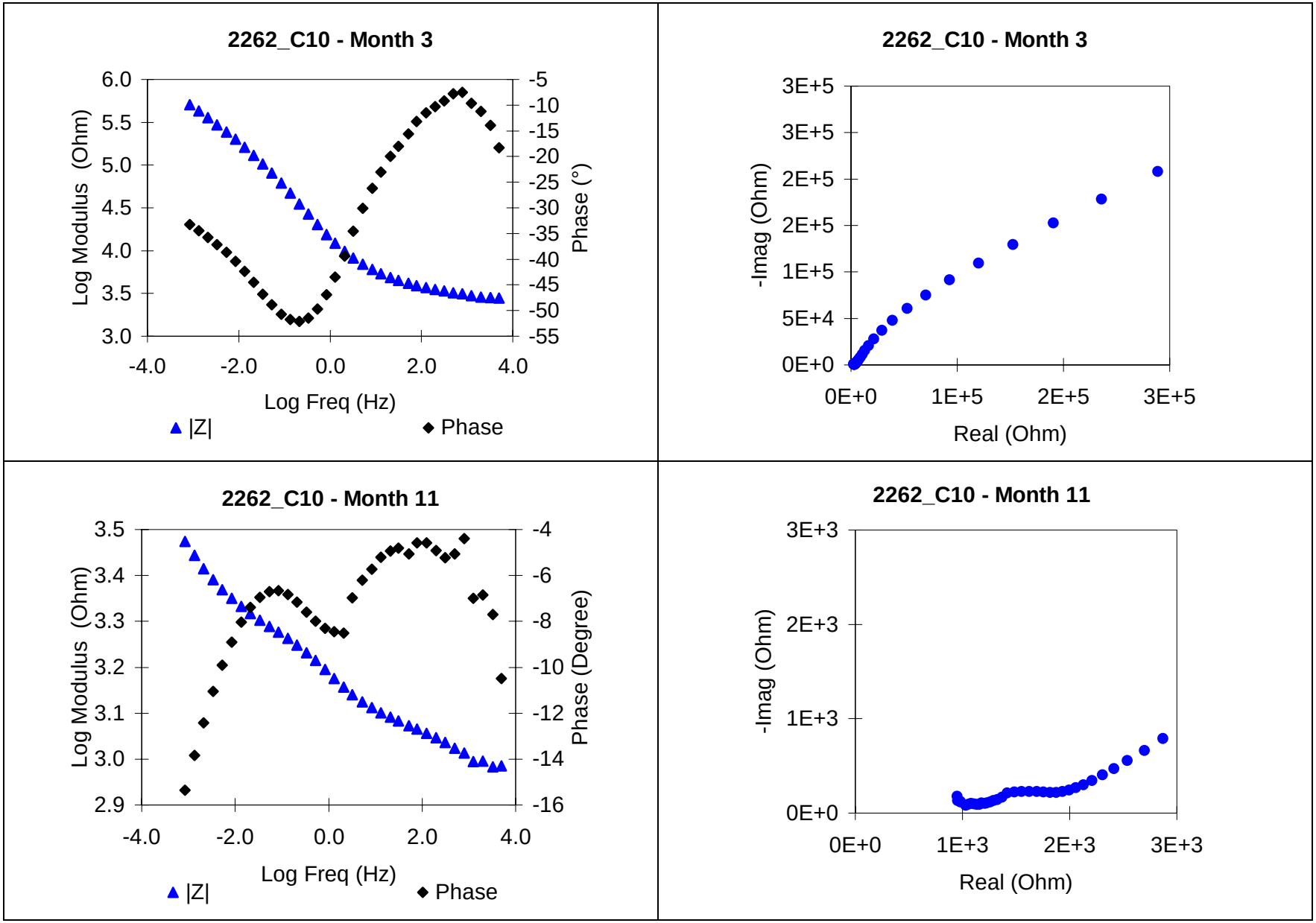

Figure 21 Typical Bode and Nyquist Plots for ECR Before and After Initiation

In general, non-corroding ECR specimens exhibited a modulus of impedance at 1 mHz on the order of 10^6 ohms. A few specimens had impedances as high as 10^8 ohms, and correspondingly noble potential values, usually more positive than –200 mV CSE. Actively corroding ECR specimens had a corresponding modulus of impedance less than 10^5 ohms, and often less than 10^4 ohms.

By observing the trends of open-circuit potential with time, changes in the system could be identified by the occurrence of sudden changes in slope or magnitude. Correlating changes in potential with shifts in impedance and phase allowed a reasonable estimation of the time of corrosion initiation, to the nearest month, which was the interval between measurements. Figure 22 presents a typical group of graphs for bare steel that convey the trends of potential and, impedance and phase angle for scan frequencies of 1 mHz, 1 Hz, and 5 kHz. For this specimen, corrosion appeared to initiate in the 13^{th} month of treatment. Figure 23 represents the same information for a typical ECR sample. Corrosion for the specimen in Figure 23 initiated in the sixth month.

The time to corrosion initiation was determined from electrochemical impedance measurements, and the time to cracking was determined by visual identification of cracks on the top surface of the treated specimens. The corrosion propagation period was defined as the difference between the time to initiation and the time to cracking. Table 9 through Table 18 present these observed time benchmarks for each of the specimens, grouped by the respective bridge from which they were obtained. Specimens which have not yet initiated corrosion, or not yet cracked, are denoted by "-" in the respective column. The bare steel bridges, numbers 6037 and 6128, are presented in Table 17 and Table 18, respectively, and are preceded by the bridges containing ECR. Specimen names are designated by bridge number, followed by a core-type abbreviation and sample number. The abbreviation "CR" designates cores targeted in the field as containing surface cracks, and "C" represents cores that did not contain cracks.

Chloride Concentrations at Time of Field Sampling and After Cracking

As outlined previously, acid-soluble chloride concentrations were obtained at two elevations of the cores above the section subject to laboratory treatment. After specimens had cracked, chloride concentrations in concrete samples taken directly above and adjacent to the active corrosion sites on the bars were also determined. Table 19 through Table 26 present the chloride concentrations before and after treatment for each specimen in the eight bridges containing ECR. Table 27 and Table 28 provide similar information for the two bridges constructed with bare steel reinforcement. Values for specimens that have not yet cracked are designated by "-". The truncated specimens from the ECR bridges also have reported values of chloride concentration "after cracking", but, of course, these would represent the concentrations at the time that treatment was terminated, since cracking never occurred for these specimens. Truncated specimens are designated by "*" in the tables.

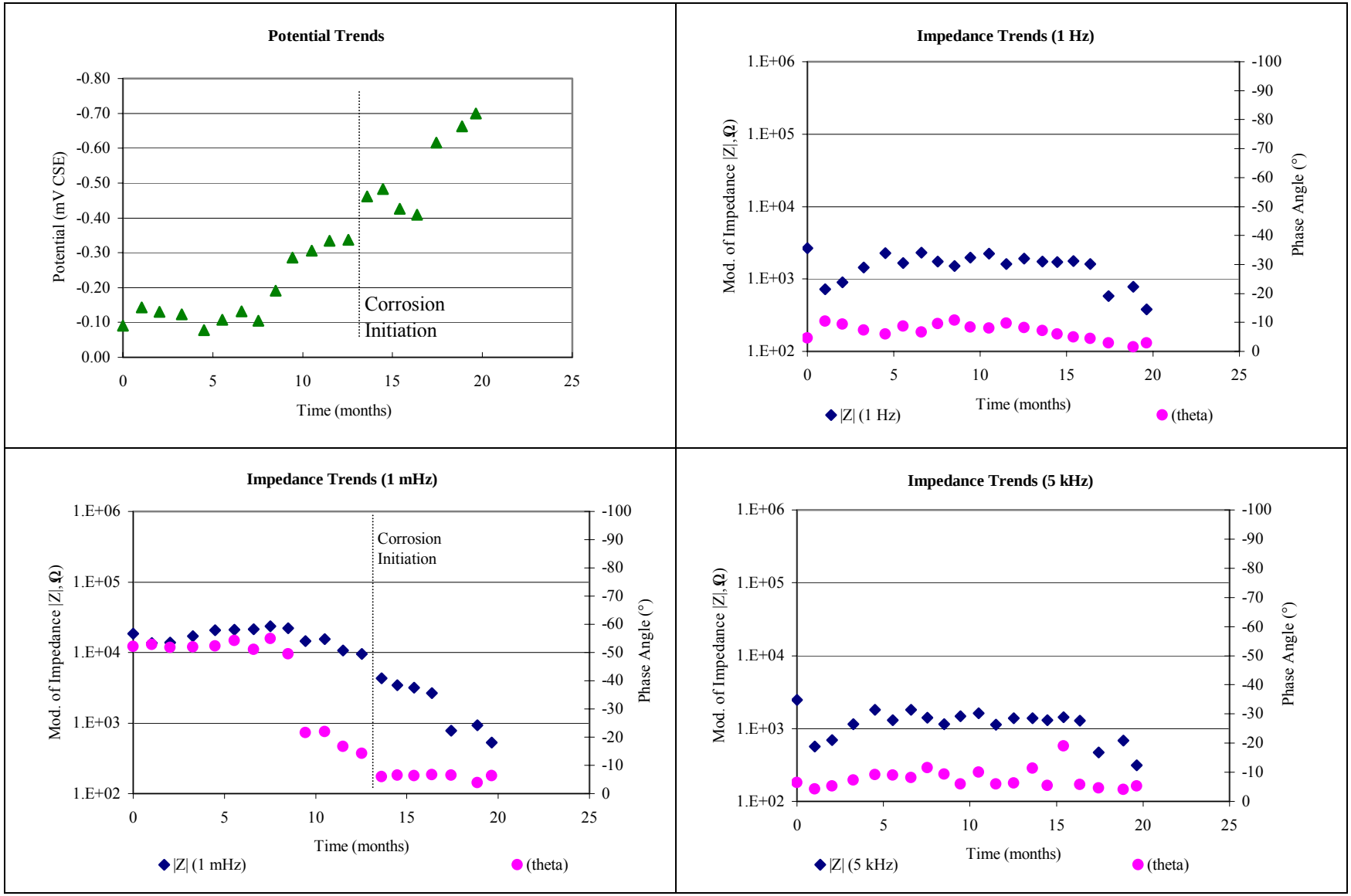

Figure 22 Potential and Impedance Trends for Bare Steel Specimens (typical)

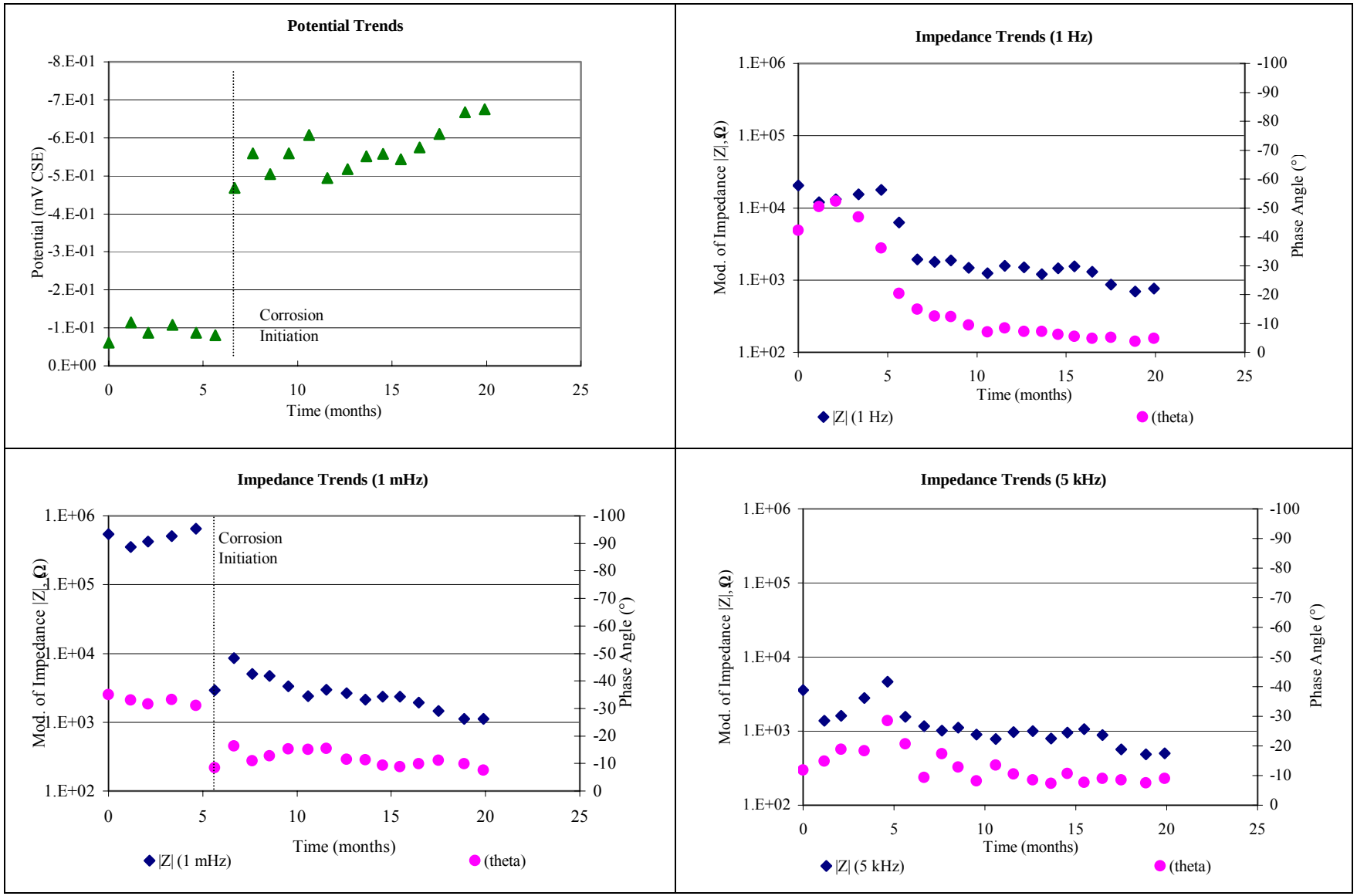

Figure 23 Potential and Impedance Trends for ECR Specimens (typical)

Table 9 Initiation and Cracking Period (to date) – Bridge 1001/ECR

Specimen	Time to Initiation (yrs)	Time to Cracking (yrs)	Propagation time (yrs)
1001_C1	-	-	-
1001_C2	0.90	1.89	0.99
1001_C3	-	-	-
1001_C4	-	-	-
1001_C5	-	-	-
1001_C6	-	-	-
1001_C7	-	-	-
1001_C8	-	-	-
1001_C9	-	-	-
1001_C11	-	-	-
1001_C12	-	-	-
1001_CR1	0.18	-	-
1001_CR2	0.18	-	-
1001_CR3	-	-	-

Table 10 Initiation and Cracking Period (to date) – Bridge 1004_3/ECR

Specimen	Time to Initiation (yrs)	Time to Cracking (yrs)	Propagation time (yrs)
1004_3_C1	0.18	1.93	1.75
1004_3_C2	0.38	-	-
1004_3_C3	0.81	1.93	1.12
1004_3_C4	-	-	-
1004_3_C5	0.81	-	-
1004_3_C6	-	-	-
1004_3_C7	-	-	-
1004_3_C8	-	-	-
1004_3_C9	0.57	-	-
1004_3_C10	0.27	-	-
1004_3_C11	0.18	-	-
1004_3_C12	0.72	1.83	1.11
1004_3_CR2	-	-	-
1004_3_CR3	0.57	-	-

Table 11 Initiation and Cracking Period (to date) – Bridge 1004_6/ECR

Specimen	Time to Initiation (yrs)	Time to Cracking (yrs)	Propagation time (yrs)
1004_6_C1	-	-	-
1004_6_C2	1.57	-	-
1004_6_C3	-	-	-
1004_6_C4	-	-	-
1004_6_C5	-	-	-
1004_6_C6	-	-	-
1004_6_C7	0.09	1.86	1.78
1004_6_C8	-	-	-
1004_6_C10	-	-	-
1004_6_C12	-	-	-
1004_6_CR1	1.74	-	-
1004_6_CR2	0.18	1.02	0.85
1004_6_CR3/C11	0.55	1.02	0.48

Table 12 Initiation and Cracking Period (to date) – Bridge 1015/ECR

Specimen	Time to Initiation (yrs)	Time to Cracking (yrs)	Propagation time (yrs)
1015_C1	1.18	1.85	0.67
1015_C2	1.18	-	-
1015_C3	0.48	-	-
1015_C4	1.30	-	-
1015_C5	0.57	-	-
1015_C6	0.09	-	-
1015_C7	0.10	-	-
1015_C8	0.10	1.91	1.81
1015_C9	0.09	-	-
1015_C10	0.09	1.94	1.85
1015_CR1	0.09	-	-
1015_CR2	0.09	-	-
1015_CR3	0.09	1.85	1.76
1015_CR1B	0.09	-	-

Table 13 Initiation and Cracking Period (to date) – Bridge 1019/ECR

Specimen	Time to Initiation (yrs)	Time to Cracking (yrs)	Propagation time (yrs)
1019_C1	-	-	-
1019_C2	0.95	-	-
1019_C3	-	-	-
1019_C4	0.95	-	-
1019_C5	-	-	-
1019_C6	-	-	-
1019_C7	-	-	-
1019_C8	-	-	-
1019_C9	0.95	-	-
1019_C10	-	-	-
1019_CR1	-	-	-
1019_CR2	0.87	-	-
1019_CR3	0.39	1.08	0.69

Table 14 Initiation and Cracking Period (to date) – Bridge 1136/ECR

Specimen	Time to Initiation (yrs)	Time to Cracking (yrs)	Propagation time (yrs)
1136_C1	-	-	-
1136_C2	-	-	-
1136_C3	-	-	-
1136_C4	-	-	-
1136_C5	1.14	-	-
1136_C6	0.81	-	-
1136_C7	0.10	1.61	1.52
1136_C8	-	-	-
1136_C9	-	-	-
1136_C10	-	-	-
1136_C11	0.10	-	-
1136_C12	0.81	-	-
1136_CR1	0.81	-	-
1136_CR2	-	1.61	1.61
1136_CR3	-	1.61	1.61

Table 15 Initiation and Cracking Period (to date) – Bridge 2021/ECR

Specimen	Time to Initiation (yrs)	Time to Cracking (yrs)	Propagation time (yrs)
2021_C1	0.95	-	-
2021_C2	1.36	-	-
2021_C3	0.95	-	-
2021_C4	-	-	-
2021_C5	0.87	-	-
2021_C6	0.09	1.04	0.96
2021_C7	0.55	-	-
2021_C8	-	-	-
2021_C9	0.55	-	-
2021_C10	-	-	-
2021_C11	0.87	-	-
2021_C12	1.64	-	-
2021_CR1	0.55	1.04	0.50
2021_CR2	-	-	-
2021_CR3	-	-	-

Table 16 Initiation and Cracking Period (to date) – Bridge 2262/ECR

Specimen	Time to Initiation (yrs)	Time to Cracking (yrs)	Propagation time (yrs)
2262_C1	1.05	-	-
2262_C2	1.75	-	-
2262_C3	-	-	-
2262_C4	0.18	1.66	1.48
2262_C5	-	-	-
2262_C6	1.05	-	-
2262_C7	0.80	-	-
2262_C8	0.18	1.66	1.48
2262_C9	1.38	-	-
2262_C10	0.47	1.66	1.19
2262_C11	-	-	-
2262_C12	0.72	-	-
2262_CR1	0.71	-	-
2262_CR2	0.10	1.91	1.81
2262_CR3	-	-	-

Table 17 Initiation and Cracking Period (to date) – Bridge 6037/Bare

Specimen	Time to Initiation (yrs)	Time to Cracking (yrs)	Propagation time (yrs)
6037_C1	0.08	0.67	0.58
6037_C2	0.08	0.67	0.58
6037_C3	0.17	1.45	1.28
6037_C5	0.08	1.72	1.64
6037_C7	0.46	1.43	0.96
6037_C8	0.08	0.67	0.58
6037_C9	0.79	1.70	0.91
6037_C10	0.46	-	-
6037_C11	0.08	0.73	0.64
6037_C12	0.47	1.90	1.43
6037_CR1/C4	0.08	1.72	1.64
6037_CR2/C6	0.08	1.43	1.34

Table 18 Initiation and Cracking Period – Bridge 6128/Bare

Specimen	Time to Initiation (yrs)	Time to Cracking (yrs)	Propagation time (yrs)
6128_C1	0.07	1.44	1.36
6128_C2	0.07	1.05	0.98
6128_C3	0.27	0.96	0.69
6128_C4	0.07	0.96	0.88
6128_C5	0.17	1.28	1.11
6128_C6	0.27	0.68	0.41
6128_C7	0.17	0.94	0.77
6128_C8	0.07	1.44	1.36
6128_C9	0.17	0.87	0.70
6128_C10	0.17	0.94	0.77
6128_C11	0.63	0.87	0.24
6128_C12	0.08	1.44	1.36
6128_CR1	0.07	0.87	0.80
6128_CR2	0.07	0.68	0.61
6128_CR3	0.08	1.00	0.92
6128_CR4	0.08	1.44	1.36

Table 19 Chloride Concentrations – Bridge 1001/ECR

Sample	Before Treatment		After Cracking	
	Cl^- at 12mm below surface (kg/m^3)	Cl^- at 19mm above the bar (kg/m^3)	Ave Cl^- at bar depth (kg/m^3)	Ave. Cl^- above bar (kg/m^3)
1001_C1	1.78	0.00	-	-
1001_C2	2.38	0.00	10.87	9.05
1001_C3	1.99	0.07	-	-
1001_C4	1.84	0.00	-	-
1001_C5	2.06	0.21	-	-
1001_C6	2.74	0.91	-	-
1001_C7	2.81	0.00	-	-
1001_C8	2.81	0.64	-	-
1001_C9	2.21	0.00	-	-
1001_C11	2.29	0.00	-	-
1001_C12	2.35	0.00	-	-
1001_CR1	1.93	1.18	-	-
1001_CR2	2.00	0.75	-	-
1001_CR3	1.83	0.00	-	-

*Specimens were randomly selected and observations were truncated prior to cracking

Table 20 Chloride Concentrations – Bridge 1004_3/ECR

Sample	Before Treatment		After Cracking	
	Cl^- at 12mm below surface (kg/m^3)	Cl^- at 19mm above the bar (kg/m^3)	Ave Cl^- at bar depth (kg/m^3)	Ave. Cl^- above bar (kg/m^3)
1004_3_C1	2.97	1.18	9.60	6.85
1004_3_C2	4.11	0.44	-	-
1004_3_C3	3.71	0.21	9.78	7.21
1004_3_C4	3.52	0.40	-	-
1004_3_C5	4.99	0.90	-	-
1004_3_C6	3.58	0.56	-	-
1004_3_C7	3.87	0.40	-	-
1004_3_C8	4.34	0.22	-	-
1004_3_C9*	3.97	0.70	10.26	6.58
1004_3_C10	3.88	0.44	-	-
1004_3_C11	4.73	1.68	-	-
1004_3_C12	3.66	1.18	8.82	11.45
1004_3_CR2	3.87	0.00	-	-
1004_3_CR3	4.42	0.00	-	-

*Specimens were randomly selected and observations were truncated prior to cracking

Table 21 Chloride Concentrations – Bridge 1004_6/ECR

Sample	Before Treatment		After Cracking	
	Cl^- at 12mm below surface (kg/m^3)	Cl^- at 19mm above the bar (kg/m^3)	Ave Cl^- at bar depth (kg/m^3)	Ave. Cl^- above bar (kg/m^3)
1004_6_C1	0.74	0.00	-	-
1004_6_C2	0.94	0.00	-	-
1004_6_C3*	0.62	0.00	10.36	9.97
1004_6_C4	0.88	0.00	-	-
1004_6_C5	1.06	0.00	-	-
1004_6_C6	0.55	0.00	-	-
1004_6_C7	1.31	0.16	9.52	14.16
1004_6_C8*	0.74	0.00	9.14	13.67
1004_6_C10	0.69	0.00	-	-
1004_6_C12*	0.79	0.00	12.93	13.48
1004_6_CR1	0.79	0.20	-	-
1004_6_CR2	1.23	0.36	6.30	11.30
1004_6_CR3/C11	0.75	0.50	6.38	6.27

*Specimens were randomly selected and observations were truncated prior to cracking

Table 22 Chloride Concentrations – Bridge 1015/ECR

Sample	Before Treatment		After Cracking	
	Cl^- at 12mm below surface (kg/m^3)	Cl^- at 19mm above the bar (kg/m^3)	Ave Cl^- at bar depth (kg/m^3)	Ave. Cl^- above bar (kg/m^3)
1015_C1	3.78	0.54	9.96	16.83
1015_C2	3.05	1.16	-	-
1015_C3	4.92	1.82	-	-
1015_C4*	6.17	3.07	9.50	12.00
1015_C5	5.86	2.98	-	-
1015_C6	4.80	2.90	-	-
1015_C7	5.81	1.17	-	-
1015_C8	5.72	1.86	9.30	14.35
1015_C9*	5.06	2.84	9.84	8.37
1015_C10	4.79	3.49	13.18	12.54
1015_CR1*	4.42	3.67	7.40	9.98
1015_CR2	7.08	0.99	-	-
1015_CR3	4.50	0.48	10.95	15.99
1015_CR1B	2.76	0.41	-	-

*Specimens were randomly selected and observations were truncated prior to cracking

Table 23 Chloride Concentrations – Bridge 1019/ECR

Sample	Before Treatment		After Cracking	
	Cl^- at 12mm below surface (kg/m^3)	Cl^- at 19mm above the bar (kg/m^3)	Ave Cl^- at bar depth (kg/m^3)	Ave. Cl^- above bar (kg/m^3)
1019_C1	1.67	0.10	-	-
1019_C2	2.11	0.02	-	-
1019_C3	1.25	0.01	-	-
1019_C4	2.34	0.07	-	-
1019_C5	1.51	0.07	-	-
1019_C6	2.90	0.24	-	-
1019_C7	1.96	0.17	-	-
1019_C8	2.48	0.45	-	-
1019_C9	2.19	0.29	-	-
1019_C10	2.00	0.28	-	-
1019_CR1	1.26	0.47	-	-
1019_CR2*	1.53	0.76	10.22	12.53
1019_CR3	2.27	0.76	6.71	6.76

*Specimens were randomly selected and observations were truncated prior to cracking

Table 24 Chloride Concentrations – Bridge 1136/ECR

Sample	Before Treatment		After Cracking	
	Cl^- at 12mm below surface (kg/m^3)	Cl^- at 19mm above the bar (kg/m^3)	Ave Cl^- at bar depth (kg/m^3)	Ave. Cl^- above bar (kg/m^3)
1136_C1	4.19	0.03	-	-
1136_C2	6.79	0.08	10.64	2.90
1136_C3	7.17	0.35	-	-
1136_C4	5.81	0.04	-	-
1136_C5	2.85	0.00	-	-
1136_C6	3.62	0.00	-	-
1136_C7	3.25	0.04	7.73	15.92
1136_C8*	4.09	0.00	5.29	16.35
1136_C9	4.62	0.00	-	-
1136_C10	3.78	0.00	-	-
1136_C11*	3.27	0.00	10.99	3.39
1136_C12	4.84	0.00	-	-
1136_CR1	7.29	0.16	-	-
1136_CR2	5.83	0.17	11.32	10.41
1136_CR3	5.41	0.33	7.92	13.17

*Specimens were randomly selected and observations were truncated prior to cracking

Table 25 Chloride Concentrations – Bridge 2021/ECR

Sample	Before Treatment		After Cracking	
	Cl^- at 12mm below surface (kg/m^3)	Cl^- at 19mm above the bar (kg/m^3)	Ave Cl^- at bar depth (kg/m^3)	Ave. Cl^- above bar (kg/m^3)
2021_C1	0.60	0.06	-	-
2021_C2	0.84	0.04	-	-
2021_C3	0.72	0.00	-	-
2021_C4*	0.79	0.08	11.74	13.40
2021_C5	0.60	0.45	-	-
2021_C6	1.09	0.52	6.29	8.83
2021_C7	1.60	0.67	-	-
2021_C8*	0.36	0.02	5.25	6.93
2021_C9	0.76	0.01	-	-
2021_C10	1.03	0.00	-	-
2021_C11	1.23	0.53	-	-
2021_C12	1.22	0.00	-	-
2021_CR1	0.56	0.04	6.33	12.35
2021_CR2*	0.34	0.20	12.18	5.66
2021_CR3	0.60	0.00	-	-

*Specimens were randomly selected and observations were truncated prior to cracking

Table 26 Chloride Concentrations – Bridge 2262/ECR

Sample	Before Treatment		After Cracking	
	Cl^- at 12mm below surface (kg/m^3)	Cl^- at 19mm above the bar (kg/m^3)	Ave Cl^- at bar depth (kg/m^3)	Ave. Cl^- above bar (kg/m^3)
2262_C1	2.61	1.30	-	-
2262_C2*	2.46	1.47	12.36	9.45
2262_C3	2.07	0.60	-	-
2262_C4	2.26	1.01	9.43	8.27
2262_C5	1.91	1.08	-	-
2262_C6	3.63	2.19	-	-
2262_C7*	1.34	0.23	11.61	5.36
2262_C8	1.87	0.91	10.48	9.50
2262_C9	1.46	0.88	-	-
2262_C10	0.67	0.50	9.85	10.17
2262_C11*	1.20	0.07	7.42	8.46
2262_C12	2.33	0.00	-	-
2262_CR1	0.24	3.43	-	-
2262_CR2	0.35	0.39	10.02	6.35
2262_CR3	3.13	0.20	-	-

*Specimens were randomly selected and observations were truncated prior to cracking

Table 27 Chloride Concentrations – Bridge 6037/Bare

Sample	Before Treatment		After Cracking	
	Cl^- at 12mm below surface (kg/m^3)	Cl^- at 19mm above the bar (kg/m^3)	Ave Cl^- at bar depth (kg/m^3)	Ave. Cl^- above bar (kg/m^3)
6037_C1	0.83	-	2.23	12.72
6037_C2	0.74	-	4.88	10.14
6037_C3	0.78	-	7.93	15.27
6037_C5	0.00	-	7.23	10.93
6037_C7	0.14	0.00	7.10	15.67
6037_C8	0.76	0.21	3.42	6.87
6037_C9	0.34	0.14	8.18	14.20
6037_C10	0.16	0.63	-	-
6037_C11	0.78	-	5.69	14.40
6037_C12	0.18	0.06	13.39	18.12
6037_CR1/C4	0.44	0.23	7.76	19.06
6037_CR2/C6	0.34	0.25	9.50	14.96

Table 28 Chloride Concentrations – Bridge 6128/Bare

Sample	Before Treatment		After Cracking	
	Cl^- at 12mm below surface (kg/m^3)	Cl^- at 19mm above the bar (kg/m^3)	Ave Cl^- at bar depth (kg/m^3)	Ave. Cl^- above bar (kg/m^3)
6128_C1	0.15	0.00	12.42	16.01
6128_C2	0.17	0.00	8.42	14.82
6128_C3	0.15	0.00	4.98	8.56
6128_C4	0.25	0.00	7.09	10.95
6128_C5	0.00	0.00	8.09	7.35
6128_C6	0.09	0.02	4.39	13.65
6128_C7	0.08	0.06	6.48	9.54
6128_C8	0.16	0.02	9.04	14.66
6128_C9	0.15	0.02	6.98	11.26
6128_C10	0.12	0.10	7.42	14.32
6128_C11	0.13	0.01	6.38	7.09
6128_C12	0.10	0.05	8.91	10.72
6128_CR1	0.15	0.00	3.91	5.35
6128_CR2	0.11	0.13	6.41	7.60
6128_CR3	0.31	0.20	5.54	6.65
6128_CR4	0.20	0.04	8.03	6.03

ANALYSIS AND DISCUSSION

Crack Frequency and Influence on Durability

Bridge deck cracks other than those associated with constituent material, physical-chemical actions and construction practices manifest themselves as linear cracks. Early-life pattern or map cracks, such as result from plastic shrinkage, do not fall within this category, and may generally be prevented with appropriate attention at the time of construction. Linear cracks may be either transverse or longitudinal relative to the direction of the traffic. Causes of linear cracking include individual or synergistic mechanisms of material subsidence, drying shrinkage, thermal expansion or contraction, and bending conditions. The influence of cracks on corrosion service life is presently controversial (Manning, D. G., 1981; Beeby, A. W., 1978). One viewpoint is that cracks reduce service life and the other is that cracks may accelerate the onset of localized corrosion but have little influence on overall service life of a deck. The difference in viewpoint is related to the width, intensity, and orientation of the cracks (parallel or perpendicular to the reinforcing bar). Cracks parallel and directly above the reinforcing steel have much greater influence than cracks perpendicular to the bar (Beeby, A. W., 1978). With respect to crack width, it has been shown that cracks of width less than 0.3 mm have little influence on corrosion (Atimay, E. & Ferguson, P. M., 1974). However, others have shown that surface crack width has no influence on corrosion (Tremper, B., 1947; Martin, H. & Schiessl, P., 1962; Raphael, M. & Shalon, R., 1971).

The controversy over the influence of crack width on the field performance of structures exposed to chlorides may be related to the environmental exposure conditions. For coastal structures, the reinforced concrete components are continuously exposed to wetting and drying cycles of chloride-laden water. Whereas, for bridge decks in deicing salts environments, the deck is exposed to periodic cycles of chloride-laden water only during the winter months. The remaining months the deck is exposed to periodic wetting and drying cycles of rain and condensates. If chloride ions are carried into cracks during the winter months, they can also be removed during the spring-summer-fall months. This mechanism for reduction of chloride ion concentration has been clearly demonstrated in uncracked bridge deck concrete (Schiessl, P. & Raupach, M., 1997).

Equally controversial is the role of ECR in cracked concrete bridge deck sections. It has been stated that in cracked concrete sections "the reinforcing steel itself is the last line of defense against corrosion, and the use of a barrier system on the reinforcing steel, such as epoxy coating, another organic coatings, or metallic coatings, is more critical" (Smith, J. L. & Virmani, Y. P., 2000). However, no evidence is provided as to how effective ECR is in cracked sections. Others have shown that ECR for corrosion protection was least effective in cracked sections and in relatively high permeable bridge deck concrete (Fanous, F. S. et al., 2000; Weyers, R. E. et al., 1997). It has also been stated that the "use of ECR bars has probably increased the number and width of deck cracks" (Krauss, P. D. & Rogall, E. A., 1996).

Field Crack Frequency

Table 29 presents the crack frequency for the longitudinal and transverse cracks less than and equal to 0.30 mm and greater than 0.30 mm. As shown, the crack frequency was significantly less for the transverse cracks than the longitudinal cracks, 0.283 and 0.049 and 0.049 and 0.003,

respectively for cracks less than and equal to 0.30 mm and greater than 0.30 mm. The crack frequency of the BS decks appears to be less than the crack frequency of the ECR decks. The average crack frequency for the 10 decks in this study was found to be 0.383 linear meters of crack per square meter of deck.

Table 29 Bridge Crack Frequency

Survey Age (years)	Crack Frequency (m/m^2)			
	Crack Width ≤ 0.30 mm		Crack Width > 0.30 mm	
	Longitudinal	Transverse	Longitudinal	Transverse
4	0.201	0.123	0.017	0.014
6	0.394	0.208	0.008	0.000
7	0.301	0.123	0.000	0.004
9	0.475	0.065	0.084	0.003
12	0.072	0.000	0.072	0.000
14	0.735	0.000	0.015	0.000
15*	0.079	0.038	0.044	0.006
16*	0.000	0.000	0.000	0.000
16	0.416	0.000	0.111	0.000
18	0.179	0.000	0.088	0.000
Sample Frequency	0.283	0.049	0.049	0.003

* Designates decks containing bare steel. Remaining decks were constructed with ECR.

Frequency of Cracks ≤ 0.30 mm wide	0.331 m/m^2
Frequency of Cracks > 0.30 mm wide	0.051 m/m^2
Cumulative Sample Crack Frequency	0.383 m/m^2

Crack Width and Depth in Cores

Various forms of regression fit, including linear, polynomial and logarithmic equations, were used to try to describe a relation between crack width and crack depth. Figure 24 presents a second-order polynomial model that best fit the data for core crack depth as a function of core crack width. As shown, there is not a strong correlation between crack width and depth. The correlation coefficient, R^2, was only 0.403. Also, no correlation could be found between crack surface width and age or crack depth and age. Thus, a visible surface crack does not, in most cases, extend to the depth of the reinforcing steel. Also, a wider surface crack does not mean the crack is deeper, and ages greater than 3 years are not a strong factor in crack development.

Chloride Concentration at Cracks and in Uncracked Locations

Average chloride concentration penetrating to depths of about 13 mm below the surface and about 19 mm above the bar depth were measured and plotted as a function of age, as shown in Figure 25 and Figure 26, respectively. However, note that background chloride content of samples of the same concrete mixture typically varies by 0.2 kg/m^3 (Brown, M. C. et al., 2001). Thus, chloride contents in a crack sample would have to be more than 0.2 kg/m^3 greater than the chloride content adjacent to the crack to clearly indicate a significant increase in chloride due to the crack.

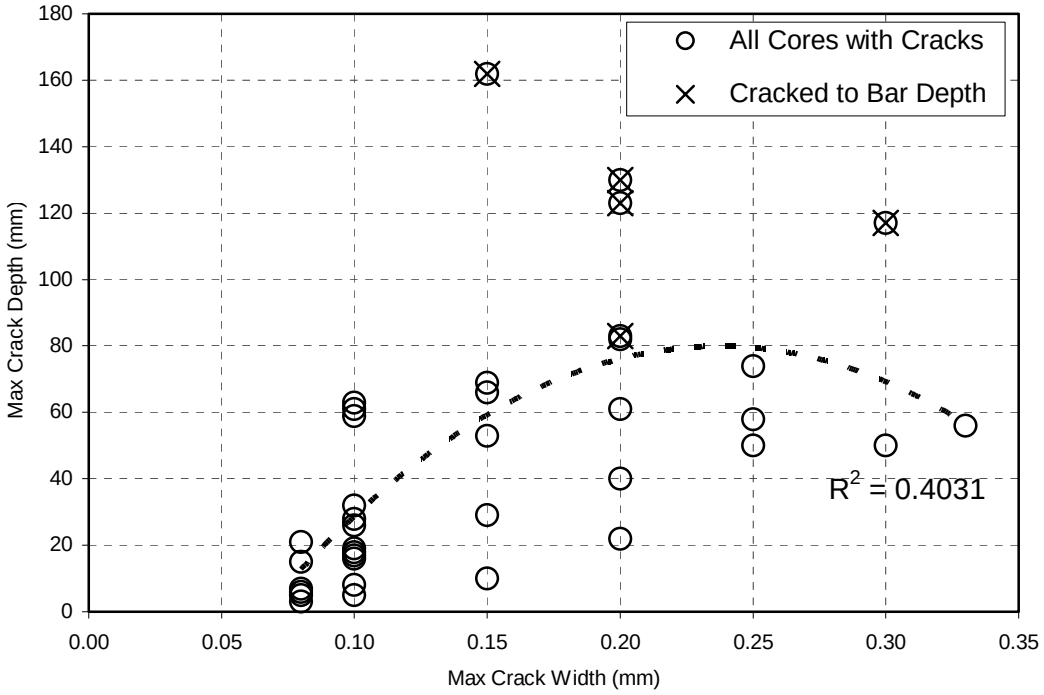

Figure 24. Crack Width and Depth

While investigating the influence of cracks, the relation to surface width of chloride content at 13 mm below the surface and 19 mm above the bar resulted in poor correlation coefficients of $R^2 = 0.18$ and $R^2 = 0.10$ for the best-fit models, respectively. When considering the influence of crack depth, the strongest correlation for chloride concentration at 13 mm below the surface was a polynomial curve, with an $R^2 = 0.20$, still a poor indicator. For the relation of chloride concentration to crack depth at 19 mm above the bar, the best correlation coefficient was only $R^2 = 0.14$. Thus, chloride concentration at cracks could not be predicted by crack width or crack depth.

Figure 25 presents the chloride concentrations at a depth of 13 mm at individual cracks versus the 95% confidence interval of chloride concentrations derived from the sample distributions of cores from uncracked locations on the same decks. Note that the chloride contents are not solely a function of age, but relate to age and route location. Ten chloride contents were within the 95% confidence limits (CL), 8 were less than the 95% lower limit (LL) and 10 were greater than the 95% upper limit (UL). Also, the average increase for those values exceeding the 95% upper confidence limits was small, approximately 18.6%. Considering a similar the number of concentration values that were less than the expected range of uncracked sections, there appears to be no difference between chloride contents at cracks and uncracked sections at a depth of 13 mm, but the variability between individual locations seems to be higher.

Figure 26 presents a comparison between individual chloride contents at cracks and the 95% confidence limits of uncracked core sections at a depth of 19 mm above the bar. Of the 18 chloride contents at 19 mm above the bar at cracks, 7 were within the CL and 11 were above the

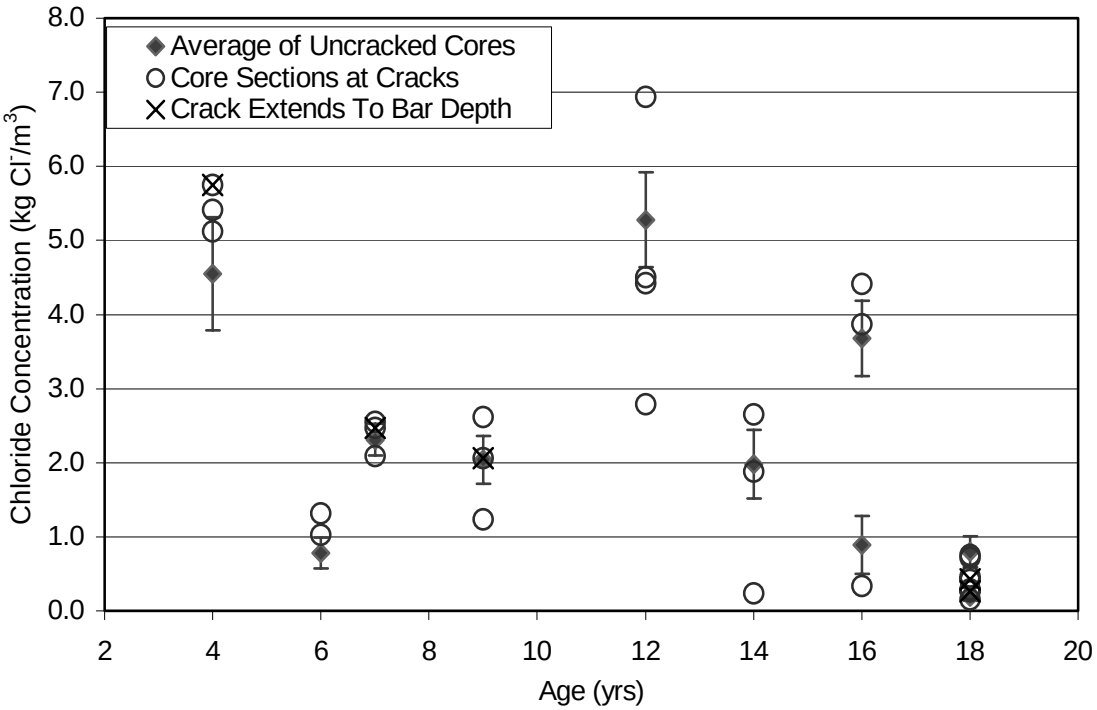

Figure 25 Comparisons of Chloride Concentration at 13mm below Surface

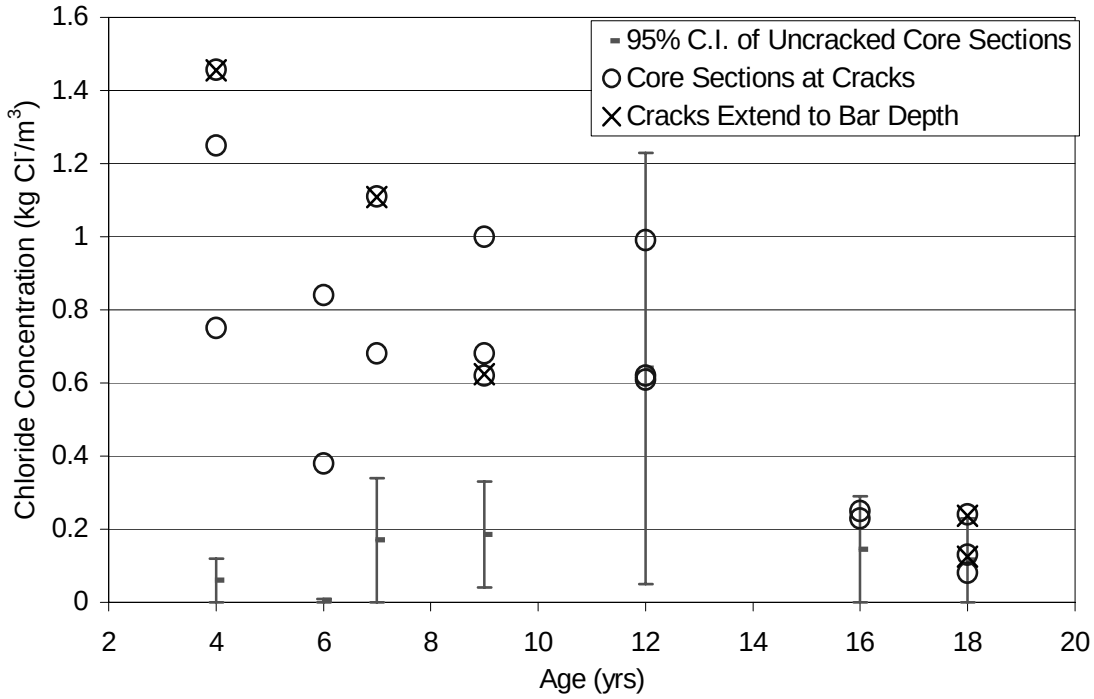

Figure 26 Comparisons of Chloride Concentration at 19mm above the Bar

95% UL. Thus, it appears that cracks influence the chloride content at a depth 19 mm above the reinforcement 61% of the time. In these instances, the average increase in chloride concentration appeared to be about 0.6 kg per cubic meter of concrete beyond the 95% UL. As is clear from Figure 26, all of the instances of increased chloride concentration at this depth were observed in decks less than 10 years of age, whereas decks greater than 10 years of age showed no significant difference in chloride concentration relative to cracks. The lack of influence of cracks on chloride penetration at later ages may be related to autogenous healing and/or carbonation products. Such reactions may result in the accumulation of products that serve to fill the crack and impede chloride ingress.

It is important to consider the overall impact of increased chloride penetration. If increased chloride from a crack centered above and parallel to the reinforcement induces corrosion and spalling, it could be reasoned that the spall-related cracks from that bar radiate to the surface at approximately a 45° angle on either side of the bar. If the average clear cover depth over the bar were 65 mm, as observed in this study, then the tributary width of the spall along the crack would be approximately 130 mm.

Some consider the crack corrosion influence zone to be 3 times the bar diameter or in this case about 100 mm wide (Babaei, K. & Hawkins, N. M., 1988; Lorentz, T. & French, C., 1995). However, this generally pertains to influence along the length of a bar, from a transversely intersecting crack, and does not likely apply to diffusion about a bar into non-fractured cement paste regions.

Nonetheless, as a worst-case, consider for a total crack frequency of 0.383 m/m^2 (Table 29) and a corrosion influence zone 130 mm wide, that all 61 percent of the cracks where the chloride content at the crack is greater than uncracked sections are located in a single span lane. The resulting deck area affected by this cracking is projected to be 3.0 percent. Twelve and one-half percent damage in the worst span-lane is considered the rehabilitation damage level (Fitch, M. G. et al., 1995). Thus, the cracking frequency of the worst span-lane would have to be about 5 times the cracking frequency measured in this study to influence the time to rehabilitation. Further, 2.5% to 3.0% damage may be associated with the level of deterioration at the time of first repair. Therefore, damage induced by linear cracking, may accelerate the onset of the first repair activities, but once addressed, is unlikely to significantly shorten the bridge deck service life.

Accelerated Laboratory Treatment and Monitoring

Laboratory treatment and monitoring were undertaken to assess the relative times to corrosion initiation, times to cracking, and associated chloride concentrations at the reinforcement for both bare steel and ECR. Comparisons were then made to determine what expected service life benefit is attributable to the use of ECR.

Time to Corrosion Initiation and Cracking

Table 30 presents the average time from first application of the ponding treatment required to initiate corrosion, the time until cracking was observed, and the propagation time which passed between those benchmarks. The information is summarized for bare steel and for ECR specimens for which observations are available to date. Note that corrosion has initiated for a

significant number of specimens in the ECR group that have not yet reached cracking. Hence, the average propagation time does not necessarily correspond to the difference between average time to initiation and average time to cracking.

Table 30 Average Times to Initiation and Cracking for Bare Steel and ECR

		Time to Initiation (yrs)	Time to Cracking (yrs)	Propagation time (yrs)
Bare Steel	Average	0.20	1.15	0.96
	StDev	0.19	0.38	0.38
	CoV (%)	98%	34%	40%
	n	28	27	27
ECR	Average	0.62	1.62	1.28
	StDev	0.48	0.35	0.47
	CoV (%)	78%	21%	36%
	n	65	21	21

To visualize the relative rates of corrosion initiation, the cumulative probability of initiation of bare steel versus ECR has been plotted in Figure 27. Note that the number of points for each distribution does not match the total number of observations for each bar type, since some observations occurred at the same age, and therefore overlap. Although the chloride concentrations at bar depth prior to ponding treatment were predicted to be very low for most specimens, more than 50% of the bare steel specimens initiated corrosion within the first two months of treatment. Although the sample size was greater, it took approximately 1.2 years for a corresponding percentage of the ECR bars to initiate corrosion. These observations will be discussed further in the chloride diffusion rates and concentrations sections.

Since the time to corrosion initiation depends upon the arrival of chlorides at the steel surface, and some period of exposure is necessary to depassivate the steel, it was not deemed appropriate to make final judgments based upon a direct comparison of time-to-initiation for the two groups. Variations in diffusion rates and surface concentrations between different decks, comprised of different concrete mixtures, even under the same specification, would significantly impact the initiation of corrosion.

Figure 28 presents the cumulative probability for the time to cracking for the bare steel and the ECR groups. Again, age at cracking was the same for some specimens, resulting in overlapping data points. At this time, approximately 22% of the ECR specimens (excluding the truncated specimens) have cracked, compared to 98% of the bare steel specimens. Comparing the 12^{th} percentile of the groups shows an increase in time to cracking of approximately 1 year for the ECR, as compared to the bare steel, whereas the range is a low of about 0.5 years to 1.2 years at 21%. Time to cracking results for ECR to date are significantly less than in previous laboratory studies that compared bare and new ECR, where the epoxy coating was well bonded to the steel substrate (Clear, K. C., 1992). The plot for ECR in Figure 28 shows an extrapolated line, projecting the future rate of cracking, based on observations to date. Future observations of cracking in the remaining ECR specimens will determine whether this trend continues.

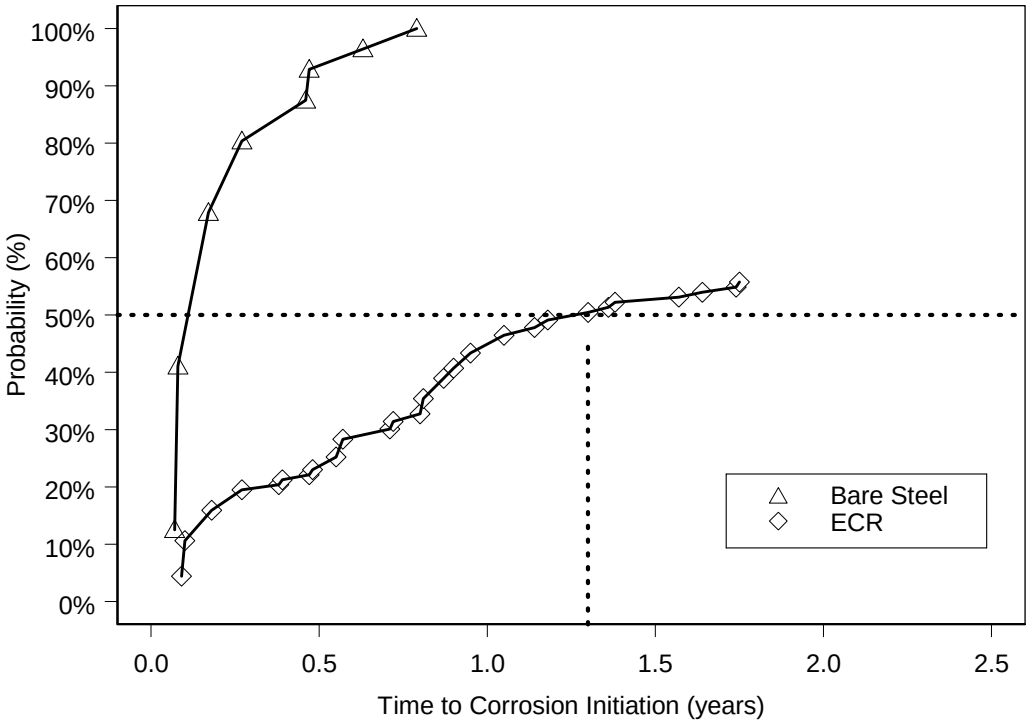

Figure 27 Comparison of Time to Initiation under Laboratory Exposure

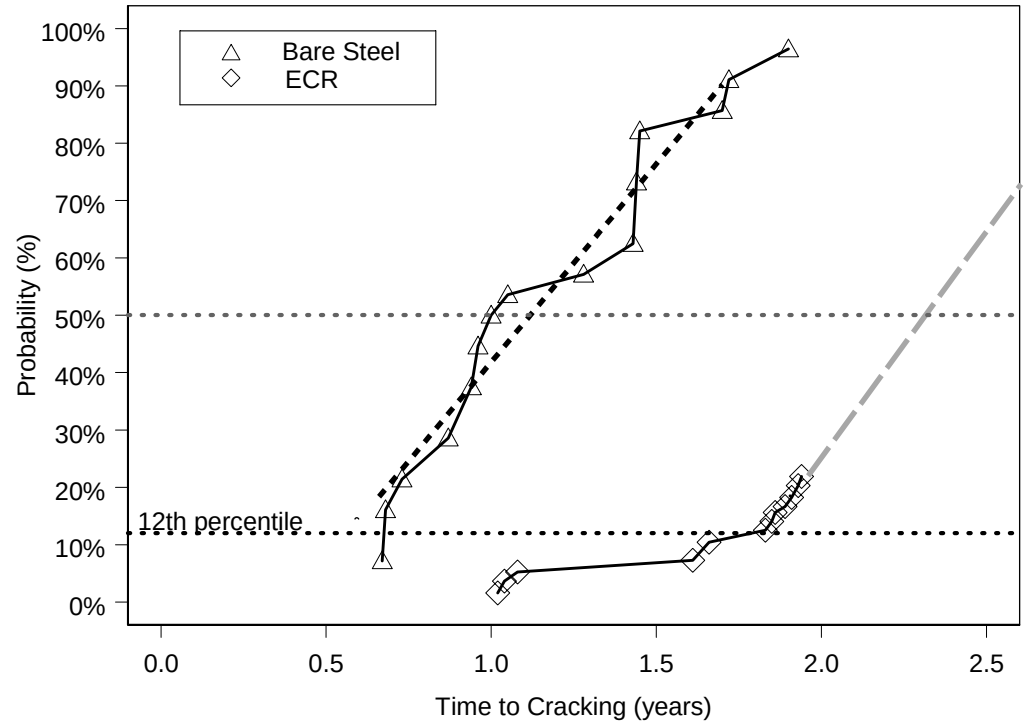

Figure 28 Comparison of Time to Cracking under Laboratory Exposure

Propagation Time

Subtracting the time-to-initiation from time-to-cracking gives the active corrosion propagation time, during which corrosion products accumulate, pressure develops, and finally the cover concrete fractures. The average propagation time for bare steel was 0.96 years in this study, and the average propagation time the ECR specimens cracked to date was 1.29 yrs.

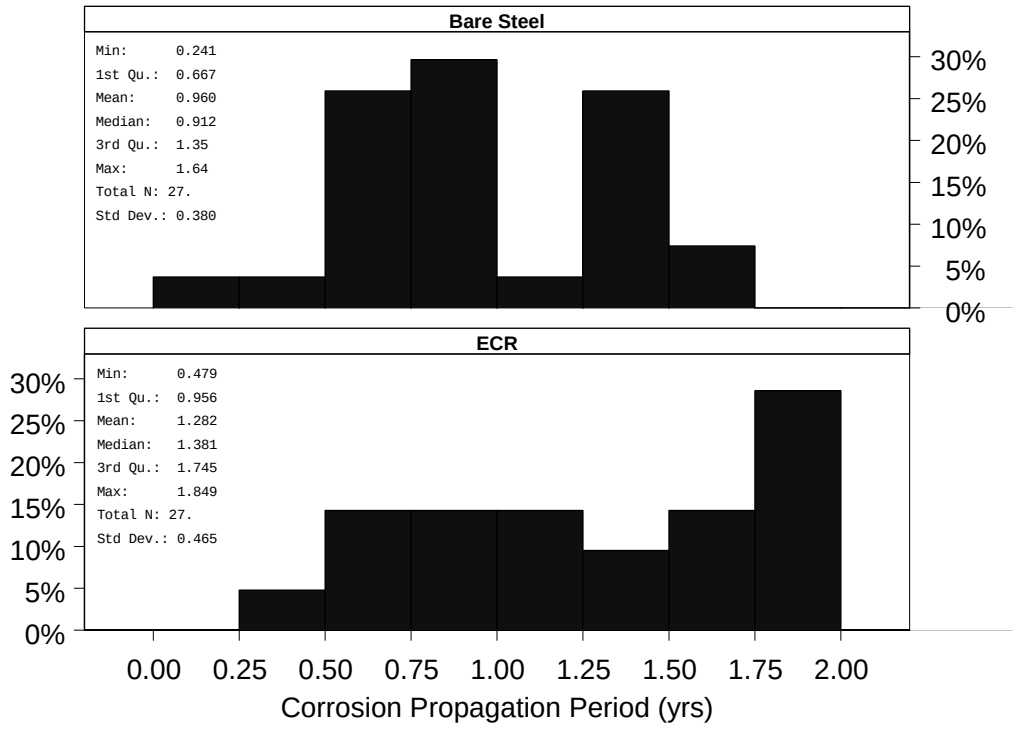

Figure 29 Histograms of Corrosion Propagation Period for BS and ECR

It might be argued that the rate of corrosion could be influenced both by the rate at which chloride concentration increases at the bar, and by the resistivity of the concrete between anode and cathode sites on the steel. Under the accelerated test conditions, it is possible that the corrosion rate in some or all of the specimens is cathodically limited by the availability of oxygen at the cathode(s), which is also a function of the concrete diffusivity and degree of saturation. Since corrosion anode and cathode reactions must be balanced, a "starved" cathode will slow the anodic reaction. However, the mechanism of corrosion underneath a disbonded coating becomes altogether different, and no longer depends upon the diffusion of oxygen to the cathode. The confined electrolyte beneath the coating becomes more acidic, promoting the corrosion reaction.

The specimens in this study were taken from locations directly adjacent to those of a preceding study, usually within 0.5 m, and along the same bar. Thus, the condition of the coating was assumed to be similar at the time of sampling to that of the companion specimens from the previous study. An attempt was made to correlate the observed time-to-cracking with available data that may be used as predictors of performance. The coating parameters considered were holidays, percent surface damage, and thickness, all of which were taken from observations in

the previous study, in which the bars were extracted from the deck and directly observed for various parameters (Pyc, W., 1998). Concrete parameters included the moisture absorption capacity, degree of saturation, effective field diffusion coefficients, and clear cover depth of the original core obtained in this study.

For bare steel, the strongest correlation to time-to-cracking was the degree of saturation of the concrete prior to ponding. A higher initial degree of saturation corresponded to a greater time to cracking. The correlation, however, was very weak ($R^2 = 0.053$), and would be a poor predictor of performance. For ECR, time-to-cracking could be best modeled as a function of the percent of damaged surface area of the coating, as mashes, dents, or scrapes, and the effective rate of diffusion estimated from the core chloride data at 13 mm below the surface and 19 mm above the bar. The correlation coefficient, R^2, was 0.86. Other concrete and coating parameters did not appear to improve the prediction. Although percent damage was a strong predictor, the percent damage to coatings was very low, ranging from none to 2.1%, with a mean of 0.2% among bars that did exhibit damage. The range of holes per bar was 0 to 1, with a mean of 0.04, and coating holidays ranged from 0 to 10, with a mean of 1.9, respectively, for companion specimens of ECR bars cracked to date.

Results from the previous study suggested a relation might be found between the degree of coating disbondment and the time to cracking. The regression analysis considered this possible relation, but did not find a correlation. This is likely due in part to the time that passed, two years, between field sampling in the two studies. During this time, additional adhesion loss between the coating and the steel may have occurred. In addition, the difference in physical locations of the respective specimens, even though they were from the same reinforcement bar and less that 0.5 m apart, could contribute to variability when comparing results from the two studies. Therefore, the lack of correlation of these results does not necessarily indicate that no relation exists between degree of disbondment and time to cracking.

Time to corrosion initiation and cracking were determined for accelerated laboratory exposures. Therefore, further analysis was required to predict corrosion in field structures based on the laboratory observations.

Chloride Concentration at Reinforcement Depth after Cracking

Since direct comparison of initiation and cracking times could not be directly related to field conditions, analysis was conducted on the concentrations of chloride after cracking occurred and estimates of chloride concentration at the reinforcement depth at the time of initiation.

Truncated Observations

As outlined previously, 17 ECR specimens were selected for evaluation prior to cracking to surmise the present status of the ECR specimens that had not yet cracked. Figure 30 shows the histograms of chloride concentration at reinforcement depth for 17 ECR specimens for which observations were truncated, as compared to those that have proceeded to the point of cracking. Based upon impedance measurements, nine specimens were not believed to have initiated corrosion. The absence of corrosion was corroborated by visual observations of the bars after cutting. The nine non-corroded specimens were omitted from further comparisons.

The remaining eight specimens subject to truncation of observations, for which corrosion initiation had been indicated by impedance measurements, were compared to the group of specimens which had already cracked. A two sample t-test indicated no difference in concentration at the 95% confidence level (p-value = 0.2913). Therefore, cracking was considered to have been imminent for the eight truncated specimens that had initiated corrosion and they were incorporated into the ECR group for further comparisons. Although it is possible that more chloride may have accumulated in these specimens prior to cracking, this method of evaluation was deemed to give a conservative estimate of ECR performance, and provided sufficient additional observations to continue the analysis. Any actual differences which may have occurred will likely be observed as additional ECR cores reach the end of treatment.

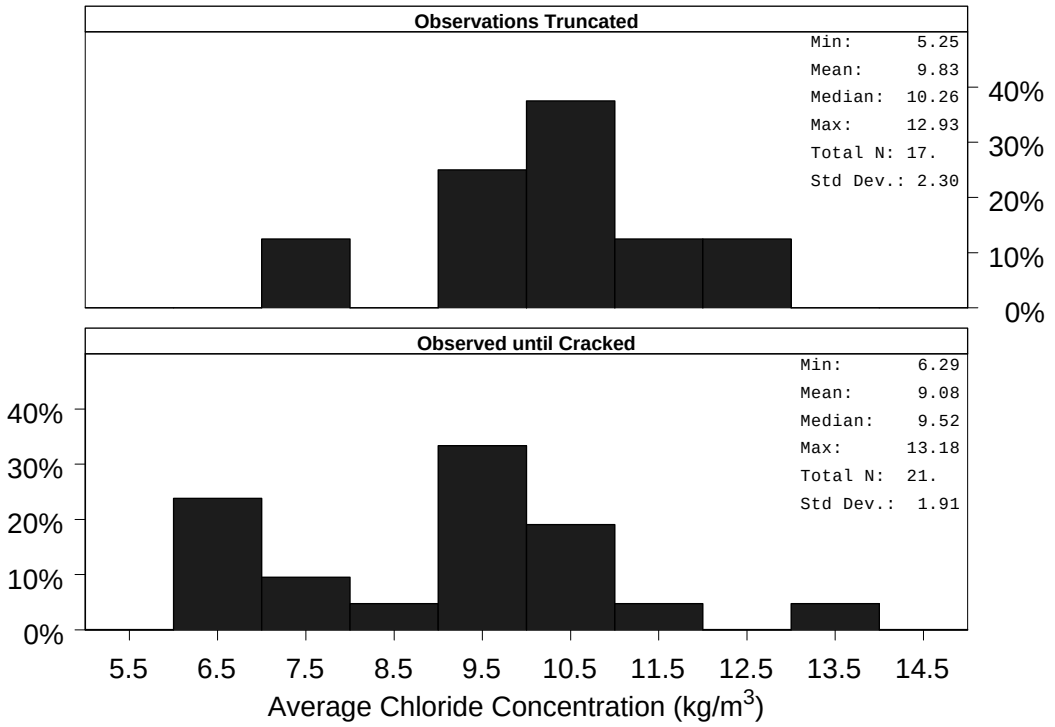

Figure 30 Chloride Concentration at ECR Depth for Truncated Observations and Cracked Specimens

Figure 31 presents histograms of the chloride concentration at the steel depth at the time of cracking, as an average of concentrations measured in concrete immediately to the left and the right of the actively corroding section of the reinforcement. Concentrations were expressed on the basis of weight per unit volume of concrete, assuming a nominal concrete density of 2,323 kg/m^3, and reduced by the nominal background chloride concentration for each bridge to reflect "diffused" chloride. The distributions of chloride concentration for bare steel and ECR were each approximately normal in shape. The average concentration for the two chloride contents at the active corrosion site for bare steel ranged from 2.23 kg/m^3 to 13.39 kg/m^3, with a group average concentration of 7.10 kg/m^3. For ECR, the concentrations ranged from 5.25 to 13.18 kg/m^3, with a group average chloride concentration of 9.41 kg/m^3.

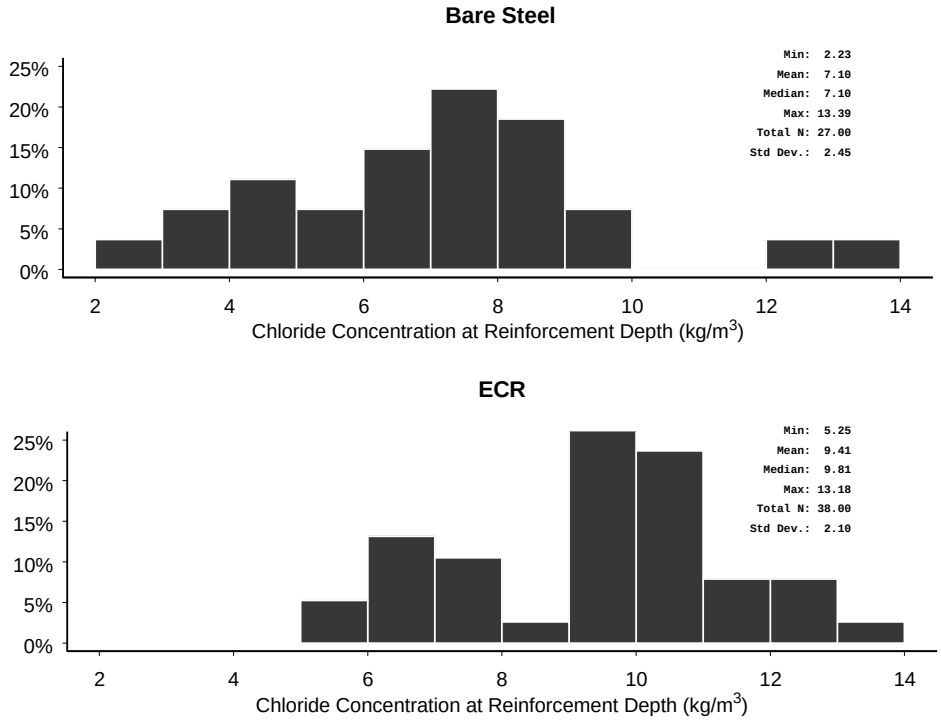

Figure 31 Chloride Concentration at Reinforcement Depth after Cracking

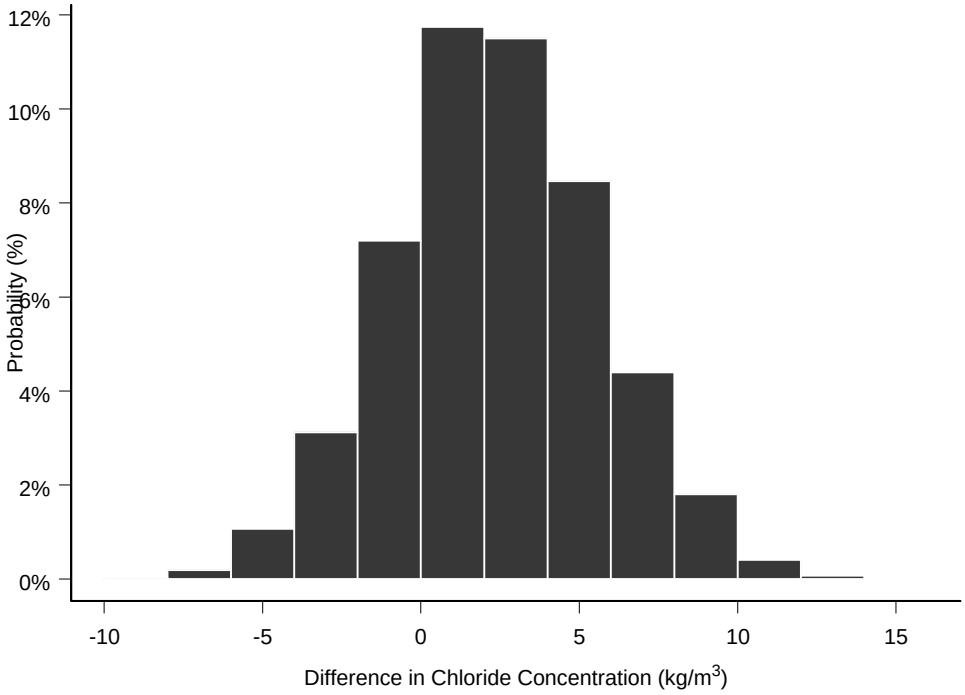

Figure 32 Chloride Concentration Difference: ECR minus Bare Steel (ΔCl^-_{cr}) under Laboratory Treatment

Using a direct sampling method, a quick simulation was run to determine the approximate range and distribution of differences between chloride concentrations after cracking for ECR and bare steel. By selecting at random an observed chloride concentration at the reinforcement depth after cracking for ECR, and subtracting from it an observed chloride concentration after cracking for bare steel, also selected at random, an approximate ΔCl^-_{cr} was determined. Repetition of this operation for 10,000 iterations revealed an approximate distribution for ΔCl^-_{cr}, as shown in Figure 32. Thus, based on the observed laboratory chloride concentrations, ECR required an average of 2.35 kg/m^3 more chloride than bare steel to induce cracking. However, 95% confidence intervals for this estimated ΔCl^-_{cr} ranged from -4.04 to 8.75 kg/m^3. Therefore, there is no guarantee that ECR will outlast bare steel in all cases. Since these values were from accelerated laboratory tests, during which diffusion rates appeared to be an order of magnitude greater than those observed for field concrete, further analysis was warranted.

Estimating Chloride Concentration at Reinforcement Depth at Corrosion Initiation

Using the age of the structures at the time of sampling, initial chloride concentration measurements at 13 mm from the deck surface and at 19 mm above the reinforcing steel, and the measured clear cover depths of the reinforcing bars, the effective diffusion rate of chloride under field exposure was approximated. Next, the computed chloride profile for each core was used to approximate the concentration of diffused chloride at the reinforcing steel depth. Most of the specimens were projected to have chloride concentrations no greater than background levels.

Bar influence

Recent literature has also brought to light the potential for significant influence by the bar on chloride accumulation at the leading face of the reinforcing steel (Kranc, S. C. et al., 2002). The presence of the rebar acts as a local barrier to diffusion within the concrete matrix. The authors stress that the presence of the bar can significantly increase the rate of chloride concentration increase at the leading face of the bar, leading to overestimations of the time to corrosion initiation. The effect becomes more severe as the ratio of bar diameter to clear cover increases, but reaches a limiting value, dependent upon the ratio of surface concentration to the initiation concentration at the bar. However, if chloride concentration is determined from samples obtained directly adjacent to the reinforcement, the authors speculate the resulting effective diffusion rate may inherently address the effect of the rebar as a barrier. A derating factor was proposed, dependent upon ratios of bar diameter to clear cover, and surface concentration to threshold initiation concentration.

In this study, effective diffusion rates were determined at two stages, first from the cover concrete of the original core, prior to treatment, and then from the treated sample, after cracking. In the former case, the ratio of bar diameter to clear cover depth was approximately 0.25. If these values were used to directly project time-to-initiation, the associated derating factor would be between 0.7 and 0.8, dependent upon the chloride ratios identified. In the case of the treatment diffusion, the ratio of bar diameter to clear cover was nearly 1, implying a significant effect of the rebar on diffusion. However, chloride concentrations for this case were determined immediately adjacent to the steel, and the increased rate of chloride accumulation at the bar is assumed to be inherently addressed within the apparent diffusion coefficient. Since the clear

cover and nominal bar diameter, and chloride treatment was approximately the same for all specimens, any actual influence should not greatly affect direct comparisons of the study groups.

Capillarity

For the treatment phase of this study, it is noted that the cores were at a relatively low saturation level when ponding initiated. Capillary action is expected to have had a significant influence on chloride uptake during the initial ponding. However, once saturated, the specimens were likely to have reverted to behavior more closely resembling diffusion-controlled chloride migration.

Therefore, the ingress of chloride through the concrete cover to the reinforcing steel depth during the cyclic ponding treatment was also modeled using the same one-dimensional solution to Fick's Second Law of Diffusion. After cracking and chloride evaluation at and above bar depth of the treatment cores, the rate of diffusion and approximate driving chloride concentration were calculated, where possible. The resulting pseudo-diffusion coefficients were generally an order of magnitude greater than the effective diffusion coefficients calculated for field exposures, and C_o concentrations were generally between 10 kg/m^3 and 20 kg/m^3.

To better understand the potential distribution of chloride within the pore system, it was useful to know whether it is possible for such concentrations to be contained entirely within the pore solution, or if some level of chloride binding or other physical phenomena was required. The authors investigated the saturation limit of chloride in a simulated concrete pore solution (Diamond, S., 1981). The saturation concentration of NaCl in pure water is approximately 360 g/L. The average of three simple laboratory trials revealed a saturation concentration of NaCl in simulated pore solution of approximately 339 g/L, or 15.2% Cl^-. The average absorption of concrete in this study was 5.76 percent by weight. For normal weight concrete (2322 kg/m^3), the pore solution could then be estimated to account for 130 kg/m^3. The resulting saturation concentration of Cl^- in concrete pore solution is estimated to be 20 kg/m^3 (33 lb/yd^3). Thus, the chloride represented in the observed C_O concentrations could be contained entirely within the pore solution under saturated condition.

Using the pseudo-diffusion rates and surface chloride concentrations, in conjunction with the observed propagation period, the amount of chloride that would have diffused during active corrosion was calculated, again using a one-dimensional solution of Fick's Second Law of Diffusion. Subtracting the estimate of chloride diffused during active corrosion from the total chloride present after cracking resulted in an approximation of the chloride present at bar depth at the time of corrosion initiation.

Figure 33 compares histograms of the estimated chloride at initiation for ECR and bare steel in cores that have cracked to date. The estimated chloride initiation level for bare steel ranged from 0.39 kg/m^3 to 9.08 kg/m^3, with an average of 2.79 kg/m^3 and standard deviation of 2.32 kg/m^3. These values are in reasonable agreement with other reports of chloride initiation under field exposure, which ranged from 0.59 to 8.75 kg/m^3 (Glass, G. K. & Buenfeld, N. R., 1997; Stratfull, R. F. et al., 1975; Vassie, P., 1984; Matsushima, M. et al., 1998).

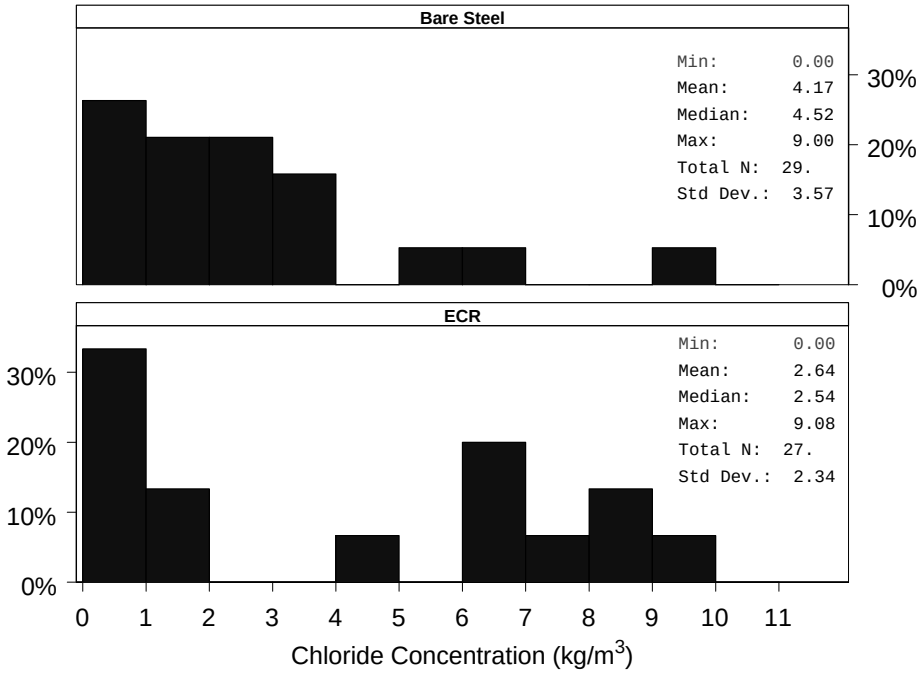

Figure 33 Estimate of Chloride Concentration at Reinforcement Depth at Corrosion Initiation

The estimated initiation range for ECR was broader, and appears to be bimodal. The range was from 0.08 kg/m^3 to 9.00 kg/m^3, with an average of 4.14 kg/m^3. However, it might be considered that the set represents two distinct groups. The group of lower initiation concentration values appears to range from 0.08 to 1.78 kg/m^3, with an average of 0.79 kg/m^3. The higher initiation concentrations range from 4.5 to 9.0 kg/m^3, with an average concentration of 7.2 kg/m^3.

The cause(s) and significance of the two groups of chloride initiation concentrations were investigated by considering the direct and interactive relationships of chloride concentrations to various coating and concrete parameters. As with the time-to-cracking correlations, the coating parameters considered were holidays, percent surface damage, and thickness, all of which were taken from observations in the previous phase of study, in which the bars were extracted from the deck and directly observed for various parameters (Pyc, W., 1998). Concrete parameters included the moisture absorption capacity, degree of saturation, effective field diffusion coefficients, and clear cover depth of the original core.

The strongest correlation between bar and concrete parameters and the estimated chloride initiation concentration was the concrete saturation level prior to ponding ($R^2 = 56$). However, this observation is of limited use, as it is based upon only 7 observations for which both chloride initiation estimates and companion core coating and concrete data were available. What is of interest is that the percent damage to the coating or number of holidays could not be correlated within this small subset of cores, as it was with the time-to-cracking. Even so, the percent damage for the observed cores was low, ranging from none to 2.1% in one case. The average of percent damage was only 0.2%. The number of holidays was also low, ranging from 0 to 10, with an average of less than 2. These observations are generally within the ranges applicable at the time of construction, as well as current specifications (ASTM, 2001).

Probabilistic Model

Recently, it has been recognized that deterioration of field structures can be better estimated by stochastic modeling based on samples obtained from individual structures or a system of structures, rather than by deterministic models using fixed input values. One such model employs a solution to Fick's Second Law of Diffusion, for one-dimensional diffusion into a semi-infinite slab, to describe the ingress of chloride and the initiation of corrosion for bare steel in concrete bridge decks (Kirkpatrick, T. J. et al., 2001b). The four variables, driving surface concentration, C_o, effective diffusion coefficient, D_c, clear cover depth, x, and the chloride concentration at the bar depth necessary to initiate corrosion, $C_{(x,t),}$ can be represented as distributions, rather than single values for a given structure or system of structures. The distributions can be selected by fitting to measured values obtained from field testing. Using a statistical re-sampling technique referred to as bootstrap methods, the distribution of each input variable can be implemented into the physical model. Repeated sampling at random from each of the input distributions and calculation of the physical model using these selected inputs results in a distribution for the output value, in this case time to corrosion initiation.

Two specific methods can be used for the selection of input values from the respective distributions. The first, known as the parametric bootstrap method, relies upon proper selection of the probability distribution function that best describes the measured parameter. For the diffusion model, the clear cover depth has been shown previously to conform to a normal distribution, whereas the surface concentration and effective diffusion coefficients appear to conform to gamma distributions. The distribution of the chloride initiation concentration is still uncertain.

The second method of input selection, referred to as a simple bootstrap, circumvents the uncertainties associated with assuming a distribution function. It simply involves direct sampling, at random, from the available measured data for the system in question. The obvious limitation is the number of measurements available for sampling for each input parameter. However, the method has proven successful in predicting life expectancy of bridge decks subject to chloride-induced corrosion, and has been validated against historic bridge performance data in Virginia (Kirkpatrick, T. J. et al., 2001a).

The referenced study, in which the stochastic modeling technique was developed, used field data from individual bridge decks to predict the service life of each deck. In this study, we will consider the distribution of parameters as representative of Virginia's bridge decks as a system of bridge components. Since the study includes structures from interstate, primary, secondary and rural routes, as well as a variety of geographic locations, it is representative of geography and route types of the system of bridges in Virginia (Kirkpatrick, T. J. et al., 2001b). The purpose will be to compare the time to initiation for bare steel and ECR decks, as a system.

Simulation Input Data

The clear cover depths, x, measured in the field were compiled for all 21 bridges surveyed in the phase II study (Pyc, W., 1998), as well as the 3 bridge decks observed in the phase I study (Zemajtis, J. et al., 1997). The eight ECR decks of this phase were a subset of phase II. However, the bare steel decks were unique to this study, and the clear cover depths for those two decks were also incorporated, for a total of 26 decks comprising 2478 observations ranging from

41 mm to 116 mm. Previous research funded by the Strategic Highway Research Program established a consensus among bridge officials around the country that the level of damage necessitating rehabilitation of a bridge deck is the delamination and spalling, including asphalt patches, of approximately 12% of the surface area of the worst span-lane of a bridge (Fitch, M. G. et al., 1995). Thus, for the system in question, it was determined that the deterioration time should consider the shallowest 12% of cover depths for each of the bridges. Once these first 12% of the bars reach corrosion initiation and propagation, then the deck would be considered to require rehabilitation. Therefore, the distribution of cover depths used in the stochastic models included all measurements less than or equal to the 12^{th} percentile depth for each deck, for a total of 140 observations, which range from 46 mm to 66 mm.

The driving chloride surface concentrations were obtained from acid-soluble chloride concentrations determined from core and powder samples at a depth range of 6 to 19 mm from the surface of the concrete. Previous research has established that chloride concentrations above this elevation are highly variable and fluctuate with time, in regions of deicing salt application. Variations may be due to the effects of wet and dry precipitation cycles, chloride application during the winter season, and chloride leaching during alternate seasons. However, at an elevation of approximately 13 mm below the surface, the driving chloride concentration reaches a maximum, and becomes relatively stable over time (Cady, P. D. & Weyers, R. E., 1983). Thirty-six values were obtained from three bridges in the phase I study, 202 observations gathered from 21 bridges in the phase II study, and 139 observations from the cores in this study, for a total of 377 observations from 26 bridge decks with a range of 0.08 kg/m^3 to 10.46 kg/m^3.

As discussed previously, effective diffusion coefficients, D_c, were calculated using the one-dimensional solution of Fick's Second Law of Diffusion. Thirty-five values were obtained from powdered concrete chloride profiles obtained in three bridge decks during the phase I study (Weyers, R. E. et al., 1997). In addition, 31 diffusion coefficients were estimated from the powdered concrete chloride profiles of the 10 bridge decks in this study. Finally, 131 effective diffusion coefficients were estimated for cores obtained in this study, based upon the chloride concentrations measured at 13 mm from a top surface in 19 mm above the bar. Approximately four of the latter values, which exceeded 500 mm^2/yr, were discarded as outliers. The total number of diffusion coefficients employed was 197, from 13 bridge decks. The diffusion coefficients ranged from 10 mm^2/yr to 417 mm^2/yr.

The final parameter for the diffusion model, and by far the most controversial and least understood, is the chloride concentration necessary to initiate corrosion. For modeling, values presented in the earlier section on Estimating Chloride at Bar at Initiation were employed. Separate groups of values were developed for bare steel bars and ECR bars. Approximately 17 values representing bare steel and 11 values representing ECR were used to describe the initiation concentration. As previously stated, these results are in agreement with other field studies of structures containing bare bar (Glass, G. K. & Buenfeld, N. R., 1997).

Estimating Service Life from Chloride Concentration at Corrosion Initiation

Using the probabilistic technique presented by Kirkpatrick with the simulation data outlined above, the service life probability distribution was projected. Note that, since the 12^{th} percentile cover depths were used, the output prediction would be the time to reach rehabilitation (defined

as corrosion of 12 percent of the system surface area). The C_o values are indicative of environmental exposures in Virginia, and the D_c parameters are functions primarily of the concrete properties, as well as the age and degree of saturation of the concrete. The $C_{(x,t)}$ used to represent corrosion initiation would be primarily a function of the quality and condition of the coating, where present, the maturity of the passive layer on the steel, and the local environment within the concrete, which affects pH, resistivity, and potential gradients.

For bare steel, all of the input properties appeared to be consistent with previously documented conditions in Virginia bridge decks. Using the simulation, the resulting cumulative distribution of time to corrosion initiation was projected, as shown in Figure 34. The findings indicate that over 50% of Virginia bridge decks constructed with bare steel under specifications in place over the last 20 years are never expected to initiate corrosion, no matter what age they reach. In addition, less than 25% of the decks are projected to initiate corrosion over sufficient area to necessitate rehabilitation within 100 years of construction. Only about 12% of the decks would begin sufficient corrosion to necessitate rehabilitation within the first 34 years. Further, this projection does not consider the propagation period associate with corrosion deterioration, which has been estimated at approximately 3 to 7 years for bare steel decks under continuous corrosion (Weyers, R. E. et al., 1993).

Extending our simulation to ECR, we observed projected time to corrosion on the same order of magnitude. In this case, over 60% of the reinforcement was found to never be susceptible to corrosion, and only about 21% were expected to corrode within 100 years. Although the average initiation concentration for the ECR was found to be greater, the distribution was also more variable, and those values which are associated with the early deterioration corresponded closely to bare steel. For ECR, the first 12% is expected to initiate within 30 years of construction, which is of the same order as that projected for bare steel.

The fact that time to initiation for some ECR bars is no different than for bare steel should not come as a surprise. It has been clearly established that placement of a perfectly intact coating, without damage or holidays, is impractical (Clear, K. C. et al., 1995). Any bare bar surface at a breach in the coating would be expected to corrode as easily as uncoated steel.

Estimating Service Life from Chloride Concentration after Cracking

A similar projection was conducted using the chloride contents observed at the time of cracking, rather than at initiation, recognizing that chloride will continue to diffuse into the concrete after corrosion has initiated. Figure 36 and Figure 37 show the projected cumulative probability curves for the first 100 years of service of the population of Virginia bridge decks, based upon chloride measured after cracking in the laboratory specimens. For both bare steel and ECR, the calculation predicted that less than 1 percent of the deck areas in Virginia would reach rehabilitation. This prediction is not at all consistent with experience, and can easily be explained by the accelerated rate of diffusion under laboratory conditions during the test, which allowed chloride to accumulate at the bar during the propagation period much more quickly than would occur in the field. Therefore, projections of service life based directly upon chloride content after cracking were not useful. Thus, the question remained of how to assess the corrosion propagation period for ECR.

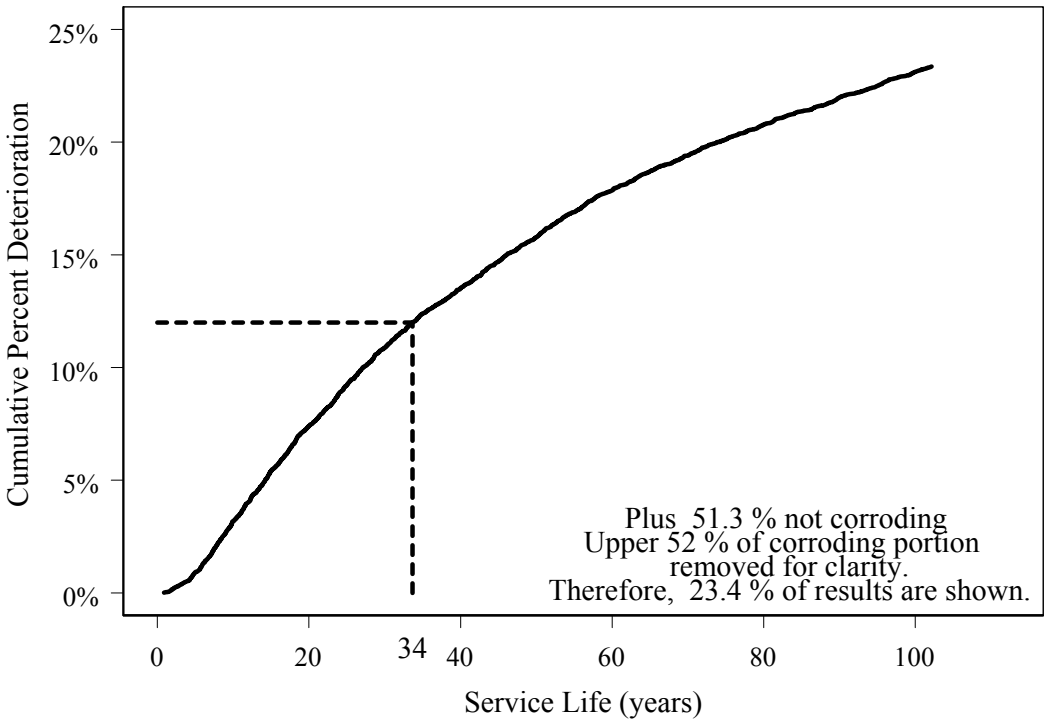

Figure 34 Cumulative Time to Corrosion Initiation for Bare Steel

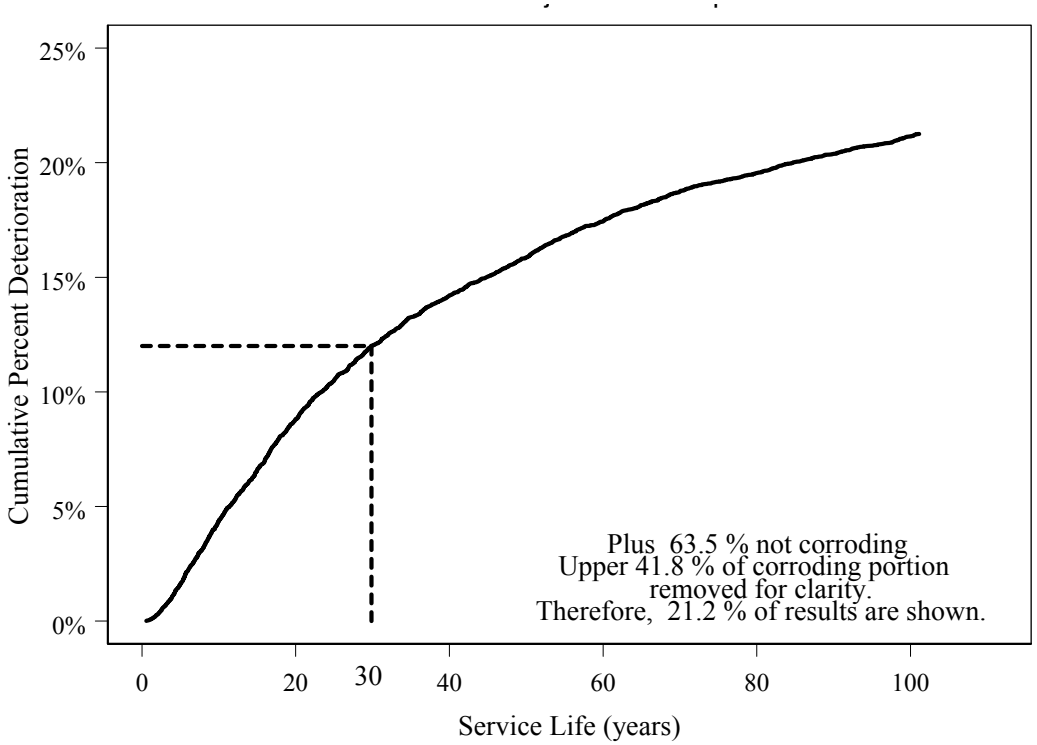

Figure 35 Cumulative Time to Corrosion Initiation for ECR

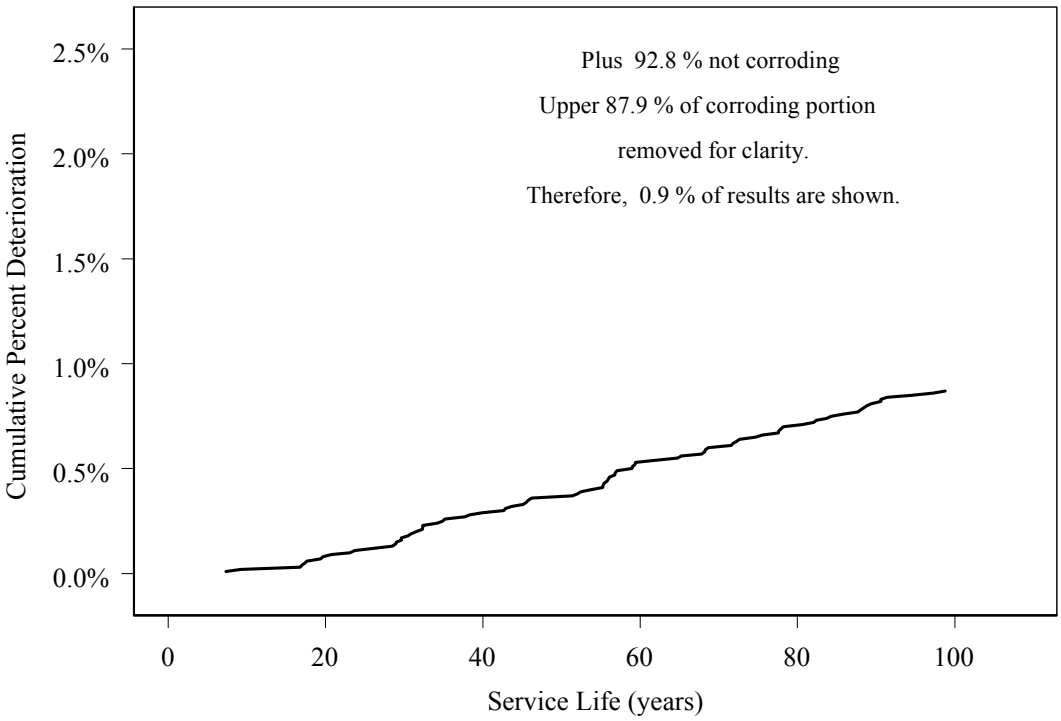

Figure 36 Cumulative Time to Cracking for Bare Steel

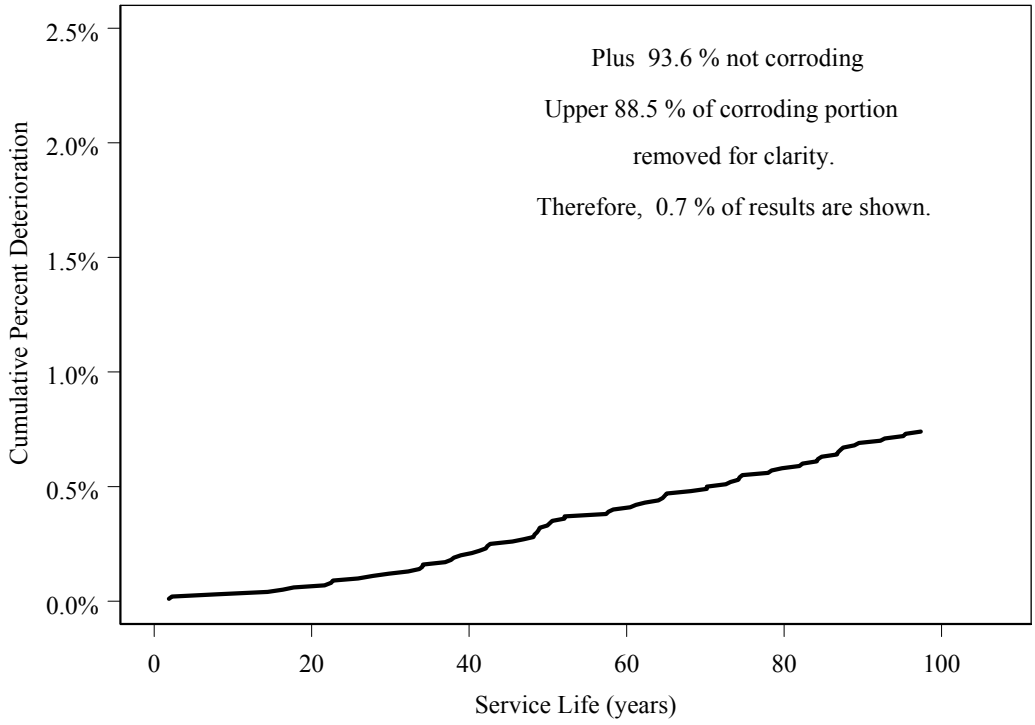

Figure 37 Cumulative Time to Cracking for ECR

Determining Corrosion Rate Ratios of ECR/Bare Steel

Sagüés and others investigated the critical amount of corrosion product necessary to induce cracking, and its relation to the degree of localization of the corrosion anode, where iron-oxide compounds accumulate (Torres-Acosta, A. A., 1999; Sagues, A. A. et al., 2001). Under the study conditions, the average steel depth lost to corrosion, at the time of cracking, x_{crit}, could be approximated as follows:

$$x_{crit}(mm) \sim 0.011\left(\frac{x_c}{\Phi}\right)\left(\frac{x_c}{L}+1\right)^{1.8}$$

Equation 32

where x_c = clear cover depth (mm)
Φ = bar diameter (mm)
L = length of the corroded anode site (mm)
with limits: $(1 \lesssim x_c/\Phi \lesssim 7)$ and $(0 \lesssim x_c/L \lesssim 3)$

After cracking, bare steel specimens corroded, on average, along approximately 25% of their length, or about 25mm. ECR specimens had corrosion products in 80% of the locations where coating was removed for observation, which translates to an average corrosion length of ~80mm. Using data from the current study, x_{crit} was determined for two cases, the first bare steel and the second ECR, using parameters x_c = 13mm (0.5 in.), Φ = 16mm (#5), and L = 25mm (1 in.) and 80 mm (3.1 in.), respectively, as follows:

$$\text{Bare: } x_{crit} = 0.011\left(\frac{13}{16}\right)\left(\frac{13}{25}+1\right)^{1.8} = 0.019 \text{ mm}$$

$$\text{ECR: } x_{crit} = 0.011\left(\frac{13}{16}\right)\left(\frac{13}{80}+1\right)^{1.8} = 0.012 \text{ mm}$$

Assuming corrosion rate, *C.R.*, is constant with time, Sagüés reasoned that the propagation period, t_p, could be determined by:

$$t_p = C.R./x_{crit}$$

Equation 33

Using the assumption of constant corrosion rate with time, a proportional comparison of the propagation times during treatment and the calculated x_{crit} for ECR and bare steel resulted in the following estimated relation between corrosion rates of ECR and of bare steel:

$$\frac{t_{p(ECR)}}{t_{p(BARE)}} = \frac{\left(\frac{CR_{(ECR)}}{x_{crit\,(ECR)}}\right)}{\left(\frac{CR_{(BARE)}}{x_{crit\,(BARE)}}\right)} = \frac{CR_{(ECR)} \times x_{crit(BARE)}}{CR_{(BARE)} \times x_{crit(ECR)}}$$

Equation 34

$$\frac{CR_{(ECR)}}{CR_{(BARE)}} = \left(\frac{x_{crit(ECR)}}{x_{crit(BARE)}}\right)\left(\frac{t_{p(ECR)}}{t_{p(BARE)}}\right)$$

Thus, substituting experimental values for x_{crit} and t_p revealed the following average proportional rate of corrosion for ECR relative to bare steel:

$$\frac{CR_{(ECR)}}{CR_{(BARE)}} = \left(\frac{0.012}{0.019}\right)\left(\frac{1.28}{0.96}\right) = (0.63)(1.33) = 0.84$$

The corrosion rate ratio of ECR to bare steel at the 2.5 percentile level of laboratory propagation times is as follows:

Given $t_{p(ECR)} = 0.49$; $t_{p(BARE)} = 0.35$ at the 2.5 percentile of propagation times:

$$\frac{C.R._{(ECR)}}{C.R._{(BARE)}} = \frac{t_{(ECR)}}{t_{(BARE)}} \times \frac{x_{crit(ECR)}}{x_{crit(BARE)}} = \left(\frac{0.49}{0.35}\right)\left(\frac{0.012}{0.019}\right) = 0.88$$

Table 31 presents the respective corrosion rate ratios for ECR versus bare steel at selected percentiles of propagation times from the laboratory observations. The average ratio of ECR to bare steel corrosion rates was 0.78, with a standard deviation of 0.093, or coefficient of variation of 12%. Thus, the ratio of corrosion rates has not varied greatly over a range of propagation times.

Table 31 Percentiles of Propagation Times (ECR vs. Bare)

Percentile Propagation Time (%)	Propagation, $t_{p(ECR)}$ (years)	Propagation, $t_{p(BARE)}$ (years)	$t_{p(ECR)} - t_{p(BARE)}$ (years)	Corrosion Rate Ratio $C.R._{(ECR)}/C.R._{(Bare)}$
2.5	0.49	0.35	0.14	0.88
5.0	0.50	0.46	0.04	0.68
10.0	0.67	0.58	0.09	0.73
12.0	0.68	0.58	0.10	0.73
20.0	0.85	0.61	0.24	0.88
			Average:	0.78

Influence of Cover Depth on Laboratory Propagation Time

Sagüés' relation indicates that the degree of corrosion necessary to induce cracking is a function of clear cover depth. Liu performed a study of reinforcing steel in large scale slab specimens subject to various chloride levels, and also determined that cracking was in part a function of clear cover (Liu, Y. & Weyers, R. E., 1998). To project the corrosion propagation period for ECR in a field structure, it is necessary to convert the observed laboratory corrosion rate relationship to account for the greater cover depths in field structures.

The average cover depth in Virginia bridge decks is 65mm, with a standard deviation of 8.9 mm. Thus, the shallowest 2.5 percentile of cover depths are estimated to be less than or equal to 47 mm. The critical penetration depth, x_{crit}, at x_c = 47mm could be estimated for ECR and bare steel as follows:

$$\text{ECR: } x_{crit} = 0.011\left(\frac{47}{16}\right)\left(\frac{47}{80}+1\right)^{1.8} = 0.074 \text{ mm}$$

$$\text{Bare: } x_{crit} = 0.011\left(\frac{47}{16}\right)\left(\frac{47}{25}+1\right)^{1.8} = 0.217 \text{ mm}$$

Results of similar calculations at selected cover depth percentiles are presented in Table 32.

Table 32 Critical Depth of Penetration for ECR vs. Bare Steel

Percentile of Field Cover Depth (%)	Cover Depth (mm)	$x_{crit(ECR)}$ (mm)	$x_{crit(BARE)}$ (mm)
2.5	47	0.074	0.217
5.0	50	0.082	0.248
10.0	54	0.094	0.294
12.0	55	0.097	0.307
20.0	57	0.103	0.332

Correlation to Field Results

Since the corrosion rate ratios and the corrosion product necessary to induce cracking are based upon accelerated corrosion rates, it is useful to make a comparison to specimens corroded under field conditions. Liu investigated the depth of penetration of bars under field exposures with varying cover depths of 25.4, 50.8, and 76.2 mm (1, 2 and 3 in.)(Liu, Y., 1996). Considering these cover depths, the predicted critical penetration depths for bare steel, according to Equation 32 would be:

$$\text{25.4 mm (1 in.): } x_{crit} = 0.011\left(\frac{25.4}{16}\right)\left(\frac{25.4}{25}+1\right)^{1.8} = 0.062 \text{ mm (2.4 mils)}$$

$$\text{50.8 mm (2 in.): } x_{crit} = 0.011\left(\frac{50.8}{16}\right)\left(\frac{50.8}{25}+1\right)^{1.8} = 0.253 \text{ mm (9.96 mils)}$$

$$\text{76.2 mm (3 in.): } x_{crit} = 0.011\left(\frac{76.2}{16}\right)\left(\frac{76.2}{25}+1\right)^{1.8} = 0.649 \text{ mm (25.5 mils)}$$

These values are corroborated by the reported findings of Spellman and Stratfull, who indicated that field results showed corrosion penetration depths up to 29 mils (0.736 mm) (Spellman, D. L. & Stratfull, R. F., 1970). Interpretation of results presented by Clear suggested 0.094 mm. Thus, the critical penetration values are consistent with previously reported corrosion penetration depths under field exposures.

Liu presented a physical model to determine the depth of steel penetration by corrosion and its relation to corrosion rate and development of expansive corrosion products (Liu, Y. & Weyers,

R. E., 1998). The cross-sectional area, A_c, lost to corrosion, assuming a round bar for simplicity, can be physically related to the depth of penetration as follows:

D_O = outside diameter (prior to corrosion)

D_I = inside diameter (after corrosion)

$x_{crit} = D_O - D_I$ = depth of penetration

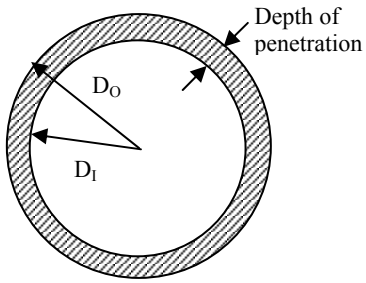

$$A_c = \frac{\pi D_O^{\,2}}{4} - \frac{\pi D_I^{\,2}}{4} = \frac{\pi\left(D_O^{\,2} - D_I^{\,2}\right)}{4}$$

Equation 35

Multiplying A_c by the density of steel, 7.87 g/cm^3 gives the mass of steel that has been lost to corrosion. As an example, consider the estimated depth of penetration for 25.4 mm (1 in.) cover:

Given x_c = 25.4 mm; x_{crit} = 0.062 mm

D_I = 15.875 – 0.062 = 15.813 mm

$$A_{c(BARE)} = \frac{\pi\left(15.875^2 - 15.813^2\right)}{4} \times 7.87 \frac{g}{cm^3} \times 0.001 \frac{cm^3}{mm^3} = 0.303g = 303mg$$

The surface area of the bare bar can be estimated as:

$\pi \times D \times L$ = (3.14) (1.587 cm) (2.5 cm) = 12.5 cm^2

Thus, the weight loss can be normalized to bar length by dividing total mass loss by bar surface area:

303 mg / 12.5 cm^2 = 24.2 mg/cm^2

Table 33 Projected Mass Loss for Bare Steel

Cover Depth (mm)	D_I (mm)	Total Mass Loss (g)	Estimated Mass Loss per Bar Area (mg/cm^2)	Normalized Mass Loss reported by Liu (mg/cm^2)
25.4	15.813	0.303	24.2	29.8
50.4	15.616	1.260	101	39.3
76.2	15.221	3.141	252	60.1

Considering the cover depths of 25.4, 50.8, and 76.2 mm (1, 2 and 3 in.) reported by Liu (Liu, Y., 1996), the normalized mass loss for bare steel is presented in Table 33. The latter two columns contain estimated values as calculated using Equation 32, and the actual values reported by Liu for field exposure specimens, respectively. For shallow depths, less than ~ 50 mm, the normalized mass loss projected using Sagüés' equation were of the same order as those reported by Liu for field specimens. Similar evaluation for ECR, considering a corroded bar length of 80 mm, and corresponding surface area of 39.8 cm^2, gives the results presented in Table 34.

Table 34 Projected Mass Loss for ECR

Cover Depth (mm)	D_I (mm)	Total Mass Loss (g)	Estimated Mass loss per Bar area (mg/cm^2)	Normalized Mass Loss reported by Liu (mg/cm^2)
25.4	15.846	0.455	11.4	29.8
50.4	15.790	1.330	33.4	39.3
76.2	15.699	2.746	68.9	60.1

As it happens, the predicted mass loss values for ECR are in even closer agreement than the bare steel mass loss projections, when compared with those reported by Liu for field exposures. It is possible that the corroded bar sites in Liu's large-scale field specimens were less localized than those in the laboratory cores of this study. Thus, if the values reported by Liu were increased by a factor of 80mm/25mm = 3.2, it is possible to observe closer agreement between the bare steel specimens in this study and the field observations, giving a general agreement between the projected values calculated herein and the field values for cover depths on the order of 51 mm (2 in.), as found in Virginia bridge decks.

Estimating ECR Propagation Time under Field Conditions

Larson and others reported the time from corrosion initiation to cracking for bare steel was approximately 3 to 5 years (Larson, T. D. et al., 1969). Liu and Weyers projected that the field service corrosion damage propagation period for bare steel varies from about 3 to 7 years as a function of cover depth and assuming a typical corrosion rate for bare steel in field concrete of approximately 1.1 $\mu A/cm^2$ (1 mA/ft^2) corrosion rate (Liu, Y. & Weyers, R. E., 1998; Sagues, A. A. & Zayed, A. M., 1991). Thus, the field service corrosion propagation period for bare steel, $t_{p(BARE,Field)}$, based upon clear cover depth, can be estimated from Liu and Weyers.

Considering again the relation of corrosion rates and propagation times for ECR and bare steel, as presented in Equation 34, the propagation time for ECR under field exposure can be estimated for various cover depths, using the corrosion rate information determined previously. For example, for the 2.5 percentile cover depth, ($x_{c(2.5\%)}$ = 47 mm), the bare steel propagation period is approximately 3 years, thus the relative propagation period for ECR can be estimated as follows:

$$\frac{t_{p(ECR)}}{t_{p(BARE)}} = \frac{CR_{(ECR)} \times x_{crit(BARE)}}{CR_{(BARE)} \times x_{crit(ECR)}} = (0.88)\left(\frac{0.217}{0.074}\right) = 2.58$$

$$t_{p(ECR,Field)} = t_{p(BARE,Field)} \times 2.58 = 3.0 \times 2.58 = 8 \text{ years}$$

Subtracting the propagation period for bare steel gives an additional propagation period for ECR of 5 years beyond bare steel.

For the percentiles of cover, as discussed previously, Table 35 presents the expected propagation times for bare steel and ECR, and shows the additional corrosion propagation time provided by ECR, $t_{p(ECR,Field)} - t_{p(BARE,Field)}$, beyond bare steel in field service.

Table 35 Estimated Propagation Times for ECR in Field Service

Percentile (%)	Cover Depth (mm)	$t_{p(BARE,Field)}$ (yr)	C.R. ratio	$t_{p(ECR,Field)}$ (yr)	$t_{p(ECR,Field)} - t_{p(BARE,Field)}$ (yr)
2.5	47	3.0	2.58	8	5
5.0	50	3.5	2.06	7	3
10.0	54	4.0	2.28	9	5
12.0	55	4.0	2.31	9	5
20.0	57	4.5	2.75	12	7
Average		4	2.29	9	5

Thus, the average service life extension contributed by ECR during the corrosion propagation phase can be estimated at 5 years.

Presently no effective method exists for the rehabilitation of concrete bridge components built with ECR. The removal of chloride-contaminated cover concrete is not likely to alleviate corrosion of ECR, once initiated, because the corrosion takes place under the coating. The removal of cover concrete does not remove the chloride from beneath the coating, and does nothing to address the development of an acidic, therefore corrosive, localized environment beneath the coating. In addition, no existing corrosion condition assessment method is amenable to field survey work. Therefore, there are significant but unquantifiable risks in the continued use of ECR as the primary method of corrosion prevention.

Stainless Steel as a Cost Effective Alternative

Stainless steel is being employed on a limited basis in several states to address corrosion problems in high-chloride environments. As a brief analysis of the cost effectiveness of stainless steel reinforcement as an alternative to ECR, consider the increase in construction costs of stainless steel, compared to black steel or ECR at the present time. In a previous report, the life-cycle costs of corrosion prevention alternatives were discussed, based upon 1997 cost information from the Virginia Department of Transportation.(Pyc, W. A. et al., 2000) Inquiries into the current prices for reinforcement, also to include stainless steel (316LN or Duplex 2205), show that bare steel and ECR prices are more or less the same as previously reported. Table 36 presents the material and installed costs for bare steel, ECR and stainless steel reinforcement (Pianca, F., 2002).

Table 36 Reinforcement Costs

Type	Material Cost Only ($/lb)	Installed price ($/lb)
Bare	$ 0.20	$ 0.49
ECR	$ 0.35	$ 0.62
Stainless Steel	$ 1.50	$ 2.36

A typical bridge deck, containing identical top and bottom mats, with #5 (16 mm) primary reinforcement at approximate 200 mm (8 in.) centers and 13-mm diameter (#4) temperature/shrinkage reinforcement at 300 mm (12 in.) centers, contains approximately 5 pounds of reinforcement per square foot.

Both the material costs and the installed cost for this "model" bridge deck can thus be projected, and the differences in costs versus bare steel estimated, as shown in Table 37. The price of a concrete overlay, including milling, patching, and traffic control, for a deck which reaches rehabilitation prior to the 75-year design life was estimated at $10.38 per square foot in 1995 (Pyc, W. A. et al., 1998). Using an effective annual inflation rate of 2.13% from 1995 to present, as determined from both construction cost and general U.S. inflation indices, the estimated current cost of this overlay would be $12.03 (Economic History Services, 2002; Engineering News-Record, 2002). Thus, the additional cost for stainless steel reinforcement, $9.35 per square foot more than bare steel and $8.70 per square foot more than ECR, is less than the cost of one concrete overlay, including traffic control costs.

Table 37 Unit Costs for Deck Reinforcement

Type	Material Only		Installed	
	Unit Cost ($/ft^2)	Cost Increase over Bare ($/ft^2)	Unit Cost ($/ft^2)	Cost Increase over Bare ($/ft^2)
Bare	$ 1.00	-	$ 2.45	-
ECR	$ 1.75	$ 0.75	$ 3.10	$ 0.65
Stainless Steel	$ 7.50	$ 6.50	$ 11.80	$ 9.35

It is important to note that stainless steel reinforcement, though a proven prevention method, has not yet come into common use, and therefore, has yet to reach fair market value (McDonald, D. B. et al., 1998). As its use increases, economies of scale and competition in the market can be expected to reduce prices, in much the same manner as occurred with ECR during its initial implementation (Manning, D. G., 1996). A significant portion of the in-place cost of stainless steel reinforcement is reported to be associated with the "fixtures", such as chairs, tie-wire, and conduits. Many specifications require that such ancillary items also be composed of stainless steel, thus driving up the current in-place cost. As stainless steel reinforcement becomes more common, it is likely that the price premium associated with its use will decrease.

A previous report evaluated the service lives and life cycle costs associated with a number of construction alternatives for reinforced concrete bridge decks(Pyc, W. A. et al., 2000). Using price data from Virginia Department of Transportation, the relative service lives and life cycle costs of ECR with normal Class A4 bridge deck concrete was compared with that of low permeability concrete. Using prices presented in that report, adjusting for inflation at an annual

rate of 2.13%, comparisons can be made regarding the cost-effectiveness of corrosion prevention alternatives.

The time to corrosion initiation of bare steel and ECR can be determined from Figure 34 and Figure 35, respectively, for selected percentiles of bridge deck area throughout Virginia. Using the propagation periods calculated for bare steel and ECR, service life predictions and times of rehabilitative overlay activities can be projected for alternative corrosion prevention systems. Consider three reinforcement bar alternatives, all employing low-permeability concrete: bare steel, ECR, and stainless steel (316LN). Low-permeability concrete has been found to extend the time to corrosion initiation by approximately 18 years beyond that of conventional A4 bridge deck concrete (Kirkpatrick, T. J. et al., 2001a). A rehabilitative concrete overlay in Virginia lasts an average of 24 years before further rehabilitation is required (Pyc, W. A. et al., 2000). Table 38 presents the expected rehabilitation times for each deck system at various corrosion probability levels in Virginia.

Table 38 Rehabilitation Times of Corrosion Prevention Systems

Corrosion Percentile (%)	Age(s) at Rehabilitation (yrs)			Number of Overlays Required		
	Bare	ECR	SS	Bare	ECR	SS
5	38,62	43,67	-	2	2	0
10	50	55	-	1	1	0
15	75	80	-	0	0	0
20	98	103	-	0	0	0

Therefore, the cumulative costs over the 75-year life of a structure, including initial construction and rehabilitation with traffic control for the various options can be estimated, as shown in Table 39. The total expenditure is the sum of the initial costs, plus the overlay costs at the rehabilitation age(s) using an annual inflation rate of 2.13%.

Table 39 Total Expenditures for Corrosion Prevention Systems

Corrosion Percentile	A4-LPC Concrete (in 2002)	Reinforcement Installed Price (in 2002)			Overlay w/ traffic control (in 2002)	Total Expenditure over Life of the Deck*		
		Bare	ECR	SS		Bare	ECR	SS
(%)	($/sf)	($/sf)	($/sf)	($/sf)	($/sf)	($/sf)	($/sf)	($/sf)
5	10.25	2.45	3.10	11.80	12.03	83.92	92.51	**22.05**
10	10.25	2.45	3.10	11.80	12.03	47.23	51.73	**22.05**
15	10.25	2.45	3.10	11.80	12.03	**12.70**	13.35	22.05
20	10.25	2.45	3.10	11.80	12.03	**12.70**	13.35	22.05

* Does not include routine inspection and minor maintenance costs

From the viewpoint of total expenditures over a 75-year service life, Table 39 shows that ECR is never a cost-effective corrosion prevention alternative in Virginia bridge decks. The only way that ECR could be cost-effective is if it prevents the need for an overlay, as compared to bare steel. For the greatest chloride exposure conditions in Virginia, it is clear that stainless steel is a least-cost alternative.

Benefits versus Risks of Corrosion Prevention Methods

Items considered in evaluating the cost effectiveness of current or proposed solutions generally include initial construction costs and projected maintenance costs. However, such evaluations should also consider the influence of the prevention method in question on future maintenance and rehabilitation options. Is there a greater risk involved in adopting a corrosion prevention strategy for which the benefit is not clearly quantified, and the costs and difficulties involved in mitigating it, should it not perform, are even less well understood?

Findings regarding projected time-to-corrosion for decks containing bare steel suggest that the severity of the corrosion-related deterioration issue has been overestimated, at least for Virginia bridge decks. Interestingly, a summary of Virginia records indicated that, as of 1998, more than 42% of bridge decks in service had been built prior to 1950, indicating a significant number of structures built under less stringent concrete and cover parameters were still performing adequately (Kerley, M., 1998). Of course, this data does not indicate whether overlays or other rehabilitation had been undertaken to extend lifespan. However, recent analysis showed that 25% of bridge decks built about 30 years ago (1968-1972) have received a maintenance overlay (polymer concrete) and only 13% had received a concrete overlay (Kirkpatrick, T. J. et al., 2001a). Conversely, records do not indicate whether bridges taken out of service were the result of corrosion related deterioration, other structural deterioration, or functional obsolescence.

With an additional increase in cover requirement, improved concrete specifications, and more recently, the adoption of high-performance, low permeable concretes to prevent alkali-silica reaction, the threat due to reinforcement corrosion in Virginia bridge decks appears to be limited to regions of intense salt usage, which can be correlated to both regional weather patterns and traffic volume (Dadson, D. K., 2001). Within Virginia, the areas of highest risk appear to be in the Northern Virginia, Culpeper and Staunton Engineering Districts, in locations with higher than average traffic counts, where deicing operations due to inclement winter weather are more common and more intense.

At present, federal guidelines require the use of a corrosion prevention method in bridge deck construction. Currently, ECR is the most widely accepted method. Best estimates have shown that ECR is not cost effective in Virginia bridge decks. A more prudent approach to application of limited highway construction and maintenance funds would be to differentiate between regions or structures based on severity of environment and traffic exposure. Structures in less severe exposures are sure to benefit from improvements in concrete quality and increased cover depth, whereas high risk areas might be more effectively addressed on a case-by-case basis, by implementing a more reliable method, such as stainless steel reinforcement.

CONCLUSIONS

Significance of Increased Chloride Penetration at Cracks

Most cracks in Virginia bridge decks are less than 0.30 mm in surface width, and longitudinal cracking was more commonly observed than transverse cracks. A relatively small number of visible cracks in bridge decks extend to the depth of reinforcement, and no apparent relation exists between crack width and crack depth. Although at early ages the presence of cracks appears to increase the chloride concentration of by an average of 0.61 kg chloride per cubic meter of concrete in about 61% of cracks, the effect appears to decline with age. As a worst-case condition, bridge deck cracking in Virginia may decrease the time to first repair, but will not significantly reduce the bridge deck service life.

Service Life Extension of ECR

In approximately the worst 20% of cases where performance is most critical, ECR provided no significant increase in projected time to corrosion initiation over that of bare steel. For a 100-year lifespan, ECR reduced the proportion of Virginia bridge deck areas expected to corrode by less than 2.5%. Comparing the expected field propagation periods of bare steel and ECR, service life was extended by approximately 5 years using ECR.

The 5 year service life extension estimated in this study is in agreement with a previous study (Weyers, R. E. et al., 1997). The 5 year service life extension provided by ECR is not a cost effective corrosion protection method for bridge decks in Virginia.

RECOMMENDATIONS

The first recommendation is that this study be continued through cracking of the majority, if not all, of the remaining ECR specimens.

Based on observations in this work, future research would be desirable in characterizing the field condition of ECR decks. Electrochemical impedance is not readily applicable to field structures, due to the complexity of the results and the myriad uncertainties concerning the observed systems. Therefore, development of simplified field condition assessment for ECR systems, to be employed by bridge officials in assessing service life and rehabilitation schedules is still needed.

In addition, it is apparent that at least some of the existing ECR decks in service will not achieve the anticipated design life. Repair procedures and remediation strategies must be specifically developed to address ECR. Some procedures, such as cathodic protection, may not be successfully implemented in such structures. Removal of chloride contaminated concrete and installing overlays above ECR that has initiated corrosion may prove insufficient, since corrosion beneath the coating may progress under completely different mechanisms once initiated.

Further investigation of the effects of recent specification changes, such as the adoption of pozzolanic admixtures and high-performance, low-permeability concretes, may help in identifying the critical exposures and allow targeted application of more rigorous corrosion control in locations where they are most needed.

For critical structures, such as those structures on Interstates and U.S. Routes in the Northern Virginia, Staunton, and Culpeper districts and other locations with a high rate of deicer salt usage, the use of stainless steel (316LN) reinforcing bar is recommended as the bridge deck corrosion protection system. The use of stainless steel (316LN) reinforcing steel is also recommended for coastal substructures. This report has demonstrated that the additional cost of stainless steel reinforcement is less than the cost of a single rehabilitative overlay for a bridge deck that does not reach 75-year design life. Stainless steel reinforcement may be implemented selectively for decks subject to the most severe exposures. Since 75% of structures are predicted not to reach the chloride corrosion concentration threshold during their expected life, low permeability concrete (<1500 coulomb per ASTM C 1202-97) is recommended for all other structures at this time.

REFERENCES

"National Transportation Statistics 1999". 2000. Bureau of Transportation Statistics (BTS) of the U.S. Department of Transportation. 2000.

Aguilar, A., Sagüés, A.A., and Powers, R.G., "Corrosion Measurements of Reinforcing Steel in Partially Submerged Concrete Slabs.", *ASTM Special Technical Publication* n. (1065), 66-85. 1990.

Alonso, C. et al., "Chloride threshold values to depassivate reinforcing bars embedded in a standardized OPC mortar," *Cement and Concrete Research*, v. 30, n. 7 (2000): 1047-1055.

Andrade, C. and Alonso, C., "Progress on Design and Residual Life Calculation With Regard to Rebar Corrosion of Reinforced-Concrete", Berke, N.S., Escalante, E., Nmai, C.K., and Whiting, D.Ed., Techniques to Assess the Corrosion Activity of Steel Reinforced Concrete Structures, 23-40 . 1996. W Conshohocken, American Society Testing and Materials. American Society for Testing And Materials Special Technical Publication.

ASTM, "C 1152-90, Standard Test Method for Acid-Soluble Chloride in Mortar and Concrete", *ASTM Annual Book of ASTM Standards* v. 04.02 Concrete and Aggregates. 1990.

ASTM, "C 876-91, Standard Test Method for Half-Cell Potentials of Uncoated Reinforcing Steel in Concrete", *ASTM Annual Book of ASTM Standards* v. 04.02n. (Concrete and Aggregates). 1991.

ASTM, "C 642-97, Standard Test Method for Density, Absorption, and Voids in Hardened Concrete", ASTM Annual Book of ASTM Standards, v. 04.02n. (Concrete and Aggregates). 1997.

ASTM, "C 702-98, Standard Practice for Reducing Samples of Aggregate to Testing Size", ASTM Annual Book of ASTM Standards, v. 04.02n. (Concrete and Aggregates). 1998.

ASTM, "A 775/A 775M - 01, Standard Specification for Epoxy-Coated Steel Reinforcing Bars", *ASTM Annual Book of ASTM Standards* v. 01.05 Steel Reinforcement. 2001.

Atimay, E. and P. M. Ferguson, "Early Chloride Corrosion of Reinforcing - A Test Report," *Materials Performance*, v. 13, n. 12 (1974): 18-21.

Babaei, Khossrow and Neil M. Hawkins, "Evaluation of Bridge Deck Protective Strategies," *Concrete International*, v. 10, n. 12 (1988): 56-66.

Bazant, Zdenik P., "Physical Model for Steel Corrosion in Concrete Sea Structures -- Application," *Journal of the Structural Division*, v. 105, n. ST6 (1979): 1155-1166.

Beeby, A. W., "Corrosion of Reinforcing Steel in Concrete and Its Relation to Cracking," *The Structural Engineer (London)*, v. 56A, n. 3 (1978): 77-81.

Bentur, A., S. Diamond, and N. Berke. *Steel Corrosion in Concrete.* London: Chapman & Hall, 1997.

Broomfield, J. P. *Corrosion of Steel in Concrete: Understanding, Investigation and Repair.* London: Chapman & Hall, 1997.

Brown, M. C., "Assessment of Commercial Corrosion Inhibiting Admixtures for Reinforced Concrete ", Virginia Polytechnic Institute & State University, Blacksburg, Virginia, 1999).

Brown, M. C., R. E. Weyers, and M. M. Sprinkel, "Effect of Corrosion-Inhibiting Admixtures on Material Properties of Concrete," *ACI Materials Journal*, v. 98, n. 3 (2001): 240-250.

Byfors, Kajsa, "Chloride binding in cement paste," *Nordic Concrete Research*, v. 5 (1986): 27-38.

Cady, P.D., "Corrosion of Reinforcing Steel in Concrete - A General Overview of the Problem", Tonini, D.E. and Dean, S.W., Chloride Corrosion of Steel in Concrete, v. ASTM STP 629, 3-11. 1977. Philadelphia, PA, ASTM. 1977.

Cady, P. D. and R. E. Weyers, "Chloride Penetration and the Deterioration of Concrete Bridge Decks," *Cement, Concrete and Aggregates*, v. 5, n. 2 (1983): 81-87.

Cady, Philip D and Richard E Weyers, "Deterioration Rates of Concrete Bridge Decks," *Journal of Transportation Engineering*, v. 110, n. 1 (1984): 34-44.

Clear, K.C., W.H. Hartt, J. McIntyre, and S. K. Lee, Performance of Epoxy-Coated Reinforcing Steel in Highway Bridges. 1995. Washington, D.C., National Academy Press.

Clear, K.C., "Effectiveness of Epoxy-Coated Reinforcing Steel.", *Concr-Int.* v. V 14n. (N 5), 58,60-62. 1992.

Covino, B.S., Cramer, S.D., Holcomb, G.R., Russell, J.H., Bullard, S.J., Dahlin, C., and Tinnea, J.S., Performance of Epoxy-Coated Steel Reinforcement in the Deck of the Perley Bridge. 2000. Albany, OR, U.S. Dept. of Energy.

Dadson, D. K., "Impact of Environmental Classification on Steel Girder Bridge Elements Using Bridge Inspection Data", Virginia Polytechnic Institute & State University, 2001).

Diamond, Sidney, "Effects of Two Danish Flyashes on Alkali Contents of Pore Solutions of Cement-Flyash Pastes," *Cement and Concrete Research*, v. 11 (1981): 383-394.

Economic History Services, "What Was the Inflation Rate Then?". 2002.

EG&G Princeton Applied Research, Basics of Electrochemical Impedance Spectroscopy (EIS). 1989. Princeton, NJ, EG&G Princeton Applied Research.

Engineering News-Record, "Construction Cost Index History (1908-2002)". 2002.

Fanous, F.S., Wu, H., and Pape, J., Impact of Deck Cracking on Durability. 2000. Ames, IA, Center for Transportation Research and Education, Iowa State University.

Fanous, F.S., Wu, H., and Pape, J., "Performance of Epoxy Coated Rebars in Bridge Decks (Preprint)", 80th Annual Meeting Preprint CD-ROM, Paper No. 01-2447. 2001. Washington, D.C., Transportation Research Board.

Feliu, S., Gonzalez, J.A., Feliu, S.Jr., and Andrade, M.C., "Confinement of the Electrical Signal for in Situ Measurement of Polarization Resistance in Reinforced Concrete.", *Aci-Mater-J.* v. 87n. (5), 457-460. 1990.

Fitch, M.G., Weyers, R.E., and Johnson, S.D. , "Determination of End of Functional Service Life for Concrete Bridge Decks", *Transportation Research Record* n. (1490), 60-66. 1995.

Gamry Instruments, I., "EIS Theory - Primer". 1999. Gamry Instruments, Inc. 2000.

Geenen, F. M., "Characterization of Organic Coatings With Impedance Measurements", Delft Univ. of Technology, 1991).

Giancoli, Douglas C. *Physics for Scientists and Engineers with Modern Physics.* 2nd ed. Englewood Cliffs, NJ: Prentice Hall, 1989.

Glass, G.K. and Buenfeld, N.R., "Presentation of the Chloride Threshold Level for Corrosion of Steel in Concrete", *Corrosion Science* v. 39n. (5), 1001-1013. 1997.

Jones, D. A. *Principles and Prevention of Corrosion.* 2 ed. Upper Saddle River, NJ: Prentice Hall, Inc., 1996.

Kerley, Malcolm. Personal Communication with Richard E. Weyers, 6 April 1998.

Kirkpatrick, T.J., R.E.Weyers, and M.M. Sprinkel, Service Life of Concrete Bridges in Virginia With and Without Epoxy Coated Reinforcement. 2000.

Kirkpatrick, T. J. et al., "Impact of Specification Changes on Chloride Induced Corrosion Service Life of Bridge Decks," *submitted for publication to Cement and Concrete Research* (2001a).

Kirkpatrick, T. J. et al., "Probabilistic Model for the Chloride Induced Corrosion Service Life of Bridge Decks," *submitted for publication to Cement and Concrete Research* (2001b).

Kobayashi, K. and K. Takewaka, "Experimental Studies on Epoxy Coating Reinforcing Steel for Corrosion Protection," *Journal of Cement Composites and Lightweight Concrete*, v. 6, n. 2 (1984).

Kranc, S. C., A. A. Sagüés, and F. J. Presuel-Moreno, "Decreased Corrosion Initiation Time of Steel in Concrete due to Reinforcing Bar Obstruction of Diffusional Flow," *ACI Materials Journal*, v. 99, n. 1 (2002): 51-53.

Krauss, P.D. and Rogall, E.A., Transverse Cracking in Newly Constructed Bridge Decks. 1996. Washington, D.C., Transportation Research Board.

Larson, T.D., Cady, P.D., and Theisen, J.C., Durability of Bridge Deck Concrete. 1969. State College, PA, Pennsylvania State University.

Liu, Youping, "Modeling the Time-to-Corrosion Cracking of the Cover Concrete in Chloride Contaminated Reinforced Concrete Structures", Virginia Polytechnic Institute & State University, 1996).

Liu, Y. and Weyers, R.E., "Modeling the Time-to-Corrosion Cracking in Chloride Contaminated Reinforced Concrete Structures", *ACI-Materials-Journal* v. 95n. (6), 675-681. 1998.

Lorentz, T. and French, C., "Corrosion of Reinforcing Steel in Concrete: Effects of Materials, Mix Composition, and Cracking", *Aci-Materials-Journal-(American-Concrete-Institute).* v. V 92n. (N 2), 181-190. 1995.

Manning, D.G., "Corrosion Resistant Design of Concrete Structures", Proceedings, Canadian Structural Concrete Conference, 199-223. 1981. University of Toronto.

Manning, D.G., "Corrosion Performance of Epoxy-Coated Reinforcing Steel: North American Experience", *Construction and Building Materials* v. 10n. (5), 349-365. 1996.

Martin, H. and Schiessl, P., "The Influence of Cracks on the Corrosion of Steel in Concrete", International Symposium on the Durability of Concrete, v. 2. 1962. RILEM .

Matsushima, M. et al., "A Study of the Application of Reliability Theory to the Design of Concrete Cover," *Magazine of Concrete Research*, v. 50, n. 1 (1998): 5-16.

McDonald, D.B., Pfeifer, D.W., and Sherman, M.R., McDonald, D.B., Corrosion Evaluation of Epoxy-Coated, Metallic-Clad and Solid Metallic Reinforcing Bars in Concrete. 1998. Springfield, Virginia, National Technical Information Services.

Neville, Adam M. *Properties of Concrete.* 4th ed. London & Marshfield, MA: Pitman Publishing, 1996.

Newhouse, C.D. and Weyers, R.E., "Modeling the Measured Time to Corrosion Cracking", Berke, N.S., Escalante, E., Nmai, C.K., and Whiting, D.Ed., Techniques to Assess the Corrosion Activity of Steel Reinforced Concrete Structures, 3-22. 1996. W Conshohocken, American Society Testing and Materials. American Society for Testing and Materials special Technical Publication.

Pantazopoulou, S.J. and Papoulia, K.D., Modeling Cover-Cracking Due to Reinforcement Corrosion in R.C. Structures.

Pianca, Frank. 15 April 2002.

Piens, M. and R. Verbist. Electrochemical Values: Their Significance When Applied to a Coated Substrate. In *Corrosion Control by Organic Coatings.* Edited by Jr. H. Leidheiser. Houston, TX: NACE, 1981.

Pyc, W.A., Weyers, R.E., and Sprinkel, M.M., Corrosion Protection Performance of Corrosion Inhibitors and Epoxy-Coated Reinforcing Steel in a Simulated Concrete Pore Water Solution. 1998. Charlottesville, Virginia, VTRC.

Pyc, W.A., Weyers, R.E., Weyers, R.M., Mokarem, D.W., Zemajtis, J., Sprinkel, M.M., and Dillard, J.G., Field Performance of Epoxy-Coated Reinforcing Steel in Virginia Bridge Decks. 2000. Charlottesville, VA, Virginia Transportation Research Council.

Pyc, Wioleta, "Field Performance of Epoxy-Coated Reinforcing Steel in Virginia Bridge Decks", Virginia Polytechnic Institute & State University, 1998).

Raphael, M. and Shalon, R., "A Study of the Influence of Climate on Corrosion and Reinforced Concrete", Proceedings, RILEM Symposium on Concrete and Reinforced Concrete in Hot Climates, 77-96. 1971.

Revie, R. W. *Uhlig's Corrosion Handbook.* 2nd ed. New York, NY: John Wiley & Sons, Inc., 2000.

Rieger, Philip H. *Electrochemistry.* 2 ed. New York & London: Chapman & Hall, 1994.

Sagüés, A., Powers, R., and Zayed, A., "Marine Environment Corrosion of Epoxy-Coated Reinforcing Steel", Page, C.L., Treadaway, K.W.J., and Bamforth, P.B., Corrosion of Reinforcement in Concrete, 539-50. 1990. Elsevier Applied Science Ltd.

Sagüés, A.A. and others, Corrosion of Epoxy-Coated Rebar in Florida Bridges, Final Report to Florida DOT. 1994. Tampa, FL, University of South Florida.

Sagüés, A.A., Kranc, S.C., Presuel-Moreno, F., Rey, D., Torres-Acosta, A., and Yao, L., Corrosion Forecasting for 75-Year Durability Design of Reinforced Concrete. 2001. 12/31/01, Florida Department of Transportation.

Sagüés, A.A., Perez-Duran, H.H., and Powers, R.G., "Corrosion Performance of Epoxy-Coated Reinforcing Steel in Marine Substructure Service", *Corrosion* v. Vol. 47n. (No. 11), 884-893. 1991.

Sagüés, A.A. and Powers, R.G., "Effect of Concrete Environment on the Corrosion Performance of Epoxy-Coated Reinforcing Steel", Corrosion 90, Paper Number 311. 1990. Houston, TX, NACE.

Sagüés, A.A., Powers, R.G., and Kessler, R., "Corrosion Performance of Epoxy-Coated Rebar in Florida Keys Bridges", PREPRINT: Corrosion 2001. 2001. Houston, TX, NACE.

Sagüés, A.A. and Zayed, A.M., Corrosion of Epoxy Coated Reinforcing Steel in Concrete -- Phase 1. 1989. Gainesville, Florida, Florida Department of Transportation, Materials Office.

Sagüés, A.A. and Zayed, A.M., "Low-Frequency Electrochemical Impedance for Measuring Corrosion of Epoxy-Coated Reinforcing Steel in Concrete", *Corrosion* v. 47n. (11), 852-859. 1991.

Sagüés, A.A., Kranc, S.C., and Moreno, E.I., "Evaluation of Electrochemical Impedance With Constant Phase Angle Component From the Galvanostatic Step Response of Steel in Concrete", *Electrochimica Acta* v. 41n. (7-8), 1239-1243. 1996.

Salparanta, L., Epoxy-Coated Concrete Reinforcements. 1988. Espoo, Finland, Vation teknillinen tutkimuskeskus (VTT).

Satake, J. et al. Chapter 21: Long-term Corrosion Resistance of Epoxy-Coated Reinforcing Bars. In *Corrosion of Reinforcement in Concrete Construction.* UK: Ellis Horwood, LTD, 1983.

Scantlebury, J.D. and Sussex, G.A.M., "Impedance Techniques for the Study of Organic Coatings", Leidheiser, Jr.H., Corrosion Control by Organic Coatings, 51-55. 1981. Houston, TX, National Association of Corrosion Engineers. 1981.

Schiessl, Peter. *Corrosion of Steel in Concrete.* London, New York: Chapman and Hall, 1988.

Schiessl, P. and Raupach, M., "Laboratory Studies and Calculations on the Influence of Crack Width on Chloride-Induced Corrosion of Steel in Concrete", *ACI Materials Journal* v. 94n. (1), 56-62. 1997.

Seymour, R. B. and H. F. Mark. *Handbook of Organic Coatings: A Comprehensive Guide for the Coatings Industry.* New York & London: Elsevier, 1990.

Smith, J.L. and Virmani, Y.P., Materials and Methods for Corrosion Control of Reinforced and Prestressed Concrete Structures in New Construction. 2000. McLean, VA, Federal Highway Administration.

Sohanghpurwala, A.A. and Scannell, W.T., Verification of Effectiveness of Epoxy-Coated Rebars. 1998. Harrisburg, PA, Pennsylvania Department of Transportation.

Spellman, D.L. and Stratfull, R.F., "Chlorides and Bridge Deck Deterioration", *Highway Research Record* n. (328,), 38-49. 1970.

St. John, D. A., A. B. Poole, and I. Sims. *Concrete Petrography: A Handbook of Investigative Techniques*. New York, NY: John Wiley & Sons, 1998.

Standish, J.V. and Leidheiser, Jr.H., "Properties and Behavior of Corrosion-Protective Organic Coatings As Determined by Electrical Impedance Measurements", Leidheiser, Jr.H., Corrosion Control by Organic Coatings, 38-44. 1981. Houston, TX, National Association of Corrosion Engineers. 1981.

Stratfull, R.F., Jurkovich, W.J., and Spellman, D.L., "CORROSION TESTING OF BRIDGE DECKS.", *Transportation Research Record* n. (539), 50-59. 1975.

Torres-Acosta, A. A., "Cracking Induced by Localized Corrosion of Reinforcement in Chloride Contaminated Concrete", University of South Florida, 1999).

Torres-Acosta, A.A. and Sagüés, A.A., "Concrete Cover Cracking Due to Corrosion of the Reinforcing Steel (Draft Preprint)", 5th CANMET/ACI International Conference on Durability of Concrete. 1999.

Tremper, Bailey, "The Corrosion of reinforcing Steel in Cracked Concrete," *ACI Journal*, v. 43, n. 10 (1947): 1137-1144.

Vassie, P., "Reinforcement Corrosion and the Durability of Concrete Bridges", *Proceedings of the Institution of Civil Engineers (London)* v. 76n. (pt 1), 713-723. 1984.

Weyers, R.E. and others, " Service Life Estimates", Concrete Bridge Protection and Rehabilitation: Chemical and Physical Techniques. 1994. Washington, D.C., Strategic Highway Research Program.

Weyers, R.E., Prowell, B.D., Sprinkel, M.M., and Vorster, M., Concrete Bridge Protection, Repair, and Rehabilitation Relative to Reinforcement Corrosion: A Methods Application Manual. 1993. Washington, D.C., Strategic Highway Research Program - National Research Council.

Weyers, R.E., Protocol for In-Service Evaluation of Bridges With Epoxy-Coated Reinforcing Steel. 1995. Washington, D.C., Transportation Research Board.

Weyers, R.E., Sprinkel, M.M., Pyc, W., Zemajtis, J., Liu, Y., and Mokarem, D.W., Field Investigation of the Corrosion Protection Performance of Bridge Decks and Piles Constructed With Epoxy-Coated Reinforcing Steel in Virginia . 1997. Charlottesville, VA, Virginia Transportation Research Council.

Zayed, A.M. and Sagüés, A.A., "Corrosion of Epoxy Coated Reinforcing Steel in Concrete ", CORROSION 89, 379. 1989. NACE, Houston, TX.

Zayed, A.M. and Sagüés, A.A., "Corrosion at Surface Damage on an Epoxy-Coated Reinforcing Steel", *Corrosion Science* v. 30n. (10), 1025-1044. 1990.

Zemajtis, J., Weyers, R.E., and Sprinkel, M.M., Performance Evaluation of Epoxy-Coated Reinforcing Steel. 1997. Charlottesville, VA, Virginia Transportation Research Council.

Zemajtis, J., Weyers, R.E., and Sprinkel, M.M., An Evaluation of the Performance of Epoxy-Coated Reinforcing Steel in Concrete Exposure Specimens. 1998. Charlottesville, VA, Virginia Transportation Research Council.

APPENDICES

A SUPPORTING DATA

Table 40 Summary Field Data for Bridge 1001

Number	Cover Depth x (mm)	Surface Chloride Content C_o (kg/m^3)	Diffusion Coefficient D_c (mm^2/year)
1	45.7	2.26	90.0
2	45.7	2.64	28.0
3	51.8	1.78	11.2
4	52.8	2.38	14.0
5	54.9	1.99	36.7
6	55.9	1.84	10.2
7	56.9	2.06	17.3
8	57.9	2.74	44.7
9	58.9	2.81	10.2
10	59.9	2.81	48.3
11	59.9	2.21	17.8
12	59.9	2.29	20.6
13	59.9	2.35	15.9
14	61.0		
15	61.0		
16	61.0		
17	61.0		
18	61.0		
19	62.0		
20	62.0		
21	62.0		
22	63.0		
23	63.0		
24	64.0		
25	64.0		
26	65.0		
27	65.0		
28	65.0		
29	66.0		
30	66.0		
31	66.0		
32	66.0		
33	66.0		
34	67.1		
35	68.1		
36	68.1		
37	70.1		
38	71.1		
39	71.1		
40	71.1		
Average	61.93	2.32	28.06
Std. Dev.	6.02	0.35	22.63
Number	40	13	13

Table 41 Summary Field Data for Bridge 1004_3

Number	Cover Depth x (mm)	Surface Chloride Content C_o (kg/m^3)	Diffusion Coefficient D_c (mm^2/year)
1	65.0	1.66	17.0
2	66.0	4.15	15.0
3	66.0	4.24	21.0
4	66.0	4.11	31.9
5	66.0	3.71	24.5
6	67.1	3.52	32.8
7	67.1	4.99	57.4
8	68.1	3.58	52.7
9	69.1	3.87	37.5
10	69.1	4.34	29.6
11	69.1	3.97	50.4
12	69.1	3.88	34.1
13	69.1	4.73	72.1
14	69.1	3.66	74.9
15	69.1		
16	70.1		
17	70.1		
18	70.1		
19	70.1		
20	70.1		
21	70.1		
22	71.1		
23	71.1		
24	71.1		
25	71.1		
26	71.1		
27	71.1		
28	71.1		
29	71.1		
30	72.1		
31	73.2		
32	75.2		
33	76.2		
34	76.2		
35	76.2		
36	77.2		
37	78.2		
38	81.3		
39	82.3		
40	79.2		
Average	71.30	3.89	39.35
Std. Dev.	4.23	0.77	19.29
Number	40	14	14

Table 42 Summary Field Data for Bridge 1004_6

Number	Cover Depth x (mm)	Surface Chloride Content C_o (kg/m^3)	Diffusion Coefficient D_c (mm^2/year)
1	56.9	0.54	7.0
2	57.9	0.76	4.0
3	57.9	0.24	1.0
4	58.9	1.06	13.1
5	59.9	0.55	12.5
6	61.0	0.74	18.5
7	61.0	0.69	17.1
8	61.0	0.79	15.7
9	61.0		
10	62.0		
11	62.0		
12	62.0		
13	65.0		
14	65.0		
15	65.0		
16	66.0		
17	66.0		
18	67.1		
19	68.1		
20	70.1		
21	70.1		
22	70.1		
23	71.1		
24	71.1		
25	72.1		
26	72.1		
27	73.2		
28	74.2		
29	79.2		
30	81.3		
Average	66.28	0.67	11.10
Std. Dev.	6.33	0.24	6.39
Number	30	8	8

Table 43 Summary Field Data for Bridge 1015

Number	Cover Depth x (mm)	Surface Chloride Content C_o (kg/m^3)	Diffusion Coefficient D_c (mm^2/year)
1	43.7	5.09	26.0
2	44.7	6.61	34.0
3	46.7	6.05	74.0
4	46.7	3.78	25.6
5	46.7	3.05	79.6
6	47.8	4.92	61.1
7	49.8	6.17	83.3
8	49.8	5.86	76.4
9	49.8	4.80	57.7
10	50.8	5.81	25.0
11	50.8	5.72	39.7
12	50.8	5.06	36.9
13	51.8		
14	51.8		
15	52.8		
16	53.8		
17	53.8		
18	53.8		
19	54.9		
20	54.9		
21	54.9		
22	54.9		
23	55.9		
24	55.9		
25	57.9		
26	58.9		
27	59.9		
28	59.9		
29	61.0		
30	61.0		
31	61.0		
32	61.0		
33	62.0		
34	62.0		
35	62.0		
36	63.0		
37	64.0		
38	66.0		
39	66.0		
40	67.1		
Average	55.50	5.24	51.61
Std. Dev.	6.29	1.03	22.84
Number	40	12	12

Table 44 Summary Field Data for Bridge 1019

Number	Cover Depth x (mm)	Surface Chloride Content C_o (kg/m^3)	Diffusion Coefficient D_c (mm^2/year)
1	45.7	1.13	8.0
2	46.7	2.40	36.0
3	46.7	1.42	34.0
4	48.8	2.61	23.7
5	48.8	2.11	16.7
6	49.8	1.25	12.9
7	49.8	2.34	21.5
8	49.8	1.51	17.9
9	49.8	2.90	41.4
10	49.8	1.96	36.1
11	49.8	2.48	36.7
12	49.8	2.19	48.0
13	49.8	2.00	41.5
14	49.8		
15	49.8		
16	50.8		
17	50.8		
18	50.8		
19	50.8		
20	50.8		
21	50.8		
22	50.8		
23	50.8		
24	51.8		
25	51.8		
26	51.8		
27	52.8		
28	53.8		
29	54.9		
30	55.9		
31	56.9		
32	56.9		
33	56.9		
34	57.9		
35	62.0		
36	62.0		
37	63.0		
38	65.0		
39	67.1		
40	71.1		
Average	53.31	2.02	28.81
Std. Dev.	5.83	0.55	12.63
Number	40	13	13

Table 45 Summary Field Data for Bridge 1136

Number	Cover Depth x (mm)	Surface Chloride Content C_o (kg/m^3)	Diffusion Coefficient D_c (mm^2/year)
1	53.8	6.29	12.0
2	54.9	3.86	5.0
3	55.9	3.56	22.0
4	55.9	4.19	14.8
5	55.9	6.79	23.3
6	55.9	8.17	32.0
7	55.9	5.81	21.4
8	55.9	2.85	10.1
9	56.9	3.62	15.3
10	57.9	3.25	25.6
11	57.9	4.09	16.1
12	57.9	4.62	15.1
13	58.9	3.78	13.1
14	58.9	3.27	15.3
15	59.9	4.84	11.4
16	59.9		
17	59.9		
18	59.9		
19	61.0		
20	61.0		
21	61.0		
22	61.0		
23	61.0		
24	62.0		
25	63.0		
26	65.0		
27	65.0		
28	65.0		
29	66.0		
30	66.0		
31	66.0		
32	66.0		
33	67.1		
34	67.1		
35	67.1		
36	68.1		
37	69.1		
38	69.1		
39	69.1		
40	71.1		
Average	61.72	4.60	16.83
Std. Dev.	4.80	1.52	6.86
Number	40	15	15

Table 46 Summary Field Data for Bridge 2021

Number	Cover Depth x (mm)	Surface Chloride Content C_o (kg/m^3)	Diffusion Coefficient D_c (mm^2/year)
1	41.7	0.61	4.0
2	46.7	0.87	3.0
3	47.8	0.21	6.0
4	47.8	0.60	9.7
5	49.8	0.84	8.3
6	50.8	0.72	2.2
7	51.8	0.79	9.2
8	52.8	0.36	5.0
9	53.8	0.76	4.3
10	54.9	1.03	2.7
11	54.9	1.22	3.2
12	54.9		
13	56.9		
14	56.9		
15	56.9		
16	56.9		
17	57.9		
18	58.9		
19	58.9		
20	59.9		
21	61.0		
22	61.0		
23	61.0		
24	61.0		
25	61.0		
26	62.0		
27	63.0		
28	64.0		
29	64.0		
30	65.0		
31	65.0		
32	65.0		
33	66.0		
34	67.1		
35	67.1		
36	68.1		
37	68.1		
38	69.1		
39	70.1		
40	70.1		
Average	59.23	0.73	5.24
Std. Dev.	7.05	0.28	2.69
Number	40	11	11

Table 47 Summary Field Data for Bridge 2262

Number	Cover Depth x (mm)	Surface Chloride Content C_o (kg/m^3)	Diffusion Coefficient D_c (mm^2/year)
1	45.7	2.90	40.0
2	46.7	0.42	27.0
3	47.8	2.09	38.0
4	47.8	2.61	18.5
5	47.8	2.46	47.7
6	52.8	2.07	14.6
7	52.8	2.26	18.6
8	54.9	1.91	44.0
9	54.9	1.34	21.6
10	55.9	1.87	51.3
11	55.9	1.20	8.2
12	56.9	2.33	4.1
13	56.9		
14	57.9		
15	57.9		
16	57.9		
17	58.9		
18	61.0		
19	61.0		
20	61.0		
21	62.0		
22	62.0		
23	63.0		
24	65.0		
25	67.1		
26	68.1		
27	68.1		
28	71.1		
29	71.1		
30	77.2		
Average	58.89	1.95	27.80
Std. Dev.	7.84	0.68	15.95
Number	30	12	12

Table 48 Summary Field Data for Bridge 6037

Number	Cover Depth x (mm)	Surface Chloride Content C_o (kg/m^3)	Diffusion Coefficient D_c (mm^2/year)
1	30.5	0.35	7.0
2	34.5	0.24	17.0
3	36.6	0.86	1.0
4	37.6	0.14	1.2
5	38.6	0.76	9.6
6	38.6	0.34	26.2
7	39.6	0.18	16.2
8	39.6		
9	39.6		
10	39.6		
11	39.6		
12	39.6		
13	40.6		
14	40.6		
15	40.6		
16	40.6		
17	40.6		
18	41.7		
19	41.7		
20	41.7		
21	41.7		
22	42.7		
23	42.7		
24	42.7		
25	42.7		
26	43.7		
27	43.7		
28	43.7		
29	43.7		
30	43.7		
31	43.7		
32	43.7		
33	44.7		
34	44.7		
35	44.7		
36	45.7		
37	45.7		
38	45.7		
39	45.7		
40	45.7		
41	47.75		
42	47.75		
43	48.77		
44	49.78		
45	50.80		
46	51.82		
47	52.83		
48	53.85		
49	53.85		

50	59.94		
Average	43.61	0.41	11.17
Std. Dev.	5.26	0.29	9.18
Number	50	7	7

Table 49 Summary Field Data for Bridge 6128

Number	Cover Depth x (mm)	Surface Chloride Content C_o (kg/m^3)	Diffusion Coefficient D_c (mm^2/year)
1	49.8	0.15	21.0
2	49.8	0.29	65.0
3	52.8	0.19	64.0
4	53.8	0.15	59.0
5	54.9	0.09	20.7
6	54.9	0.16	10.5
7	55.9	0.15	17.6
8	56.9	0.10	54.7
9	56.9		
10	56.9		
11	57.9		
12	57.9		
13	57.9		
14	57.9		
15	57.9		
16	57.9		
17	57.9		
18	58.9		
19	58.9		
20	58.9		
21	59.9		
22	59.9		
23	59.9		
24	61.0		
25	61.0		
26	61.0		
27	61.0		
28	61.0		
29	61.0		
30	61.0		
31	61.0		
32	61.0		
33	63.5		
34	64.0		
35	65.0		
36	65.0		
37	65.0		
38	65.0		
39	66.0		
40	70.1		
Average	59.42	0.16	39.07
Std. Dev.	4.22	0.06	23.53
Number	40	8	8

Table 50 Density, Absorption, Permeable Voids and Saturation of Field Cores

District - County - Route	Age @ Sampling (yrs)	Absorption after boiling (%)		Bulk Density, as received (g/cm3)		Bulk density, after boiling (g/cm3)		Apparent Density (g/cm3)		Pore space (%)		Saturation (%)	
		Ave	StDev	Ave	StDev	Ave	StDev	Ave	StDev	Ave	StDev	Ave	StDev
1 - Wise - SR 72	4	6.67%	0.71%	2.34	0.06	2.38	0.06	2.62	0.06	14.8%	1.3%	76.4%	3.5%
6 - Northumberland - SR 200	6	5.96%	0.77%	2.31	0.05	2.35	0.05	2.56	0.05	13.2%	1.5%	68.4%	5.5%
7 - Culpeper - US 29	7	6.27%	0.77%	2.25	0.24	2.30	0.24	2.50	0.29	13.6%	2.2%	66.8%	6.0%
7 - Culpeper - SR 522	9	6.30%	0.52%	2.28	0.02	2.33	0.02	2.54	0.02	13.8%	1.0%	66.7%	4.1%
2 - Giles - SR 100	12	6.35%	0.66%	2.34	0.03	2.38	0.03	2.61	0.02	14.2%	1.3%	72.2%	4.7%
9 - Fairfax - Vaden Drive	14	6.04%	0.83%	2.40	0.06	2.46	0.05	2.70	0.03	14.0%	1.6%	54.6%	4.1%
2 - Franklin - SR 740	15	6.43%	0.49%	2.36	0.03	2.42	0.03	2.67	0.03	14.6%	1.0%	57.5%	6.4%
3 - Nelson - SR 6	16	6.63%	0.72%	2.32	0.03	2.37	0.03	2.61	0.02	14.7%	1.4%	63.9%	2.4%
1 - Grayson - SR 662	16	5.92%	0.67%	2.40	0.05	2.45	0.05	2.68	0.04	13.6%	1.3%	68.4%	7.3%
5 - Greensville - I-95	18	6.50%	0.84%	2.29	0.04	2.34	0.03	2.56	0.02	14.2%	1.5%	60.6%	6.4%
10-bridge Average		6.33%	0.74%	2.33	0.10	2.38	0.10	2.60	0.11	14.1%	1.5%	60.4%	17.7%

Table 51 Potential and Impedance At Initiation – Bridges 1001 & 1004_3

Specimen	Initiation Date	E_{OC} (V)		$\|Z\|_{1\ mHz}$ (Ω)		$\|Z\|_{5\ kHz}$ (Ω)		$\theta_{1\ mHz}$ (°)		$\theta_{5\ kHz}$ (°)	
		before	after	before	After	before	after	before	after	before	after
1001											
1001_C1											
1001_C2	2/23/2001	-0.357	-0.487	1.19E+05	2.42E+04	1.02E+04	5.42E+03	-16	-13	-65	-39
1001_C3											
1001_C4											
1001_C5											
1001_C6											
1001_C7											
1001_C8											
1001_C9											
1001_C11											
1001_C12											
1001_CR1	6/7/2000	-0.109	-0.565	4.48E+04	2.31E+04	7.26E+03	6.04E+03	-19	-5	-60	-42
1001_CR2	6/7/2000	-0.088	-0.494	1.34E+06	1.10E+05	2.49E+03	1.43E+03	-35	-25	-13	-15
1001_CR3											
1004_3											
1004_3_C1	6/5/2000	-0.123	-0.536	8.12E+04	2.66E+04	6.38E+03	3.53E+03	-20	-17	-25	-28
1004_3_C2	8/17/2000	-0.101	-0.391	1.22E+05	1.27E+05	7.64E+03	6.56E+03	-14	-13	-74	-75
1004_3_C3	1/18/2001	-0.144	-0.597	7.88E+04	4.93E+04	5.77E+03	5.57E+03	-18	-13	-63	-53
1004_3_C4											
1004_3_C5	1/18/2001	-0.116	-0.444	5.29E+05	2.35E+05	9.92E+03	1.86E+04	-7	-25	-95	-54
1004_3_C6											
1004_3_C7											
1004_3_C8											
1004_3_C9	10/23/2000	-0.277	-0.374	3.14E+04	1.41E+04	4.98E+03	3.64E+03	-22	-20	-47	-28
1004_3_C10	7/6/2000	-0.116	-0.368	3.99E+03	2.13E+04	3.23E+03	3.23E+03	55	-25	-45	-27
1004_3_C11	6/5/2000	-0.258	-0.400	4.12E+04	2.21E+04	4.99E+03	3.15E+03	-23	-19	-43	-44
1004_3_C12	12/18/2000	-0.299	-0.492	2.07E+04	3.19E+03	2.61E+03	1.74E+03	-22	-6	-25	-20
1004_3_CR2											
1004_3_CR3	10/23/2000	-0.213	-0.344	8.24E+04	4.29E+04	6.62E+03	5.14E+03	-25	-27	-64	-52

Table 52 Potential and Impedance At Initiation – Bridges 1004_6 & 1015

Specimen	Initiation Date	E_{oc} (V)		$\|Z\|_{1\ mHz}$ (Ω)		$\|Z\|_{5\ kHz}$ (Ω)		$\theta_{1\ mHz}$ (°)		$\theta_{5\ kHz}$ (°)	
		before	after	before	after	before	after	before	after	before	after
1004_6											
1004_6_C1											
1004_6_C2	11/16/2001	-0.168	-0.318	2.30E+05	1.73E+05	1.35E+04	1.08E+04	-28	-23	-38	-59
1004_6_C3											
1004_6_C4											
1004_6_C5											
1004_6_C6											
1004_6_C7	5/24/2000	-0.132	-0.452	3.15E+04	8.45E+03	5.85E+03	3.11E+03	-25	-7	-45	-24
1004_6_C8											
1004_6_C10											
1004_6_C12											
1004_6_CR1	1/18/2002	-0.120	-0.146	1.94E+05	2.95E+05	1.08E+04	1.62E+04	-29	-30	-33	-46
1004_6_CR2	6/26/2000	-0.184	-0.167	9.37E+04	9.82E+04	7.90E+03	7.98E+03	-18	-18	-74	-74
1004_6_CR3/C11	11/7/2000	-0.286	-0.260	1.27E+04	1.56E+04	2.32E+03	2.80E+03	-24	-17	-20	-22
1015											
1015_C1	5/31/2001	-0.512	-0.493	3.89E+03	3.23E+03	1.89E+03	1.54E+03	-8	-9	-12	-10
1015_C2	5/31/2001	-0.365	-0.480	1.17E+04	5.87E+03	4.80E+03	2.85E+03	-16	-12	-26	-17
1015_C3	9/15/2000	-0.225	-0.332	4.42E+04	1.75E+04	2.39E+03	2.01E+03	-25	-14	-16	-14
1015_C4	7/12/2001	-0.213	-0.462	1.96E+05	7.13E+04	8.61E+03	8.73E+03	-19	-10	-77	-74
1015_C5	10/18/2000	-0.155	-0.357	5.41E+05	1.17E+05	8.62E+03	1.12E+04	-17	3	-39	-53
1015_C6	4/28/2000	-0.182	-0.565	8.75E+04	6.31E+03	1.03E+04	2.38E+03	-19	-5	-34	-10
1015_C7	4/29/2000	-0.086	-0.576	1.18E+06	1.48E+04	1.68E+04	3.35E+03	-49	-5	-26	-11
1015_C8	4/29/2000	-0.283	-0.604	2.42E+05	1.54E+04	1.81E+04	5.42E+03	-6	-9	-12	-10
1015_C9	4/28/2000	-0.410	-0.627	2.08E+04	1.02E+04	6.70E+03	3.10E+03	-16	-20	-24	-13
1015_C10	4/28/2000	-0.500	-0.528	9.75E+03	7.46E+03	3.41E+03	2.35E+03	-13	-21	-15	-13
1015_CR1	4/28/2000	-0.203	-0.490	1.08E+05	4.13E+04	3.21E+03	3.12E+03	-24	-8	-10	-10
1015_CR1B	4/28/2000	-0.218	-0.612	2.49E+05	1.69E+04	6.91E+03	1.08E+03	-34	-20	-13	-11
1015_CR2	4/28/2000	-0.330	-0.588	9.99E+04	8.28E+04	7.94E+03	1.63E+04	-18	-5	-16	-47
1015_CR3	4/28/2000	-0.168	-0.566	3.15E+05	4.39E+04	1.50E+04	3.97E+03	-45	-20	-12	-30

Table 53 Potential and Impedance At Initiation – Bridges 1019 & 1136

Specimen	Initiation Date	E_{oc} (V)		$\|Z\|_{1\ mHz}$ (Ω)		$\|Z\|_{5\ kHz}$ (Ω)		$\theta_{1\ mHz}$ (°)		$\theta_{5\ kHz}$ (°)	
		Before	after	before	after	before	after	before	after	before	after
1019											
1019_C1											
1019_C2	4/4/2001	-0.091	-0.370	1.36E+06	4.43E+05	1.15E+04	1.77E+04	-27	-21	-75	-38
1019_C3											
1019_C4	4/4/2001	-0.129	-0.339	1.15E+06	1.60E+05	9.89E+03	7.09E+03	-29	-25	-22	-43
1019_C5											
1019_C6											
1019_C7											
1019_C8											
1019_C9	4/4/2001	-0.427	-0.452	8.04E+05	2.94E+05	1.41E+04	7.89E+03	-16	-12	-73	-96
1019_C10											
1019_CR1											
1019_CR2	3/6/2001	-0.379	-0.588	8.90E+04	1.49E+04	6.26E+03	5.25E+03	-13	-7	-82	-52
1019_CR3	9/11/2000	-0.212	-0.583	1.92E+05	5.24E+04	5.44E+03	5.24E+03	-19	-11	-43	-41
1136											
1136_C1											
1136_C2											
1136_C3											
1136_C4											
1136_C5	5/18/2001	-0.095	-0.428	2.62E+06	6.37E+05	3.44E+04	3.45E+04	-48	-28	-72	-78
1136_C6	1/16/2001	-0.195	-0.400	4.41E+05	2.15E+05	2.44E+04	1.82E+04	-15	-18	-45	-40
1136_C7	5/3/2000	-0.357	-0.595	1.05E+05	4.41E+04	1.53E+04	5.58E+03	-19	-16	-9	-15
1136_C8											
1136_C9											
1136_C10											
1136_C11	5/2/2000	-0.184	-0.487	9.82E+05	1.09E+05	2.33E+04	6.08E+03	-31	-29	-39	-25
1136_C12	1/16/2001	-0.183	-0.532	3.08E+05	2.67E+04	3.59E+03	3.54E+03	-31	-8	-23	-23
1136_CR1	1/16/2001	-0.213	-0.589	7.09E+05	1.94E+05	2.56E+04	2.30E+04	-29	-18	-71	-61
1136_CR2	3/28/2000	N/A	-0.571	N/A	1.38E+04	N/A	7.64E+03	N/A	-8	N/A	-17
1136_CR3	3/28/2000	N/A	-0.577	N/A	2.02E+04	N/A	2.77E+03	N/A	-18	N/A	-11

N/A ≡ Not Available – typically for specimens that initiated corrosion in the first month, thus no previous data was available.

Table 54 Potential and Impedance At Initiation – Bridges 2021 & 2262

Specimen	Initiation Date	E_{oc} (V)		$\|Z\|_{1\ mHz}$ (Ω)		$\|Z\|_{5\ kHz}$ (Ω)		$\theta_{1\ mHz}$ (°)		$\theta_{5\ kHz}$ (°)	
		before	after	before	after	before	after	before	after	before	after
2021											
2021_C1	3/29/2001	-0.184	-0.539	6.51E+05	1.03E+05	9.73E+03	8.39E+03	-12	-5	-85	-68
2021_C2	8/24/2001	-0.175	-0.199	1.34E+05	2.67E+05	9.82E+03	9.52E+03	-5	-25	-81	-82
2021_C3	3/29/2001	-0.166	-0.595	9.80E+06	6.85E+05	2.98E+04	2.73E+04	-9	-5	-87	-81
2021_C4											
2021_C5	2/28/2001	-0.290	-0.566	1.18E+05	1.35E+04	8.46E+03	4.65E+03	-22	-13	-75	-39
2021_C6	5/17/2000	-0.227	-0.227	4.25E+04	4.25E+04	4.71E+03	4.71E+03	-35	-35	-23	-23
2021_C7	10/31/2000	-0.126	-0.408	1.26E+05	2.07E+04	7.88E+03	4.31E+03	-21	-18	-56	-28
2021_C8											
2021_C9	10/31/2000	-0.143	-0.485	4.70E+04	2.88E+04	4.24E+03	3.04E+03	-28	-13	-45	-52
2021_C10											
2021_C11	2/28/2001	-0.239	-0.322	3.82E+05	8.59E+04	6.67E+03	4.91E+03	-21	-22	-82	-62
2021_C12	12/5/2001	-0.277	-0.305	1.90E+04	1.84E+04	2.13E+03	2.42E+03	-41	-40	-16	-19
2021_CR1	10/31/2000	-0.252	-0.252	5.36E+04	5.36E+04	4.49E+03	4.49E+03	-27	-27	-34	-34
2021_CR2											
2021_CR3											
2262											
2262_C1	4/25/2001	-0.259	-0.445	1.11E+06	1.64E+05	1.11E+04	1.05E+04	-38	-15	-78	-72
2262_C2	1/5/2002	-0.201	-0.400	6.03E+05	2.56E+05	1.66E+04	1.89E+04	-25	-23	-43	-46
2262_C3											
2262_C4	7/17/2000	-0.182	-0.475	3.46E+05	2.23E+04	1.69E+04	7.48E+03	-22	-13	-64	-43
2262_C5											
2262_C6	4/25/2001	-0.072	-0.072	3.35E+06	3.35E+06	2.34E+04	2.34E+04	-14	-14	-82	-82
2262_C7	1/22/2001	-0.227	-0.227	1.81E+05	1.81E+05	9.32E+03	9.32E+03	-44	-44	-66	-66
2262_C8	6/9/2000	-0.074	-0.326	1.25E+05	2.90E+04	9.97E+03	7.25E+03	-39	-24	-45	-18
2262_C9	8/21/2001	-0.155	-0.510	8.07E+05	1.56E+05	1.57E+04	8.80E+03	-10	-13	-60	-71
2262_C10	9/25/2000	-0.087	-0.081	6.46E+05	2.90E+03	4.64E+03	1.55E+03	-31	-9	-29	-21
2262_C11											
2262_C12	12/23/2000	-0.215	-0.476	3.00E+05	9.11E+04	8.07E+03	9.51E+03	-42	-14	-65	-67
2262_CR1	12/22/2000	-0.184	-0.203	4.71E+05	4.52E+04	8.07E+03	8.83E+03	-23	-14	-59	-68
2262_CR2	5/11/2000	-0.149	-0.523	2.88E+05	8.96E+03	3.18E+03	1.70E+03	-35	-6	-12	-11
2262_CR3											

Table 55 Potential and Impedance At Initiation – Bridges 6037 & 6128

Specimen	Initiation Date	E_{oc} (V)		$\|Z\|_{1\ mHz}$ (Ω)		$\|Z\|_{5\ kHz}$ (Ω)		$\theta_{1\ mHz}$ (°)		$\theta_{5\ kHz}$ (°)	
		before	after	before	after	before	after	before	after	before	after
6037											
6037_C1	5/12/2000	-0.072	-0.471	1.32E+04	1.36E+03	2.16E+03	8.95E+02	-63	-8	-3	-16
6037_C2	5/12/2000	-0.070	-0.466	1.23E+04	1.99E+03	1.59E+03	5.94E+02	-61	-12	-3	-3
6037_C3	6/13/2000	-0.107	-0.388	1.67E+04	3.78E+03	8.26E+02	7.57E+02	-54	-9	-11	-5
6037_C5	5/12/2000	-0.109	-0.576	0.00E+00	2.46E+03	4.77E+03	5.02E+02	0	-12	-2	-3
6037_C7	9/27/2000	-0.211	-0.250	1.36E+04	1.16E+04	3.40E+03	1.14E+03	-38	-33	-16	-5
6037_C8	5/12/2000	-0.260	-0.605	6.65E+03	1.56E+03	2.74E+03	4.08E+02	-30	-17	-5	-3
6037_C9	1/24/2001	-0.497	-0.553	2.20E+03	1.68E+03	2.29E+03	6.63E+02	-7	-5	-6	-8
6037_C10	9/27/2000	-0.486	-0.486	1.81E+03	1.81E+03	2.67E+03	2.67E+03	-6	-6	-3	-3
6037_C11	5/12/2000	-0.090	-0.143	1.86E+04	1.36E+04	2.47E+03	5.67E+02	-52	-53	-6	-4
6037_C12	9/28/2000	-0.210	-0.330	6.84E+03	4.13E+03	1.64E+03	1.31E+03	-33	-16	-14	-8
6037_CR1/C4	5/12/2000	-0.076	-0.433	1.42E+04	2.21E+03	7.17E+02	3.84E+02	-66	-15	-5	-5
6037_CR2/C6	5/12/2000	-0.084	-0.142	9.55E+03	6.61E+03	6.67E+02	4.07E+02	-51	-49	-5	-6
6128											
6128_C1	5/15/2000	N/A	-0.471	N/A	2.30E+03	N/A	2.63E+03	N/A	-14	N/A	-4
6128_C2	5/15/2000	N/A	-0.359	N/A	3.21E+03	N/A	3.79E+02	N/A	-29	N/A	-3
6128_C3	7/24/2000	-0.139	-0.516	1.29E+04	1.53E+03	1.29E+03	3.37E+02	-53	-11	-26	-10
6128_C4	5/15/2000	N/A	-0.345	N/A	3.97E+03	N/A	2.79E+02	N/A	-22	N/A	-3
6128_C5	6/20/2000	-0.305	-0.543	4.22E+03	1.30E+03	2.49E+02	9.06E+02	-30	-10	-3	-18
6128_C6	7/24/2000	-0.118	-0.514	9.41E+03	9.01E+02	5.30E+02	2.90E+02	-63	-8	-6	-5
6128_C7	6/20/2000	-0.144	-0.553	1.01E+04	1.20E+03	6.08E+02	3.80E+02	-54	-17	-30	-5
6128_C8	5/15/2000	N/A	-0.092	N/A	1.60E+05	N/A	5.93E+04	N/A	-8	N/A	-21
6128_C9	6/20/2000	-0.206	-0.418	7.76E+03	1.24E+03	3.08E+02	4.12E+02	-49	-6	-4	-5
6128_C10	6/20/2000	-0.154	-0.527	8.66E+03	9.68E+02	2.44E+02	2.52E+02	-61	-8	-5	-7
6128_C11	12/4/2000	-0.274	-0.494	9.08E+03	1.37E+03	6.51E+02	3.44E+02	-31	-7	-9	-10
6128_C12	5/16/2000	N/A	-0.504	N/A	1.24E+03	N/A	2.84E+02	N/A	-13	N/A	-5
6128_CR1	5/15/2000	N/A	-0.349	N/A	2.73E+03	N/A	3.54E+02	N/A	-19	N/A	-6
6128_CR2	5/15/2000	N/A	-0.500	N/A	1.07E+03	N/A	2.04E+02	N/A	-11	N/A	-7
6128_CR3	5/16/2000	N/A	-0.534	N/A	1.82E+03	N/A	2.06E+02	N/A	-20	N/A	-5
6128_CR4	5/16/2000	N/A	0.000	N/A	1.53E+04	N/A	4.55E+02	N/A	-51	N/A	-3

N/A ≡ Not Available – typically for specimens that initiated corrosion in the first month, thus no previous data was available.

B POTENTIAL AND IMPEDANCE TRENDS

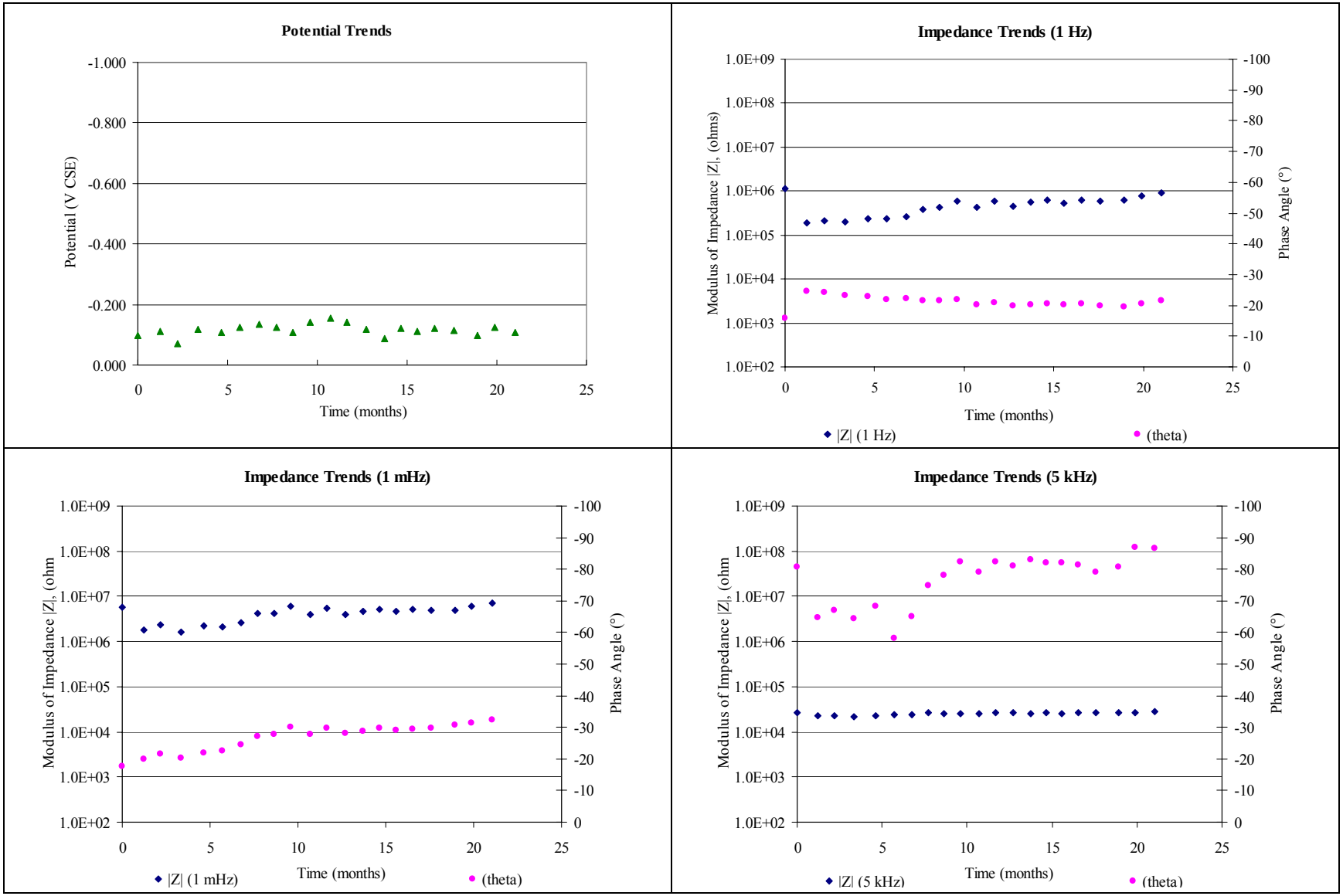

Figure B-1 Potential and Impedance Summary for Specimen 1001_C1

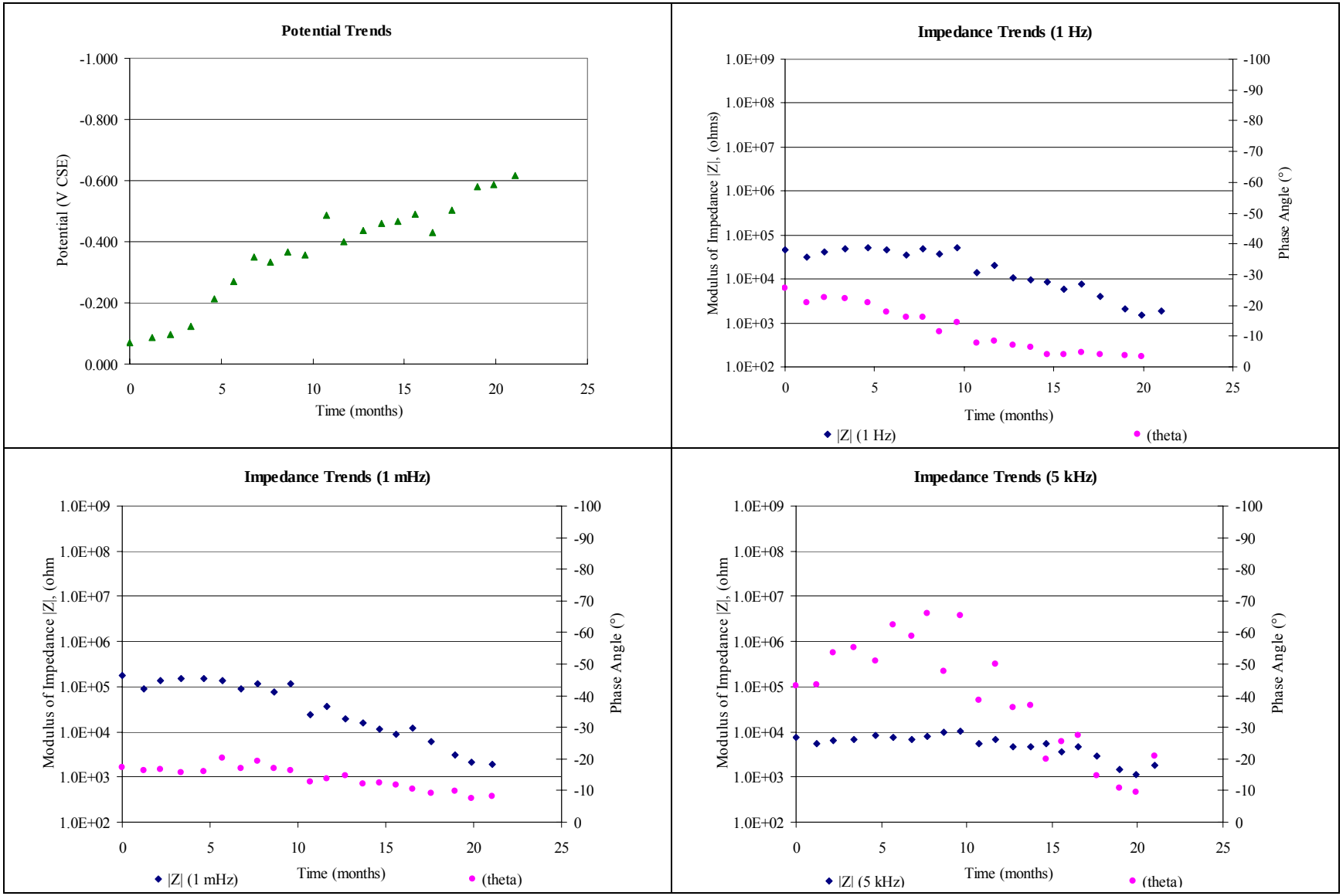

Figure B-2 Potential and Impedance Summary for Specimen 1001_C2

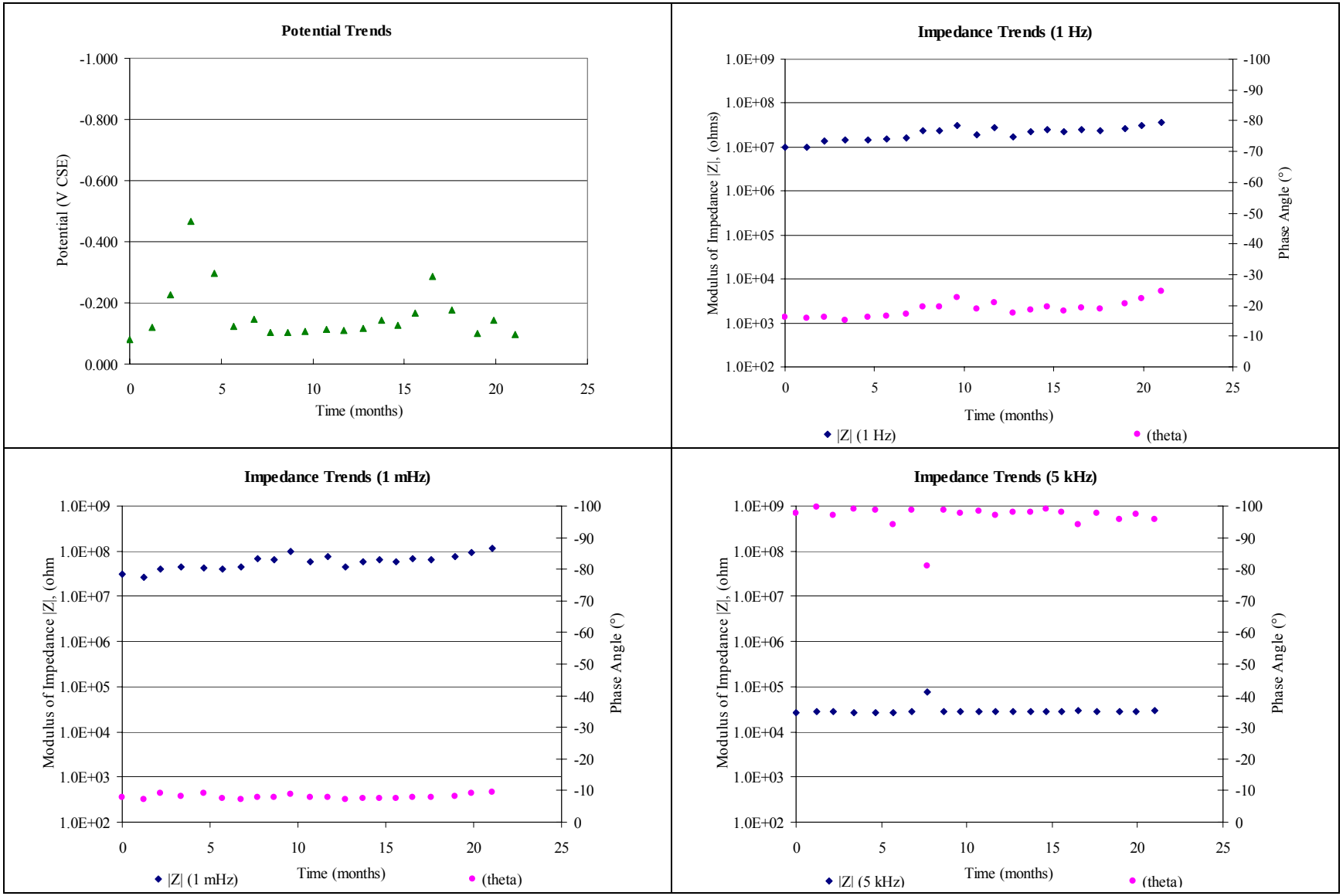

Figure B-3 Potential and Impedance Summary for Specimen 1001_C3

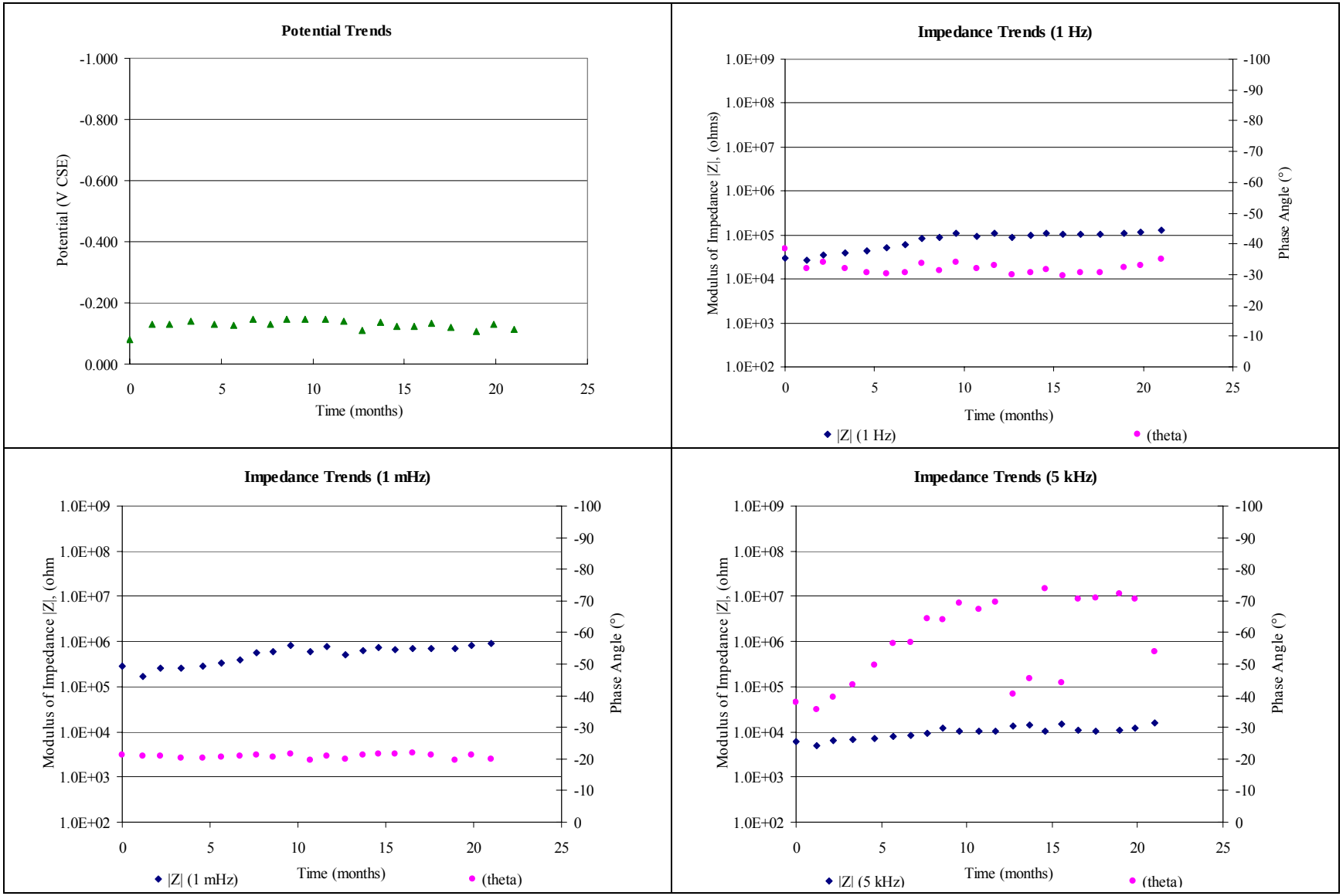

Figure B-4 Potential and Impedance Summary for Specimen 1001_C4

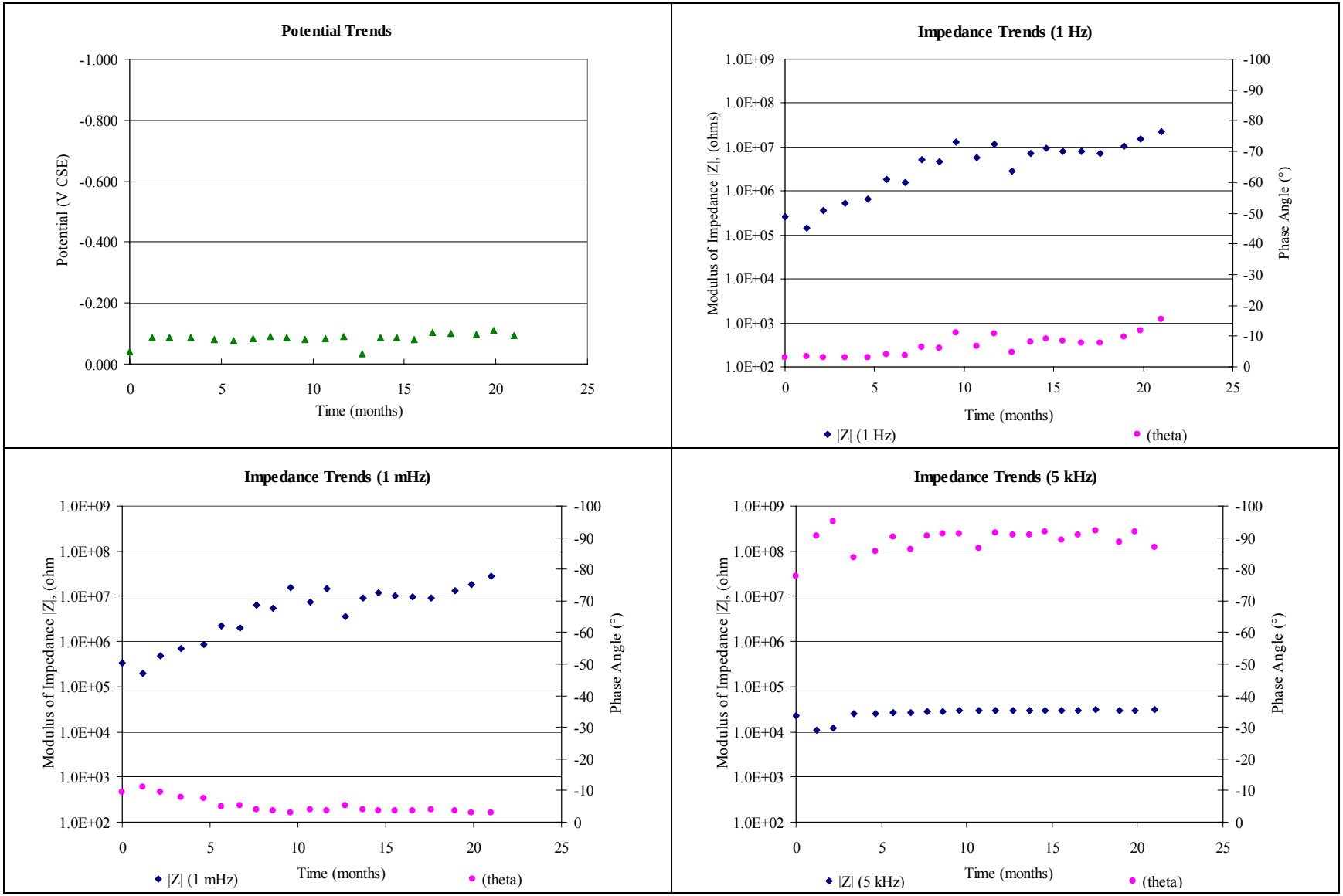

Figure B-5 Potential and Impedance Summary for Specimen 1001_C5

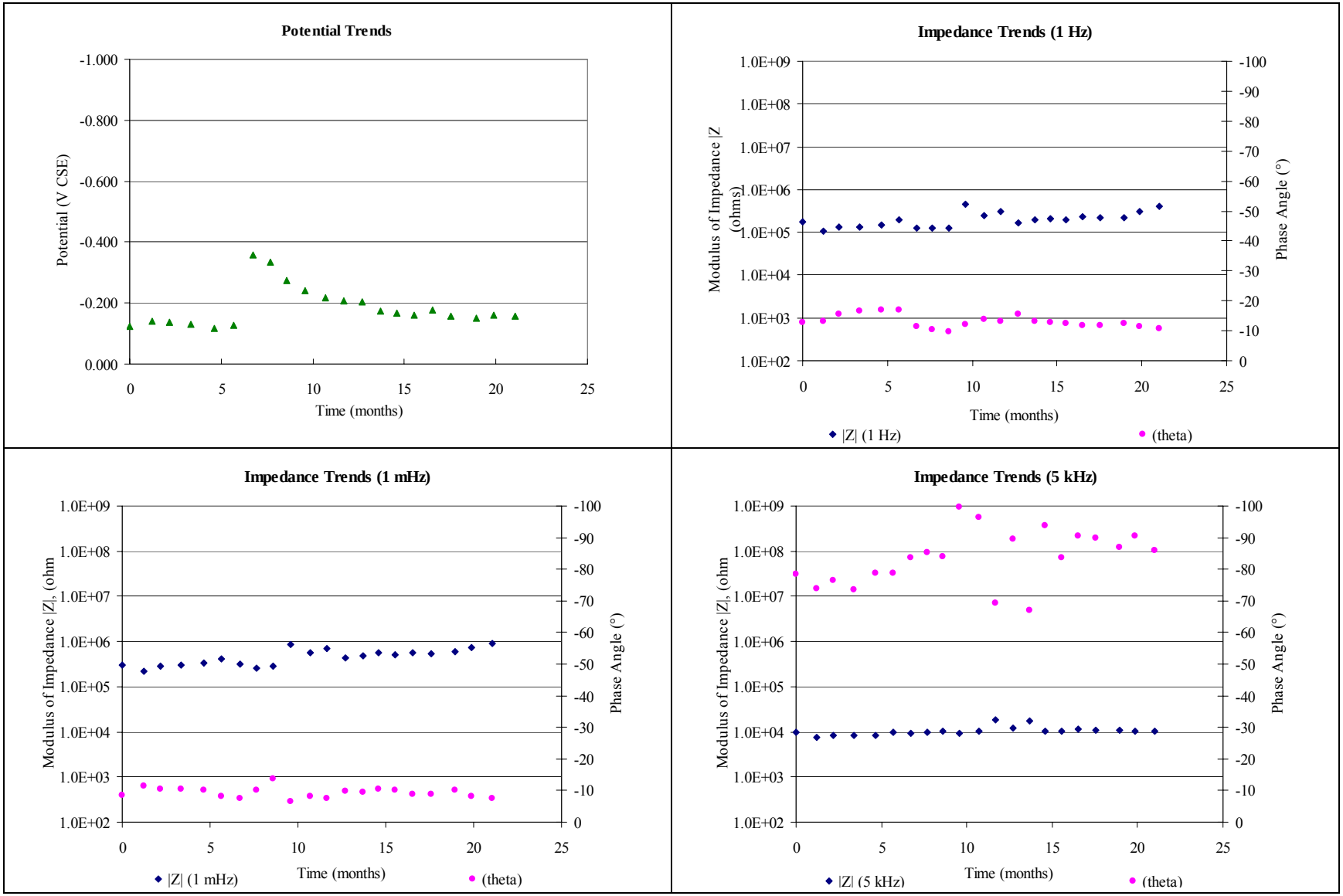

Figure B-6 Potential and Impedance Summary for Specimen 1001_C6

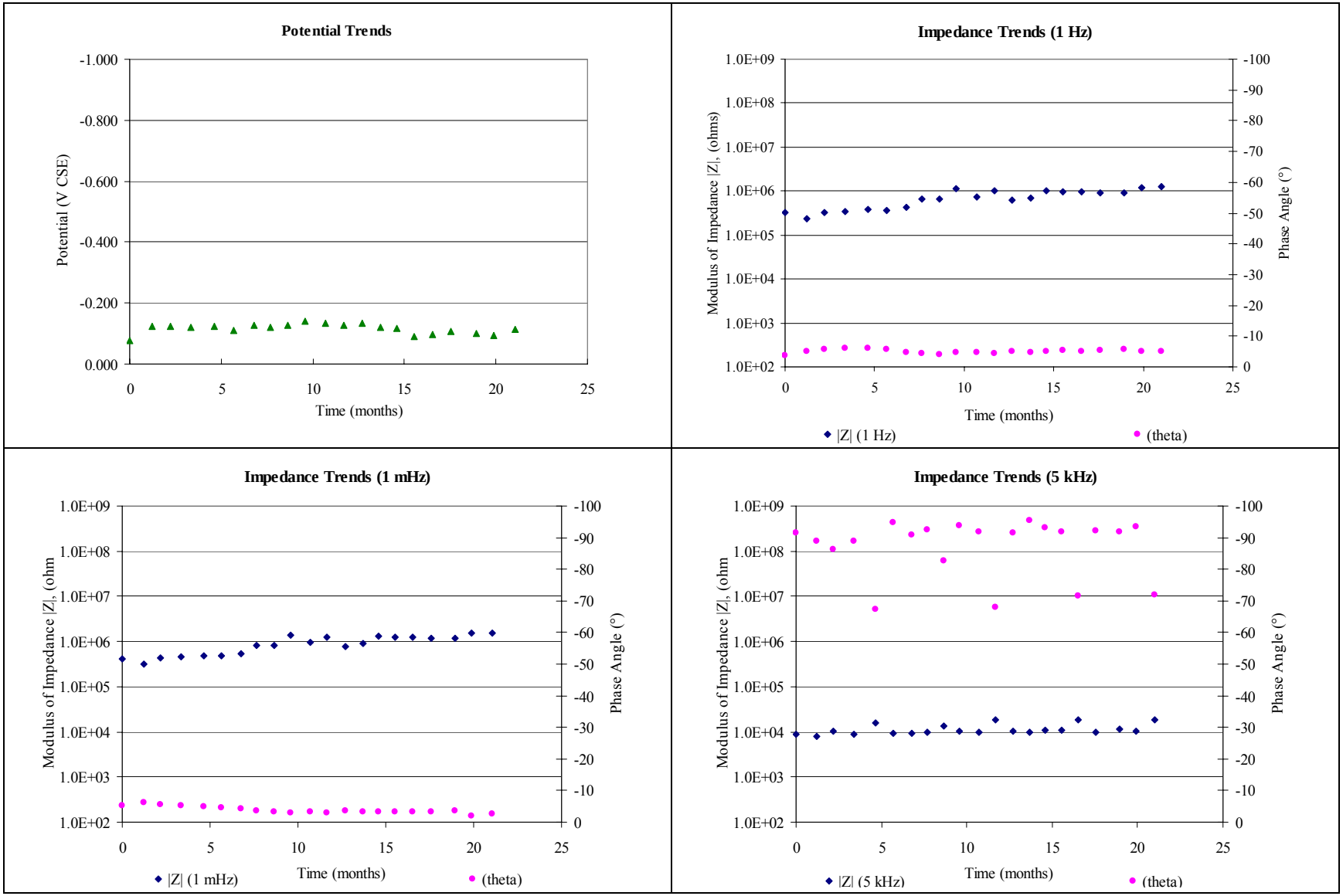

Figure B-7 Potential and Impedance Summary for Specimen 1001_C7

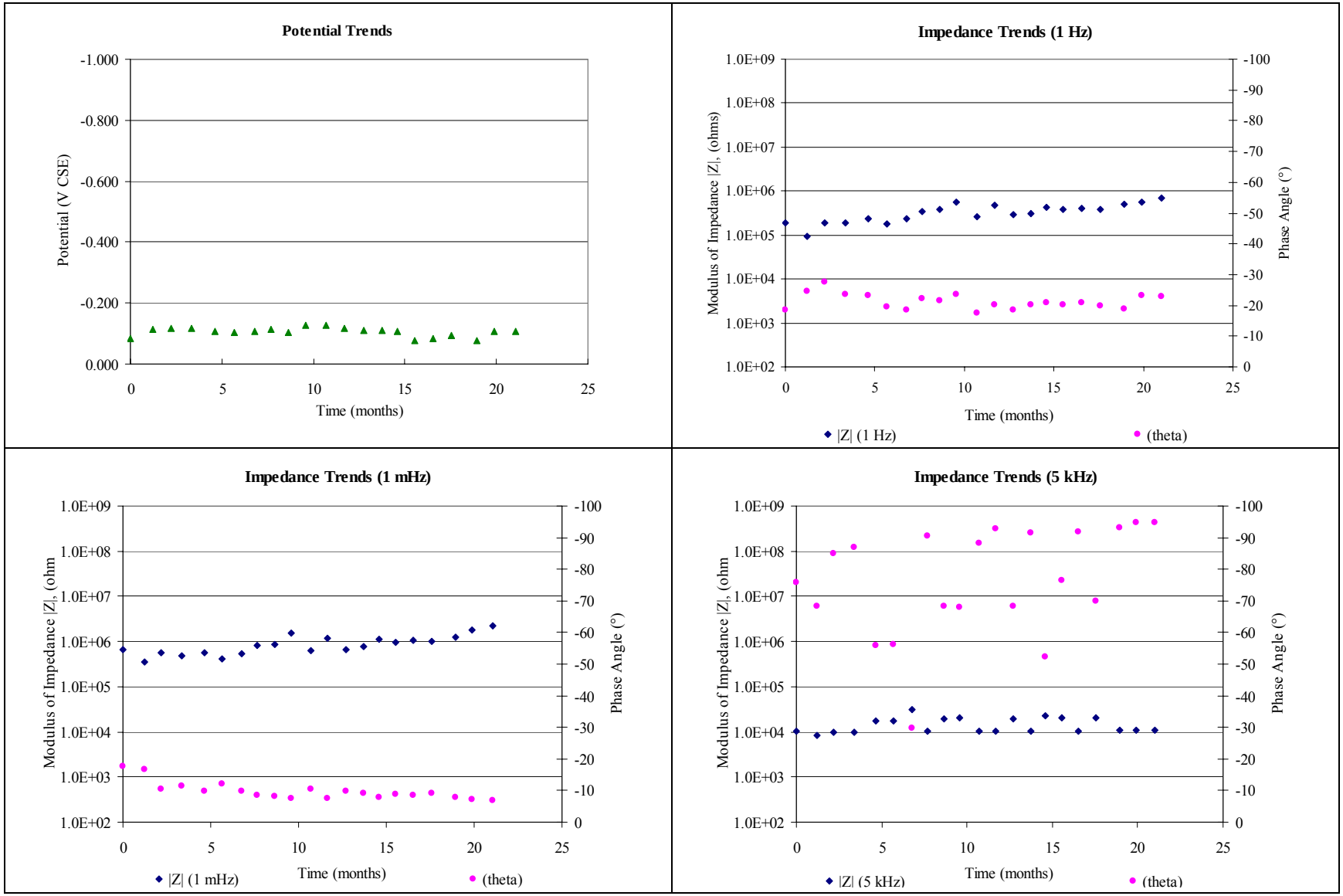

Figure B-8 Potential and Impedance Summary for Specimen 1001_C8

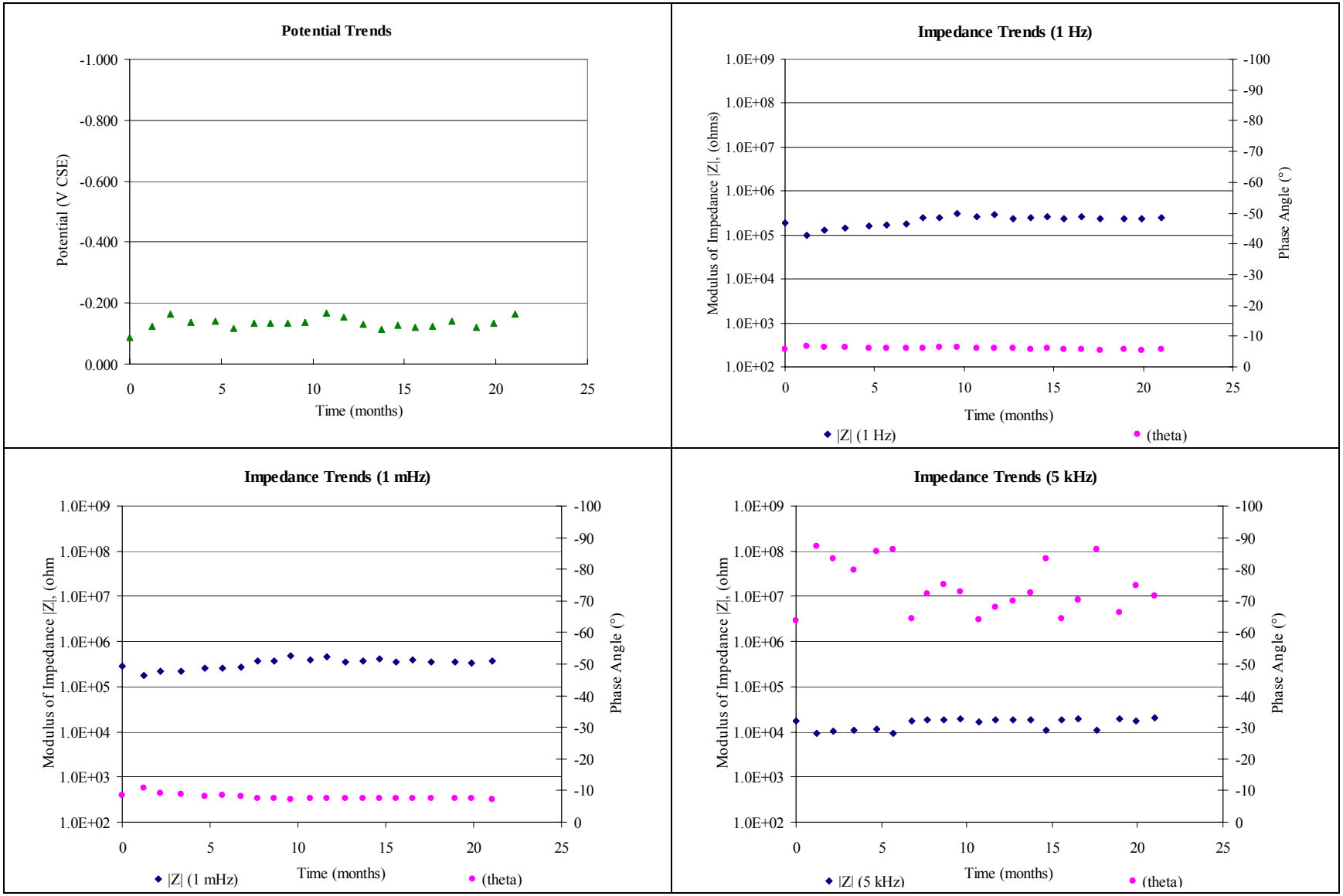

Figure B-9 Potential and Impedance Summary for Specimen 1001_C9

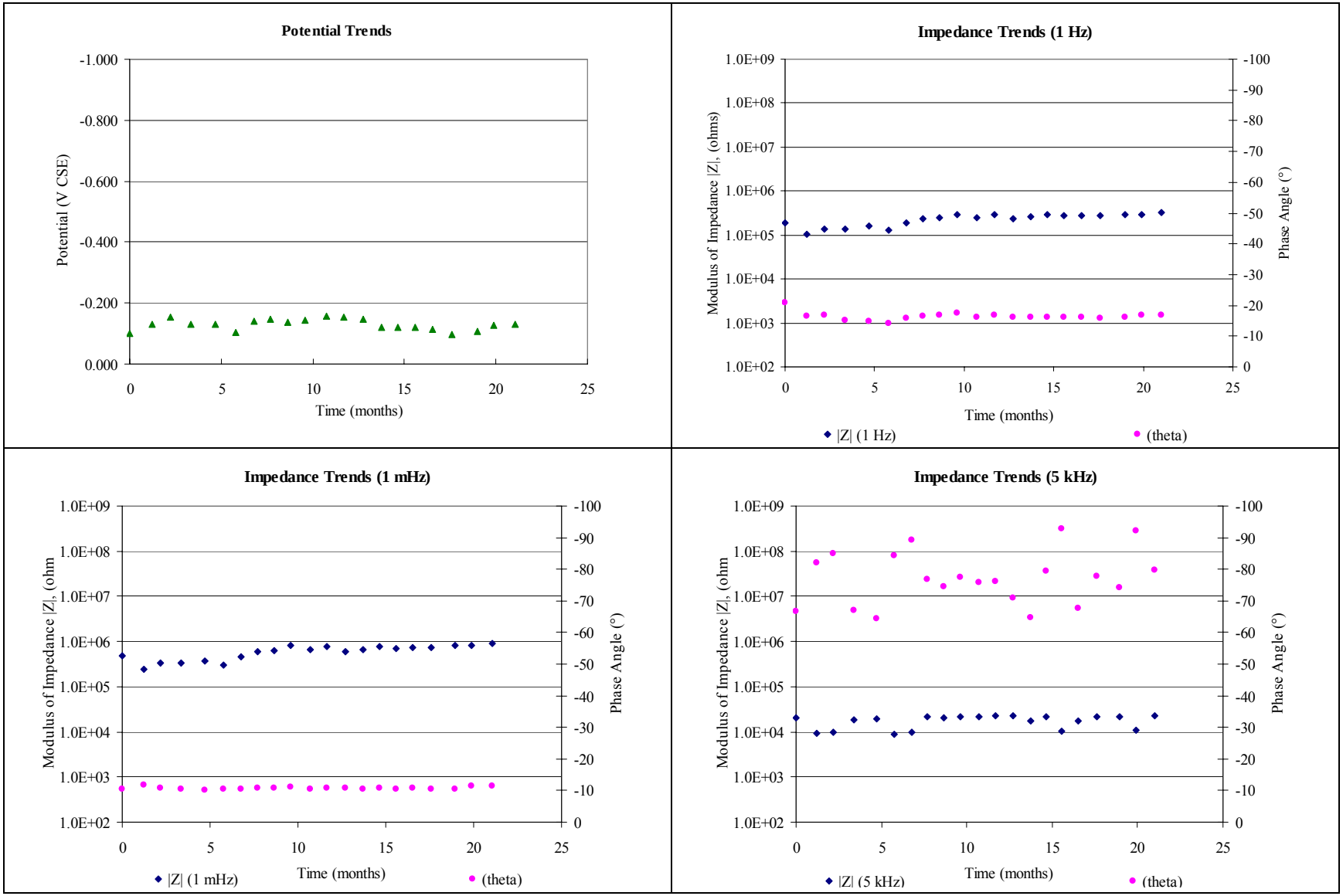

Figure B-10 Potential and Impedance Summary for Specimen 1001_C10

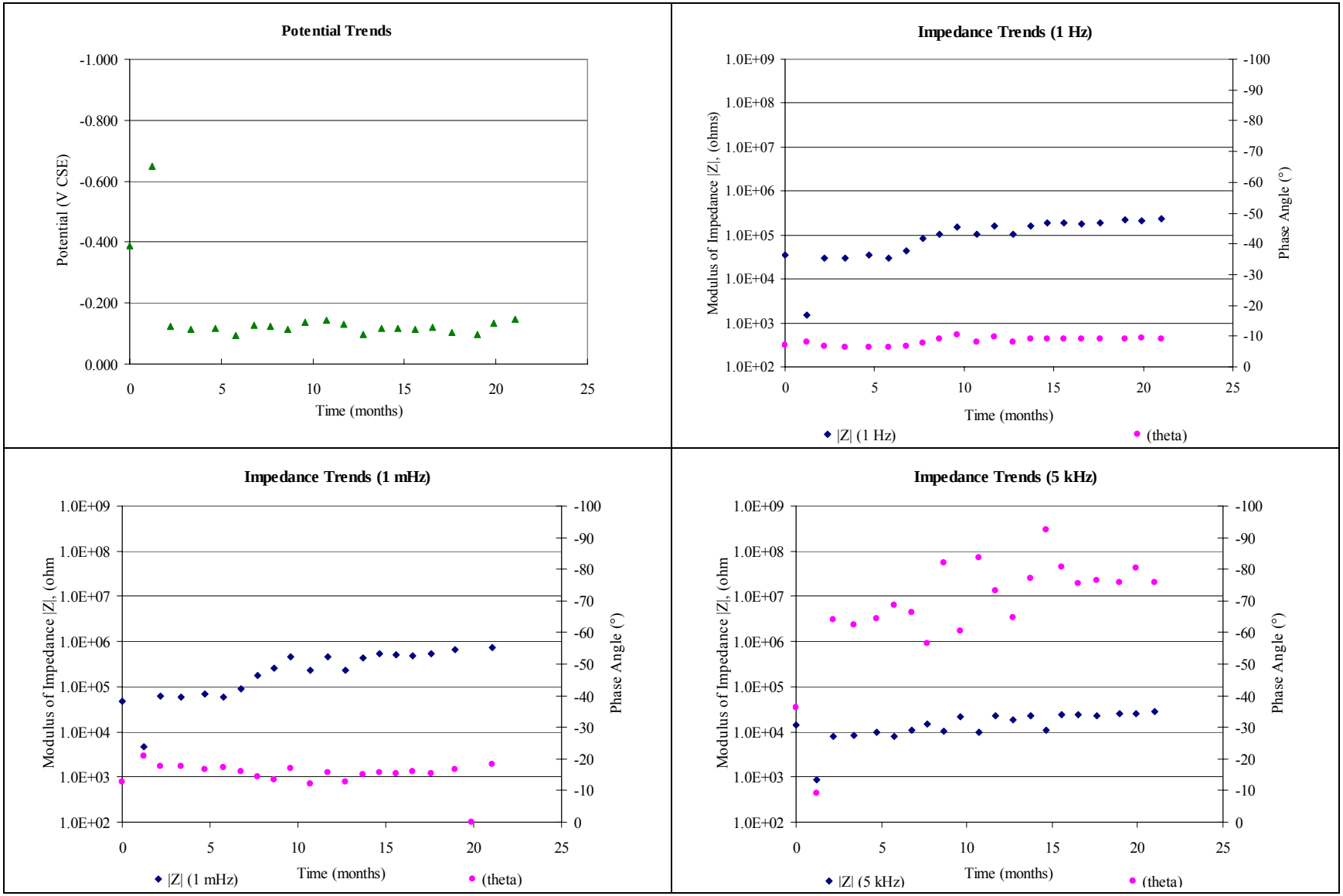

Figure B-11 Potential and Impedance Summary for Specimen 1001_C11

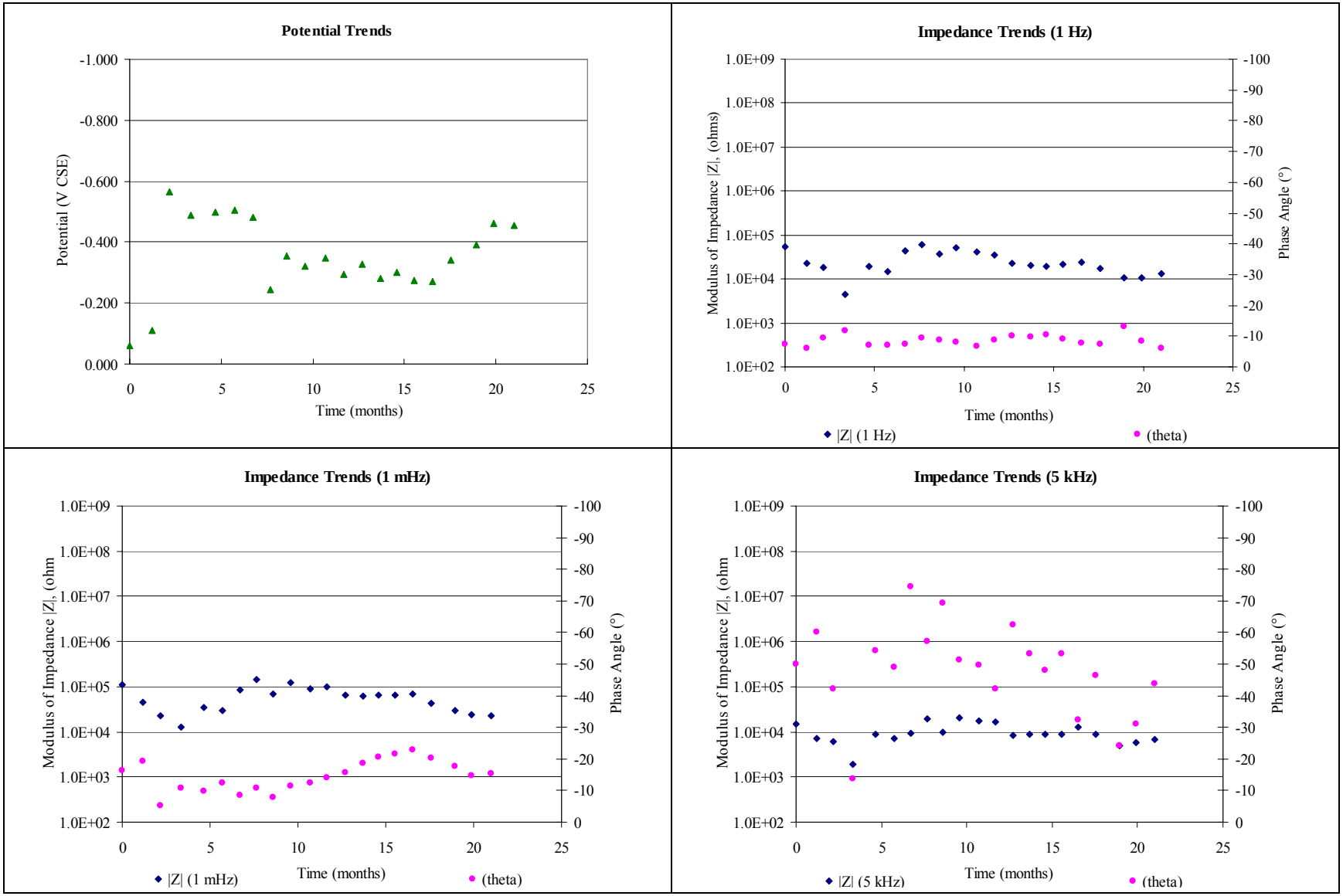

Figure B-12 Potential and Impedance Summary for Specimen 1001_CR1

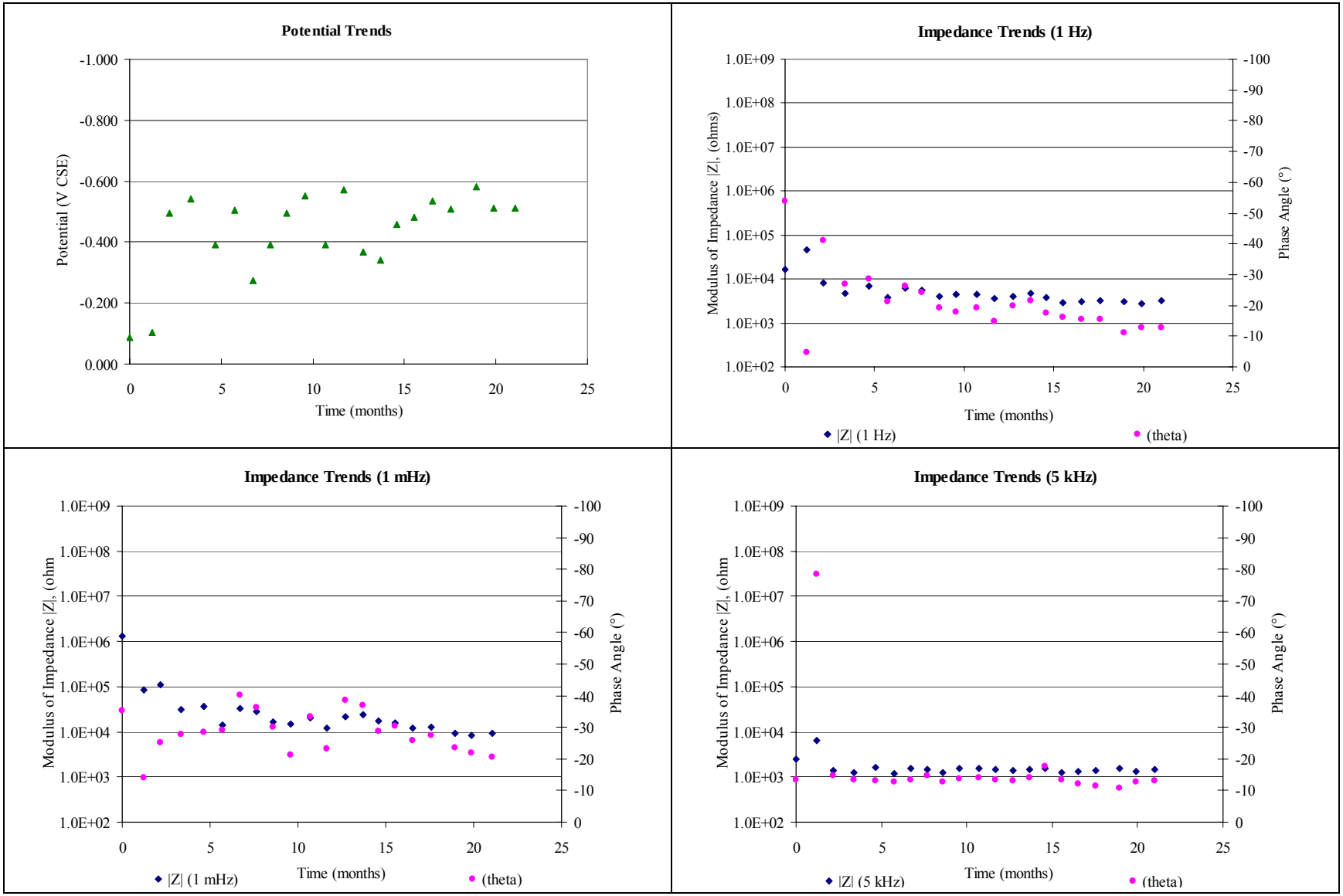

Figure B-13 Potential and Impedance Summary for Specimen 1001_CR2

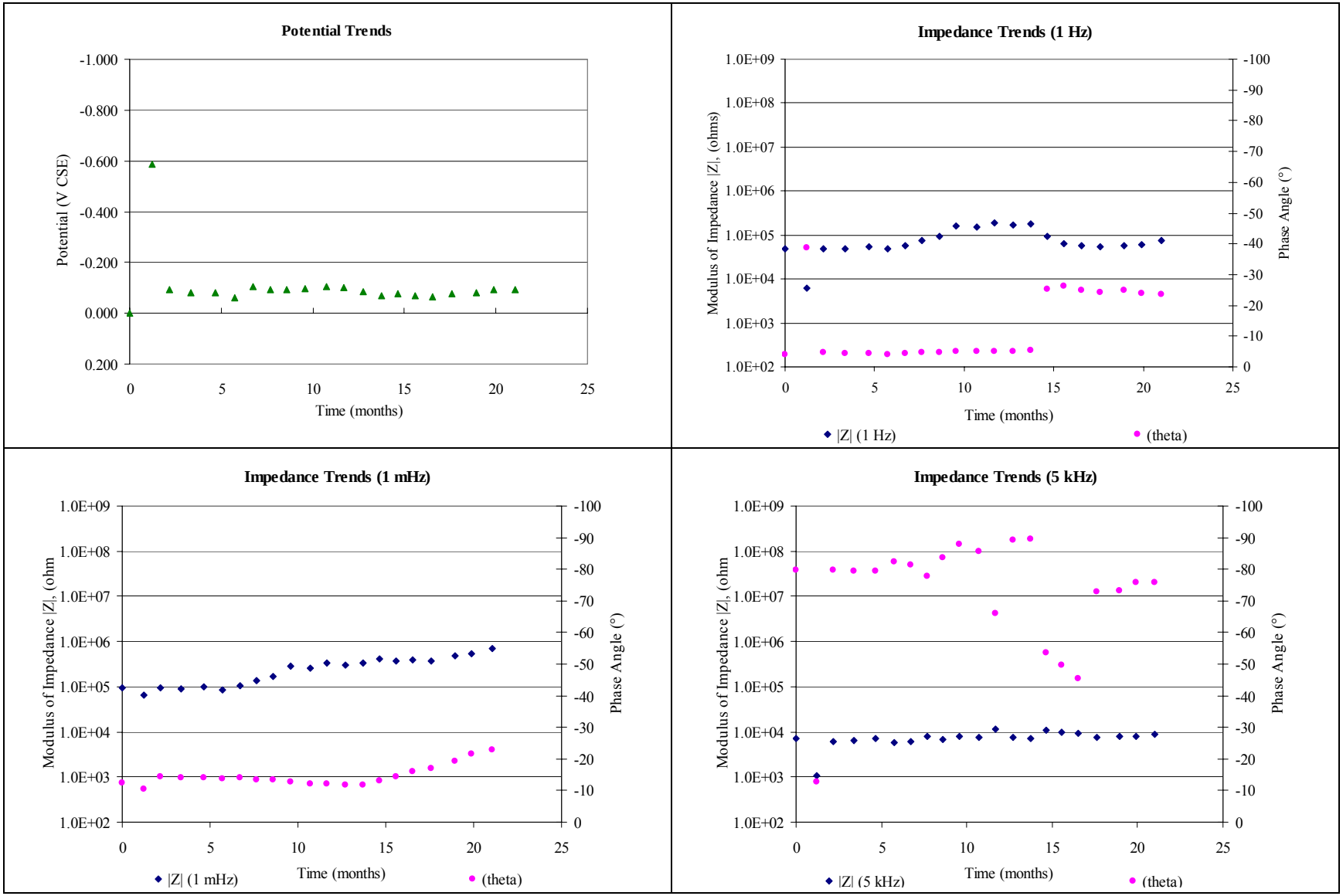

Figure B-14 Potential and Impedance Summary for Specimen 1001_CR3

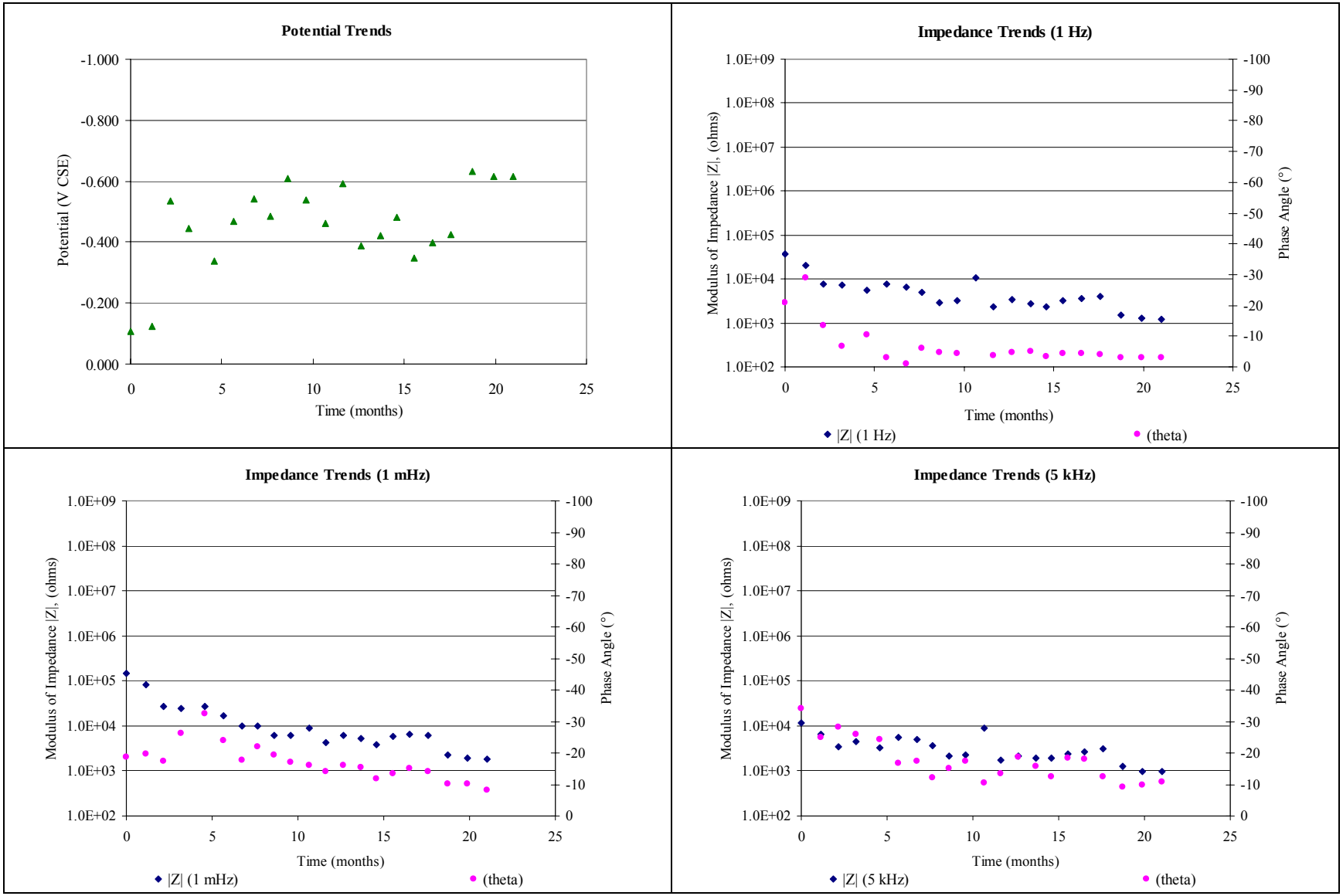

Figure B-15 Potential and Impedance Summary for Specimen 1004_3_C1

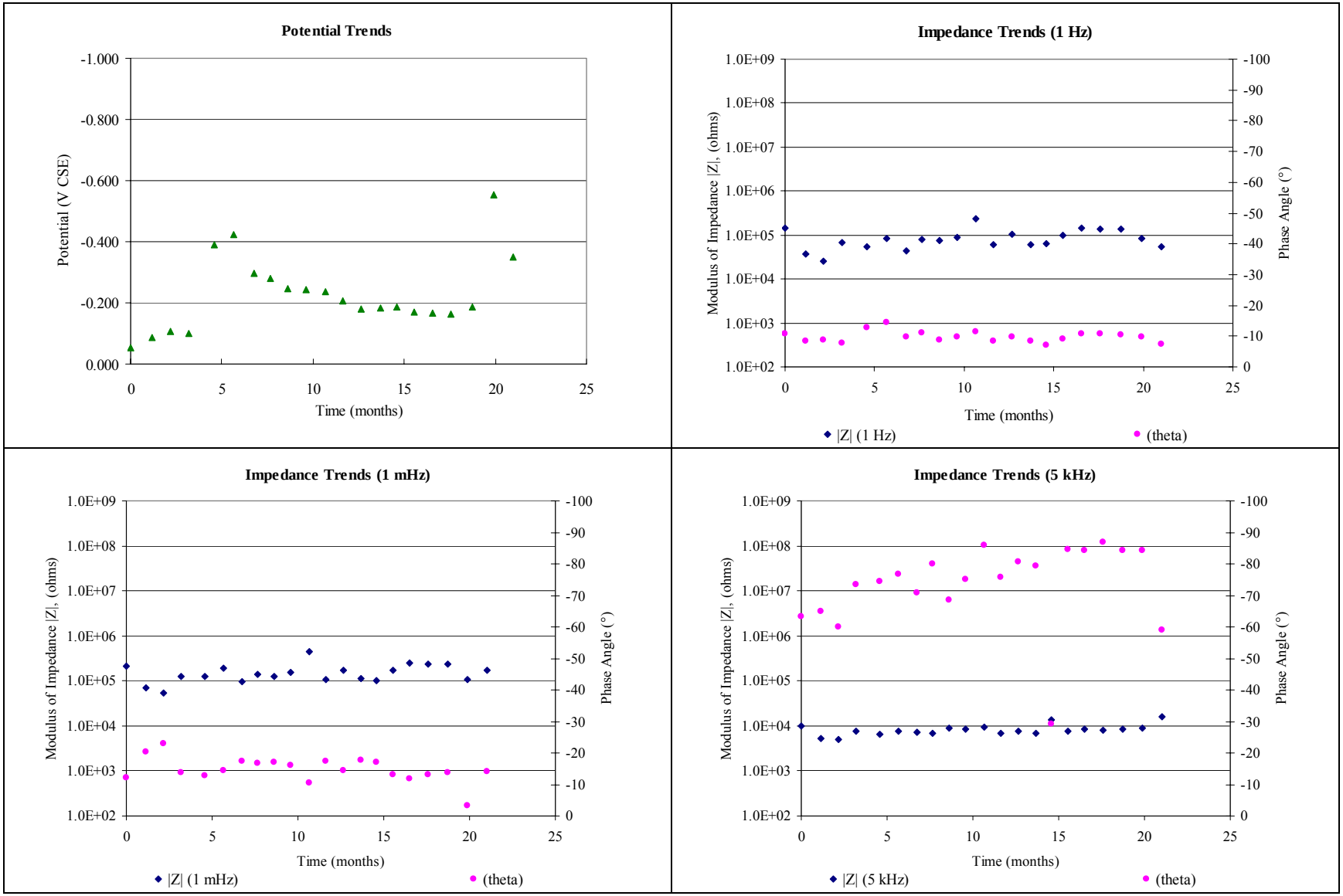

Figure B-16 Potential and Impedance Summary for Specimen 1004_3_C2

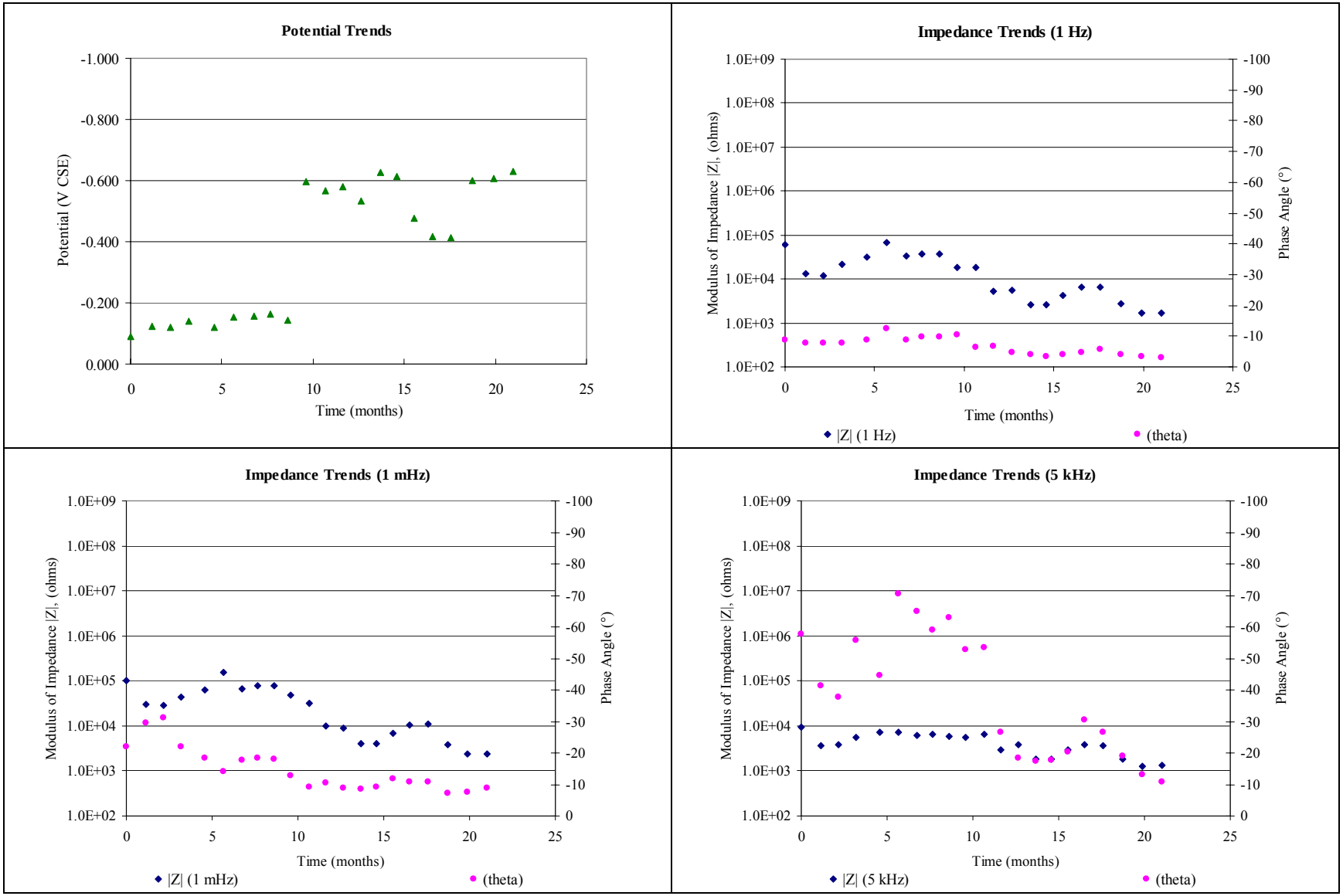

Figure B-17 Potential and Impedance Summary for Specimen 1004_3_C3

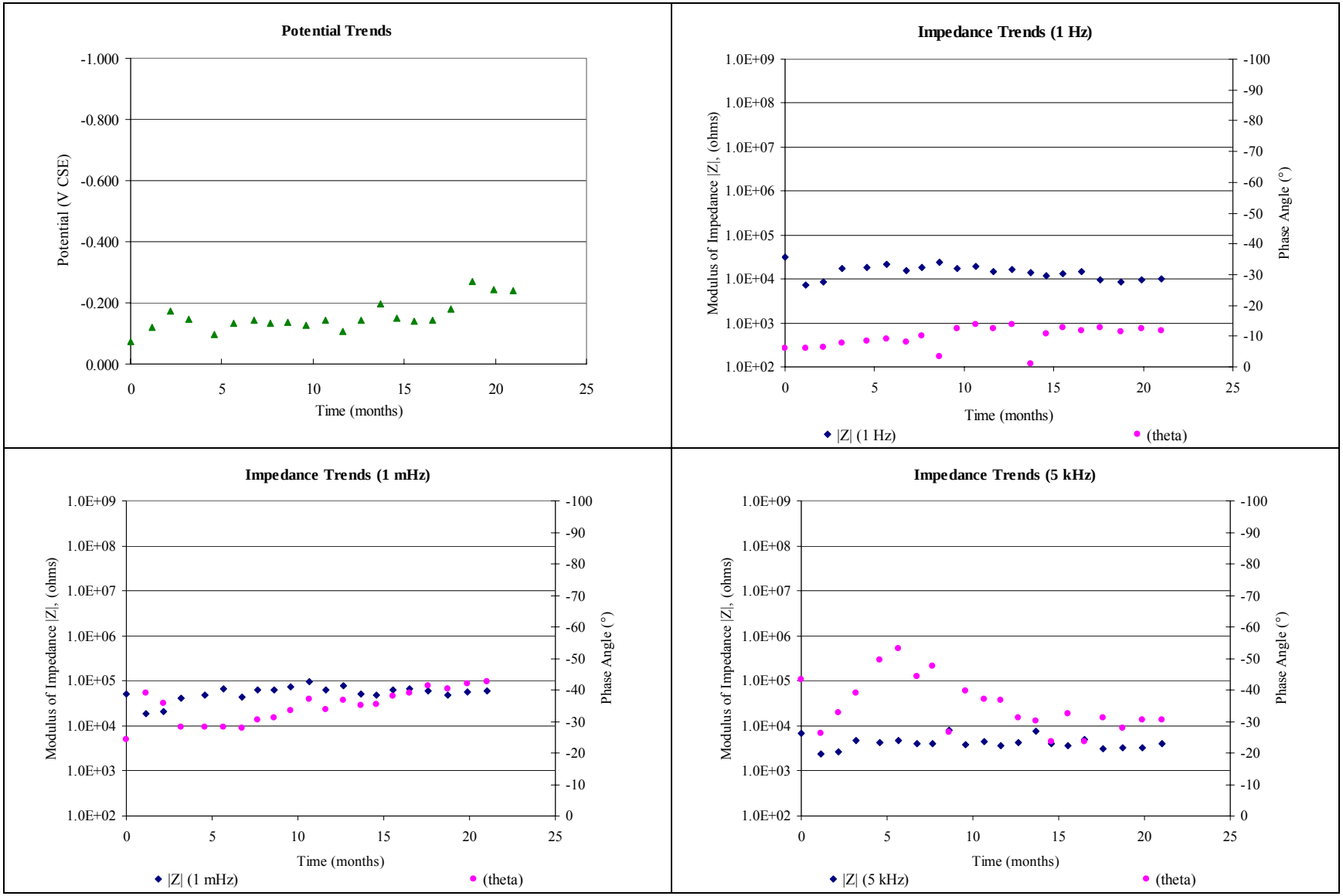

Figure B-18 Potential and Impedance Summary for Specimen 1004_3_C4

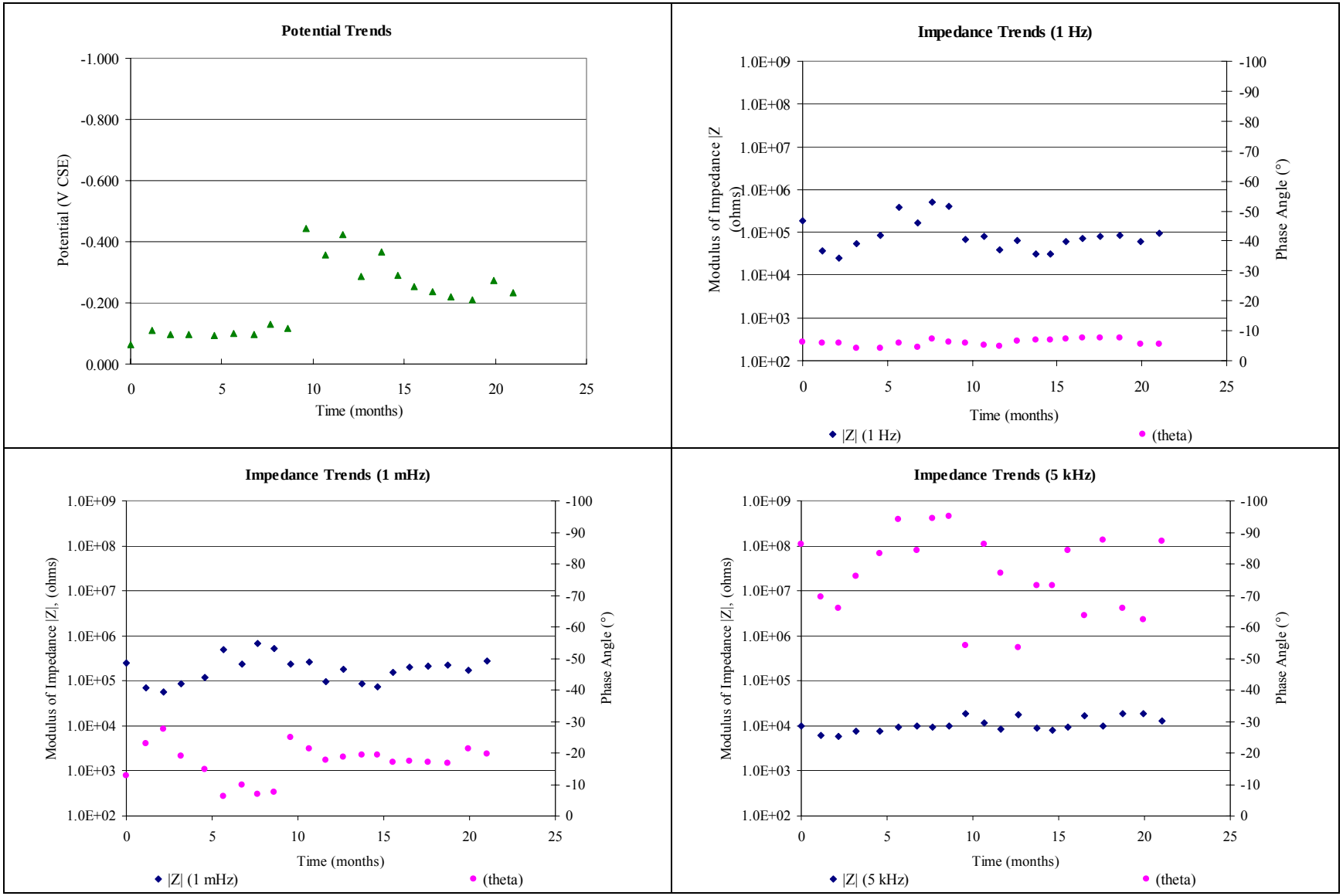

Figure B-19 Potential and Impedance Summary for Specimen 1004_3_C5

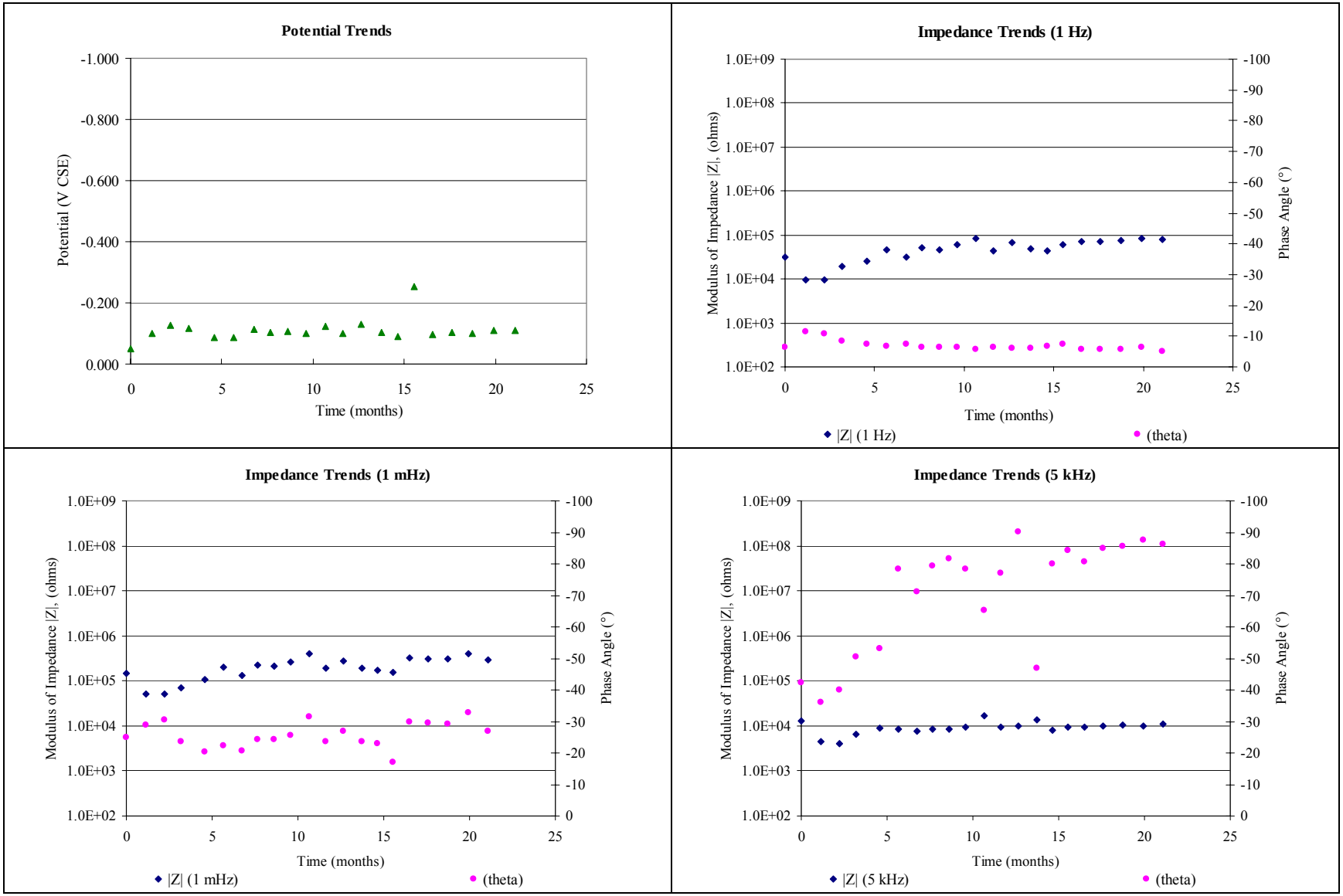

Figure B-20 Potential and Impedance Summary for Specimen 1004_3_C6

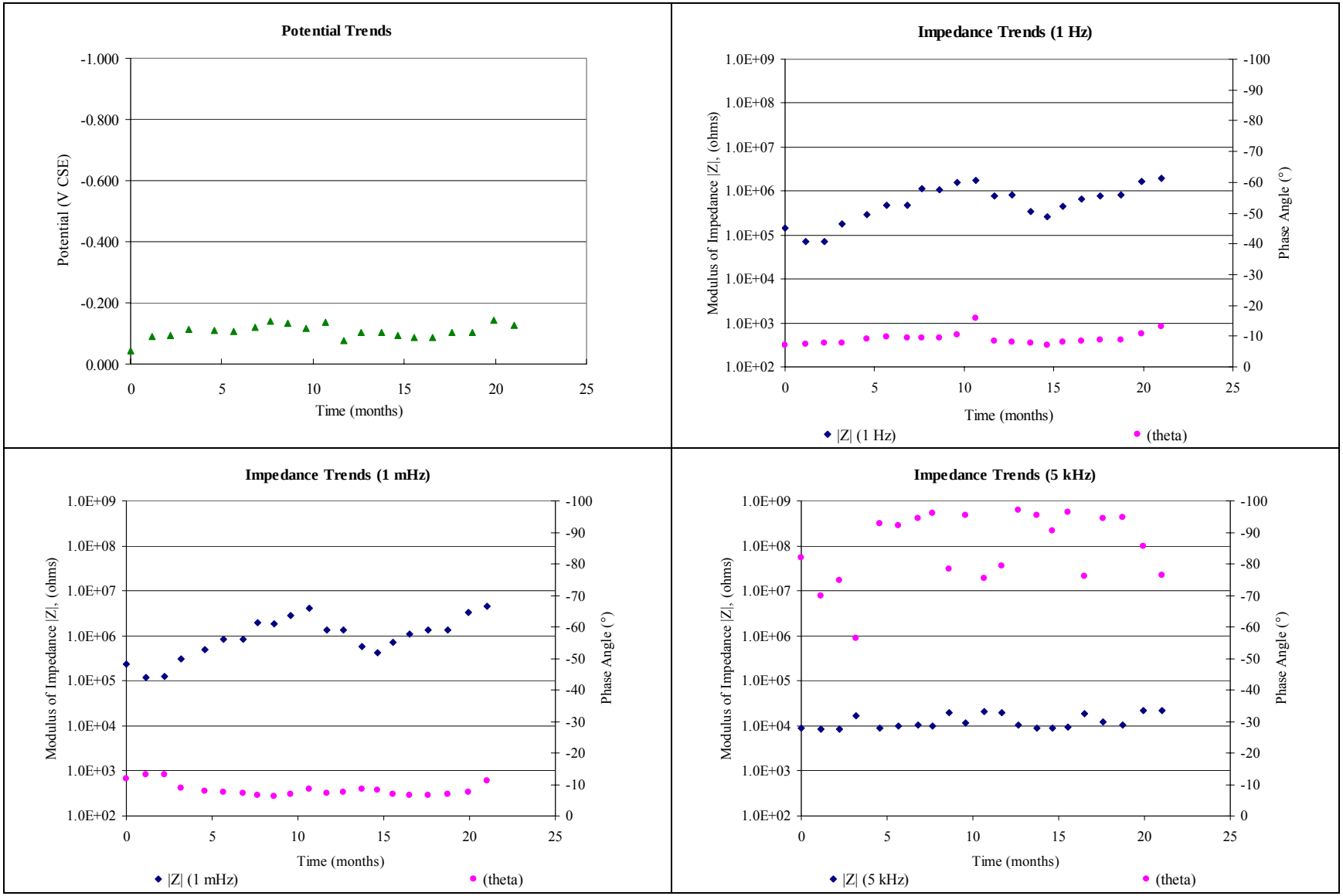

Figure B-21 Potential and Impedance Summary for Specimen 1004_3_C7

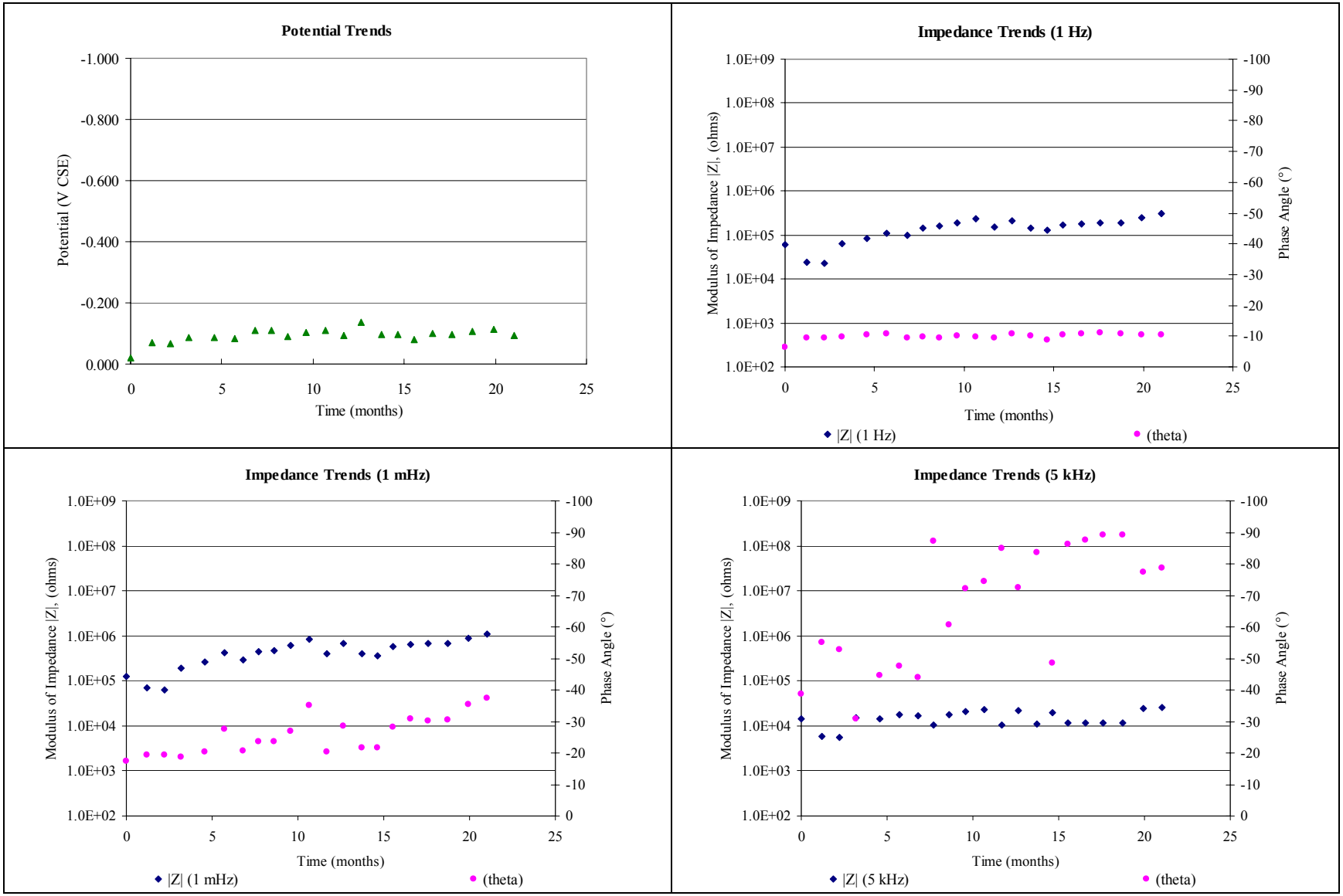

Figure B-22 Potential and Impedance Summary for Specimen 1004_3_C8

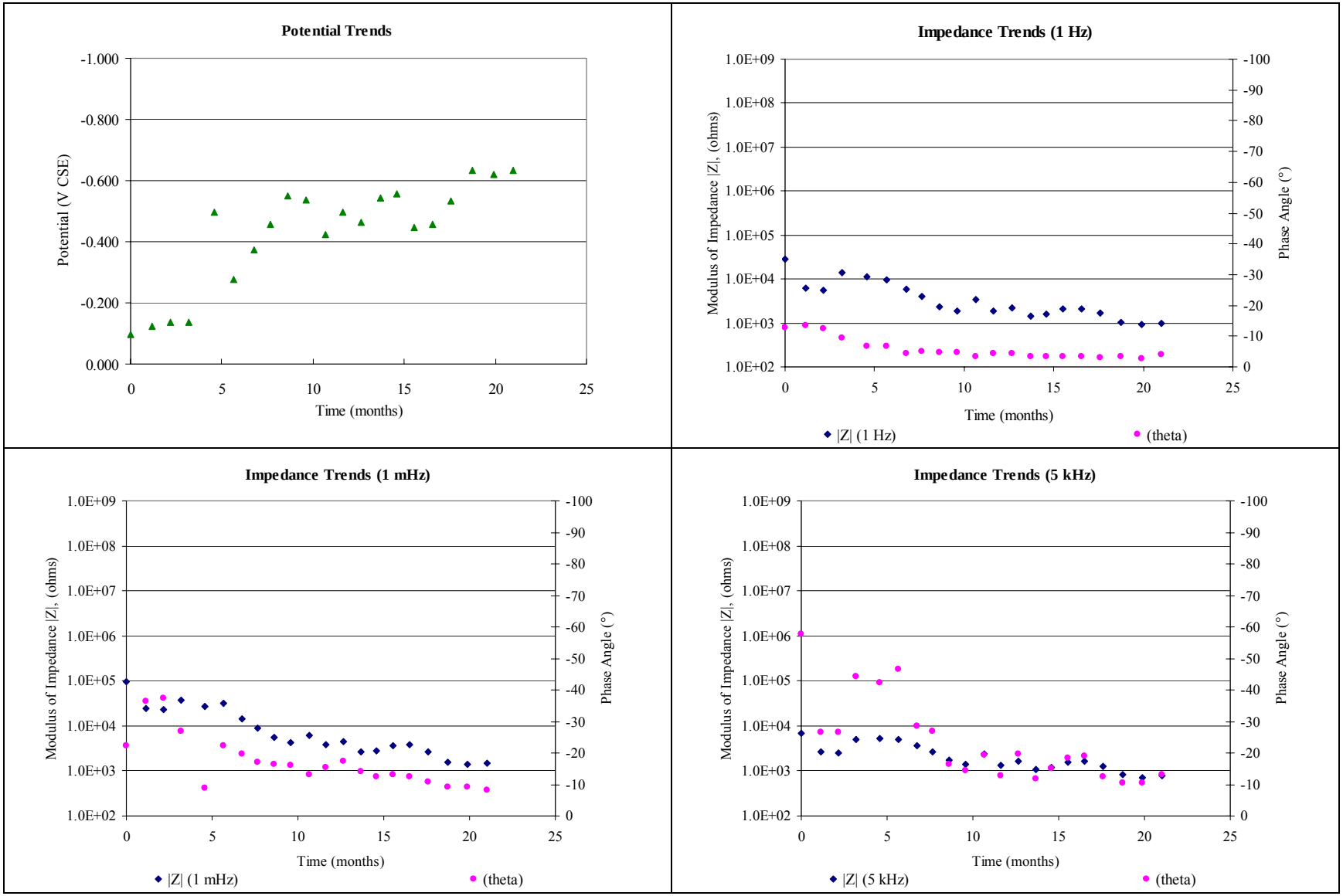

Figure B-23 Potential and Impedance Summary for Specimen 1004_3_C9

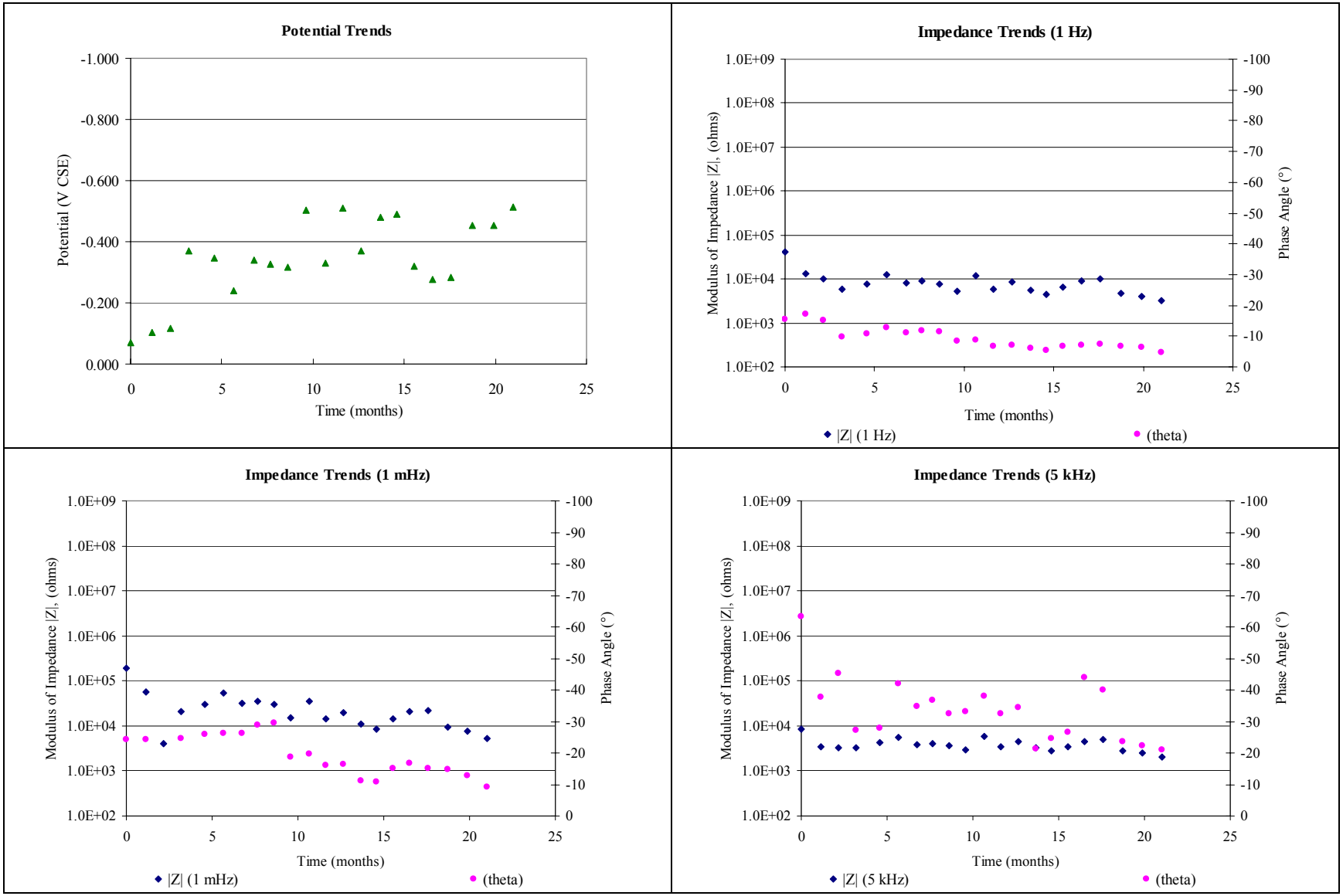

Figure B-24 Potential and Impedance Summary for Specimen 1004_3_C10

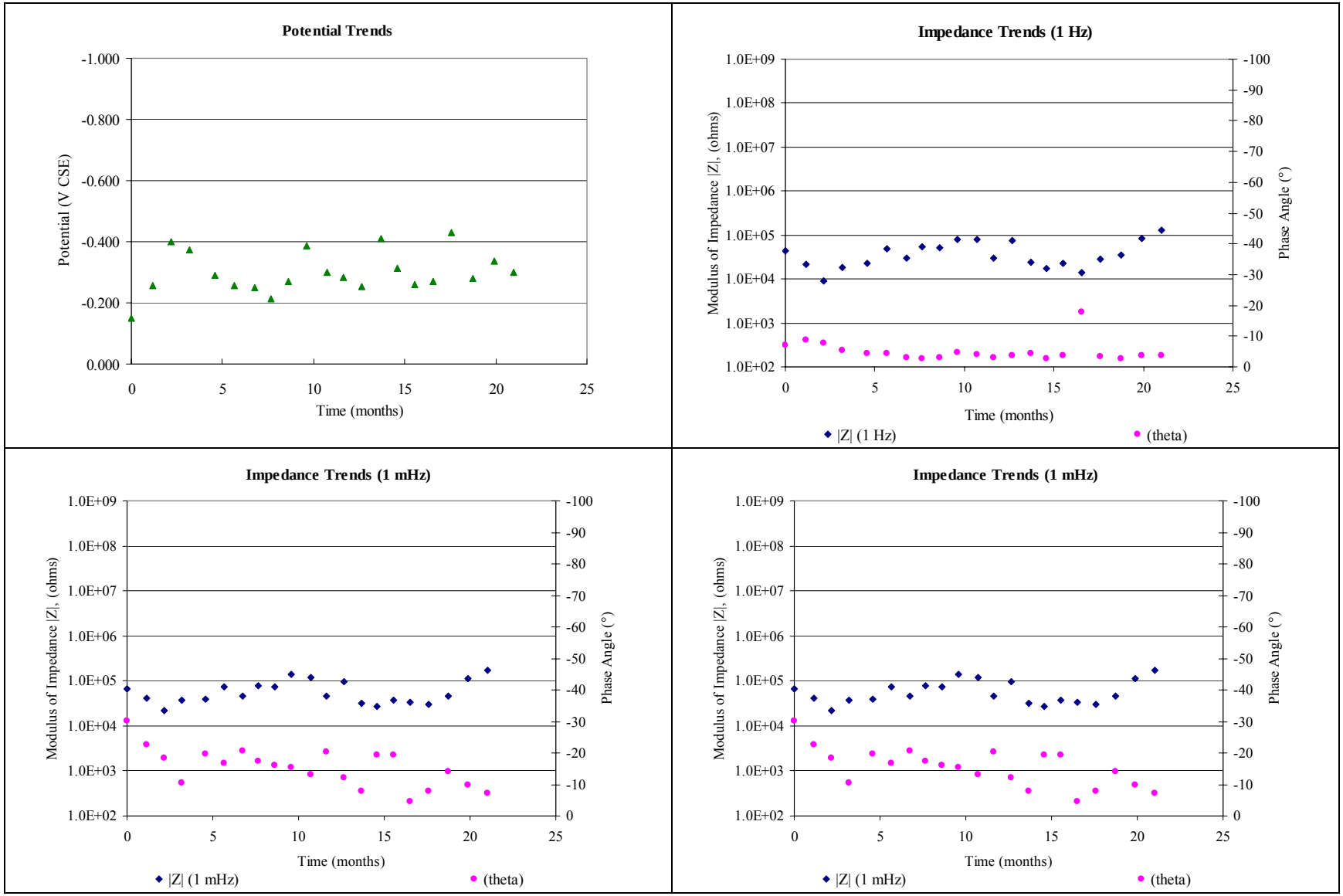

Figure B-25 Potential and Impedance Summary for Specimen 1004_3_C11

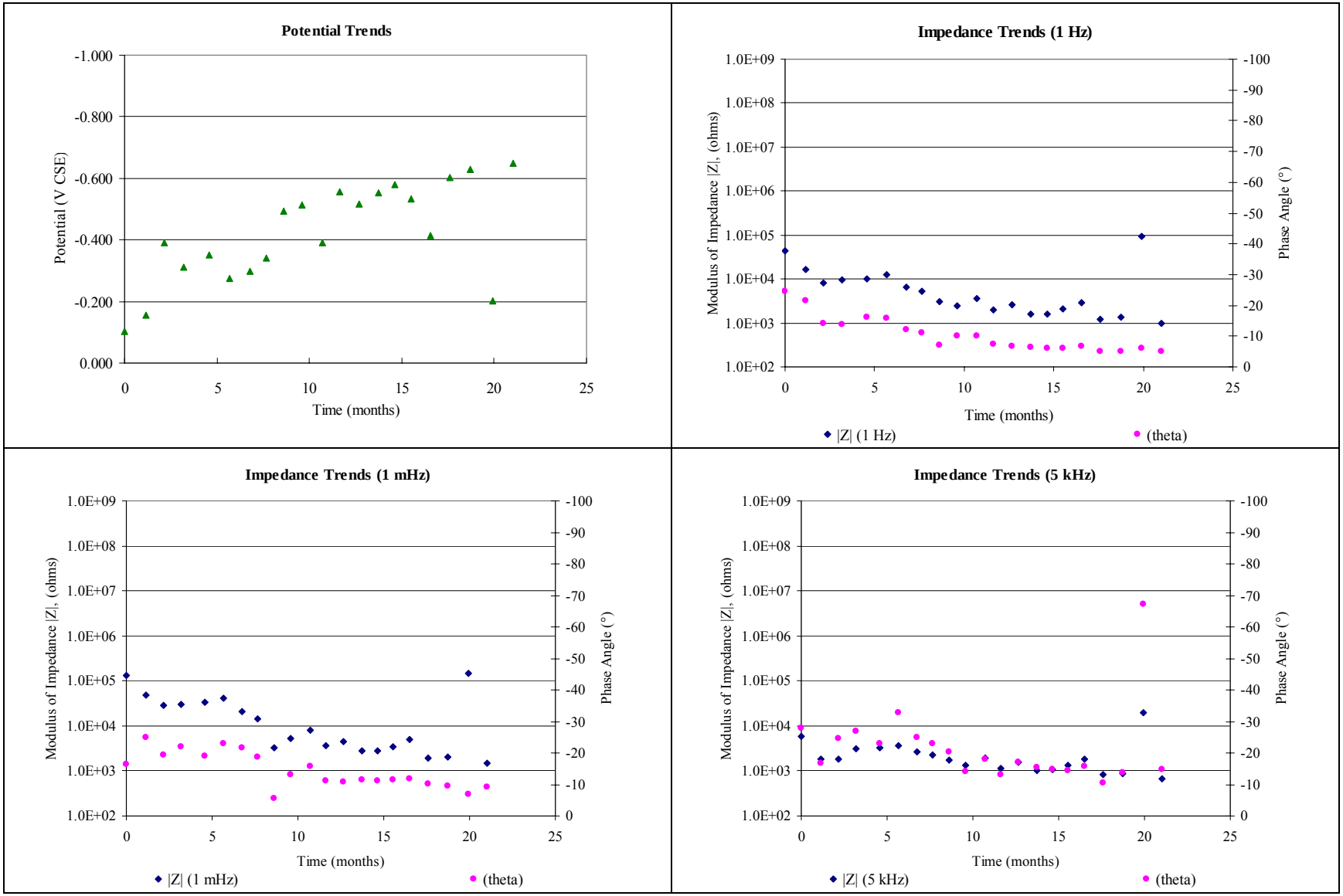

Figure B-26 Potential and Impedance Summary for Specimen 1004_3_C12

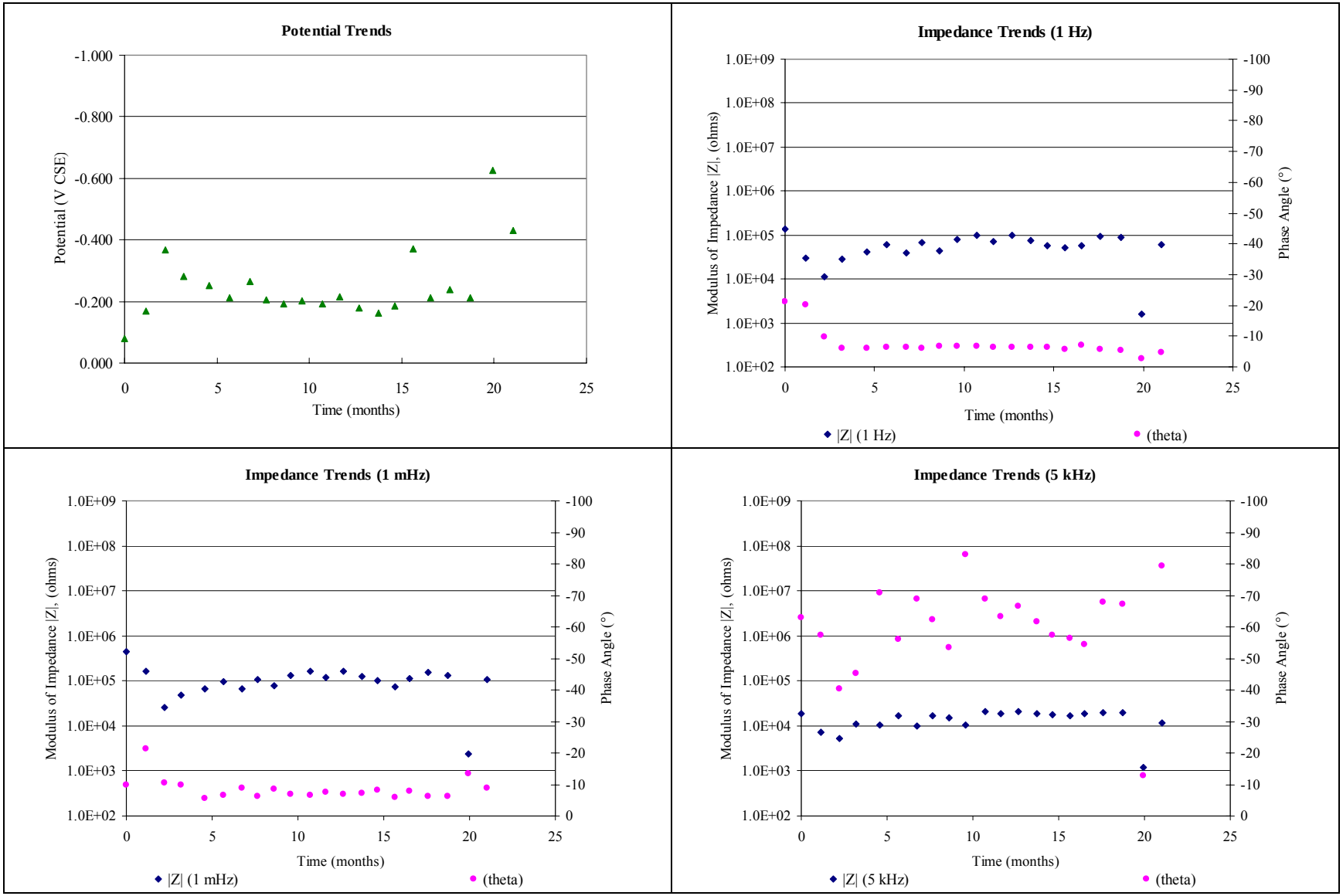

Figure B-27 Potential and Impedance Summary for Specimen 1004_3_CR2

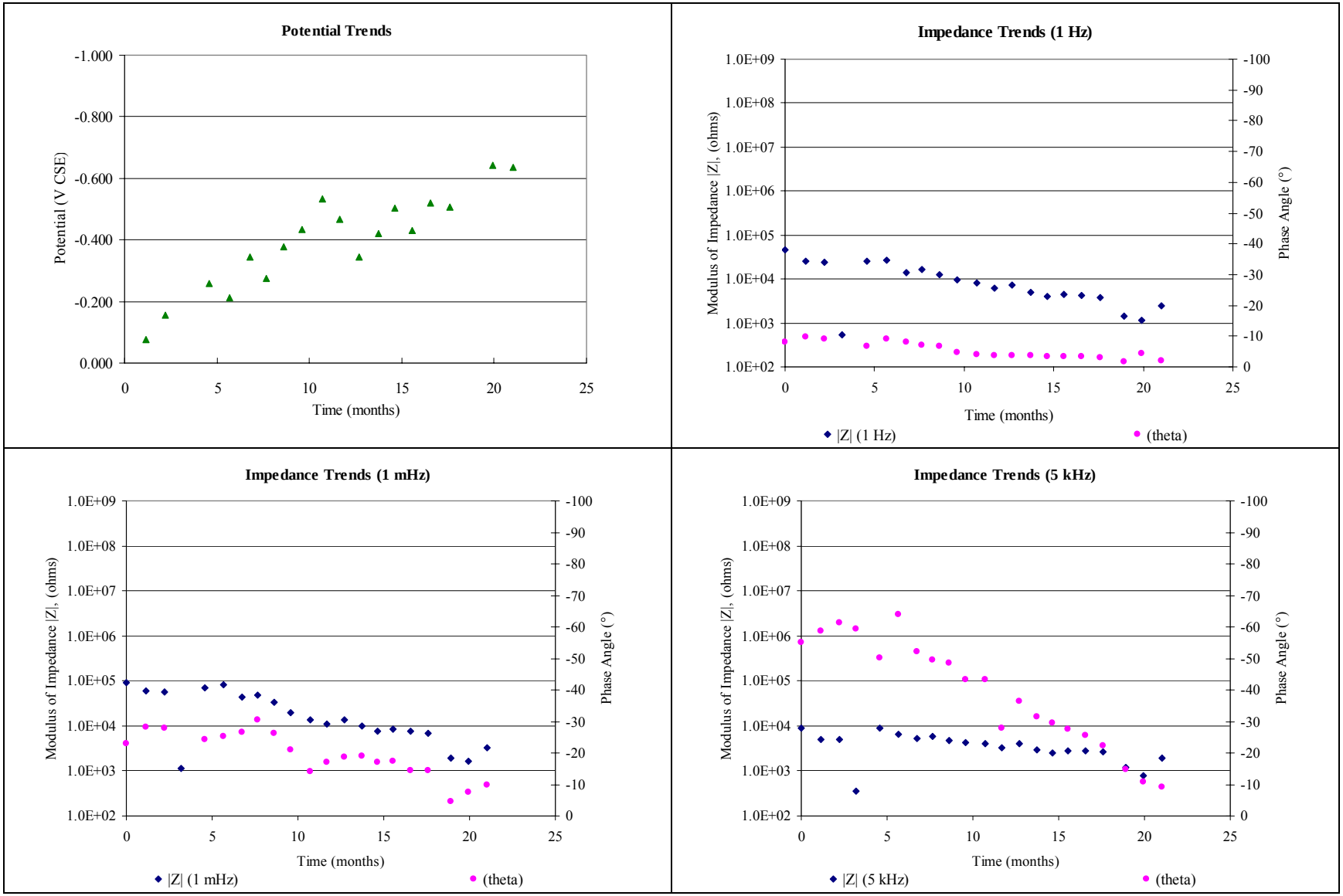

Figure B-28 Potential and Impedance Summary for Specimen 1004_3_CR3

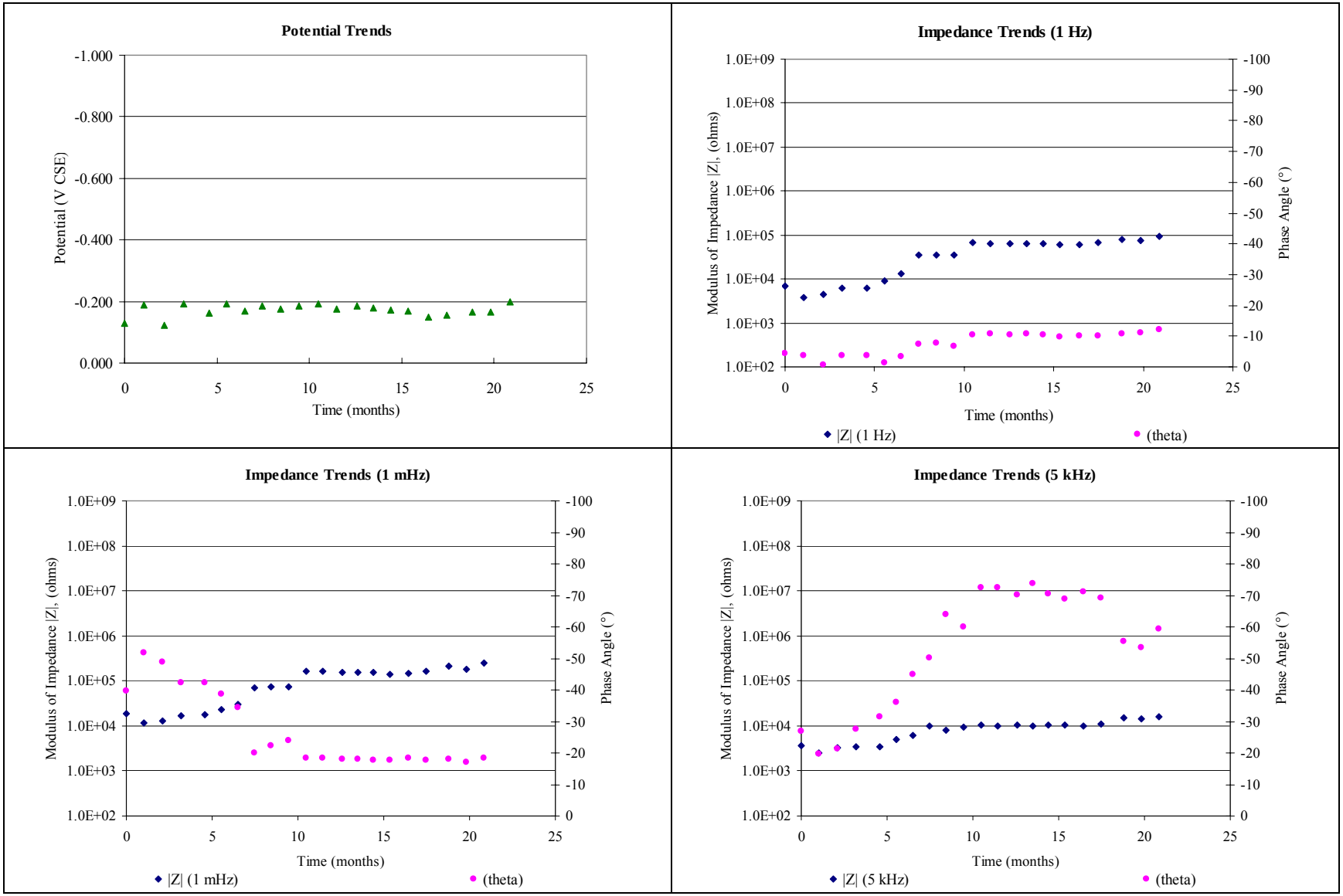

Figure B-29 Potential and Impedance Summary for Specimen 1004_6_C1

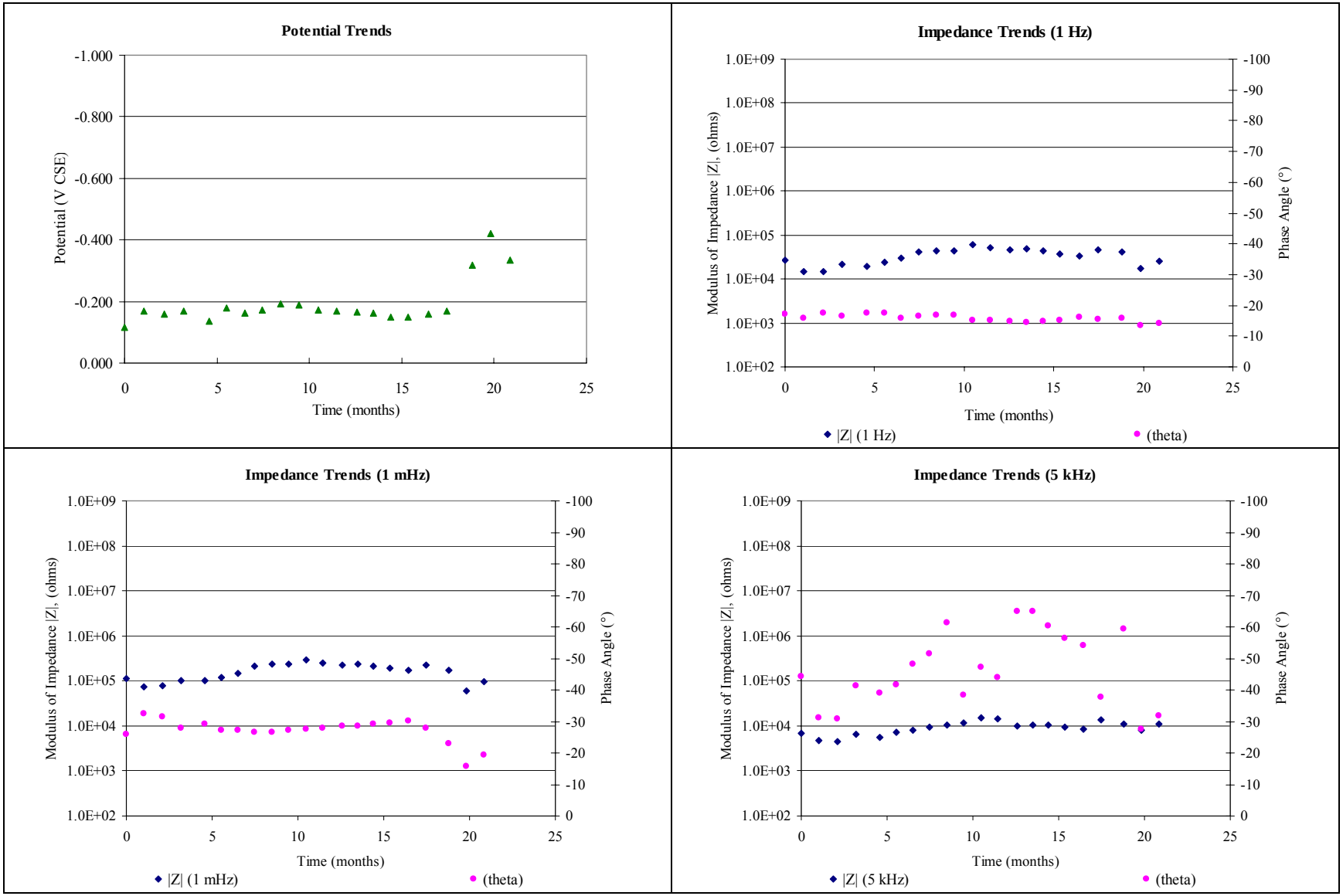

Figure B-30 Potential and Impedance Summary for Specimen 1004_6_C2

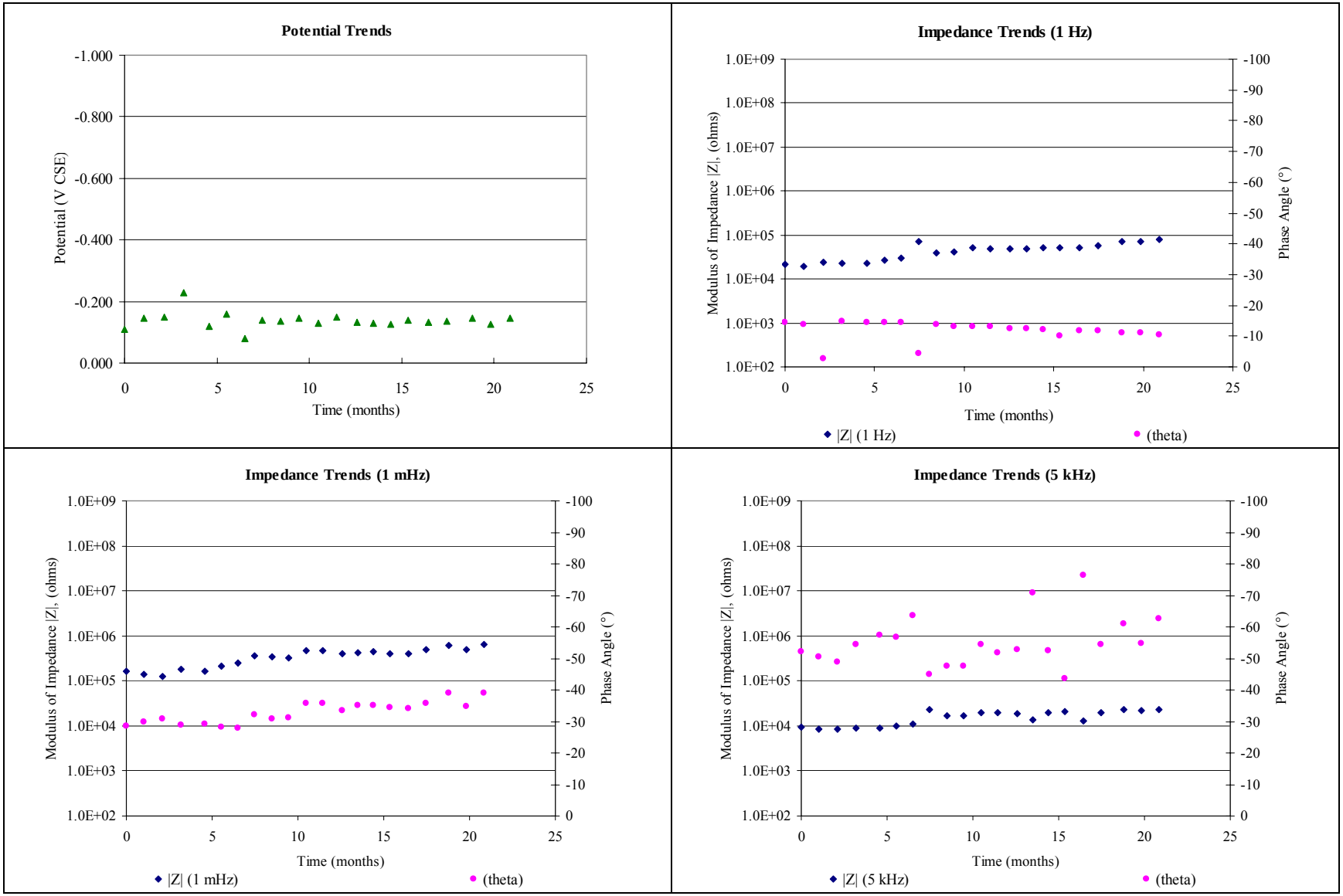

Figure B-31 Potential and Impedance Summary for Specimen 1004_6_C3

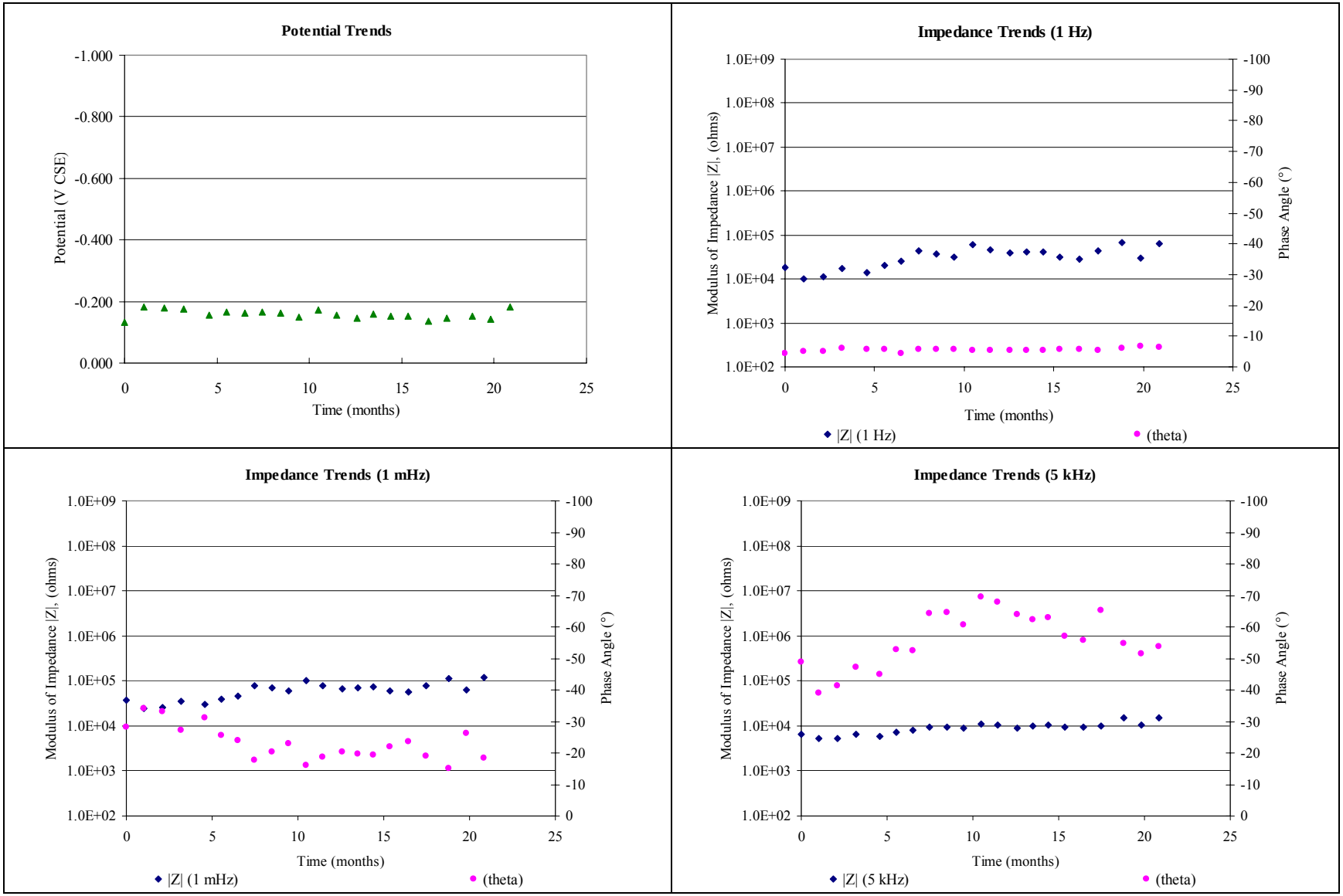

Figure B-32 Potential and Impedance Summary for Specimen 1004_6_C4

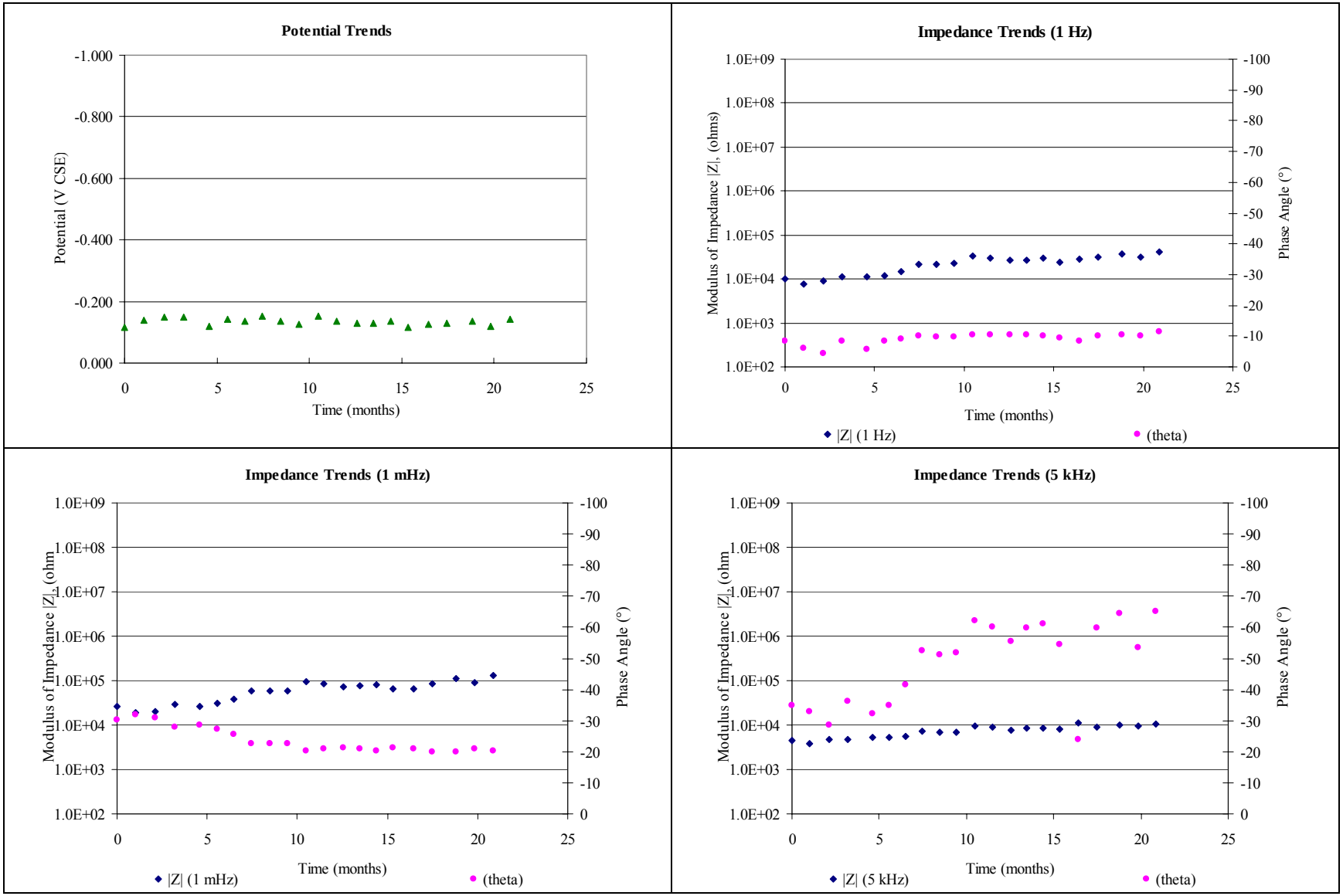

Figure B-33 Potential and Impedance Summary for Specimen 1004_6_C5

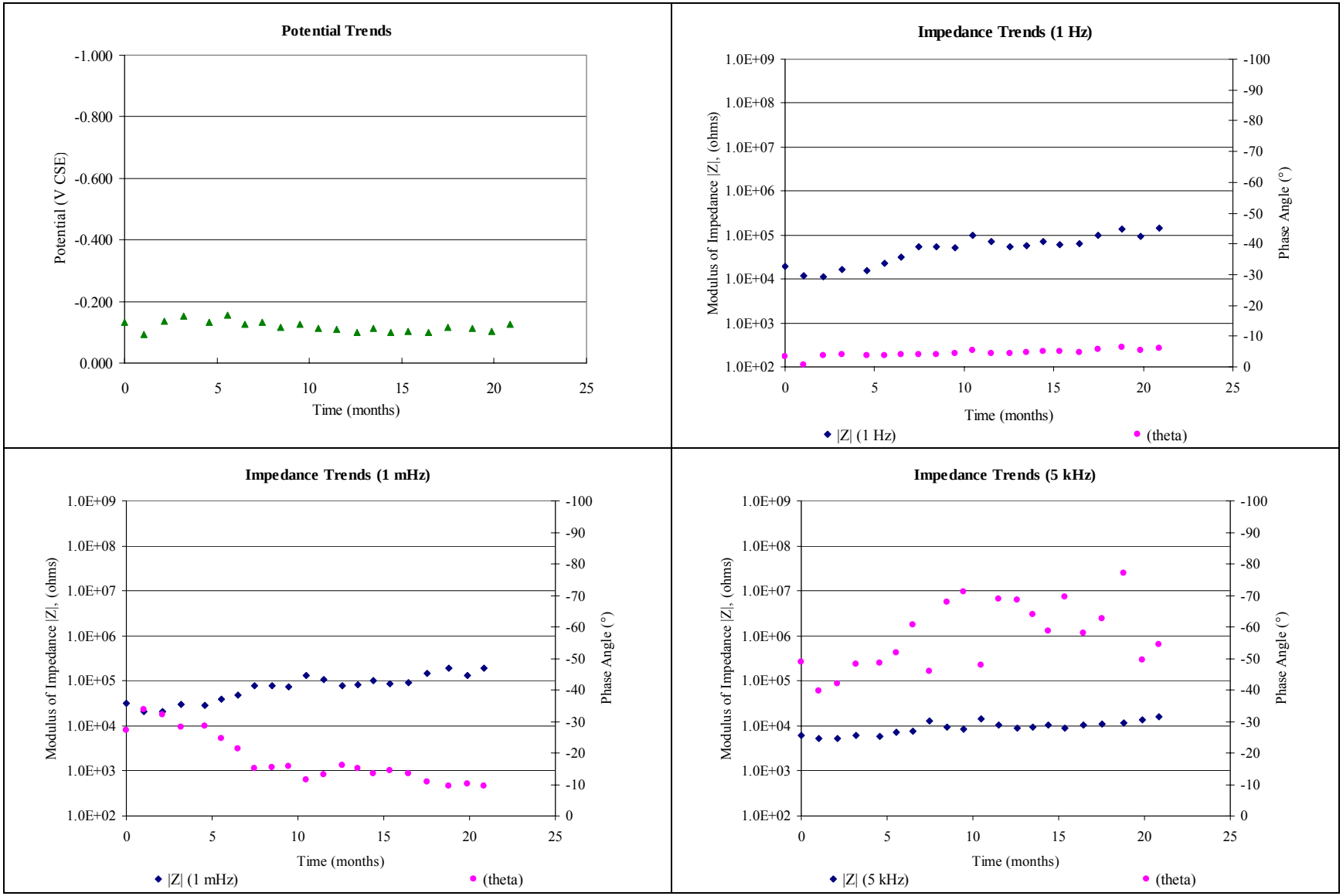

Figure B-34 Potential and Impedance Summary for Specimen 1004_6_C6

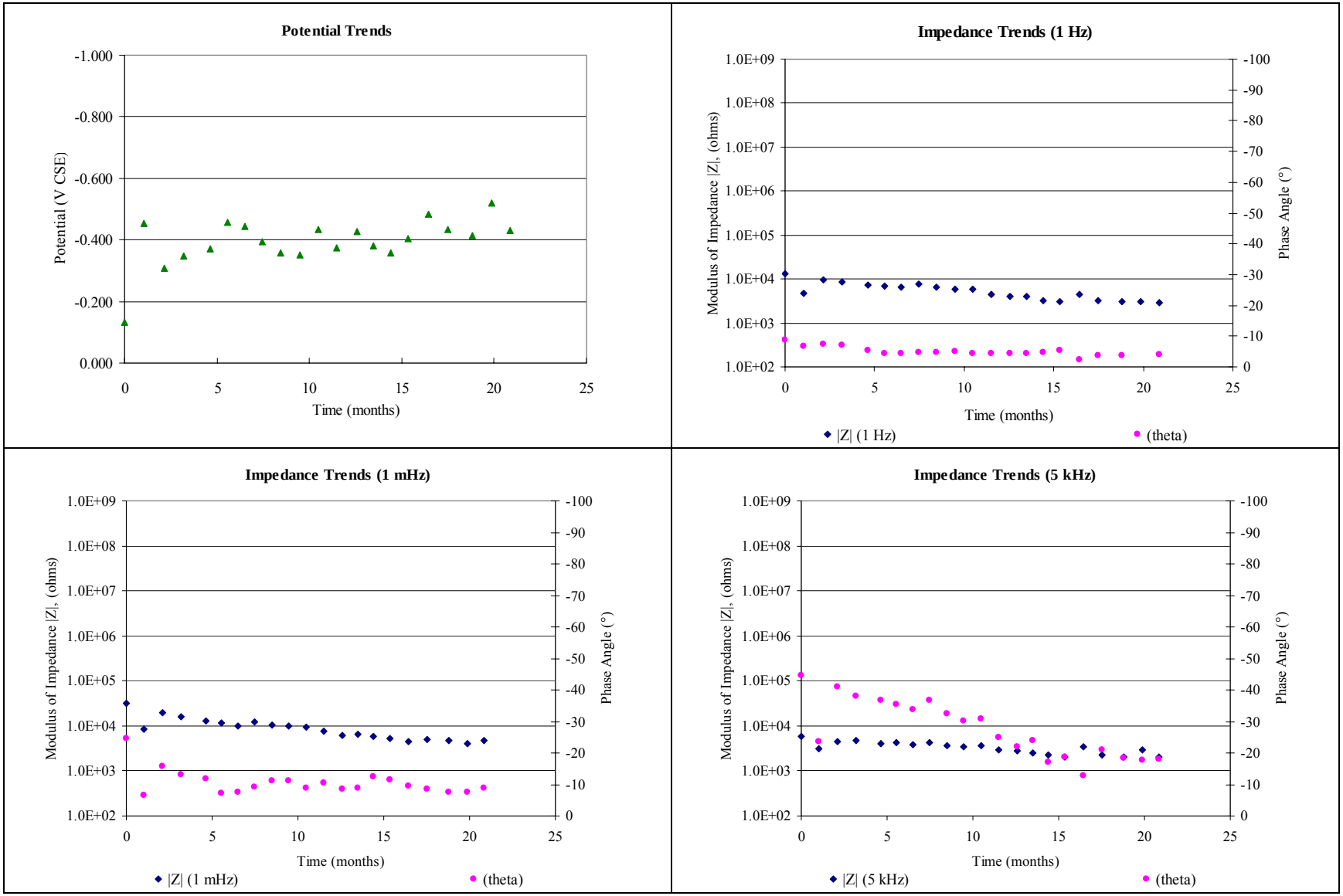

Figure B-35 Potential and Impedance Summary for Specimen 1004_6_C7

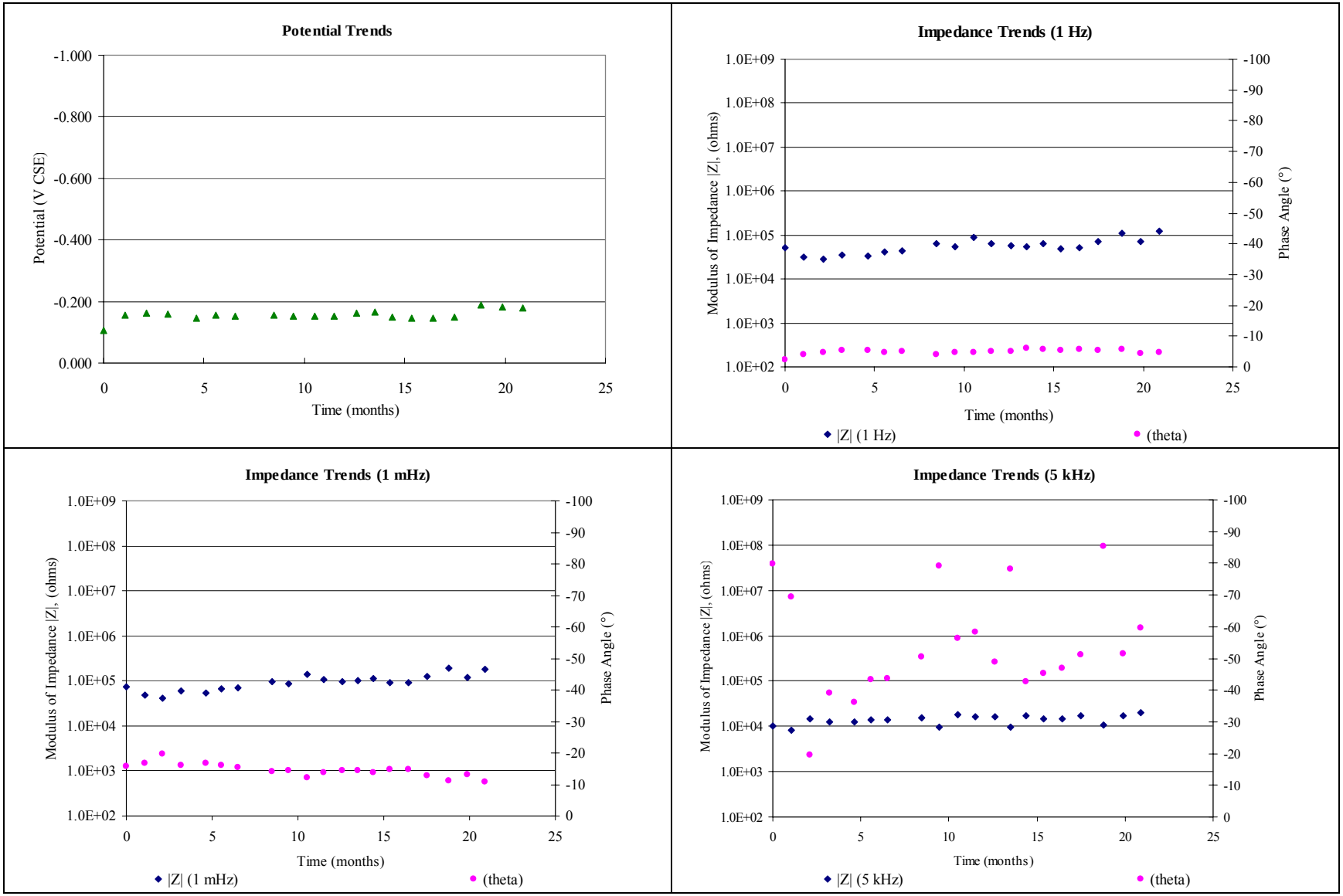

Figure B-36 Potential and Impedance Summary for Specimen 1004_6_C8

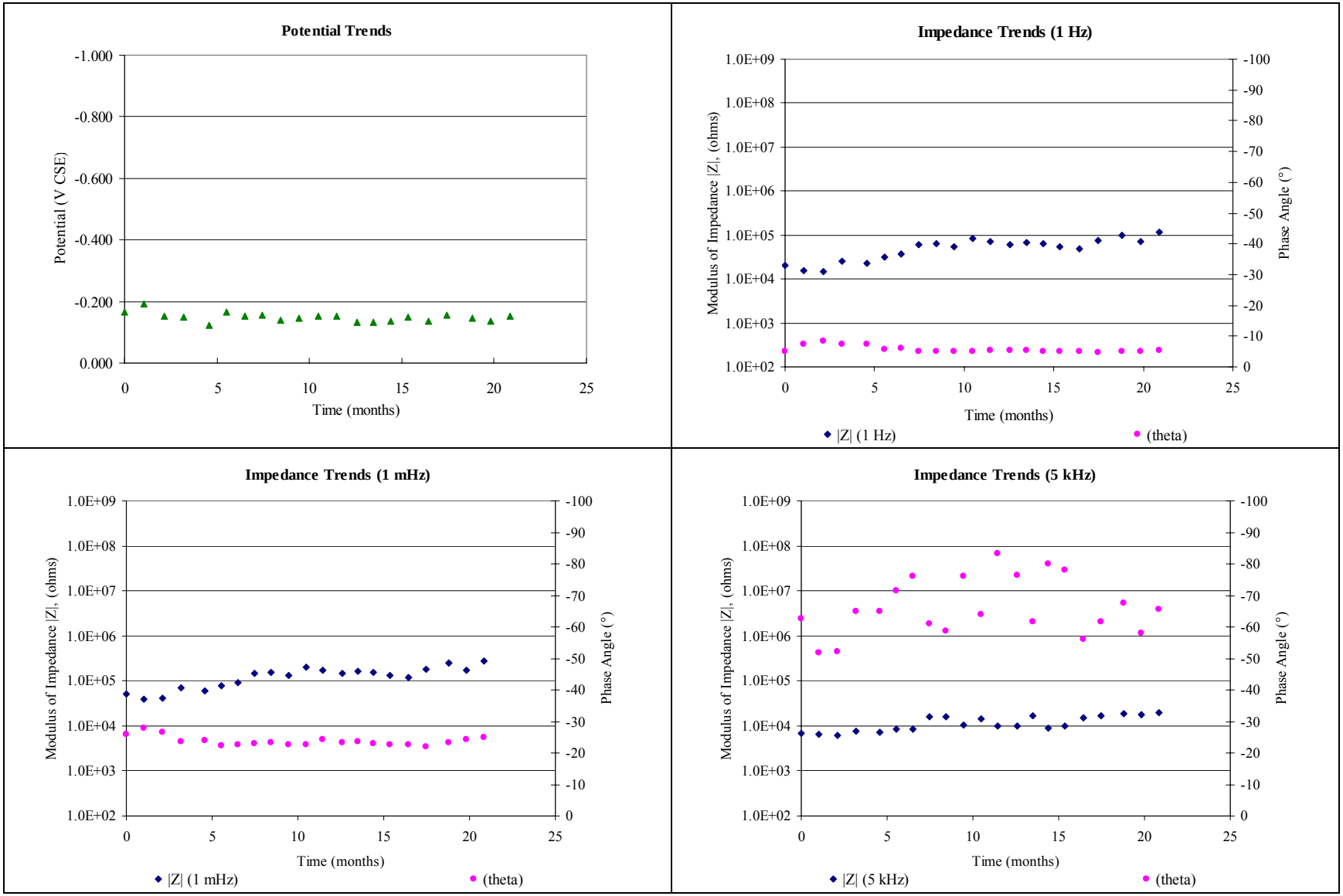

Figure B-37 Potential and Impedance Summary for Specimen 1004_6_C10

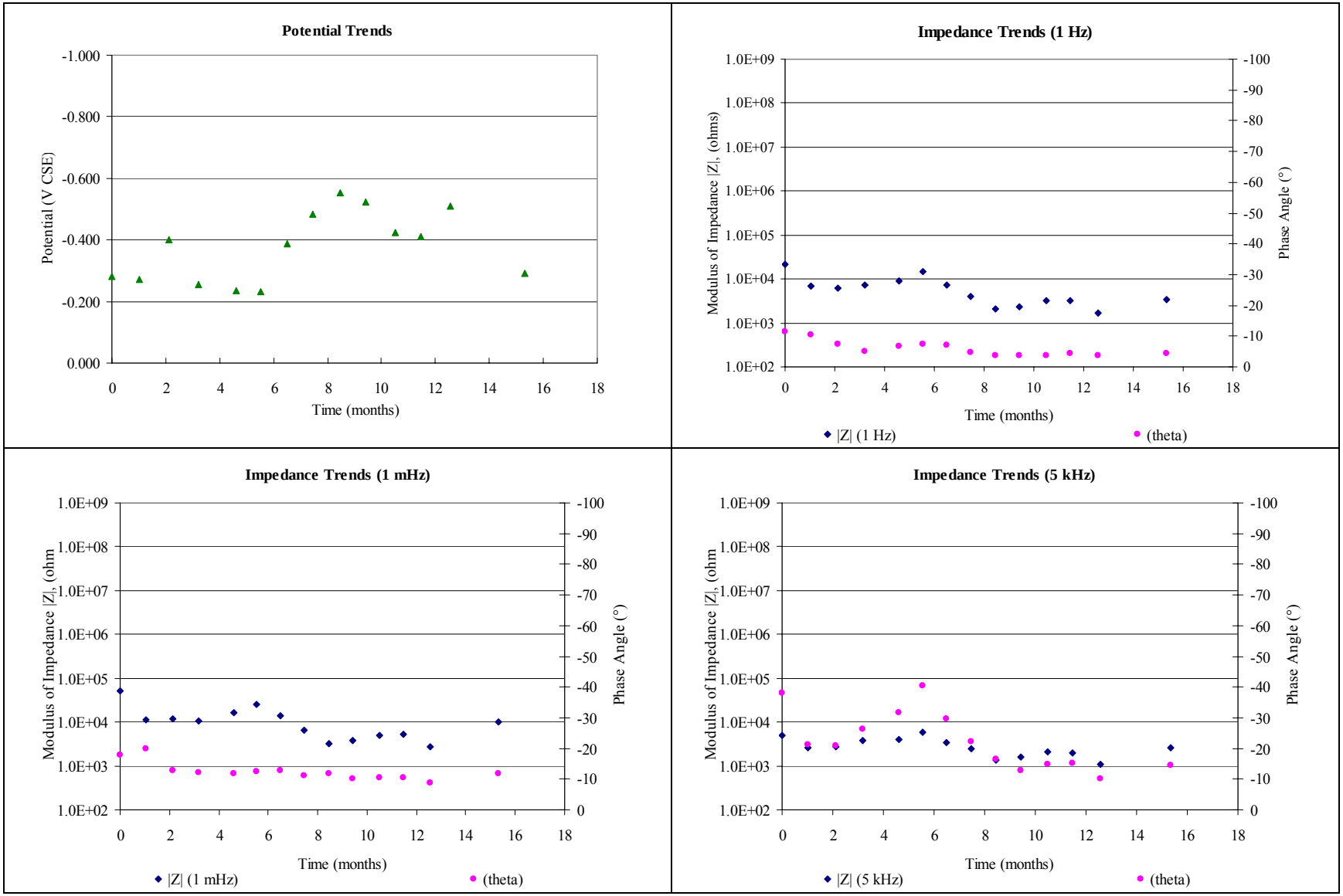

Figure B-38 Potential and Impedance Summary for Specimen 1004_6_C11/CR3

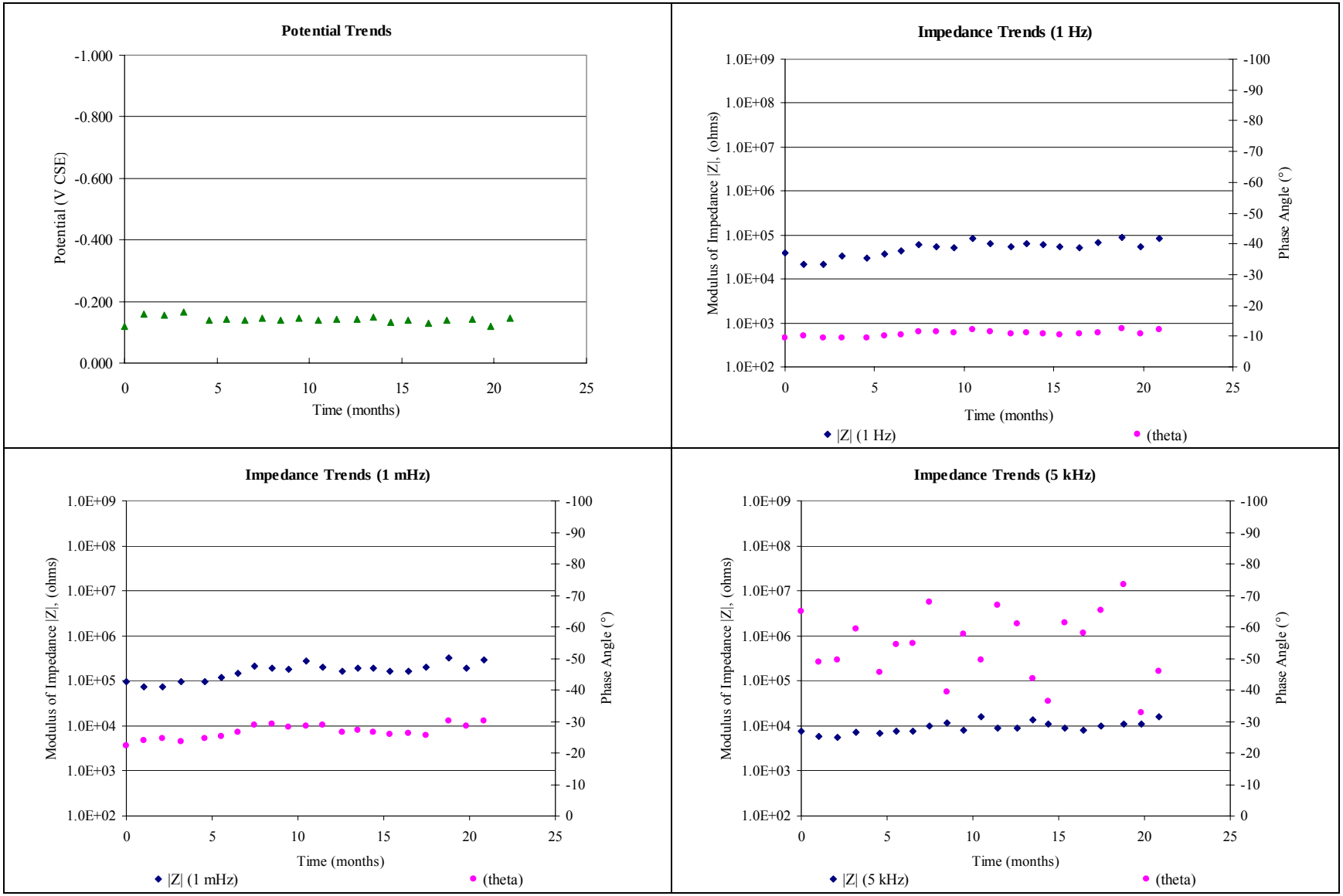

Figure B-39 Potential and Impedance Summary for Specimen 1004_6_C12

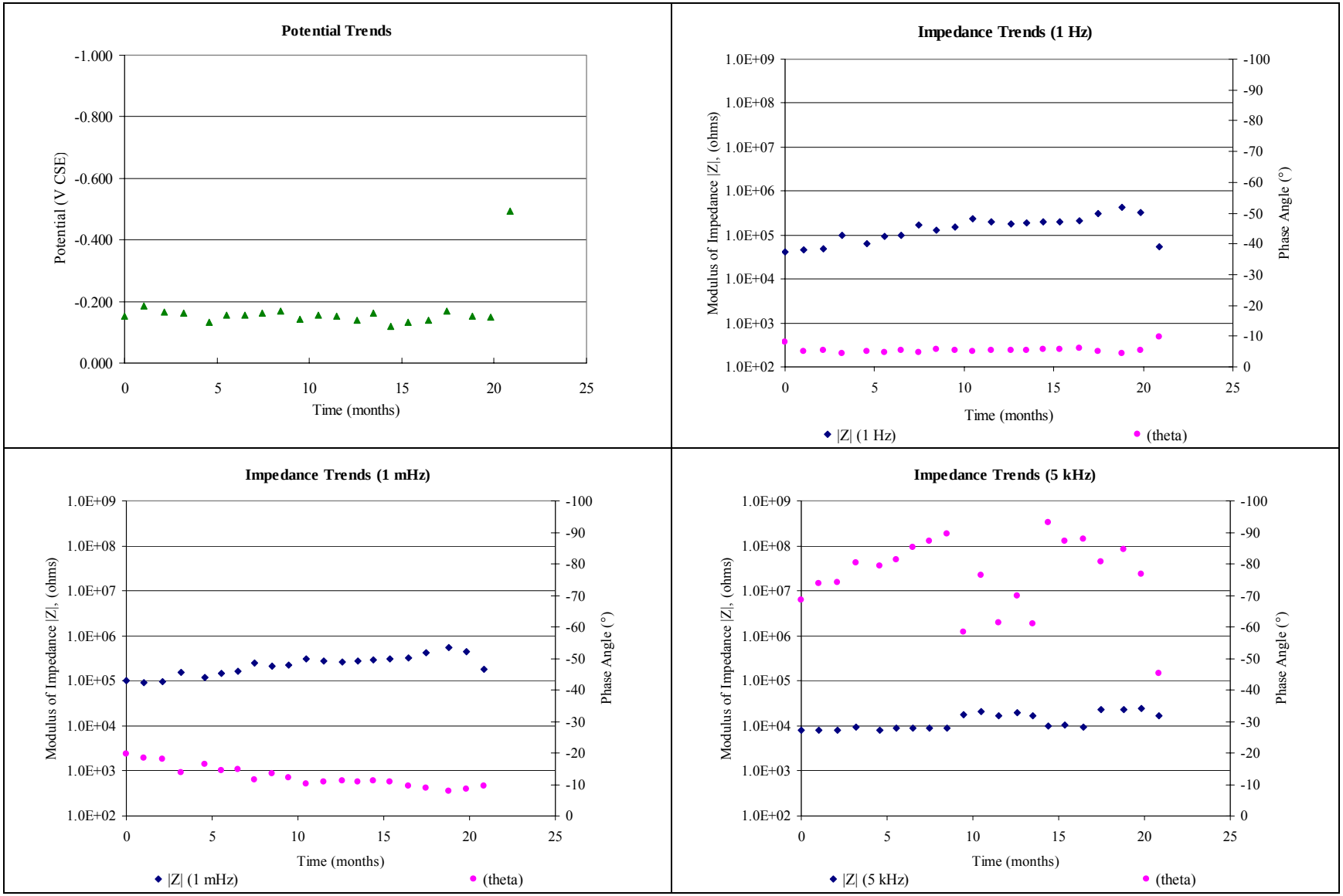

Figure B-40 Potential and Impedance Summary for Specimen 1004_6_CR1

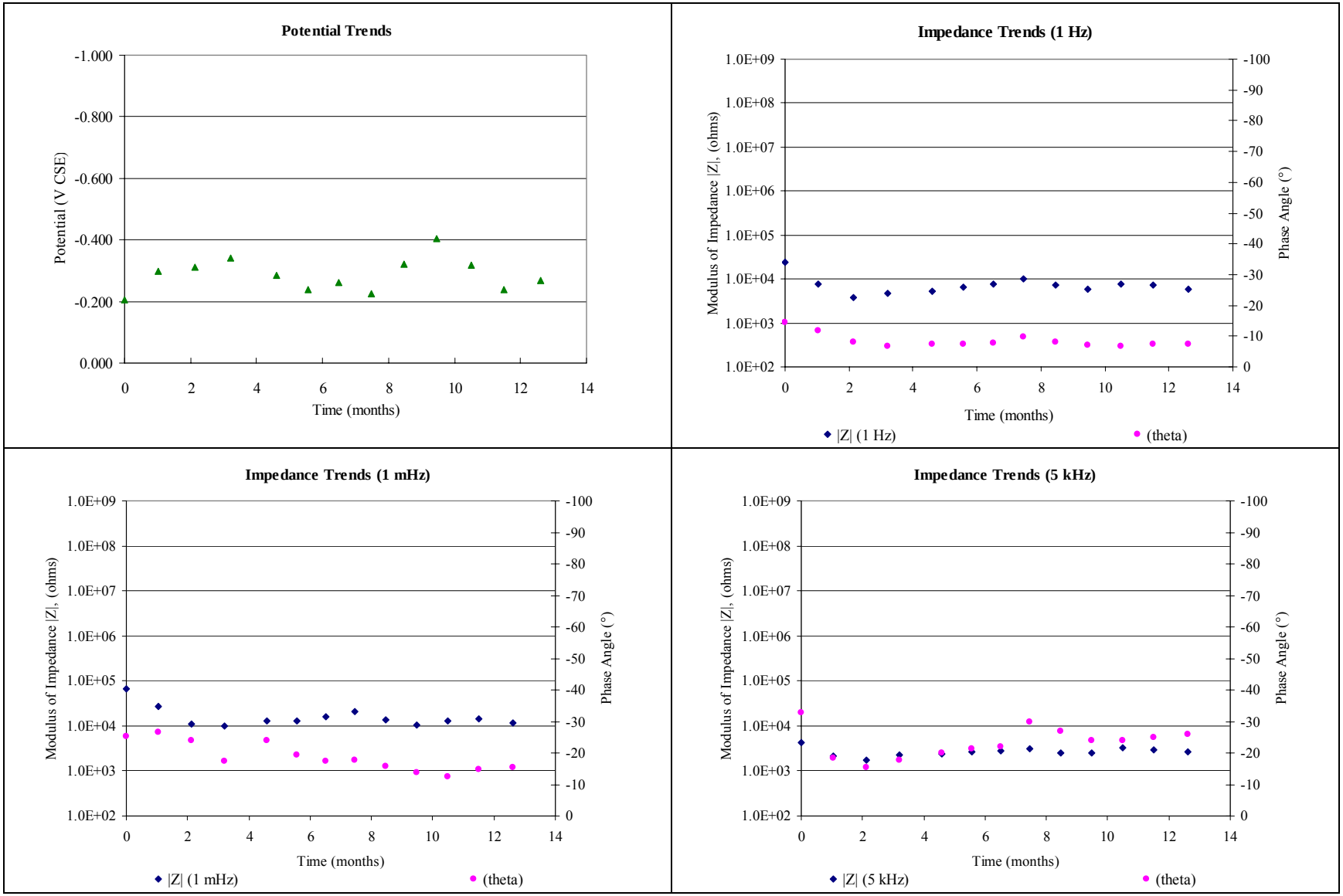

Figure B-41 Potential and Impedance Summary for Specimen 1004_6_CR2

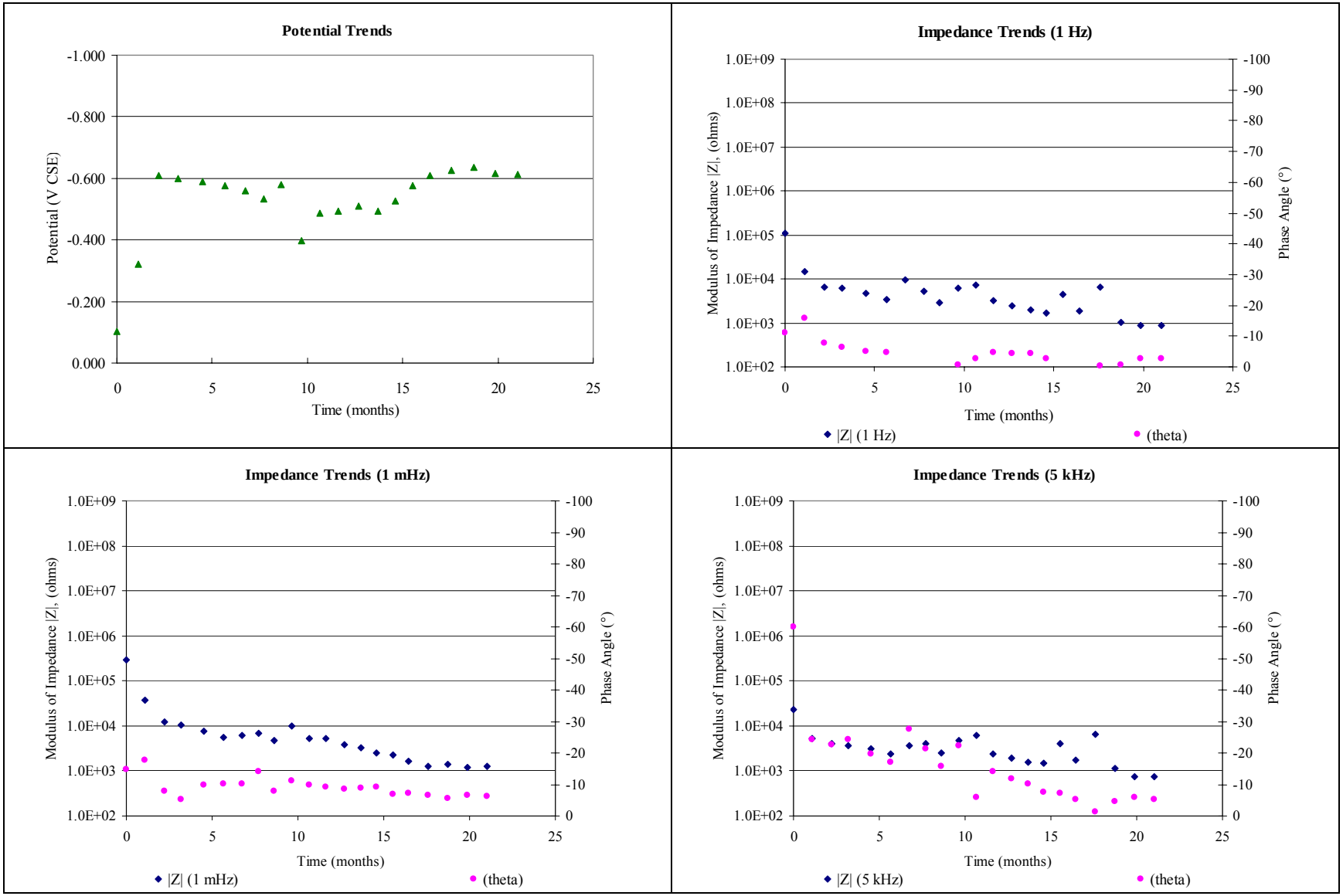

Figure B-42 Potential and Impedance Summary for Specimen 1015_C1

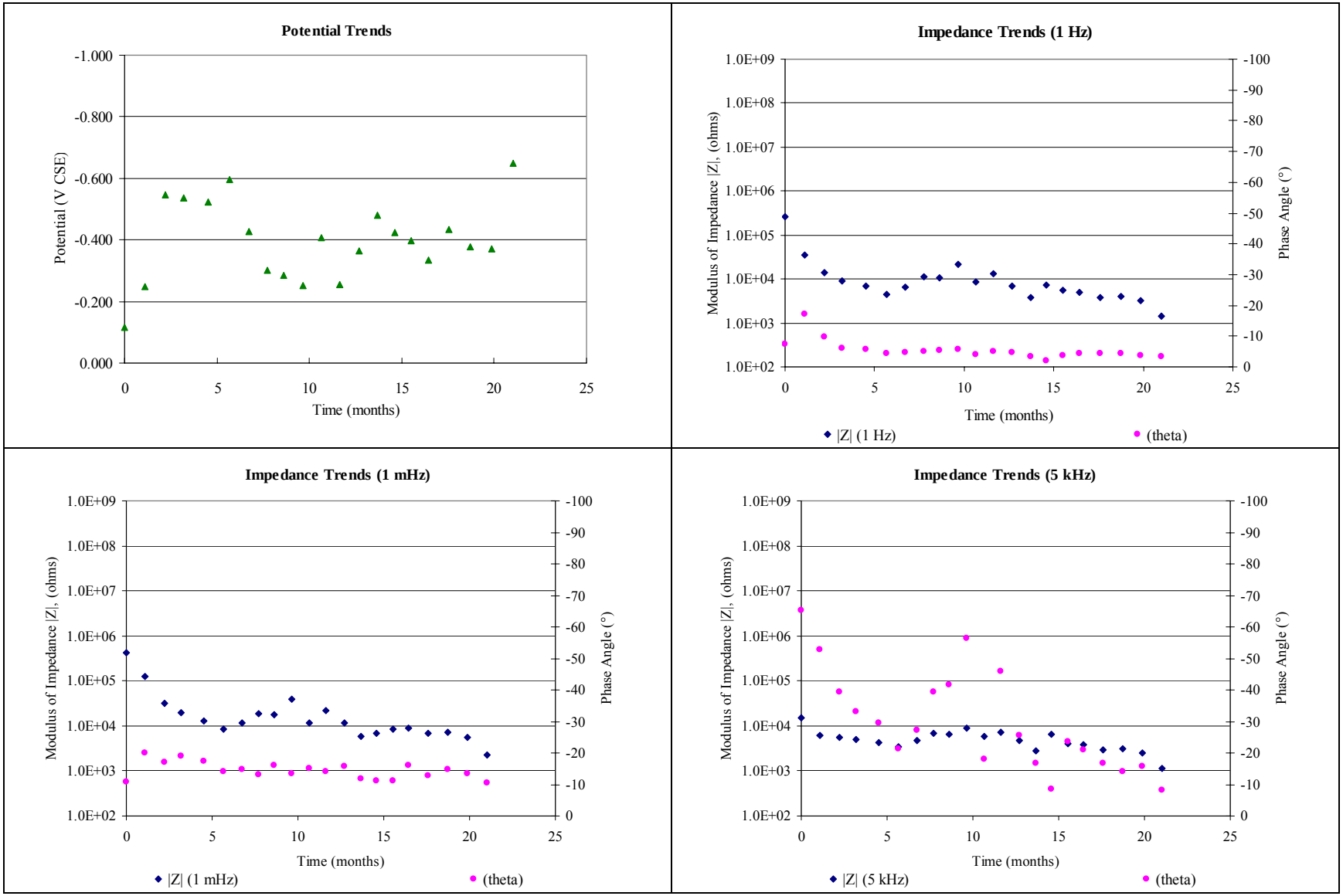

Figure B-43 Potential and Impedance Summary for Specimen 1015_C2

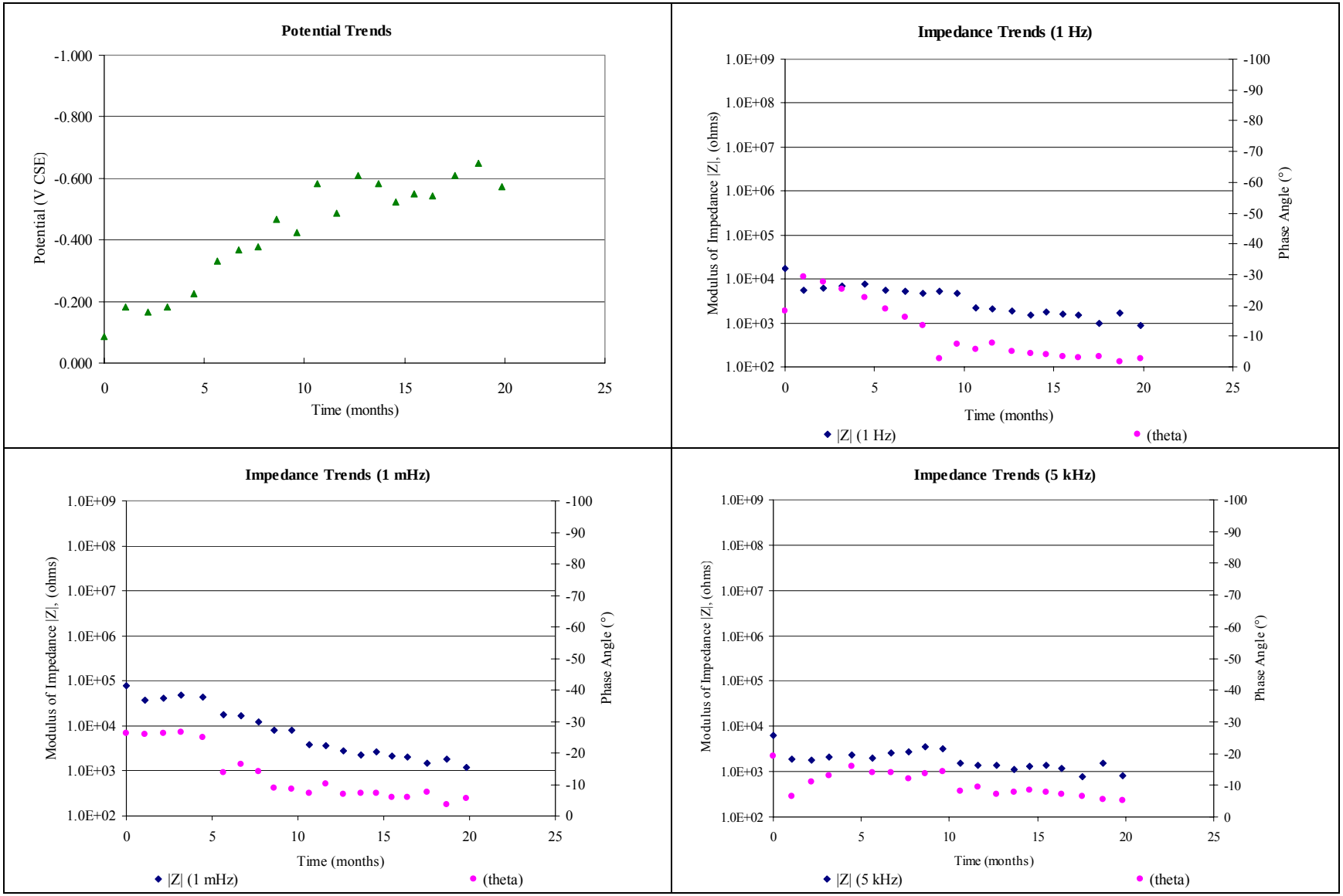

Figure B-44 Potential and Impedance Summary for Specimen 1015_C3

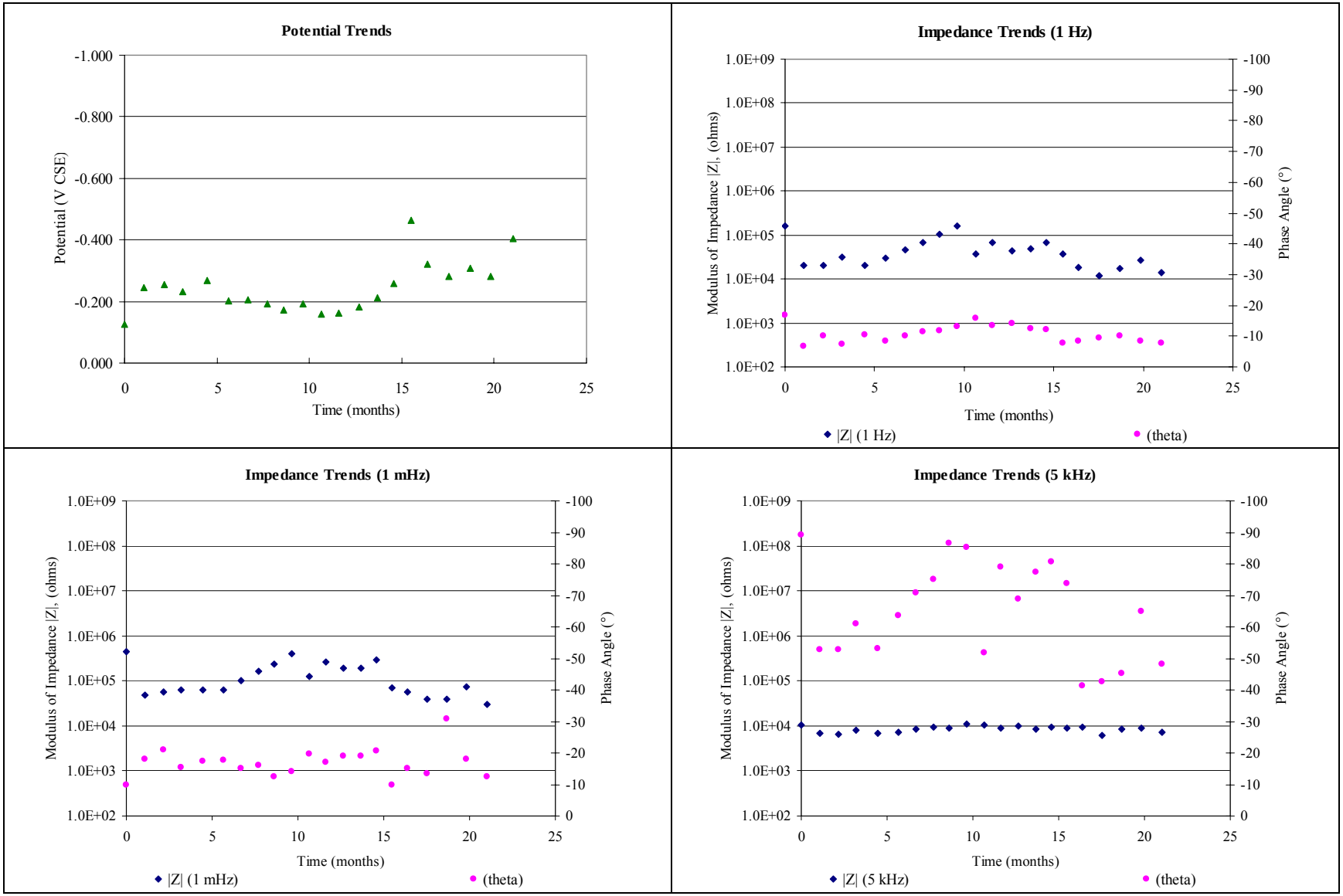

Figure B-45 Potential and Impedance Summary for Specimen 1015_C4

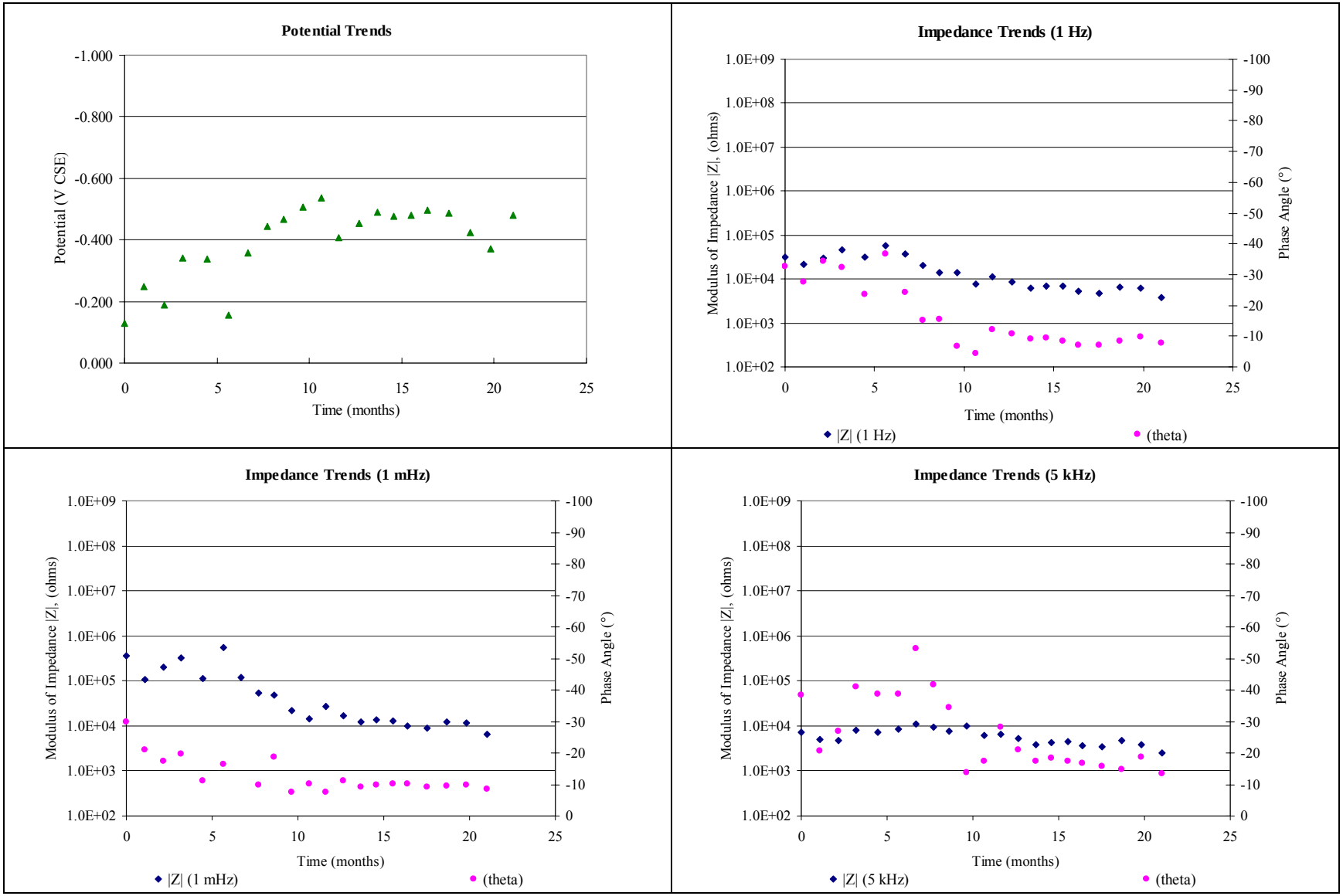

Figure B-46 Potential and Impedance Summary for Specimen 1015_C5

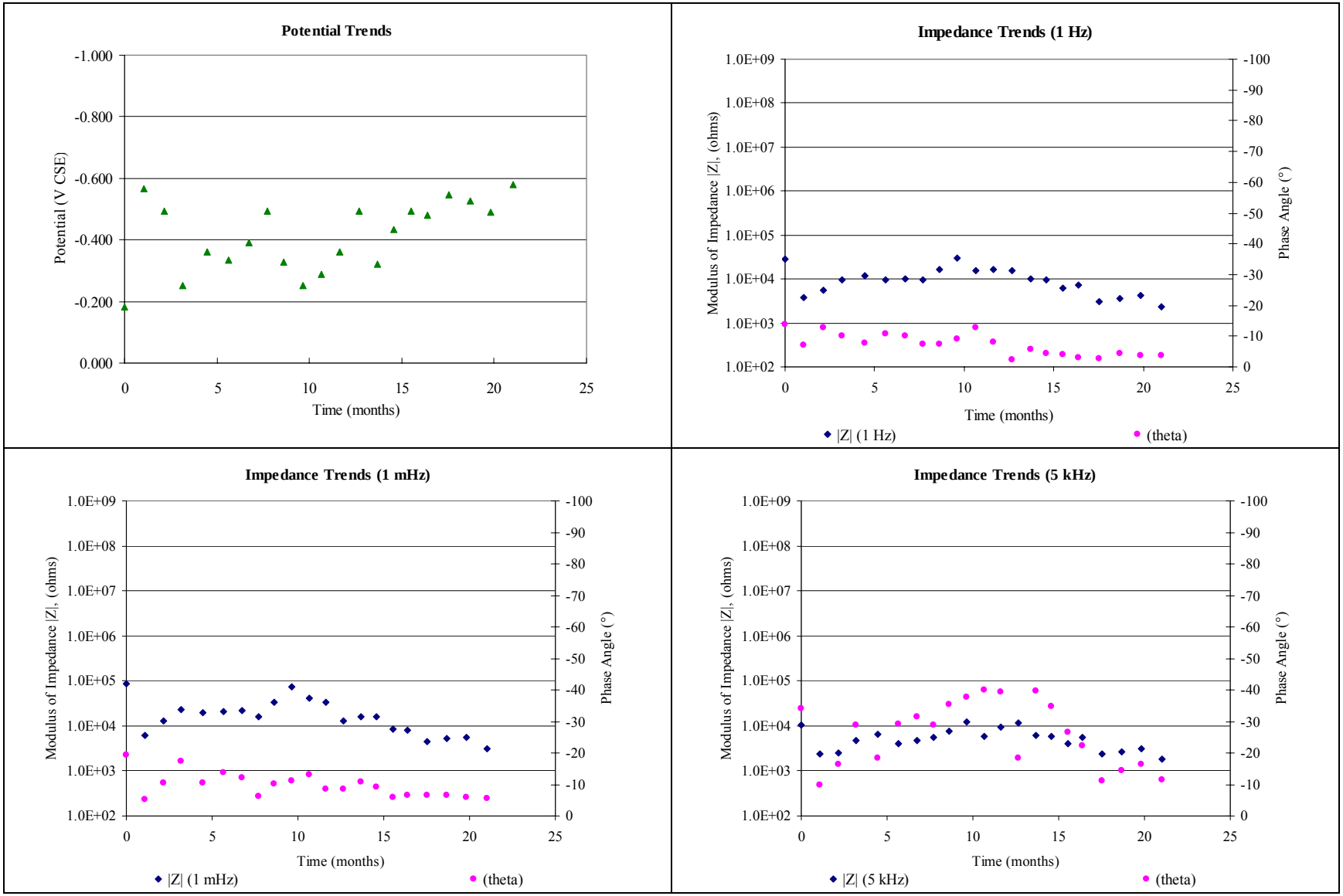

Figure B-47 Potential and Impedance Summary for Specimen 1015_C6

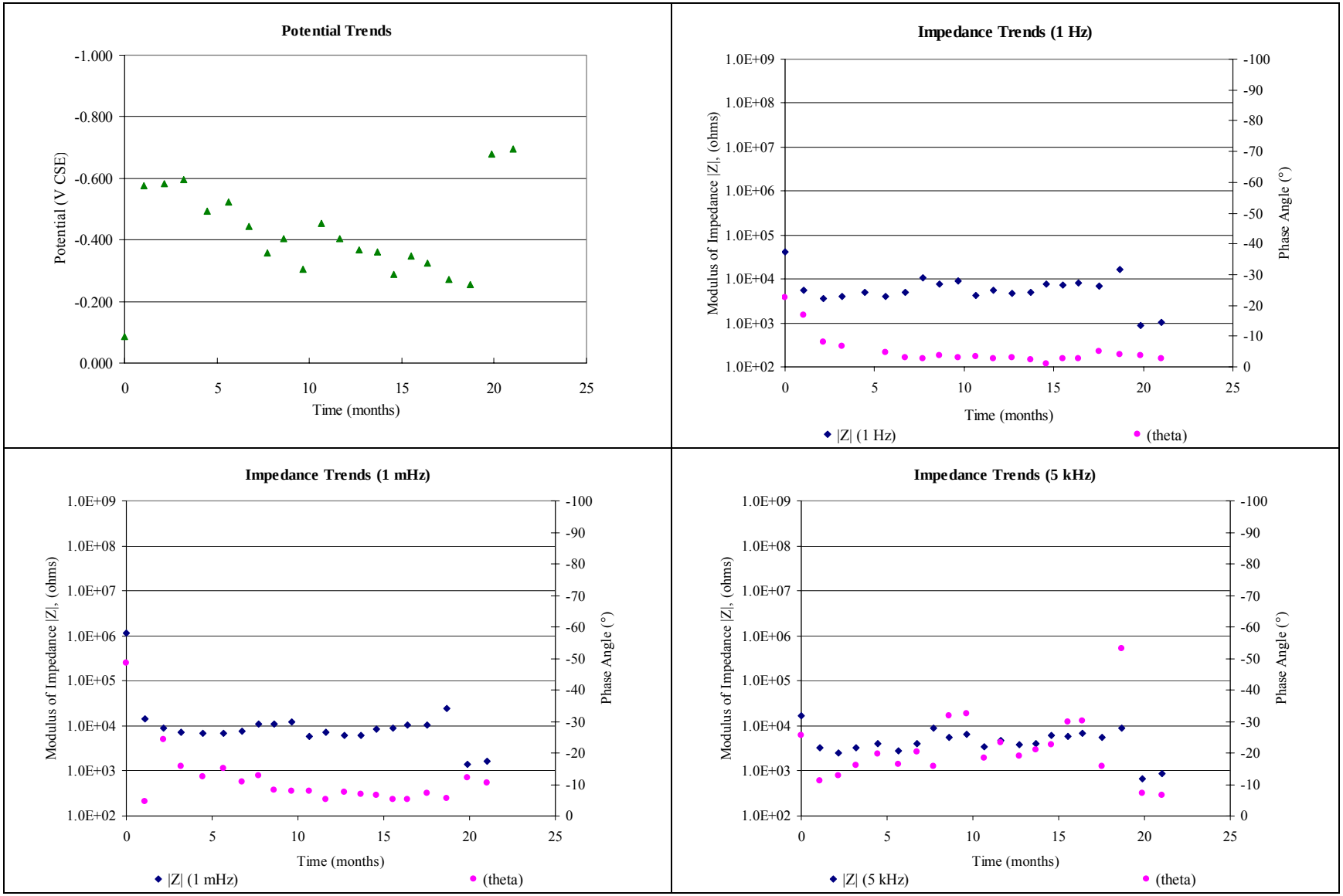

Figure B-48 Potential and Impedance Summary for Specimen 1015_C7

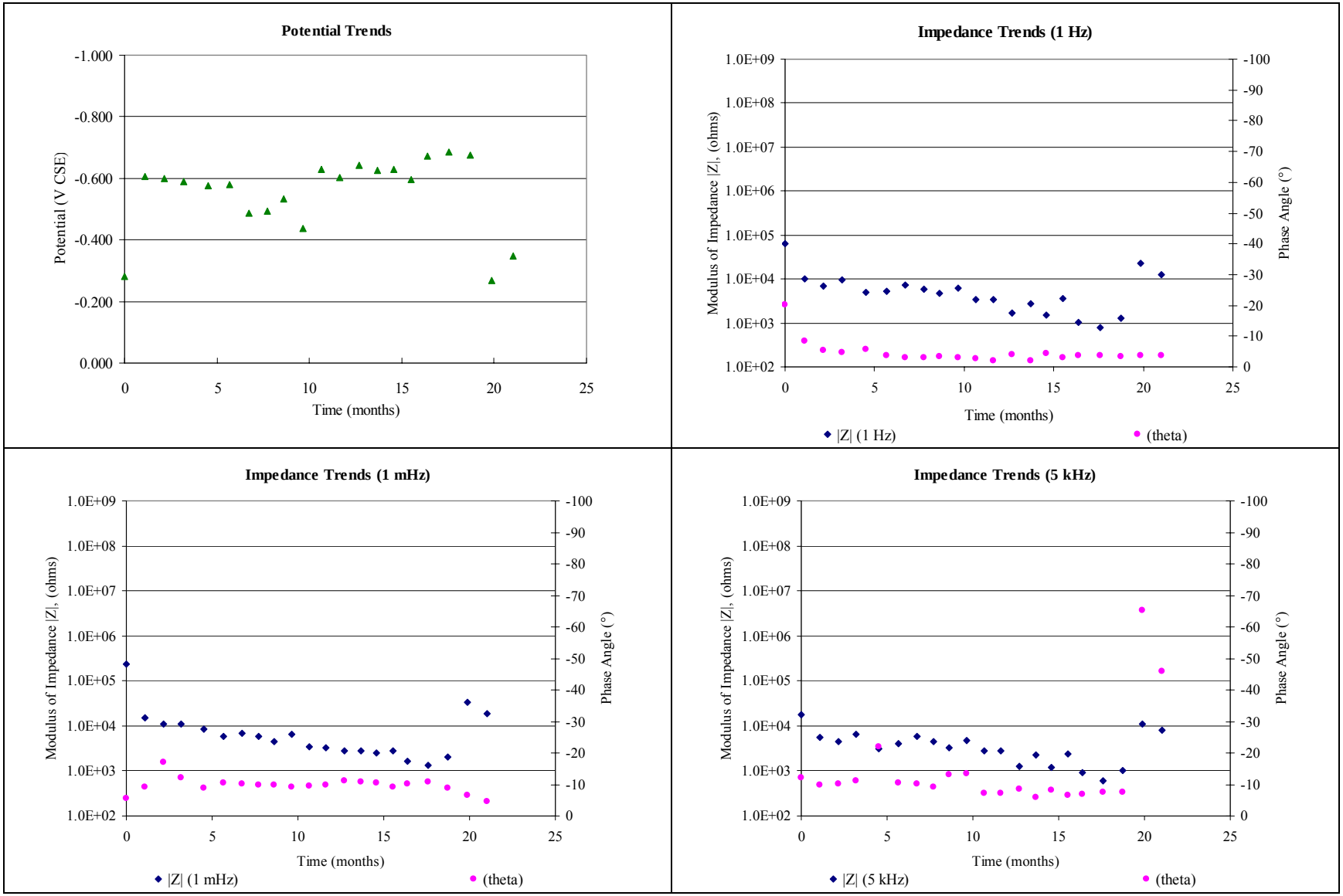

Figure B-49 Potential and Impedance Summary for Specimen 1015_C8

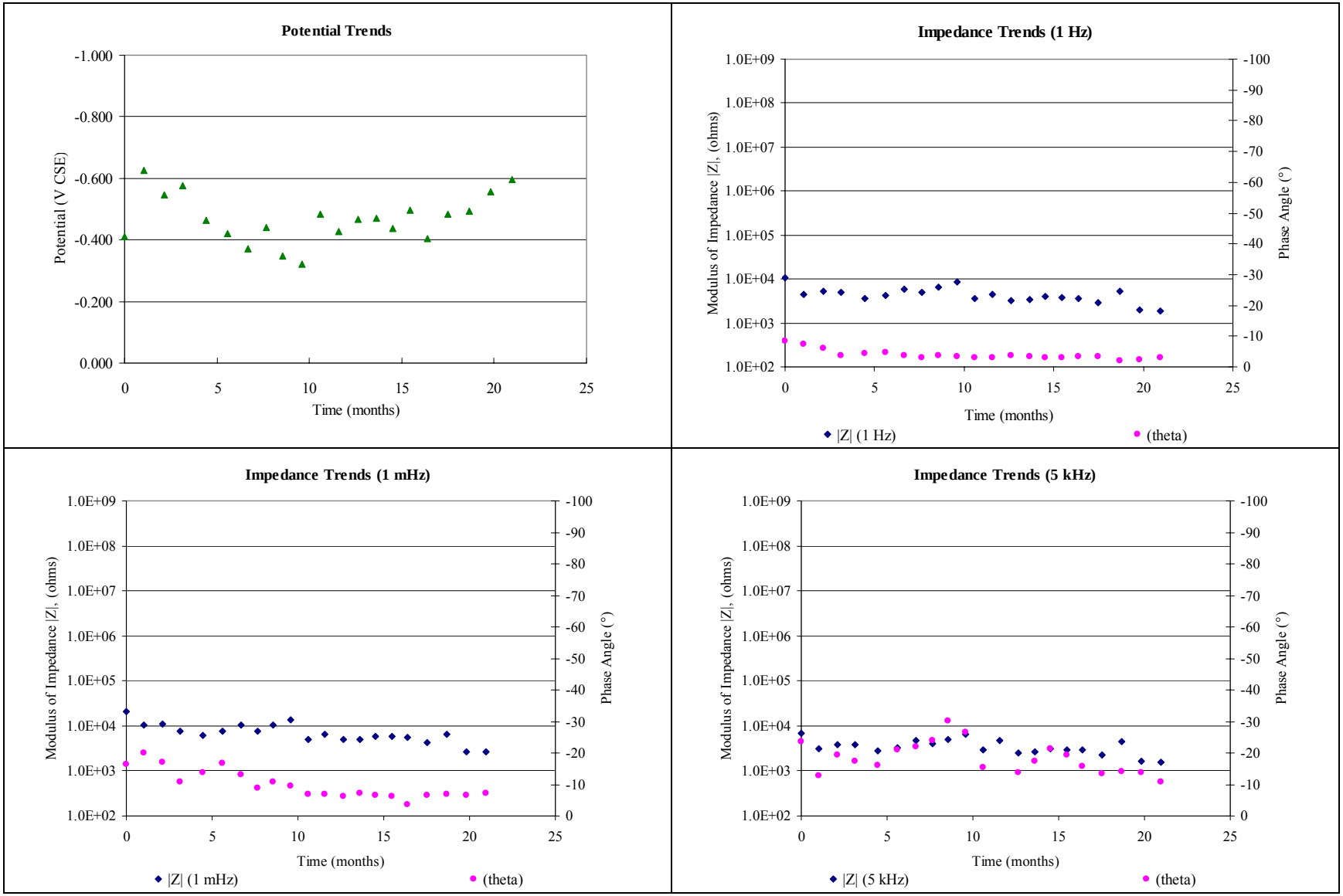

Figure B-50 Potential and Impedance Summary for Specimen 1015_C9

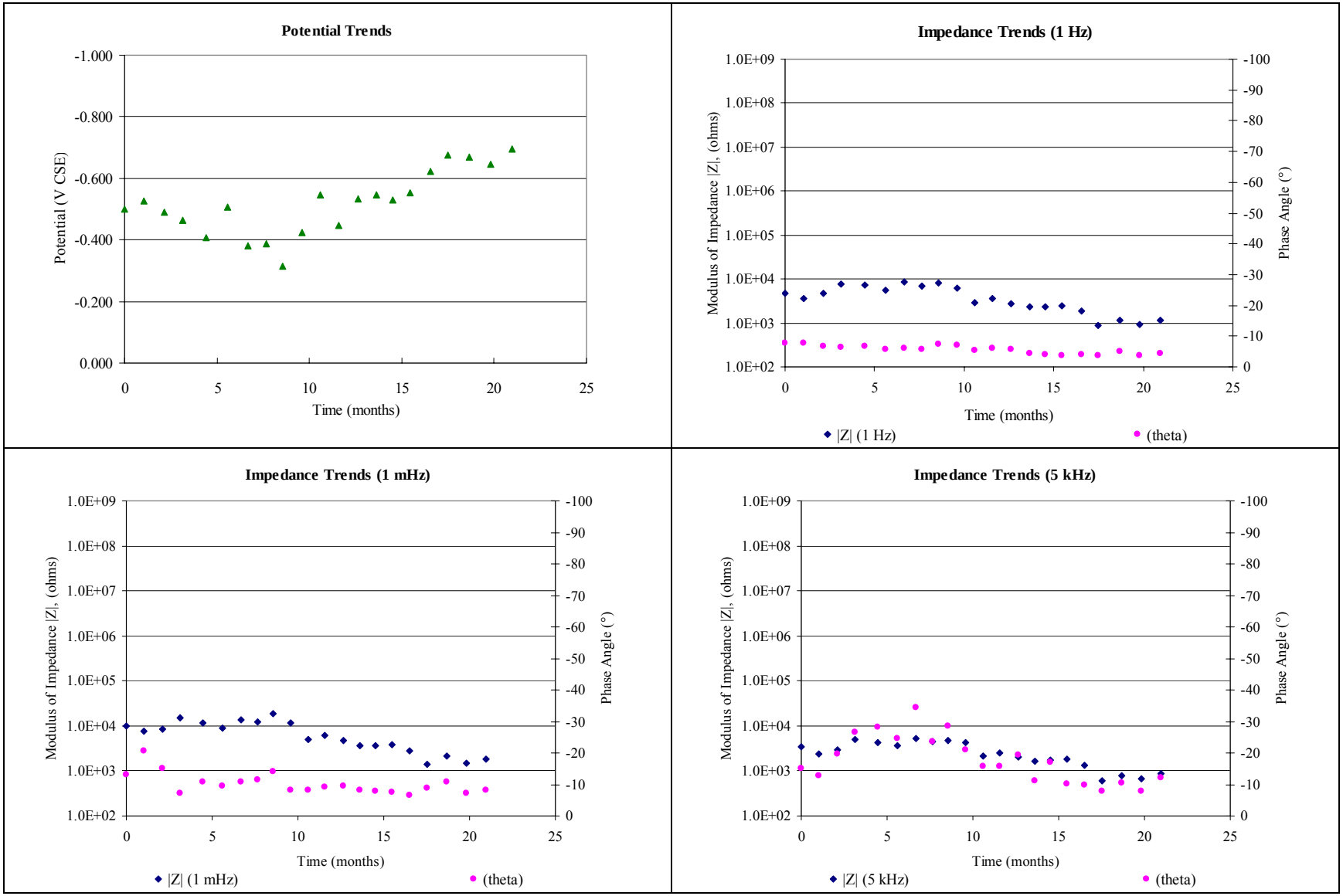

Figure B-51 Potential and Impedance Summary for Specimen 1015_C10

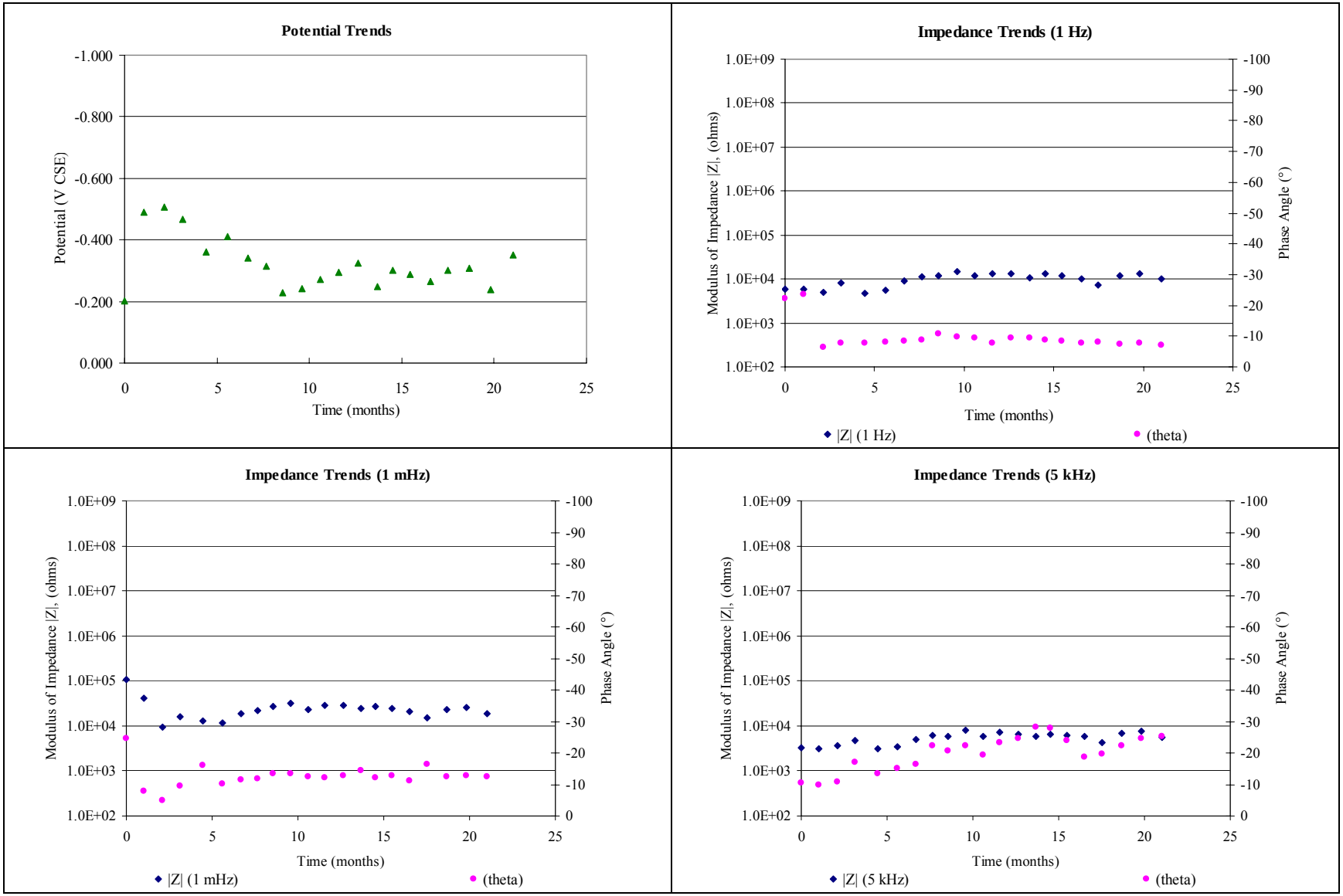

Figure B-52 Potential and Impedance Summary for Specimen 1015_CR1

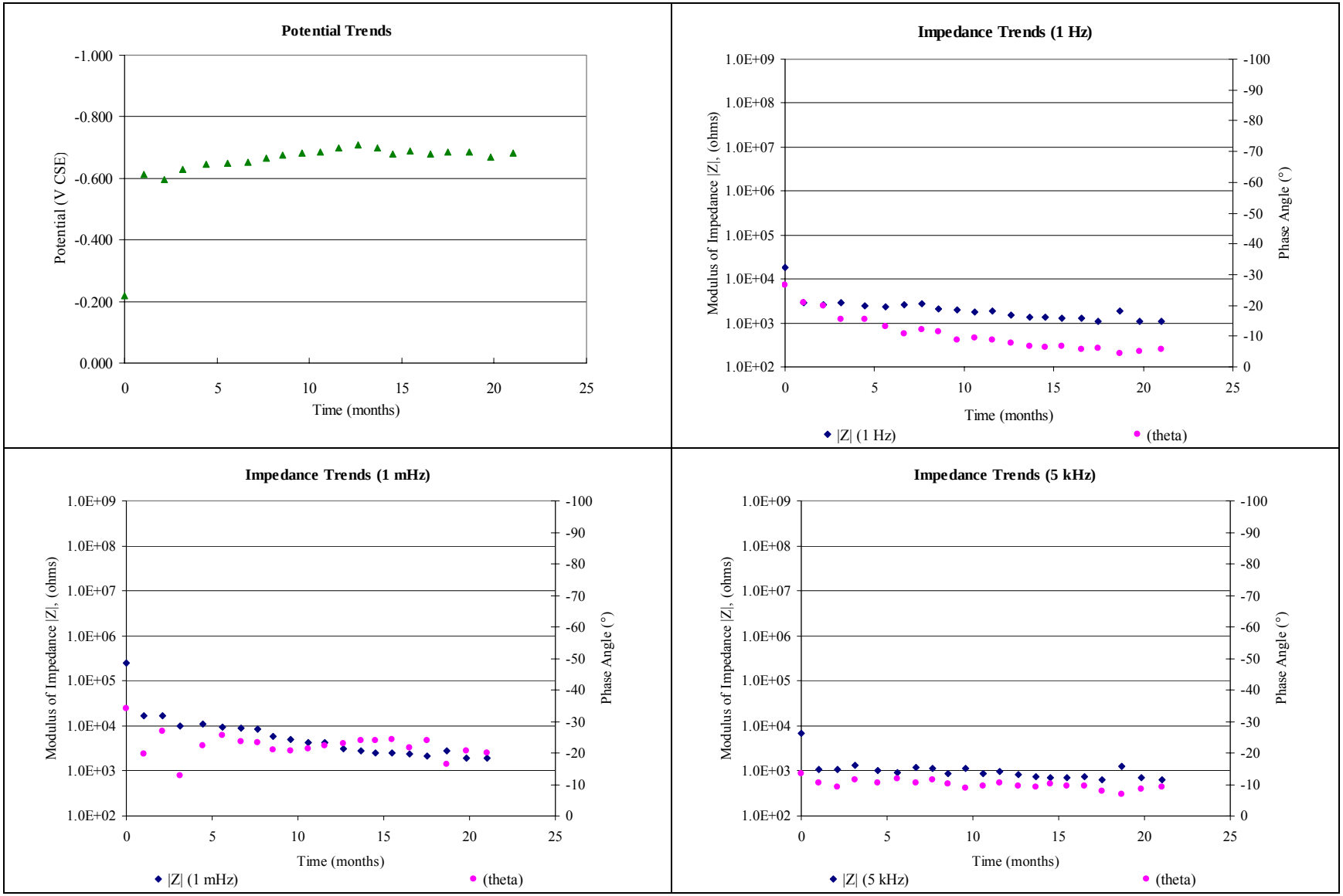

Figure B-53 Potential and Impedance Summary for Specimen 1015_CR1b

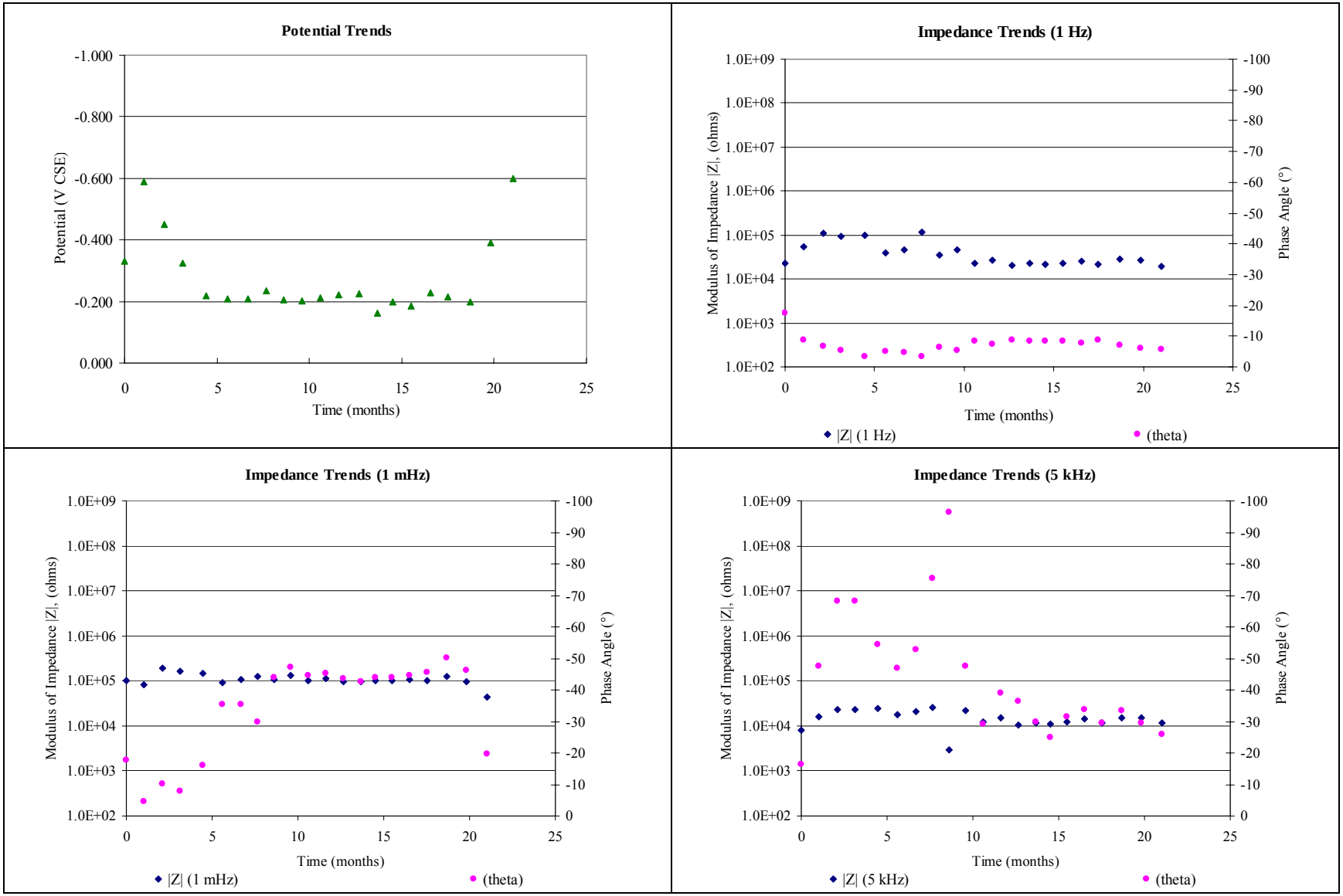

Figure B-54 Potential and Impedance Summary for Specimen 1015_CR2

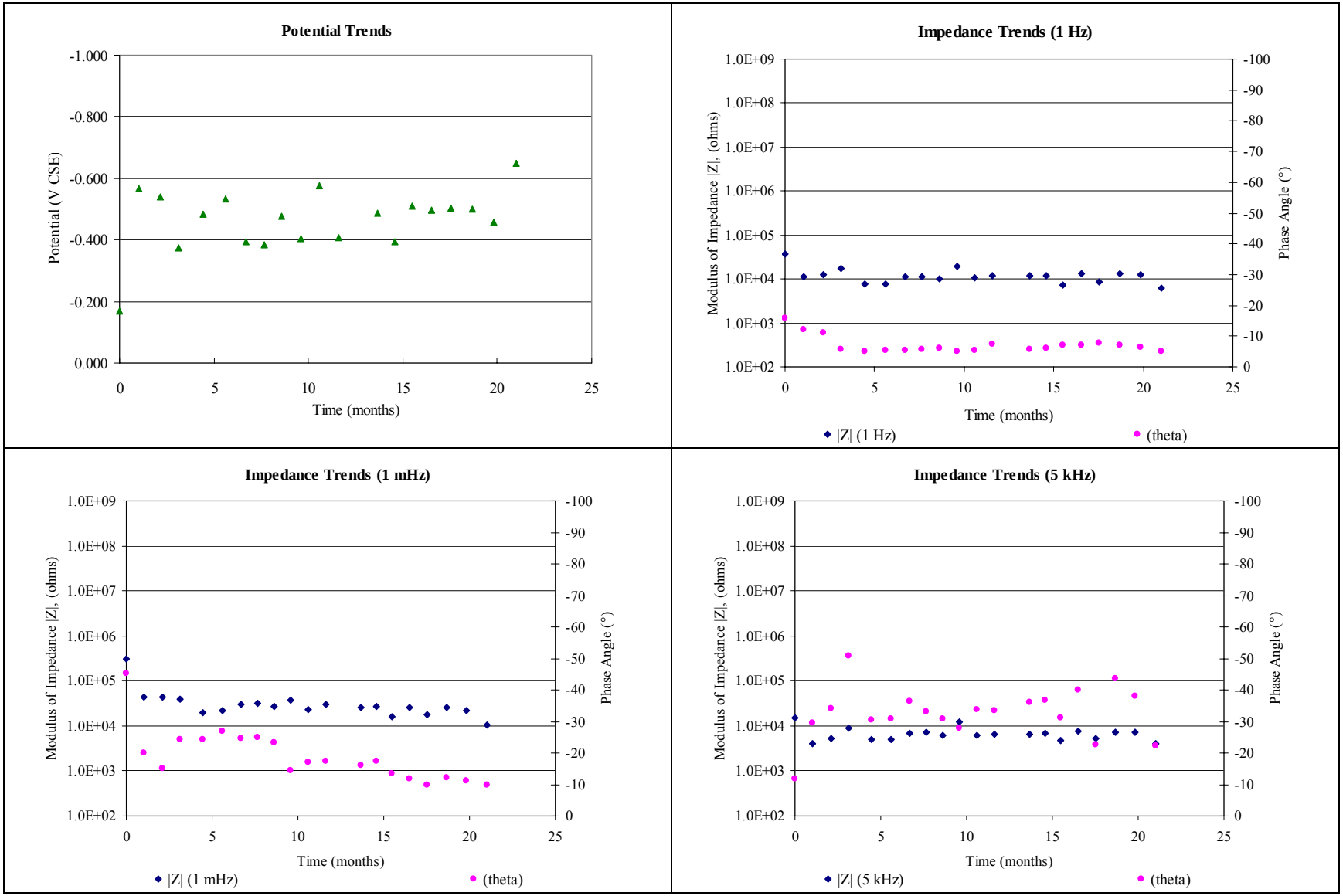

Figure B-55 Potential and Impedance Summary for Specimen 1015_CR3

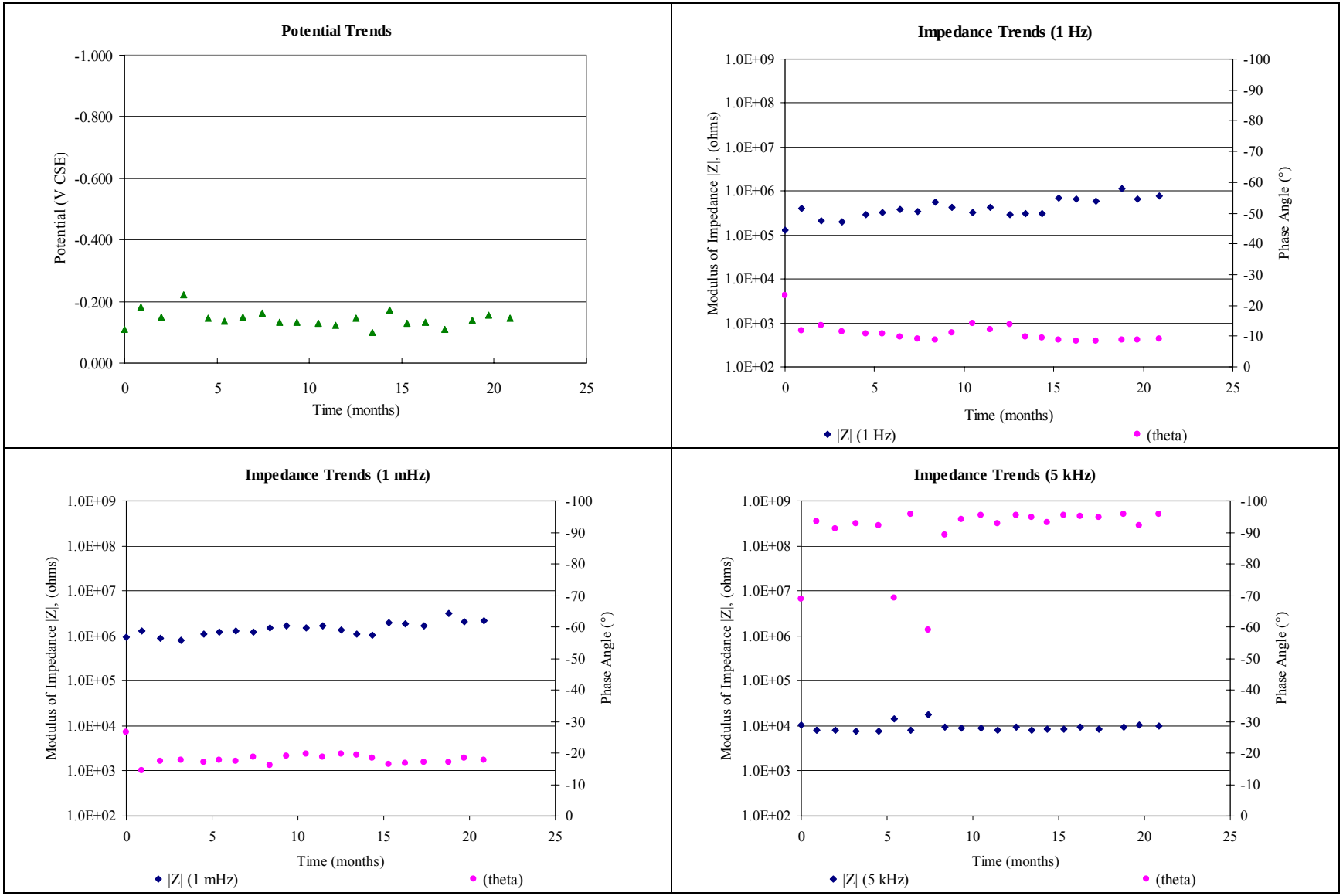

Figure B-56 Potential and Impedance Summary for Specimen 1019_C1

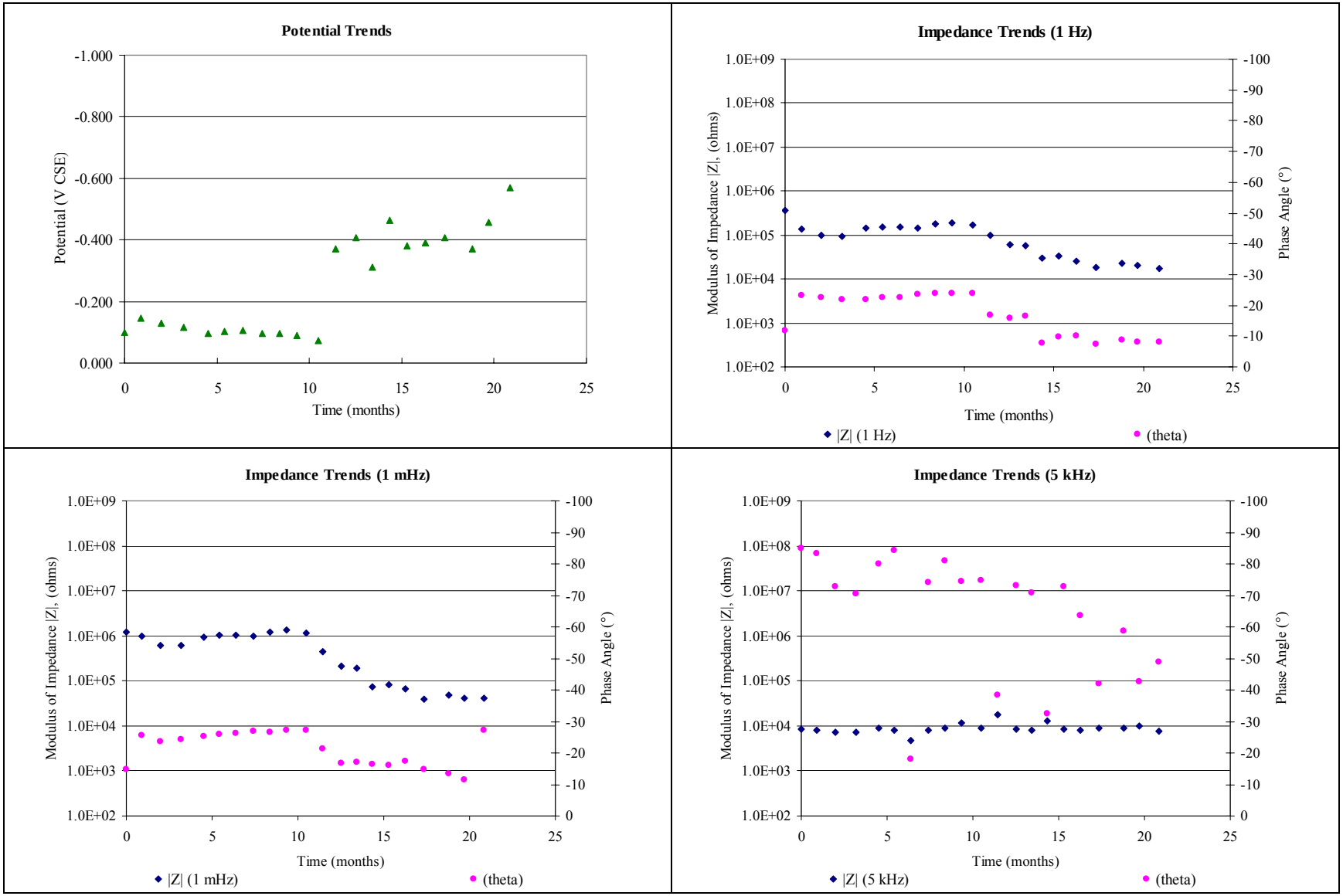

Figure B-57 Potential and Impedance Summary for Specimen 1019_C2

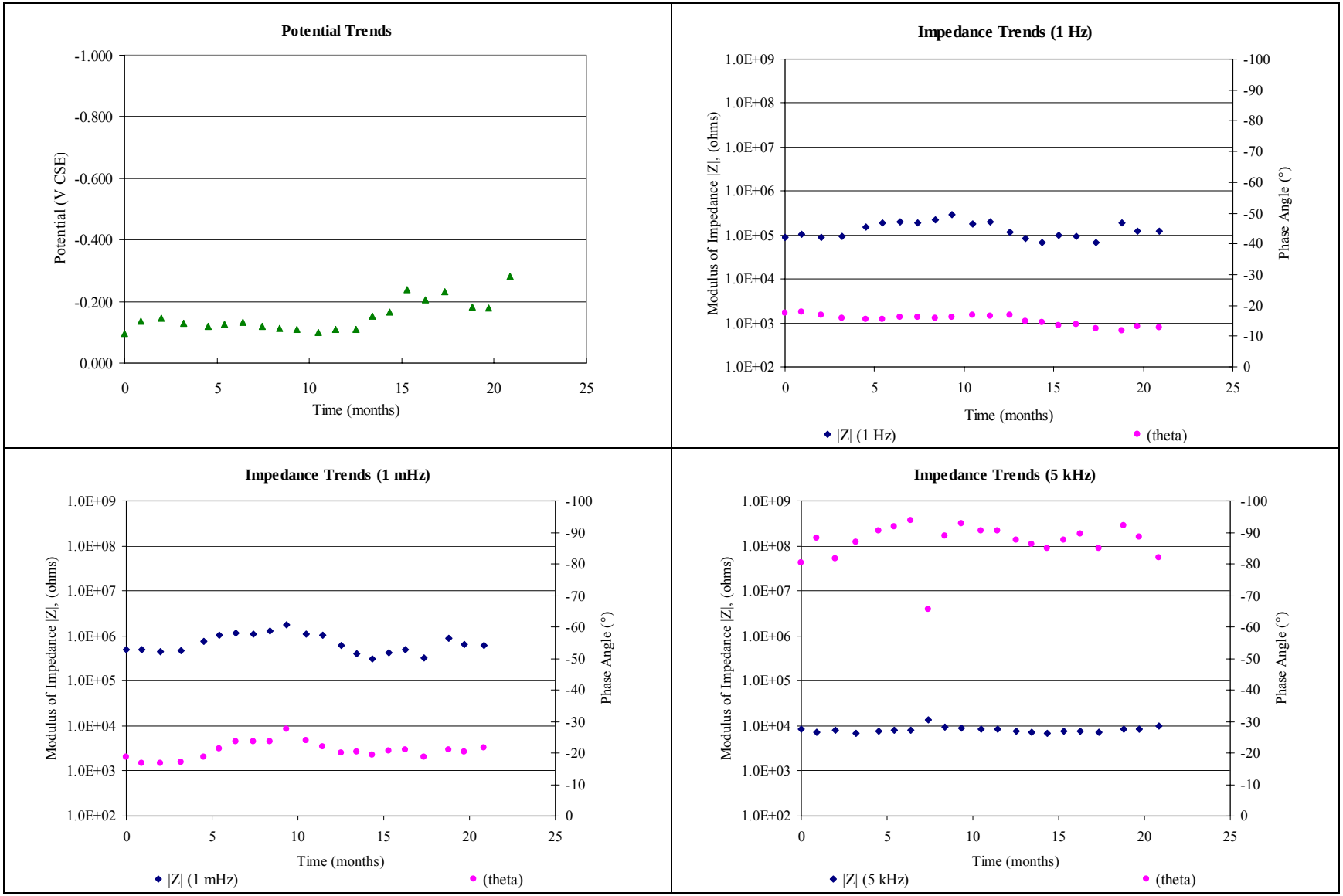

Figure B-58 Potential and Impedance Summary for Specimen 1019_C3

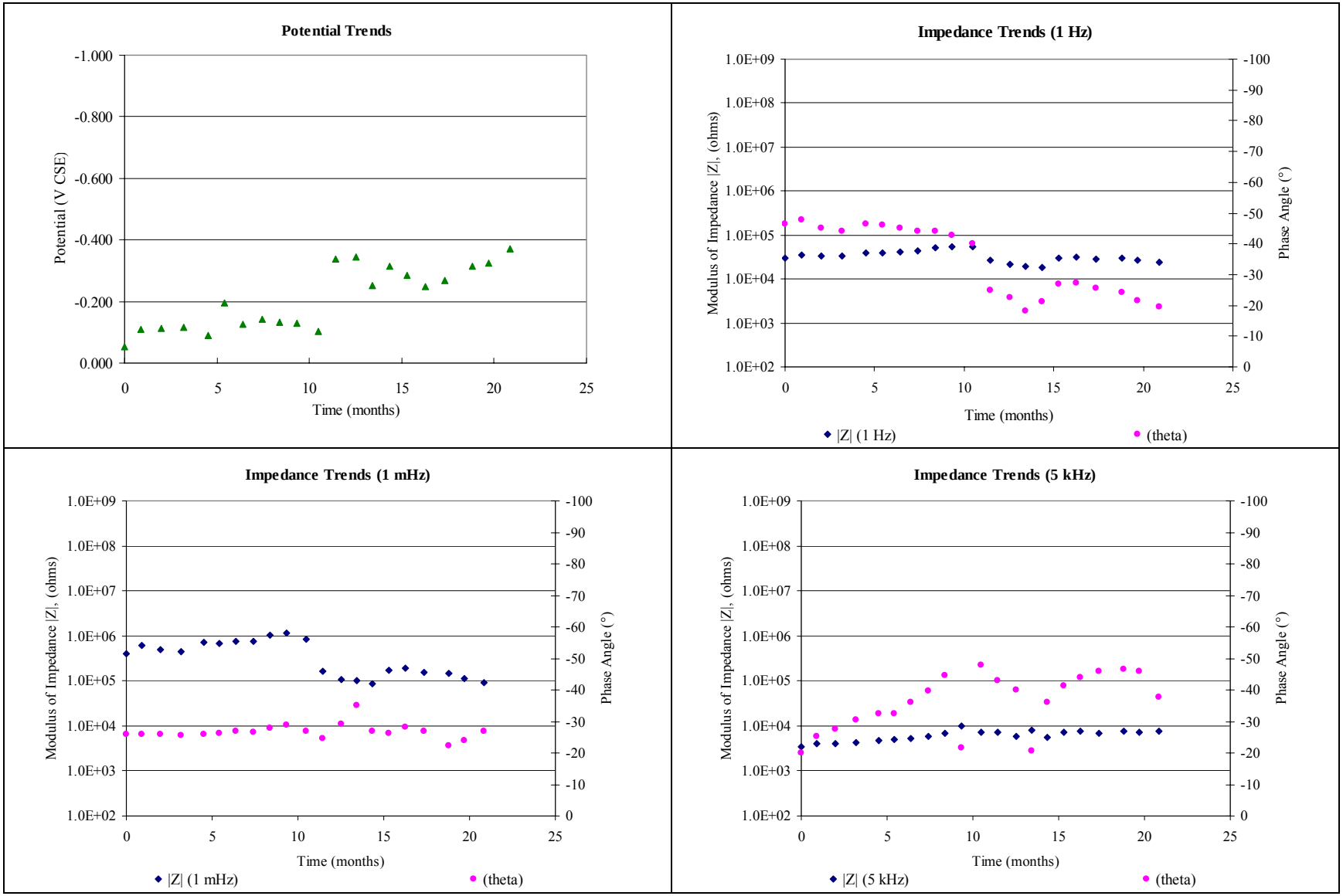

Figure B-59 Potential and Impedance Summary for Specimen 1019_C4

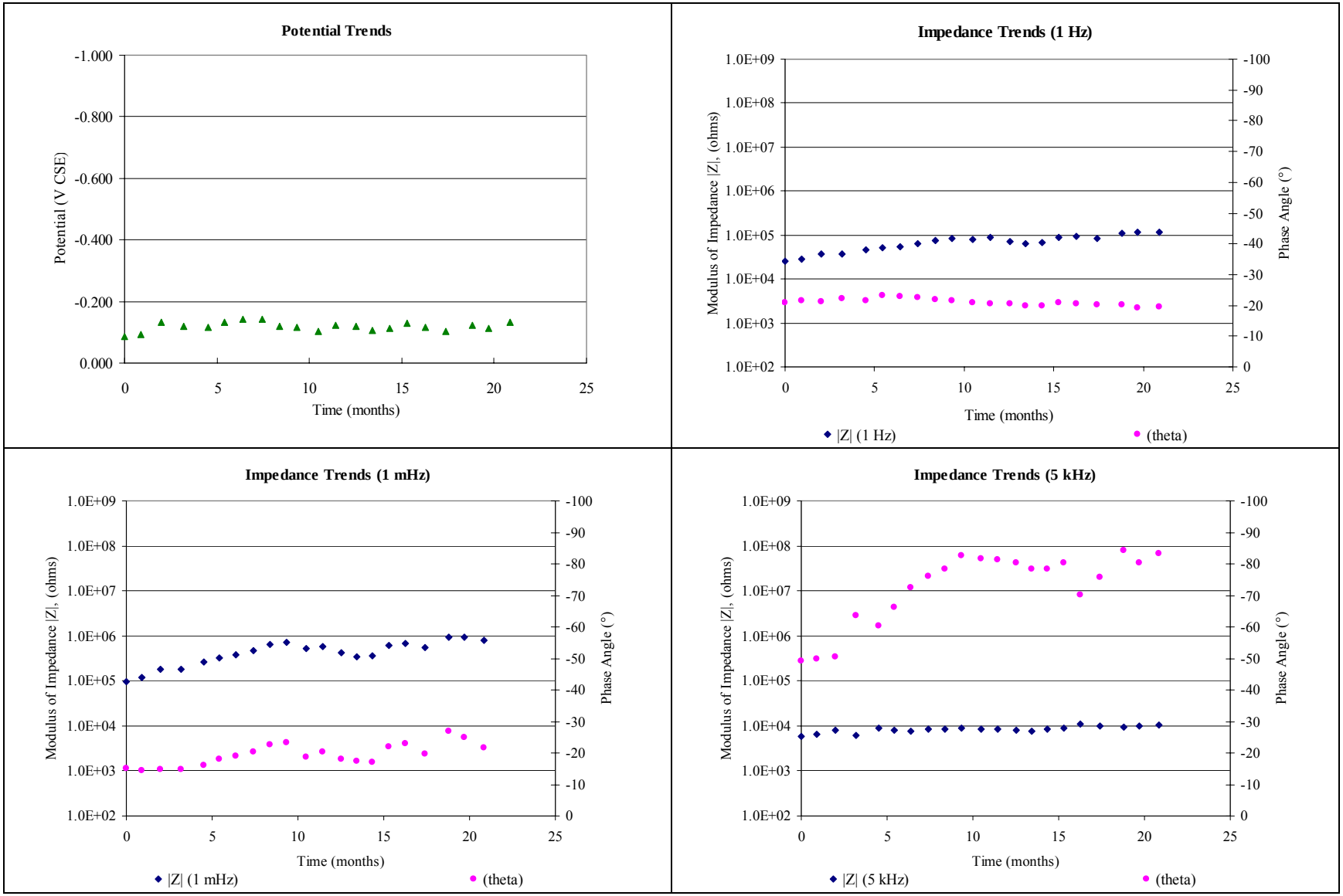

Figure B-60 Potential and Impedance Summary for Specimen 1019_C5

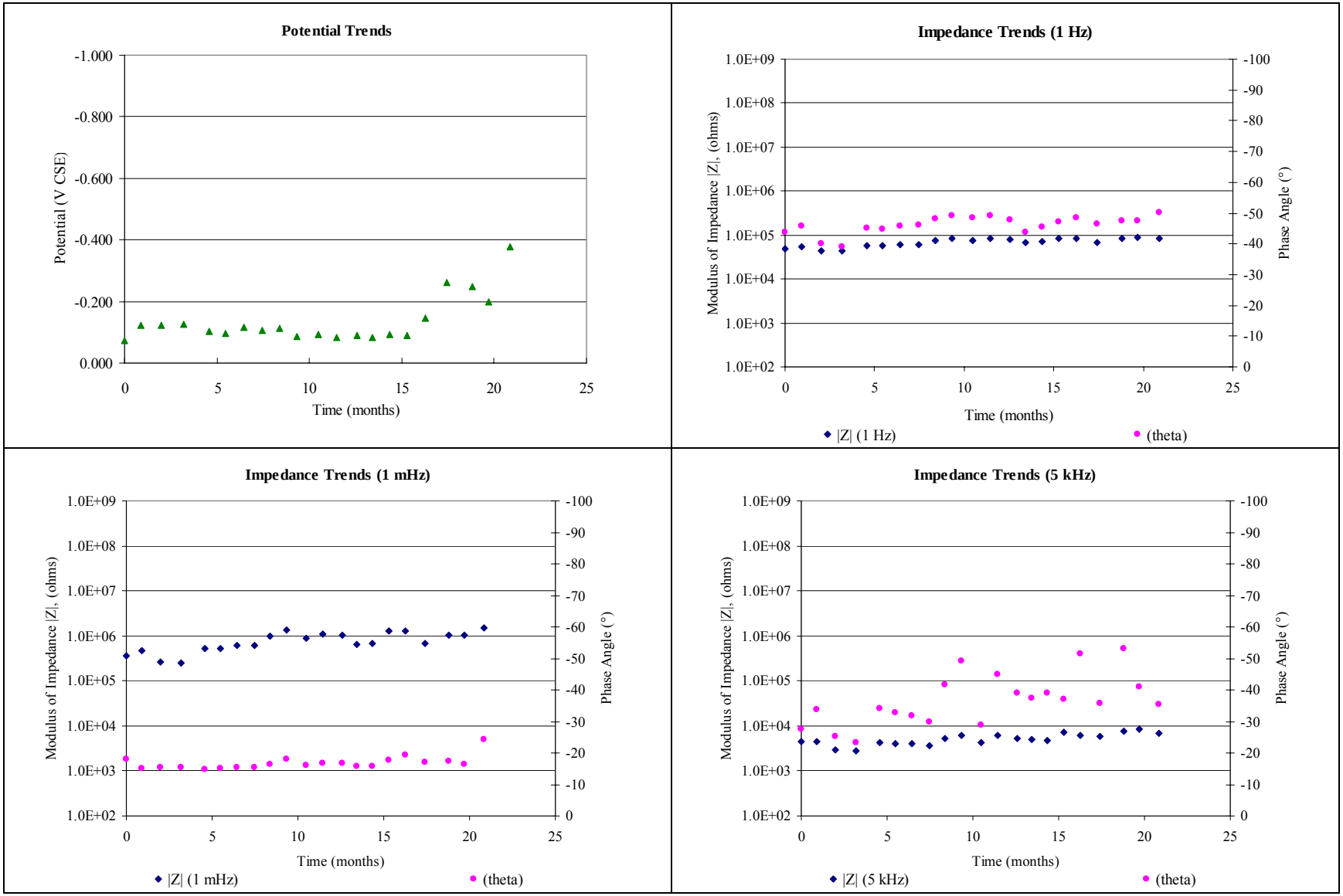

Figure B-61 Potential and Impedance Summary for Specimen 1019_C6

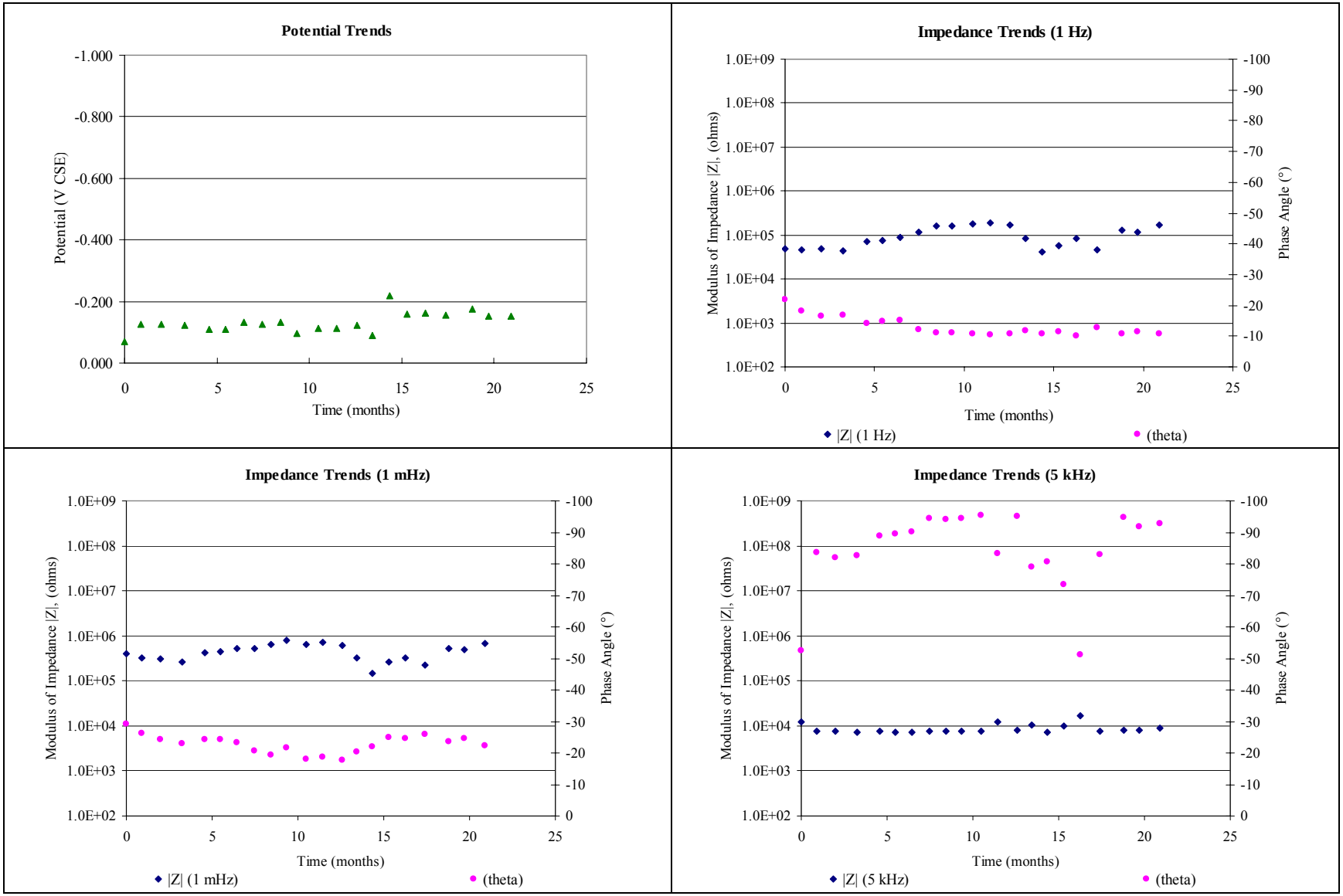

Figure B-62 Potential and Impedance Summary for Specimen 1019_C7

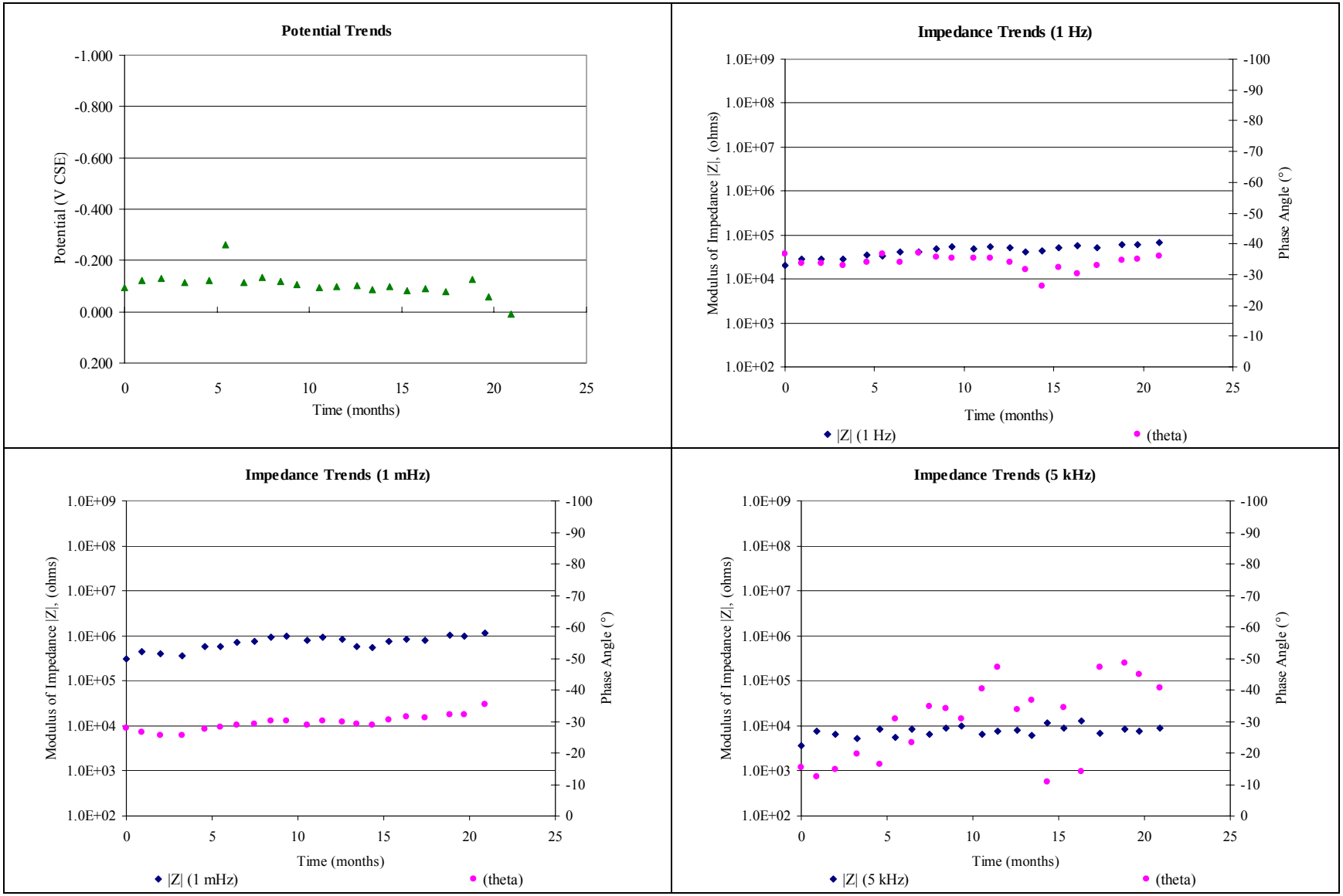

Figure B-63 Potential and Impedance Summary for Specimen 1019_C8

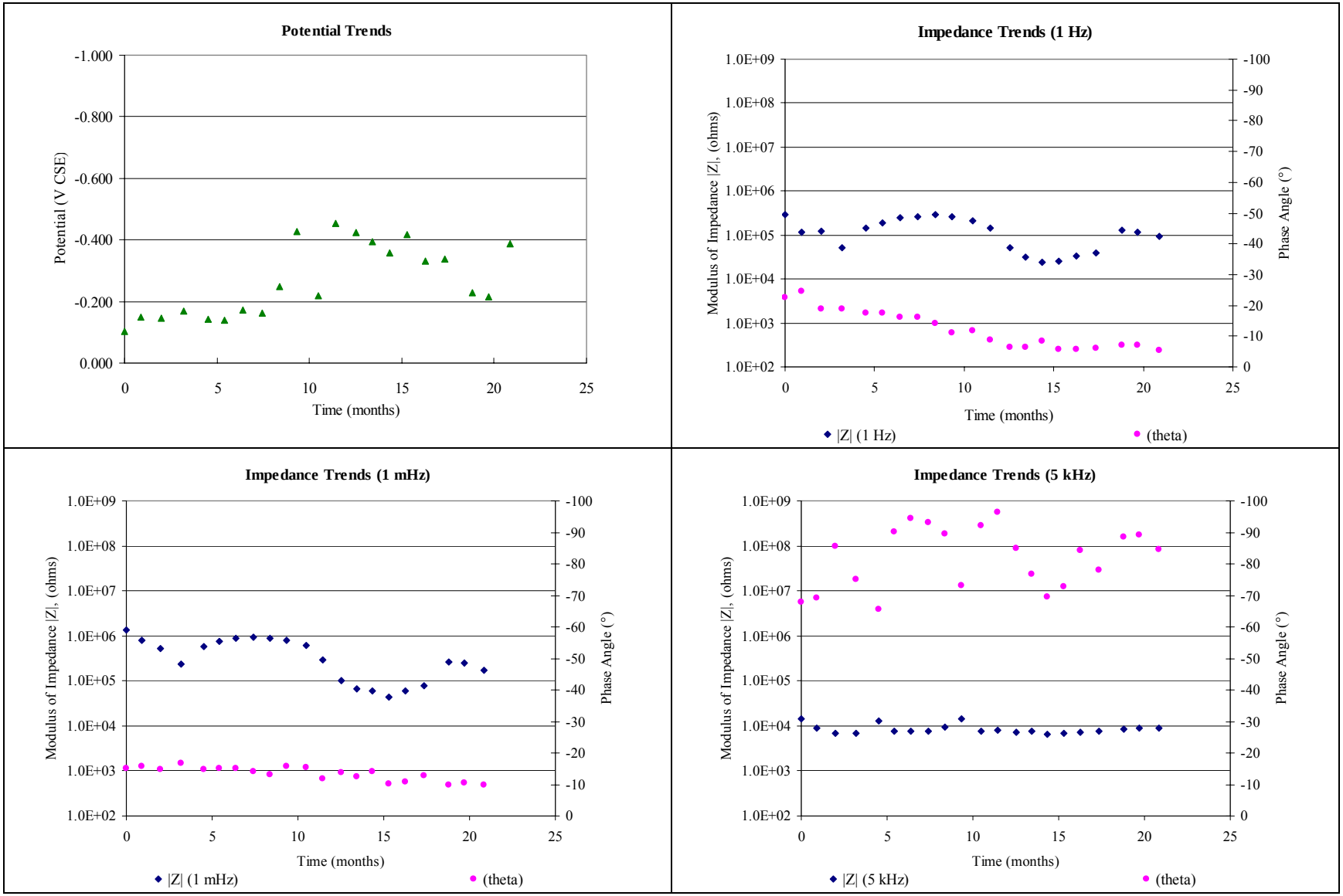

Figure B-64 Potential and Impedance Summary for Specimen 1019_C9

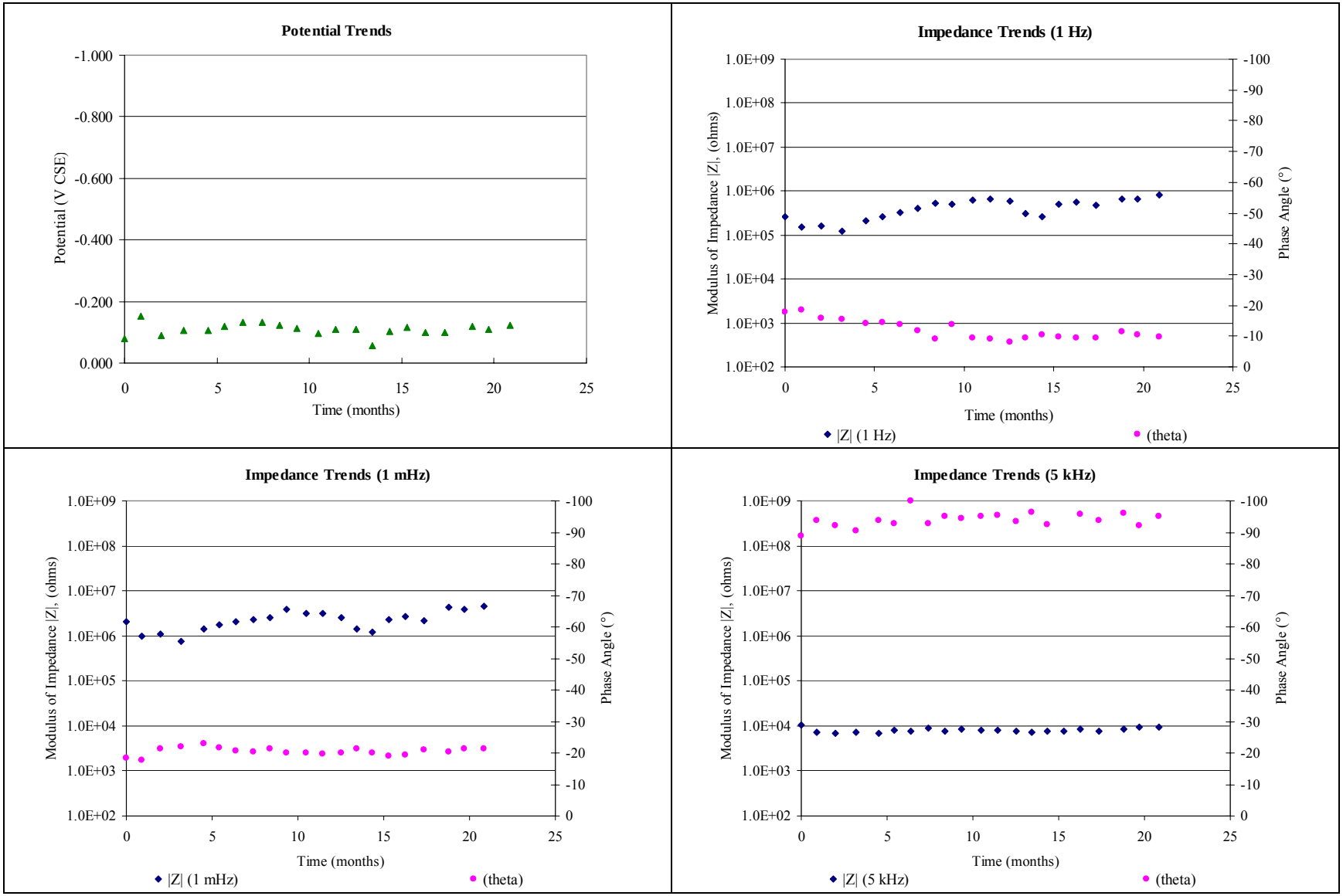

Figure B-65 Potential and Impedance Summary for Specimen 1019_C10

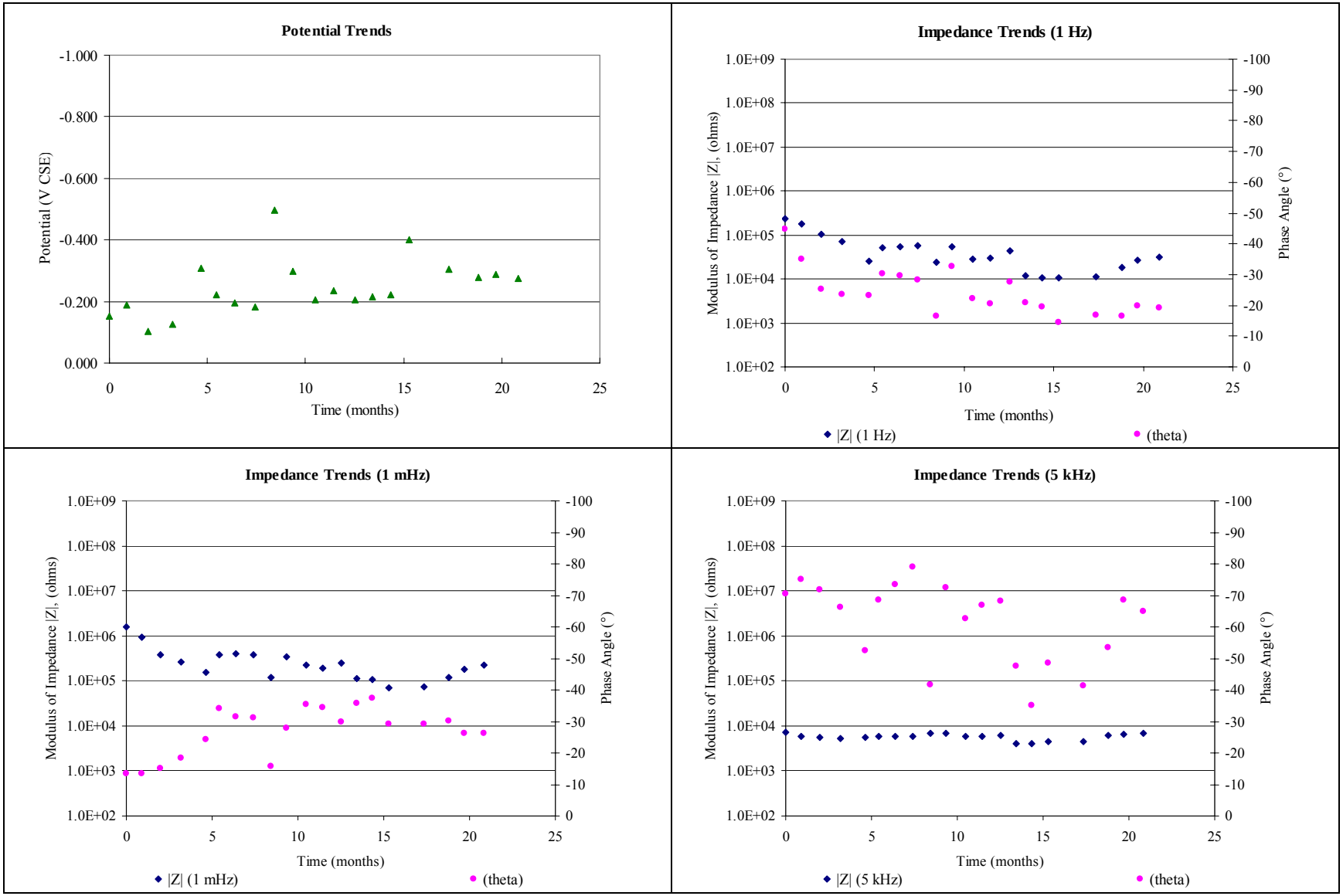

Figure B-66 Potential and Impedance Summary for Specimen 1019_CR1

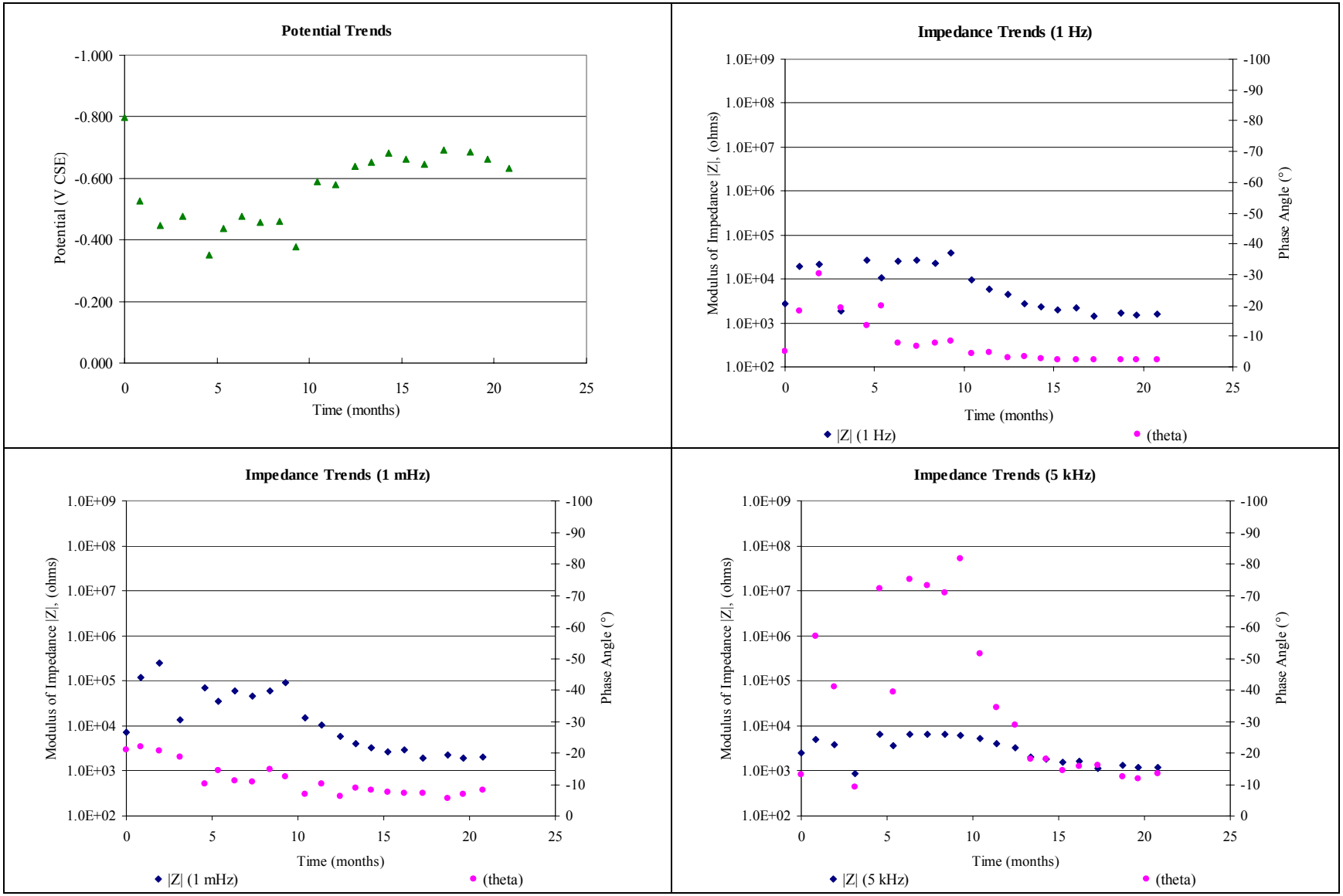

Figure B-67 Potential and Impedance Summary for Specimen 1019_CR2

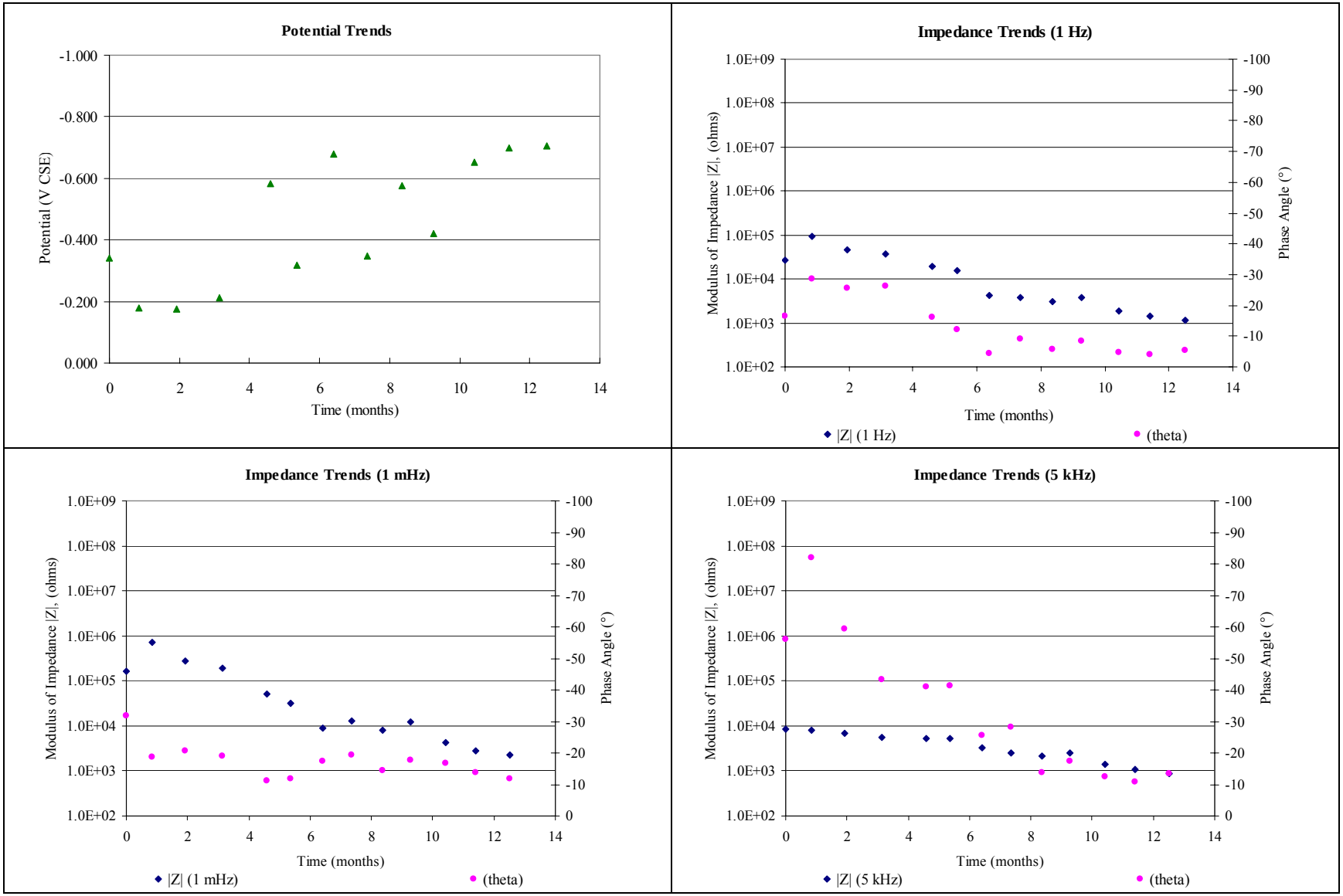

Figure B-68 Potential and Impedance Summary for Specimen 1019_CR3

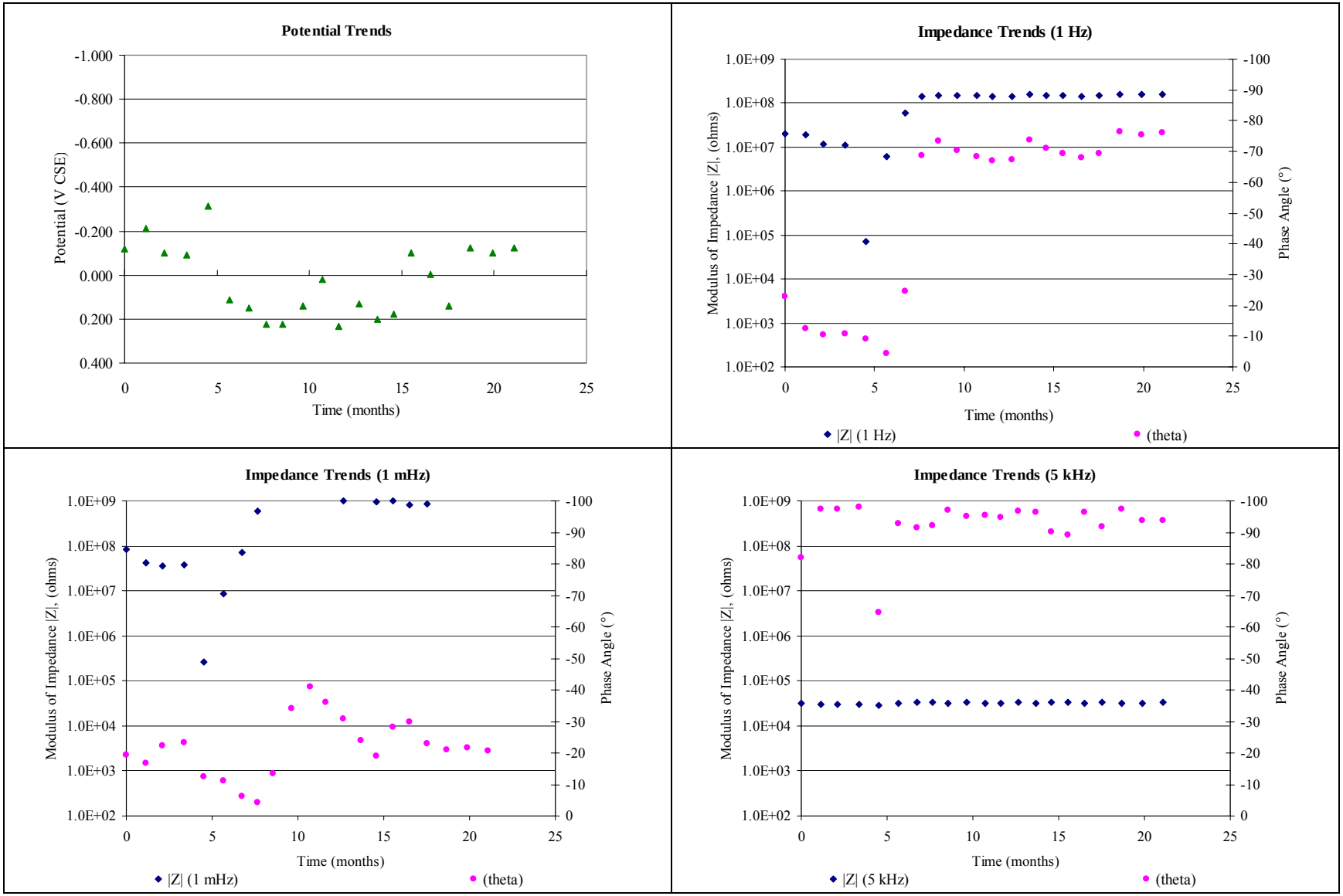

Figure B-69 Potential and Impedance Summary for Specimen 1136_C1

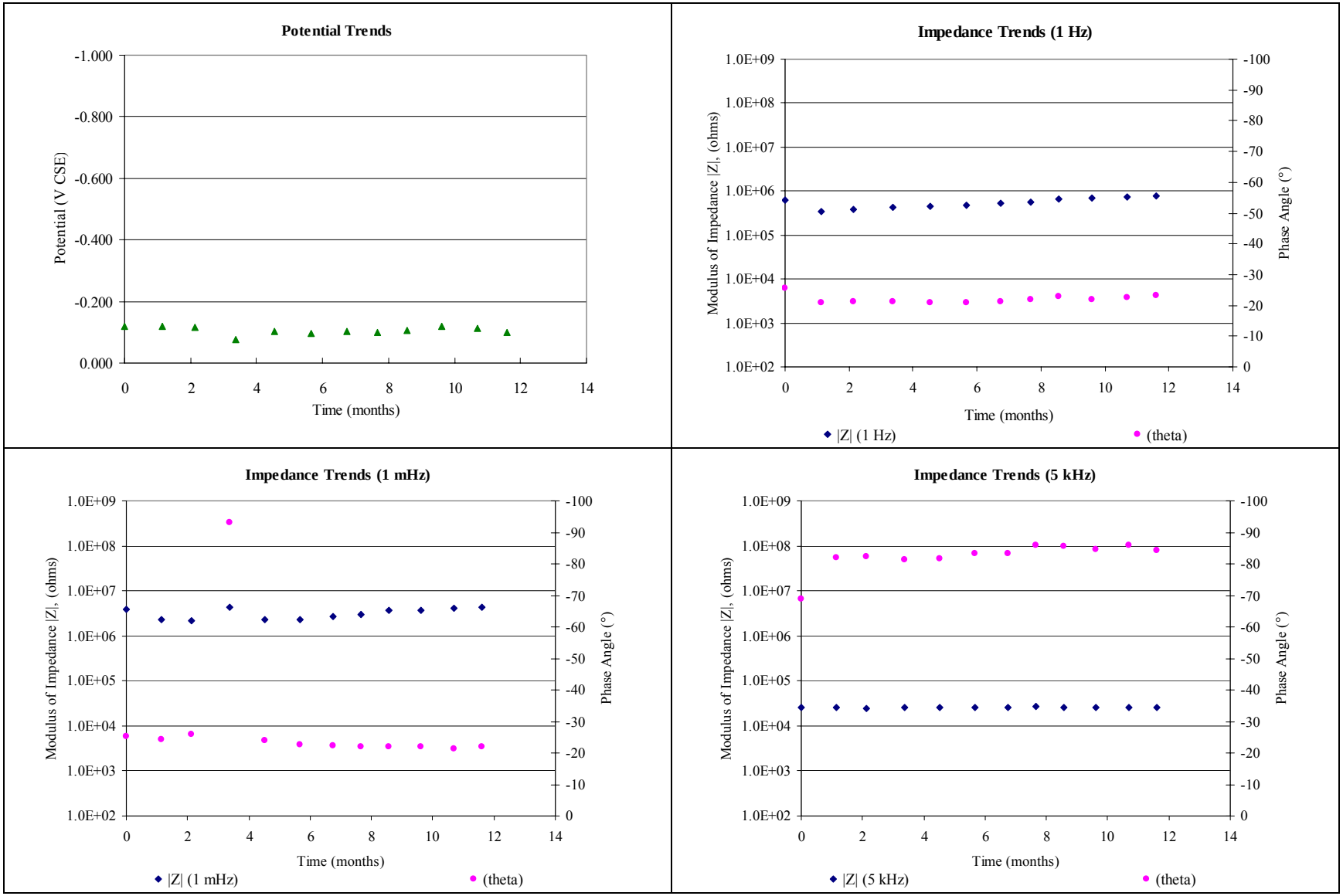

Figure B-70 Potential and Impedance Summary for Specimen 1136_C2

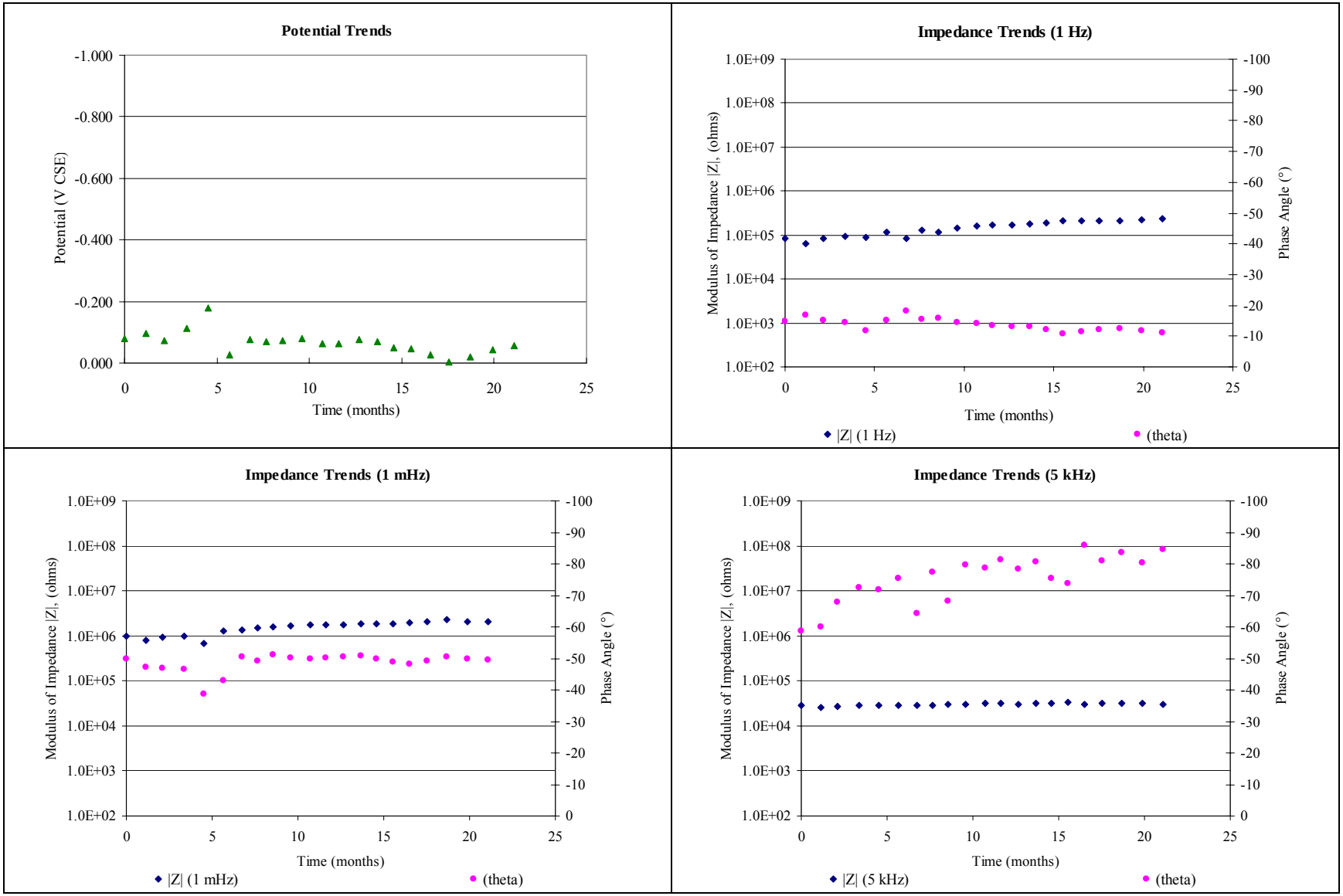

Figure B-71 Potential and Impedance Summary for Specimen 1136_C3

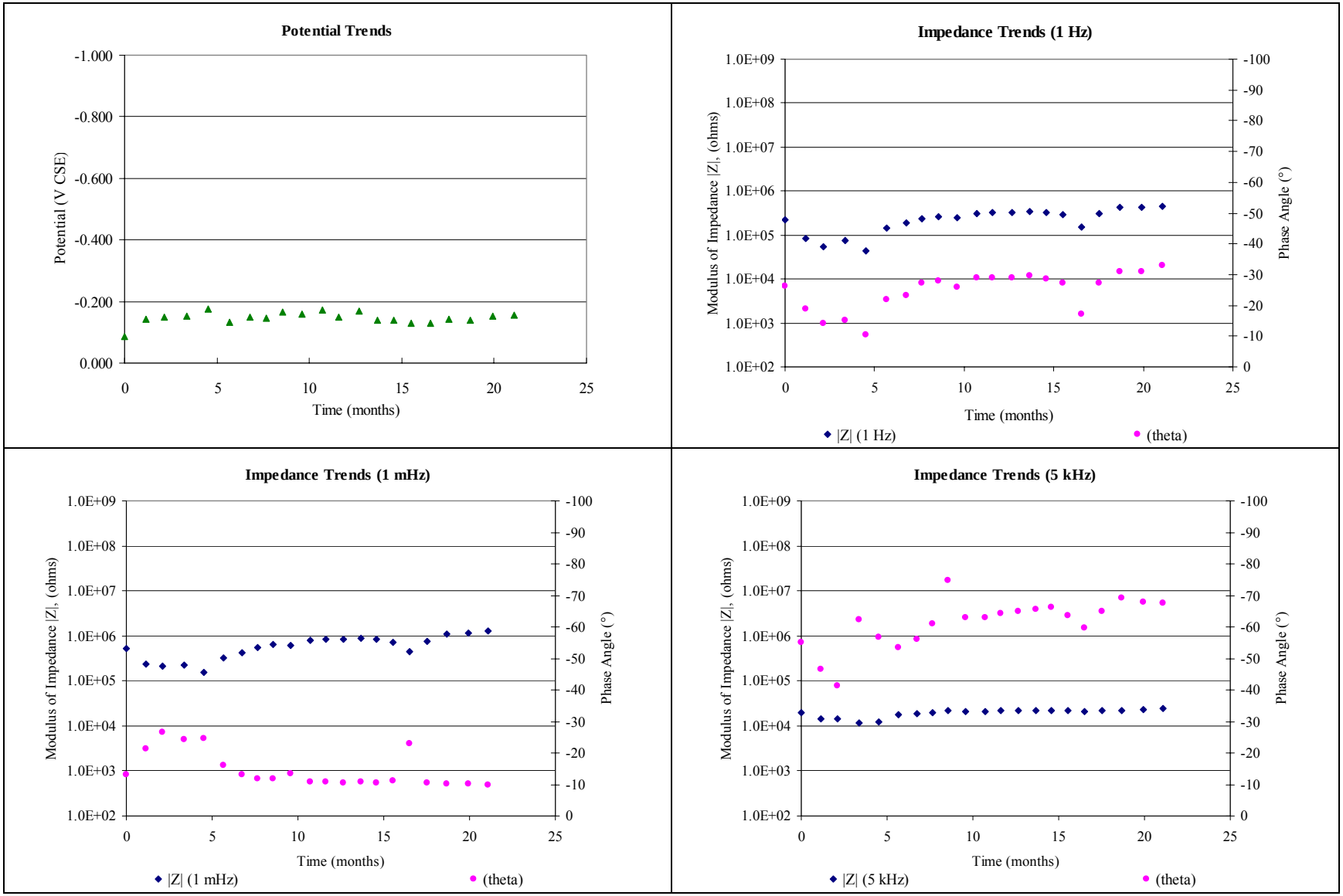

Figure B-72 Potential and Impedance Summary for Specimen 1136_C4

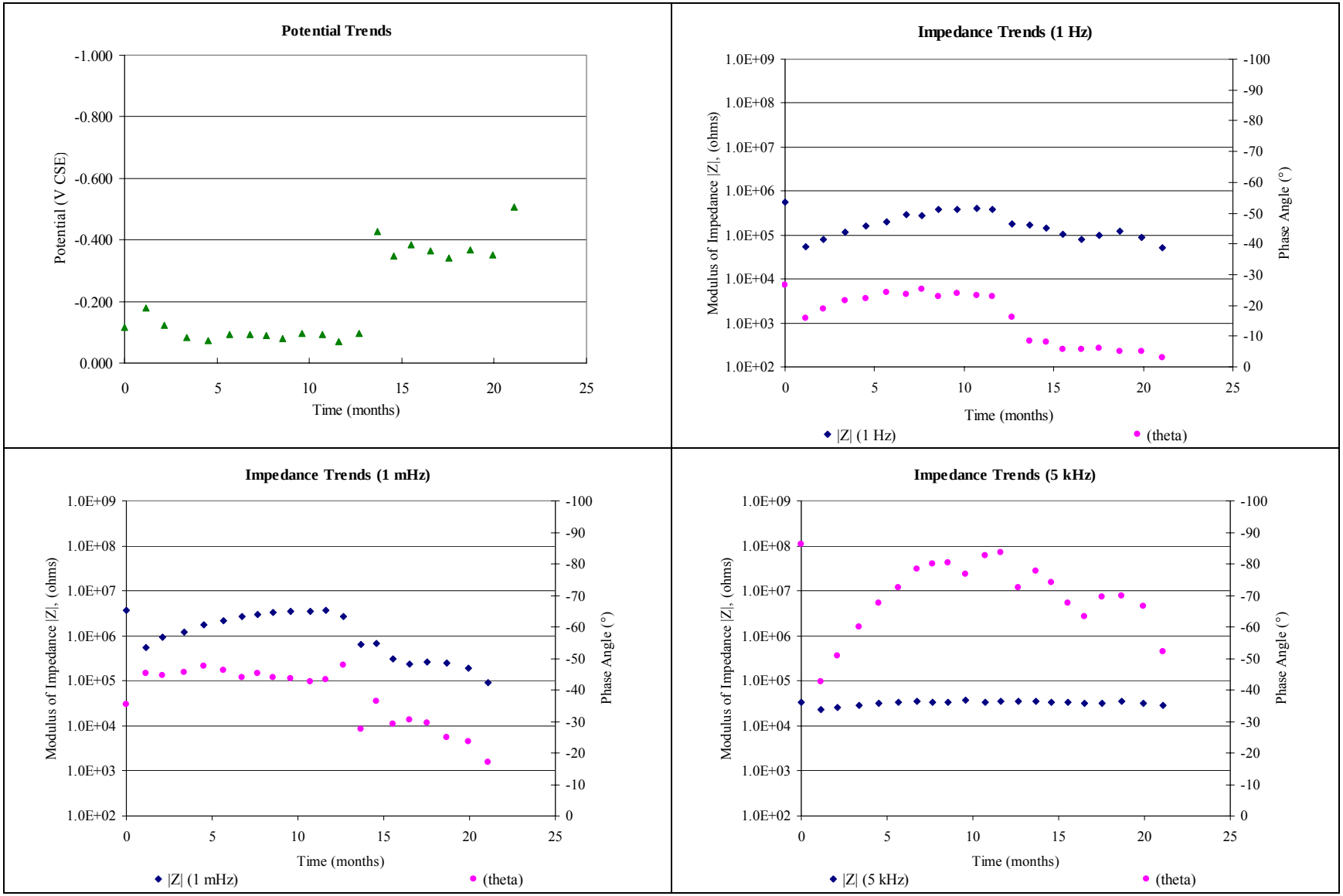

Figure B-73 Potential and Impedance Summary for Specimen 1136_C5

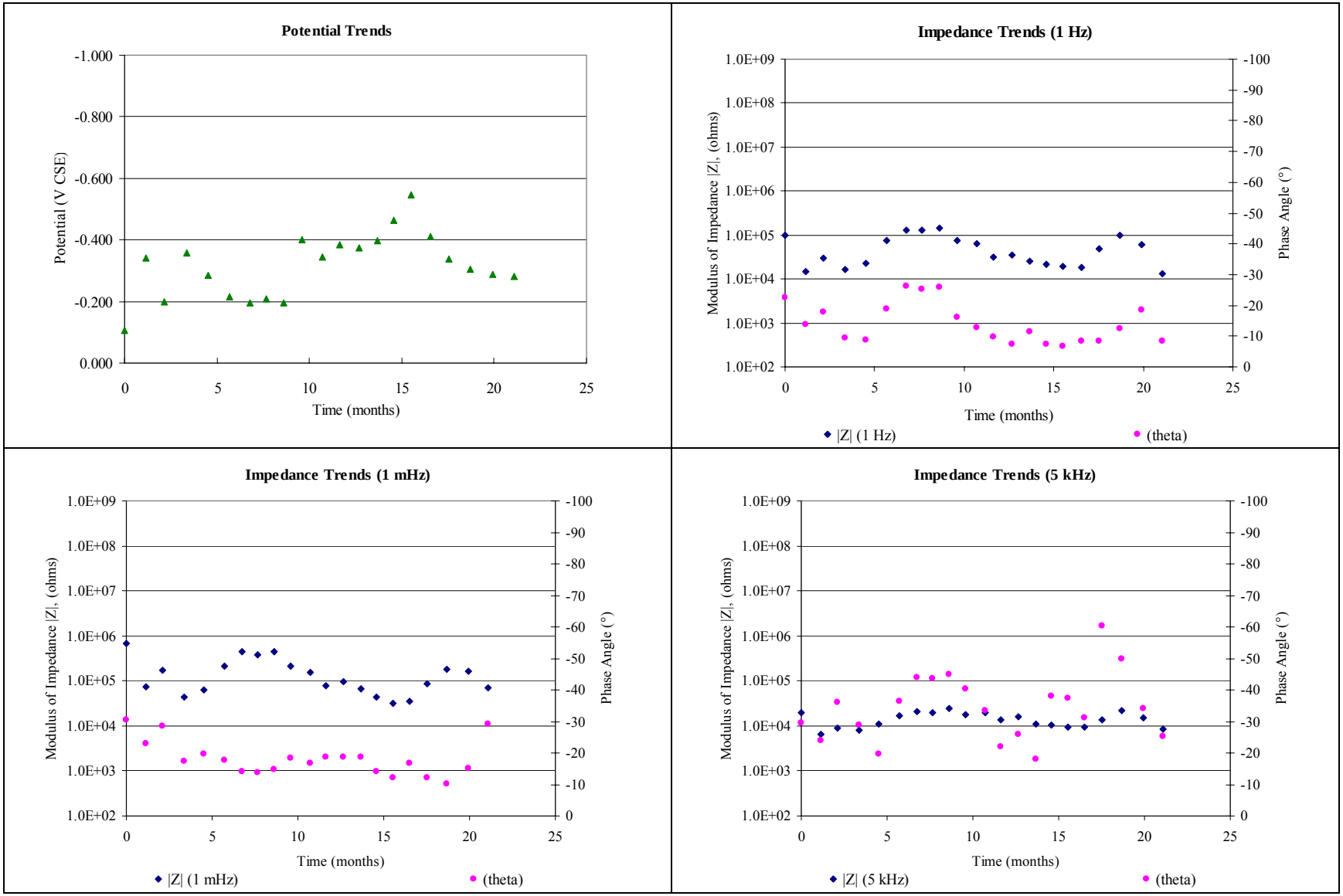

Figure B-74 Potential and Impedance Summary for Specimen 1136_C6

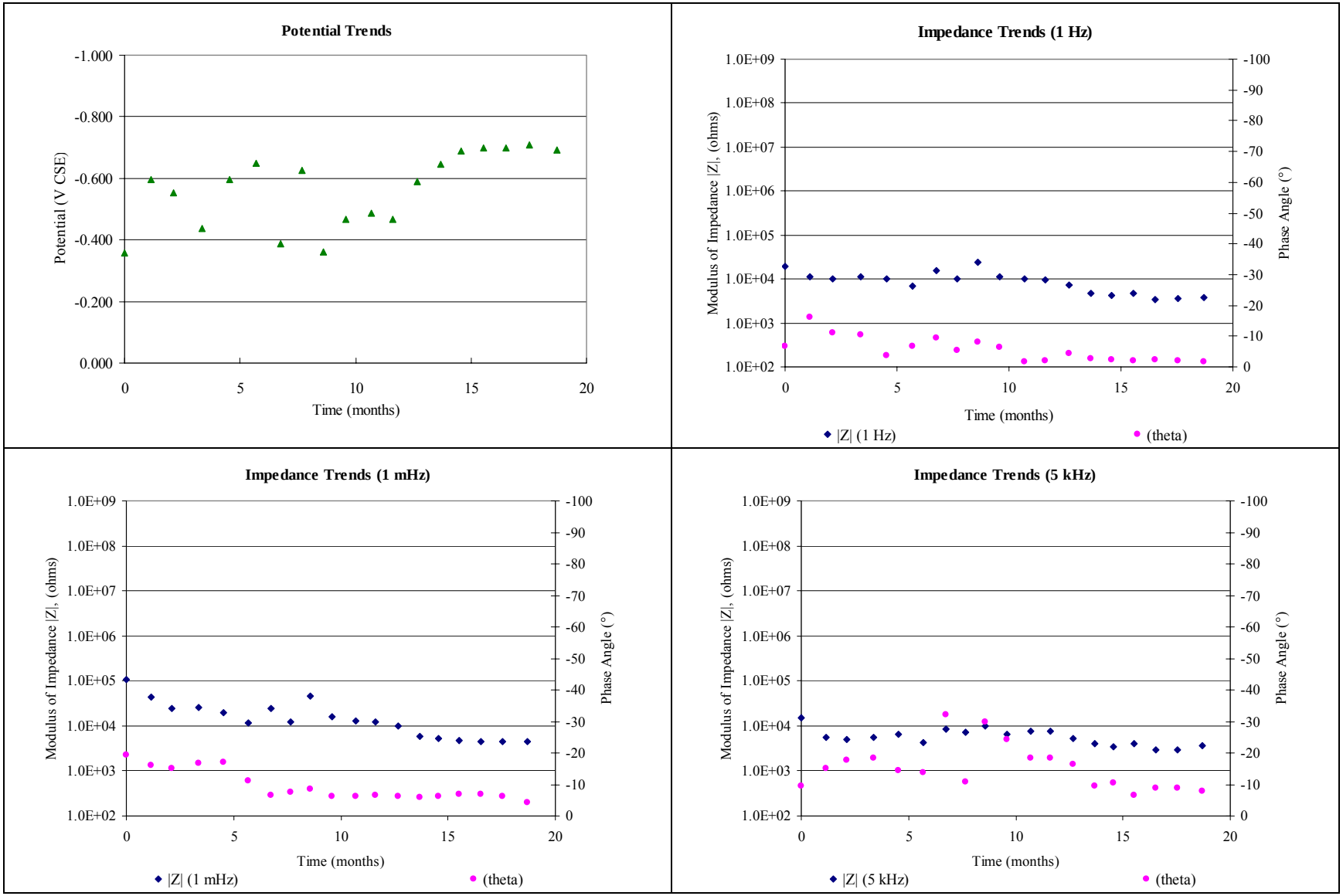

Figure B-75 Potential and Impedance Summary for Specimen 1136_C7

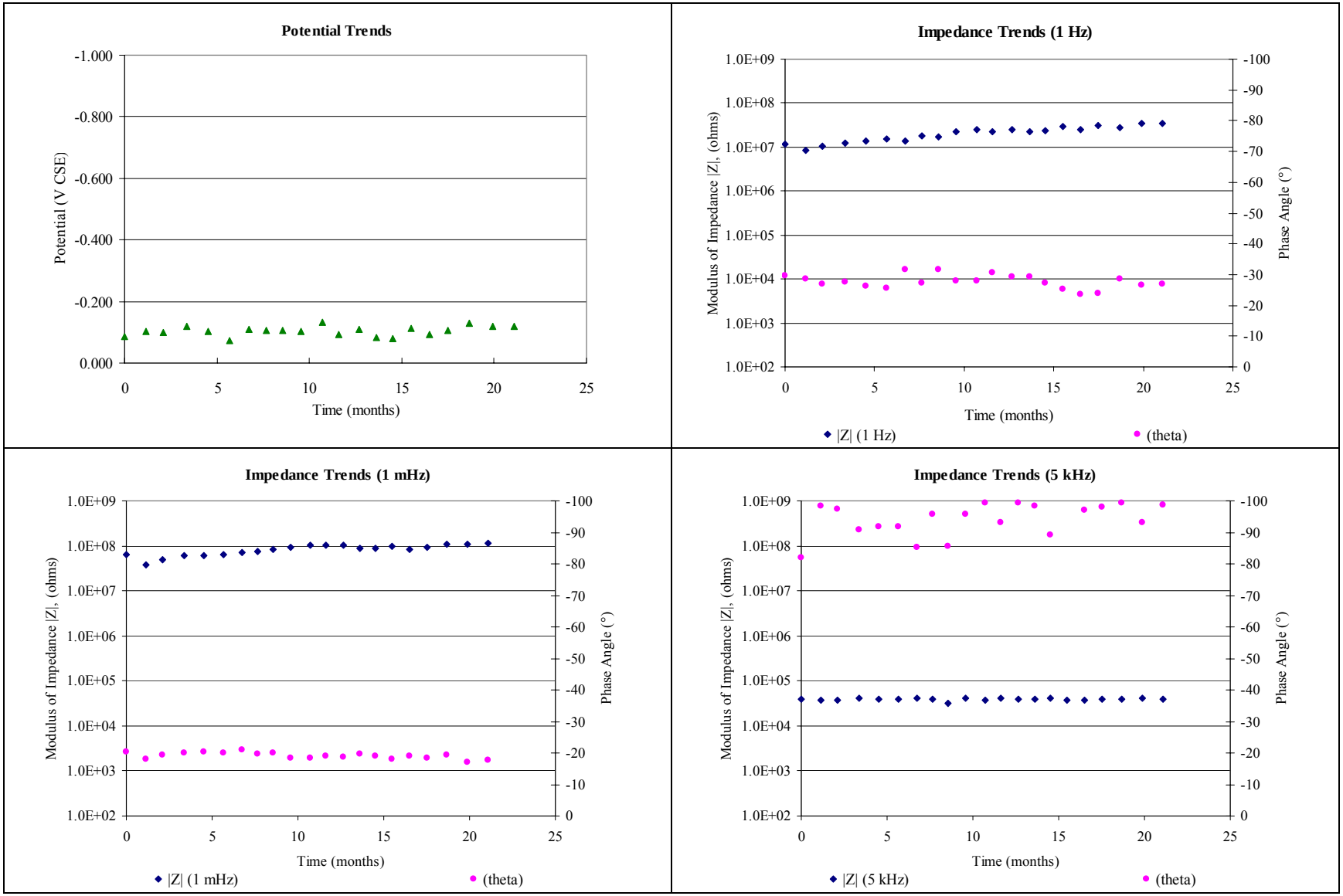

Figure B-76 Potential and Impedance Summary for Specimen 1136_C8

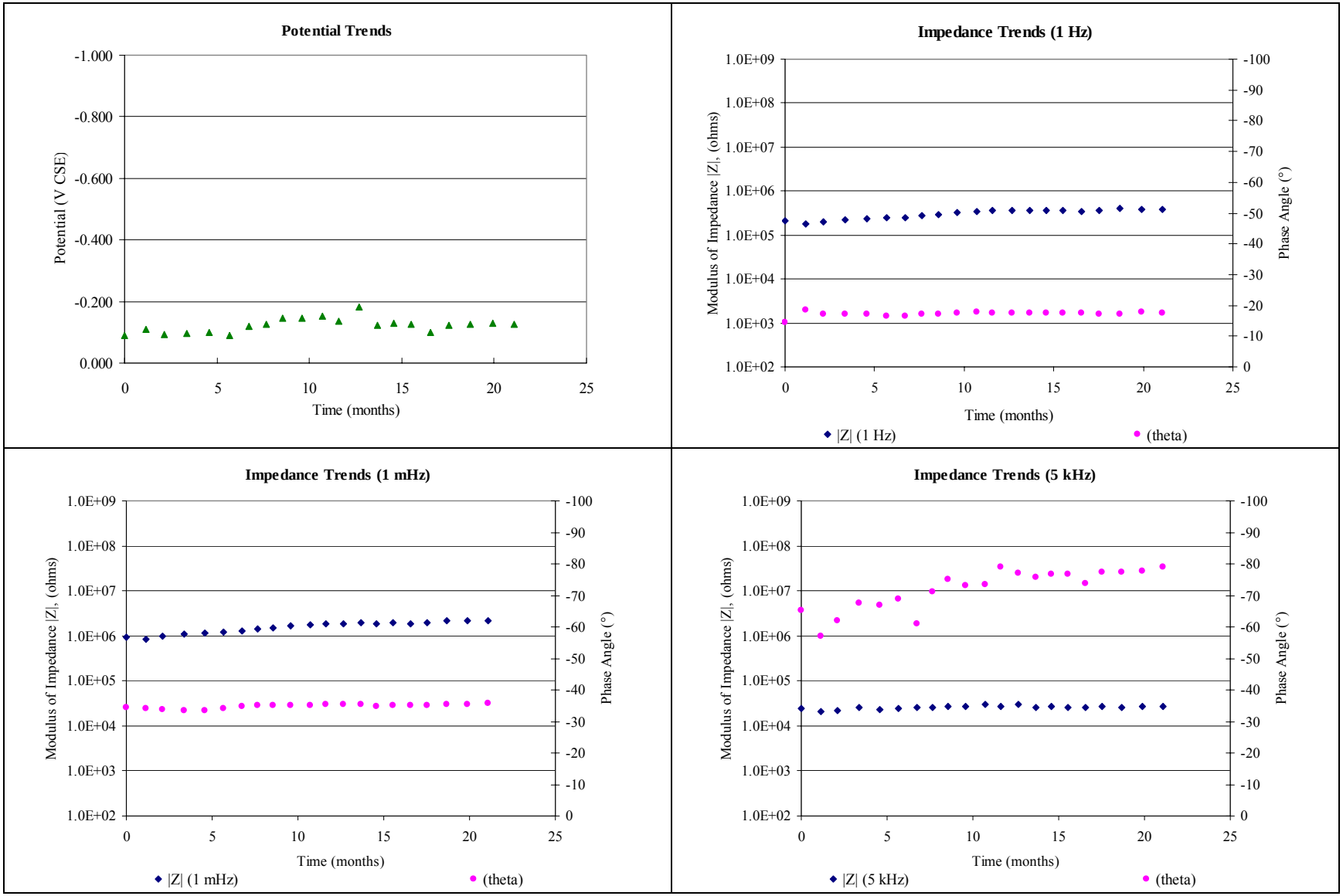

Figure B-77 Potential and Impedance Summary for Specimen 1136_C9

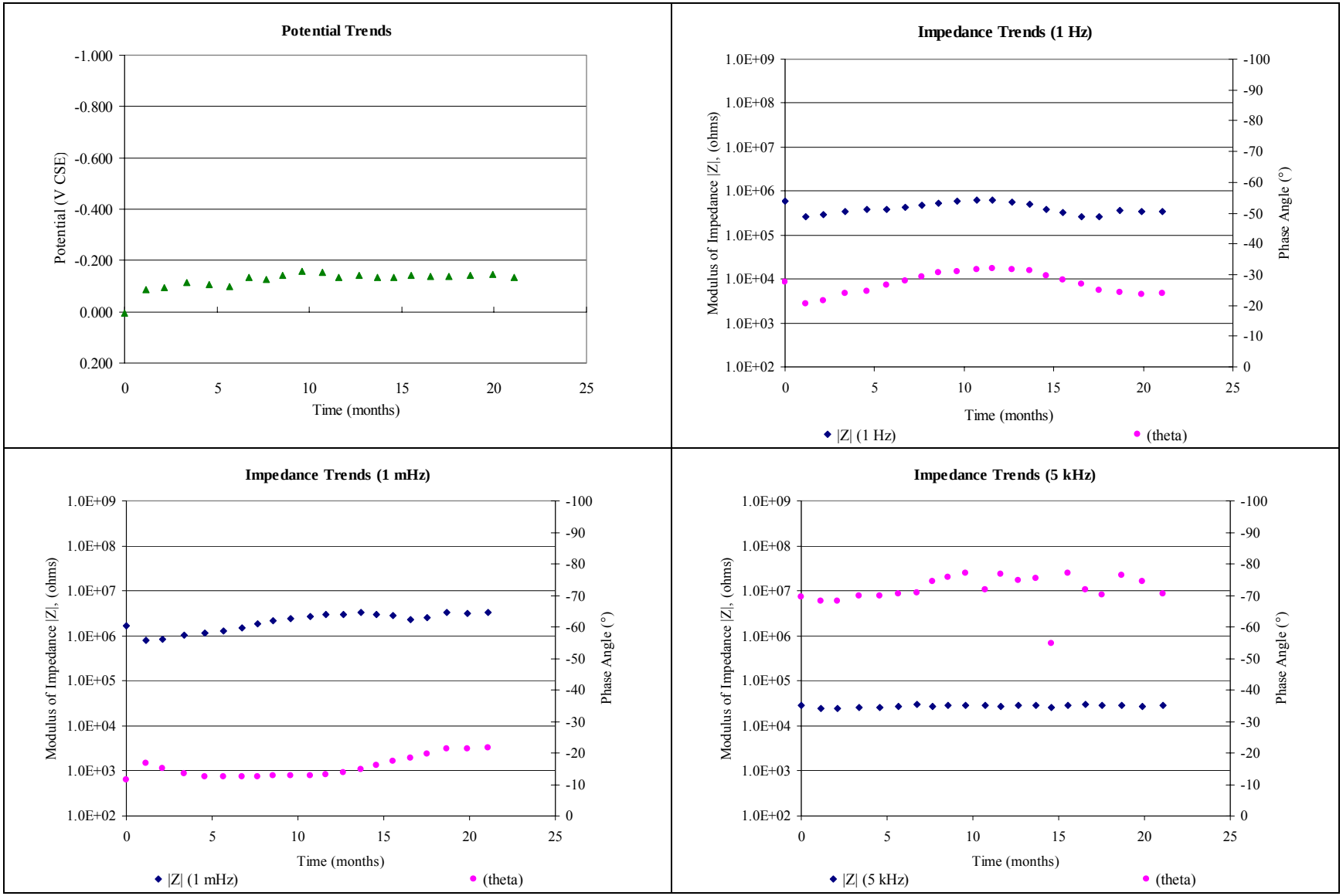

Figure B-78 Potential and Impedance Summary for Specimen 1136_C10

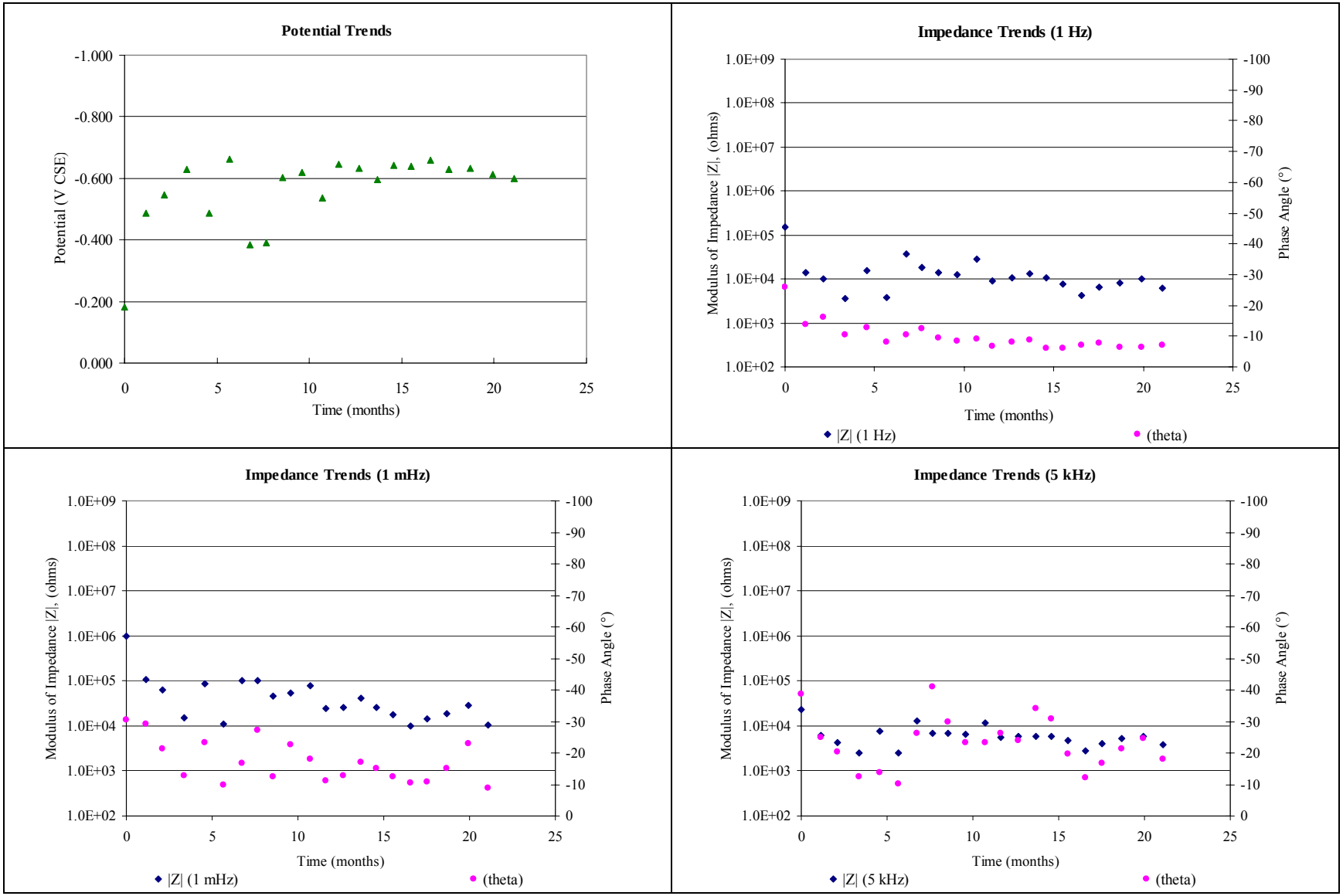

Figure B-79 Potential and Impedance Summary for Specimen 1136_C11

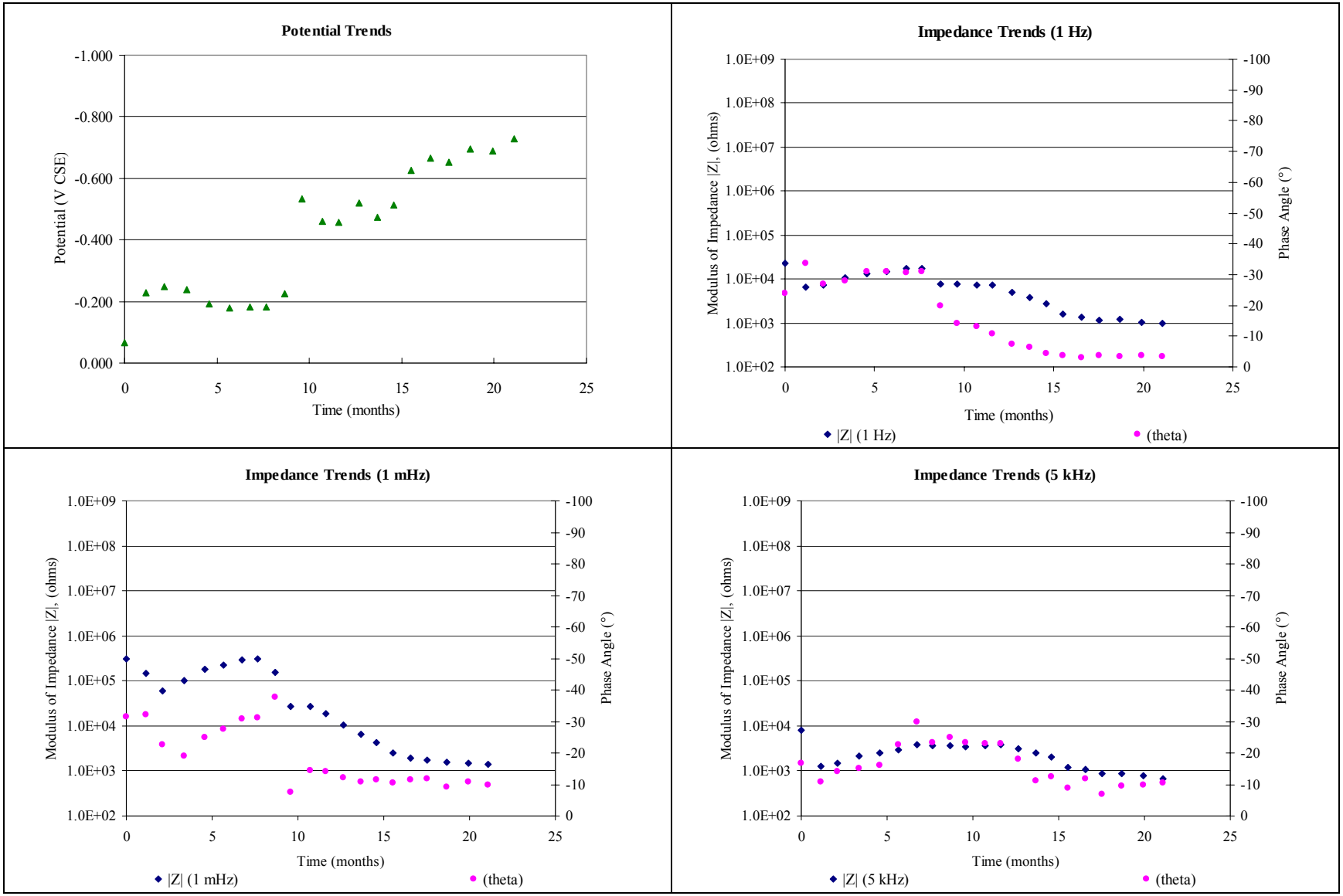

Figure B-80 Potential and Impedance Summary for Specimen 1136_C12

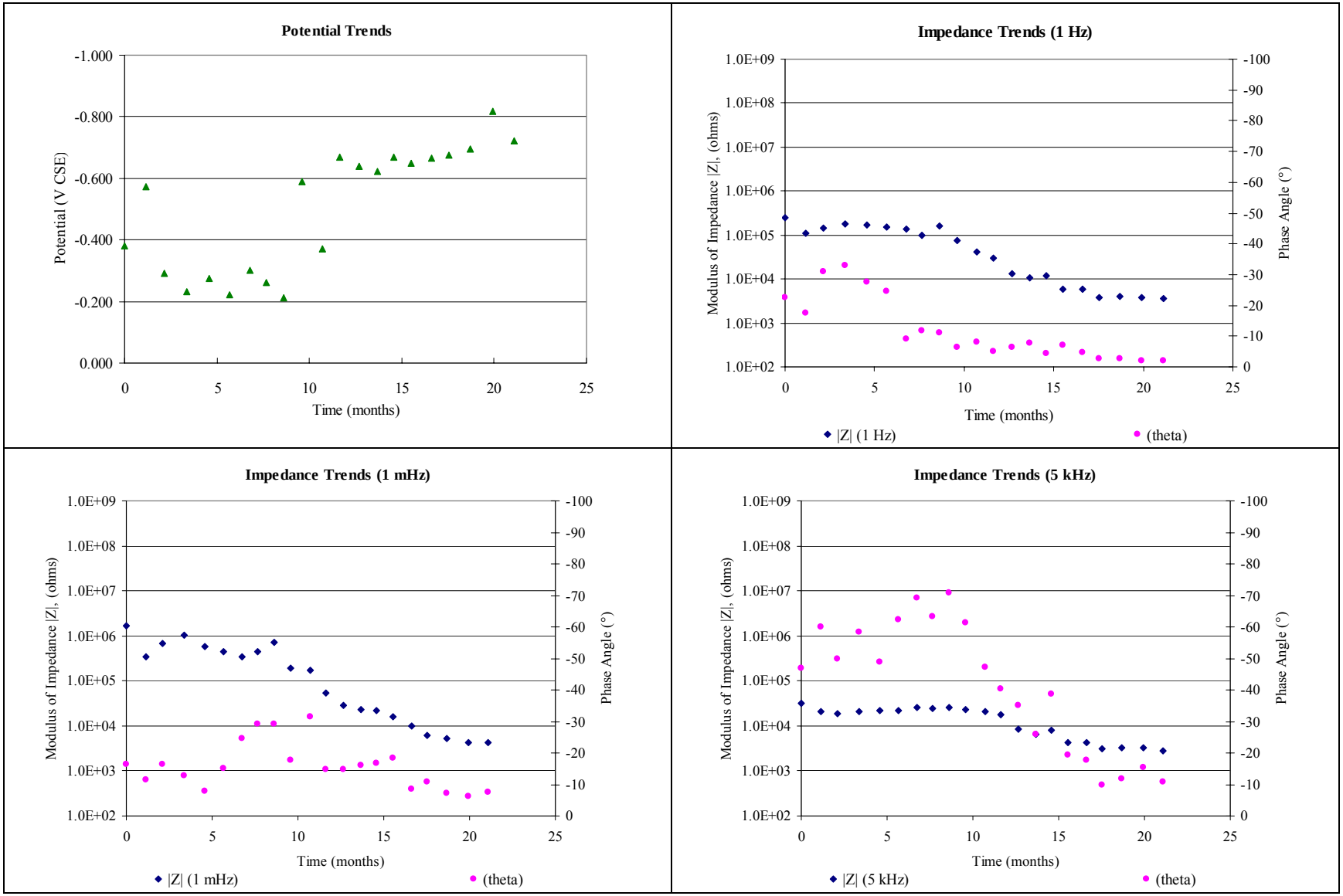

Figure B-81 Potential and Impedance Summary for Specimen 1136_CR1

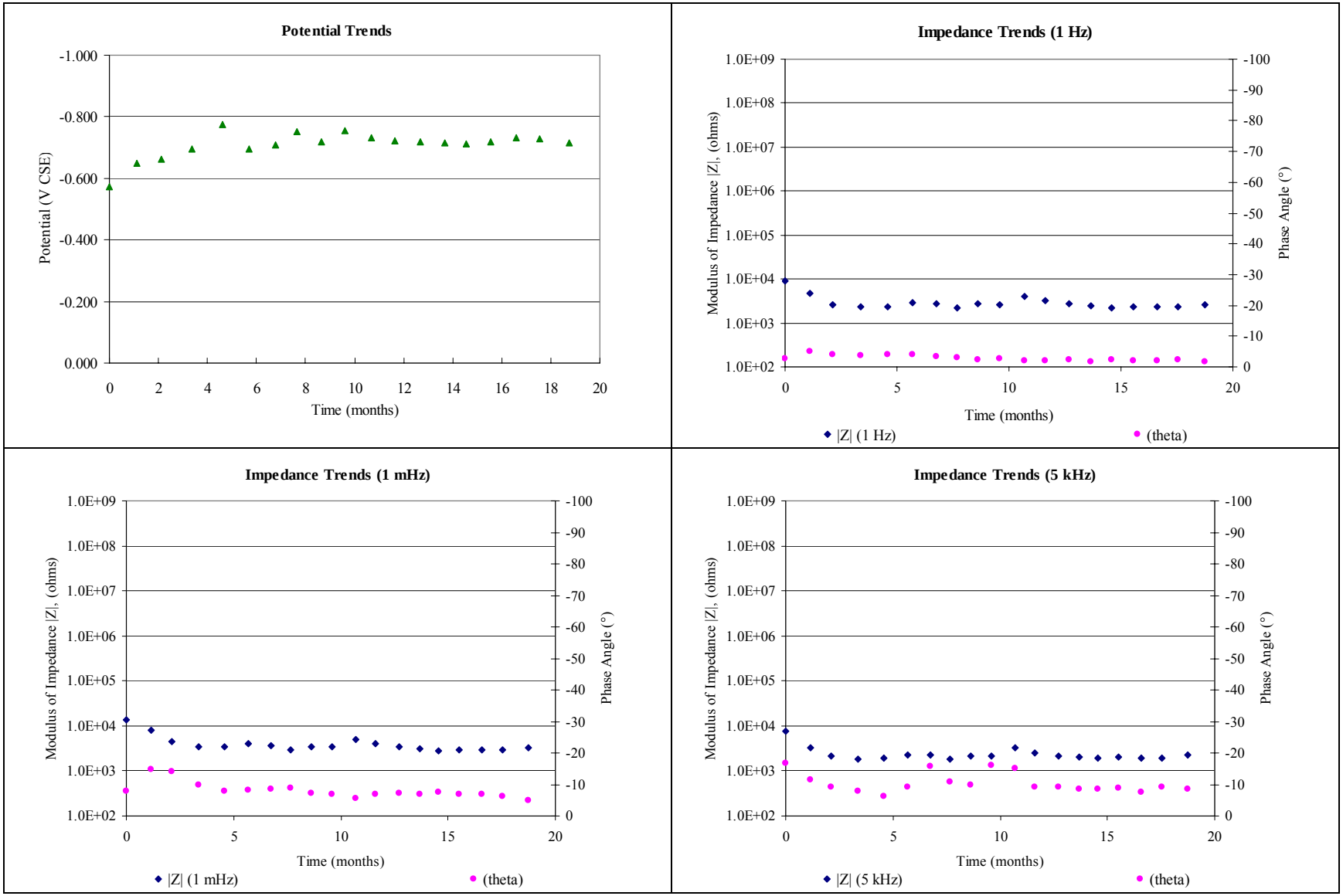

Figure B-82 Potential and Impedance Summary for Specimen 1136_CR2

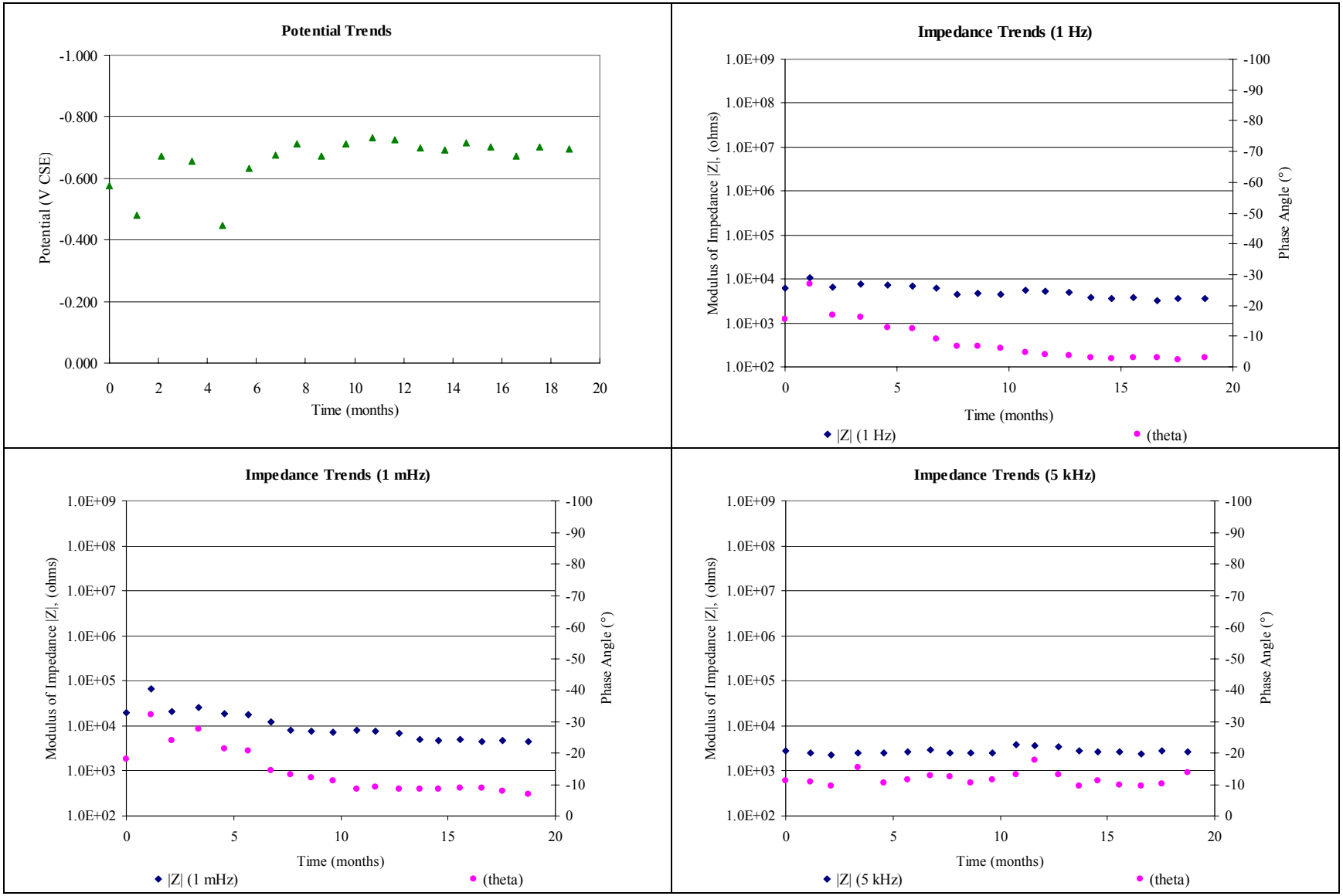

Figure B-83 Potential and Impedance Summary for Specimen 1136_CR3

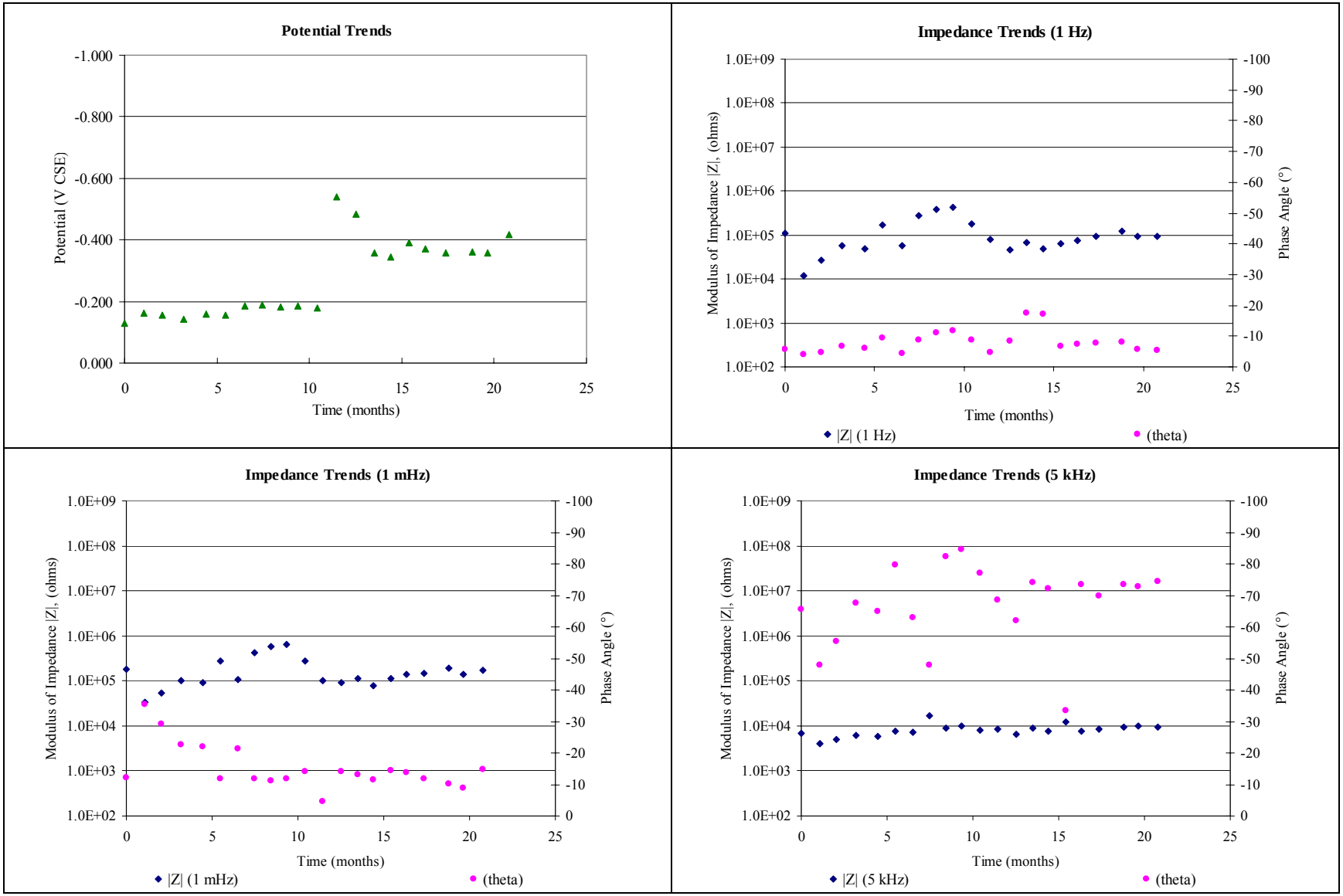

Figure B-84 Potential and Impedance Summary for Specimen 2021_C1

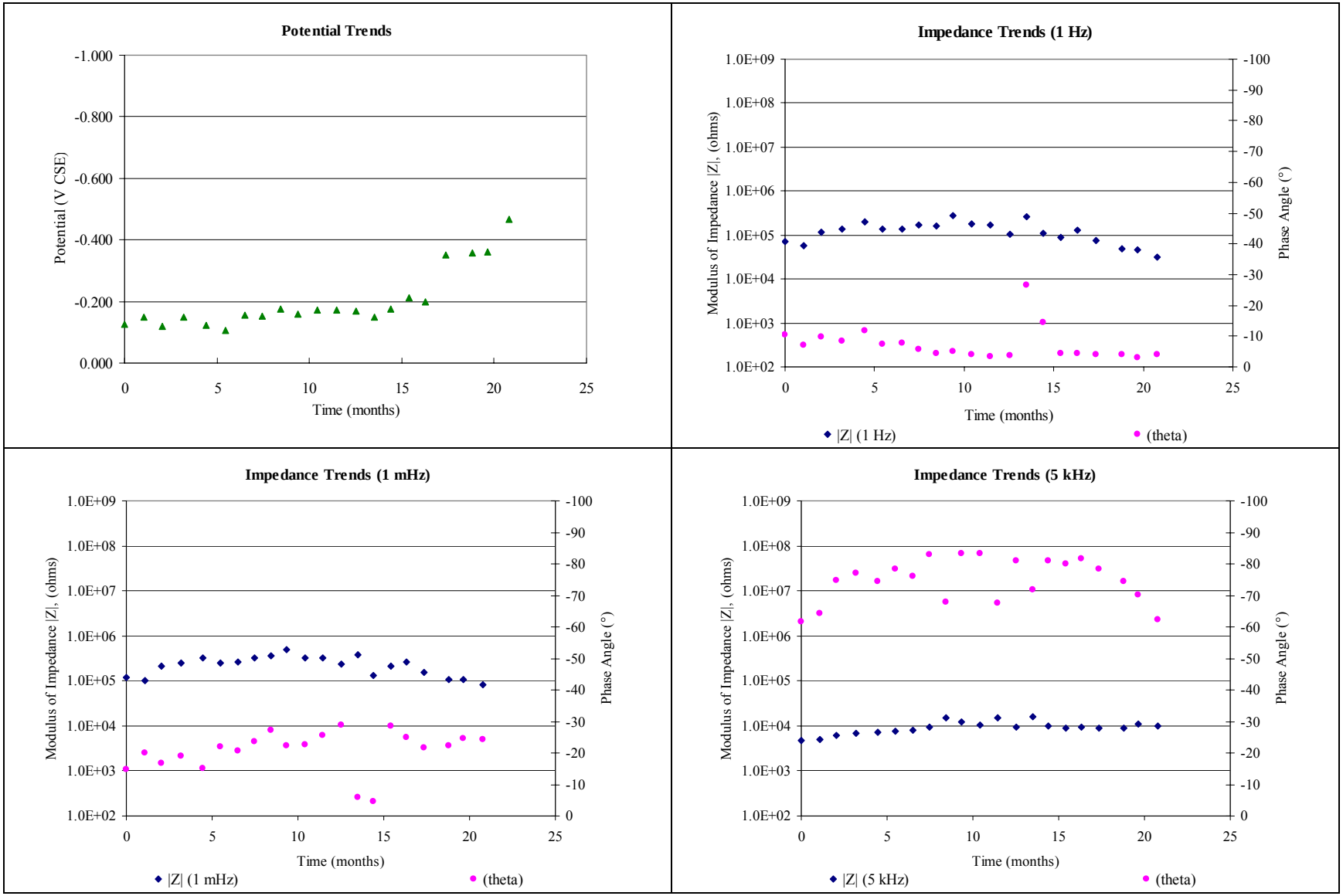

Figure B-85 Potential and Impedance Summary for Specimen 2021_C2

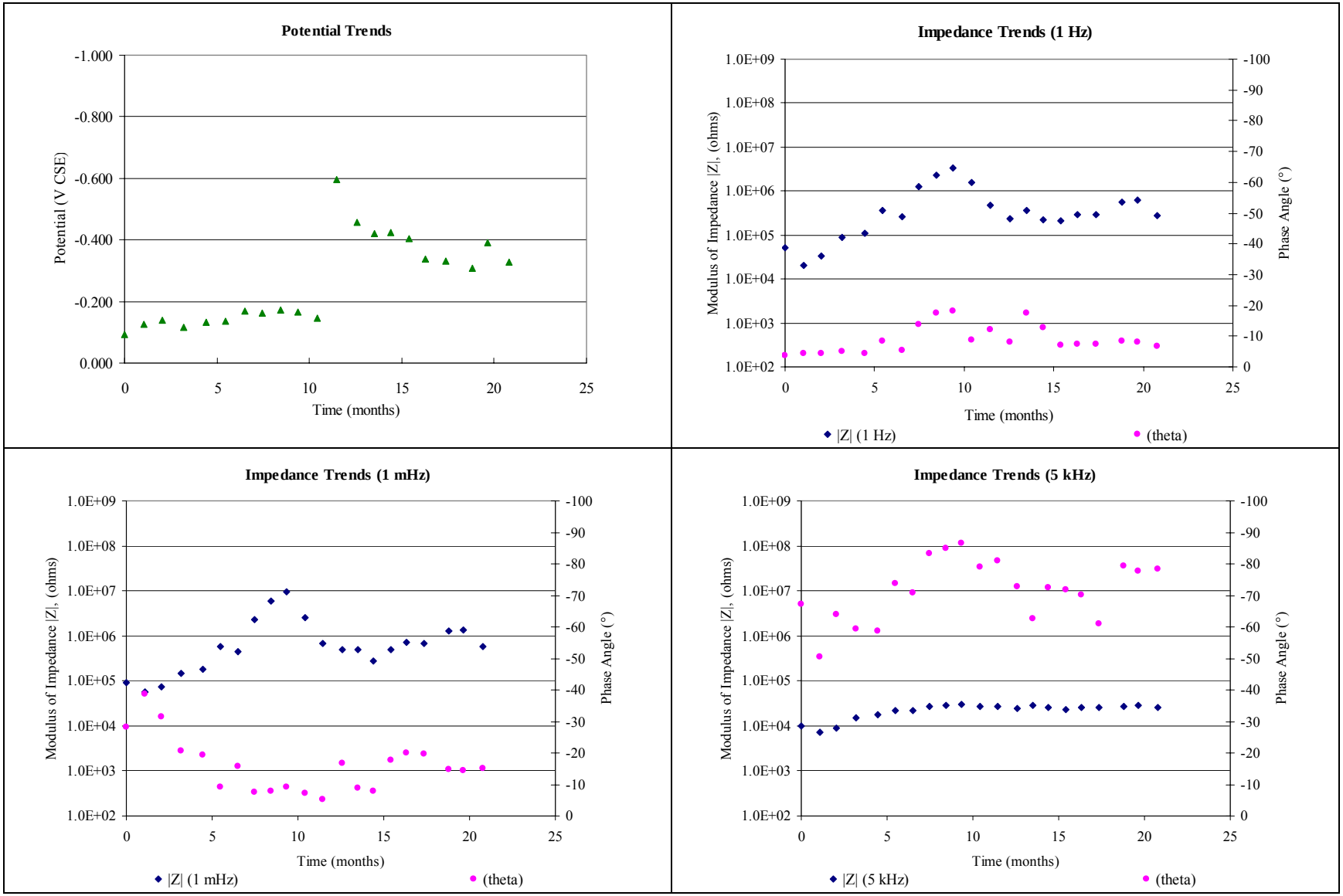

Figure B-86 Potential and Impedance Summary for Specimen 2021_C3

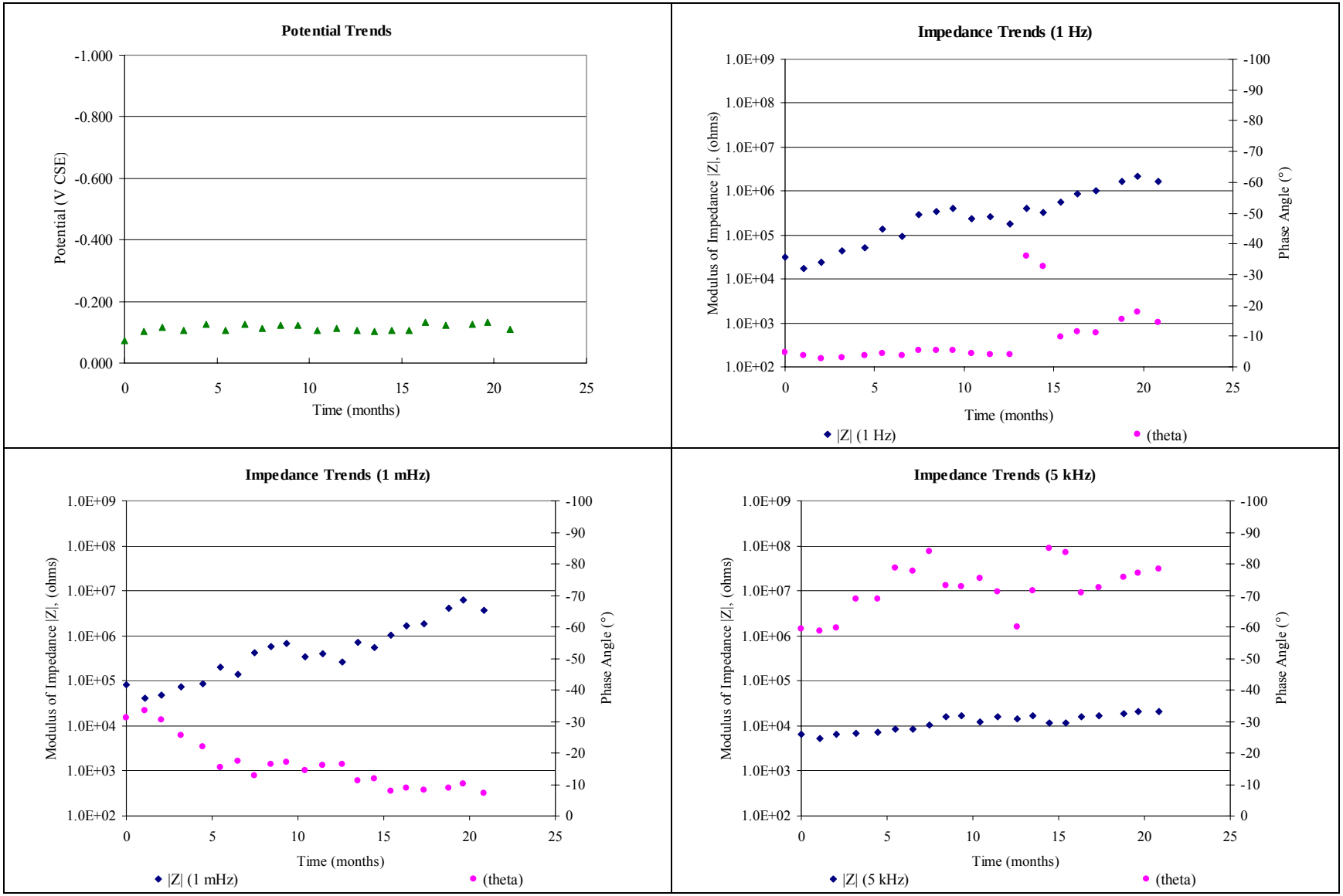

Figure B-87 Potential and Impedance Summary for Specimen 2021_C4

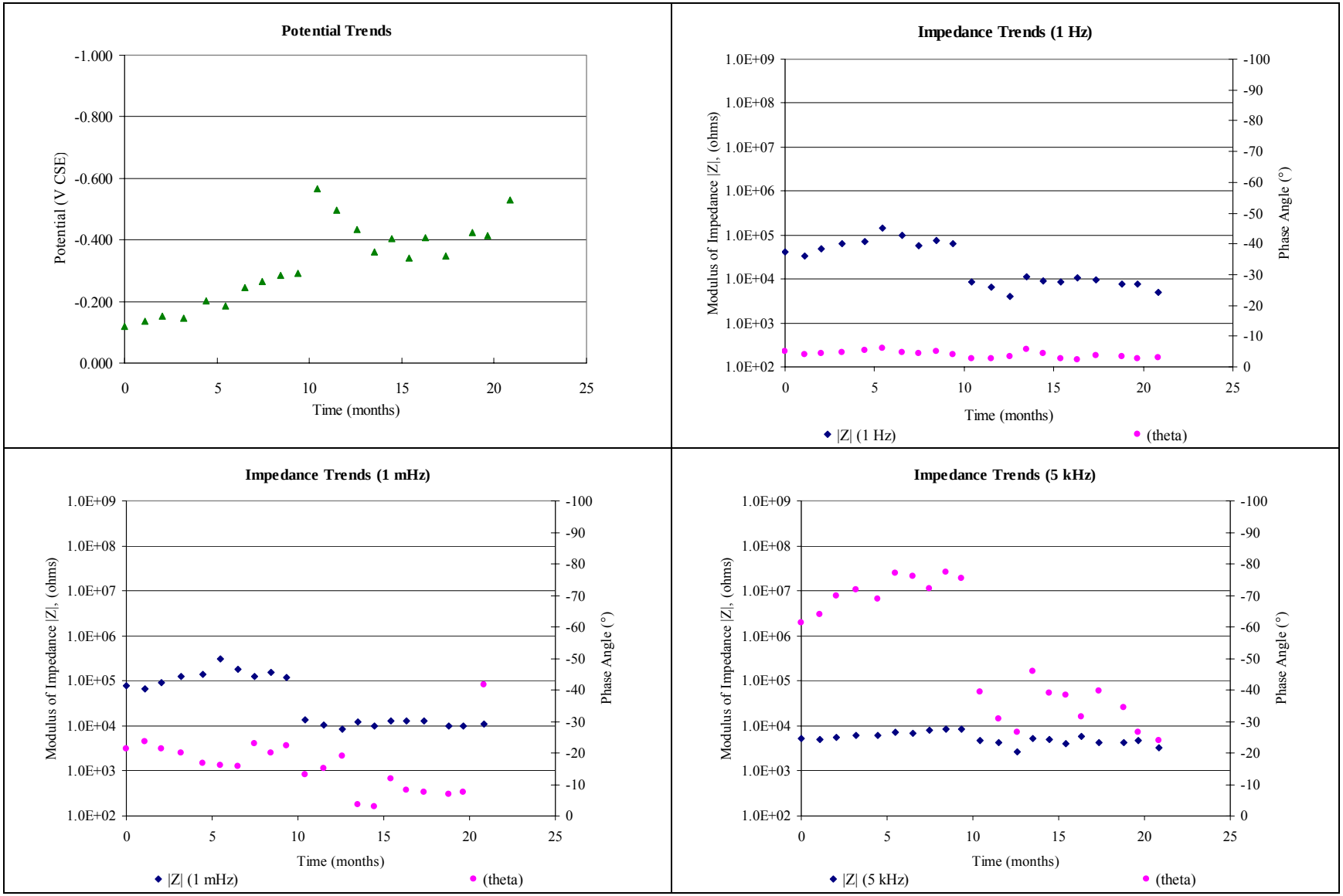

Figure B-88 Potential and Impedance Summary for Specimen 2021_C5

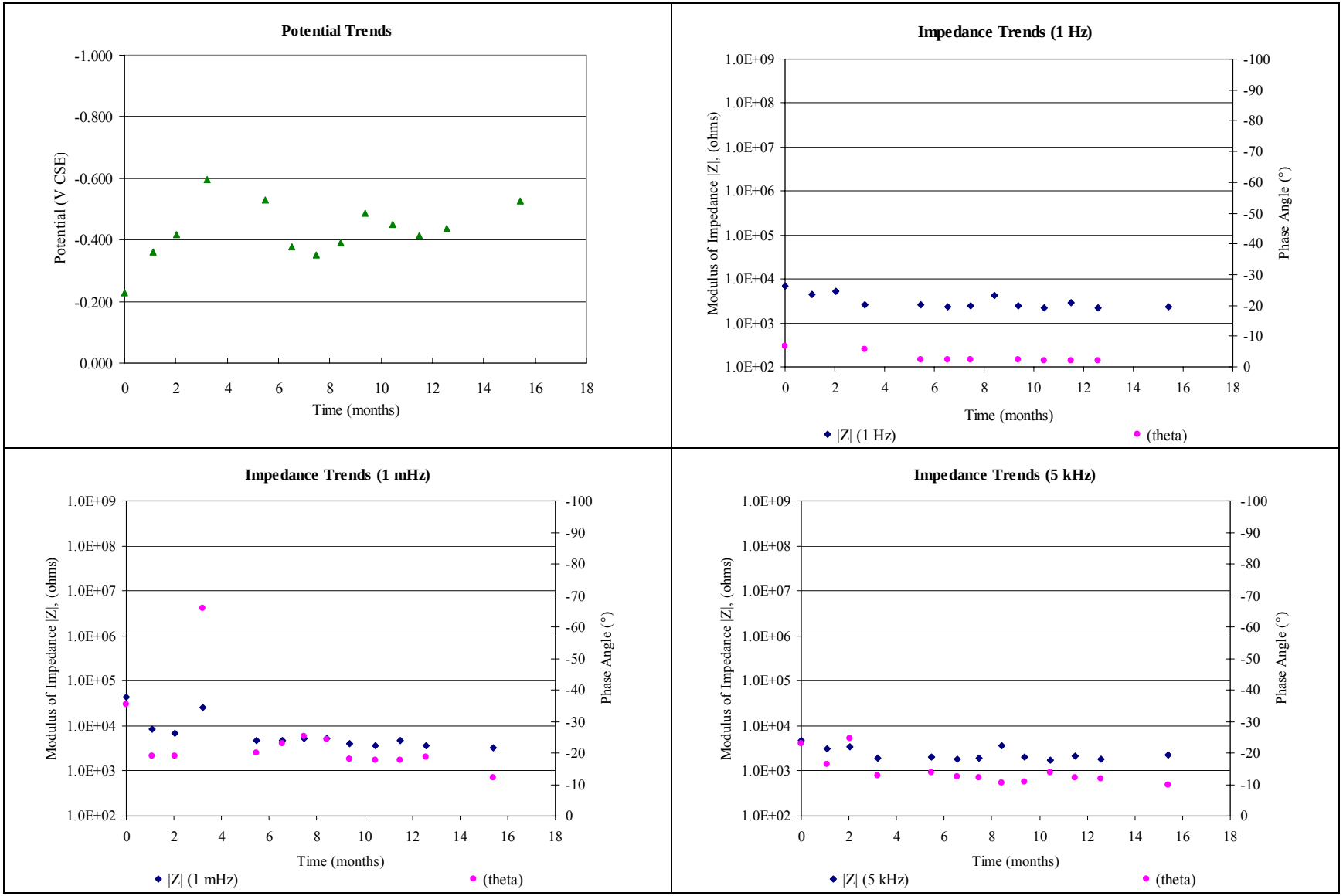

Figure B-89 Potential and Impedance Summary for Specimen 2021_C6

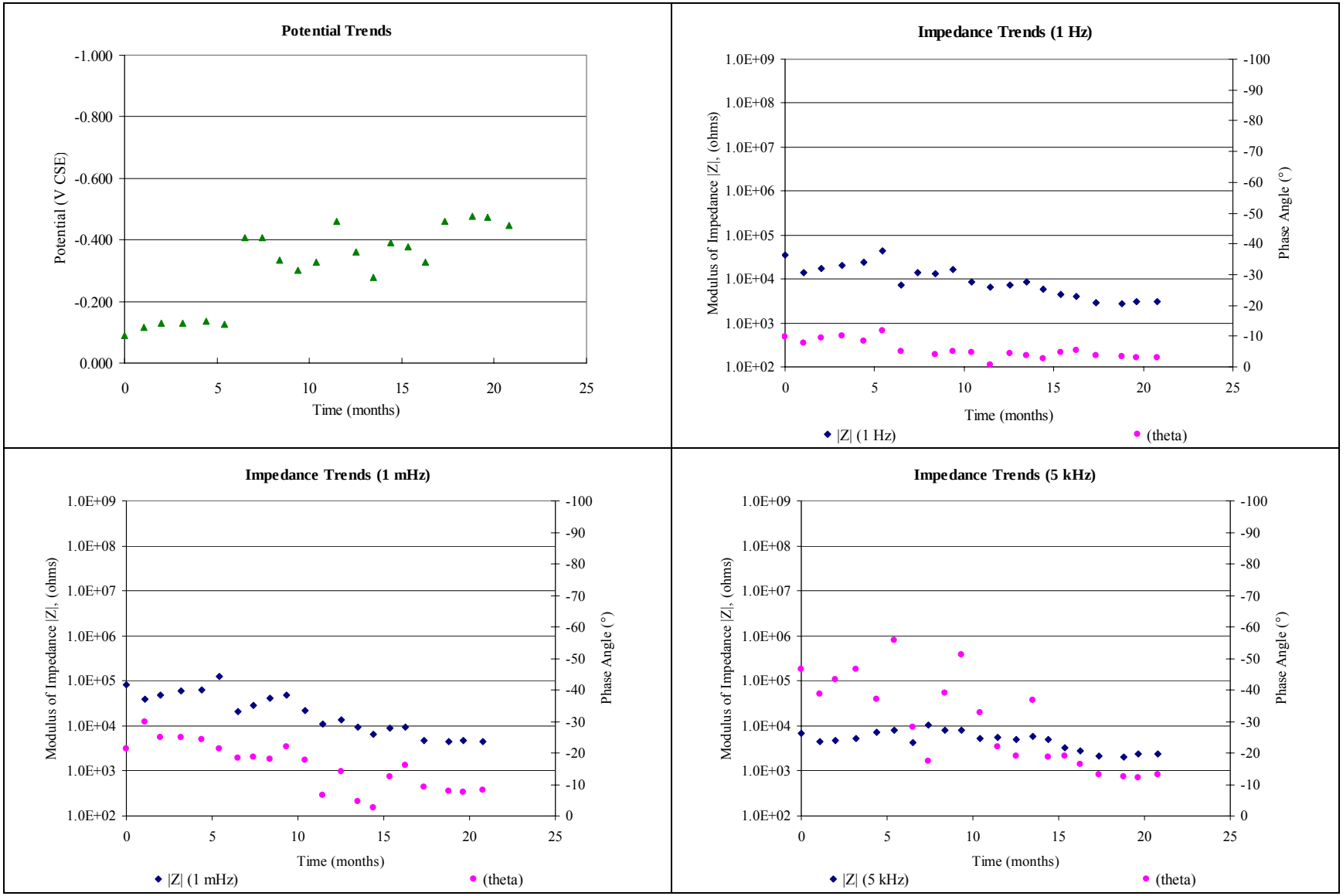

Figure B-90 Potential and Impedance Summary for Specimen 2021_C7

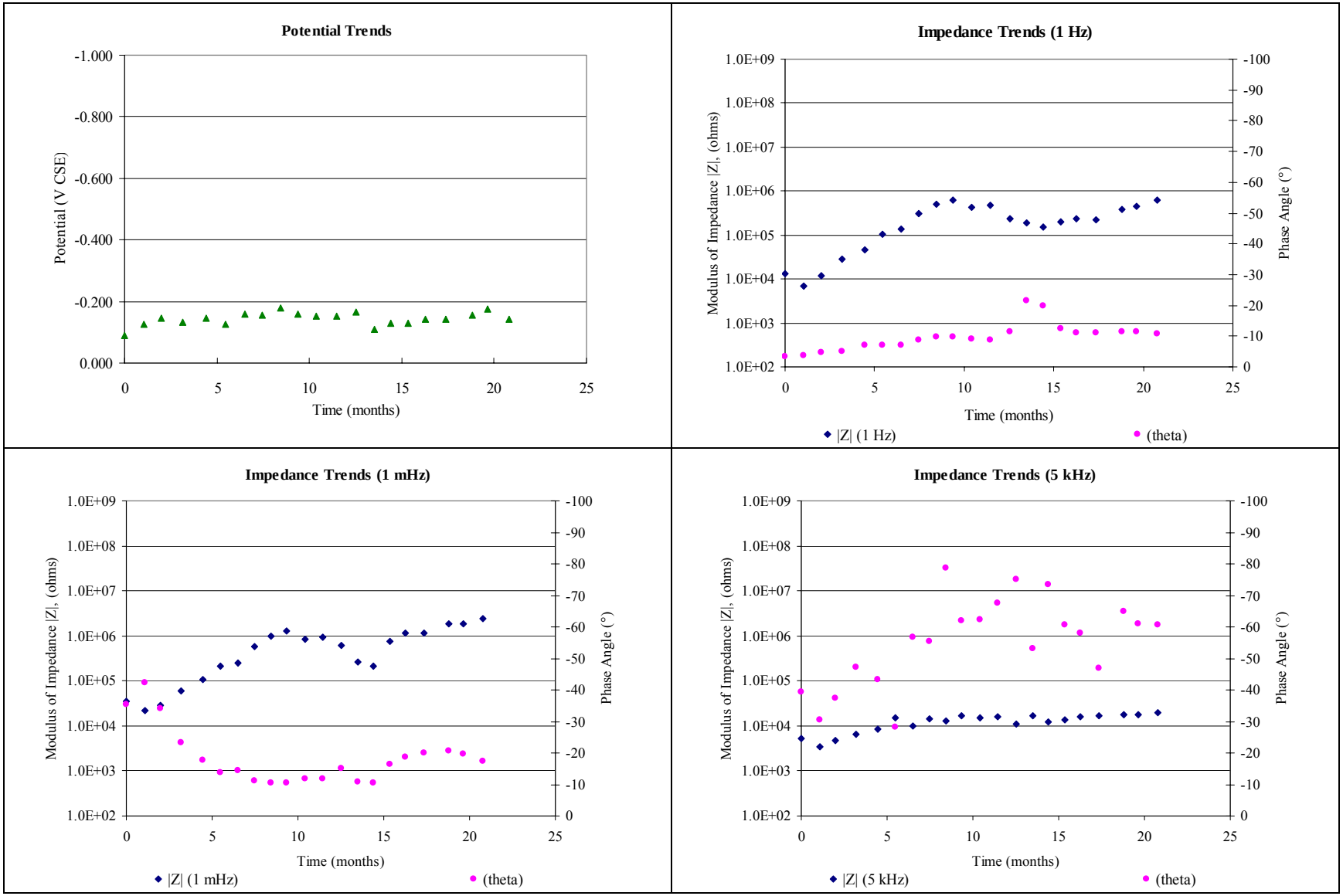

Figure B-91 Potential and Impedance Summary for Specimen 2021_C8

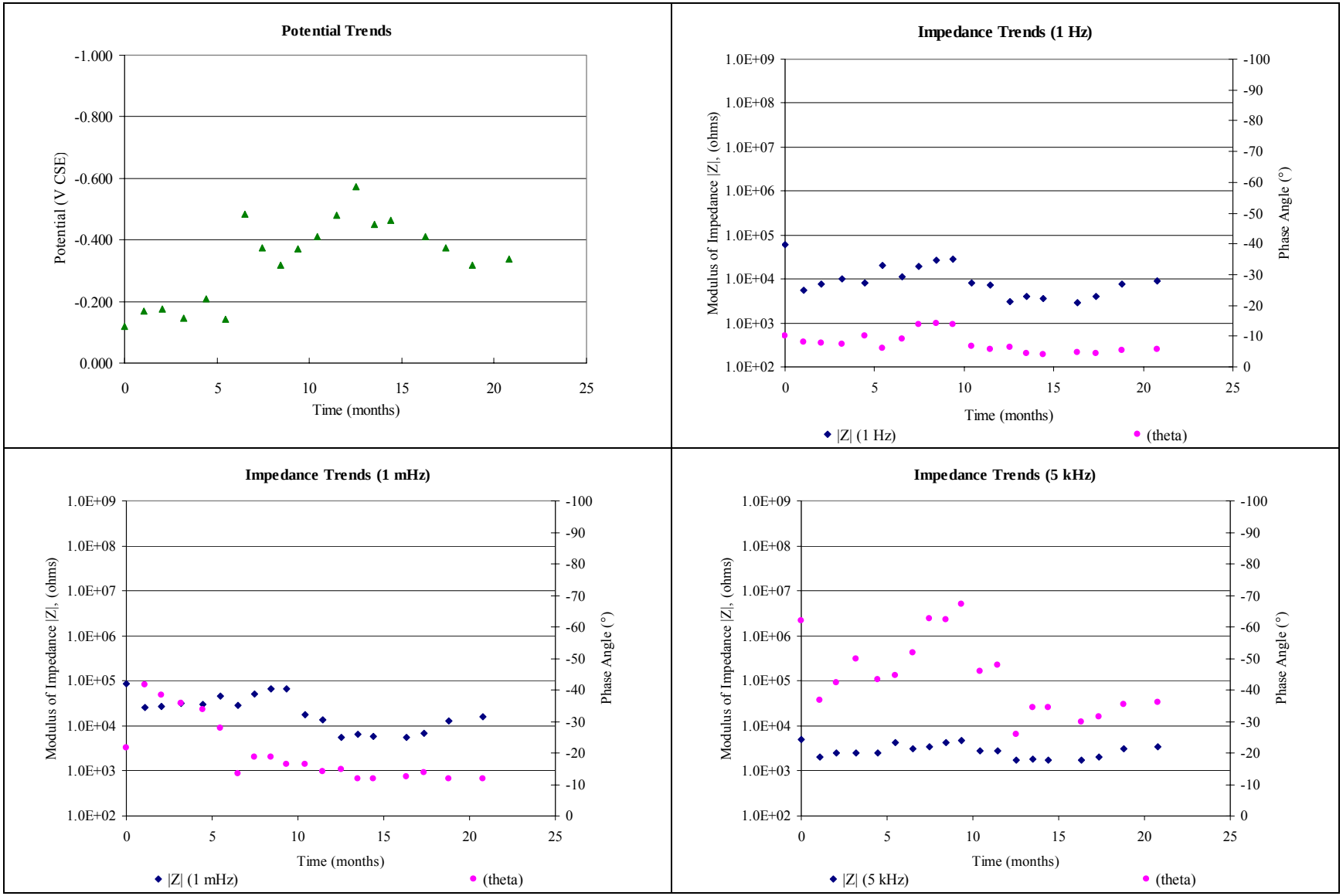

Figure B-92 Potential and Impedance Summary for Specimen 2021_C9

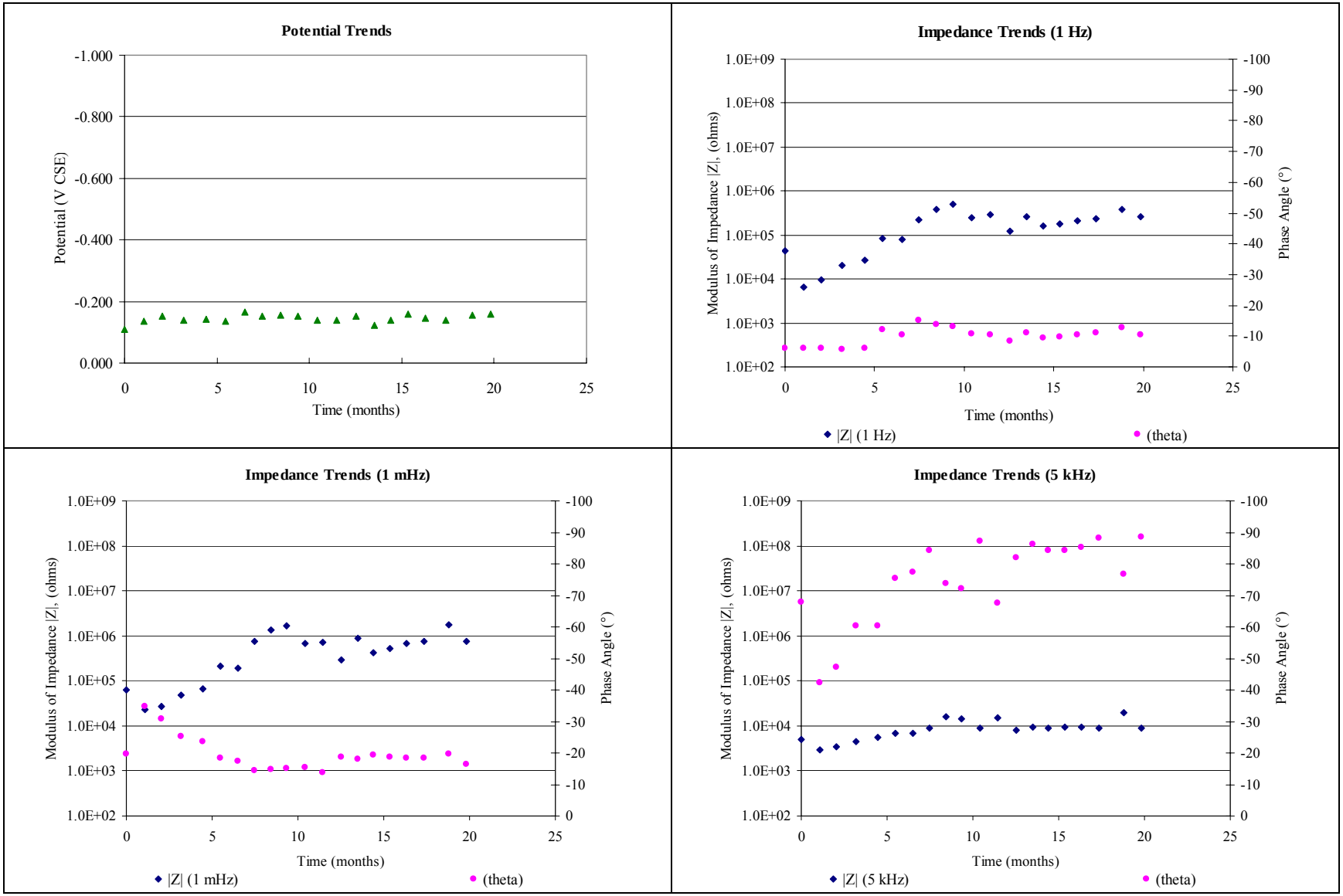

Figure B-93 Potential and Impedance Summary for Specimen 2021_C10

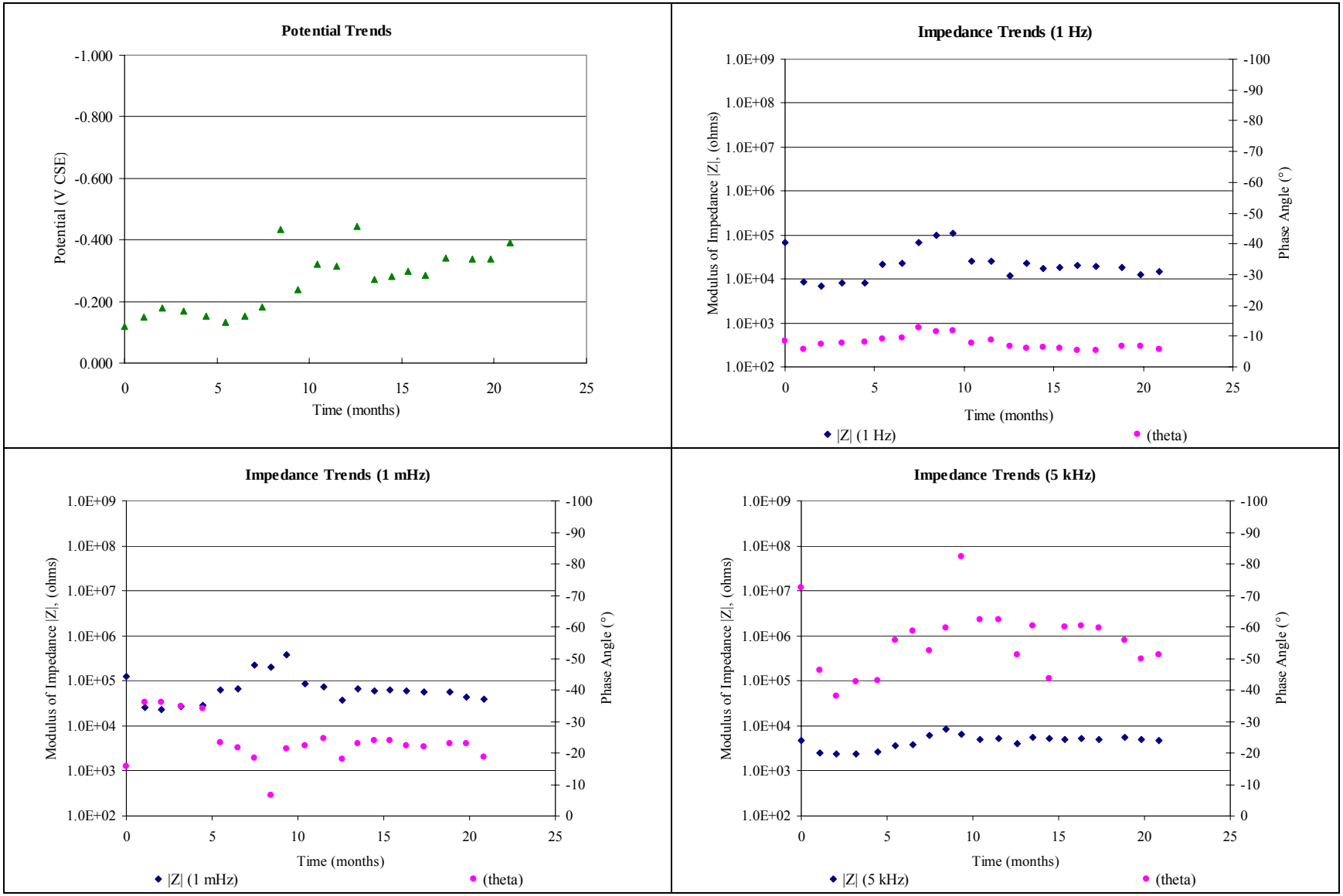

Figure B-94 Potential and Impedance Summary for Specimen 2021_C11

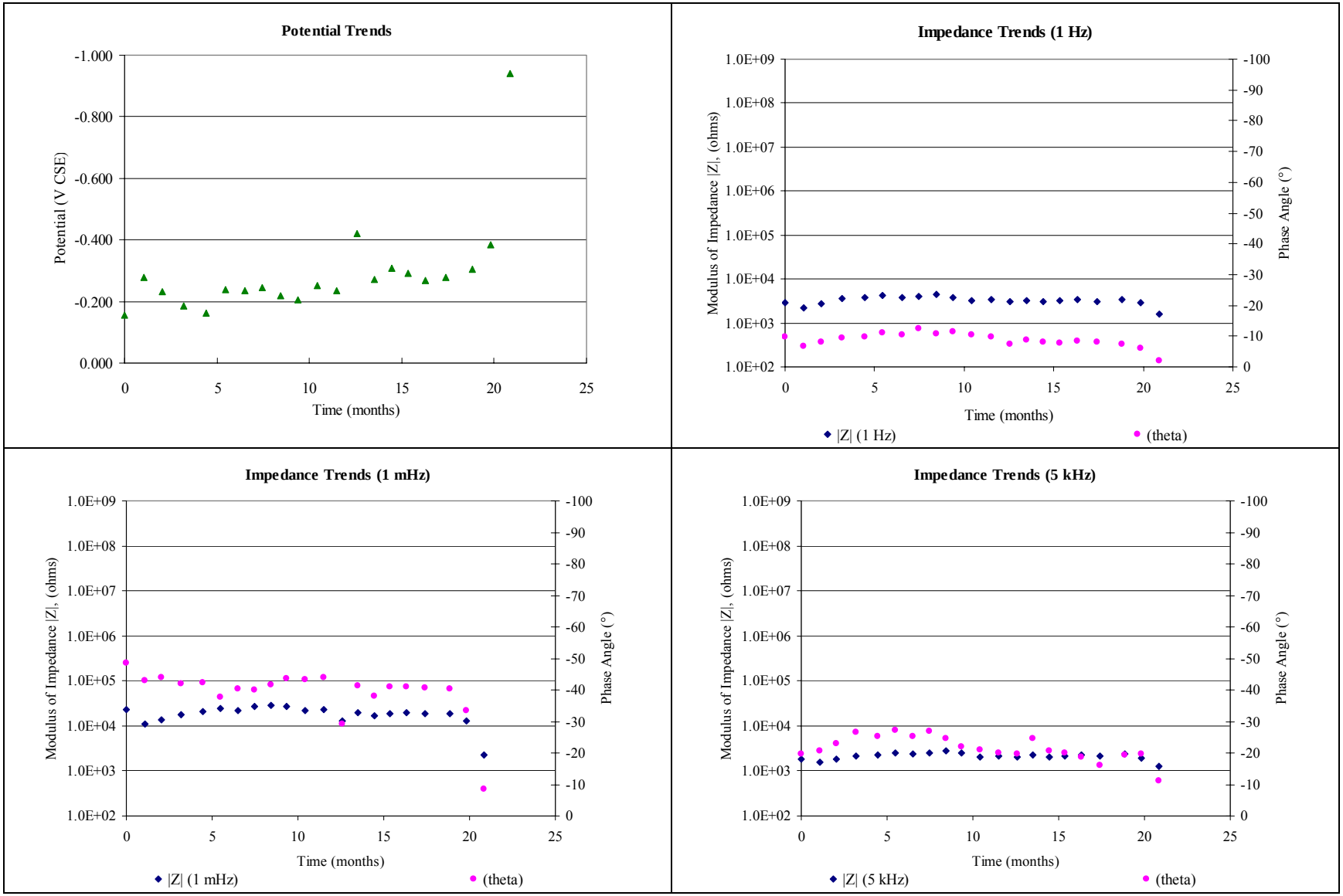

Figure B-95 Potential and Impedance Summary for Specimen 2021_C12

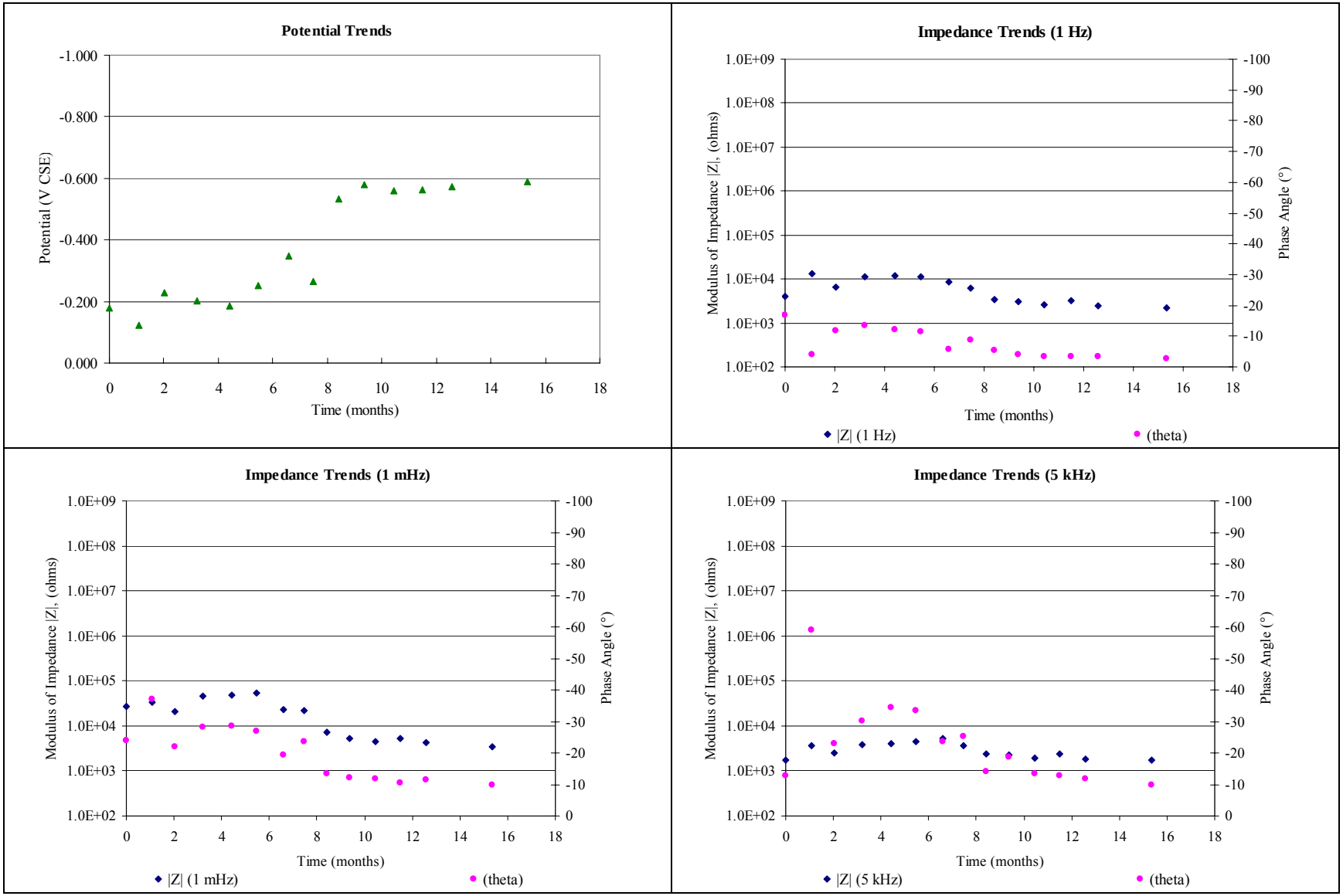

Figure B-96 Potential and Impedance Summary for Specimen 2021_CR1

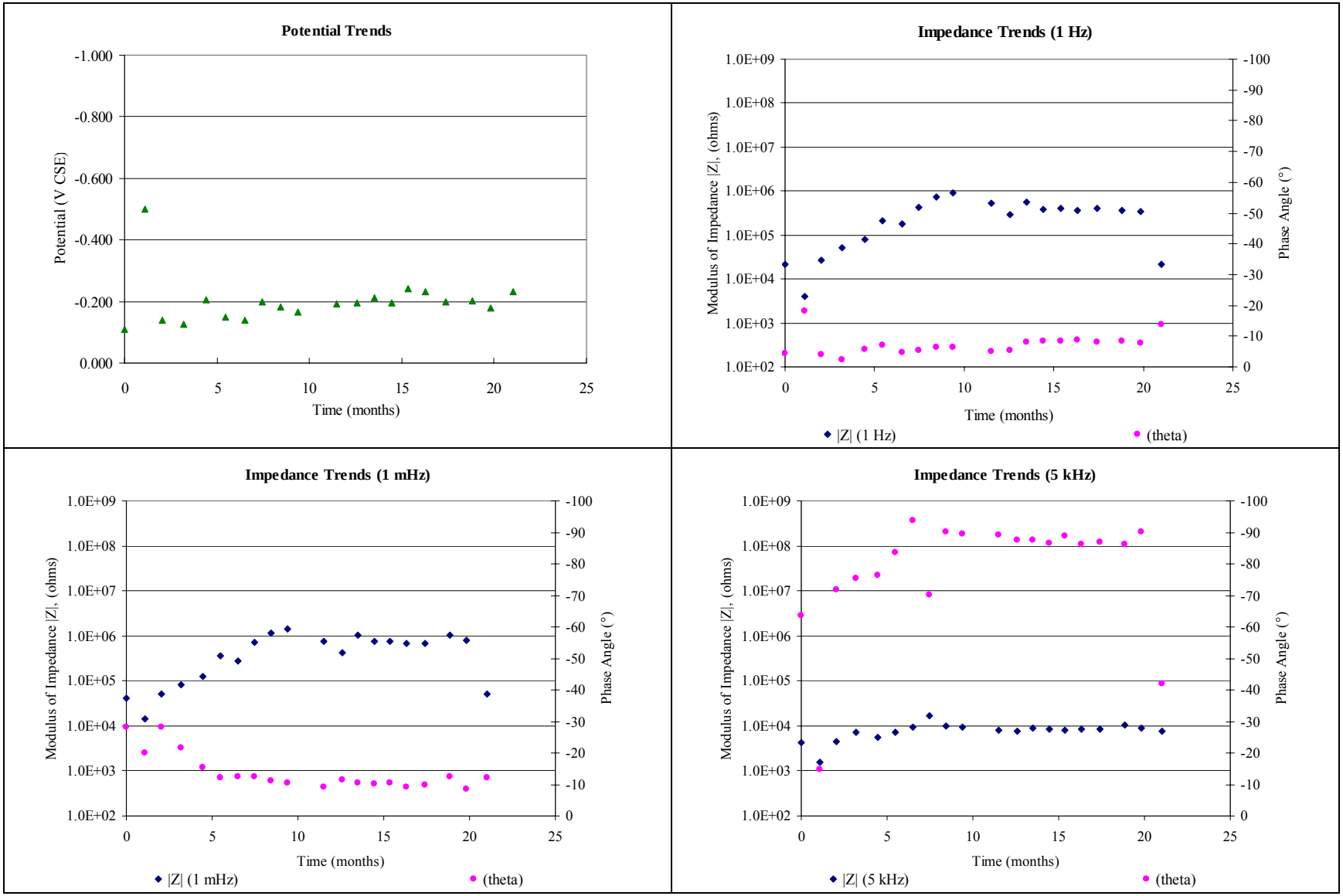

Figure B-97 Potential and Impedance Summary for Specimen 2021_CR2

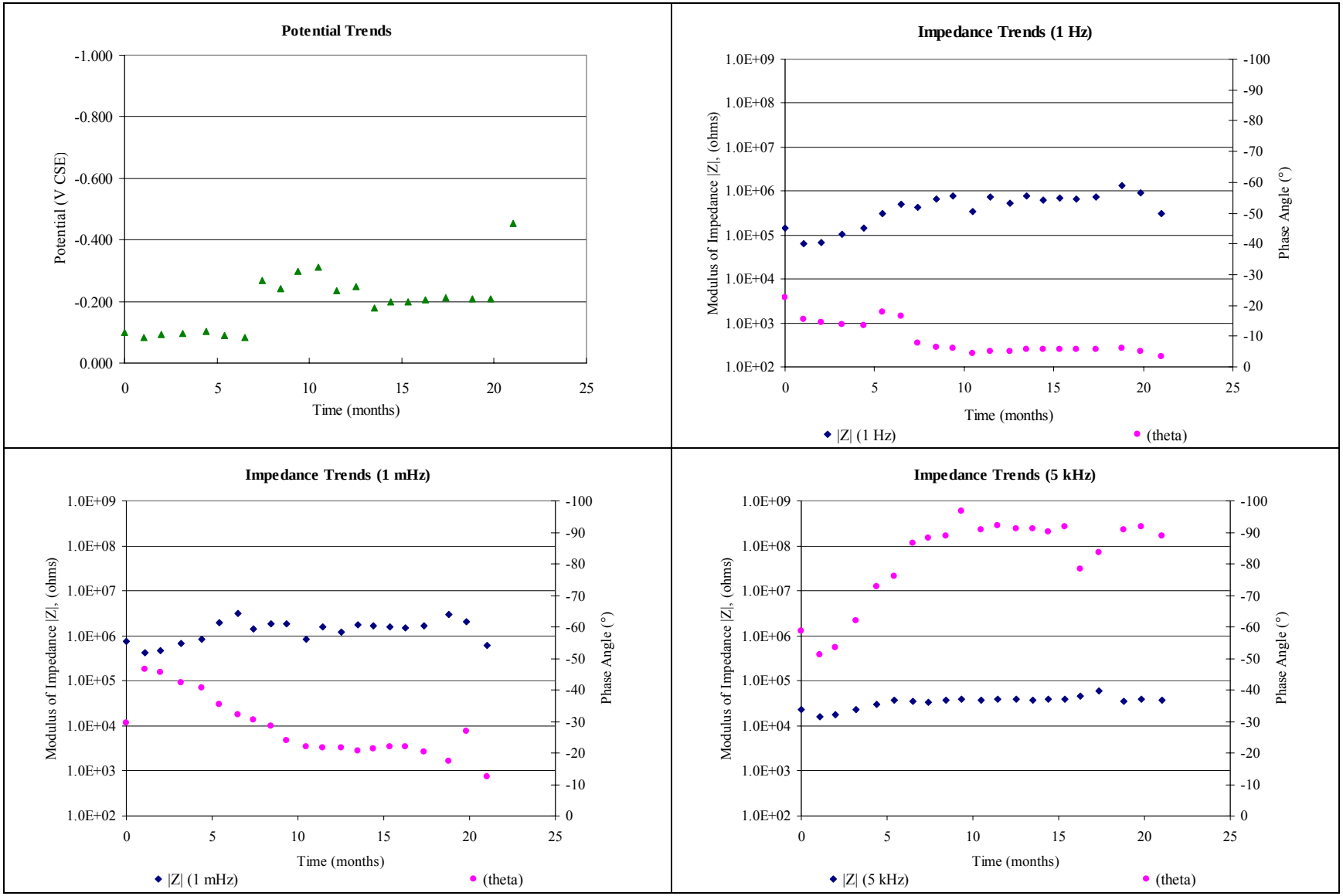

Figure B-98 Potential and Impedance Summary for Specimen 2021_CR3

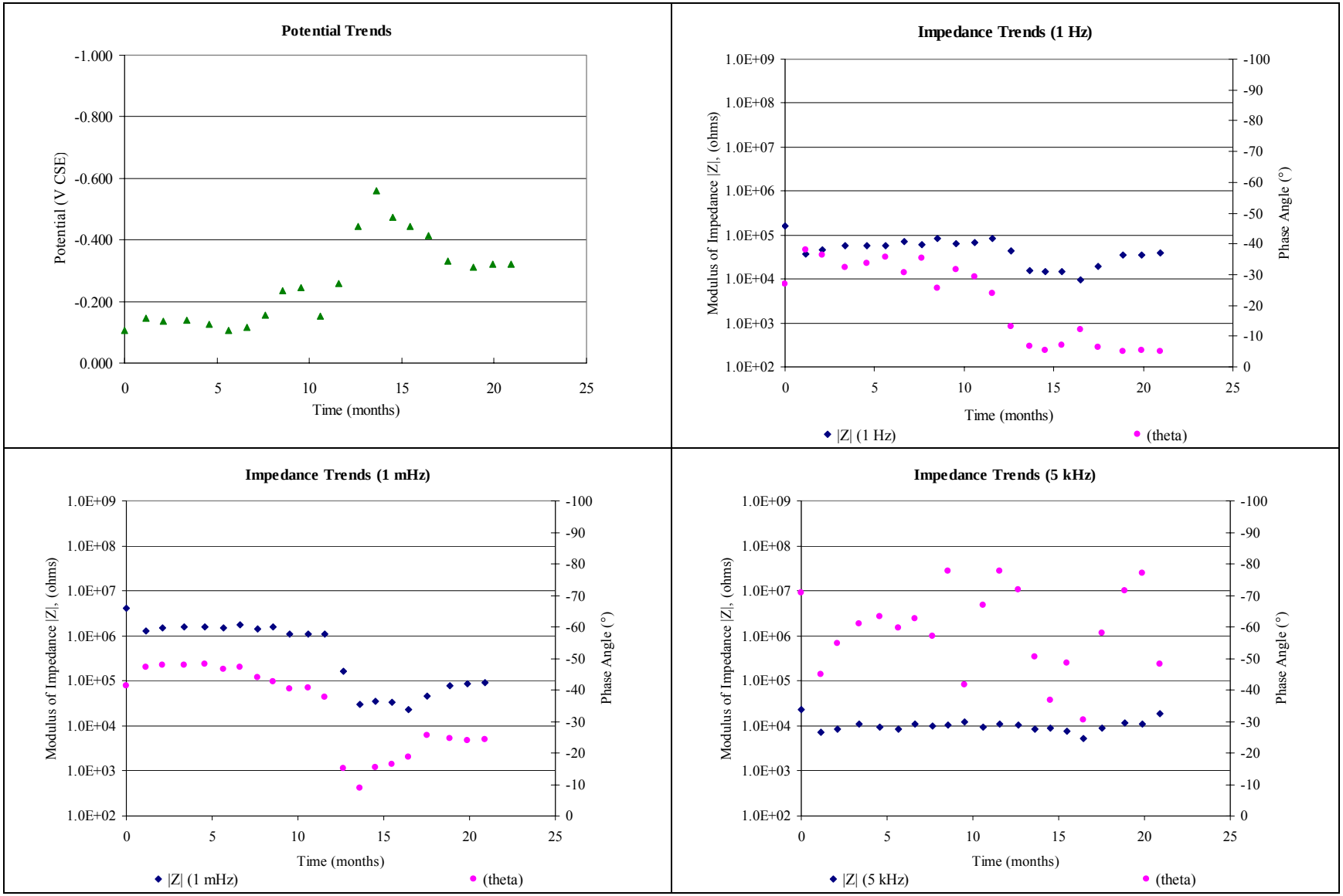

Figure B-99 Potential and Impedance Summary for Specimen 2262_C1

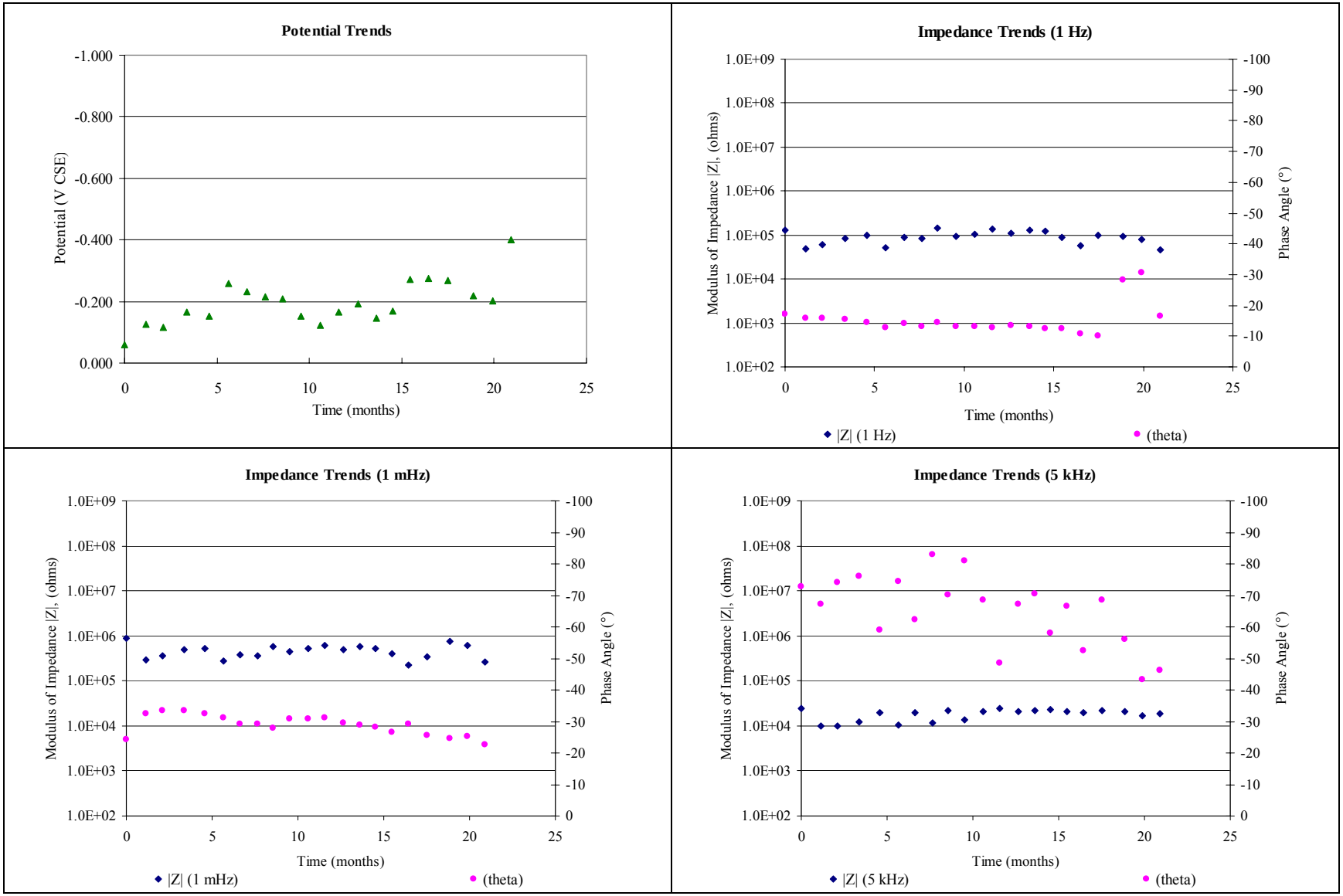

Figure B-100 Potential and Impedance Summary for Specimen 2262_C2

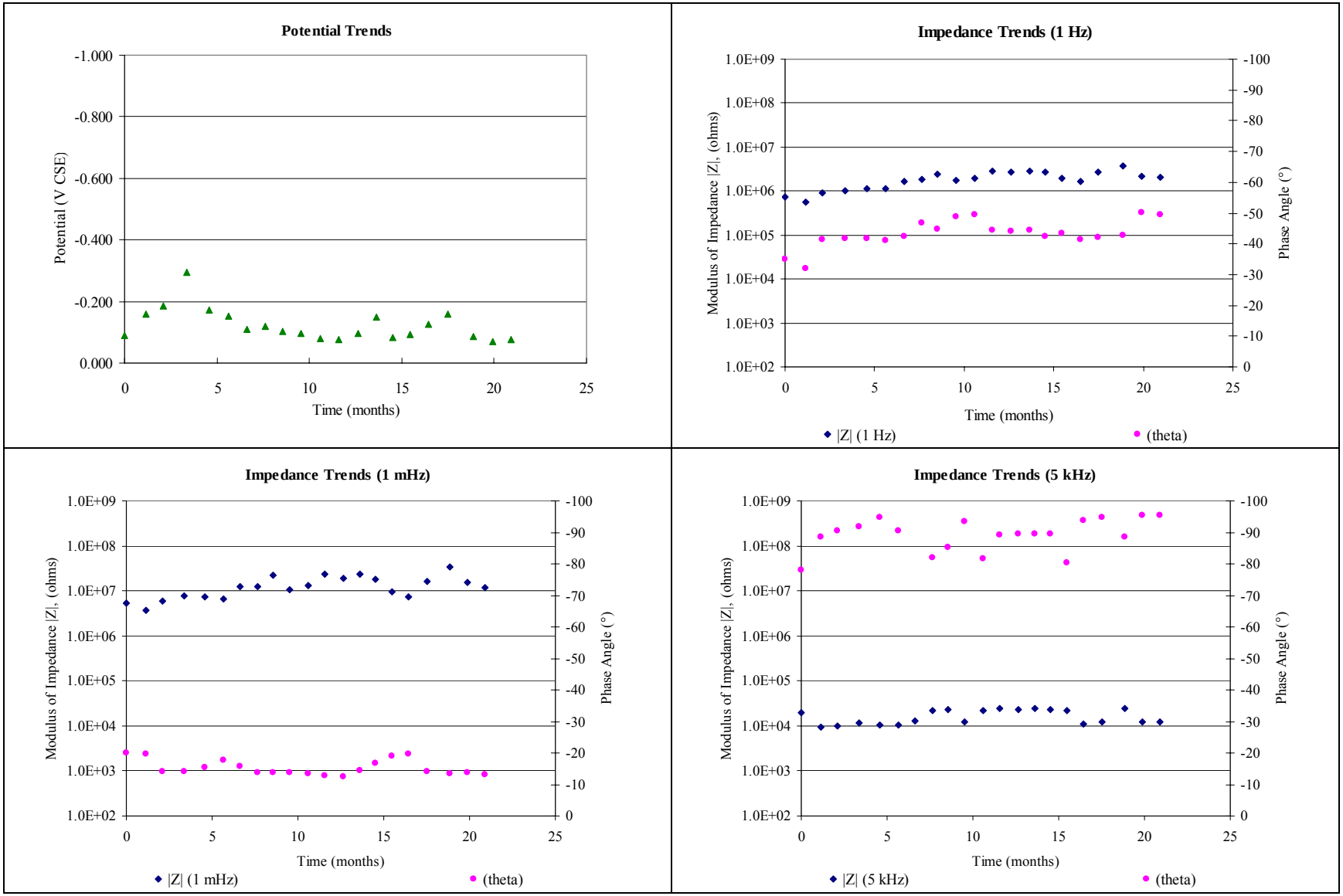

Figure B-101 Potential and Impedance Summary for Specimen 2262_C3

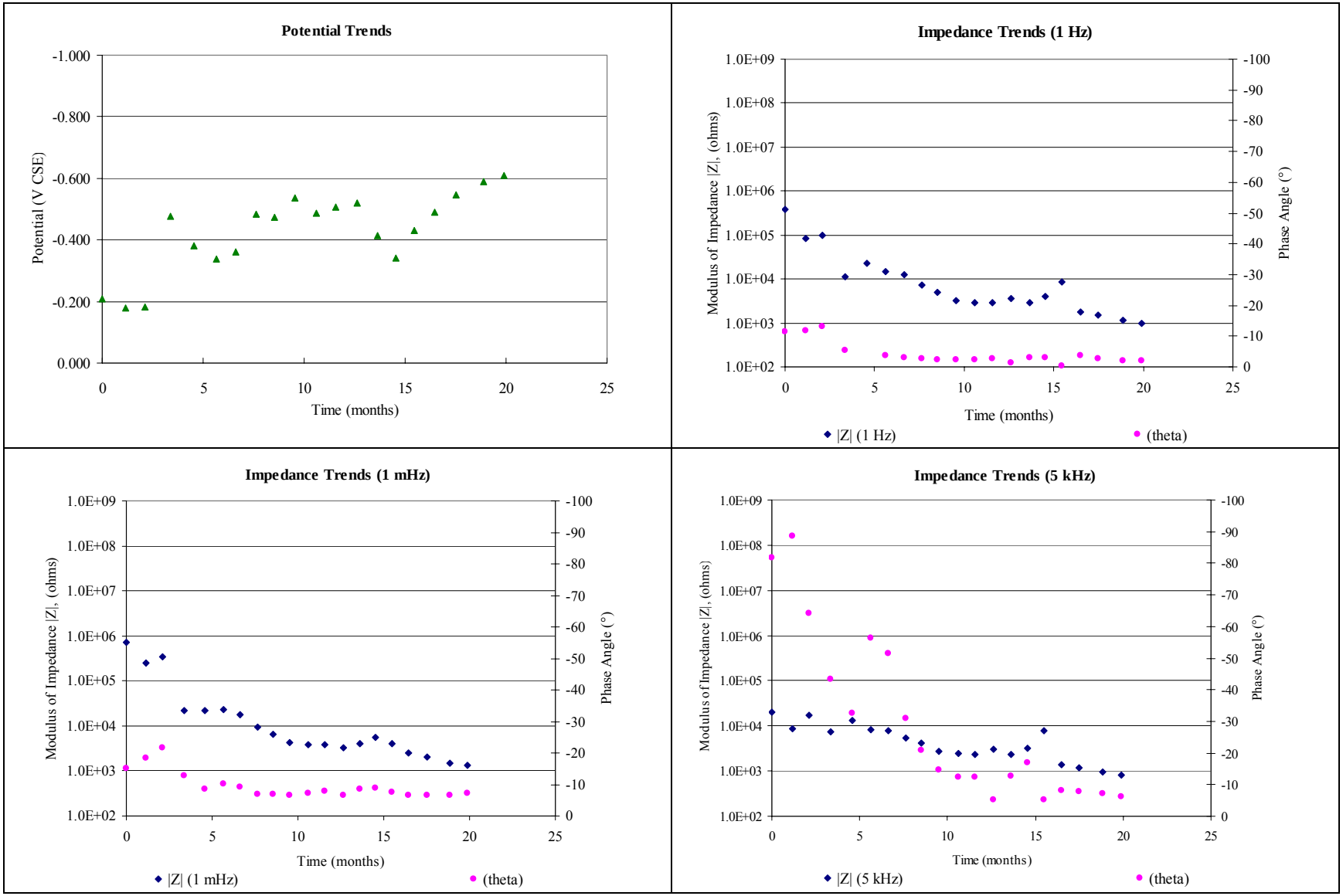

Figure B-102 Potential and Impedance Summary for Specimen 2262_C4

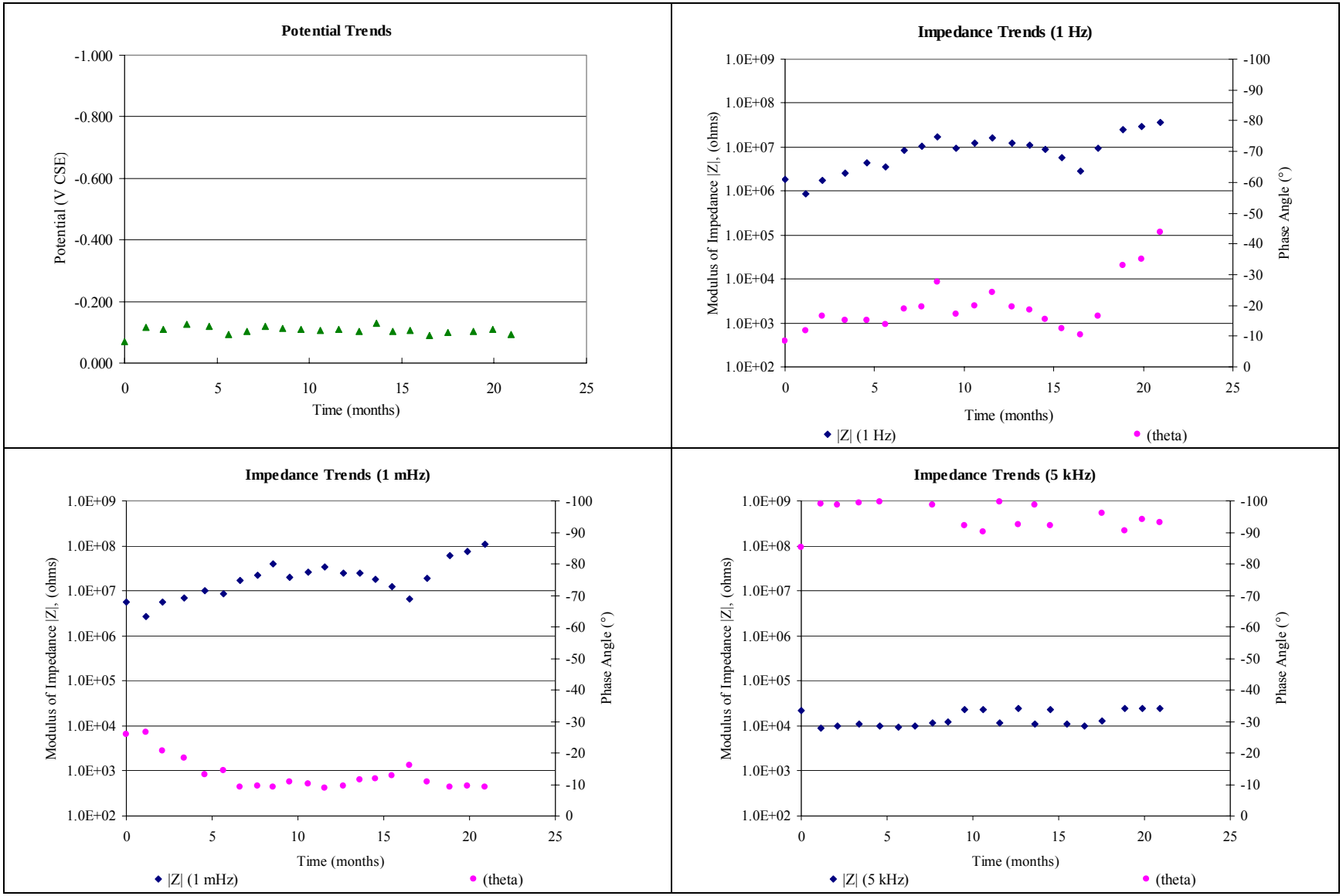

Figure B-103 Potential and Impedance Summary for Specimen 2262_C5

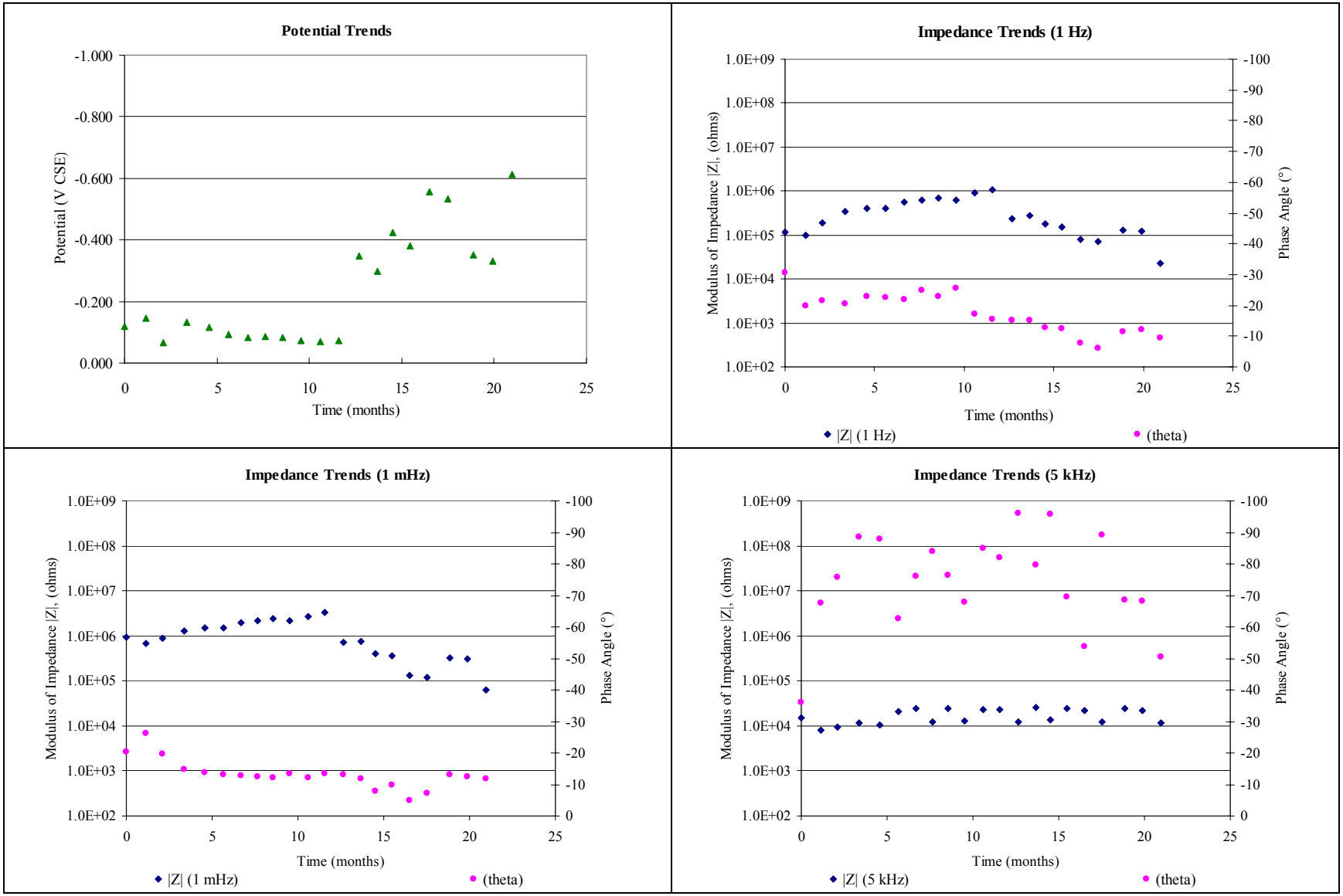

Figure B-104 Potential and Impedance Summary for Specimen 2262_C6

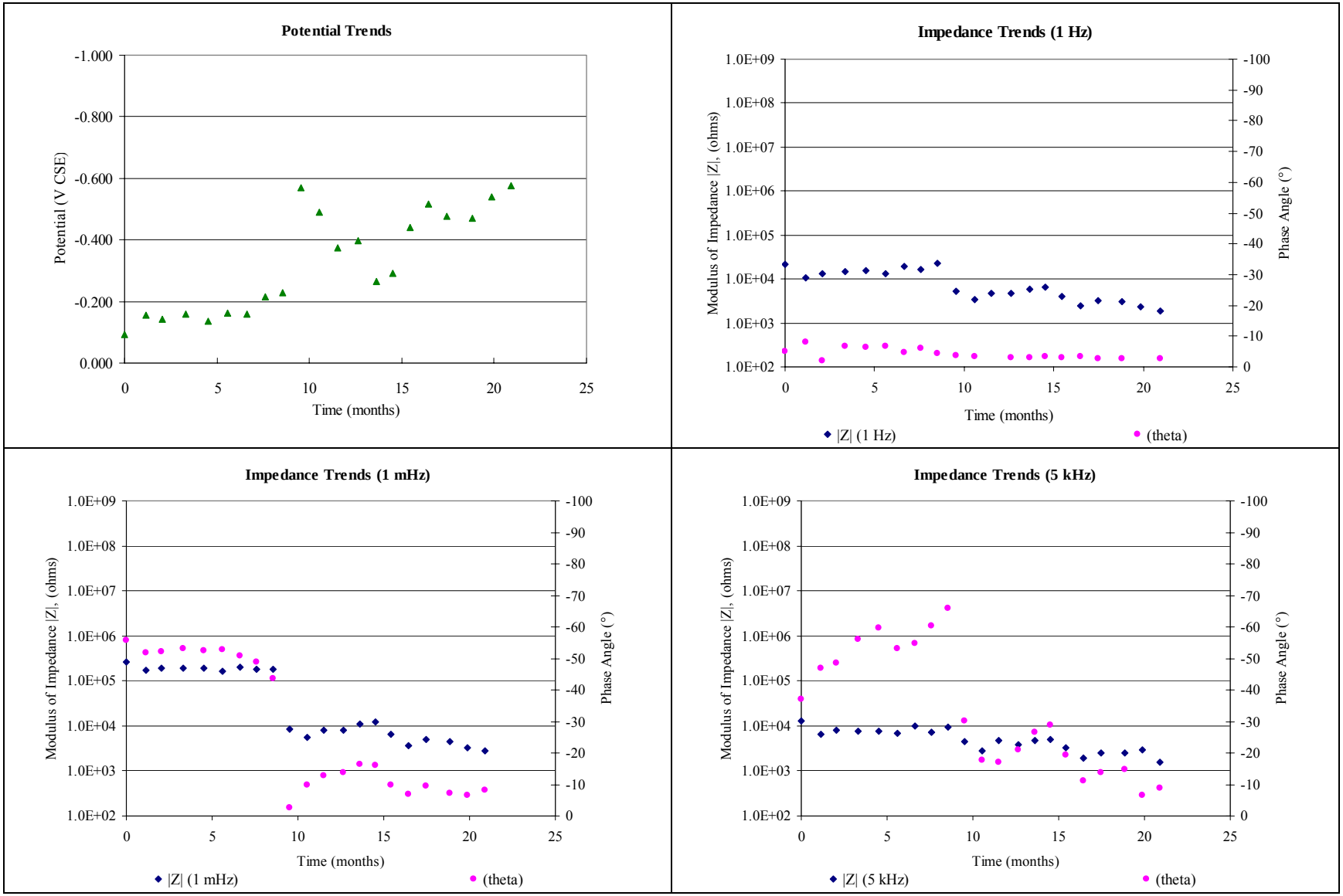

Figure B-105 Potential and Impedance Summary for Specimen 2262_C7

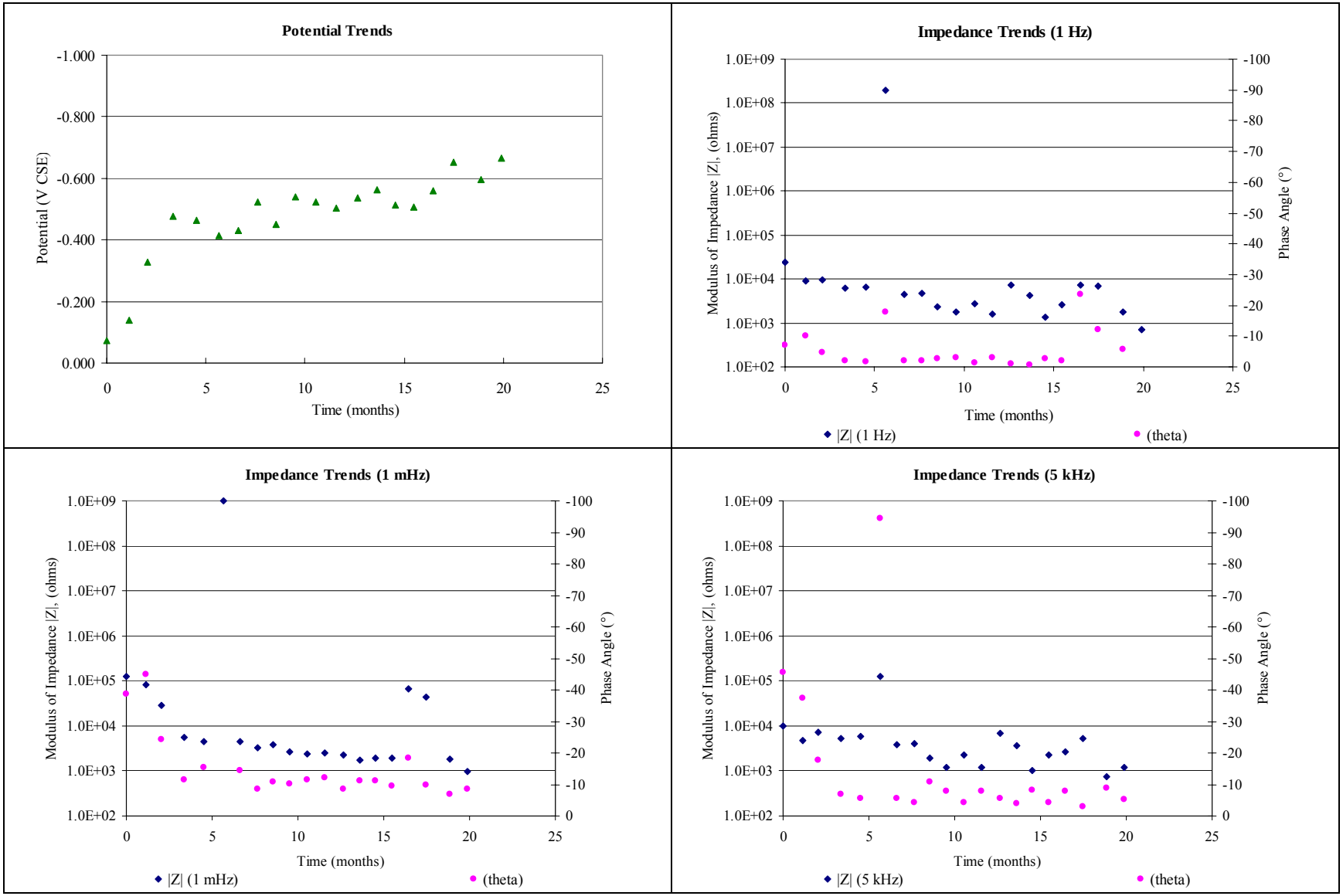

Figure B-106 Potential and Impedance Summary for Specimen 2262_C8

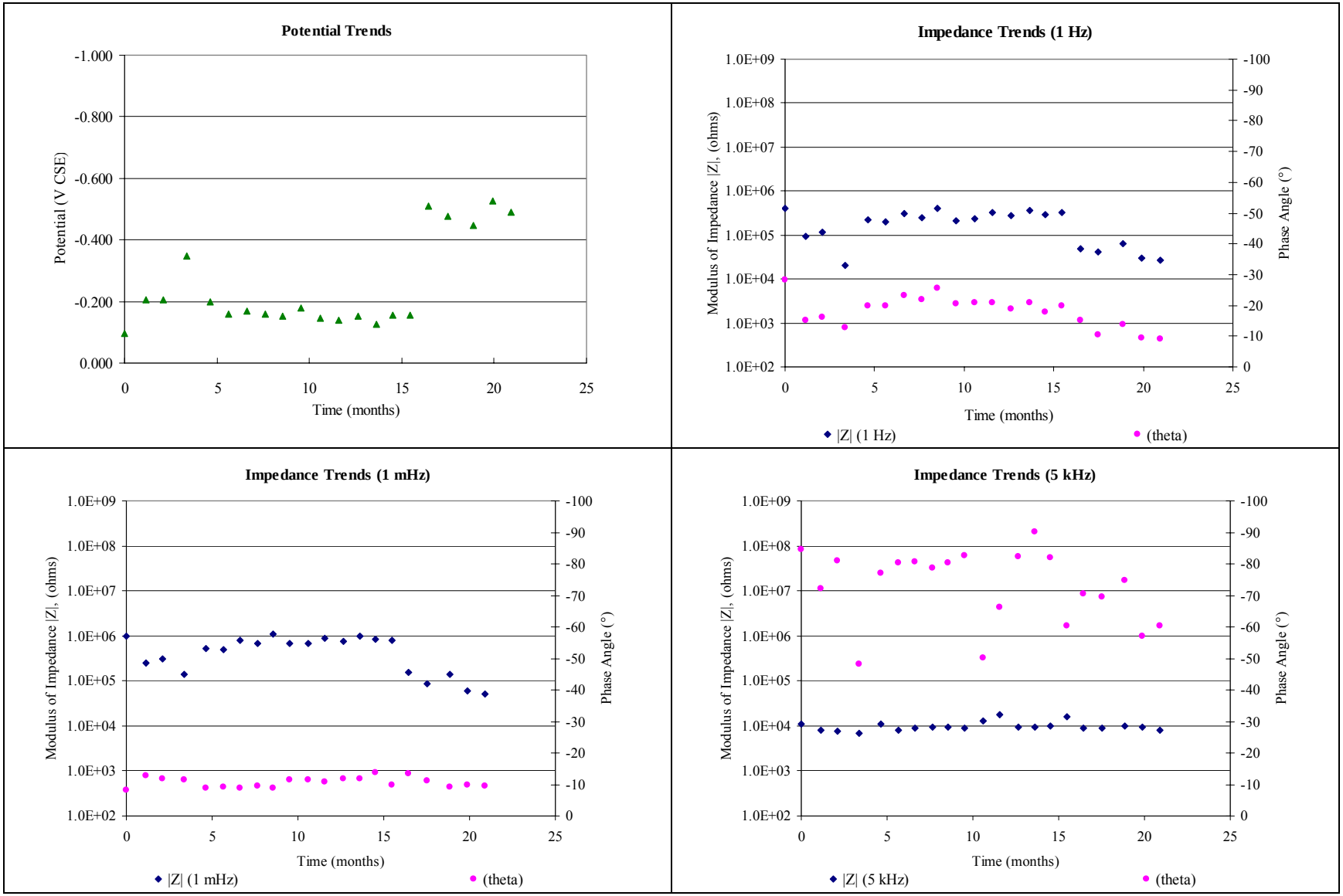

Figure B-107 Potential and Impedance Summary for Specimen 2262_C9

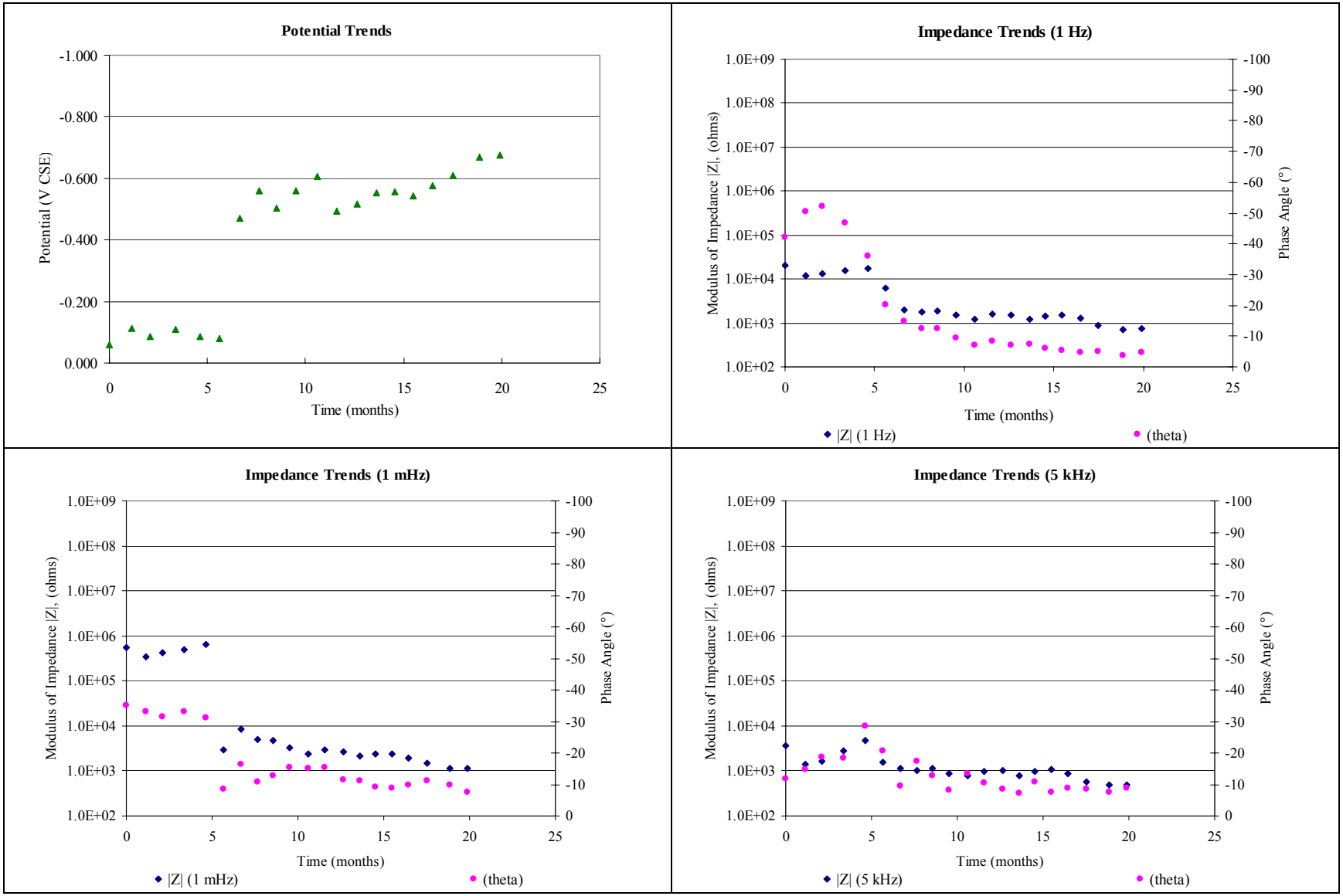

Figure B-108 Potential and Impedance Summary for Specimen 2262_C10

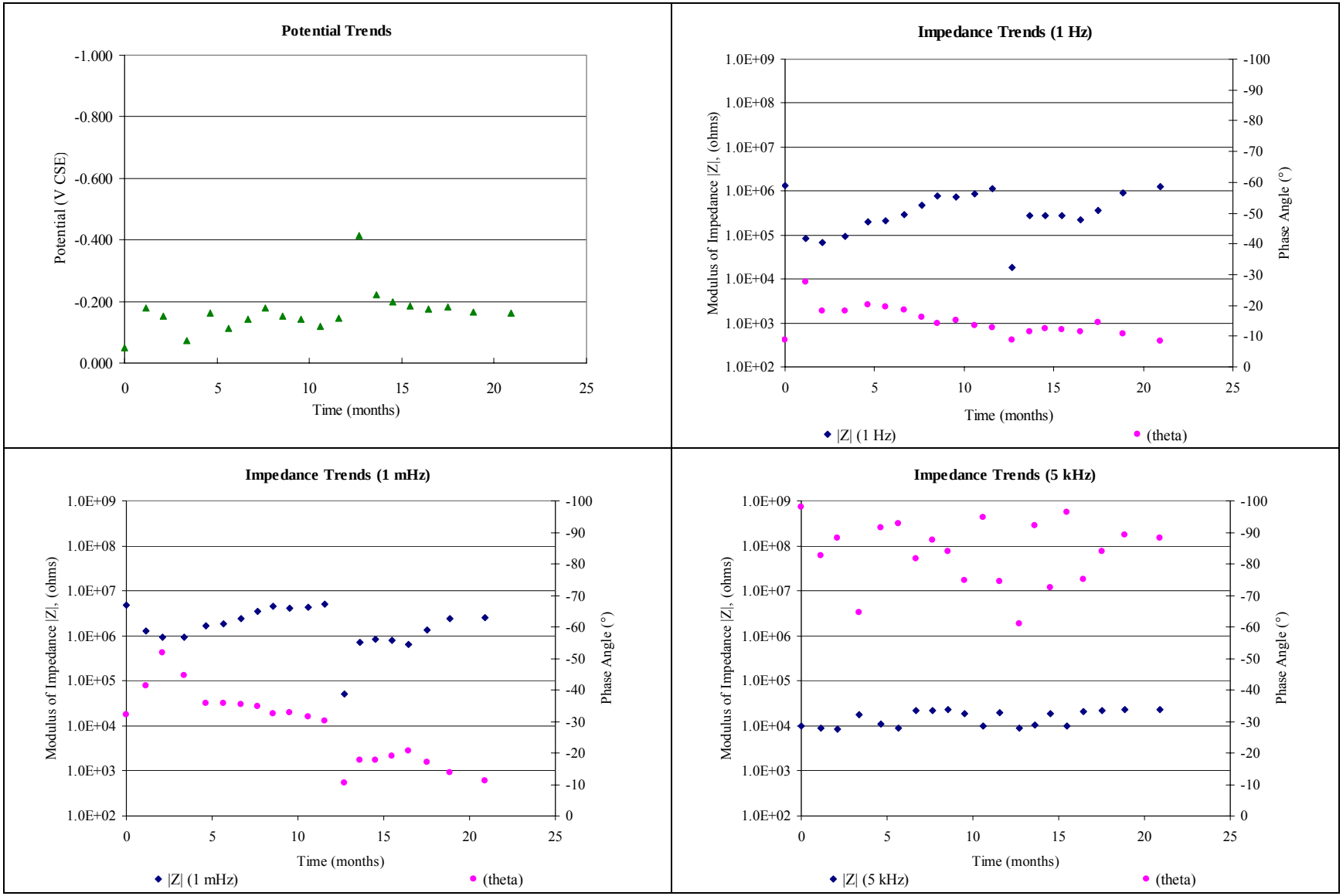

Figure B-109 Potential and Impedance Summary for Specimen 2262_C11

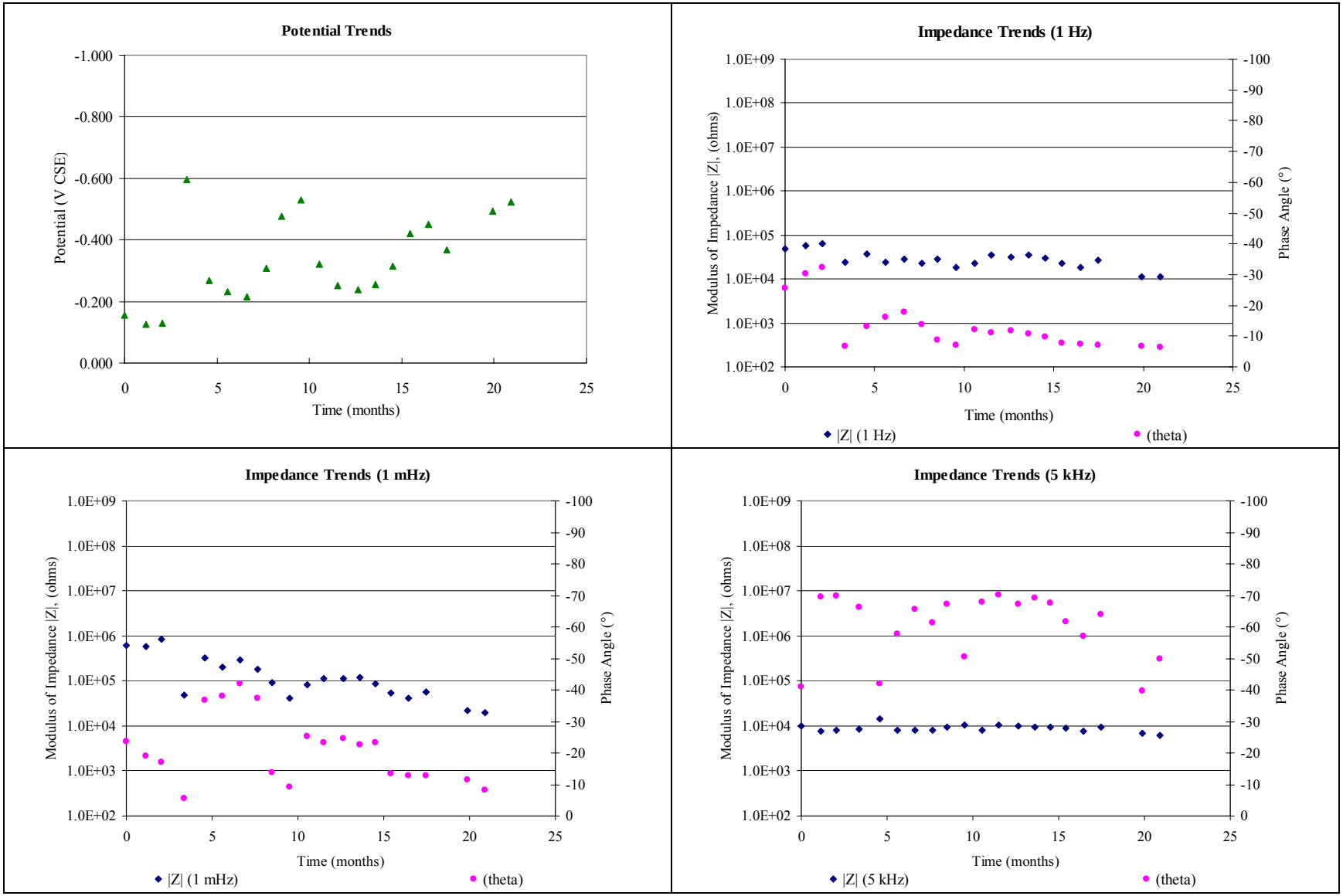

Figure B-110 Potential and Impedance Summary for Specimen 2262_C12

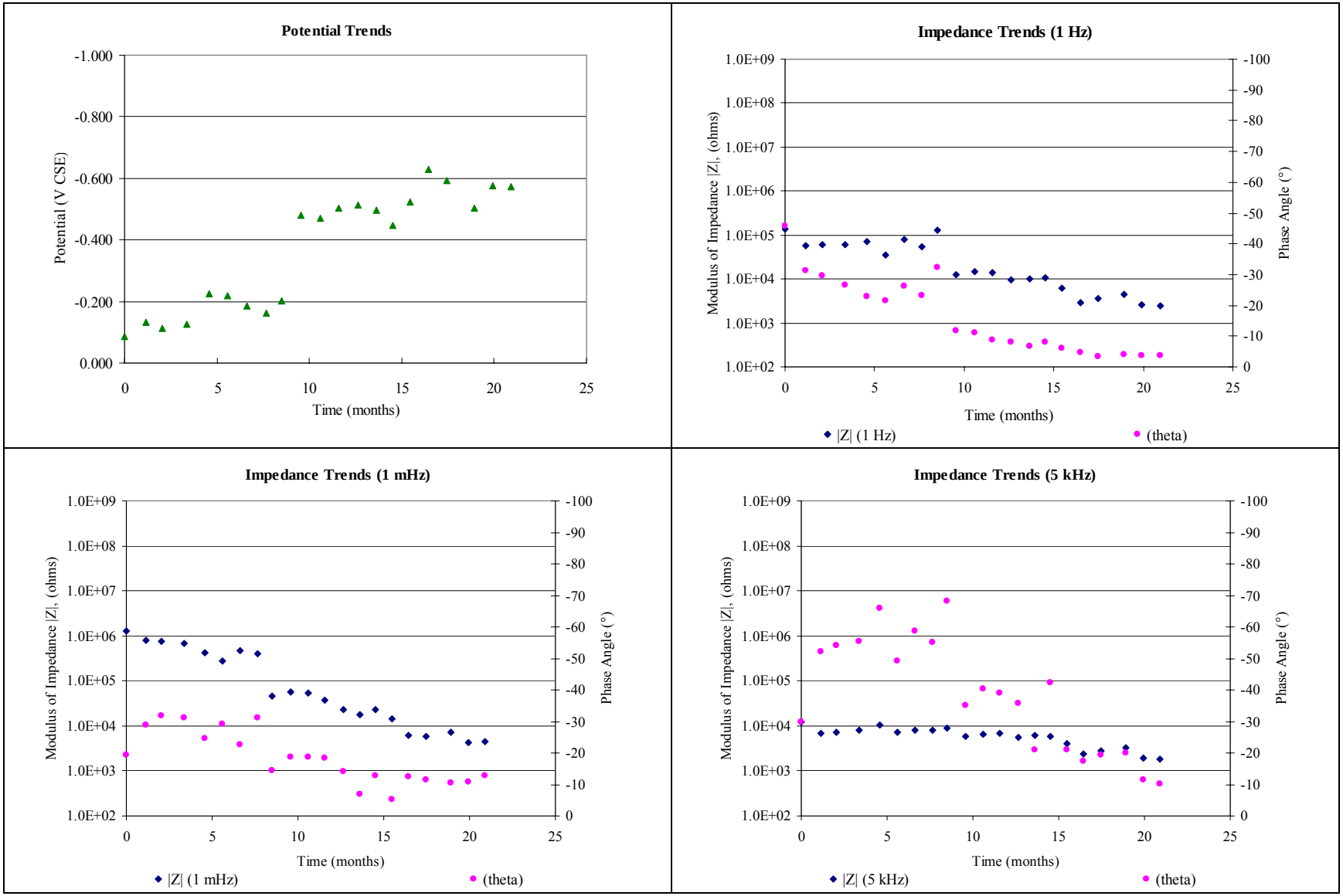

Figure B-111 Potential and Impedance Summary for Specimen 2262_CR1

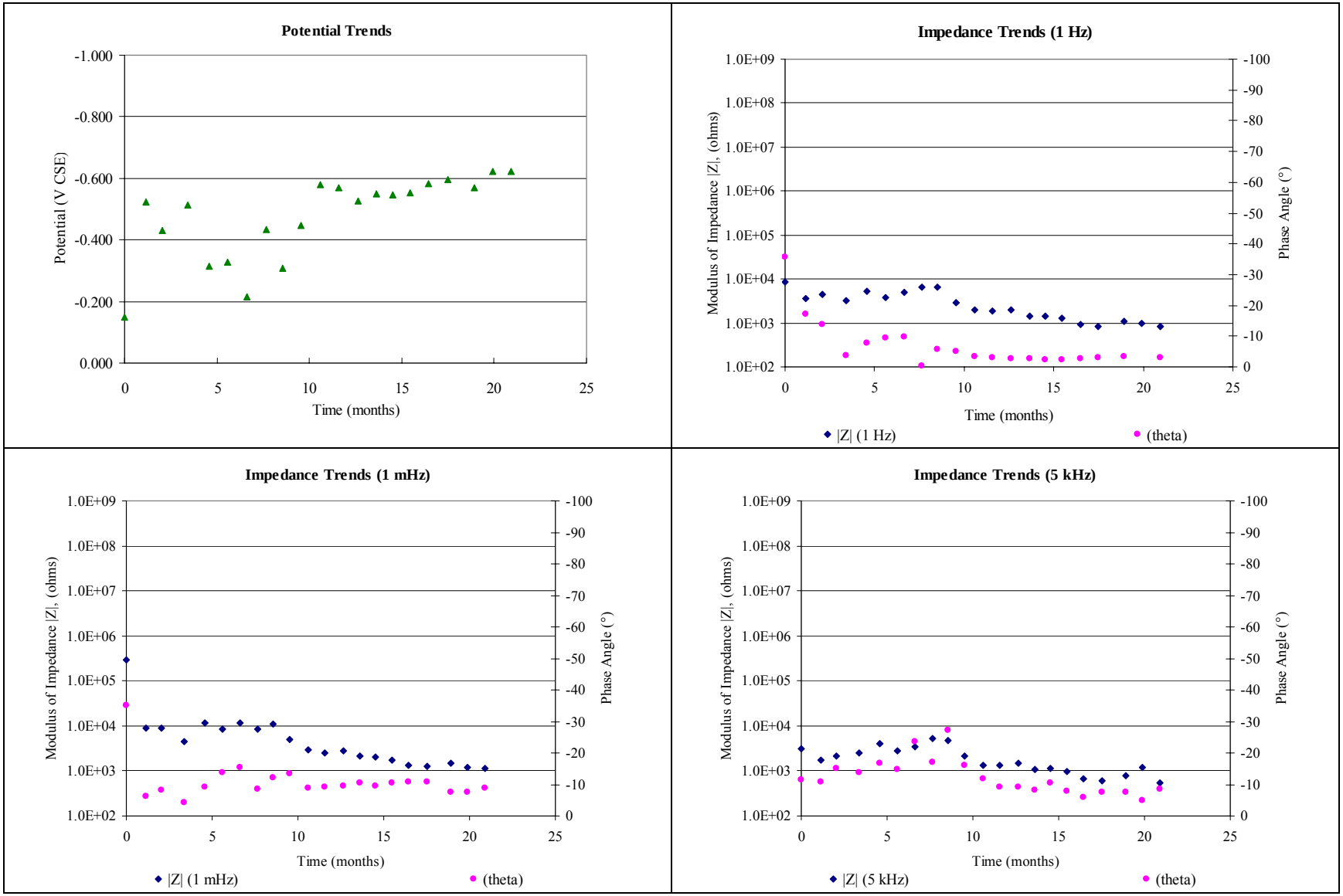

Figure B-112 Potential and Impedance Summary for Specimen 2262_CR2

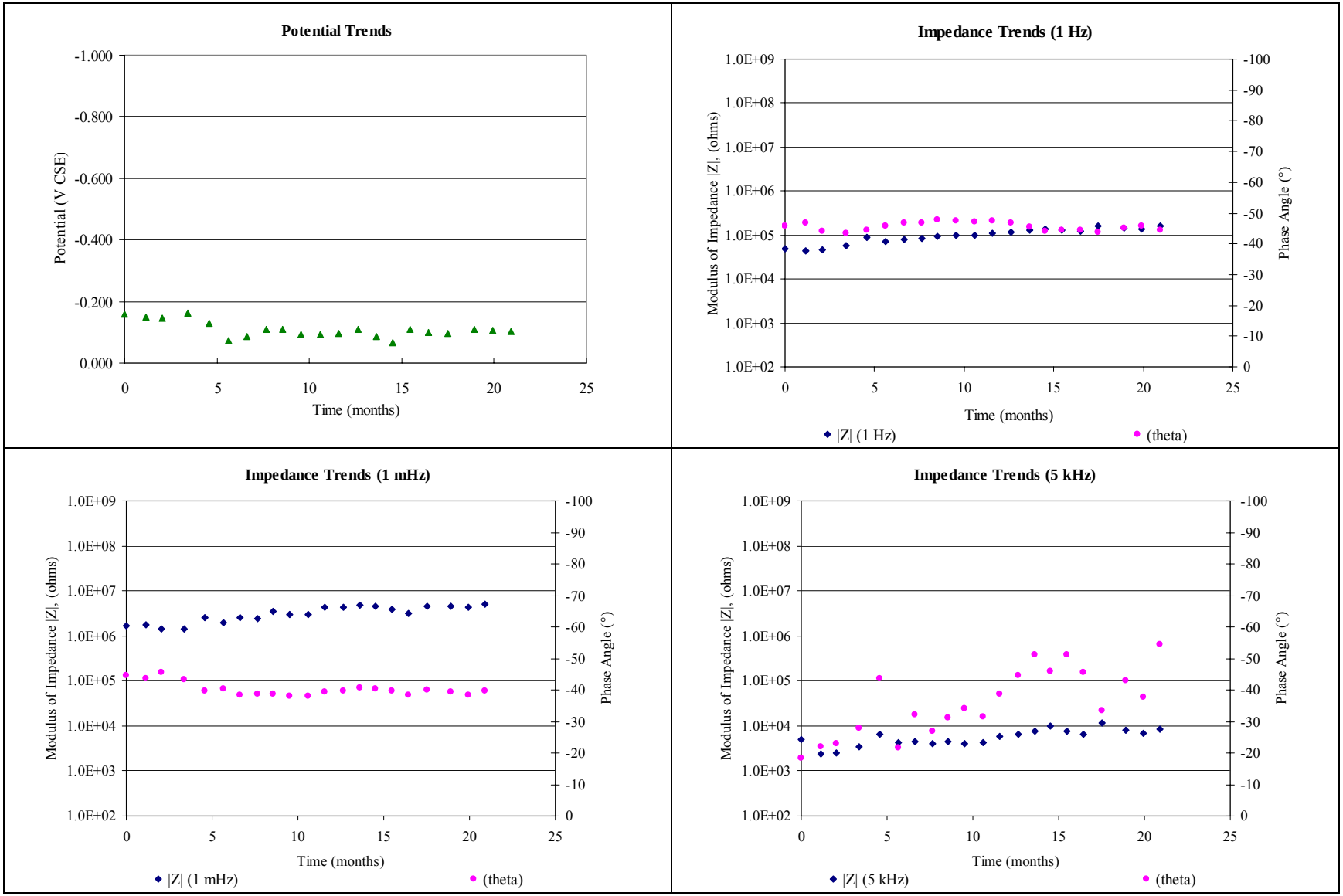

Figure B-113 Potential and Impedance Summary for Specimen 2262_CR3

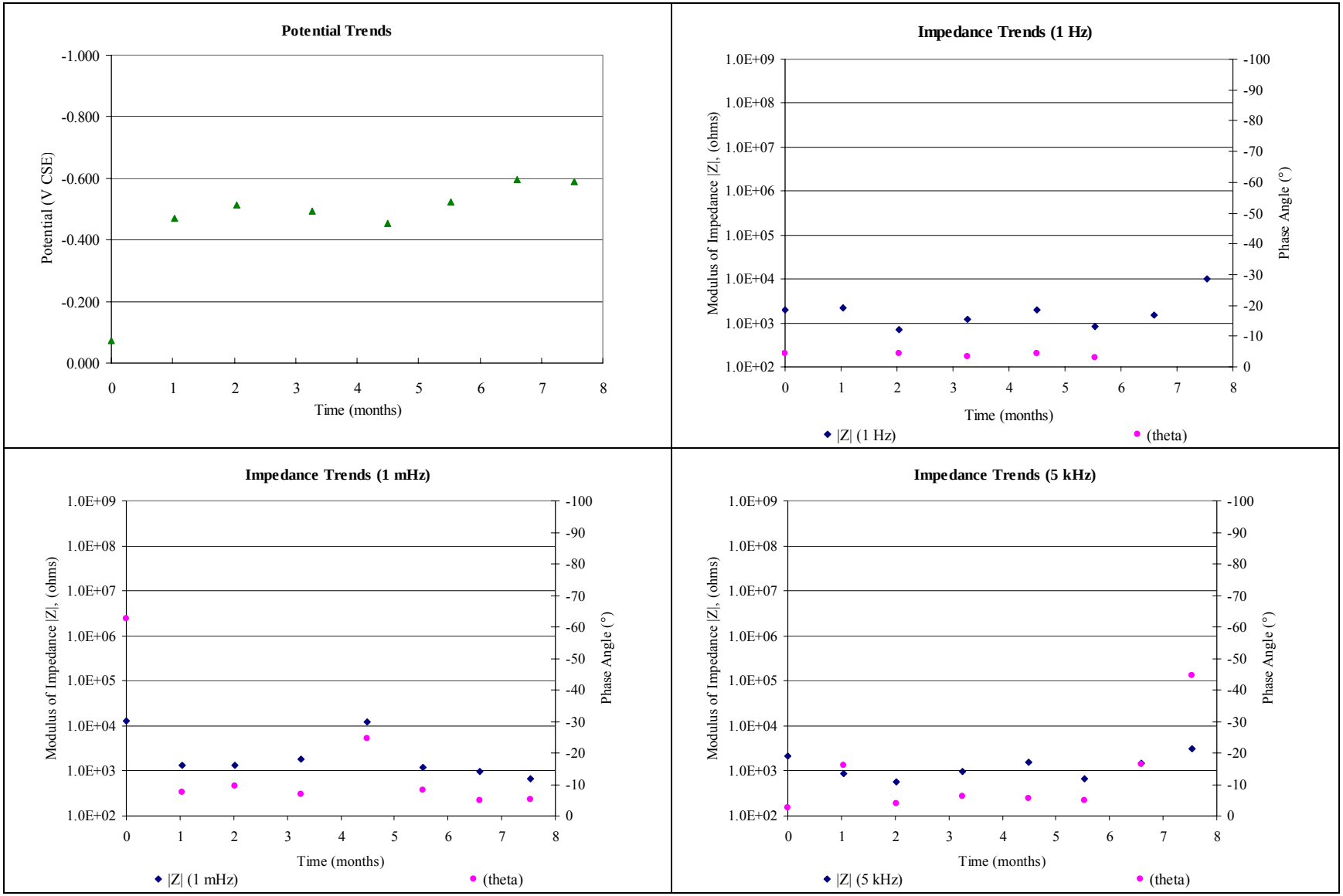

Figure B-114 Potential and Impedance Summary for Specimen 6037_C1

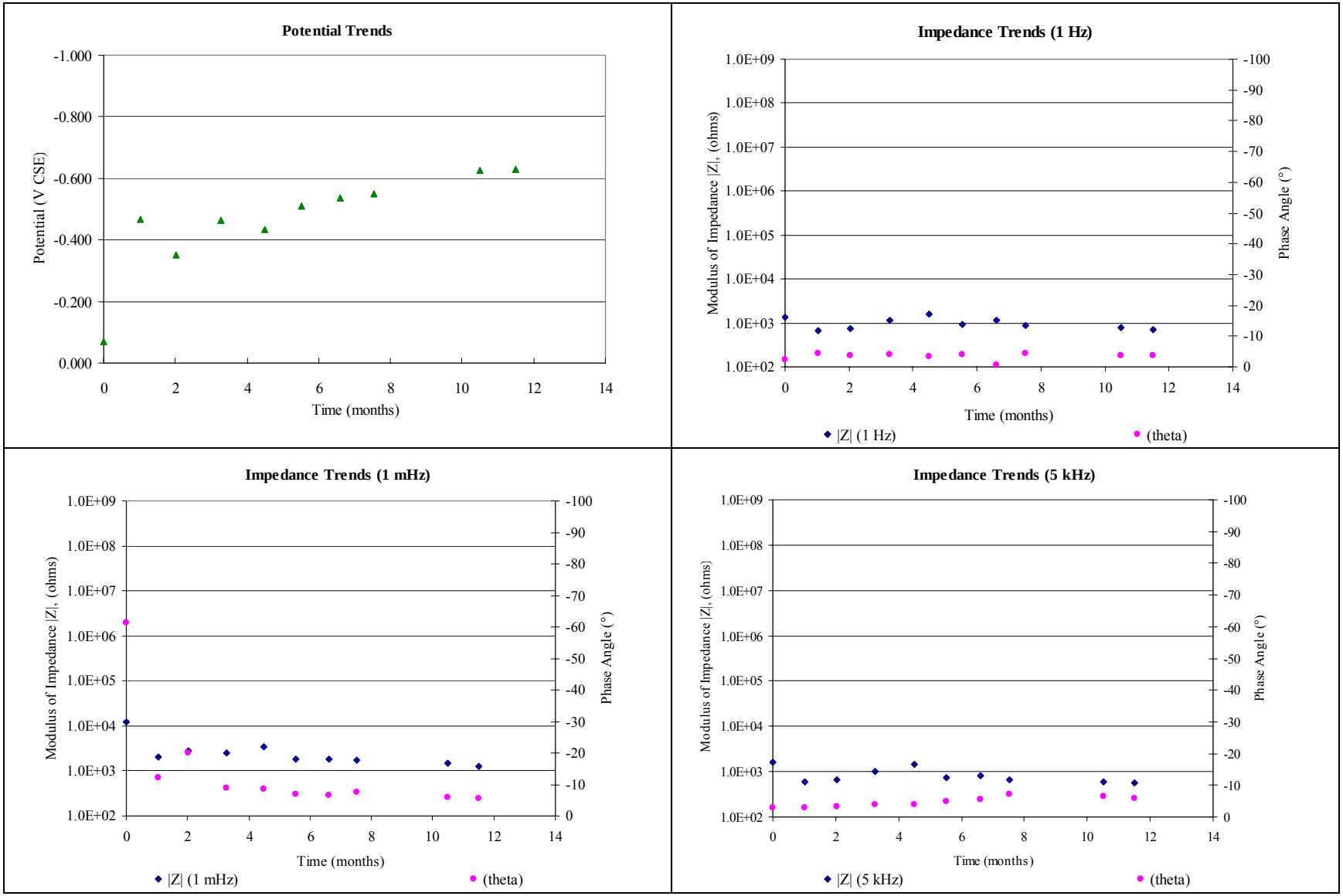

Figure B-115 Potential and Impedance Summary for Specimen 6037_C2

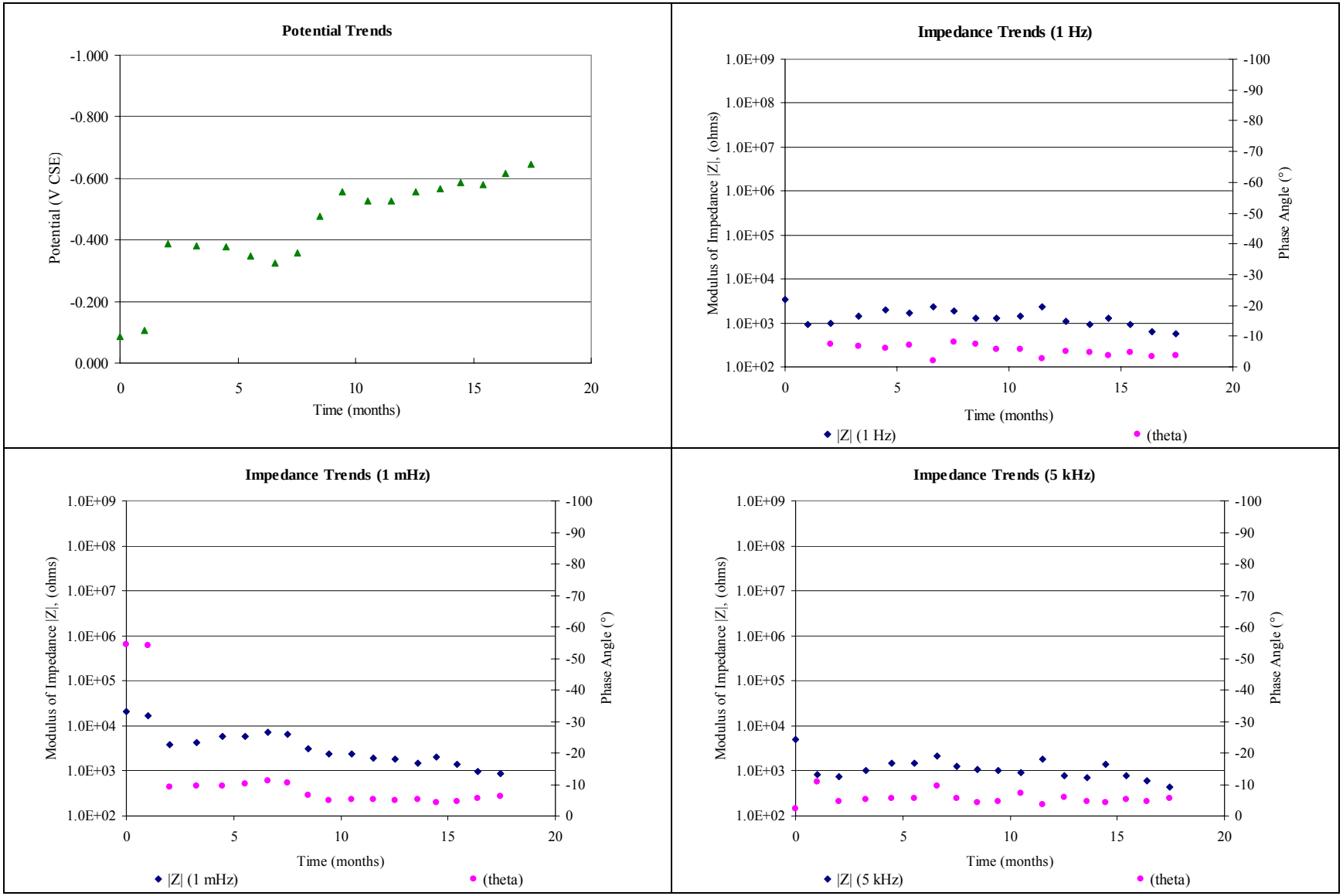

Figure B-116 Potential and Impedance Summary for Specimen 6037_C3

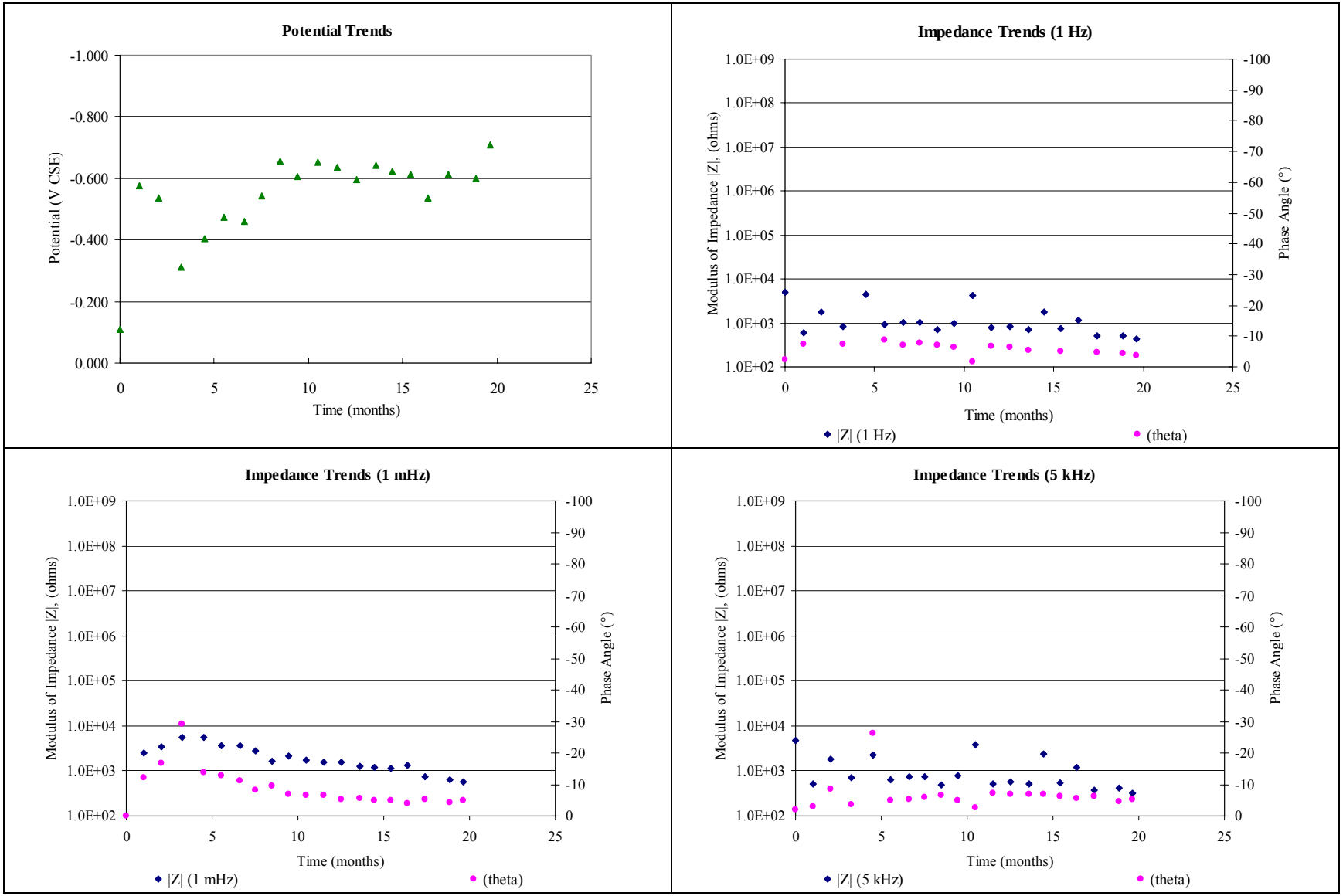

Figure B-117 Potential and Impedance Summary for Specimen 6037_C4/CR1

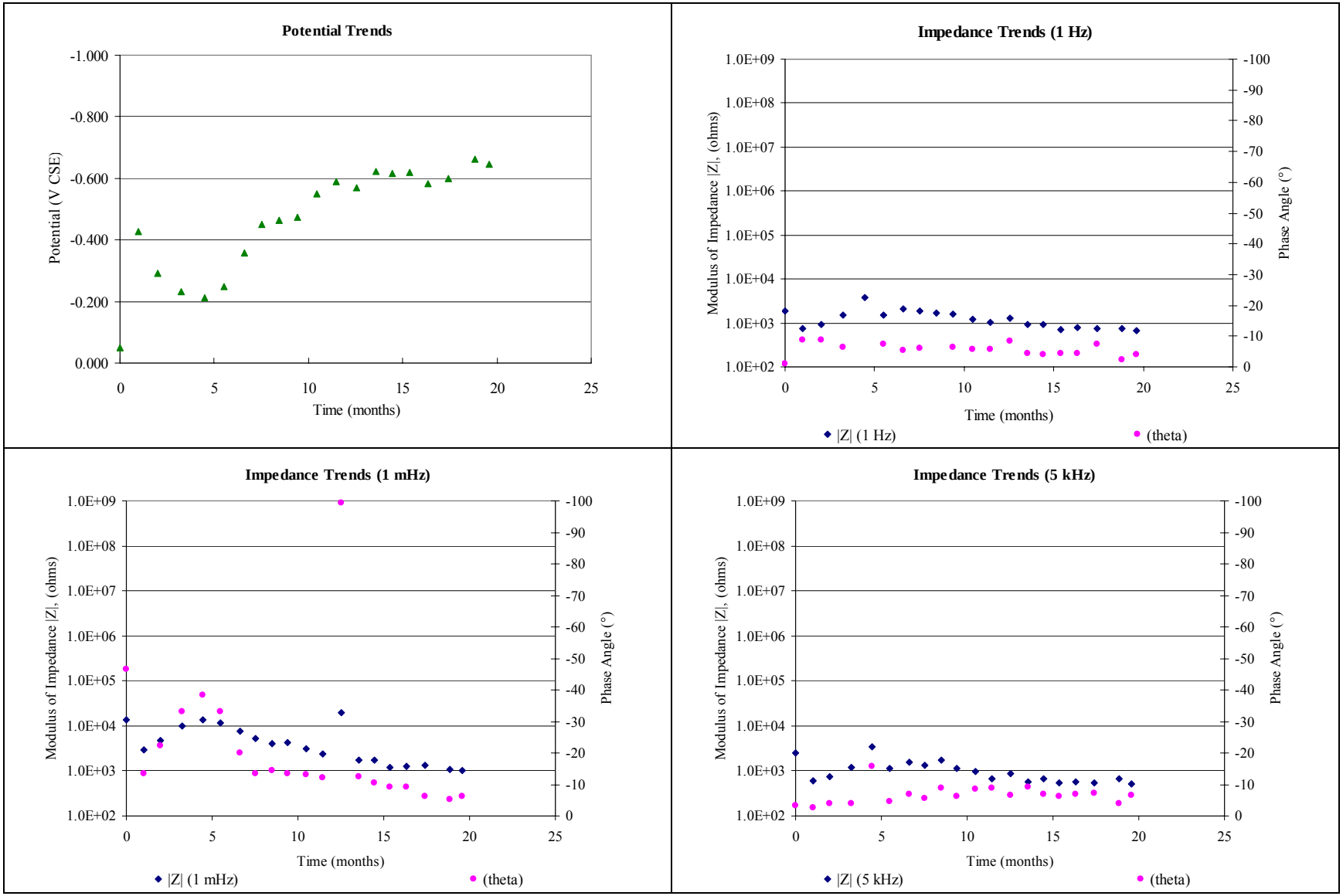

Figure B-118 Potential and Impedance Summary for Specimen 6037_C5

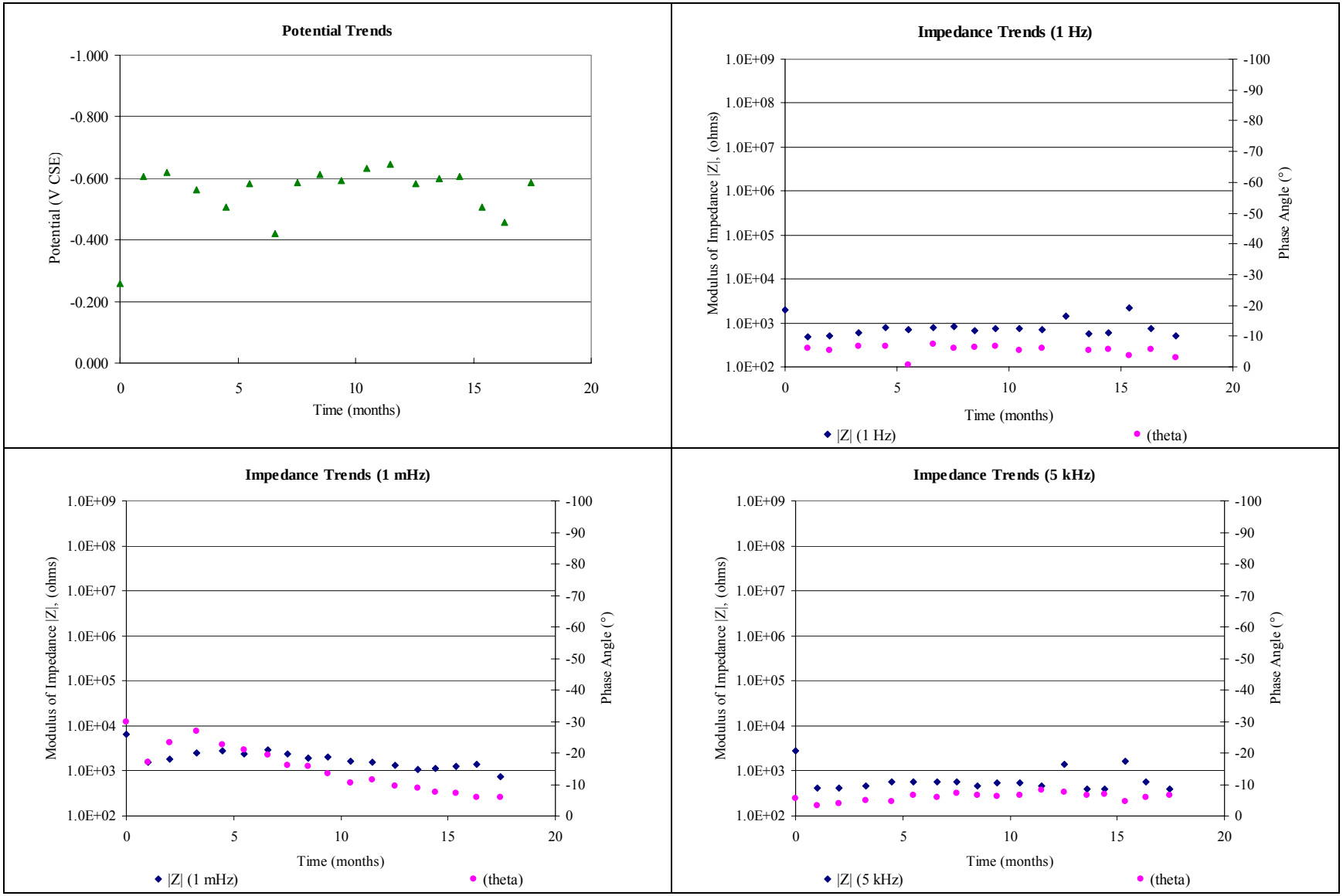

Figure B-119 Potential and Impedance Summary for Specimen 6037_C6/CR2

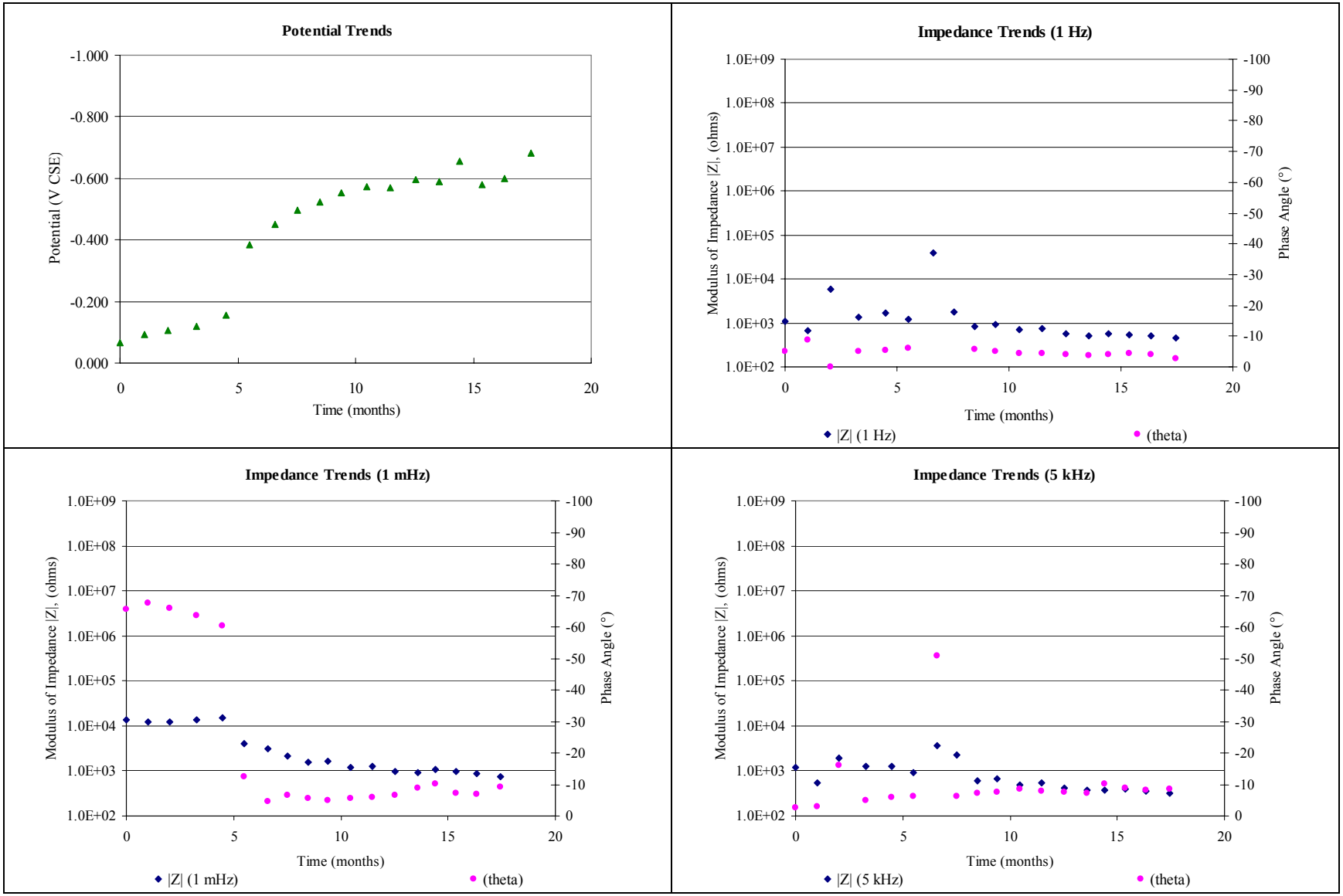

Figure B-120 Potential and Impedance Summary for Specimen 6037_C7

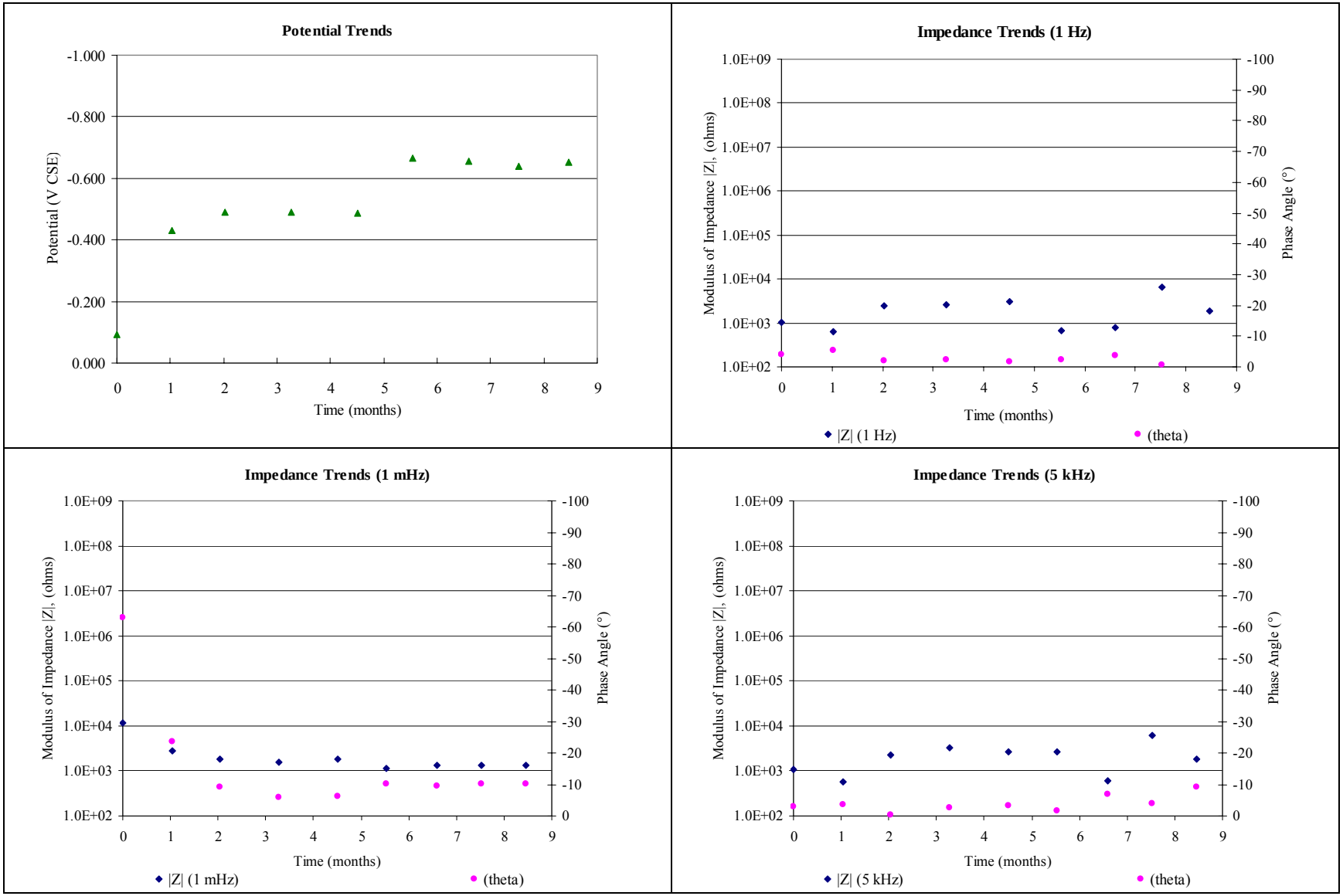

Figure B-121 Potential and Impedance Summary for Specimen 6037_C8

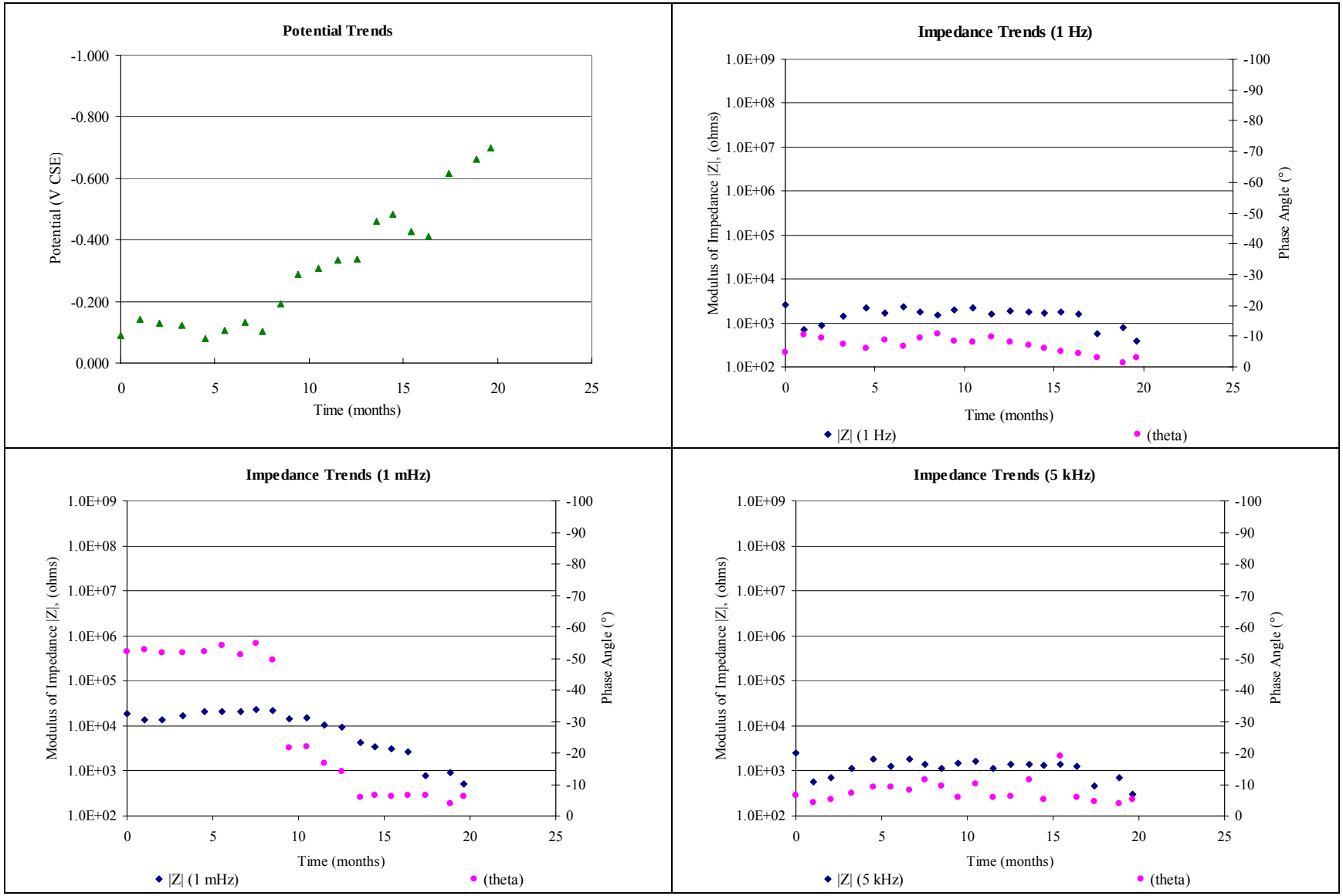

Figure B-122 Potential and Impedance Summary for Specimen 6037_C9

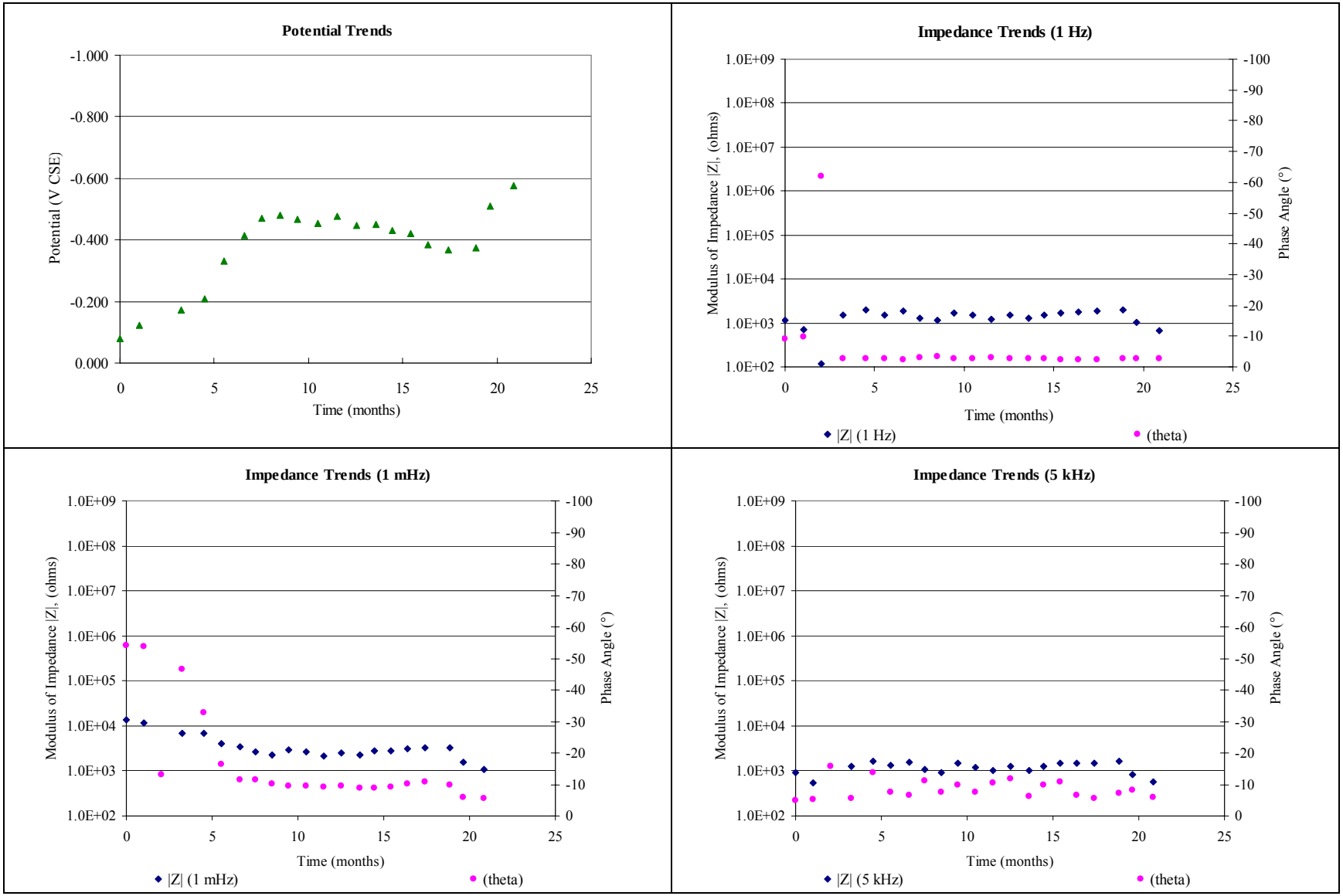

Figure B-123 Potential and Impedance Summary for Specimen 6037_C10

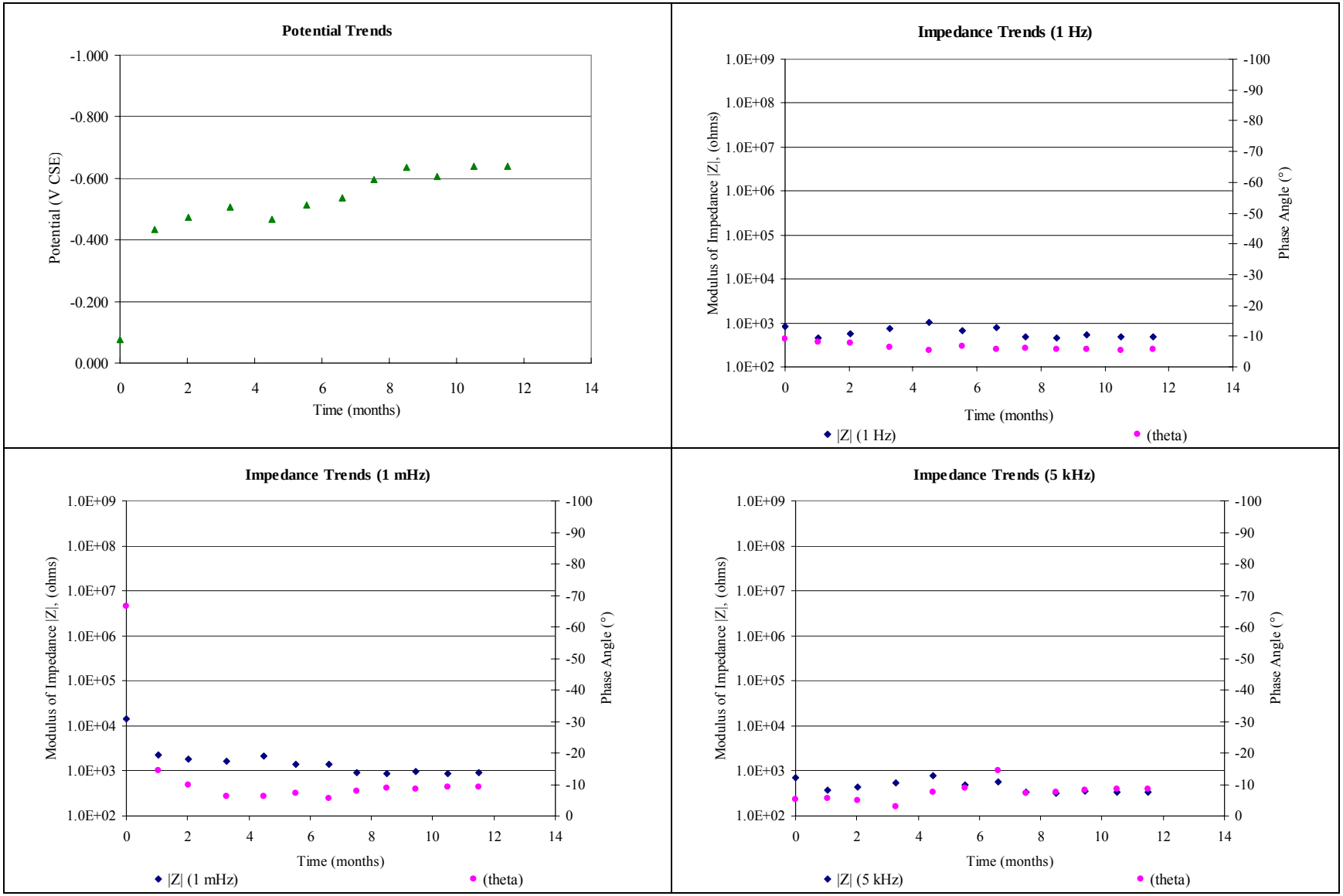

Figure B-124 Potential and Impedance Summary for Specimen 6037_C11

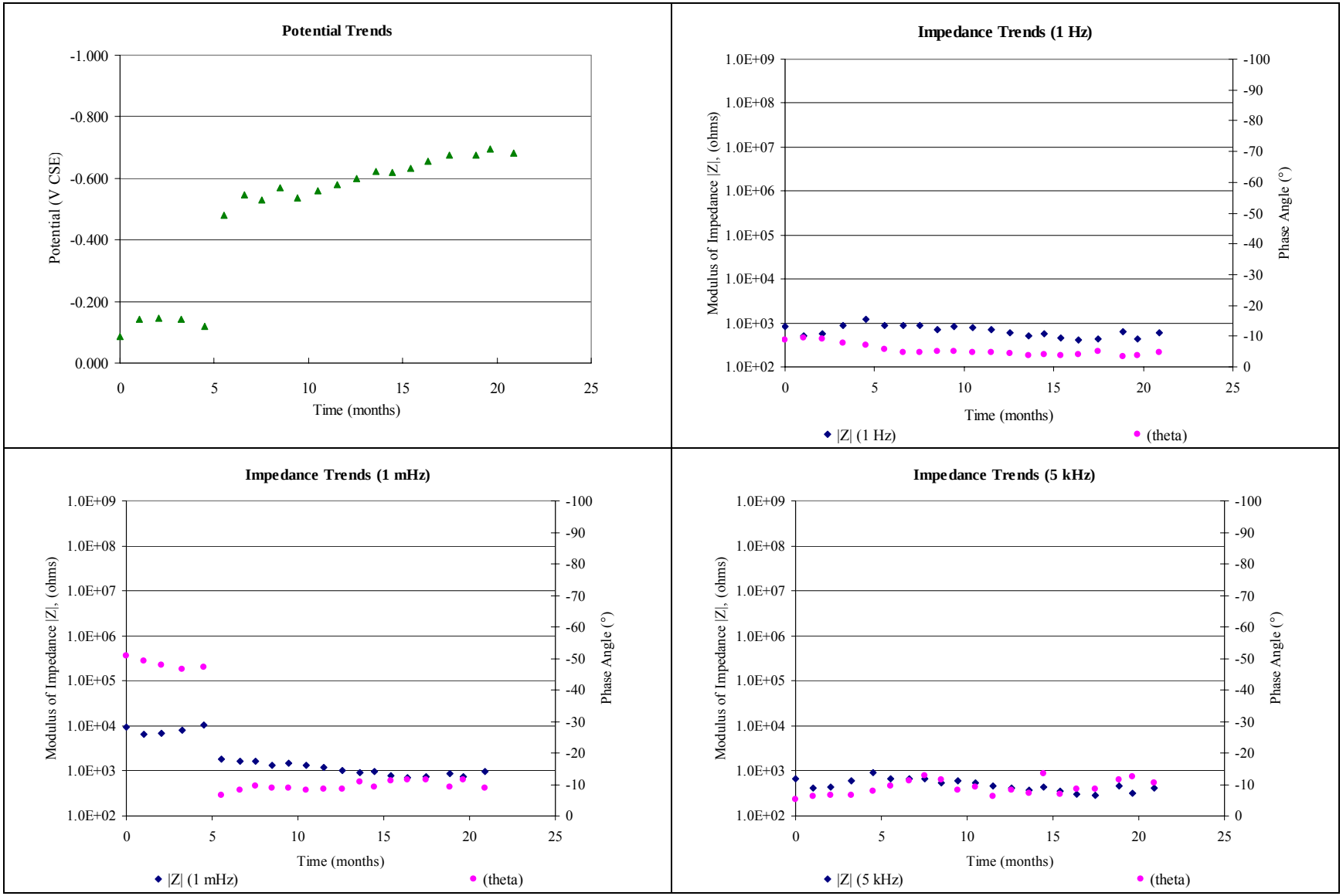

Figure B-125 Potential and Impedance Summary for Specimen 6037_C12

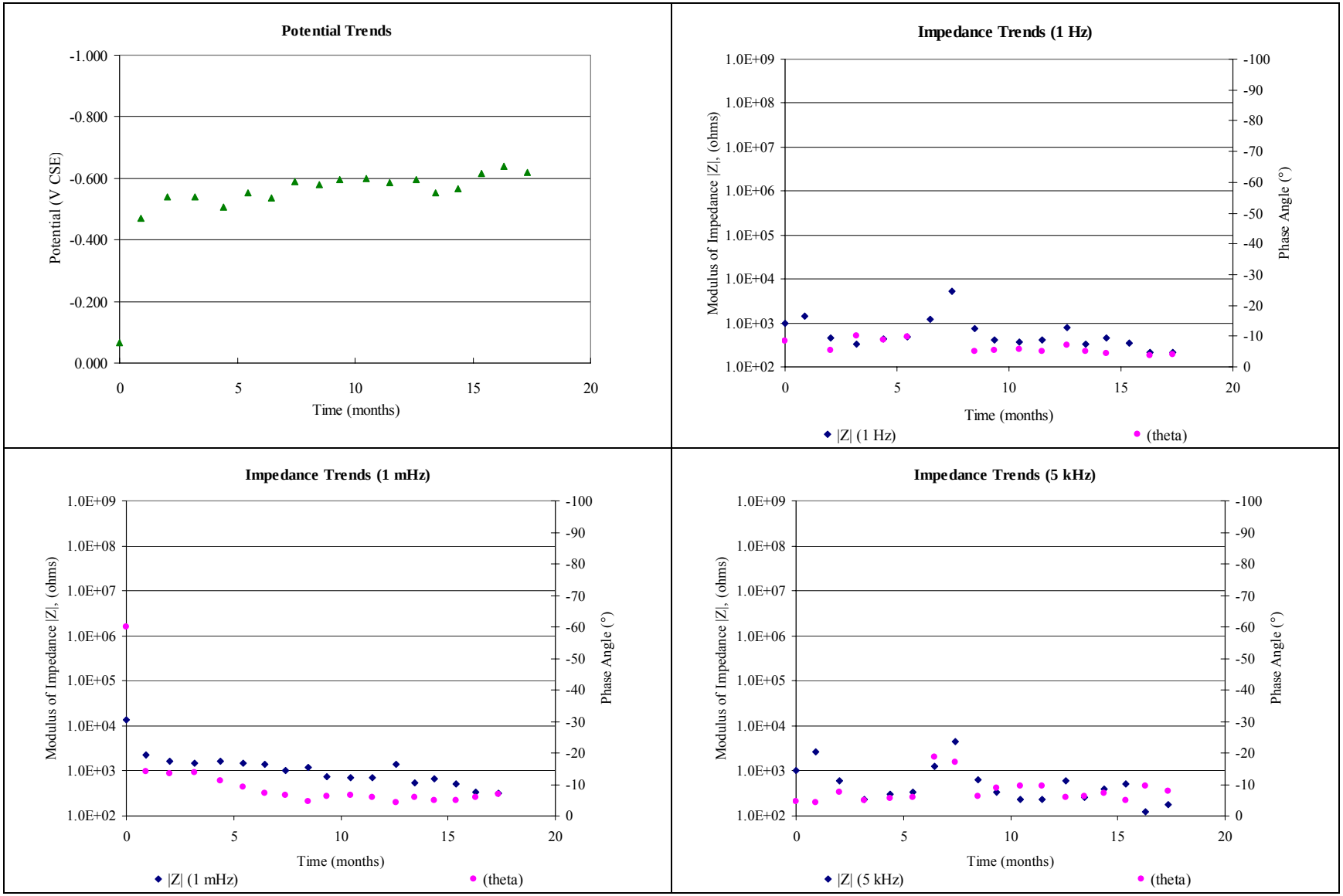

Figure B-126 Potential and Impedance Summary for Specimen 6128_C1

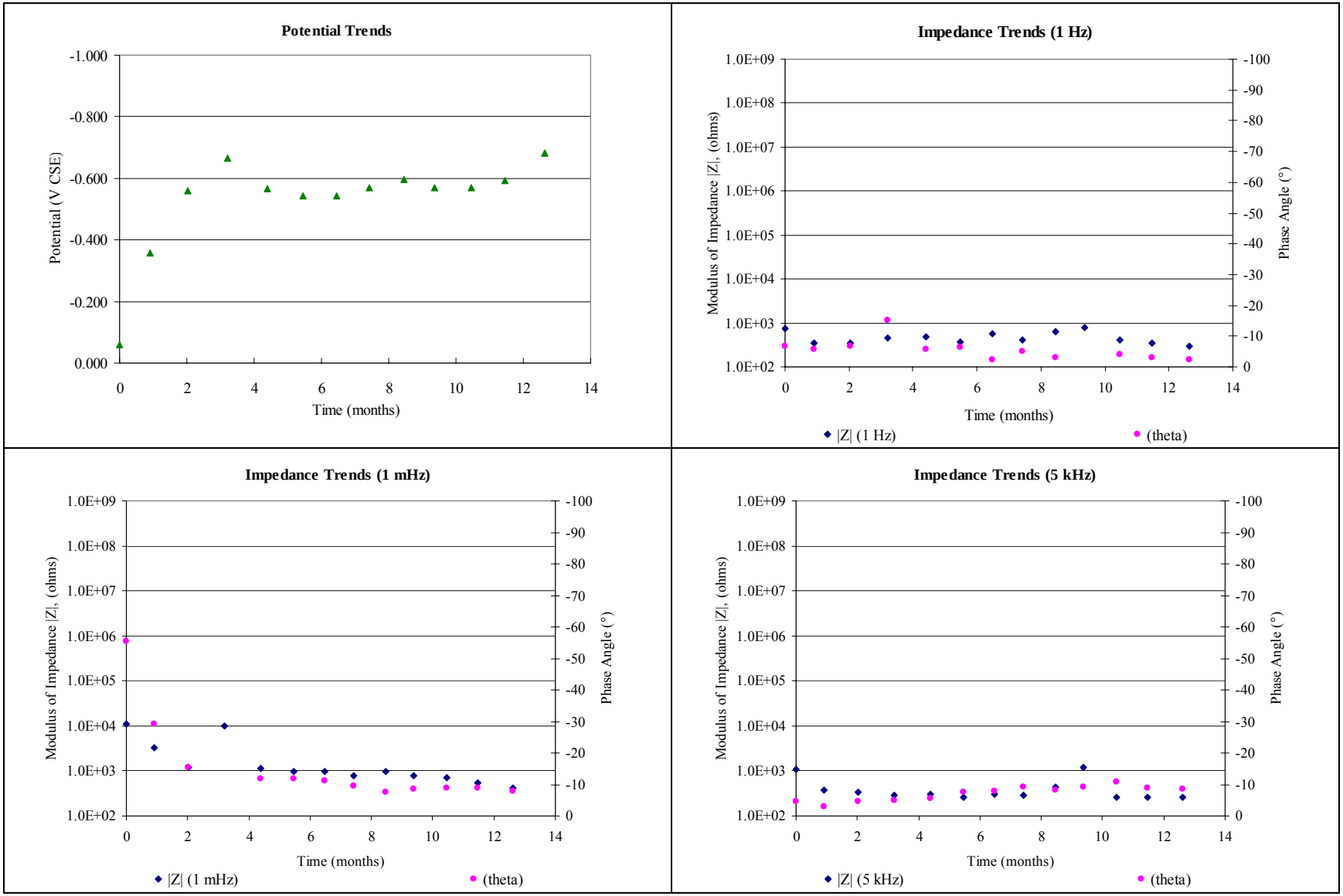

Figure B-127 Potential and Impedance Summary for Specimen 6128_C2

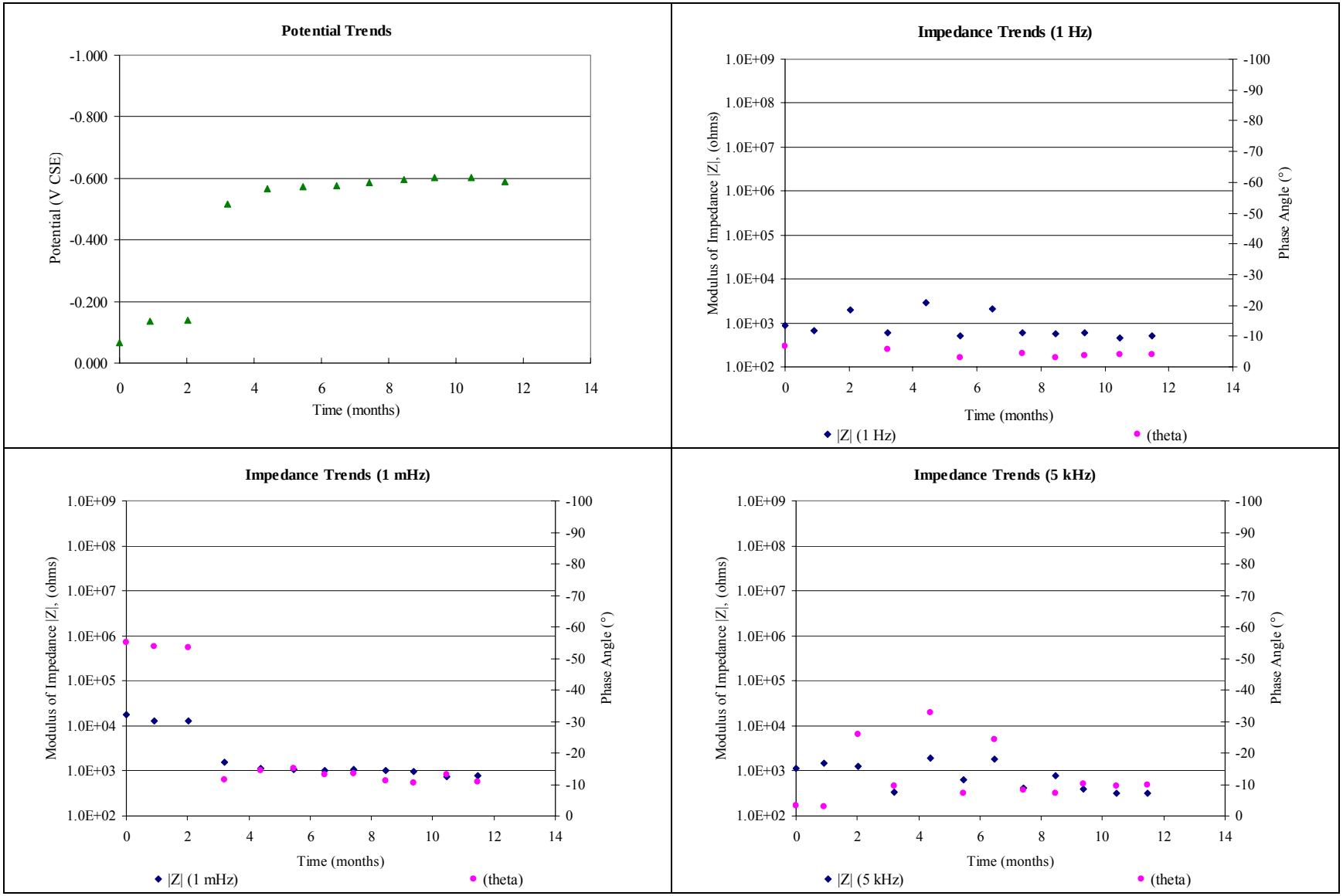

Figure B-128 Potential and Impedance Summary for Specimen 6128_C3

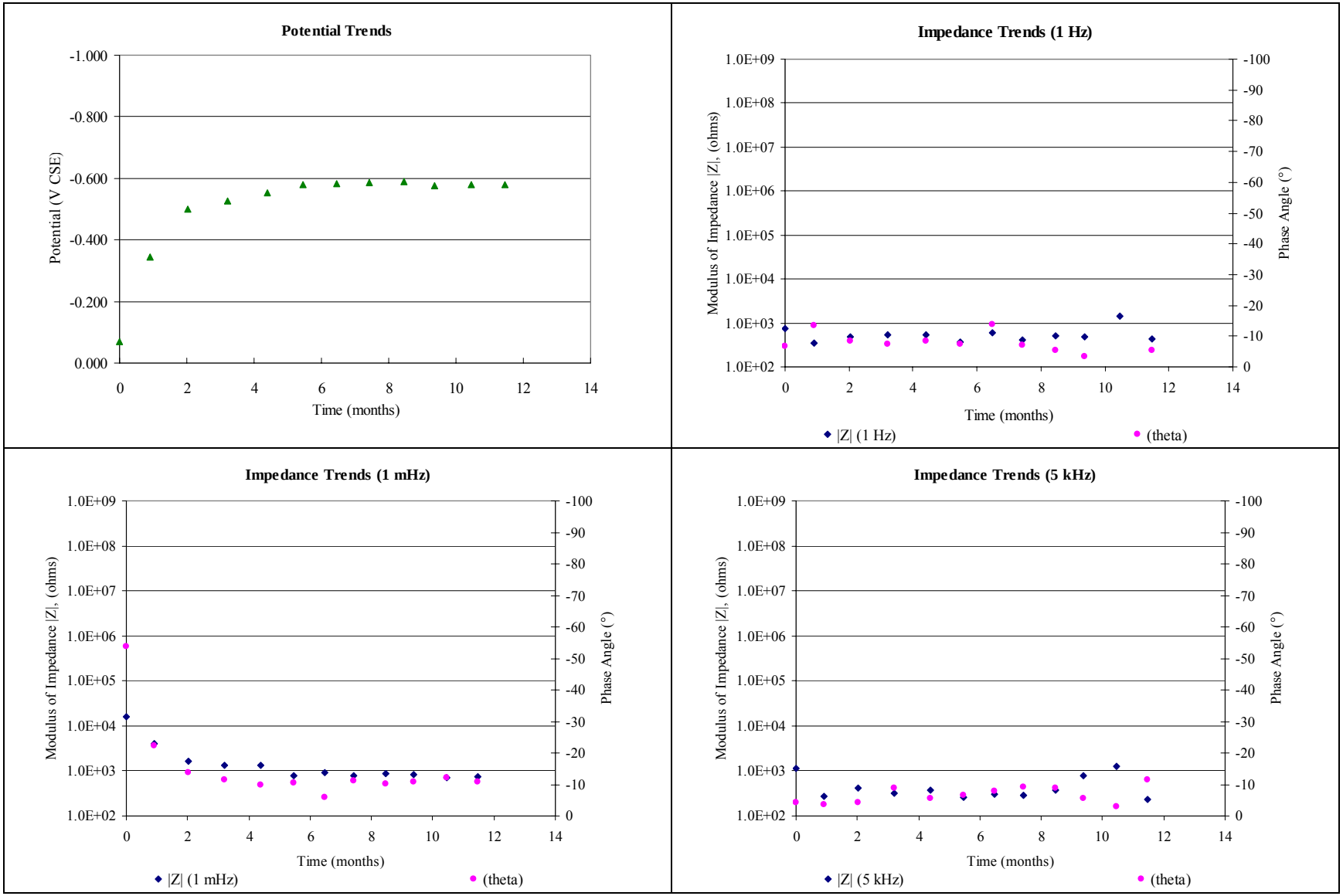

Figure B-129 Potential and Impedance Summary for Specimen 6128_C4

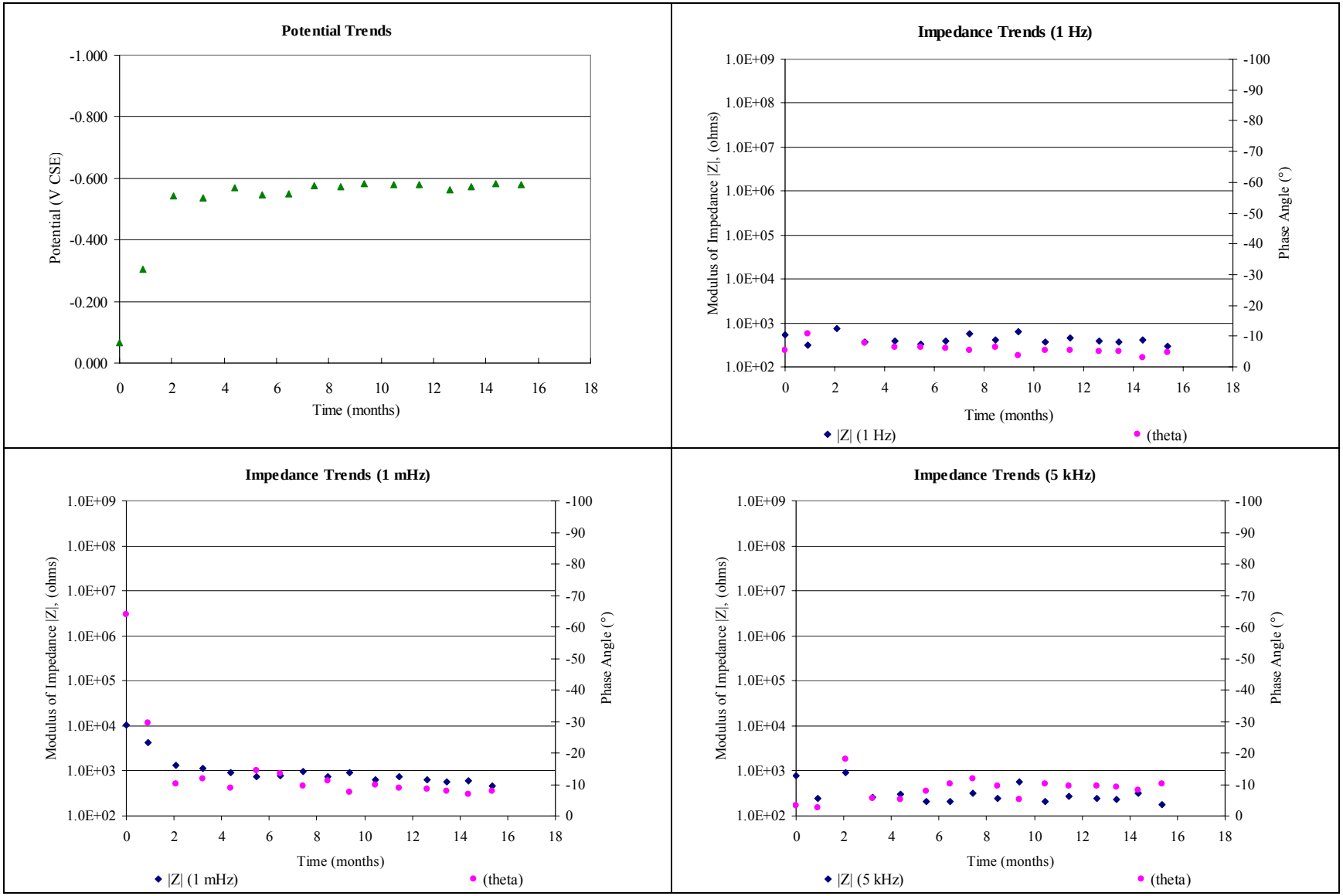

Figure B-130 Potential and Impedance Summary for Specimen 6128_C5

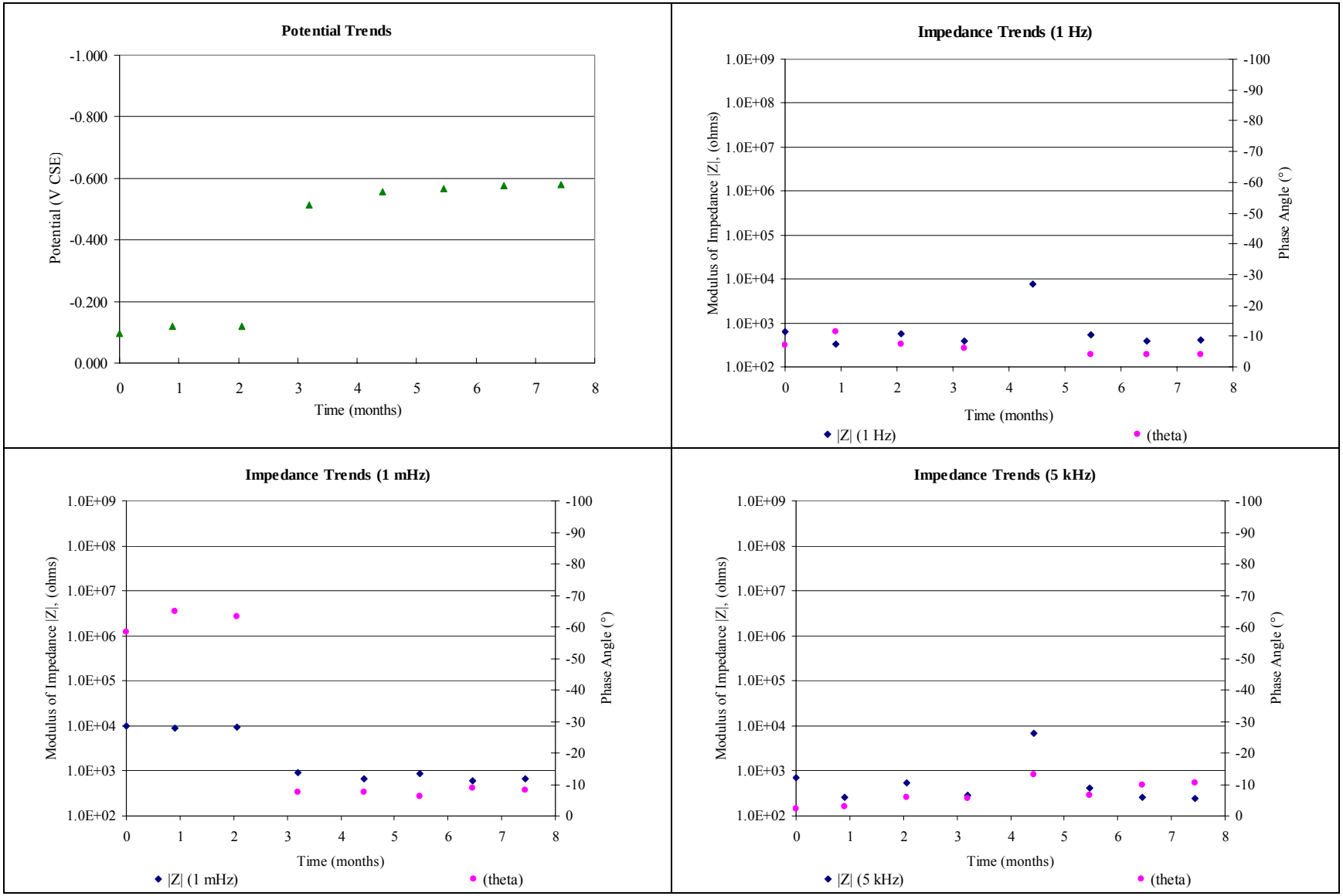

Figure B-131 Potential and Impedance Summary for Specimen 6128_C6

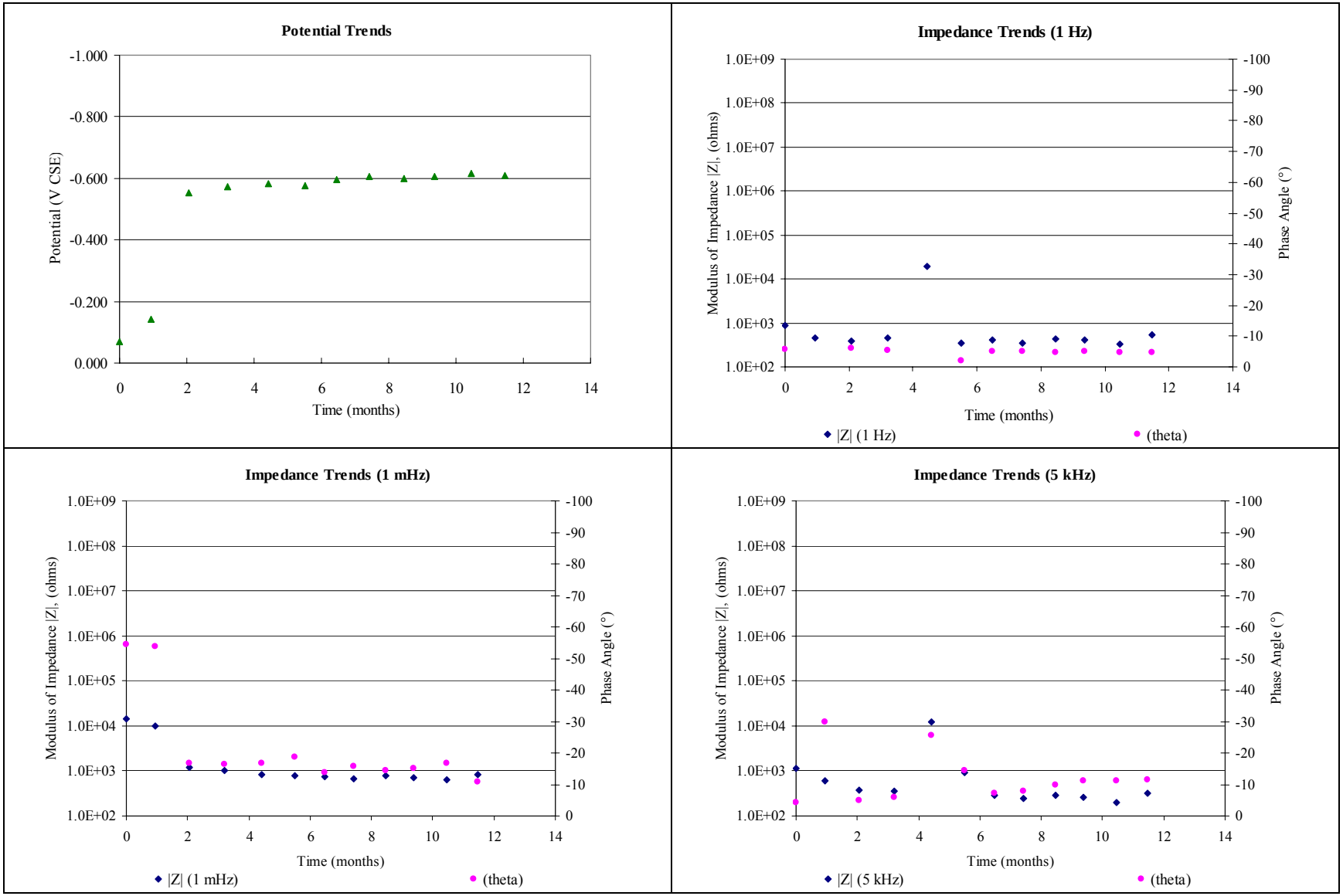

Figure B-132 Potential and Impedance Summary for Specimen 6128_C7

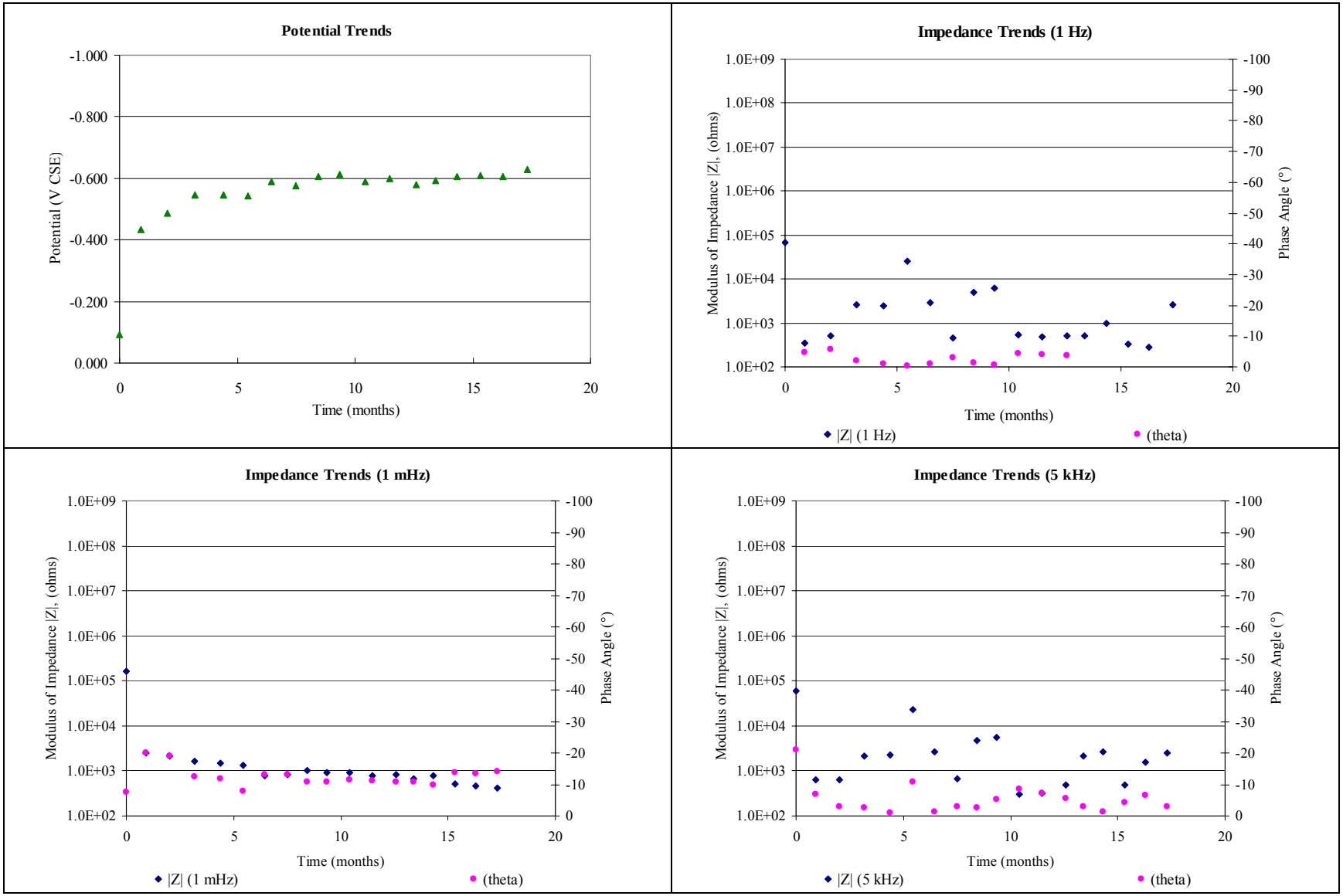

Figure B-133 Potential and Impedance Summary for Specimen 6128_C8

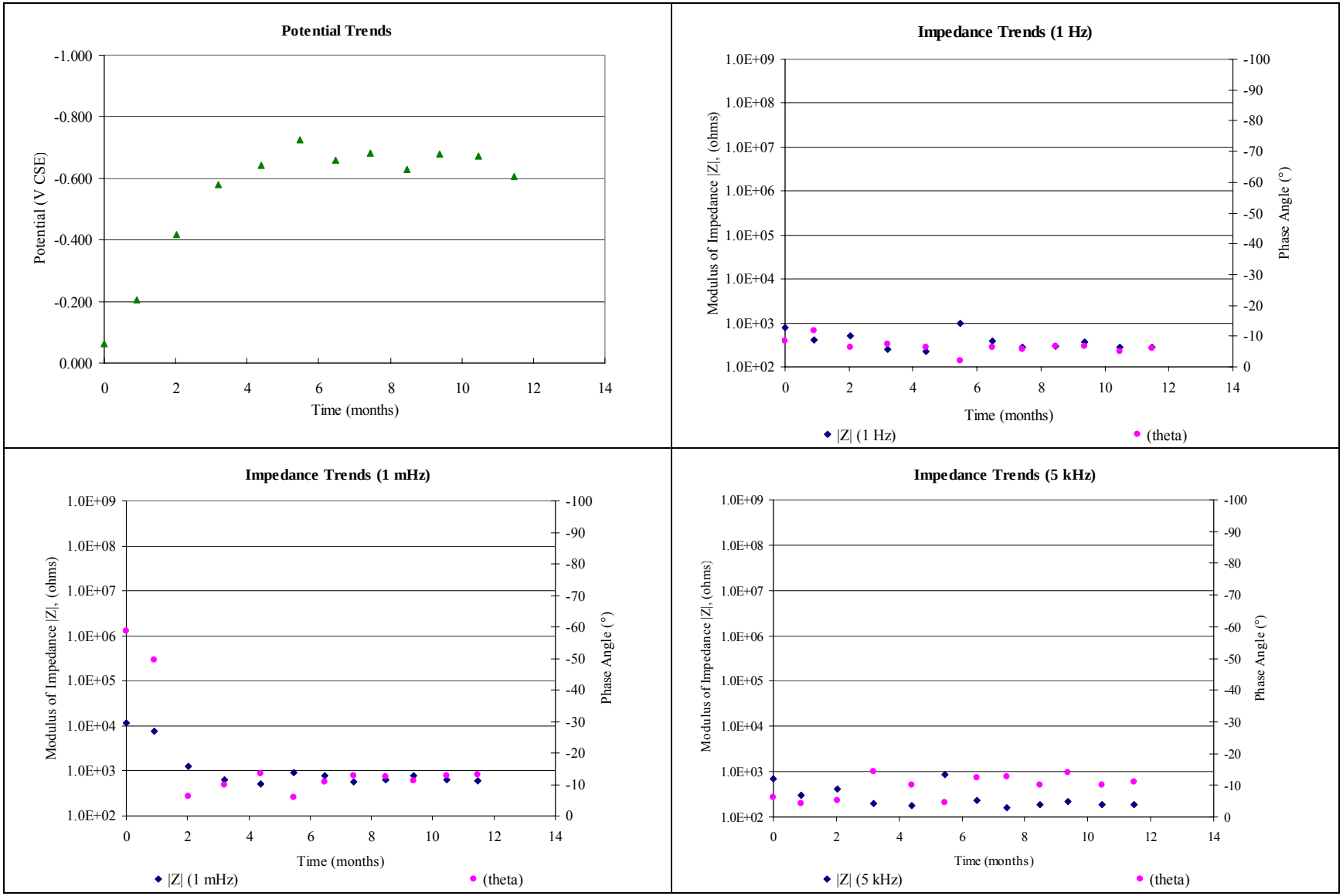

Figure B-134 Potential and Impedance Summary for Specimen 6128_C9

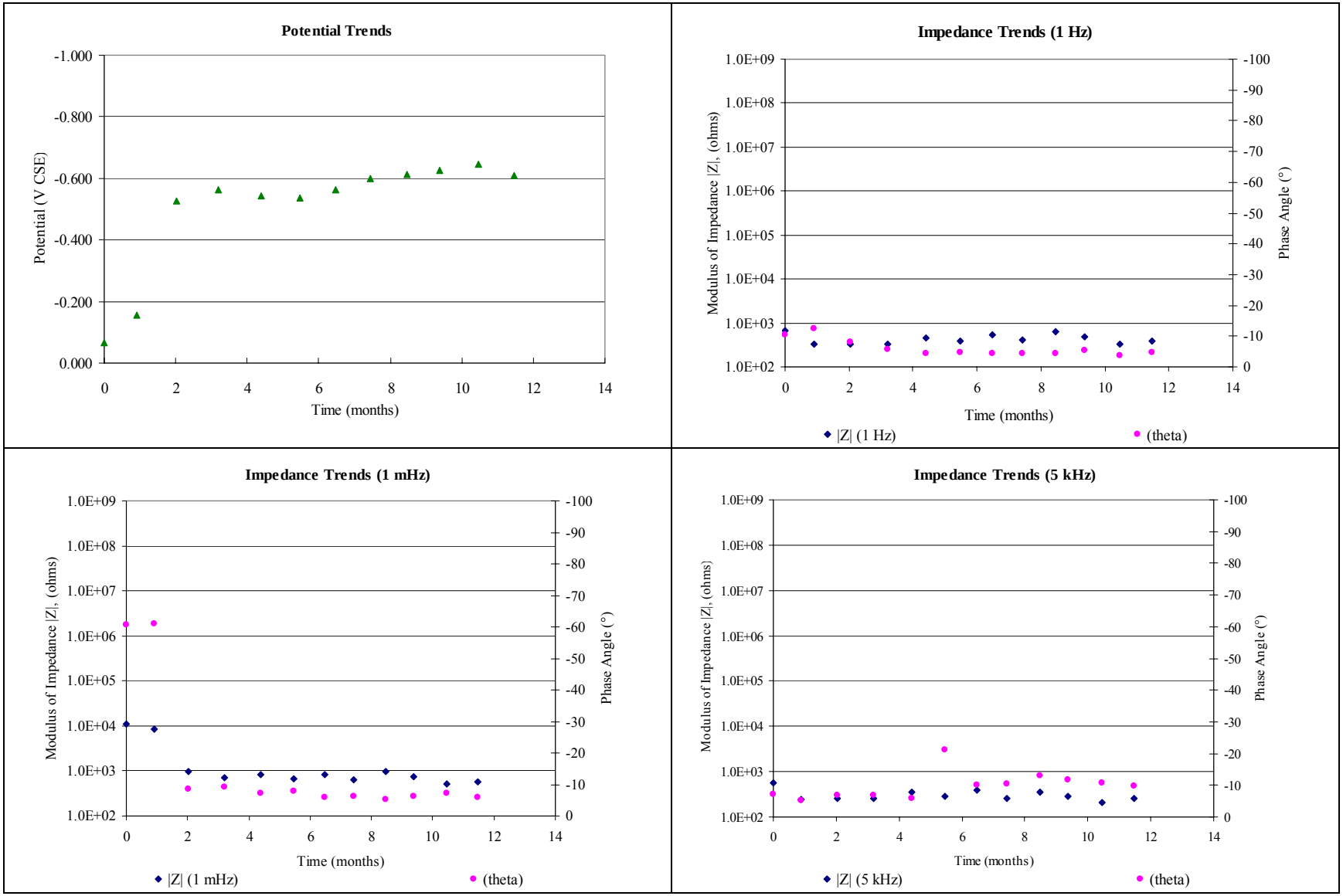

Figure B-135 Potential and Impedance Summary for Specimen 6128_C10

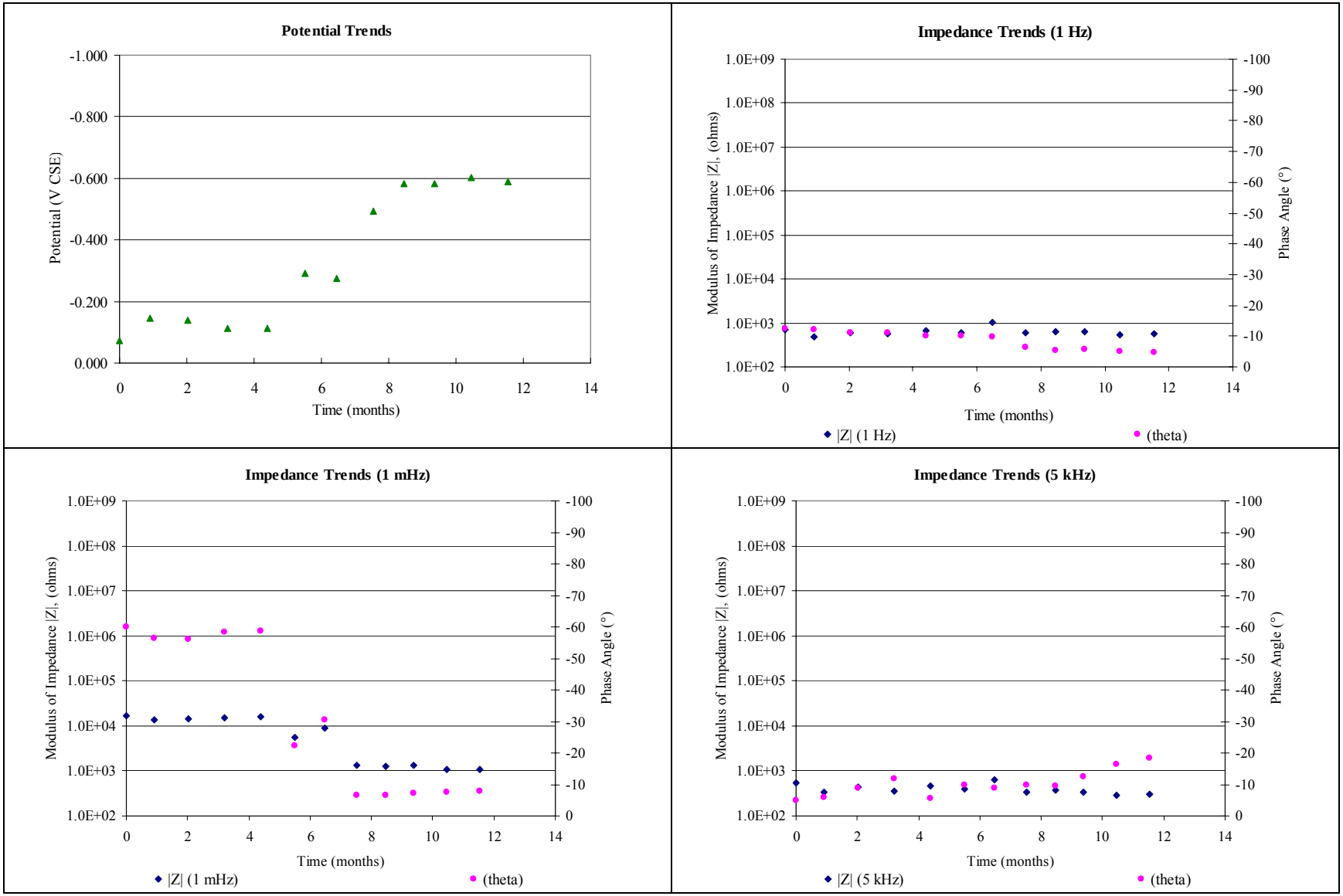

Figure B-136 Potential and Impedance Summary for Specimen 6128_C11

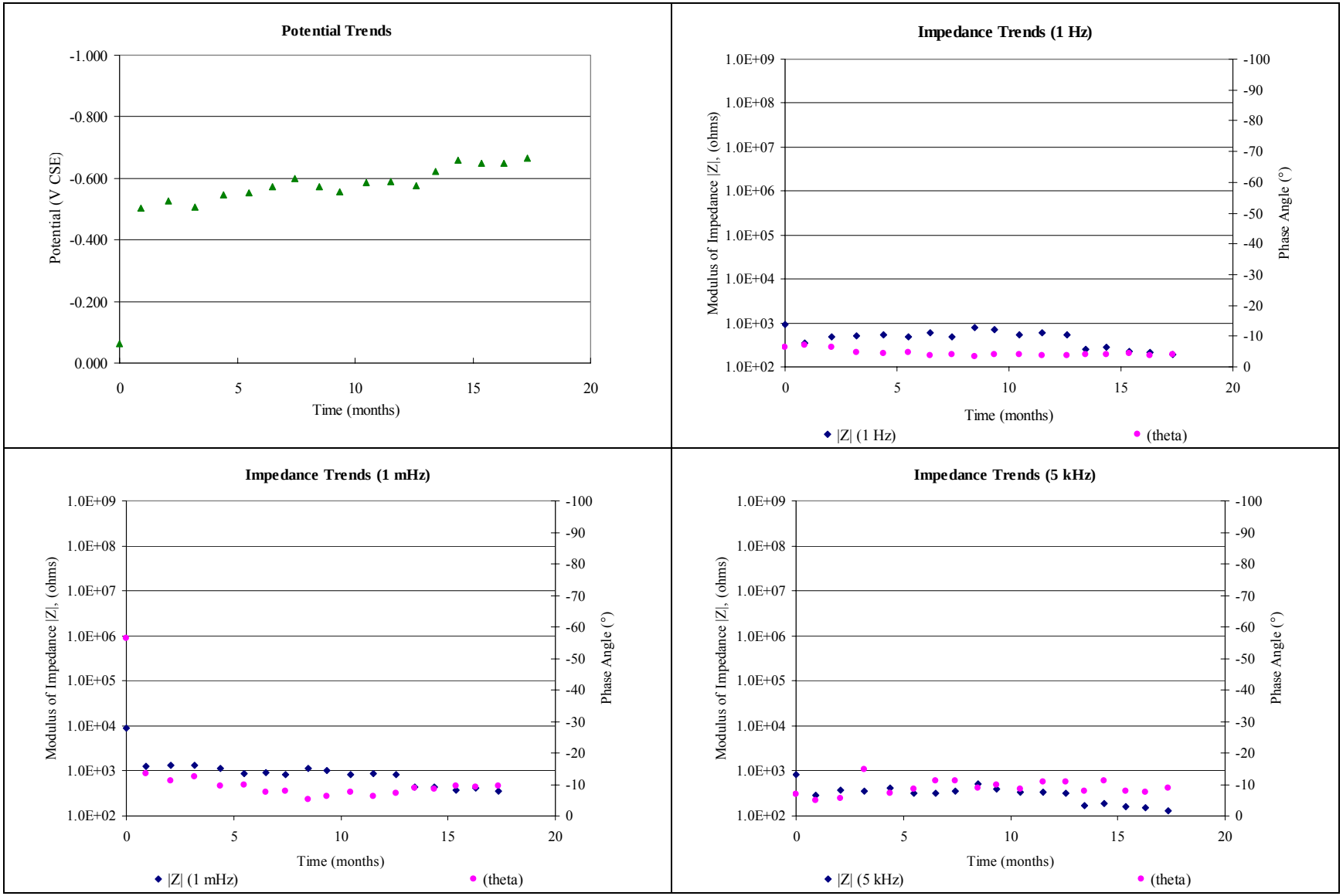

Figure B-137 Potential and Impedance Summary for Specimen 6128_C12

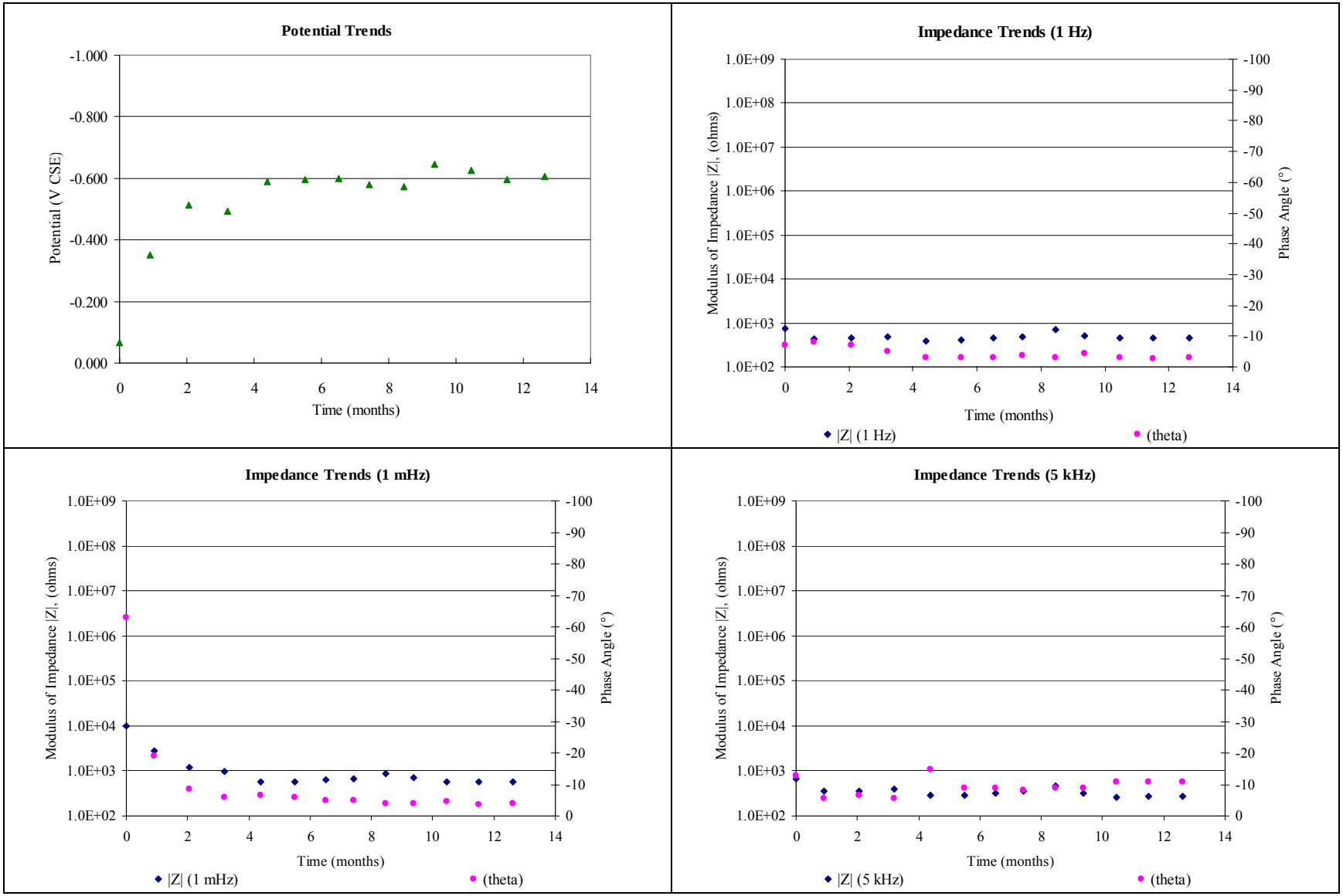

Figure B-138 Potential and Impedance Summary for Specimen 6128_CR1

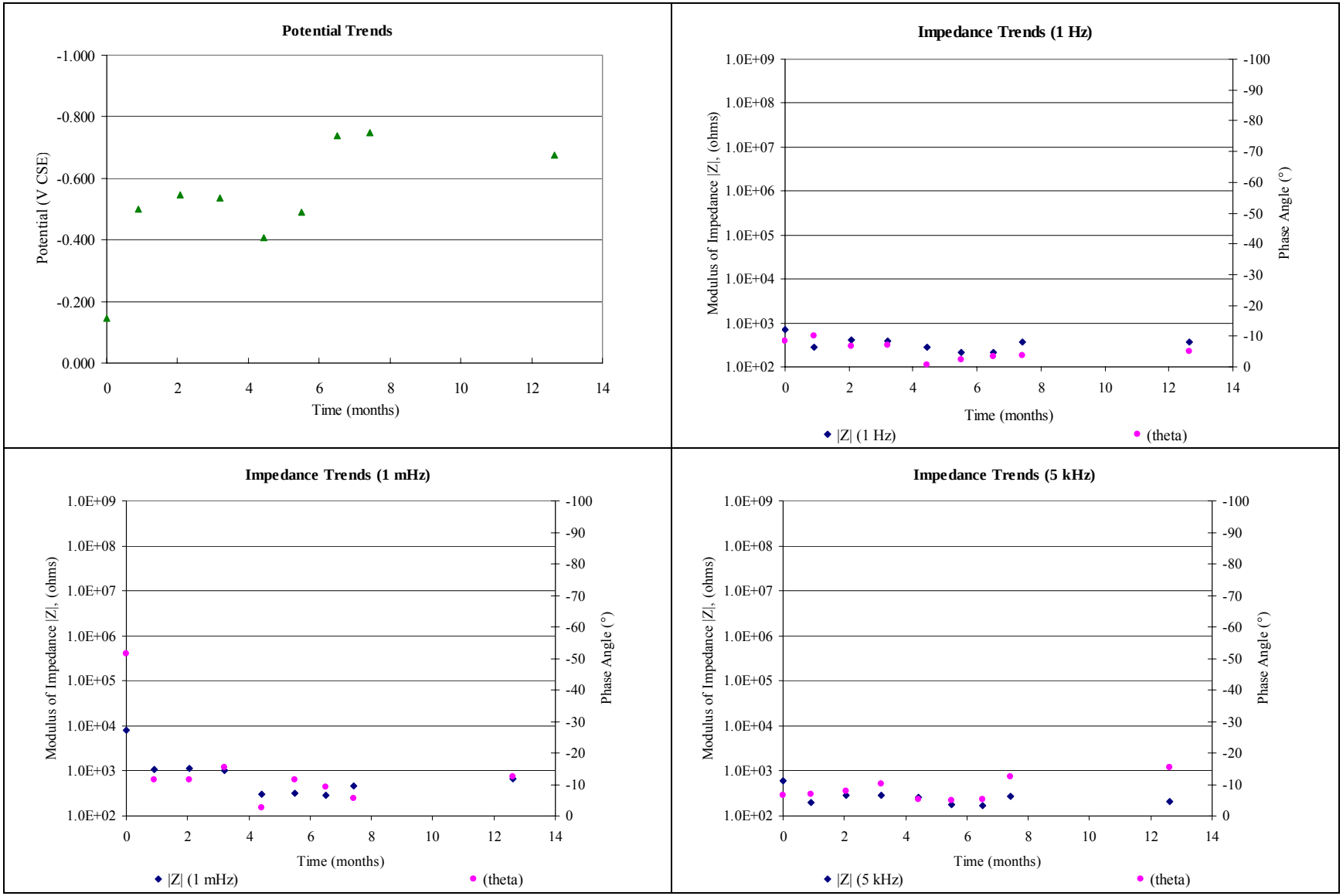

Figure B-139 Potential and Impedance Summary for Specimen 6128_CR2

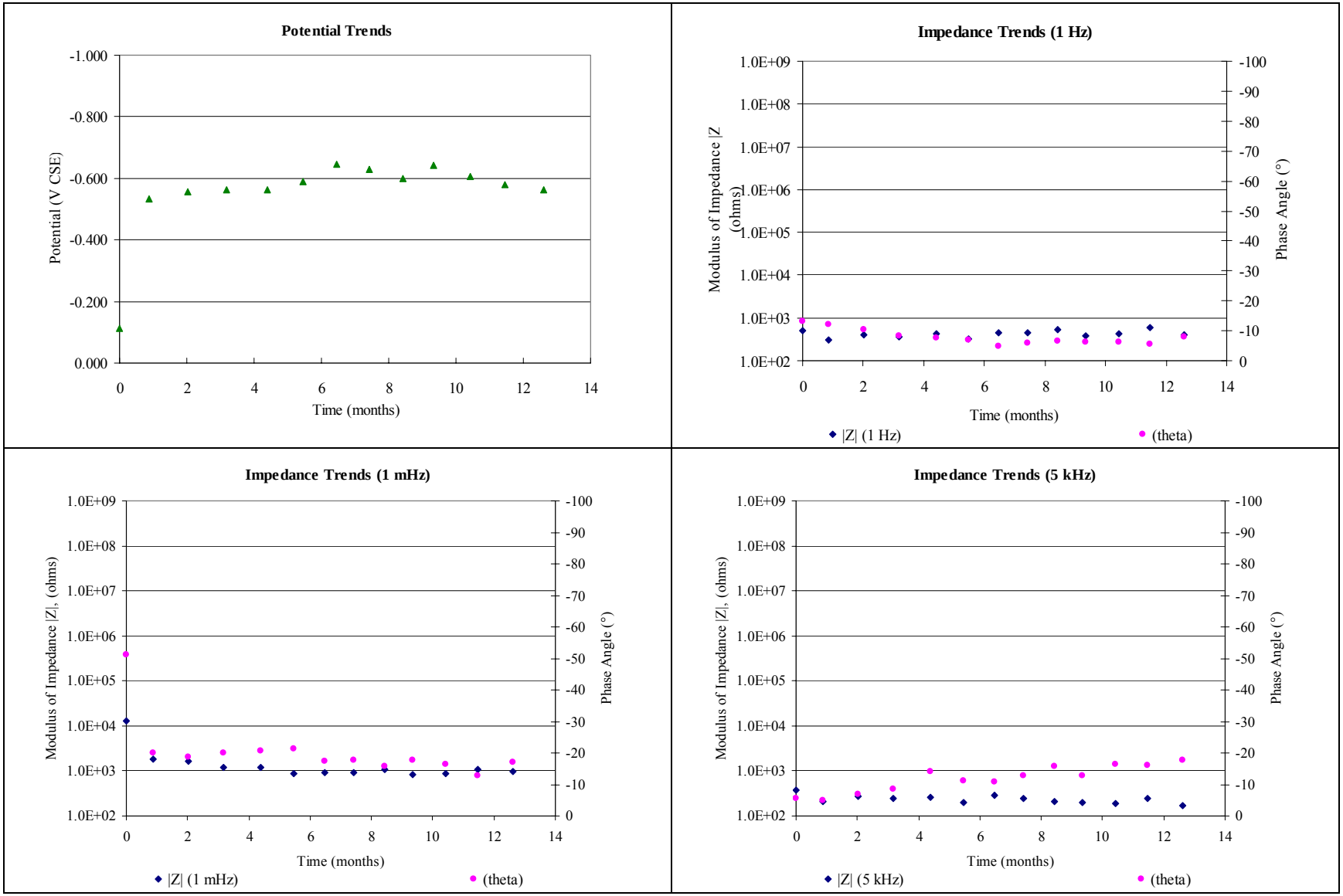

Figure B-140 Potential and Impedance Summary for Specimen 6128_CR3

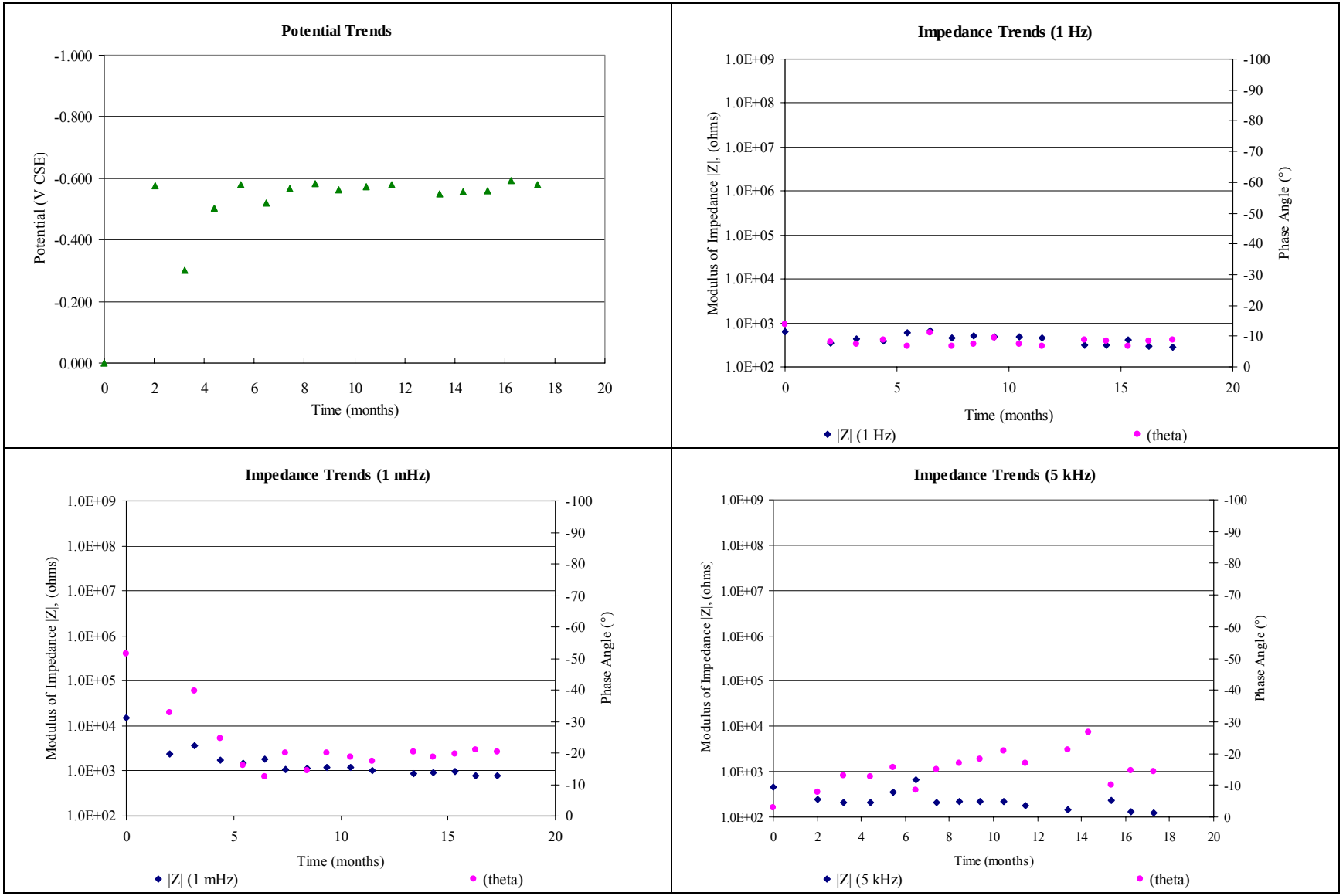

Figure B-141 Potential and Impedance Summary for Specimen 6128_CR4

VITA

Michael Carey Brown was born in Alexandria, Virginia on February 3, 1969, as the first son of Ronald Carey and Jeanne Margaret Brown. The family moved from Alexandria in 1972 to Onancock, Virginia, located on the Eastern Shore Peninsula. There he lived for seven years and began grade school. In 1979, the family moved to Virginia Beach, Virginia, where Michael graduated from Kempsville High School in June 1987.

In August 1987, Michael enrolled at Virginia Tech and began studies in Engineering. He received his Bachelor of Science degree in Civil Engineering in December 1991. From April 1992 to October 1996, Michael worked as a Materials and Project Engineer for Law Engineering and Environmental Services, Inc., in Chantilly, Virginia. While at LAW, Michael conducted assessments and designed repairs of aging structures, and found an enduring interest in the rehabilitation of structures. Under a research fellowship from the National Science Foundation, Michael returned to Virginia Tech in January 1997 to pursue Masters and Doctoral degrees in Civil Infrastructure Systems. Michael completed his Master of Science degree in December 1999, for which he investigated corrosion inhibiting admixtures for reinforced concrete. He continued graduate research in corrosion, focusing on service life prediction for epoxy-coated reinforcement in his doctoral program.

Michael is married to JulieAnne Blancher Brown, who also attended Kempsville High School in Virginia Beach. They are the parents of two children, Alexander and Meghan.